

PAPER

Magnetic and transport properties of the mixed $3d-5d-4f$ double perovskite $\text{Sm}_2\text{CoIrO}_6$

To cite this article: Suman Kalyan Pradhan *et al* 2021 *J. Phys.: Condens. Matter* **33** 335801

View the [article online](#) for updates and enhancements.



IOP | ebooks™

Bringing together innovative digital publishing with leading authors from the global scientific community.

Start exploring the collection—download the first chapter of every title for free.

Magnetic and transport properties of the mixed $3d-5d-4f$ double perovskite $\text{Sm}_2\text{CoIrO}_6$

Suman Kalyan Pradhan¹, Biswajit Dalal¹, Rafikul Ali Saha¹, Raktim Datta², Subham Majumdar²  and Subodh Kumar De^{1,*} 

¹ School of Materials Sciences, Indian Association for the Cultivation of Science, 2A & 2B Raja S.C. Mullick Road, Jadavpur, Kolkata 700032, India

² School of Physical Sciences, Indian Association for the Cultivation of Science, 2A & 2B Raja S.C. Mullick Road, Jadavpur, Kolkata 700032, India

E-mail: msskd@iacs.res.in

Received 25 February 2021, revised 12 May 2021

Accepted for publication 28 May 2021

Published 25 June 2021



CrossMark

Abstract

Iridium-based double perovskites having mixed $3d-5d-4f$ magnetic sub-lattices are expected to exhibit exotic magnetic phenomenon. In this paper, we report a study of structural, magnetic and transport properties of the mixed $3d-5d-4f$ double perovskite $\text{Sm}_2\text{CoIrO}_6$ (SMCO), which crystallizes in monoclinic structure with space group $P2_1/n$ and the crystal symmetry remains same throughout the measured temperature down to 15 K. High resolution synchrotron x-ray diffraction reveals an isostructural phase transition around 104 K. Magnetization measurements on polycrystalline samples indicate that SMCO orders ferrimagnetically at $T_{\text{FiM}} = 104$ K; while, a second transition is observed below 10 K due to the rare-earth (Sm^{3+}) ordering. The ferrimagnetic transition is well-understood by Néel's two-sublattice model, which is primarily ascribed to antiferromagnetic coupling between Co^{2+} and Ir^{4+} sub-lattices. Electronic transport measurement shows the insulating behaviour of SMCO, which follows Mott variable-range hopping conduction mechanism. However, dielectric measurements as a function of temperature rules out the presence of magneto dielectric coupling in this compound.

Keywords: double perovskite, ferrimagnetism, 3D Mott VRH

(Some figures may appear in colour only in the online journal)

1. Introduction

Double perovskite oxides $\text{A}_2\text{BB}'\text{O}_6$ containing alkaline or lanthanide ions at the A site and $3d-4d(5d)$ transition-metal (TM) ions at the B and B' sites offer a unique playground for exploring novel electronic and magnetic phenomena, due to their comparable energies of strong spin-orbit coupling (SOC), on-site Coulomb and crystal-field interactions [1]. Thus, from the perspective of new materials designing, double perovskites provide wide flexibility by virtue of choosing not only the TM

ions but also the alkaline and lanthanide ions. In addition, these double perovskites are found to exhibit a variety of interesting physical properties, such as half-metallic tunneling-type magnetoresistance, high-Curie-temperature ferrimagnetic (FiM) half-metals and insulators, multiferroicity, magnetocaloric, and exchange bias [2–12], enabling them to become a great prospect for spintronic applications. In general, the magnetic ground state and the temperature and magnetic field-dependent magnetization behavior for most of these materials are mainly determined by the TM ions at the B and B' sites through superexchange interaction [13–15]. However, the 12-coordinated alkaline ions do not take part directly in determining the magnetic properties of double perovskite, or otherwise influenc-

* Author to whom any correspondence should be addressed.

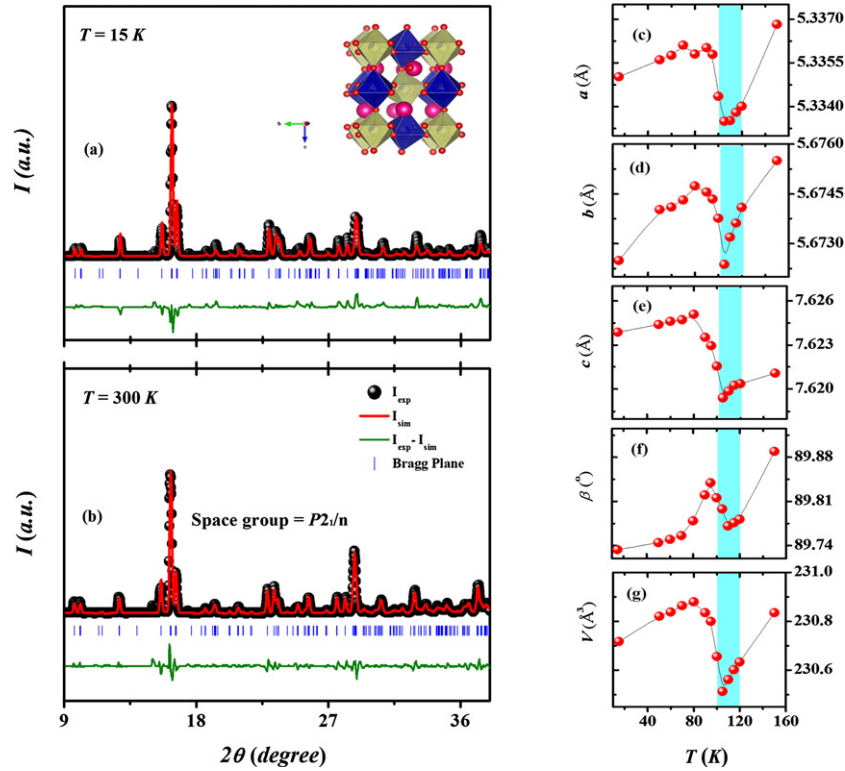


Figure 1. (a) and (b) show the synchrotron x-ray diffraction patterns of $\text{Sm}_2\text{CoIrO}_6$ measured at 15 and 300 K, respectively. Filled black circles represent the experimental data and the continuous red line represents the simulated pattern. The blue scattered lines are the Bragg peak. The green line represents the difference between the experimental and simulated pattern. The inset of (a) represents the refined crystal structure at 15 K. (c)–(g) Thermal variation of lattice parameters a , b , c , β and unit cell volume V .

ing indirectly through lattice distortion. On the other hand, lanthanide ions, in particular, rare-earth (RE) ions having unfilled $4f$ shell are especially interesting in magnetism due to their single-ion anisotropy effect (contribution from the large unquenched orbital angular momentum). Although, the d – f exchange interactions are weaker than d – d exchange interactions as the nature of $4f$ orbitals in RE atoms are strongly localized, these weak exchange interactions however can induce fascinating magnetic phenomenon in the double perovskites [16].

Iridates, more explicitly, iridium (Ir)-based double perovskites have gained a lot of attention in recent days and turned into a rapidly growing research topic in condensed matter physics as $5d$ Ir ions bring strong and unusual SOC, which results in diverse magnetic ground states. In case of $5d^4$ systems i.e., Ir^{5+} ions in an octahedral crystal field of A_2BIrO_6 (with A^{2+} and B^{3+} cations) compounds, it is expected that the strong SOC associated with the Ir ions drives the system into a ' $J_{\text{eff}} = 0$ ' nonmagnetic ground state. However, there are certain controversies in literature regarding the perfect ' $J_{\text{eff}} = 0$ ' ground state, and in most of the cases, it hasn't been achieved due to the presence of either electronic many-body effects or defects (chemical disorder and/or off-stoichiometry) [17–21]. In contrast, the systems having Ir^{4+} ions ($5d^5$, t_{2g}^5)

within octahedral oxygen cages lead to a ' $J_{\text{eff}} = 1/2$ ' Mott-insulating state, as the strong SOC splits t_{2g} level into a fully occupied $J_{\text{eff}} = 3/2$ quartet and a partially-filled $J_{\text{eff}} = 1/2$ doublet states [22]. Furthermore, the double perovskite iridates having strongly correlated $3d$ ions at the other B site are found to show exotic magnetic phenomenon along with the complex magnetic ground states. For instance, among the $\text{La}_2\text{B}(\text{IrO}_6)$ iridates, $\text{B} = \text{Mn}$ is found to show ferromagnetic (FM) ground state [23], the noncollinear antiferromagnetic (AFM) ground state (as well as a weak FM component) is reported for $\text{B} = \text{Ni}$, Fe , Co and Cu compounds [24–31], and the $\text{B} = \text{Mg}$ (Zn) exhibits AFM (canted) ground state [30, 32]. Recently, it is observed that the FM cluster glass and exchange bias behavior have emerged upon Cr-doping at the Cu site of $\text{La}_2\text{CuIrO}_6$ compound [31].

Although earlier studies have reported that $\text{La}_2\text{CoIrO}_6$ shows FM-like components at low temperature (from hysteresis loop measurements) [25, 27], more recent investigations have predicted a FiM ground state resembling to the AFM coupling between a weak FM moment of canted Co^{2+} spins and Ir^{4+} cations with a negative moment [28]. In contrast, a reentrant spin-glass magnetic state also has been found in this compound recently [33]. Since, the other members of this $\text{Ln}_2\text{CoIrO}_6$ family with Ln-site magnetic RE elements

Table 1. The Rietveld refined crystallographic parameters, such as fractional atomic coordinates (with Wyckoff positions), isotropic thermal parameters (B_{iso}) obtained from the $T = 15$ K, x-ray diffraction pattern of $\text{Sm}_2\text{CoIrO}_6$. Occ corresponds to site occupancies.

Space group: $P2_1/n$

$a = 5.3350 \text{ \AA}$, $b = 5.6724 \text{ \AA}$, $c = 7.6238 \text{ \AA}$, $\beta = 89.7325^\circ$

Unit-cell volume (V) = 230.7150 \AA^3

$R_p = 8.2$, $R_{wp} = 10$, $\chi^2 = 5$

| Atom | x/a | y/b | z/c | B_{iso} | Occ |
|-------------|----------|----------|----------|------------------|------|
| Sm ($4e$) | 0.015 33 | 0.573 00 | 0.747 60 | 0.083 | 1.0 |
| Co ($2b$) | 0 | 0 | 0.5 | 0.715 | 0.85 |
| Ir ($2b$) | 0 | 0 | 0.5 | 0.715 | 0.15 |
| Ir ($2a$) | 0 | 0 | 0 | 0.715 | 0.85 |
| Co ($2a$) | 0 | 0 | 0 | 0.715 | 0.15 |
| O1 ($4e$) | 0.100 50 | 0.029 00 | 0.248 30 | 0.916 | 1.0 |
| O2 ($4e$) | 0.187 50 | 0.297 00 | -0.05070 | 0.574 | 1.0 |
| O3 ($4e$) | 0.201 80 | 0.303 60 | 0.548 80 | 0.671 | 1.0 |

could bring a paramagnetism complexity in magnetism due to the interactions between three magnetic cations, researchers now focus on studying the physical properties of hetero-tri-spin $3d-5d-4f$ systems [34]. In this context, it is worthwhile to mention that $\text{Ln}_2\text{CoIrO}_6$ double perovskites with $\text{Ln} = \text{Eu}$, Tb and Ho show a high-temperature FiM transition and moderate magnetocaloric effects (MCEs); while, both $\text{Tb}_2\text{CoIrO}_6$ and $\text{Ho}_2\text{CoIrO}_6$ compounds exhibit a temperature-induced FiM-to-AFM phase transition and a field-induced spin-flop-like transition below AFM Néel temperature [35]. However, no reports have been found in literature till now to understand the complex magnetic and electrical behaviours of SMCO double perovskite having hetero-tri-spin configuration.

In this report, we have investigated the magnetic and transport behaviours of the polycrystalline double perovskite compound SMCO, synthesized by standard solid-state-reaction method. The powder diffraction pattern analysis confirms that SMCO crystallizes in the monoclinic structure with space group $P2_1/n$, alike other hetero-tri-spin systems in this $\text{Ln}_2\text{CoIrO}_6$ family [35]. Temperature and magnetic field-dependent magnetization measurements reveal that sample shows FiM transition at $T_{\text{FiM}} = 104$ K as well as the RE Sm^{3+} ions ordering at $T_{\text{R}}^{\text{Sm}} = 10$ K. However, the conventional Arrott plot rules out the validity of mean-field theory near paramagnetic-FiM phase transition. Temperature dependence of electrical resistivity measurement suggests that SMCO is an insulator, and shows Mott variable-range hopping (VRH) conduction behaviour. Dielectric measurements reveal the absence of magneto dielectric coupling in this as studied sample.

2. Experimental details

Polycrystalline sample of SMCO was prepared by the conventional solid-state-reaction method from stoichiometric amount of Sm_2O_3 (Sigma Aldrich, 99.99%), $\text{CoCO}_3 \cdot x\text{H}_2\text{O}$ (Sigma Aldrich, 99%) and IrO_2 (Sigma Aldrich, 99.99%). At first, these raw oxides and carbonate were mixed and ground thoroughly in an agate mortar, and heated at 873 K for 16 h in air. Then the mixture was reground and sintered at 1323 K

for 24 h in air, and subsequently furnace-cooled to room temperature. This process was repeated 3–5 times to get good quality homogeneous sample. The high resolution temperature dependent powder x-ray diffraction (XRD) measurements were performed using synchrotron facility ($\lambda = 0.77 \text{ \AA}$) at Photon Factory, National Laboratory for High Energy Physics (KEK) Japan, within temperature range 300 K to 15 K. Rietveld refinement [36] of the XRD data was performed using the FullProf software package [37] and the chemical unit cell has been drawn using the software VESTA [38]. The dc magnetization measurements were carried out on a Quantum Design superconducting quantum interference device magnetometer between 2 and 300 K, and applied magnetic field up to 70 kOe. The resistivity of the sample as a function of temperature was measured from 50 to 230 K using the standard four-probe method with dc current in a Physical Properties Measurement System (PPMS, Cryogenic Ltd., UK). The dielectric measurements were performed in the temperature range 5–270 K using low temperature facility (Cryogenics Ltd., UK) and frequency 1 kHz–1 MHz using LCR meter (KEYSIGHT E4980A).

3. Results and discussions

3.1. Crystal structure

The structural refinements of room temperature synchrotron XRD of SMCO has been carried out by considering monoclinic space group $P2_1/n$ (No. 14). Temperature dependent XRD patterns have been taken over a wide temperature range of 15–300 K. The Rietveld refinements of these XRD patterns have been performed using the same monoclinic space group $P2_1/n$ down to 15 K. The refined XRD patterns of both 15 K and room temperature (300 K) are presented in figures 1(a) and (b) respectively. The obtained lattice constants, unit cell volume, and the Wyckoff positions of individual atoms are summarized in table 1 for $T = 15$ K data. Thermal variations of refined lattice parameters, a , b , c , β and V are shown in figures 1(c)–(g). An anomaly at around 104 K is observed in the temperature dependent lattice parameters, signifying a structural phase transition happens in SMCO (shape variation of hkl plane (-112) and (200) are presented from 90–110 K temperature range in the appendix). Due to possible very small changes in the position coordinates across the phase transition, the present Rietveld refinements cannot conclusively determine the true symmetry of low temperature phase. Such kinds of difficulties are not unusual when the lattice distortions are weak [39, 40]. This probably originates from exchange striction results from the lattice degrees of freedom. Such a scenario causes the magnetically interacting atoms to change their relative distance so that the system gains the magnetic energy in lieu of the elastic energy [41]. A careful analysis of the XRD data at 15 K shows the presence of antisite disorder in the system. The best fit is obtained for a disorder of 15% in the system. The peak corresponding to ordering is $2\theta = 10^\circ$. However, the crystal structure consists of alternating octahedral of Co and Ir along three crystallographic directions, as shown in inset of

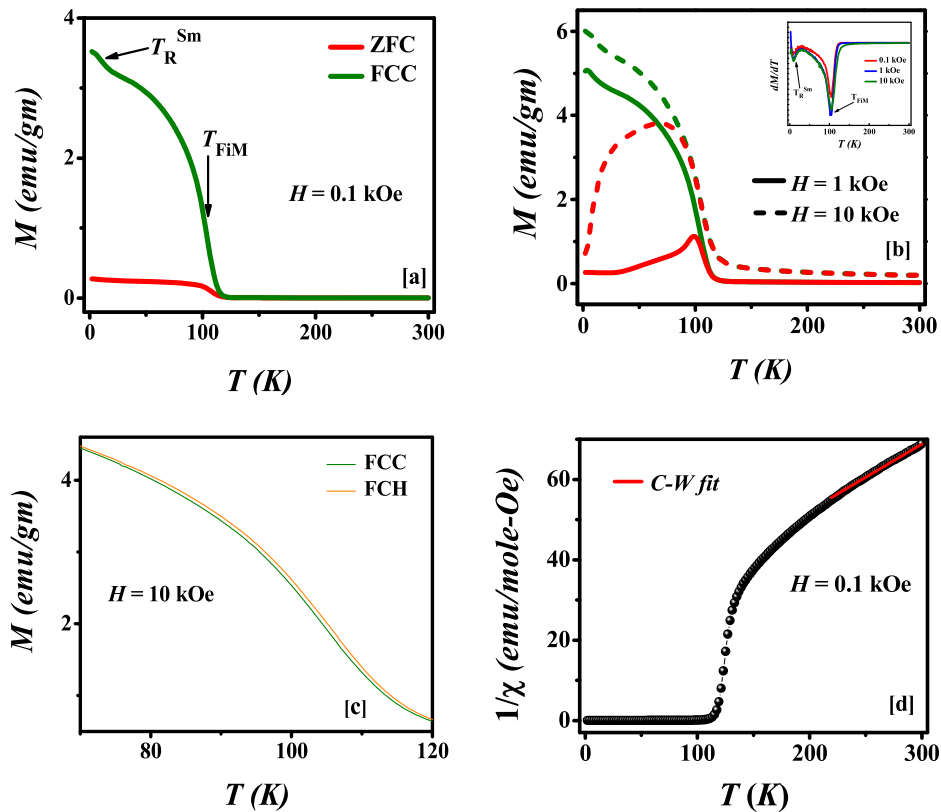


Figure 2. Temperature (T) dependent zero-field-cooled (ZFC: red) and field-cooled-cooling (FCC: green) magnetization (M) at various applied magnetic fields, $H =$ (a) 0.1 kOe (b) 1 kOe and 10 kOe (inset of (b) displays the first-order derivative spectra ($\frac{dM}{dT}$) of FCC $M(T)$ as a function of T for different H). (c) Variation of FCC and FCH data at $H = 10$ kOe in the temperature (T) interval 70–120 K. (d) The magnetic inverse susceptibility ($1/\chi$) as a function of temperature (T) under $H = 0.1$ kOe. Solid red line denotes Curie–Weiss (C–W) behavior at high temperature.

figure 1(a). The crystal structure also reveals that IrO_6 octahedra is connected with CoO_6 octahedra via corner sharing. These connectivities satisfy the Co–O–Ir bond angle $\sim 147.2^\circ$. In addition, we have also calculated the Goldschmidt tolerance factor (t) for this double perovskite compound, as it often gives an indication regarding the stability of crystalline phases. We obtain $t = 0.84$ for this double perovskite considering the ionic radius of $\text{Sm}^{3+} = 1.079 \text{ \AA}$, $\text{Co}^{2+} = 0.745 \text{ \AA}$, $\text{Ir}^{4+} = 0.625 \text{ \AA}$, and $\text{O}^{2-} = 1.40 \text{ \AA}$ [42]. It is well-known that the value $t \leq 0.96$ usually belongs to either orthorhombic or monoclinic structure [43], and the observed monoclinic structural model of SMCO is consistent with this t -value.

3.2. Magnetism

The thermal variations (2–300 K) of the dc magnetization (M) have been measured in the zero-field-cooled (ZFC), field-cool-cooling (FCC) and field-cool-heating (FCH) protocols under different applied magnetic fields. Figures 2(a) and (b) show the ZFC and FCC $M(T)$ data measured at external magnetic fields (H) = 0.1 kOe, 1 kOe, and 10 kOe. As the temperature decreases from room-temperature, both ZFC and FCC magnetizations increase slowly up to a particular temperature. A sudden jump in both ZFC and FCC magnetizations and a large contrast between them below this temperature

($T = 104$ K) indicate the onset of an FM-like ordering. Instead of T_C , we define this particular magnetic ordering temperature as T_{FiM} here, and the reason behind such preference is discussed later. With further decrease of temperature, FCC magnetization curve shows an extra anomaly around 10 K, which is attributed to the ordering (T_{R}^{Sm}) of RE Sm^{3+} spins. Both these magnetic transitions are clearly visible in the thermal variation of the first-order derivative of FCC magnetization ($\frac{dM}{dT}$) (see inset of figure 2(b)); however we observe very weak anomaly in the derivative spectra of ZFC magnetization at lower applied field due to ordering of RE ions, which is not shown here. In addition, we note that the shape of ZFC curve changes with increasing the external magnetic field. At lower applied field (say $H = 0.1$ kOe), no peak exists in the ZFC curve; while, a peak appears just below T_{FiM} for $H = 1$ kOe, which shifts to lower temperature and becomes broader with further increase of external magnetic field (in case of $H = 10$ kOe). This kind of characteristics of ZFC $M(T)$ peak is quite similar to that of the other double perovskite compound, such as $\text{Eu}_2\text{CoIrO}_6$ [35], in this series. Moreover, the bifurcation between ZFC and FCC magnetizations, along with a broad maximum in ZFC curve, signals the presence of large magnetocrystalline anisotropy in this compound.

A wide and thin hysteresis between the FCC and FCH data is observed around 104 K (110–120 K, slightly higher than

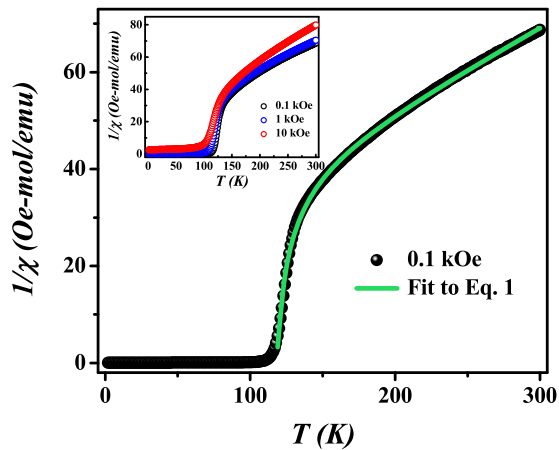


Figure 3. Green solid line suggests the agreement of the Neel's expression at high temperature. (Inset shows the inverse magnetic susceptibility $\{\chi^{-1}(T)\}$ as a function of temperature (T) for different applied magnetic field (H)).

the ordering temperature) (see figure 2(c)) for $H = 10$ kOe, which coincides with the anomaly of the temperature dependent refined lattice parameters (mentioned in section 3.1), signifying the phase transition. This similar kind of trend has been observed for $M(T)$ data measured at other external magnetic fields (H).

The effective magnetic moment of SMCO is calculated from the well-fitted $\chi^{-1}(T)$ data (using $H = 0.1$ kOe FCC data) by the Curie–Weiss (C–W) law, $\chi = C/(T - \theta)$ in the temperature range 230–300 K, where C is the Curie constant and θ is the C–W temperature (see figure 2(d)). The obtained effective magnetic moment (μ_{eff}) and C–W temperature (θ) from the fit are $6.95 \mu_{\text{B}}/\text{f.u.}$ and -117 K, respectively. The negative value of θ indicates the AFM interaction of the compound and is consistent with the Kanamori–Goodenough rule [15] as reflected by the Co–O–Ir bond angle (147.2° , as mentioned in the section 3.1). Since the theoretically calculated value ($\mu_{\text{Sm}}^{\text{theo}} = 0.84 \mu_{\text{B}}$, using $\mu_{\text{Sm}}^{\text{theo}} = g_{\text{Sm}} \sqrt{J_{\text{Sm}}(J_{\text{Sm}} + 1)}$ where g_{Sm} is the Landé g -factor) of effective moment of Sm^{3+} differs significantly from the experimentally observed value of $\mu_{\text{Sm}}^{\text{exp}} = 1.5 \mu_{\text{B}}$ [44], we consider $\mu_{\text{Sm}} = 1.5 \mu_{\text{B}}$, $\mu_{\text{Co}} = 4.8 \mu_{\text{B}}$ (for high-spin Co^{2+} in related double perovskites [35]), and $\mu_{\text{Ir}} = 1.4 \mu_{\text{B}}$ (taking the maximum value in these Ir-based double perovskites [35]) to calculate the expected effective moment of SMCO using the relation $\mu_{\text{eff}} = \sqrt{2\mu_{\text{Sm}}^2 + \mu_{\text{Co}}^2 + \mu_{\text{Ir}}^2}$. The calculated value of $5.43 \mu_{\text{B}}/\text{f.u.}$ is lower than the value obtained experimentally; though, the exact reason is unclear. However, we predict that the large difference between the experimental and theoretical effective moment values might be related to the canted AFM spin states associated with Dzyaloshinskii–Moriya interaction. We also believe that the C–W fitting to $\chi^{-1}(T)$ data for much higher magnetic field would provide better approximation of the theoretical μ_{eff} value.

To investigate the nature of magnetism in this double perovskite and its magnetic ground state, we plot the thermal variation of inverse dc susceptibility $\chi^{-1}(T)$ using $H = 0.1$ kOe FC magnetization data in figure 3. The $\chi^{-1}(T)$ exhibits true paramagnetic nature, and follows conventional C–W behaviour above 225 K. Below this temperature, $\chi^{-1}(T)$ significantly

deviates from C–W behaviour, and shows a sharp downturn (stair-like) before reaching the ordering temperature. This kind of stair-like feature in $\chi^{-1}(T)$, just above the ordering temperature, is often suggested the presence of Griffith's phase, and characterized by the short-range FM clustering due to competing magnetic interactions [45, 46]; however, almost field-independent behaviour of this stair-like feature (remains intact even at higher external applied field, see inset of figure 3) rules out the possibility of formation of Griffith's phase in the vicinity of magnetic ordering temperature. It is important to note that $\chi^{-1}(T)$ shows hyperbolic-kind of variation around the magnetic phase transition, which is in sharp contrast to the typical characteristic of FM materials. Nevertheless, the hyperbolic behaviour of $\chi^{-1}(T)$ above the onset of magnetic ordering is a distinctive of FiM materials, and can be analyzed by Néel's equation [47],

$$\chi^{-1}(T) = \frac{T - \Theta}{C} - \frac{\xi}{T - \Theta'}, \quad (1)$$

where the first term symbolizes simple C–W behaviour at high-temperature region, and last term is responsible for hyperbolic behaviour near FiM ordering [48, 49]. Here, Θ' and ξ are the fitting parameters, and their origins have been described in the two sub-lattice model of FiM [49]. The green solid line in figure 3 is the fitted curve to $\chi^{-1}(T)$ according to equation (1), and an exact fit thus establishes the FiM ordering around $T = 104$ K in this compound. The obtained parameters from this fitting are as follows, $C = 5.17 \text{ emu K mole}^{-1} \text{ Oe}^{-1}$, $\Theta = -137.55 \text{ K}$, $\Theta' = 109.84 \text{ K}$, and $\xi = 350.77 \text{ mole K emu}^{-1} \text{ Oe}^{-1}$. The FiM ordering in this compound mainly originates from the AFM coupling between the canted Co^{2+} and Ir^{4+} spins, as predicted for other compounds $\text{Ln}_2\text{CoIrO}_6$ ($\text{Ln} = \text{La}$, [28, 30] Eu , Tb , and Ho [35]) in this series. The ZFC isothermal magnetization $M(H)$ curves at various temperatures for SMCO are displayed in figure 4(a). The $M(H)$ curves at $T = 150$ K and 120 K do not show any hysteretic behaviour, and magnetization linearly increases with increasing field, implying the true paramagnetic state of the sample. With the decrease of temperature from 120 K to 110 K, the shape of the $M(H)$ curve slightly changes; while, the $M(H)$ curve at $T = 100$ K reveals thin hysteresis loop, and the magnetization starts to show linear field dependency from $H \geq 5$ kOe, thus indicating a typical FiM ground state. From figure 4(a), it is clear that the $M(H)$ curves show well-defined hysteresis loop as the temperature further decreases below 100 K, and the coercive field (H_C) and the remanent magnetization continuously increase with decreasing temperature. From the isothermal $M(H)$ curves measured at different temperatures, the estimated values of H_C are plotted as a function of temperature in figure 4(b), which clearly shows a sudden change in slope near the onset of FiM ordering, and H_C gradually increases with decreasing temperature below FiM ordering temperature and reaches the maximum value at $T = 2$ K. The strong linear field dependence of magnetization beyond the FiM hysteresis can be attributed to the gradual field alignment of the canted Co^{2+} and Ir^{4+} moments [35], and as a result, $M(H)$ curves do not show any sign of saturation at $H = 70$ kOe. It is worthwhile to mention that M does not saturate even up to 60 T

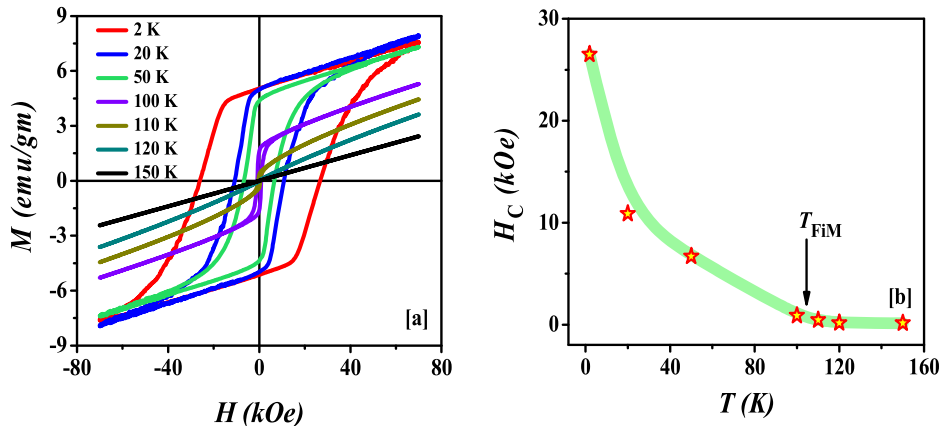


Figure 4. (a) Magnetization (M) vs Magnetic Field (H) loop ranging from -70 to 70 kOe at various temperatures, (b) temperature (T) dependence of obtained coercive field (H_C) from ZFC $M(H)$ loops.

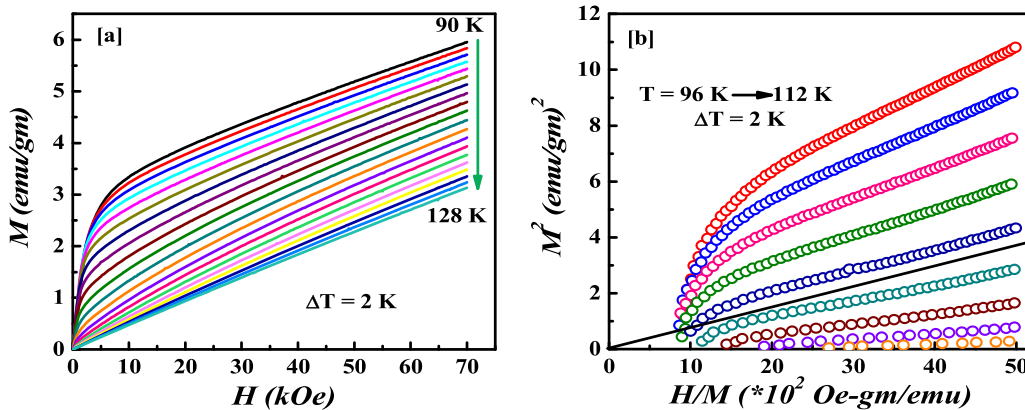


Figure 5. (a) M vs H isotherm (Virgin curve) around T_{FiM} , from temperature (T) between 90 and 128 K at the interval of 2 K. (b) Basic Arrott plots constructed from M - H data.

magnetic field (varies linearly with field) in similar Ir-based double perovskite materials [35].

To understand the nature of magnetic phase transition in-depth, we have carried out isothermal magnetization measurements in the vicinity of PM-FiM transition. Figure 5(a) shows a series of initial $M(H)$ isotherms (virgin legs) in between 90 – 128 K at an interval $\Delta T = 2$ K, showing a gradual change between PM and FiM states. However, it is advantageous to use the conventional Arrott plot (M^2 vs H/M) method [50] to determine the order of phase transition. Figure 5(b) displays the Arrott plot for this compound in between 96 – 112 K. The positive slope of M^2 vs H/M isotherms indicates that the PM-FiM phase transition in this compound is second order, which is in accordance with the Banerjee criteria [51]. Furthermore, according to the mean-field theory, M^2 vs H/M isotherms at different temperatures should manifest a set of parallel straight lines near the magnetic phase transition, and the line at $T = T_{\text{FiM}}$ must traverse the origin. In contrast, a non-linear variation of M^2 vs H/M curves has been found for SMCO, exhibiting a significant downward curvature at low-field region possibly due to the mutually misaligned magnetic domains [52]; while, the high-field linear portions show clear divergence. Hence, the mean-field theory fails to interpret the observed phase transi-

tion in SMCO, indicating the presence of critical fluctuations. Therefore modified Arrott plot method may be a good option to analyze the criticality [53].

The MCE has been investigated in order to understand the isothermal magnetic entropy change ΔS_M of the magnetic material when it is subjected to a changing external magnetic field, and to explore the possible applications in magnetic refrigeration technology. Besides the direct measurement through calorimetry method, it is well-established that ΔS_M can be calculated indirectly from magnetization measurements using Maxwell’s thermodynamic relation:

$$\Delta S_M = \int_0^H \left(\frac{\partial M(T, H)}{\partial T} \right) dH.$$

It is found that $-\Delta S_M$ reaches a maximum value around the magnetic ordering temperature, T_{FiM} at each field, where the value of $-\Delta S_M$ has been calculated from the isothermal $M(H)$ virgin curves of figure 5(a). The temperature and field dependence of $-\Delta S_M$ for SMCO is displayed in figure 6 through a three-dimensional surface plot. The magnitude of $-\Delta S_M$ increases with increasing field, and the maximum value of $-\Delta S_M$ is found to be $0.716 \text{ J kg}^{-1} \text{ K}^{-1}$ at $H = 70$ kOe, which

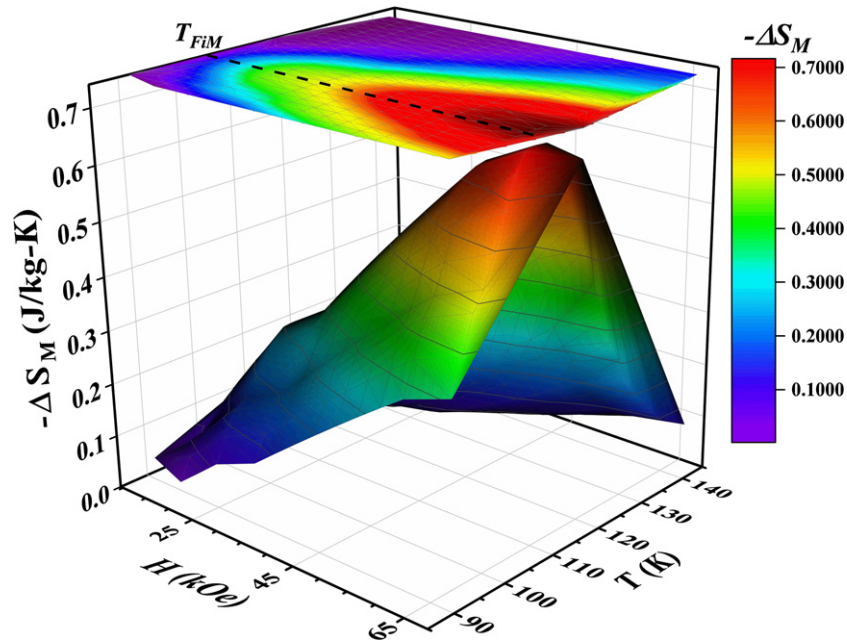


Figure 6. Thermal profile of field induced magnetic entropy change ($-\Delta S_M$) under the applied field changing from 10–70 kOe.

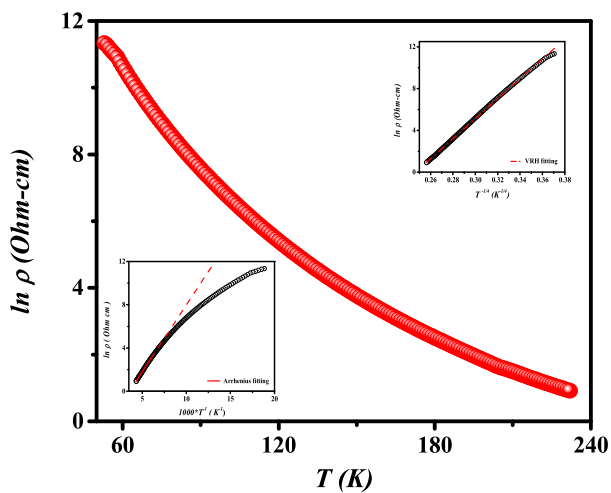


Figure 7. Temperature (T) dependence of resistivity (ρ) for SMCO. Upper and lower insets show the fitting results using VRH and Arrhenius model respectively.

is slightly higher than that of the value reported for $\text{Eu}_2\text{CoIrO}_6$ at $H = 8 \text{ T}$ [35]. A colour map of the $-\Delta S_M$ as a function of temperature, T , and magnetic field, H is also projected at the top of figure 6, where clear indications of the maximum value of $-\Delta S_M$ for all fields are found around at T_{FIM} .

In addition, the value of relative cooling power (RCP), which represents the refrigerant capacity of a magnetic material, can be evaluated for SMCO using the relation [54]:

$$\text{RCP} = -\Delta S_M^{\text{max}} \times \delta T_{\text{FWHM}},$$

where first and second terms denote the maximum value of magnetic entropy ($-\Delta S_M$) and the full-width at half-

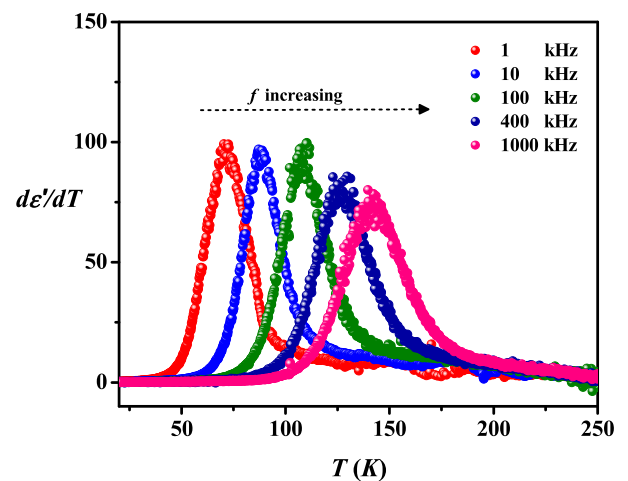


Figure 8. Thermal variation of first-order derivative of ϵ' with temperature (T) for different frequencies (f).

maximum of $-\Delta S_M$ peak at a particular magnetic field, respectively. RCP values are found to be 12.5 J kg^{-1} and 30 J kg^{-1} for $H = 10 \text{ kOe}$ and 70 kOe , respectively, showing a gradual increase with increasing external magnetic field.

3.3. Resistivity

The temperature dependent resistivity $\rho(T)$ measurement in the range 50–230 K (figure 7) shows that SMCO is an insulator, possibly due to large separation between the B-site cations, as also seen in nearly all double perovskites [55]. From Arrhenius fit (using the equation $\rho = \rho_0 \exp(E_a/k_B T)$) in the temperature interval 165–230 K, an activation energy of $E_a \sim 100 \text{ meV}$ is estimated from the slope of $\ln \rho$ ver-

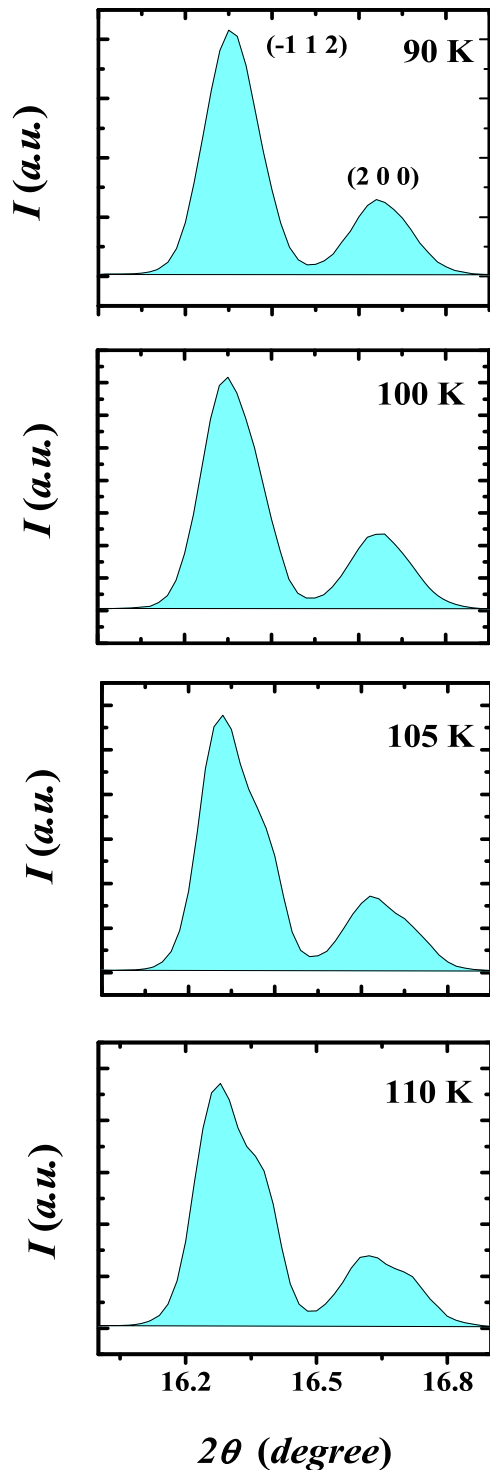


Figure 9. Plot of (-112) and (200) peak in the Intensity (I) vs 2θ plot from 90–110 K temperature range.

sus $(k_B T)^{-1}$ curve (lower inset of figure 7), which is worthy of comparison with other strongly insulating Ir-based oxides [56–58]. It is clear that linear fitting to the data in figure 7 deviates above 165 K, and hence, prompts us to understand the electrical conduction mechanism through other models. However, the linear dependence of $\ln \rho$ on $T^{-1/4}$ throughout the temperature range (50–230 K) indicates that Mott VRH

($\rho = \rho_0 \exp(T_0/T)^{1/4}$ in three-dimension) is the possible conduction mechanism in this compound (see upper inset of figure 7). Obtained parameters from VRH fitting are $\rho_0 \sim 6.22 \times 10^{-11} \Omega \text{ cm}$ and Mott characteristic temperature $T_0 \sim 83 \times 10^6 \text{ K}$.

3.4. Dielectric behaviour

Recently, our group has reported [59] the dielectric and impedance property of SMCO. No anomaly (or, peak) has been observed in ϵ' vs T spectra around the magnetic ordering temperature T_{FiM} , and ϵ' almost attains a constant value above 250 K. It is to be mentioned that the peak in thermal variation of first-order derivative of ϵ' with respect to temperature ($d\epsilon'/dT$) spectra for $f = 1 \text{ kHz}$ is centered around 70 K, which is well below the magnetic ordering temperature; whereas, this peak is positioned at 88 K (still below the T_{FiM}) for $f = 10 \text{ kHz}$ data (see in figure 8). Thus, the step-like features in ϵ' vs T spectra do not have any magnetic origin, implying the absence of significant magneto-dielectric coupling in this particular double perovskite.

4. Conclusions

In summary, we have successfully synthesized the mixed $3d-5d-4f$ double perovskite compound SMCO in polycrystalline form, and investigated the structural, magnetic and transport properties. SMCO crystallizes in the monoclinic structure with space group $P2_1/n$, and shows FiM order below $T_{\text{FiM}} = 104 \text{ K}$, likely arising from the AFM coupling between Co^{2+} and Ir^{4+} sub-lattices. A second magnetic transition is observed in $M(T)$ data around 10 K, which is associated with the ordering of RE Sm^{3+} spins. A moderate MCE is found around FiM transition, having maximum RCP value of 30 J kg^{-1} for $H = 70 \text{ kOe}$. Smaller magnetic moment of Sm^{3+} ion, $\mu(\text{Sm}) = 0.85 \mu_B$, directly gives negligible contribution to the overall magnetic coupling between $3d-5d-4f$ systems, in comparison with other compounds containing more f electrons. In general, crystalline anisotropy controls the spin configuration of $3d-5d$ sub-lattices at high temperature in case of oxide materials. However, the interaction of the d -sublattices and RE moments becomes significant at low temperature, which perhaps overcomes crystalline anisotropy forces and induces spin-reorientation, as observed in case of $\text{Ln}(\text{Tb, Ho})_2\text{CoIrO}_6$ double perovskites. In contrast, due to the presence of weak $f-d$ interaction between Co–Ir sublattices and Sm^{3+} moments (small moments) and large magneto-crystalline anisotropy, we probably have not seen any spin-reorientation phenomenon in this compound. So, eventually, Sm moments have significant role in determining the magnetic properties and behaviour of SMCO compound, although it has small moment. Electrical resistivity measurements suggest the insulating behaviour of the sample, in which Mott VRH conduction mechanism is detected. At the same time temperature dependent dielectric measurements of this as studied sample suggests it is not related to magnetic ordering. We hope our results will inspire more investigations of theoretical calculations, as well as experimental studies employing doping elements.

Acknowledgments

One of the authors, SKP, is thankful to Department of Science and Technology, Government of India for providing DST INSPIRE Fellowship (IF150147) and IACS during the tenure of work. RAS is thankful to CSIR, India and IACS for supporting fellowship. RD is thankful to SERB for providing fellowship during the tenure of the work. This work is funded by the Science and Engineering Research Board, Government of India, File No. EMR/2016/005437. Authors thank UGC-DAE Kolkata Centre for providing the dielectric measurement facility. Authors also thank the Department of Science and Technology, India for the financial support during the experiments at the Indian Beamline, PF, KEK, Japan, and Proposal No. 2018-IB-30.

Data availability statement

All data that support the findings of this study are included within the article (and any supplementary files).

Appendix

Figure 9 shows the modulation of (-112) and (200) hkl plane within temperature (T) range 90–110 K of SMCO. -112 plane is the most intense in the XRD data throughout the temperature scan. After 100 K; from the 105 K data the peak shapes are changed, justifies the structural phase transition happens in the as studied sample.

ORCID iDs

Subham Majumdar  <https://orcid.org/0000-0001-6136-1588>

Subodh Kumar De  <https://orcid.org/0000-0002-6385-3129>

References

- [1] Kim B J, Ohsumi H, Komesu T, Sakai S, Morita T, Takagi H and Arima T 2009 *Science* **323** 1329–32
- [2] Kobayashi K-I, Kimura T, Sawada H, Terakura K and Tokura Y 1998 *Nature* **395** 677–80
- [3] Kato H, Okuda T, Okimoto Y, Tomioka Y, Takenoya Y, Ohkubo A, Kawasaki M and Tokura Y 2002 *Appl. Phys. Lett.* **81** 328–30
- [4] Krockenberger Y *et al* 2007 *Phys. Rev. B* **75** 020404
- [5] Aréval-López A M, McNally G M and Attfield J P 2015 *Angew. Chem., Int. Ed.* **54** 12074–7
- [6] Feng H L *et al* 2016 *Phys. Rev. B* **94** 235158
- [7] Sakai M, Masuno A, Kan D, Hashisaka M, Takata K, Azuma M, Takano M and Shimakawa Y 2007 *Appl. Phys. Lett.* **90** 072903
- [8] Yáñez-Vilar S *et al* 2011 *Phys. Rev. B* **84** 134427
- [9] Moon J Y, Kim M K, Choi Y J and Lee N 2017 *Sci. Rep.* **7** 16099
- [10] Moon J Y, Kim M K, Oh D G, Kim J H, Shin H J, Choi Y J and Lee N 2018 *Phys. Rev. B* **98** 174424
- [11] Feng H L, Adler P, Reehuis M, Schnelle W, Pattison P, Hoser A, Felser C and Jansen M 2017 *Chem. Mater.* **29** 886–95
- [12] Feng H L, Reehuis M, Adler P, Hu Z, Nicklas M, Hoser A, Weng S-C, Felser C and Jansen M 2018 *Phys. Rev. B* **97** 184407
- [13] Anderson P W 1950 *Phys. Rev.* **79** 350–6
- [14] Goodenough J B 1955 *Phys. Rev.* **100** 564–73
- [15] Kanamori J 1959 *J. Phys. Chem. Solids* **10** 87–98
- [16] Campbell I A 1972 *J. Phys. F: Met. Phys.* **2** L47–50
- [17] Cao G, Qi T F, Li L, Terzic J, Yuan S J, DeLong L E, Murthy G and Kaul R K 2014 *Phys. Rev. Lett.* **112** 056402
- [18] Dey T *et al* 2016 *Phys. Rev. B* **93** 014434
- [19] Corredor L T *et al* 2017 *Phys. Rev. B* **95** 064418
- [20] Kayser P, Kennedy B J, Ranjbar B, Kimpton J A and Avdeev M 2017 *Inorg. Chem.* **56** 2204–9
- [21] Terzic J, Zheng H, Ye F, Zhao H D, Schlottmann P, DeLong L E, Yuan S J and Cao G 2017 *Phys. Rev. B* **96** 064436
- [22] Kim B J *et al* 2008 *Phys. Rev. Lett.* **101** 076402
- [23] Demazeau G, Siberchicot B, Matar S, Gayet C and Largeteau A 1994 *J. Appl. Phys.* **75** 4617–20
- [24] Powell A V, Gore J G and Battle P D 1993 *J. Alloys Compd.* **201** 73–84
- [25] Currie R C, Vente J F, Frikkee E and Ijdo D J W 1995 *J. Solid State Chem.* **116** 199–204
- [26] Uhl M, Matar S F and Siberchicot B 1998 *J. Magn. Magn. Mater.* **187** 201–9
- [27] Narayanan N, Mikhailova D, Senyshyn D, Trots D M, Laskowski R, Blaha P, Schwarz K, Fuess H and Ehrenberg H 2010 *Phys. Rev. B* **82** 024403
- [28] Kolchinskaya A *et al* 2012 *Phys. Rev. B* **85** 224422
- [29] Manna K *et al* 2016 *Phys. Rev. B* **94** 144437
- [30] Iakovleva M *et al* 2018 *Phys. Rev. B* **98** 174401
- [31] Pradhan S K, Dalal B, Kumar R, Majumdar S and De S K 2020 *J. Phys.: Condens. Matter* **32** 305803
- [32] Cao G *et al* 2013 *Phys. Rev. B* **87** 155136
- [33] Song J, Zhao B, Yin L, Qin Y, Zhou J, Wang D, Song W and Sun Y 2017 *Dalton Trans.* **46** 11691–7
- [34] Ferreira T, Morrison G, Yeon J and Zur Loye H-C 2016 *Cryst. Growth Des.* **16** 2795–803
- [35] Ding X, Gao B, Krenkel E, Dawson C, Eckert J C, Cheong S-W and Zapf V 2019 *Phys. Rev. B* **99** 014438
- [36] Rietveld H M 1969 *J. Appl. Crystallogr.* **2** 65–71
- [37] Rodríguez-Carvajal J 1993 *Physica B* **192** 55–69
- [38] Momma K and Izumi F 2011 *J. Appl. Crystallogr.* **44** 1272–6
- [39] Saha R A, Halder A, Saha-Dasgupta T, Fu D, Itoh M and Ray S 2020 *Phys. Rev. B* **101** 180406
- [40] Basu T *et al* 2014 *Sci. Rep.* **4** 5636
- [41] Strässle T, Juranyi F, Schneider M, Janssen S, Furrer A, Krämer K W and Güdel H U 2004 *Phys. Rev. Lett.* **92** 257202
- [42] Shannon R D 1976 *Acta Crystallogr. A* **32** 751
- [43] Philipp J B *et al* 2003 *Phys. Rev. B* **68** 144431
- [44] Kittel C 1976 *Introduction to Solid State Physics* (New York: Wiley)
- [45] Dalal B, Sarkar B and De S K 2016 *J. Alloys Compd.* **667** 248–54
- [46] Pathak A K, Paudyal D, Jayasekara W T, Calder S, Kreyssig A, Goldman A I, Gschneidner K A Jr and Pecharsky V K 2014 *Phys. Rev. B* **89** 224411
- [47] Néel M L 1948 *Ann. Phys., NY* **12** 137
- [48] Winkler E, Blanco Canosa S, Rivadulla F, López-Quintela M A, Rivas J, Caneiro A, Causa M T and Tovar M 2009 *Phys. Rev. B* **80** 104418
- [49] Dalal B, Sarkar B, Rayaprol S, Das M, Siruguri V, Mandal P and De S K 2020 *Phys. Rev. B* **101** 144418
- [50] Arrott A 1957 *Phys. Rev.* **108** 1394–6
- [51] Banerjee B K 1964 *Phys. Lett.* **12** 16–7
- [52] Aharoni A 1971 *Introduction to the Theory of Ferromagnetism* (New York: Oxford University Press)
- [53] Arrott A and Noakes J E 1967 *Phys. Rev. Lett.* **19** 786–9
- [54] Pecharsky V K, Gschneidner K A and Tsokol A O 2005 *Rep. Prog. Phys.* **68** 1479
- [55] Vasala S and Karppinen M 2015 *Prog. Solid State Chem.* **43** 1–36

- [56] Okabe H *et al* 2011 *Phys. Rev. B* **83** 155118
- [57] Singh Y, Manni S, Reuther J, Berlijn T, Thomale R, Ku W, Trebst S and Gegenwart P 2012 *Phys. Rev. Lett.* **108** 127203
- [58] Krajewska A, Takayama T, Dinnebier R, Yaresko A, Ishii K, Isobe M and Takagi H 2020 *Phys. Rev. B* **101** 121101
- [59] Datta R, Pradhan S K, Chatterjee S, Majumdar S and De S K 2021 *J. Alloys Compd.* **876** 160158

Cyanobacteria of the Indian Sundarbans: A Potential Source of Powerful Therapeutic Agents

Shayontani Basu¹, Veerabadhran Maruthanayagam¹, Sandeep Chakraborty¹, Arnab Pramanik², Anushree Achari³, Dr. Parasuraman Jaisankar³, Dr. Joydeep Mukherjee*¹

¹School of Environmental Studies, Jadavpur University, Kolkata 700032, India,

²Department of Biochemistry, University of Calcutta, 35, Ballygunge Circular Road, Kolkata 700 019,

³India Indian Institute of Chemical Biology, Kolkata- 700032, India

Abstract:

Mangrove forests occupy the estuarine ecotone and harbor a wide range of microorganisms along with a rich diversity of flora and fauna. Marine and estuarine organisms are known to produce unique molecules due to the aggressive, exigent, and competitive surroundings that are unlike those produced in the terrestrial environment. Marine cyanobacteria are a vast resource for new bioactive natural products useful in the development of therapeutics. The Sundarbans mangrove ecosystem harbours various unique microorganisms having different interesting properties. Discovery of a unique alkaline serine protease enzyme tolerant to bleach, detergent, high salt concentration and solvent, isolation and identification of obligately halophilic, euryhaline novel cyanobacteria from intertidal soil surface of the Sundarbans and identification of a pair of novel *Streptomyces* represent a few of the ongoing endeavors undertaken to explore the mostly untapped microbial diversity of the Sundarbans. This study focuses on two novel strains of cyanobacteria isolated from the intertidal soil surface biofilm of the Indian Sundarbans, which were cultivated on a large scale to yield a significant quantity of biomass for the extraction of secondary metabolites. The cyanobacterial biomass was extracted with a range of polar and non-polar solvents and the ethyl acetate fractions showed significant anti-angiogenic activity when tested against sunitinib (a protein kinase inhibitor). The extracts also showed significantly greater anti-inflammatory activity compared to dexamethasone, which has been shown to reduce the 28 day mortality rate of patients affected by COVID-19.

Keywords: Halophilic cyanobacteria, Indian Sundarbans, anti-inflammatory activity, anti-angiogenic activity.

Introduction

Modern day trends in drug discovery from natural sources stress the investigation of marine environment to yield numerous biologically active compounds many of which are antimicrobial in nature (Burja et al., 2001). The intertidal areas considered as interfaces of the ocean, atmosphere, and terrestrial environments harbour diverse microbial biofilm communities that are subjected to fluctuations in metal ion concentrations, temperature, desiccation, UV irradiation, and wave activities. The organisms in intertidal zones essentially spend part of their lives in extreme, arid conditions during emersion and half of their lives in stable, benign seawater. These conditions lead to the development of unique and specific characteristics of the inhabiting organisms (Zhang et al., 2013). These ecosystems experience tidal flooding, which causes environmental factors such as salinity and nutrient availability to be highly variable resulting in unique and specific characteristics of the inhabiting

organisms. The microbiome is one of the important communities of the mangrove ecosystem as the abundance of carbon and other nutrients sustains a large number of microbial communities which are adapted to the brackish and fluctuating environmental conditions (Pramanik et al., 2011). Marine cyanobacteria are a vast resource for new bioactive natural products useful in basic research, biomedical sciences, and the development of therapeutics (Gogineni et al., 2018).

Natural products of pharmacological importance derived from cyanobacteria

Cyanobacterial natural products are grouped according to their biosynthetic origins such as polyketides, cyanopeptides, alkaloids, isoprenoids and other metabolites. While major research has been towards investigating toxicity, many studies have shown cyanobacteria to produce compounds that are of pharmaceutical and biotechnological interest. Cyanobacterial compounds comprise 40% lipopeptides, 5.6% amino acids, 4.2% fatty acids, 4.2% macrolides and 9% amides. Most of the bioactivity shown by cyanobacteria tends to be from lipopeptides like cytotoxic (41%), antitumor (13%), antiviral (4%), antibiotics (12%) and the remaining 18% include anti-malarial, antimycotics, multi-drug resistance reversing agents, herbicides and immunosuppressive agents. A major part of cyanobacterial secondary metabolites are peptides or possess peptidic structures. Many important classes of cancer cell toxins with apoptotic properties have been characterized from marine cyanobacteria over the past years. Effects of cyclic peptides as anticancer agent with multitude targets have been reviewed. *Lyngbya majuscula* among other cyanobacterial genera collected from various coastal and deep-sea regions of the marine environment worldwide has proved to be one of the main sources for the production of natural products with anti-tumor and anti-cancer properties, regardless of their geographical distribution (Nagarajan et al., 2012). Many of the secondary metabolites secreted by cyanobacteria were found active against different mammalian cancer cell lines. Some important compounds isolated from cyanobacteria that target cancers are given as follows: colon cancers are targeted by minutissamides, microcystilide A, laxaphycins, cylindrocyclophanes and bauerines A-C while breast cancers are targeted by carbamidocyclophanes, dendroamide, hapalosin and tolyporphins; lung cancer is targeted by pahayokolide A; and prostate cancer by tychonamide. A few secondary metabolites isolated from cyanobacteria were shown to have profound activity against certain parasites causing deadly diseases. A compound isolated from freshwater cyanobacterium *Nostoc* displayed antiprotozoal activity against *Trypanosoma* and *Leishmania* and significant toxicity to malaria parasite. Pharmacologically important metabolites have been isolated from marine benthic and planktonic cyanobacteria that inhibit growth of severe bacterial, fungal and protozoal pathogens. Studying active concentration, active modules and mechanism of action of bioproducts on both prokaryotic and eukaryotic pathogens and/or parasites will help in their selection for clinical evaluation. A class of antifungal lipopeptides known as lobocyclamides were isolated from marine cyanobacterium *L. confervoides* collected from Cay Lobos, Bahamas (Nagarajan et al., 2012; Raja et al., 2016). Freshwater and terrestrial cyanobacteria are also proven to have the potential to produce compounds displaying cytotoxic, protease inhibiting and growth controlling properties on parasites, pathogens and harmful algae. Further studies on these metabolites may make synthesis of drugs containing the bioactive key components possible. Thus, a new vista may

open towards the treatment of life-threatening diseases (Nagarajan et al., 2012). Despite the wide range of natural products found in cyanobacteria, exploitation of these products is still not widespread.

Studies on the cyanobacteria of the Indian Sundarbans

The Sundarbans mangrove ecosystem harbours various unique cyanobacteria having pharmacologically important properties. Isolation and subsequent identification of obligately halophilic, euryhaline novel cyanobacteria from intertidal soil surface of the Sundarbans (Pramanik et al., 2011) represents one of the endeavors undertaken to explore the vastly unexplored microbial diversity of the Indian Sundarbans, under the guidance of Dr. J. Mukherjee (School of Environmental Studies, Jadavpur University). Based on morphological characteristics, six of the isolated cyanobacteria were assigned to the *Lyngbya-Phormidium-Plectonema* (LPP) group B, and one each was assigned to *Oscillatoria* and *Synechocystis* genera. A polyphasic approach-based taxonomic characterisation was performed for the cyanobacteria, which led to the discovery of four novel strains, out of which two are a novel species *O. aestuarii* belonging to the genus *Oxynema*. Cross walls in the apical portion of cells of the strains AP17 and AP24 were absent while the same were present in CCALA960. Additionally, optimal growth of AP17 and AP24 was recorded at 5–8% salinity and salinity above 14% inhibited growth of both strains, which were isolated from the intertidal soil surface; whereas *O. thaianum* CCALA960 which was found in a hypersaline environment could grow at 40% salinity. Differences between the internal transcribed spacer (ITS) sequences of the two strains isolated from the Indian Sundarbans and the reference strain included the insertion of 9 nucleotides in the D2 with spacer region, insertion of 2 nucleotides in the pre Box B spacer region, deletion of 2 nucleotides in the post Box B spacer region, deletion of 8 nucleotides in the D4 region, deletion of 8 nucleotides in V3 region and insertion of 2 nucleotides in the D5 region of the ITS sequences of AP17 and AP24, which were observed in comparison to the analogous regions of CCALA960. Structural details of Box B helices of AP17 and AP24 revealed that though their lengths were identical with that of the reference strain, their sequences were completely different from CCALA960. Four nucleotide substitutions were present in different positions in the Box B helix of *O. thaianum* CCALA960. Secondary structures of the V3 regions of both AP17 and AP24 (containing 51 nucleotides) showed a small terminal bulge and a bigger bilateral bulge while the analogous structure of *O. thaianum* CCALA 960 (comprising of 59 nucleotides) showed one additional bilateral bulge in comparison to AP17 and AP24. Therefore, based on morphological, ecological and molecular differences in comparison to *O. thaianum* CCALA960, isolates AP17 and AP24 were proposed to be members of a second novel species in the *Oxynema* genus, for which the name *Oxynema aestuarii* sp. nov. has been proposed (Chakraborty et al., 2018). The other two strains AP9F and AP25 are monophyletic taxa designated as *Euryhalinamamangrovii* and *Leptolongatuslitoralis* (gen. nov., sp. nov.). The cells of AP9F and AP25 were highly elongated whereas the cells of the reference strains (*Leptolyngbyaboryana* and *Nodosilineanodulosa*) were occasionally elongated to isodiametrical. Terminal cells of AP9F and AP25 appeared as flattened corners (as opposed to rounded), which was different from the cell structure of other

Leptolyngbyaceae members. 16S rRNA gene sequences of AP9F (1366 bp) and AP25 (1408 bp) showed 95% and 92% similarities respectively with the non-redundant (nr) nucleotide sequences of their closest relatives of the *Leptolyngbya* genus. Test strains occupied a clade in the phylogenetic tree that was different from the ones containing the type species. A single operon containing both tRNA^{ile} and tRNA^{ala} genes were present in the ITS regions of AP9F and AP25 as compared to the presence of two operons in the ITS region of the reference genera *Leptolyngbya* and *Nodosilinea*: one in which both tRNA^{ile} and tRNA^{ala} genes are present and the other lacking both the genes. The secondary structures of the traditionally conservative D-stem region as well as the Box B helix and V3 regions of the ITS operons showed significant variation between the test strains and also when compared with the corresponding sequences of *L. boryana* and *N. nodulosa*. Molecular, phylogenetic and morphological data suggested AP9F and AP25 to be monophyletic taxa for which the names *Euryhalinemamangrovii* gen. nov., sp. nov. and *Leptoelongatuslitoralis* gen. nov., sp. nov. were proposed respectively (Chakraborty et al., 2019). Thus, the strains AP17, AP24, AP9F and AP25 isolated from the Sagar Island and Lothian Island of the Indian Sundarbans differed from the reference strains (*Oxynemathaiianum* CCALA960 for *Oxynemaestuariae*, *Leptolyngbyaboryana*, and *Nodosilineanodulosa* for *Euryhalinemamangrovii* and *Leptoelongatuslitoralis*) in terms of morphology, ecology and 16S- 23S ITS sequences (Chakraborty et al., 2018, Chakraborty et al., 2019). The aforementioned novel strains have been deposited and cryopreserved in the Microbial Culture Collection (MCC), India having accession numbers MCC 3874 (AP17), MCC 3873 (AP24), MCC 3171 (AP9F) and MCC 3170 (AP25).

Material and methods

Cyanobacterial isolates were established by aseptic collection of cyanobacterial soil surface biofilm, inoculation in artificial sea nutrient (ASN-III) medium, and subsequent incubation in fluorescent irradiance maintaining a 12-h:12-h light:dark cycle at 25±1°C, and plating the serially diluted homogenized biomass obtained after 40 days of growth. Individual colonies of filamentous cyanobacteria were isolated after 30 days on ASN-III plates, observed microscopically, and grown in liquid ASN-III medium supplemented cycloheximide and triple-antibiotic solution (containing penicillin G, chloramphenicol, and streptomycin sulfate) to prevent culture contamination. The cyanobacterial cell suspension so obtained was subsequently grown in antibiotic-free ASN-III medium for 30 days, and culture purity was confirmed by the absence of microbial growth in tryptone-yeast extract-glucose (TYG) broth (Pramanik et al., 2011; Chakraborty et al., 2018). Mass cultivation of the established cyanobacterial monoculture strains was done by growing them individually in 20 litre capacity plastic jars disinfected by washing with benzalkonium chloride followed by addition of 12 litres of sterile ASN III media and ~5 gm (wet mass) of cyanobacterial culture added to each of the jars as inoculum. Aeration was achieved with the use of pumps to ensure proper mixing of the media components, along with maintenance of the light and temperature conditions for growth (Pramanik et al., 2011). The cyanobacterial biomass of each of the two strains (one belonging to *Oscillatoria* sp. and the other being *Oxynemaestuariae*) thus obtained (~200g each) was dried at 50°C, divided into two parts and both parts extracted separately using ethyl acetate and n-butanol. The extracts were dried in vacuo and tested for anti-inflammatory activity and anti-angiogenic activity. The test for anti-inflammatory activity was performed using human

monocytic leukemia THP-1 cells that were pre-treated for 12h with standard compound Dexamethasone (1 μ M). Subsequently, pretreated cells were stimulated with LPS- 50 ng/ml for 4h. After treatments, cell supernatant was collected for TNF measurement using ELISA. (According to Clin Chem. 2005; 51(12):2252-6). Measurement of anti- angiogenic activity is based on the principle that the formation of capillary-like structures among endothelial cells plated at sub- confluent densities in matrigel matrix in the presence of the compound under investigation extrapolates to angiogenesis (Goodwin, 2007). The cell line used for this *in- vitro* assay is the EA.hy926 endothelial cell line obtained by the hybridization of human umbilical vein endothelial cells with the A549/8 human lung carcinoma cell line (Aranda et al., 2009).

Results and discussion

Secondary metabolites obtained from the cyanobacterial biomass extracts (with ethyl acetate) have shown promising anti- inflammatory activity and anti- angiogenic activity (the ability to prevent endothelial cells to form capillary-like structures) compared to the standards Dexamethasone and Sunitinib respectively (tested at CDRI, Lucknow) (unpublished report). Both the extracts from the cyanobacterial strains showed anti- angiogenic activity by reducing the capillary structures (>25% inhibition compared to standard compound, Sunitinib) at the initial 100 μ g/ml test dose (Table 1). Both extracts also showed \geq 75% inhibition of inflammatory activity compared to Dexamethasone at the initial 100 μ g/ml test dose (Table 2). Thus, the ethyl acetate extracts of these cyanobacterial strains can be further purified by column chromatography and HPLC for reduction of possible cytotoxicity.

| Serial number | Extract Code | % Tubulogenesis inhibition |
|-----------------|------------------------------|---------------------------------|
| 1 | “Ethyl Acetate Extract” AP20 | Active, lower dose to be tested |
| 2 | “Ethyl Acetate Extract” AP24 | Active, lower dose to be tested |
| Standard | Sunitinib | ~40 |

Table 1: Test results of ethyl acetate extracts of AP20 (*Oscillatoria* sp.) and AP24 (*Oxynema aestuarii*) for anti- angiogenic activity against Sunitinib (standard). Concentration of extract tested: 100 μ g/ml.

Source: Unpublished report, CDRI Lucknow.

| Anti- inflammatory activity | | |
|-----------------------------|------------------------------|--------------|
| Serial number | Extract Code | % inhibition |
| 1 | “Ethyl Acetate Extract” AP20 | \geq 85 |
| 2 | “Ethyl Acetate Extract” AP24 | \geq 85 |
| Standard | Dexamethasone | ~78 |

Table 2: Test results of ethyl acetate extracts of AP20 (*Oscillatoria* sp.) and AP24 (*Oxynema aestuarii*) for anti-inflammatory activity against Dexamethasone (standard). Concentration of extract tested: 100µg/ml.

Source: Unpublished report, CDRI Lucknow.

Conclusion

Despite the wide range of natural products of significant pharmacological value found in cyanobacteria, exploitation of these products is still not widespread. The growth of cyanobacterial biomass is quite slow, which is certainly one of the most important limiting factors due to which massproduction of bioactive compounds is limited. Further studies on the metabolites isolated from the cyanobacterial biomass may help in the synthesis of drugs containing the key components contributing to the bioactivity possible (Nagarajan et al., 2012). The study may prove to be a beneficial step in the discovery of several compounds of pharmacological interest from the largely unexplored mangrove microbiota of the Indian Sundarbans, opening a new vista towards the treatment of life-threatening diseases.

References

1. Aranda, E., and Owen, I. G. 2009. A semi-quantitative assay to screen for angiogenic compounds and compounds with angiogenic potential using the EA.hy926 endothelial cell line. *Biol Res* 42:377-389.
2. Burja, A.M., Banaigs, B., Abou- Mansour, E., Burgess, J.G., Wright, P.C. 2001. Marine Cyanobacteria- A prolific source of natural products. *Tetrahedron report no.* 590.
3. Chakraborty, S., Maruthanayagam, V., Achari, A., Mahansaria, R., Pramanik, A., Jaisankar, P., Mukherjee, J. 2018. *Oxynema aestuarii* sp. nov. (Microcoleaceae) isolated from an Indian Mangrove forest. *Phytotaxa* 374:24-40.
4. Chakraborty, S., Maruthanayagam, V., Achari, A., Pramanik, A., Jaisankar, P., Mukherjee, J. 2019. *Euryhalinamangrovii* gen. nov., sp. nov. and *Leptoelongatus litoralis* gen. nov., sp. nov. (Leptolyngbyaceae) isolated from an Indian mangrove forest. *Phytotaxa*, 422(1), 058-074.
5. Gogineni, V. and Hamann, M.T., 2018. Marine natural product peptides with therapeutic potential: Chemistry, biosynthesis, and pharmacology. *Biochimica et Biophysica Acta (BBA)-General Subjects*, 1862(1), pp.81-196.
6. Goodwin, A.M., 2007. In vitro assays of angiogenesis for assessment of angiogenic and anti-angiogenic agents. *Microvascular research*, 74(2-3), pp.172-183.
7. Nagarajan, M., Maruthanayagam, V., & Sundararaman, M. 2012. A review of pharmacological and toxicological potentials of marine cyanobacterial metabolites. *Journal of Applied Toxicology*, 32(3), 153-185.
8. Pramanik, A., Sundararaman, M., Das, S., Ghosh, U., & Mukherjee, J. 2011. Isolation and Characterization of Cyanobacteria Possessing Antimicrobial Activity from the Sundarbans, The world's Largest Tidal Mangrove Forest. *Journal of phycology*, 47(4), 731-743.
9. Raja, R., Hemaiswarya, S., Ganesan, V. and Carvalho, I.S., 2016. Recent developments in therapeutic applications of Cyanobacteria. *Critical reviews in microbiology*, 42(3), pp.394-405.
10. Zhang, W., Wang, Y., Lee, O.O., Tian, R., Cao, H., Gao, Z., Li, Y., Yu, L., Xu, Y. and Qian, P.Y., 2013. Adaptation of intertidal biofilm communities is driven by metal ion and oxidative stresses. *Scientific reports*, 3, p.3180.

খোয়াই

ISSN 2319 – 8389, Vol : 43, Issue : 43

KHOAI
UGC Care Listed Journal
Art and Humanities
Tri - Annual Journal



সংখ্যা ৪৩ : ২৫ বৈশাখ, ১৪২৮

শান্তিনিকেতন

সূচীপত্র

| | | |
|--|--|-----|
| সম্পাদকীয় | | |
| পারিবারিক সম্পর্কের বন্ধনে 'নৌকাডুবি' | -- অসীম কুমার মুখার্জী | ৯ |
| ✓ রবীন্দ্রনাথের 'নদী': একটি অন্তরঙ্গ পাঠ | -- শুভাশিস গোস্বামী | ১৪ |
| রবীন্দ্রসঙ্গীতে বাস্তবতা, সমাজ নৈতিকতা ও বিশ্বমানবতার শিক্ষা | -- অসীম কুমার রায় | ১৯ |
| মুর্শিদাবাদের সংস্কারধর্মী প্রবাদ : সমীক্ষা ও মূল্যায়ন | -- নিবিড় কুমার ঘোষ | ৩২ |
| দারা শিকোর দার্শনিক ও আধ্যাত্মিক নিকটবর্তিতা | -- মহম্মদ ফায়েক, প্রহ্লাদ রায়, সিদ্দিকী ওয়াসিম রহমান | ৩৬ |
| সত্যজিৎ রায় পরিচালিত চলচ্চিত্রে প্রতিফলিত লোকসংস্কৃতি | -- পুলক গাঙ্গুলী | ৪১ |
| রোসাঙ রাজসভার সাহিত্যে সূফী সাধনার প্রভাব | -- তনুকা চৌধুরী | ৪৮ |
| বাংলা চলচ্চিত্রে ব্যবহৃত লোকসংগীত ও লোকনৃত্য | -- ইতি পাল | ৫৫ |
| মূল্যবোধ শিক্ষা : প্রসঙ্গ মধ্যযুগের ইংরেজি সাহিত্য | -- মৌসুমী পেড়িওয়াল | ৬২ |
| 'রঘুবংশম্' মহাকাব্যে বিজ্ঞানচেতনা | -- সঞ্জয় মণ্ডল | ৬৯ |
| 'দিবে আর নিবে, মিলাবে মিলিবে': শিক্ষার প্রাঙ্গণে বিশ্বায়ন | -- নাফিসা সনম | ৭২ |
| সমুদ্রে জাতীয়তাবাদ : ঊনবিংশ ও বিংশ শতকে ভারত- | | |
| -মহাসাগরীয় সমুদ্রবাণিজ্যে স্বদেশী প্রয়াস ও পরিণতি | -- সৌম্যজিৎ মুখার্জী | ৭৮ |
| অবনীন্দ্রনাথ ঠাকুরের 'বুড়ো আংলা' : বাংলার সমাজ ও সংস্কৃতি | -- শুভঙ্কর ঘোড়ুই | ৮৭ |
| দ্বিজেন্দ্রলাল রায়ের খয়লাঙ্গ বাংলা গান | -- চন্দ্রানী দাস | ৯৫ |
| ভারতীয় রাগসঙ্গীত ও তাঁর উদ্দেশ্য | -- অরিন্দম সেন | ১০৬ |
| সূর্য-দীঘল বাড়ী : উপন্যাসে, চলচ্চিত্রে | -- তীর্থ দাস | ১১২ |
| বাংলা কথাসাহিত্যে ঝাড়খণ্ডের জনজীবন | -- অনির্বাণ সাহু | ১১৬ |
| শিক্ষার আঙিনায় সর্ব লিঙ্গ সমন্বয় : লিঙ্গসমতার এক অধ্যায় | -- সুমেধা মুখার্জী ও উমাকান্ত প্রসাদ | ১২৪ |
| প্রগতি ও অগ্রগতি : ঊনিশ শতকে মেয়েদের জন্য বাংলা ভাষার পত্রিকা | -- সঞ্চিতা বসু | ১৩৪ |
| দূরস্থিত সংযোগ | -- ইন্দিরা দাশ | ১৪৩ |
| ইতিহাসের অন্তরালে ঊনিশ শতকের নিরিখে পট ও ব্রাত্য- | | |
| -জনগোষ্ঠী পটুয়া শিল্পীদের যাপন আখ্যানের আলোচনা | -- রাকেশ কৈবর্ত | ১৪৭ |

রবীন্দ্রনাথের 'নদী': একটি অন্তরঙ্গ পাঠ
শুভাশিস গোস্বামী

'চিত্রা' কাব্য প্রকাশিত হবার একমাস আগে (২২মাঘ, ১৩০২ বঙ্গাব্দ) রবীন্দ্রনাথের 'নদী' নামের ছন্দ কাব্যটি প্রকাশিত হয়। ভ্রাতুষ্পুত্র বলেন্দ্রনাথের শুভ পরিণয়ের দিন এই কাব্যটি তাঁকে উপহার দেওয়া হয়। ১৯০৩ খ্রীস্টাব্দে মোহিতচন্দ্র সেন যে কাব্যগ্রন্থ প্রকাশ করেন (২ আশ্বিন, ১৩১০ বঙ্গাব্দ) তার সপ্তমভাগে 'শিশু' খণ্ডের মধ্যে স্থান পেয়েছিল 'নদী'। তখন থেকে সেখানেই আছে।

'বাল্যগ্রন্থাবলী'র অন্তর্গত এই কাব্যটির 'বিজ্ঞাপন' অংশে রবীন্দ্রনাথ লিখেছিলেন,—
“এই কাব্যগ্রন্থখানি বালক বালিকাদের পাঠের জন্য রচিত হইয়াছে। পরীক্ষার দ্বারা জানিয়াছি ইহার ছন্দ শিঞ্জা সহজেই আবৃত্তি করিতে পারে। বয়স্ক পাঠকদিগকে বলা বাহুল্য যে, প্রত্যেক ছন্দের আরম্ভের শব্দটির পরে যেখানে ফাঁক দেওয়া হইয়াছে সেখানে স্বল্পকালমাত্র থামিতে হইবে।”

'নদী' কাব্যটির মূল আকর্ষণ হল রচনাভঙ্গির বিশিষ্টতা। রবীন্দ্রজীবনীকার গ্রন্থটি রচনার কিছু প্রেক্ষাপটের কথা জানিয়েছেন।^১ প্রথমত এই সময় তাঁর সন্তানদের শিক্ষাসহায়ক গ্রন্থের খুবই অভাব ছিল। বিশেষত যুক্তকর্মী কবিতা খুবই কম। কন্যা রেণুকার পাঠ সহায়ক হিসাবেও এটি রচিত হয়ে থাকতে পারে।^২

দ্বিতীয়ত, এই সময়ে চলছিল 'সহজ পাঠ' এর খসড়া তৈরির কাজ। তাই শিশুদের কল্পনাশক্তি উদ্ভিক করা ও ছন্দ সৌন্দর্য উপভোগের জন্যে নতুন কাব্য সৃষ্টির প্রয়োজনও কবি উপলব্ধি করছিলেন।

রবীন্দ্রনাথের চেষ্টা ছিল সংযুক্ত ব্যঞ্জনবর্ণ যথাসাধ্য কম ব্যবহার করা। ৩০০ ছত্রের এই কবিতাটিতে যুক্তাক্ষর আছে মাত্র বারোটি।

ইন্দিরা দেবী 'নদী' কবিতাটির সঙ্গে ইংল্যান্ডের কবি রবার্ট সাদে রচিত 'Falls of Ladore' (কবিতার প্রকৃত নাম 'Cataract of Ladore', রচনাকাল ১৮২০ খ্রীস্টাব্দ) কবিতাটির মিল খুঁজে পেয়েছিলেন।^৩ কবি সাদে কবিতাটি লিখেছিলেন তাঁর সন্তানদের জন্যে। বালকপুত্র প্রশ্ন করেছিলেন কবিকে, 'কীভাবে পাহাড়ের উপর থেকে নেমে আসে ঝর্ণাধারা ?'

" How does the water
Come down at Ladore ?
My little boy asked me
Thus, once on a time ;
And moreover he tasked me
To tell him in rhyme."

কবি সাদে অনুপম শব্দ ও ধ্বনিমাধুর্যে পাহাড়ের উঁচু কোল থেকে ছন্দিত হিল্লোল দুলাকি চালে, নৃত্যরত ভঙ্গিমায় ঝর্ণাধারার নেমে আসাকে বর্ণনা করেছেন। চার ছত্র উল্লেখ করছি --

খোয়াই

ISSN 2319 – 8389, Vol : 44, Issue : 44

KHOAI
UGC Care Listed Journal
Art and Humanities
Tri - Annual Journal



সংখ্যা ৪৪ : ২২ শ্রাবণ, ১৪২৮

শান্তিনিকেতন

Aesthetics of Raga-

লোকবিশ্বাস ও লোকসংস্কার : মহাশ্বেতা দেবীর একটি উপন্যাস-
নেল নডিংস এর শিক্ষাভাবনা-
উনবিংশ শতাব্দীর দ্বিতীয়ার্ধে উত্তরবঙ্গের নগরায়ন ও নাগরিক
পরিষেবা : প্রসঙ্গ মালদহ জেলা-
ডিজিটাল ও অনলাইন দুনিয়ায় রবীন্দ্রগানের প্রচার ও প্রসার এবং
করোনা আবহে তার ইতিবাচক ও নেতিবাচক প্রভাব -
একটি সমীক্ষা ভিত্তিক মূল্যায়ণ-

Unselfishness is the essence of Morality according
to Swami Vivekananda-

রবীন্দ্রসঙ্গীতে ভারতীয় সংস্কৃতির নবজাগরণ-

The Effectiveness of Virtual Field Trip on Academic Achievement of Students in Inclusive Classroom
with respect to Teaching Forest Resources at Higher Secondary Level-

'ধুম্রিনালের দুই সঙ্গী' গল্পে সাম্প্রদায়িক দাঙ্গা ও সংকট উত্তরণের ছবি-
ঔপনিবেশিক আমলে মালদা-র সাঁওতাল সমাজ-
চেতন্য সংস্কৃতি ও বর্তমান সময়ে তার প্রাসঙ্গিকতা-
"ইতিহাস ও ঐতিহ্যের সংস্কৃতি পৌষ সংক্রান্তি"-

Teaching-Learning Strategies for Children with Disabilities
in Inclusive Classrooms-

রবীন্দ্রনাথের 'সন্ধ্যাসংগীত' কাব্যে নদীর স্থান-
'নতুন ইহুদি' : দেশভাগের জীবন্ত দলিল-
পারিবারিক সম্পর্কের আলোকে 'চোখের বালি'-

Population Education & Geography of Surul village: a Study- Sk Rashidul Haque

'দেশ' পত্রিকার ছোটগল্পে গ্রামবাংলার লোকসংস্কার-
মহামারি করোনার করাল ছায়ায় : প্রসঙ্গ সাহিত্য প্রেম-
বাংলা মঙ্গলকাব্যের পাঠক রবীন্দ্রনাথ-
বিংশ শতাব্দীর কিংবদন্তী মহিলা সংগীতশিল্পী বেগম আখতার-

Leadership Needs a Strategic Change to Prevent Child

Labour : A Stage of Covid-19 Epidemic-

Impact of Family Environment and Mobile Phone
Addiction on the Academic Achievement

of Undergraduate Students-

Dhrupad Tradition of Vishnupur Gharana in West Bengal-

উনবিংশ শতকের পটভূমিকায় বিশ্ববোধের উন্মেষ :
বিশ্বশান্তির বাণী প্রচারে রামমোহন থেকে রবীন্দ্রনাথ-

Evolution and Growth of Market System,

Economy in Kolkata-

Genesis and Development of Drainage and Sewerage

System during Colonial period In Calcutta -1800-1948

A Historical Analysis of Ayacut settlement In

Travancore in Southern India from 1883-1911-

ভগবত গীতার আত্মতত্ত্ব: অদ্বৈত ও দ্বৈতবাদের আলোকে পুনঃমূল্যায়ণ-

বাংলার নবজাগরণ ও জোড়াসাঁকো ঠাকুরবাড়ীর সঙ্গীত শিক্ষা-

অর্থনৈতিক সংকটের প্রেক্ষাপটে দীপেন্দ্রনাথ বন্দ্যোপাধ্যায়ের জটায়ু : পুরাণের নবনির্মাণ-

EARLY PANDYA INVASIONS IN SOUTH T

Shyamal Makhai

শিশির সিং

মন্দিরা সিংহ

খাতরত গোস্বামী

শ্রী কৌস্তভ কর্মকার

Sabyasachi Mondal

অনির্বাণ সাহু

Sanjoy Dutta & Dr. Mousumi Boral

মৃদুল ঘোষ

রাজেন হেমরম

প্রবীর কুমার পাল

অঞ্জন কর

Dr.Gopal Singh Dr.Sharmila Yadav

শুভাশিষ গোস্বামী

শিরীণ মুস্তাফি

অসীম কুমার মুখার্জী

Sk Rashidul Haque

রূপশ্রী ঘোষ

সমীর প্রসাদ

মুনায় কুমার মাহাত

ড. চন্দ্রানী দাস

Pritam Pyne & Dr. Umakant Prasad

Dr. Prarthita Biwas & Dr. Shyamsundar Bairagya

Ashok Barman

সুচন্দ্রা মৈত্র

DR. CHITRALEKHA MAITI & DR. ATREYA PAUL

Dr. Atreya Paul

DR . SURESH .J

মীনাঙ্কী ভট্টাচার্য্য

সোমা দাস মণ্ডল

অর্পিতা দাস

Sajeev Singh. M. K

রবীন্দ্রনাথের 'সন্ধ্যাসংগীত' কাব্যে নদীর স্থান
শুভাশিষ গোস্বামী

রবীন্দ্রনাথ ঠাকুরের 'সন্ধ্যা সংগীত' কাব্যটির প্রকাশকাল নিয়ে সামান্য একটু বিতর্ক আছে। গ্রন্থটি ছাপা হয়েছে আরম্ভ হয় ১২৮৮ বঙ্গাব্দের চৈত্র মাসে। কিন্তু বই হিসাবে প্রকাশিত হয় ১২৮৯ বঙ্গাব্দের আষাঢ় মাসে, খ্রিষ্টাব্দের ৫ জুলাই। পুস্তকের পরিচয়পত্রে বই ছাপা আরম্ভের তারিখ ছাপা হয়েছিল।

প্রথম সংস্করণে কাব্যটিতে ছিল পঁচিশটি কবিতা, যার মধ্যে বারোটি কবিতা পূর্বে 'ভারতী' পত্রিকায় মুদ্রিত হয়েছিল। 'বিজ্ঞাপন' অংশে স্বয়ং গ্রন্থকার জানিয়েছিলেন ---- "আমার রচিত কবিতার মধ্যে যেগুলি সন্ধ্যাসংগীত নামে উক্ত হইতে পারে, সেইগুলিই এই পুস্তকে প্রকাশিত হইল। ইহার অধিকাংশ কবিতাই গত দুই বৎসরের মধ্যে রচিত হইয়াছে।" কাব্যটি সমকালে সাহিত্যসম্রাট বঙ্কিমচন্দ্র চট্টোপাধ্যায় কর্তৃক প্রশংসিত হয়েছিল।

রবীন্দ্রকবাজীবনে প্রাক 'সন্ধ্যাসংগীত' পর্বটি ছিল মূলত অনুকরণের পর্ব। বিহারীলাল চক্রবর্তী, অক্ষয়চন্দ্র বসু প্রমুখের রচনার 'কপিবুক'। কবির নিজেরই স্বীকৃতি রয়েছে 'সূচনা' অংশে, ---- "সেই কপিবুকের চৌকাঠ পরিষ্কারই প্রথম দেখা দিল সন্ধ্যাসংগীত। ... সন্ধ্যাসংগীতেই আমার কাব্যের প্রথম পরিচয়।" জীবনস্মৃতি গ্রন্থের 'সন্ধ্যাসংগীত' নামক অধ্যায়েও রবীন্দ্রনাথ তাঁর কবি হয়ে ওঠার প্রাথমিক পর্বে রচিত এই কাব্যটি রচনাকালীন তাঁর মনসিক প্রেক্ষাপটটি সবিস্তারেই তুলে ধরেছেন। স্মৃতিচারণা করতে গিয়ে লিখেছেন, ---- "কাব্য হিসাবে সন্ধ্যাসংগীতের মূল্য বেশি না হতে পারে। উহার কবিতাগুলি যথেষ্ট কাঁচা। উহার ছন্দ ভাষা ভাব মূর্তি ধরিয়া কিছুটা হইয়া উঠিতে পারে নাই। ... সে লেখটার মূল্য না থাকিতে পারে কিন্তু খুশিটার মূল্য আছে।" 'সন্ধ্যাসংগীত'কে রবীন্দ্রনাথ তাঁর 'প্রথম মুদ্রিত গ্রন্থ' বলেও স্বীকার করেছেন। এর পূর্বে রচিত সমস্ত কবিতাকেই তিনি বাদ দিয়েছিলেন তাঁর কাব্যগ্রন্থাবলী থেকে।

রবীন্দ্রনাথ তাঁর কবি হয়ে ওঠার পিছনে জ্যোতিদাদা (জ্যোতিরিন্দ্রনাথ ঠাকুর) ও নতুন বৌঠানের (কাদম্বরী দেবী) অনুপ্রেরণার কথা সশ্রদ্ধ চিত্তে স্মরণ করেছেন আজীবন। বিশেষত স্নেহে-পরিচর্যায়-প্রীতিমধুরতায় কাদম্বরী দেবী রবীন্দ্রনাথের সাহিত্য প্রতিভার অঙ্কুরোদগমের সময় যথার্থই প্রেরণাদাত্রী হয়ে উঠেছিলেন। এই কাদম্বরী দেবী ১২৯১ বঙ্গাব্দের ৮ বৈশাখ স্নেহে আত্মহননের পথ বেছে নিয়েছিলেন। জীবনীকার জানিয়েছেন, কাদম্বরী দেবী তার আগেও একবার আত্মহত্যার চেষ্টা করেছিলেন। যার ফলস্বরূপ 'পারিবারিক বিশৃঙ্খলার প্রতিঘাতে' রবীন্দ্রনাথের দ্বিতীয়বার বিলাতযাত্রা স্বর্গিত হয়ে যায়। জ্যোতিরিন্দ্রনাথ পত্নীকে সুস্থ করবার জন্যে এবং জোড়াসাঁকোর পরিবেশ থেকে সরে থাকবার জন্যে তৎকালীন বোম্বাই প্রদেশের কোনো পার্বত্য অঞ্চলে কিছুকাল অবস্থান করেছিলেন। সম্রাট ১২৮৭ বঙ্গাব্দের কার্তিক মাস নাগাদ। এই সময় জ্যোতিরিন্দ্রনাথ ও কাদম্বরী দেবী জোড়াসাঁকোর তেতলায় কাঁড়ি ছাদের যে অংশটায় থাকতেন সেটা সাময়িক রবীন্দ্রনাথের 'দখলে' আসে। সেই নির্জন দিনগুলিতে সেখানে বসেই 'সন্ধ্যাসংগীত'--এর কবিতাগুলি লেখার সূত্রপাত। এই সময়পর্বেই কাব্যরচনায় পূর্বতন সংস্কারের আবেষ্টন থেকে তিনি মুক্ত হচ্ছিলেন, ফিরে পাচ্ছিলেন নিজস্ব ছন্দও। 'জীবনস্মৃতি'--তে লিখেছেন, ---- "নদী যেমন কাটা

হিজল

বঙ্গীয় সাহিত্য-সংস্কৃতি বিষয়ক গবেষণাধর্মী বাৎসরিক

(রেফারিড জার্নাল)

বর্ষ : ২৭, সংখ্যা : ২য়

ডিসেম্বর, ২০২০

সম্পাদক

সৌরভ রায়

সূচিপত্র

১

বাঙালির খাদ্য-সংস্কৃতি : সাহিত্যে ও ইতিহাসে (মধ্যযুগ থেকে উনিশ শতকের বাংলা)

বিকাশ রায় পৃ. - ৯

২

বাংলা নাটকে উত্তরবঙ্গ : একটি সীমাবদ্ধ আলোচনা

প্রণব কুমার ভট্টাচার্য পৃ. - ২৩

৩

স্বতন্ত্রতায় বিশিষ্টতায় সত্ত্বরের উপন্যাস

সেলিম বক্স মন্ডল পৃ. - ৩২

৪

গদ্যকার রামকুমার মুখোপাধ্যায়ের দশটি ছোটগল্প : স্বতন্ত্র নির্মিতি

সাবলু বর্মণ পৃ. - ৩৭

৫

বাঙালি মহিলা ঔপন্যাসিকের উপন্যাসে দেশভাগ ও নারী স্বনির্ভরতা : অভিশাপ হয়েও আশীর্বাদ

কৃষ্ণিশ্রী ভট্টাচার্য পৃ. - ৫৫

৬

যৌনতা : ধূসর পাণ্ডুলিপি

মনিরুল ইসলাম পৃ. - ৬১

৭

জমিদারির অবসানে গণতন্ত্রের সূচনা : প্রসঙ্গ 'মহিষকুড়ার উপকথা'

মৃদুল ঘোষ পৃ. - ৬৬

৮

রবীন্দ্রনাথের 'চৈতালি' কাব্যে নদীর স্থান

শুভাশিস গোস্বামী পৃ. - ৭৪

৯

কার্তিক লাহিড়ীর ছোটগল্পে রাবীন্দ্রিকভাবনা ও রবীন্দ্রসঙ্গীত

সুলতা হালদার পৃ. - ৮৪

১০

সুভাষ মুখোপাধ্যায় : রাজনৈতিক কর্মী ও কবি সত্ত্বার দ্বন্দ্ব

দেবাশিষ সরকার পৃ. - ৯১

১১

বিনতা রায়চৌধুরীর গল্প : নারীর মনস্তাত্ত্বিক জটিলতার স্বরূপ সন্ধান

মোসাঃ রাবেয়া বাসরি পৃ. - ৯৭

রবীন্দ্রনাথের 'চৈতালি' কাব্যে নদীর স্থান

শুভাশিস গোস্বামী

'চিত্রা'-র অব্যবহিত পরেই রচিত 'চৈতালি' কাব্যগ্রন্থে ১৩০২ বঙ্গাব্দের চৈত্রমাস থেকে ১৩০৩ বঙ্গাব্দের শ্রাবণ মাস পর্যন্ত রচিত কবিতা স্থান পেয়েছে। 'চিত্রা'-র শেষ কবিতা 'সিন্ধুপারে' লেখা হয়েছিল ২০ ফাল্গুন ১৩০২ বঙ্গাব্দে। আর 'চৈতালি'র প্রথম কবিতা 'উৎসর্গ' রচিত হয়েছে ১৩০২ বঙ্গাব্দের ১৩ চৈত্র (অবশ্য এই কাব্যগ্রন্থে রচনাকালের দিক থেকে প্রথম কবিতা 'প্রভাত'। লেখা হয় ১১ চৈত্র)। কবিতাগুলির অধিকাংশই রচিত হয় পতিসরে, বাকি কয়েকটি সাজাদপুরে। যেহেতু সাজাদপুর রবীন্দ্রনাথদের জমিদারির ভাগে আর পড়ছে না, সুতরাং পদ্মা-তীরের এই অংশে বসবাসের পর্ব এবার শেষ হতে চলেছে। এইবারে তাঁর সঙ্গী হয়েছে পতিসর সংলগ্ন গ্রাম্য নদী নাগর। 'সূচনা' অংশে কবি লিখেছেন— "অল্প তার পরিসর, মন্ত্র তার স্রোত। তার একতীরে দরিদ্র লোকালয়, গোয়ালঘর, ধানের মরাই, বিচালির স্তূপ; অন্যতীরে বিস্তীর্ণ ফসল-কাটা শস্যক্ষেত ধূ ধূ করছে। কোনো এক গ্রীষ্মকাল এইখানে আমি বোট বেঁধে কাটিয়েছি।" মোহিতচন্দ্র সেন সম্পাদিত 'কাব্যগ্রন্থাবলী'র (আশ্বিন ১৩০৩ বঙ্গাব্দ) মধ্যে 'চৈতালি' প্রথম প্রকাশিত হয়। এর ভূমিকায় স্বয়ং কবি জানিয়েছিলেন— "চৈতালি শীর্ষক কবিতাগুলি লেখকের সব শেষের লেখা। তাহার অধিকাংশই চৈত্রমাসে লিখিত বলিয়া বৎসরের শেষ উৎপন্ন শস্যের নামে তাহার নামকরণ করিলাম।"

শ্রেণিগত দিক থেকে 'চৈতালি' 'সোনার তরী' বা 'চিত্রা' থেকে তেমন স্বতন্ত্র কিছু নয়। তবে বেশ বুঝতে পারা যায় যে, কবিমনের ভাবনা, কল্পনা ও অনুভূতি ধীরে ধীরে ভিন্নরূপ ধারণ করছে। আগের মত ভাবের অতিশয় আবেগ, কল্পনার মাধুর্য বা আসক্তির তীব্রতা অপেক্ষা এখানে যে সুরটি শোনা যাচ্ছে তা হল পূর্ণতার সুর, তৃপ্তির সুর। আগে যা ছিল 'সামান্য সত্য', এখন তা 'বিশিষ্ট' হয়ে উঠেছে।^১ একটি 'অখণ্ড নিসর্গানুভূতি' থেকেই এসেছে এই পূর্ণতা ও তৃপ্তির সুর।^২ 'চৈতালি'র ছোট ছোট কবিতাগুলিতেও দেখি যে, মানুষ ও প্রকৃতি মিলে একটি পূর্ণতার সুর সৃষ্টি করে কবিতাগুলিকে অপরূপ মাধুর্য দান করেছে।

'সোনার তরী'-'চিত্রা' যুগের তীব্র অনুভূতি 'চৈতালি'তে পরিণত হয়েছে গভীর উপলব্ধিতে। শান্ত সমাহিত চিন্তে কবি যেন সত্য দর্শন করেছেন আর ধীরে ধীরে তা ব্যক্ত করছেন। কবিতার আকারও অনেক সংক্ষিপ্ত হয়েছে এখানে। ভাষাতেও নেই অজস্র অলংকারের ঐশ্বর্য ও চমৎকারিত্ব। কবিতাগুলি যেন কবির উপলব্ধ সত্যের অনাড়ম্বর প্রকাশ। 'সূচনা' অংশে কবিই লিখেছেন সে কথা— "মনটা আছে ক্যামেরার চোখ নিয়ে, ছোটো ছোটো ছবির ছায়া ছাপ দিচ্ছে অন্তরে। অল্প পরিধির মধ্যে দেখছি বলেই এত স্পষ্ট করে দেখছি। সেই স্পষ্ট দেখার স্মৃতিকে ভরে রাখছিলুম নিরলংকৃত ভাষায়। অলংকার প্রয়োগের চেষ্টা জাগে মনে যখন প্রত্যক্ষবোধের স্পষ্টতা সম্বন্ধে সংশয় থাকে। যেটা দেখছি মন যখন বলে 'এটাই যথেষ্ট' তখন তার উপরে রঙ

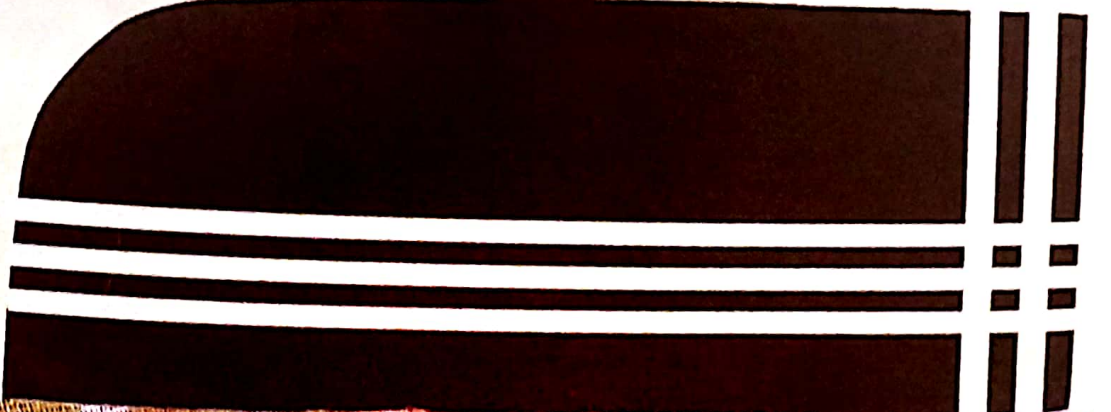
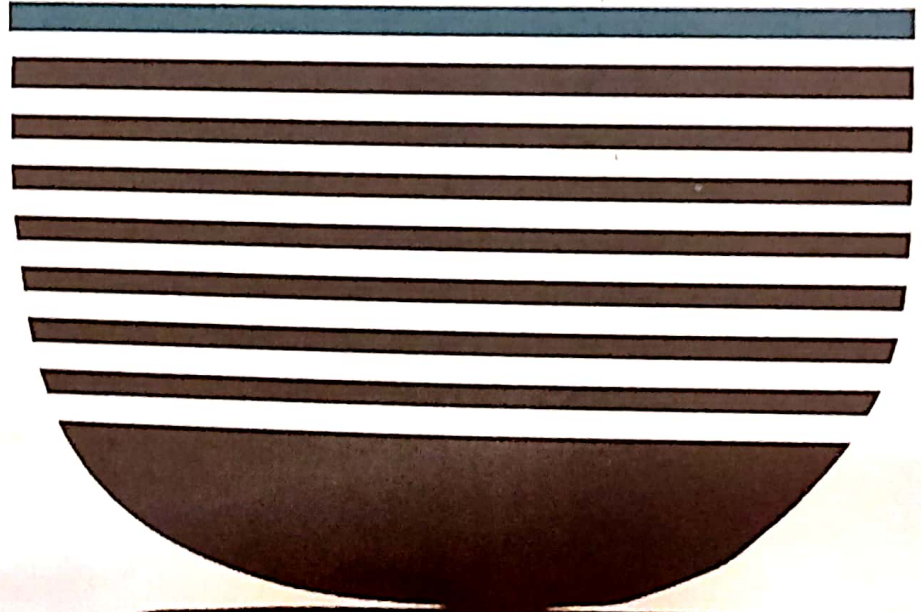
ISSN 2249-8133

নাব্যশ্ৰোত

ষান্মাসিক সমাজ ও সংস্কৃতি বিষয়ক কাগজের জমি

পঞ্চদশ বর্ষ, প্রথম ও দ্বিতীয় সংখ্যা

অগাস্ট ২০২০ ও ফেব্রুয়ারি ২০২১



✓ প্রবন্ধগুচ্ছ- দুই

রবীন্দ্রনাথের 'চিত্রা' কাব্যে নদীর স্থান

শুভাশিস গোস্বামী ১০৯

গিরিশচন্দ্র ঘোষের নাটকের সংলাপ : একটি সংক্ষিপ্ত অবলোকন

কৌশিককুমার দত্ত ১২২

ভারত-নেপাল দ্বিপাক্ষিক সম্পর্কে চীনের প্রভাব :

একটি ঐতিহাসিক বিশ্লেষণ (১৯৫০-১৯৬০)

বাসুদেব দাস ১৩২

সার্থশতবর্ষে দেশবন্ধু চিত্তরঞ্জন : এক আপোষহীন মহাপ্রাণ

গার্গী সেনগুপ্ত ১৪৩

মহর্ষি পতঞ্জলির দৃষ্টিভঙ্গিতে ধ্যান ও সমাধি : একটি পর্যালোচনা

বিপ্লব বারিক ১৫৬

রমাপদ চৌধুরীর ছোটগল্পে সমাজ ও পরিবেশের প্রভাব

ড. অর্জুন দোলই ১৭০

প্রাপ্তজনের সংকট : নলিনী বেরার 'অপৌরুষেয়'

ও কাবেরী রায়চৌধুরীর 'শ্রীমান রঞ্জাবতী'

অসীম মণ্ডল ১৭৬

প্রবন্ধগুচ্ছ- তিন

আমার আখরগুলি

ড. সৈয়দ তানভীর নাসরীন ১৯৩

রবীন্দ্রনাথের 'চিত্রা' কাব্যে নদীর স্থান

শুভাশিস গোস্বামী

'সোনার তরী' ও 'চিত্রা' কাব্যের সময়ের ব্যবধান মাত্র একমাসের। 'সোনার তরী'-র শেষ কবিতা 'নিরুদ্দেশ যাত্রা' রচিত হয় ২৭ অগ্রহায়ণ ১৩০০ বঙ্গাব্দ। আর 'চিত্রা' কাব্যগ্রন্থের প্রথম কবিতা (রচনাকালের দিক থেকে) 'জ্যোৎস্নারাত্রে' (৬ মাঘ ১৩০০ বঙ্গাব্দ)। ৬ মাঘ ১৩০০ বঙ্গাব্দ থেকে ২০ ফাল্গুন ১৩০২ বঙ্গাব্দ পর্যন্ত 'চিত্রা' কাব্যগ্রন্থের কবিতাগুলির রচনার কাল।

'সোনার তরী' ও 'চিত্রা' দুই কাব্যগ্রন্থের কবিতাগুলি রচনাকালে কবির মানসিক পরিবেশ এবং লেখার পরিপ্রেক্ষিতেও মোটের উপর একইরকম। কবি তখনও বাস করছেন বোটে। তাঁর জীবনে মনে তখনও চলেছে 'নির্জন-সজনের নিত্য সংগম'। তাছাড়া কাব্যকল্পনা ও কাব্য প্রসাধনগত দিক থেকেও দুই কাব্যের মধ্যে পার্থক্য সামান্য। কবির objective দৃষ্টিভঙ্গি যেমন 'চিত্রা' পর্বে অনেকটা গভীর হয়েছে তেমনি 'সোনার তরী'-র সময়কার সৌন্দর্যধ্যানও আরও গভীরতর রূপ লাভ করেছে। কবির অতিশয় আত্মগত ও আত্মসচেতন ভাবকল্পনা থেকে জাত জীবনদেবতার ধ্যান— 'চিত্রা'য় আরও 'দৃঢ়তর ভিত্তির উপর প্রতিষ্ঠিত হয়েছে।' সর্বোপরি 'রিয়াল' ও 'আইডিয়াল'—এর দ্বন্দ্বও কিছুটা সময় লাভ করেছে এই পর্বে।

পদ্মা ও তার শাখানদীগুলির ঘনিষ্ঠ সান্নিধ্যে থাকার কারণে রবীন্দ্রনাথের 'চিত্রা' কাব্যগ্রন্থেরও বহু কবিতায় বিভিন্নভাবে উঠে এসেছে নদী প্রসঙ্গ। আমরা তেমন প্রাসঙ্গিক কবিতাগুলি আলোচনায় অগ্রসর হব।

'চিত্রা' কাব্যগ্রন্থ প্রকাশিত হয় ২৯ ফাল্গুন ১৩০২ বঙ্গাব্দ (ইং-১১ মার্চ ১৮৯৫ খ্রি.)। প্রথমত এই কবিতা সংকলনটিতে ছিল ৩৪টি কবিতা। পরে 'সোনার তরী' থেকে নিয়ে সুখ

শুভাশিস গোস্বামী : গবেষক, রাঁচী বিশ্ববিদ্যালয় (বাংলাভাষা ও সাহিত্য বিভাগ)। সহযোগী অধ্যাপক, অহরুরাম মেমোরিয়াল কলেজ, ঝালদা, পুরুলিয়া।

'এবং মহায়া' - বিশ্ববিদ্যালয় মঞ্জুরী আয়োগ (UGC-CARE)
অনুমোদিত তালিকার অন্তর্ভুক্ত।
২০২০সালে প্রকাশিত ৮৬পৃ.তালিকার ৬০ পৃ.এবং ৮৪পৃ.উল্লেখিত।

এবং মহায়া

(বাংলা ভাষা, সাহিত্য ও গবেষণাধর্মী মাসিক পত্রিকা)

২২ তম বর্ষ, ১২৫ সংখ্যা

অক্টোবর, ২০২০

সম্পাদক

ড. মদনমোহন বেরা

সহসম্পাদক

পায়েল দাস বেরা

মৌমিতা দত্ত বেরা

যোগাযোগ :

ড. মদনমোহন বেরা, সম্পাদক।

গোলকুন্ডাচক, পোষ্টি-মেদিনীপুর, ৭২১১০১, জেলা-প.মেদিনীপুর, প.বঙ্গ।

মো.-৯১৫৩১৭৭৬৫৩

কে.কে. প্রকাশন

গোলকুন্ডাচক, মেদিনীপুর, পশ্চিমবঙ্গ।

| | |
|--|-----|
| ২৭. কুমুদরঞ্জন মল্লিকের প্রবন্ধে গ্রাম সমাজের রূপ ও রূপান্তর | |
| :: সম্রাট কুমার পাল..... | ২২৫ |
| ২৮. 'নঙ্গী কাঁথার মাঠ' এবং 'রাপসী বাংলা' : বঙ্গ প্রকৃতির রূপের বিচিত্র আলোচনা | |
| :: বাপি দত্ত..... | ২৩০ |
| ২৯. কমল কুমার মুখোপাধ্যায়ের গল্প 'মতিলাল পাদরী' : ধর্ম বিশ্বাসের আড়ালে মানবিক চেতনা | |
| :: বেবী পাত্র (সামন্ত)..... | ২৩৫ |
| ৩০. সরলা দেবী চৌধুরাণী : উপনিবেশিক বঙ্গের বিপ্লবী আন্দোলনের অন্যতম উদগাতা | |
| :: চিত্ত সেন পরামানিক..... | ২৪৫ |
| ৩১. 'কথা'র মধ্যে 'বাদ'-এর শ্রেষ্ঠত্ব বিচার | |
| :: প্রিয়াঙ্কা মাইতি (দাস)..... | ২৫৩ |
| ৩২. রবীন্দ্রসঙ্গীত : ব্যক্তিগত থেকে নৈব্যক্তিক অভিযাত্রা | |
| :: সুকান্ত চক্রবর্তী..... | ২৬৭ |
| ৩৩. কাশীদাসী মহাভারতে রাজনৈতিক ও মনোস্তাত্ত্বিক দ্বন্দ্ব | |
| :: সৌমিতা মুখার্জী..... | ২৭৪ |
| ৩৪. 'উদ্যোগ পর্ব' : এক বিশেষ সময়ের ইতিবৃত্তে গুঁরাও জীবন | |
| :: বৈশাখী কুণ্ড..... | ২৮২ |
| ৩৫. রবীন্দ্র ছোটগল্পে প্রতিবাদী নারী | |
| :: তাহমিজা খাতুন..... | ২৮৭ |
| ৩৬. "দুঃখ তোমার ঘুচবে কবে?" রবীন্দ্রনাথ | |
| :: ড. অরুণ সরকার..... | ২৯৪ |
| ৩৭. বাংলা মঙ্গলকাব্যে অস্তিত্বের সংকট | |
| :: ড. শান্তনু ভট্টাচার্য..... | ৩০৩ |
| ৩৮. বাংলা থিয়েটারে নারী : উনিশ শতক | |
| :: ড. বিপুলকুমার মণ্ডল..... | ৩১৪ |
| ৩৯. পাঠ্যপুস্তক রচয়িতা রবীন্দ্রনাথ | |
| :: ড. অর্চনা দশপাঠ..... | ৩২৪ |
| ৪০. প্রকৃতি ও প্রবৃত্তির দ্বন্দ্ব অতীন বন্দ্যোপাধ্যায়ের উপন্যাস | |
| :: ড. সুরতকুমার দে..... | ৩৩৩ |
| ৪১. এমন দিন কবে হবে তারা ; প্রসঙ্গ 'বীরাজনা কাব্য'র তারা চরিত্র | |
| :: ড. শান্তনু চট্টোপাধ্যায়..... | ৩৪৩ |

বাংলা মঙ্গলকাব্যে অস্তিত্বের সংকট

ড. শান্তনু ভট্টাচার্য

মঙ্গল কথাটির আভিধানিক অর্থ হল কল্যাণ। সাধারণভাবে যে কাব্যে দেবদেবীর তাকেই আমরা মঙ্গলকাব্য বলি। মঙ্গলকাব্য আখ্যানমূলক কাব্য। পঞ্চদশ থেকে অষ্টাদশ শতাব্দী পর্যন্ত দীর্ঘ চারশত বছর ধরে বহু কবি এই কাব্যশাখায় একাধিক কাব্যলিখেছেন। বিশিষ্ট সমালোচকের মতে, 'বাংলাদেশে খ্রীষ্টীয় পঞ্চদশ শতাব্দীর শেষভাগ হইতে অষ্টাদশ শতাব্দীর শেষার্ধ পর্যন্ত পৌরাণিক, লৌকিক এবং পৌরাণিক-লৌকিক সংমিশ্রিত দেব-দেবীর লীলামাহাত্ম্য, পূজা-প্রজ্ঞার ও ভক্তকাহিনী অবলম্বনে যে-ধরনের সম্প্রদায়গত, প্রচারধর্মী ও আখ্যানমূলক কাব্য রচিত হইয়াছে, তাহাকে বাংলা সাহিত্যের ইতিহাসে মঙ্গলকাব্য বলা হয়।' মঙ্গলকাব্য সাধারণত চারটি অংশে বিভক্ত— বন্দনা অংশ, গ্রন্থোৎপত্তির কারণ অংশ, দেবখণ্ড, নরখণ্ড। মঙ্গলদেবদেবী চরিত্রে লোকভিত্তি, পৌরাণিক দেবতাদের সঙ্গে সঙ্ঘ, মানবিক স্বভাব প্রভৃতি বিশিষ্টতা লক্ষণীয়। মঙ্গলকাব্যগুলিতে মধ্যযুগের বাঙালিদের জীবনযাত্রার তথ্যনিষ্ঠ ছবি ধরা পড়েছে। নারীগণের পতিনিন্দা, বারমাস্যা, চৌতিশা, পুরাণ কথার উদ্বেগ প্রভৃতি মঙ্গলকাব্যের রীতির অন্তর্গত।

জীবনধারণে মানবসমাজ নানা সংকটের সম্মুখীন হয়। এই সংকট আবার কখনো কখনো অস্তিত্বের সঙ্গে যুক্ত হয়ে থাকে। সাহিত্য জীবনের প্রতিচ্ছবি। তাই স্বাভাবিকভাবেই সাহিত্যেও অস্তিত্বের সংকটের প্রসঙ্গ ধরা পড়েছে নানাভাবে। মানব সমাজে অস্তিত্বের সংকট মূলত জীবন এবং জীবিকা কেন্দ্রিক। বাংলা মঙ্গলকাব্যের ধারায় দৃষ্টিপাত করলে আমরা এমন অনেক চরিত্র এবং প্রসঙ্গ পাব যাতে অস্তিত্বের সংকট নানাভাবে ফুটে উঠেছে। আলোচনার সুবিধার্থে বিশেষ কয়েকটি মঙ্গলকাব্যের বিশেষ কয়েকটি চরিত্র এবং প্রসঙ্গকে কেন্দ্র করে আমরা এগোবো যেখানে মানবসমাজের অস্তিত্বের সংকটগুলি বিশেষভাবে দৃষ্টি আকর্ষণ করে। বিজয়গুপ্তের মনসামঙ্গল, কবিকঙ্কণ মুকুন্দের চণ্ডীমঙ্গল এবং ভারতচন্দ্রের অন্নদামঙ্গল— এই কাব্যগুলিকে কেন্দ্র করে পরবর্তী অংশে আলোচ্য বিষয়ে আলোকসম্পাত করা হবে।

বিজয়গুপ্তের মনসামঙ্গল কাব্যের দিকে দৃষ্টিপাত করলে প্রথমেই যে চরিত্রে অস্তিত্বের সংকট সর্বাপেক্ষা লক্ষিত হয় সে হল কেন্দ্রীয় চরিত্র মনসা। মনসা অযোনি সন্তুতা। জন্মলগ্ন থেকেই তিনি অবহেলিতা, লাঞ্ছিতা, অপমানিতা। তার খেদোক্তি—

“জমন দুঃখিনী আমি দুঃখে গেল কাল।

যেই ডাল ধরি আমি ভাঙ্গে সেই ডাল।।

‘এবং মহুয়া’-বিশ্ববিদ্যালয় মঞ্জুরী আয়োগ(UGC-CARE list-I 2021)
অনুমোদিত তালিকার অন্তর্ভুক্ত।

২০২১সালে প্রকাশিত ১৩পৃ. তালিকার(৩১৯টির মধ্যে) ৩ পৃ. ৩০নং উল্লেখিত।

এবং মহুয়া

(বাংলা ভাষা, সাহিত্য ও গবেষণাধর্মী মাসিক পত্রিকা)

২৩তম বর্ষ, ১৩৭ সংখ্যা

আগস্ট, ২০২১

সম্পাদক

ড. মদনমোহন বেরা

সহসম্পাদক

পায়েল মাস বেরা

মৌমিতা মত বেরা

যোগাযোগ :

ড. মদনমোহন বেরা, সম্পাদক।

খোলকুয়াচক, পোষ্ট-মেদিনীপুর, ৭২১১০১, জেলা-প. মেদিনীপুর, প. বঙ্গ।

ফো. - ৯১৫৩১৭৭৬৫৩

ডে. ডে. প্রকাশন

খোলকুয়াচক, মেদিনীপুর, পশ্চিমবঙ্গ।

| | |
|--|-----|
| ৫৩ আধুনিক ভারতে যোগচর্চা | |
| :: ড. বিপ্লব সরকার..... | ৪১৫ |
| ৫৪ সংস্কৃত অলংকারশাস্ত্রে শ্রীশ্রীচেতন্য প্রবর্তিত ভক্তিরস | |
| :: ড. দিলীপ পণ্ডা..... | ৪২৩ |
| ৫৫ উনবিংশ শতাব্দীতে নারী শিক্ষা ও উত্তরপাড়ার হিতকরী সভা : | |
| একটি পর্যালোচনা:: ড. মিলন কান্তি দাস..... | ৪৩১ |
| ৫৬ ত্রিপুরার বাংলা কবিতাচর্চা :: ড. মৌসুমী পাল..... | ৪৪০ |
| ৫৭ ধর্মশাস্ত্রে আলোচ্য স্বধর্ম :: ড. মুকুল মন্ডল..... | ৪৪৭ |
| ৫৮ বিশুদ্ধ পাগলামির কারুশিল্প : অবনীন্দ্রনাথের যাত্রাপালা | |
| :: ড. প্রত্যায কুমার জানা..... | ৪৫৪ |
| ৫৯ উত্তর-পূর্ব ভারতের রাজবংশী লোকদেবতা মাশান | |
| :: ড. কৃষ্ণকান্ত রায়..... | ৪৬১ |
| ৬০ বরাক উপত্যকার সৃজন ভাবনায় উদ্বাস্ত চেতনায় : প্রসঙ্গ | |
| কবি শক্তিপদ ব্রহ্মচারী ও অতীন দাসের কবিতা | |
| :: ড. কালীপদ দাস..... | ৪৭২ |
| ৬১ মঙ্গলকাব্যের দেব-দেবী:আর্য ও অনার্য ধর্ম ও সংস্কৃতির মেলবন্ধন | |
| :: ড. শান্তনু ভট্টাচার্য..... | ৪৮১ |
| ৬২ পঞ্চাশের কবি শক্তি চট্টোপাধ্যায় : ভাবনার নিজস্ব ভুবন | |
| :: ড. সুশান্তকুমার দোলই..... | ৪৮৯ |
| ৬৩ নারীর ক্ষমতায়ণ ও রাজা রামমোহন রায় : একটি পর্যালোচনা | |
| :: ড. স্বাগতা ভট্টাচার্য..... | ৫০২ |
| ৬৪ ত্রিপুরার বাংলা ছোটগল্পে প্রান্তীয় মানুষ-জন | |
| :: ড. শংকরী দাস..... | ৫১২ |
| ৬৫ সাহিত্যের বিষয় ও কয়েকটি সাহিত্যতাত্ত্বিক প্রসঙ্গ | |
| :: ড. সুমন ঘোষ..... | ৫২১ |
| ৬৬ বাংলা গোয়েন্দা সাহিত্যের উদ্ভব | |
| :: ড. কৌষেয়ী ব্যানার্জি..... | ৫২৬ |
| ৬৭ সংগীত প্রশিক্ষণে গুরুশিষ্য পরম্পরা এবং বৈজ্ঞানিক পদ্ধতিতে | |
| ব্যবধানিক শিক্ষা :: ড. লোপামুদ্রা চক্রবর্তী..... | ৫৩০ |
| ৬৮ বিনয় মজুমদার : সৃষ্টিসুখে সমর্পিত | |
| এক কবির বিয়াদময় জীবন কথা :: ড. আশিস অধিকারী | ৫৩৫ |
| ০০লেখক পরিচিতি..... | ৫৫১ |
| ০০০UGC--CARE list..... | ৫৫৫ |

संस्कृत भाषा में लिखित एक कविता का
संग्रह (संग्रह)
ए. ए. ए. ए.

संस्कृत भाषा में लिखित एक कविता का संग्रह (संग्रह) ए. ए. ए. ए.

संस्कृत भाषा में लिखित एक कविता का संग्रह (संग्रह) ए. ए. ए. ए.

संस्कृत भाषा में लिखित एक कविता का संग्रह (संग्रह) ए. ए. ए. ए.

संस्कृत भाषा में लिखित एक कविता का संग्रह (संग्रह) ए. ए. ए. ए.

संस्कृत भाषा में लिखित एक कविता का संग्रह (संग्रह) ए. ए. ए. ए.

‘এবং মহুয়া’ -বিশ্ববিদ্যালয় মঞ্জুরী আয়োগ (UGC-CARE)

অনুমোদিত তালিকার অন্তর্ভুক্ত।

২০২১সালে প্রকাশিত ৮৬পৃ.তালিকার ৬০ পৃ.এবং ৮৪পৃ.উল্লেখিত।

এবং মহুয়া

(বাংলা ভাষা, সাহিত্য ও গবেষণাধর্মী মাসিক পত্রিকা)

২৩তম বর্ষ, ১৩২ (ক) সংখ্যা

এপ্রিল, ২০২১

সম্পাদক

ড. মদনমোহন বেরা

সহসম্পাদক

পায়েল দাস বেরা

মৌমিতা দত্ত বেরা

যোগাযোগ :

ড. মদনমোহন বেরা, সম্পাদক।

গোলকুঁয়াচক, পোস্ট-মেদিনীপুর, ৭২১১০১, জেলা-প.মেদিনীপুর, প.বঙ্গ।

মো.-৯১৫৩১৭৭৬৫৩

কে.কে. প্রকাশন

গোলকুঁয়াচক, মেদিনীপুর, পশ্চিমবঙ্গ।

U.G.C.- CARE List (2021)approved journal, Indian
Language-Arts and Humanities Group, out of 86 pages
placed in Page 60 & 84.

EBONG MAHUA

**Bengali Language, Literature, Research and Referred with
Peer-Review Journal**

23th Year, 132 (A) Volume

April, 2021

Published By

K. K. Prakashan

Golekuachawk, P.O.-Midnapur,721101.W.B.

DTP and Printed By

K.K.Prakashan

Cover Designed By

Kohinoorkanti Bera

Communication :

Dr. Madanmohan Bera, Editor.

Golekuachawk, P.O.-Midnapur, 721101. W.B.

Mob.-9153177653

Email- madanmohanbera51@gmail.com /

kohinoor bera @ gmail.com

Rs 600

| | |
|---|----------|
| ৫৭.মানবিক মূল্যবোধ গঠনে গান্ধীজীর সত্য ও অহিংসা নীতির প্রাসঙ্গিকতা :: সুমিত্র মাহাত |৪৭২ |
| ৫৮.জাতি বৈষম্য নিরসনে সাংবিধানিক বিধিবিধান :: ড. তারক নাথ জাঁতুয়া |৪৮০ |
| ৫৯.ঋগ্বেদে ধর্মনিরপেক্ষ চেতনা :: তপতী গায়েন |৪৮৭ |
| ৬০.সাঁওতালি ভাষা ও সাহিত্য বিকাশে পি.ও.বোডিং :: বাপি টুডু |৪৯২ |
| ৬১.সুনীতিকুমার চট্টোপাধ্যায়ের O.D.B.L. : বাংলা ভাষা চর্চার নানাদিক :: ড. স্বরূপ দে |৪৯৬ |
| ৬২.মহাভারতের নারী বিনির্মাণ : শাঁওলী মিত্রের 'কথা অমৃতসমান' :: সোনা মন্ডল |৫১০ |
| ৬৩.মহাশ্বেতা দেবীর উপন্যাসের আলোকে সাঁওতাল সম্প্রদায়ের ইতিবৃত্ত :: ড. অরুণাভ মুখার্জী |৫২৩ |
| ৬৪.শিশু মনে স্বদেশ-ভক্তি ও স্বদেশ -প্ৰীতি জাগরণে বাংলা ছড়া :: ড. চিত্ত সেন পরামানিক |৫২৭ |
| ৬৫.বাংলাদেশের রাখাইন উপজাতির আর্থ-সামাজিক ও রাজনৈতিক জীবনধারা :: ড. রুমকি বোস (মজুমদার) |৫৩২ |
| ৬৬.আন্তর্জাতিক রাজনীতির প্রেক্ষিতে বিশ্বায়ন ও উন্নয়ন :: মৃত্যুঞ্জয় পন্ডা |৫৪০ |
| ৬৭.লোকপাল ও লোকায়ুক্ত: তাত্ত্বিক পর্যালোচনা :: কৃষ্ণ কালি শঙ্কর সাউ |৫৪৬ |
| ৬৮.কথাসাহিত্যিক কণা বসু মিশ্রের উপন্যাসে নারী :: ড. শুদ্ধসত্ত্ব বর্মণ |৫৫০ |
| ৬৯.অনিকেতভাবনা, নিপীড়ন এবং শোষণ: ভারতী মুখার্জীর Jasmine মিশ্র সাংস্কৃতিক পরিচয় সঙ্কটের উপন্যাস :: প্রদীপ কুমার বেরা |৫৫৮ |
| ৭০.সাঁওতালি ধারাবাহিক মৌখিক সাহিত্য :: ড. কিশুন মুরমু |৫৬৫ |
| ৭১.আদিবাসী জীবন জীবিকা ও সংস্কৃতি : বিপন্নতার আলোকে :: রবীন্দ্রনাথ হাঁসদা |৫৭২ |
| ৭২.স্থানীয় রাজনীতির ক্ষেত্র বুড়ুল : প্রেক্ষিত আইন অমান্য আন্দোলন :: ড. সঞ্জয় ঢালী |৫৮২ |
| ৭৩.ইলেকট্রনিক বর্জ্য ও তার ব্যবস্থাপনা :: মধুসূদন গাঁড়াই |৫৯৪ |
| ০০লেখক পরিচিতি |৬০৪ |
| ০০০UGC--CARE list |৬০৮ |

মহাশ্বেতা দেবীর উপন্যাসের আলোকে সাঁওতাল সম্প্রদায়ের ইতিবৃত্ত

ড. অরুণাভ মুখার্জী

বাংলা সাহিত্য ধারায় মহাশ্বেতা দেবীর উপন্যাসের জগতে সাঁওতাল সম্প্রদায়ের জীবনলেখ্য একটি মাইলস্টোন হিসাবে ফুটে উঠেছে। সাঁওতাল সম্প্রদায়ের জীবন চর্চা, তথা জীবন ভাবনা উপন্যাসিক মহাশ্বেতা দেবী এতটা ব্যক্তবসম্মতভাবে চিত্রিত করেছেন যে, তা আর উপন্যাস থাকেনি - হয়ে উঠেছে জনজাতি উপজাতির জীবন্ত দলিল। আজও এই একবিংশ শতাব্দীর মুখে দাঁড়িয়ে যখন ভারতের মাটিতে অবমাননার নিয়ত নিবিড় উদ্ভাপ সঞ্চারিত করছে অর্থনৈতিক উন্নয়নের গাল ভরা প্রতিশ্রুতি, যখন ধাপে ধাপে, দফার পর দফা অর্থনৈতিক কর্মসূচিকে রূপায়িত করার জন্য শীতাতপ নিয়ন্ত্রিত হোটেল গুলিতে আলোচনাচক্রের অনুষ্ঠান করতে করতে প্রশাসনিক আমলাদের রক্তচাপ ক্রমশ বৃদ্ধি পাচ্ছে, যখন ক্ষেতমজুরদের ন্যূনতম বেতন ধার্য করে তা কার্যকর করার জন্য জনপ্রিয় সরকারের মন্ত্রীদেব চোখে ঘুম নেই - এমন এক কঠিন সময়েও সেই তালিকায় সংযুক্ত হয়নি দেশের লক্ষ লক্ষ আদিবাসী ও বিভিন্ন উপজাতি এবং বিভিন্ন প্রদেশের দুর্গম এলাকায় অবস্থিত হরিজনদের অস্তিত্ব। তাদের ভূমি নেই, বাদ্য নেই, জল নেই, শরীরের পক্ষে ন্যূনতম প্রয়োজনীয় বস্তু লবণ নেই, নারীদের নিরাপত্তা নেই, বেঁচে থাকার সার্থকতা নেই, সর্বোপরি নেই ভবিষ্যৎ। এদের বাঁচবার জন্য অবশ্য কিছু কিছু আইন আছে, ভালো ভালো প্রকল্প আছে, কিছু কিছু প্রতিশীল আমলাও আছেন। কিন্তু এই দুই মেরুর মধ্যবর্তী ভূগোলে দাঁড়িয়ে আছে এক দুর্জয় পাহাড় যা জোতদার - মহাজন - আমলাদের বহু শতাব্দী সঞ্চিত ধনা ও ষড়যন্ত্রের লোভ ও লালসার নির্মমতা ও হিংসার পাথর দিয়ে তৈরি। 'সুজলাং দুকলাং শীতলাং' ভারতবর্ষের এটিই আসল চেহারা; শিক্ষিত মধ্যবিত্তের লেখা কুল বা কলেজ পাঠ্য কবিতায়, গল্পে, গানে ও ইতিহাসে যা শেখানো হয়, এ তা নয়। প্রচলিত অর্থে এই ইতিহাসের প্রতি অনুরাগ আমাদের দেশের ডান ও বাম সব রাজনৈতিক দল নির্বিশেষে ঐকান্তিক অনুরাগ জন্মানোয় আছে, আগ্রহ আছে, কিন্তু বাস্তবায়িত আজও হয়নি। দেশের আসল ইতিহাস এত ভয়ংকর ভাবে নির্মম ও বীভৎস যে, তার মুখোমুখি হওয়ার সৎ সাহস দেখাতে কেউ সাহস পান না। তাই কৃত্রিম আন্দোলনে আদিবাসী কৃষকের রক্ত ঝরলে আমরা অভিনন্দন জানাই,

ISSN 2319 – 8389, Vol : 43, Issue : 43

KHOAI
UGC Care Listed Journal
Art and Humanities
Tri - Annual Journal

KHOAI

A Collector on Literature and Culture

Chief Editor
Kishore Bhattacharya

VOLUME 43
9 May, 2021

SANTINIKETAN, BIRBHUM, PIN- 731235, W.B. INDIA

সূচীপত্র

সম্পাদকীয়

| | | |
|--|--|-----|
| পারিবারিক সম্পর্কের বন্ধনে 'নৌকাডুবি' | -- অসীম কুমার মুখার্জী | ৯ |
| রবীন্দ্রনাথের 'নদী': একটি অন্তরঙ্গ পাঠ | -- শুভাশিস গোস্বামী | ১৪ |
| রবীন্দ্রসঙ্গীতে বাস্তবতা, সমাজ নৈতিকতা ও বিশ্বমানবতার শিক্ষা | -- অসীম কুমার রায় | ১৯ |
| মুর্শিদাবাদের সংস্কারধর্মী প্রবাদ : সমীক্ষা ও মূল্যায়ন | -- নিবিড় কুমার ঘোষ | ৩২ |
| দ্বারা শিকোর দার্শনিক ও আধ্যাত্মিক নিকটবর্তিতা | -- মহম্মদ ফায়েক, প্রহ্লাদ রায়, সিদ্দিকী ওয়াসিম রহমান | ৩৬ |
| সত্যজিৎ রায় পরিচালিত চলচ্চিত্রে প্রতিফলিত লোকসংস্কৃতি | -- পুলক গাঙ্গুলী | ৪১ |
| রোসাঙ রাজসভার সাহিত্যে সূফী সাধনার প্রভাব | -- তনুকা চৌধুরী | ৪৮ |
| বাংলা চলচ্চিত্রে ব্যবহৃত লোকসংগীত ও লোকনৃত্য | -- ইতি পাল | ৫৫ |
| মূল্যবোধ শিক্ষা : প্রসঙ্গ মধ্যযুগের ইংরেজি সাহিত্য | -- মৌসুমী পেড়িওয়াল | ৬২ |
| 'রঘুবংশম্' মহাকাব্যে বিজ্ঞানচেতনা | -- সঞ্জয় মণ্ডল | ৬৯ |
| 'দিবে আর নিবে, মিলাবে মিলিবে': শিক্ষার প্রাক্কণে বিশ্বায়ন | -- নাফিসা সনম | ৭২ |
| সমুদ্রে জাতীয়তাবাদ : ঊনবিংশ ও বিংশ শতকে ভারত- | | |
| -মহাসাগরীর সমুদ্রবাণিজ্যে স্বদেশী প্রয়াস ও পরিণতি | -- সৌম্যজিৎ মুখার্জী | ৭৮ |
| অবনীন্দ্রনাথ ঠাকুরের 'বুড়ো আংলা' : বাংলার সমাজ ও সংস্কৃতি | -- শুভঙ্কর ঘোড়াই | ৮৭ |
| হিজেন্দ্রলাল রায়ের ঝালাঙ্গ বাংলা গান | -- চন্দ্রানী দাস | ৯৫ |
| ভারতীয় রাগসঙ্গীত ও তার উদ্দেশ্য | -- অরিন্দম সেন | ১০৬ |
| সূর্য-দীঘল বাড়ী : উপন্যাসে, চলচ্চিত্রে | -- তীর্থ দাস | ১১২ |
| বাংলা কথাসাহিত্যে ঝাড়খণ্ডের জনজীবন | -- অনির্বাণ সাহ | ১১৬ |
| শিক্ষার আভিনায় সর্ব লিঙ্গ সমন্বয় : লিঙ্গসমতার এক অধ্যায় | -- সুমেধা মুখার্জী ও উমাকান্ত প্রসাদ | ১২৪ |
| প্রগতি ও অগ্রগতি : ঊনিশ শতকে মেয়েদের জন্য বাংলা ভাষার পত্রিকা | -- সঞ্জিতা বসু | ১৩৪ |
| দূরস্থিত সংযোগ | -- ইন্দীরা দাশ | ১৪৩ |
| ইতিহাসের অন্তরালে ঊনিশ শতকের নিরিখে পট ও ব্রাত্য- | | |
| -জনগোষ্ঠী পটুয়া শিল্পীদের যাপন আখ্যানের আলোচনা | -- রাকেশ কৈবর্ত | ১৪৭ |

পারিবারিক সম্পর্কের বন্ধনে 'নৌকাডুবি'

অসীম কুমার মুখার্জী

বহুদূরী প্রতিভার অধিকারী রবীন্দ্রনাথ ঠাকুর বাংলা সাহিত্যে এক সর্বজন বন্দিত নাম। দীর্ঘ আয়ুর অধিকারী রবীন্দ্রনাথ বাংলা সাহিত্যে ভাণ্ডারকে করে গেছেন সমৃদ্ধ। ছেলেবেলা থেকে শুরু করে আমৃত্যু পর্যন্ত নিজের জীবনের কাহিনী- পরিবারের কাহিনী নানা রচনায় বাজু করেছেন। তিনি ছিলেন জোড়াসাঁকো ঠাকুর বাড়ির বন্দি সন্ধ্যা। সকলের সঙ্গে ছিল তাঁর ঘনিষ্ঠ সম্পর্ক। ঠাকুরদা-ঠাকুমা, দাদামশায়-দিদিমা, বাবা-মা, জ্যাঠা-জ্যাঠিমা, কাকা-কাকিমা, কক-বোহি ভাইসে-ভাইবি, স্ত্রী-পুত্র-কন্যা ও সকল সম্পর্ক নিয়েই ছিল ঠাকুর বাড়ির অন্দরমহল। এই সম্পর্কের কথায় রবীন্দ্র উপন্যাস ও ছোট গল্পের কাহিনী নির্মাণের চয়নে ও বয়নে সাহায্য করেছে। অঙ্কন করেছেন এই পারিবারিক চিত্রের এক নির্মাণ শিল্প। যার উৎকৃষ্ট প্রমাণ 'নৌকাডুবি' উপন্যাস। পারিবারিক সম্পর্কের বন্ধনেই এই রচনার মূল প্রতিপাদ্য বিষয়।

পিতা-পুত্র: ব্রজমোহন চৌধুরী ও রমেশ:-

'নৌকাডুবি' উপন্যাসের একটা গুরুত্বপূর্ণ চরিত্র ব্রজমোহন চৌধুরী। রমেশের বাবা। ব্রজমোহনের সক্রিয়তা উপন্যাসে নশ্বল। কিন্তু পিতা হিসেবে রমেশের জীবনের একমাত্র ভাগ্য বিধাতা। ভাগ্য নিয়ন্ত্রাও বলা যায়। রমেশের আইন পরীক্ষা সমাপ্ত করে বাড়ির উদ্দেশ্যে বওনা দেওয়ার কথা। কিন্তু তোরঙ্গ সাজাবার কোনো উৎসাহ তার দেখা যায়নি। একিৎ বাড়ি অন্দর জন্য পিতা বরবর তাকে চিঠি লিখেছে। রমেশের উত্তর পরীক্ষার ফল বেরলেই বাড়ি ফিরবে। অন্দরবন্দুর হেলে যোগেন্দ্রের বসায় জমজমট চায়ের আসরে বেহারা একখানি চিঠি রমেশের হাতে ধরিয়ে দিয়ে চলে গেল। চিঠি পড়ে শশব্যস্ত হয়ে পড়লে সকলেই রমেশকে জিজ্ঞাসা করলেন এত ব্যস্ততার কারণ কি। রমেশ বলল, "বাবা দেশ হইতে আসিয়াছেন।" ব্রজমোহনবাবু পুত্রকে বললেন কালকেই দেশে যেতে হবে। কেন কোনো জরুরী কাজ আছে? পিতা বলিলেন, "এমন কিছু গুরুতর নহে।" পরের দিন ভোরের ট্রেনেই পিতা-পুত্র বাড়ির উদ্দেশ্যে যাত্রা করল।

বাড়ি পৌঁছে রমেশ বরব পেল তার বিবাহের পাত্রী এবং দিন দুটোই স্থির হয়ে গেছে। ব্রজমোহনের বন্দ্যবরু ঈশানের একমাত্র কন্যা রমেশের হবু স্ত্রী। কৃতজ্ঞতা বশত এই কন্যাকে পুত্রবধূ করার অস্বীকার করেছেন ব্রজমোহন বাবু। কারণ যখন তার আর্থিক দুরবস্থা চলছিল তখন এই ঈশানের সাহায্যেই উত্তরণ। আজকে যে বাড়িবাস্ত তও নাকি ঐ ঈশানের জ্ঞানই। তাই তার মৃত্যুর পর তার অসহায় স্ত্রী ও কন্যার প্রতি দায়বদ্ধতা থেকেই সফল সম্পর্কে প্রশ্ন তুললে ব্রজমোহনবাবু বলেন-- "ও সকল কথা আমি ভালো বুঝি না-- মানুষ তো ফুল কিংবা প্রজাপতি মত নয় যে দেবার বিচারটাই সর্বাগ্রে তুলিতে হইবে। মেয়েটির মা যেমন সতী সাধী, মেয়েটিও যদি তেমনি হয়, তবে রমেশ কেন তাহাই ভাগ্য বলিয়া জ্ঞান করে"।

বিবাহের কথায় রমেশের মুখ শুকিয়ে গেল। মনে মনে সাহস জুগিয়ে একবার বিবাহের অসম্মতির কথা

वर्ष : 2020
अंक : 14

ISSN: 2231-0525

संवाद

PEER REVIEWED YEARLY RESEARCH JOURNAL



ENLIGHTENMENT TO PERFECTION

हिन्दी विभाग
उत्तर बंग विश्वविद्यालय
राजा राममोहनपुर
दार्जिलिंग - 734013

संवाद

PEER REVIEWED YEARLY RESEARCH JOURNAL

वर्ष : 2020 ISSN : 2231-0525 अंक : 14

: संपादक :

डॉ. सुनील कुमार द्विवेदी



ENLIGHTENMENT TO PERFECTION
Accredited by NAAC with Grade 'A'

हिन्दी विभाग

उत्तर बंग विश्वविद्यालय

दार्जिलिंग-734013

भूमंडलोत्तर हिमाचली जीवन और एस. आर. हरनोट की कहानियाँ

-गीतम सिंह राणा

समकालीन हिंदी कहानीकारों में एस. आर. हरनोट का नाम कोई परिचय का मोहताज नहीं है। ये हिमाचल प्रदेश की पार्वत्य-पृष्ठभूमि पर विपुलता के साथ लिखनेवाले एक ऐसे महत्वपूर्ण कहानीकार हैं, जिनकी कहानियों से गुजरते हुए आप अनायास ही बदलते समय के साथ पिछले चार दशकों की हिमाचली धड़कनों को महसूस कर सकते हैं। साथ ही समय के विकास के तदंतर हिमाचली पार्वत्य समाज में बढ़ती मूल्यहीनता को भी इनकी कहानियों के कैनवास पर बड़ी स्पष्टता के साथ चित्रित देख सकते हैं। बीसवीं सदी के नवें दशक से निरंतर सृजनरत इस कथाकार के अब तक कुल आठ कहानी संग्रह-‘पंजा’, ‘आकाशबेल’, ‘पीठ पर पहाड़’, ‘दारोश तथा अन्य कहानियाँ’, ‘जीनकाठी तथा अन्य कहानियाँ’, ‘मिट्टी के लोग’, ‘लिटन ब्लॉक गिर रहा है’ तथा ‘कीलें’ प्रकाशित हो चुकी हैं। आठ कहानी संग्रह के अतिरिक्त इनके द्वारा रचित एक उपन्यास - ‘हिडिम्ब’ एवं हिमाचल की संस्कृति और जनजीवन पर पाँच महत्वपूर्ण पुस्तकों - ‘हिमाचल के मंदिर और उनसे जुड़ी लोक कथाएँ’, ‘यात्रा’, ‘हिमाचल से जान पहचान’, ‘हिमाचल एट ए ग्लांस (संयुक्त कार्य) तथा ‘हिमाचल प्रदेश: मंदिर और लोकश्रुतियाँ’ का भी प्रकाशन हो चुका है। हिमाचल प्रदेश के पार्वत्य क्षेत्र के चनावग गाँव(जिला-शिमला) में जन्मे इस कथाकार ने हिंदी-पाठकों के मन को अपनी कहानियों के मार्फत सबसे ज्यादा आंदोलित किया है क्योंकि बचपन से लेकर अपनी समझदारी की उम्र तक इन्होंने जिस नैसर्गिक-सौन्दर्य-संपन्न पहाड़ी जीवन को जिया और साथ ही उसके खुरदुरे यथार्थ को अनुभूत किया, उसे इन्होंने जस का तस बड़ी कोमलता के साथ अपनी कहानियों में रख दिया है। यही कारण है कि इनकी कहानियों की पृष्ठभूमि के महत्व पर बात करते हुए ज्ञानरंजन कहते हैं -“एक जबर्दस्त पराजय और बियाबान के बीच जहाँ साहित्य, संस्कृति विकास, व्यवस्था, सत्ता प्रशासन, सबकुछ लुप्त हो गया है और जहाँ मासूम बच्चे और असहाय वृद्ध ही बचे हैं, ऐसे भूखंडों में हरनोट ने अपनी रचना को केन्द्रित करने का प्रयास अपनी कहानियों के माध्यम से किया है।”

भारत के सन्दर्भ में जब भी पार्वत्य समाज की बात की जाती रही है, तभी हमारे जेहन में उसकी स्थानीय लोक संस्कृति पूरे वजन के साथ प्रस्तुत होती रही है और उस लोक संस्कृति की सबसे बड़ी खासियत उसका मानवीय व प्राकृतिक मूल्यबोध के साथ

काफी गहराई तक जुड़ा हुआ होना रहा है। रहा है कहने का तात्पर्य है कि मशीनी सभ्यता के विकास के बरक्स यह जुड़ाव कम हुआ है। कम क्या खात्मे की ओर ही अग्रसर है। इसका मूल कारण मशीनी सभ्यता के विकास की आड़ में पहाड़ तक पहुँची पूँजीवादी मानवीय मूल्यबोधहीन शक्तियों का पार्वत्य समाज को अपनी जकड़ में ले लेना व अधिकाधिक धन उगाहने के लालच में पूरे पहाड़ का अंधाधुंध दोहन करना है। इसके कारण पूरे पार्वत्य अंचल का समाज, संस्कृति व प्रकृति खतरे में पड़ चुकी है। हिमाचल का पार्वत्य अंचल इसका अपवाद नहीं है। मशीनी सभ्यता के बढ़े कदम के बरक्स इसके समाज व संस्कृति में निहित मानवीय व सांस्कृतिक मूल्यबोध में दरकन स्पष्टतः देखी जा सकती है। इस सन्दर्भ में एस. आर. हरनोट की कहानियों का अनुशीलन बहुत ज़रूरी है।

पहाड़ पर पहुँची आधुनिकता व मशीनी सभ्यता का सबसे ज्यादा प्रभाव वहाँ की पारिवारिक संरचना की मजबूत बुनावट पर पड़ा है। इसने पारिवारिक बुनावट के तंतुओं को जार-जार कर देने का काम किया है, जिससे पारिवारिक संरचना के अंग छिन्न-भिन्न होकर अलग-थलग कराहते नज़र आ रहे हैं। आधुनिकता के सम्मोहन ने पढ़े-लिखे पहाड़ी युवाओं को शहर की ओर उन्मुख कर दिया है। शहरी वातावरण में पढ़-लिखकर वे वहाँ की सुख सुविधाओं के जुगत की अंधी दौड़ में इस तरह शामिल हो गए हैं कि वे अपने पहाड़, पहाड़ीपन, पहाड़ी संस्कृति और साथ ही केवल उनके ही आसरे पहाड़ पर पड़े हुए वृद्ध अभिभावक तक से दूर हो गये हैं। इससे पहाड़ पर अपनी जिन्दगी बसर करनेवाले वृद्ध और शहर की आधुनिकता के फाँस में फँसा युवा दोनों ही एक दूसरे से कटे छटपटाहट में जीवन व्यतीत कर रहे हैं। इस परिस्थिति का दंश पहाड़ से लगाव रखनेवाले वृद्धों को ज्यादा झेलना पड़ रहा है। इस सन्दर्भ में हरनोट की 'बिल्लियाँ बतियाती हैं', 'कागभाखा', 'मोबाईल', 'मिट्टी के लोग', 'जूजू' आदि कहानियाँ काफी महत्वपूर्ण हैं।

'बिल्लियाँ बतियाती हैं' हिमाचल की पार्वत्य पृष्ठभूमि पर लिखित एक ऐसी कहानी है, जिसमें कहानीकार ने पार्वत्य ग्रामीण परिवेश व शहरी परिवेश के मध्य मानवीय मूल्यबोध की दृष्टि से आये फर्क को बयां किया है। साथ ही आधुनिकता की दस्तक से पार्वत्य समाज की बनावट-बुनावट में जो दरकनें आई हैं, उनका भी चित्रण किया है। इस बात की सच्चाई से कोई भी मुकर नहीं सकता कि भोगवाद की बढ़ती लिप्सा और उसके तदंतर प्रायोजित सांप्रदायिकता, राजनैतिक प्रपंचों के कारण शहर हिंसा, दंगे-फसाद की गिरफ्त में आ चुके हैं। यह शहर में मानवीय मूल्यबोध के पतन को बयान करता है, जबकि इसकी तुलना में पार्वत्य गाँव में शांति-सद्भाव है। इसका मूल कारण पहाड़ों तक मशीनी सभ्यता का देर से पहुँचना है। इस सन्दर्भ में कहानी की मुख्य पात्र 'देवरू काकी' के

मनोभाव को व्यक्त करनेवाला कथन द्रष्टव्य है। "शहर में कितनी बेचैनी बढ़ गई है। रोज कुछ-न-कुछ घटता ही है। दंगे-फसाद होते हैं, लाठियां-गोलियां चलती हैं। इन सभी के बीच उसके बेटे-बहू कैसे रहते होंगे। पोतू कैसे स्कूल जाता होगा। इसलिए अम्मा को अपना गाँव बड़ा भला लगता है। कहीं कुछ नहीं घटता। शांति है। चैन है।" पर पहाड़ पर पहुँची मशीनी सभ्यता की मानवीय मूल्यबोधहीन मानसिकता ने वहाँ की शांति को नष्ट करना शुरू कर दिया है। पहाड़ पर रहनेवाला साधारण किसान खेती-मजदूरी करके, जरूरत पड़ने पर कर्ज़ लेकर, अपनी ज़मीन को रेहन पर रखकर भी अपने बच्चों को शहर में बड़ी-बड़ी डिग्रियों को दिलाने के लिए पढ़ा तो रहा है, पर जब उन बच्चों को नौकरी मिल जा रही है तो वे शहर के ही तौर-तरीकों के मोहपाश में बंधे पहाड़ पर अपने वृद्ध अभिभावकों को छोड़ वहीं बस जा रहे हैं। इससे पहाड़ पर बसे ग्रामीण वृद्ध अभिभावकों की दशा बड़ी दयनीय होती जा रही है। इस सन्दर्भ में कहानी की पंक्तियाँ हैं - "उसके पिता की जिद रहती कि एक ही बेटा है, इसे अफसर नहीं बनाया तो हमारा कमाना व्यर्थ है। उसे खूब पढ़ाया-लिखाया। हजारों कर्जा सर पर ले लिया। एक-दो खेत रेहन रख दिये। कॉलेज पूरा हुआ तो नौकरी भी लग गई। लेकिन उन बूढ़ों को यह भनक भी नहीं लगी कि शहर के तौर-तरीकों और चटक ने उसे उन दोनों से बहुत दूर कर दिया है।"

आधुनिकता और मशीनी सभ्यता की दस्तक ने सौहार्द-सम्पन्न पार्वत्य समाज में किस प्रकार विष घोलने का कार्य किया है, उसका मंजर हरनोट की 'कागभाखा' कहानी में देखने को मिलता है। इस कहानी की प्रमुख पात्र दादी आज के पक्षी-विज्ञानी सलीम अली की तरह कौवों की भाषा समझती है, जो पार्वत्य प्रदेश के मानव-मानवेतर संवेदनात्मक सम्बन्ध को दर्शाता है। कहने का तात्पर्य है कि मानवीय संवेदना की गहरी पैठ पार्वत्य ग्रामीण प्रदेशों की खासियत रही है। आधुनिकता के सम्मोहन में यह प्रदेश भी संवेदनहीन होता जा रहा है, जो इसके प्राकृतिक चरित्र के एकदम विपरीत है। जहाँ दादी जैसे लोगों का निवास है, जिसमें संवेदना इतनी घनी है कि वह मानवेतर तक के साथ भावनात्मक संबंध स्थापित कर पाती है, वहाँ भी यह ऋणात्मक परिवर्तन लक्षित हो रहा है। इस सन्दर्भ में दादी के मनोभाव को व्यक्त करनेवाली कहानी की ये पंक्तियाँ द्रष्टव्य हैं- "आज का समाज देखकर दादी भीतर ही भीतर कूढ़ती है, जलती है, फूंकती है। जैसे गाँव ही बदल गया। पहले जैसे लोग नहीं रहे, दया, धर्म खत्म हो गया। ममता नहीं रही। एक-दूसरे के लिए अनजान बन गए। छोटी-छोटी बातों पर लड़ते-झगड़ते हैं। मारपीट करते हैं। भला-बुरा बोलते हैं।"

पहले कितना प्यार था। मिलजुल कर लोग आपस में रहते, एक-दूसरे के दुःख-सुख में आते-जाते, जैसे एक ही घर हो, एक ही परिवार हो।”

हिमाचल का पार्वत्य प्रदेश नैसर्गिक सौन्दर्य से सम्पन्न है, परंतु इस सौन्दर्यमय आवरण के तले निहित खुरदुरे यथार्थ को भी झुठलाया नहीं जा सकता है। देश में आज़ादी के बाद बनी सरकारों की नीतियों के कारण इन क्षेत्रों का समुचित विकास नहीं हो पाया है। आज भी पहाड़ के दूर-दराज के क्षेत्रों में गरीबी मुँह बाए खड़ी दिखती है। बतौर पेशा यहाँ के कुछ गरीबों को भिक्षावृत्ति ही चुनना पड़ता है। पूँजीवादी सोच के प्रतिनिधि के रूप में पहुँची मोबाईल कंपनियों के लोग यहाँ भी अपना षडयंत्र रचने में सफल रहते हैं। अधिकाधिक मुनाफा कमाने की भूख ने उन्हें संवेदनहीन बना दिया है। वे इन क्षेत्रों में भी अपना उत्पाद बेचने और यहाँ की सीमित जनसंख्या को भी अपने गिरफ्त में लाने का काम करते हैं। इसके लिए वे गरीब भिखारी बच्चों तक के शरीर को अपने विज्ञापनों का वाहक बनाते हैं क्योंकि पहाड़ के इन दुर्गम प्रान्तों में यातायात की सुविधा के विकास के अभाव में उनका प्रचार महँगा पड़ जाता है, जबकि नन्हों का शरीर अपेक्षाकृत बहुत सस्ता पड़ता है। इसलिए वे संवेदनहीन होकर नन्हें बच्चों का भी अपने प्रचार माध्यम के रूप में बेझिझक उपयोग करने लगे हैं। अपने लुभावने प्रचार के मार्फत वे अपने उत्पाद रूपी अफीम का स्वाद पहाड़ की बेचारी भोली-भाली जनता को भी एक बार चखाना चाहते हैं, ताकि एक बार उनके चंगुल में फँसे ग्राहकों का आजीवन आर्थिक दोहन किया जा सके। इस सन्दर्भ को हरनोट की 'मोबाइल' कहानी प्रस्तुत करती है। इस तरह के प्रकरण को देखते हुए हरनोट अपनी इस कहानी में कहते हैं . “उस मोबाईल कम्पनी ने पहाड़ों के दूरदराज के इलाकों तक पहुँचने की जद्दोजेहद में अब भोले-भाले लोगों और उनके बच्चों का पुरजोर इस्तेमाल करना शुरू कर दिया था। लेकिन लोगों के पास यह सोचने का समय ही नहीं था कि यह घुसपैठ, बाजार को उनकी बहू-बेटियों के कमरों तक ले जा रही है।”

आधुनिक मशीनी सभ्यता के विकास ने मानव को अपार सुख सुविधायें प्रदान की हैं और साथ ही बढ़ती जनसंख्या के बरक्स जन्मी खाद्य संकट की समस्या का समाधान भी किया है; पर पहाड़ी ग्रामीण पारंपरिक मजदूरों के जीवन को बड़ा कष्टमय भी बना दिया है। हरनोट ने अपनी कहानी 'मिटटी के लोग' का विषय इसी को चुना है। हिमाचली पार्वत्य ग्रामीण प्रदेश में पहले से मौजूद सामंतवाद ने किसान-मजदूरों का शोषण तो किया ही था, पर बाद में वहाँ पहुँचे मशीनी विकासवाद के दैत्यों ने वहाँ के किसान-मजदूरों के जीवन को लीलना ही शुरू कर दिया है। उसके एक मंजर को बयान करते हुए कहानीकार अपनी कहानी के मुख्य पात्र मिटटी के घर बनाकर अपना पेट पालनेवाले 'बालदू' के बारे में

कहता है . "आज बालदू बेकार है। उसके हाथ में बेशक बही हुनर है। दक्षता है। महारत है। पर काम नहीं है। चंद सालों में क्या कुछ नहीं हो गया है। सब कुछ बदल गया है।" केवल पारंपरिक मजदूरी ही नहीं बल्कि पार्वत्य घरेलू उद्योगों पर भी मशीनी सभ्यता का नकारात्मक प्रभाव पड़ा है। हिमाचल के पार्वत्य ग्रामीण प्रदेश में बकरी-भेड़ों के बाल-ऊन से खारचे-पट्टू शाल बनाने के घरेलू उद्योग का प्रचलन हमेशा से रहा था। इन उद्योगों पर पहाड़ी जनसंख्या का कुछ भाग तो प्रत्यक्षतः निर्भर था और कुछ लोगों के लिए यह थोड़ा बहुत अतिरिक्त आमदनी का साधन हुआ करता था। पर आधुनिक मशीनी सभ्यता के आगमन ने, उसके मन लुभावन प्रचारों ने भोले-भाले पहाड़ी लोगों के स्वाद को बदलने और अपने उत्पादों को खपाने में सफलता हासिल की, जिसका परिणाम यह हुआ कि पहाड़ी घरेलू उद्योग के उत्पादों की माँग घटती गई और उससे जुड़े मजदूर बेकार होते गये। ऐसे ही एक प्रकरण का उल्लेख करते हुए हरनोट अपनी कहानी के पात्र 'रामेशरी चाची' की आर्थिक बदहाली के कारण को बताते हुए कहते हैं - "एक ज़माना था जब रामेशरी चाची बकरियों की बकराथा(बाल) निकाल कर उनके खारचे (गर्म दरियाँ) बना कर बेचा करती थी। भेड़ों की ऊन निकाल कर खुद पट्टू-शालों के लिए कातती भी थी और बेच भी दिया करती थी। दाम भी बहुत अच्छे मिल जाते थे। पर आज तो मशीनों से बनी चीजों का जमाना है। भेड़-बकरियों की ऊन और बालों की कद्र अब कहाँ रही।"

हिमाचली पार्वत्य ग्रामीण समाज में महिलाओं द्वारा अपने शिशुओं को लस्सी या मक्खन के बीच रत्तीभर अफीम चटा देने का प्रचलन था। वहाँ के लिए यह एक आम घटना थी क्योंकि ऐसा करने से शिशु पल भर में खेलते-खेलते ऊँघते और फिर पाँच-छः घंटों तक के लिए सो जाते थे, जिससे गृहणियों को घरेलू काम व पालतू मवेशियों को चारा-पानी देने का अवकाश मिल जाता था। सबसे बड़ी बात तो यह है कि इससे शिशु के शारीरिक व मानसिक स्वास्थ्य पर और साथ ही मातृत्व की घनी संवेदना पर इसका कोई प्रतिकूल प्रभाव नहीं पड़ता था। पर जबसे आधुनिकता ने पार्वत्य ग्रामों में दस्तक दी है, तब से इस संवेदना में क्षरण लक्षित होने लगा है। आधुनिकता के सम्मोहन में चटक दिखने व फिगर मेंटेनेंस की भावना के कारण मातृत्व की संवेदना का क्षरण होने लगा है। शिशुओं को बचपन से ही उनके पौष्टिक आहार मातृ-दुग्ध से दूर करने का काम शुरू हो गया है, जिससे शिशुओं के शारीरिक-मानसिक स्वास्थ्य पर बुरा प्रभाव पड़ रहा है। सबसे ज्यादा सोचनीय स्थिति तो यह है कि अब पार्वत्य समाज से जुड़े लोगों के घरों में भी अफीम का स्थान दूरदर्शन के कार्टूनो ने ले लिया है। अब गृहणियाँ फुर्सत के पल निकालने के लिए शिशुओं को अफीम चटाने के बजाय दूरदर्शन का रिमोट पकड़ा देती हैं, जिसका उनके शारीरिक व

मानसिक स्वास्थ्य पर बहुत ही बुरा प्रभाव पड़ रहा है। हरनोट ने अपनी 'जूजू' कहानी में इसी प्रसंग को विषय बनाया है। कहानीकार ने इसमें बुद्धू बक्से के कार्टून की लत लग चुके शिशुओं को मनोवैज्ञानिक रोगी के रूप में दर्शाया है, जिसके लक्षण घर पर दूरदर्शन के खराब हो जाने पर प्रकट होने लगते हैं। शिशु खाना-पीना छोड़कर रोने लगता है क्योंकि शिशु की मनोवैज्ञानिक जरूरतें पूरी नहीं हो पाती हैं, जो उस उम्र में उनके लिए सबसे अधिक आवश्यक है। कहानी में एक महीने से खराब तबियत वाले शिशु का इलाज करनेवाला डॉक्टर जब पर्ची में लिखकर देता है, "मैंने पर्ची पर दवाई नहीं लिखी है: शो हिम् जूजू एंड गेट योर चाइल्ड ओके।" तब आधुनिकता के सम्मोहन के कारण फैले इस रोग की भयानकता सामने प्रकट होती है।

पार्वत्य प्रदेश की लोक संस्कृति सदैव लोक-प्रकृति मैत्री का पर्याय रही है। यहाँ की संस्कृति के अंतर्गत आनेवाले रीति-रिवाज, व्रत-त्योहार, जीवन-पद्धति, रहन-सहन आदि विभिन्न अंग गहन प्रकृति मूल्यबोध से जुड़े रहे हैं। पर इस प्रदेश में मशीनी सभ्यता के कदम पड़ते ही लोक-प्रकृति के बीच का संतुलन गड़बड़ा गया है। मशीनी सभ्यता के 'टूल्स' ने पार्वत्य प्रदेश की प्रकृति पर इतने गहरे चोट किये हैं कि उसमें दरकनें आ गई हैं। ये दरकनें भविष्य में पुरे पहाड़ पर आनेवाले विनाशकारी संकट के संकेत हैं। पहाड़ का पूरा सौन्दर्य उसके प्राकृतिक संतुलन पर आश्रित है और इस संतुलन को बनाये रखने का श्रेय पहाड़ी संस्कृति को जाता रहा है। पर आधुनिक मशीनी आकर्षक सभ्यता के आवरण तले पहाड़ तक पहुँची पूँजीवादी मानसिकता ने उस संस्कृति में क्षरण ला दिया है, जिसका सबसे ज्यादा विनाशकारी प्रभाव पहाड़ के प्रकृति-पर्यावरण पर पड़ने लगा है। पहाड़ पर पहुँची पूँजीवादी शक्तियों ने अधिकाधिक धन कमाने के लोभ से ग्रसित होकर पहाड़ का अंधाधुंध दोहन शुरू कर दिया है। इन शक्तियों ने सत्ता से साँठ-गाँठ करके अपने काम को अंजाम देना शुरू कर दिया है। बेचारी पहाड़ की सीधी सरल जनता इनकी कारस्तानियों को समझ नहीं पा रही है और जो पढ़े लिखे समझदार लोग इस पड़यंत्र को समझ भी रहे हैं, वे इस साँठ-गाँठ की शक्ति के आगे निरीह बने हुए हैं। बीच-बीच में ये संगठित होकर इसका विरोध तो कर रहे हैं पर पूँजीवादी शक्तियाँ बड़ी चालाकी से इनसे निपटकर दोहन के नित-नवीन तरीके इजाद करने में सफल होती जा रही हैं, जिससे पूरा पहाड़ संकट के सम्मुखीन है। हिमाचल का पार्वत्य प्रदेश भी इस संकट से गुजर रहा है। हरनोट अपने समय और परिवेश के सजग प्रहरी हैं। उनकी सजग आँखें इन सभी घटनाओं पर ध्यान केन्द्रित किये हुए हैं। वे खतरे में आए पहाड़ और पहाड़ीपन को बचाने के निमित्त अपनी कहानियों के मार्फत मानवीय तथा प्राकृतिक मूल्यबोध को बचाये रखने की कवायद कर रहे हैं और

साथ ही साथ इसको विनष्ट करने वाले तत्वों तथा शक्तियों की पहचान लोगों को करवाते जा रहे हैं। इस सन्दर्भ में इनकी 'माफिया', 'बेजुबान दोस्त', 'नदी गायब है', 'आभी', लोग उल्लेखनीय हैं।

एस. आर. हरनोट कृत 'माफिया' कहानी हिमाचल के जंगलायत में तैनात सरकारी अफसरों, नेता तथा मंत्री के मिलीभगत से वन तथा वन्य पशुओं के गैरकानूनी ढंग से क्रिये गये दोहन पर आधारित है। कहानी में यह दर्शाया गया है कि किस प्रकार नेता-मंत्रीगण पर्यावरण तथा वन्य जीव संरक्षण की खोखली डींगे हाँकते हैं, जबकि वास्तव में ये ही पार्वत्य प्रदेश के वन को काटकर तथा वन्य पशुओं को मारकर गैरकानूनी ढंग से इनकी खरीद-फ़रोख़्त में लिप्त हैं और इसके लिए वे प्रशासन को अपनी पूँजी और चालाकी के दम पर ढाल के रूप में उपयोग करते हैं। कहानीकार इस गोरख-धंधे से जुड़े हर एक शख्स को माफिया ही घोषित करता है। इस माफियागिरी के धंधे की सबसे बड़ी खासियत है कि इसमें नेता, मंत्री तथा प्रशासन एक तंत्र के रूप में कार्य करते हैं। कहानी का सबसे महत्वपूर्ण स्थल वह है जहाँ मंत्री जी मोर-मोरनी के निवास स्थान मोरनी-धार को राष्ट्रीय उद्यान घोषित करने के उद्घाटन में आते हैं और उनकी आवभगत में उनके कारिंदे मोरनी को ही मारकर उसके माँस को अनूठे व्यंजन के रूप में पेश करते हैं; जिसकी खबर मंत्री सहित वहाँ मौजूद उसके तंत्र को है। कहानी का पात्र चुन्नी जो एक आठ वर्षीय बालक है, जब मोर की थाह लेने की कोशिश करता है तो उसे बताया जाता है कि मोरनी बीमार है। पर इसके बाद मंत्री और उनके कारिंदों की प्रतिक्रिया विस्मय में डाल देनेवाली होती है। कहानीकार उनके दोहरे चरित्र का पर्दाफ़ाश करते हुए कहता है - "चुन्नी ने आश्चर्य से उसकी तरफ देखा-वह हँस रहा था। उसका उत्तर कुछ दूसरे जंगलायत के कर्मचारियों ने भी सुन लिया था। उन्होंने एक ठहाका लगाया।" वास्तव में उनका यह सम्मिलित दर्प भरा ठहाका वन तथा वन्य पशुओं के गैरकानूनी दोहन के बरक्स उनका अपनी कारसाजी में सफल होकर समाज को ठेंगा दिखाने जैसा ही है।

पहाड़ी जंगल वाले ज़मीन अमूमन 'डोलोमाइट' तथा चूने पत्थर की पर्याप्त उपलब्धता वाली ज़मीन होती है। उस पर पूँजीपतियों का विशेष ध्यान रहता है क्योंकि वे क्षेत्र सीमेंट उद्योग की स्थापना के सबसे अनुकूल केंद्र होते हैं, जबकि ऐसे उद्योगों की स्थापना वहाँ की प्रकृति तथा पर्यावरण को बहुत अधिक क्षति पहुँचाने वाली होती है। बावजूद इसके पूँजीवादी शक्तियाँ मोटा धन खर्च कर सरकारी व्यवस्था तथा सत्ता को अपने षडयंत्र में शामिल करने में सफल हो जाती हैं। इसके लिए सरकार पहाड़ की भोली-

भाली जनता को विकास, रोजगार सृजन तथा आरामदेह जीवन देने का लालच देकर उनकी जमीनों को बहुत ही अदना-सा मूल्य देकर पूंजीपति-कम्पनियों को सौंप देती है। जो ज़मीन-खेती प्रेमी किसान अपनी ज़मीन देने से मुकरते हैं, वे भी सीमेंट उद्योग के शुरू होने पर उससे बढ़ी मुसीबतों का सामना करने में अक्षम होकर जमीन देने के लिए बाध्य हो जाते हैं। हरनोट हिमाचली पार्वत्य पृष्ठभूमि में होनेवाली इस कारसाजी से लड़ने में अक्षम किसानों की मुसीबत को अपनी कहानी 'बेजुबान दोस्त' में बयां करते हुए कहते हैं - "जिन किसानों ने ज़मीनें नहीं दी थीं, उनकी मुसीबत भी कम नहीं थी। सीमेंट के लिए जिस पहाड़ी से पत्थर जाता, वहाँ दिन-रात ब्लास्ट होते रहते। उनसे कई मकानों में दरारें आ गई थीं। कुछ मकान तो गिर ही गए थे। मुआवज़े के नाम पर किसानों को आधी रकम भी नहीं मिल पाती थी।"¹⁰ पूंजीपति अधिकाधिक मुनाफ़ा कमाने के लोभ से ग्रसित होकर किस प्रकार पूरे पहाड़ के प्राकृतिक संतुलन को खत्म करने को आतुर हो चुके हैं और इसमें किस प्रकार पूरी व्यवस्था उनके षडयंत्र की भागीदार बनी हुई है; कहानीकार इस सच्चाई को इस कहानी में बयान करते हैं। साथ ही आनेवाले समय में पूरे पहाड़ के खतरे में आने का संकेत भी देते हैं। पहाड़ पर इस तरह का पर्यावरण संकट पैदा करनेवाली कम्पनियाँ किस प्रकार पर्यावरण प्रेमी होने का ढोंग रचती हैं, उसका चित्रण भी इस कहानी में मिलता है। उनके इस दोहरे चरित्र का पर्दाफ़ाश करते हुए कहानीकार कहता है - "पर्यावरण दिवस पर तो वे ज्यादा ही सक्रिय रहते। करोड़ों रुपये खर्च कर देते क्योंकि वे जानते थे कि फैक्ट्री लगाने से पहले पूरे प्रदेश में पर्यावरण प्रदूषित होने के डर से उनका विरोध होता रहा था।"¹¹ इसी प्रकरण पर केन्द्रित हरनोट की एक दूसरी कहानी 'लोग नहीं जानते थे उनके पहाड़ खतरे में हैं' भी है, जिसमें कहानीकार ने पूंजीवादी शक्ति और सत्ता के साथ पहाड़ों के शोषण में पूल की तरह काम करनेवाले स्थानीय सामंत, ठेकेदार, नेता के असल चरित्र का पर्दाफ़ाश किया है। सीमेंट कंपनियों के विकास के मार्फत पहाड़ी क्षेत्र के विकास के जो खोखले वादें सरकार और कम्पनी के लोग करते हैं, उसकी सच्चाई को बयान करते हुए कहानीकार कहानी के पात्र जीवन के माध्यम से कहता है - "उसे मालूम था कि जिन-जिन जगहों पर पहले इस तरह के कारखाने लगे हैं और प्राइवेट यूनिवर्सिटियाँ बनी हैं, उनकी वजह से पर्यावरण को भारी नुकसान पहुँच रहा है।.....ये लोग कंपनियों और सरकार के बीच पूल का काम किया करते, जिस पर उनके अपने स्वार्थ और सम्पन्नता की गाड़ियाँ बिना धुआं उगले चुपचाप दौड़ती रहतीं।"¹²

पार्वत्य प्रदेश में बहनेवाली छोटी-बड़ी नदियाँ वहाँ निवास करनेवाले लोगों के लिए जीवन रेखा होती हैं। खासकर हिमाचल की नदियाँ तो 'ग्लेशियर' से पिघलकर प्राप्त

जल का महत्वपूर्ण स्रोत हैं। इन नदियों से ही वहाँ के लोगों को पेय जल की प्राप्ति होती है, मवेशियों को भी इसी जल के सहारे पाला जाता है और साथ ही इसी जल पर वहाँ का कृषि कार्य भी आश्रित है। इसके अतिरिक्त जल का यह बहाव पूरे पार्वत्य प्रदेश को एक संतुलन प्रदान किये हुए है। पर आधुनिक मशीनी सभ्यता के विकास ने इनका भी अंधाधुंध दोहन कर मुनाफ़ा कमाने का काम शुरू कर दिया है। पूंजीपति बड़ी चालाकी और अपनी धन की शक्ति से सारे पर्यावरणीय नियम-कानूनों को दरकिनार कर पहाड़ पर जल विद्युत उत्पादन केंद्र खोलने की अनुमति व्यवस्था से लेने लगे हैं। उनका ध्यान सिर्फ मुनाफ़ा कमाने पर आश्रित है। वे नदियों के जल को कृत्रिम जलाशय या सुरंग बनाकर उसमें एकत्रित करते हैं और उसका उपयोग जल विद्युत-उत्पादन के लिए करते हैं। इसके लिए ज़रूरत पड़ने पर वे पहाड़ के कुछ हिस्सों को 'डायनामाइट' से फोड़कर नदियों का रास्ता तक बदल दे रहे हैं, जिससे पहाड़ के लोगों का जीवन तो संकटापन्न हुआ ही है और साथ ही पूरे पहाड़ का प्राकृतिक संतुलन खतरे में पड़ता जा रहा है। यह आनेवाले समय में पूरे पहाड़ का उसके जनजीवन के साथ ख़त्म हो जाने का संकेत है और इस घोर अप्राकृतिक कुकृत्य में सत्ता तथा प्रशासन की मिलीभगत है। पहाड़ के संकटाभिमुख होने और उसमें पूंजीपति-व्यवस्था की मिलीभगत होने को केंद्र में रखकर हरनोट ने अपनी 'नदी गायब है' कहानी का ताना-बाना बुना है। वे पहाड़ी नदियों का पूंजीवादी शक्तियों के द्वारा दोहन के बरअक्स संकट की ओर अग्रसर पहाड़ और पहाड़ी जनजीवन का चित्रण अपनी इस कहानी में करते हैं - "नदी गायब होने के साथ उनके गाँव पर एक और संकट खड़ा हो गया था। उनका गाँव ऐसे पर्वतों की तलहटी में था, जहाँ ग्लेशियरों के गिरने का खतरा हमेशा बना रहता था। अब रोज डायनामाइट के धमाकों से टनों के हिसाब से उस नदी में चट्टानें गिरनी शुरू हो गई थी और नदी के किनारे जो घराट थे, वे पूरी तरह नष्ट हो गए थे।"¹³ हरनोट ने नदियों की आज़ादी को खत्म करके उन्हें जबरन सुला देने और जमकर उसका दोहन करने के भयंकर दुष्परिणाम को दर्शाते हुए अपनी कहानी 'भागादेवी का चायघर' में कहा है - "छोटी-बड़ी परियोजनाओं के भारी-भरकम बोझों से वे थकी-हारी घाटियों के बीच सोयी दिखती है। कभी जगती हैं तो उनका आक्रोश आसमान पर होता है। वे अपने प्रतिबंधों को भारी उफ़ान से तोड़ती चलती है और उनके रास्ते जो भी आये उसे लील लेती है।"¹⁴

हरनोट कृत 'आभी' हिमाचल प्रदेश के कुल्लू जिला के दुर्गम भानी क्षेत्र में 11500 फीट की ऊँचाई पर स्थित सरेउलसर झील और नदियों से उसे साफ रखनेवाली आभी प्रजाति की चिड़ियों की कहानी है। इस दुर्गम पहाड़ी झील क्षेत्र तक पहुँच चुकी मशीनी-

पूँजीवादी मानसिकता किस प्रकार इसे प्रदूषित करने में अपनी भूमिका निभा रही है, उसका जीवंत चित्र कहानीकार ने इसमें प्रस्तुत किया है। दूरिज्म उद्योग के विकास के कदम इस दुर्गम क्षेत्र पर पड़ चुके हैं, जिसके साथ इन झीलों की प्राकृतिक सुन्दरता को खत्म करनेवाले 'टूल्स' भी पहुँच चुके हैं। इन झीलों के अस्तित्व को सबसे ज्यादा खतरे में डालनेवाली प्लास्टिक पर्यटकों के मार्फत पहुँचने लगी है। प्लास्टिक से जल-मृदा प्रदूषण का खतरा तो है ही साथ ही साथ इस जल-मृदा पर आश्रित आभी तथा अन्य जीव समुदाय का भी अस्तित्व खतरे में पड़ने लगा है। इसके कारण पहाड़ की जैव-विविधता नष्ट हो रही है, जिसने पूरे पहाड़ के अस्तित्व को ही संकट के सम्मुखीन कर दिया है। इस परिस्थिति पर दूरिज्म उद्योग से जुड़े लोगों को अपने पहाड़ को बचाने की कवायद करते हुए कहानीकार कहता है - "वे नहीं जानते कि उनकी इन हरकतों से जंगल और पहाड़ बर्बाद हो रहे हैं। वे नहीं जानते कि उनकी गाड़ियों के शोर से जंगली जानवर के एकांत खत्म हो रहे हैं और वे दूर कहीं अपनी-अपनी खोहों में डर के मारे दुबके पड़े हैं।" सबसे दिलचस्प बात यह है कि मानव को इस पूँजीवादी मानसिकता ने इतना अँधा बना दिया है कि यह जानते हुए भी कि वह प्रकृति को क्षति पहुँचाकर स्वयं कभी बच नहीं सकता; इसके बावजूद वह प्रकृति के अंधाधुंध दोहन में लीन है। पहाड़ी जंगल के वृक्षों की गैरकानूनी कटाई व कटाई करनेवालों की लगामहीन विलासिता के कारण फेंके गये जलती बीड़ी-सिगरेट के टुकड़ों से पूरा का पूरा जंगल और जंगल में रहनेवाले जीव खत्म हो रहे हैं। इस परिस्थिति में मानवीय संवेदना भी छीज रही है क्योंकि वन में लगी आग से बचने के लिए प्रत्येक श्रमिक को दूसरे श्रमिक के आग में स्वाहा हो जाने का थोड़ा भी दुःख नहीं हो रहा है। वह केवल अपनी जान बचाने के लिए बेतहाशा दौड़ रहा है। दरअसल इस आग को कहानीकार ने सांकेतिक रूप से प्रकृति की भयानक प्रतिक्रिया के रूप में दर्शाया है, जिसमें सभी का जलकर खाक हो जाना तय है - "उस आदमी के साथी अभी भी दौड़ रहे हैं। उसे उस मरते साथी की परवाह नहीं है, अपनी जान की है। वे हर हालत में बचना चाहते हैं। जीना चाहते हैं। पर उन्हें लगता है कि आग की अनगिनत लपटें उनके पीछे भागती आ रही हैं, जिनसे बचना मुश्किल है।" 16

निष्कर्षतः यह कहना कोई अत्युक्ति नहीं होगी कि हिमाचल के पार्वत्य प्रदेश पर मशीनी सभ्यता के पहुँचने के कारण वहाँ मानवीय संवेदना तथा प्राकृतिक मूल्यबोध की भावना छीज रही है। वहाँ अमानवीयता, सत्ता की निरंकुशता, साम्प्रदायिकता, बाज़ारवादी, क्रूर, हिंसक, मनुष्य विरोधी तथा सबसे अधिक प्रकृति को विनष्ट करने वाली ताकतों ने अपनी पैठ बना ली है, जिससे पूरे पहाड़ का अस्तित्व संकट में आ गया है। चूँकि

हरनोट अपने समय के सजग प्रहरी हैं, अतः वे चौकन्ने होकर इन सभी शक्तियों से लड़ने के लिए अपनी कहानियों की बुनावट करते हैं। मशीनी सभ्यता के बढ़ते कदम के बरअक्स पहाड़ में आई दरकनों तथा उसके पीछे की शक्तियों की वे शिनाख्त करते हैं और उन्हें अपनी कहानियों के मार्फत पेश करते हैं ताकि पहाड़, पहाड़ीपन और उसके नैसर्गिक सौंदर्य की रक्षा के लिए विनष्टकारी शक्तियों के विरुद्ध पहाड़ की जनता एक प्रबल प्रतिपक्ष के रूप में खड़ा हो सके। उनकी कहानियों की इस विशेषता और उनकी सजगता के सन्दर्भ में प्रो. सूरज पालीवाल का कहना है . "हरनोट की कहानियों में पहाड़ केवल पहाड़ के रूप में नहीं अपने पूरे परिवेश के साथ उपस्थित होता है। समय के विकास के साथ भूमंडलोत्तर पहाड़ी जीवन में आये बदलावों, टूटते रिश्तों, सांस्कृतिक परिवर्तनों और स्त्री-पुरुष संबंधों के साथ रूढ़ियों की टूटती जंजीरें जिस झनझनाहट के साथ हरनोट की कहानियों में आती हैं, वे विस्मय उत्पन्न नहीं करती बल्कि यह सोचने को विवश करती है कि हरनोट अपने परिवेश के प्रति कितने सजग हैं।"¹⁷

सन्दर्भ सूची :

1. ज्ञानरंजन, दारोश तथा अन्य कहानियाँ (कहानी-संग्रह), आधार प्रकाशन, पंचकूला (हरियाणा), द्वितीय संस्करण: 2012, फ्लैप
2. हरनोट, एस. आर., बिल्लियाँ बतियाती हैं, दारोश तथा अन्य कहानियाँ (कहानी-संग्रह), आधार प्रकाशन, पंचकूला (हरियाणा), द्वितीय संस्करण: 2012, पृ.14
3. वही, पृ.12
4. वही, पृ.55
5. हरनोट, एस. आर., जीनकाठी तथा अन्य कहानियाँ (कहानी-संग्रह), आधार प्रकाशन, पंचकूला (हरियाणा), द्वितीय संस्करण: 2012, पृ.40
6. हरनोट, एस. आर., मिट्टी के लोग, मिट्टी के लोग (कहानी-संग्रह), आधार प्रकाशन, पंचकूला (हरियाणा), प्रथम संस्करण: 2010, पृ.28
7. वही, पृ.26
8. हरनोट, एस. आर., जूजू, लिटन ब्लाक गिर रहा है (कहानी-संग्रह), आधार प्रकाशन, पंचकूला (हरियाणा), प्रथम संस्करण: 2014, पृ.99

9. हरनोट, एस. आर., माफिया, दारोश तथा अन्य कहानियाँ (कहानी-संग्रह), आधार प्रकाशन, पंचकूला (हरियाणा), द्वितीय संस्करण: 2012, पृ.50
10. हरनोट, एस. आर., बेजुबान दोस्त, मिट्टी के लोग (कहानी-संग्रह), आधार प्रकाशन, पंचकूला (हरियाणा), प्रथम संस्करण: 2010, पृ.13
11. वही, पृ.14
12. हरनोट, एस. आर., लोग नहीं जानते उनके पहाड़ खतरे में हैं, लिटन ब्लाक गिर रहा है (कहानी-संग्रह), आधार प्रकाशन, पंचकूला (हरियाणा), प्रथम संस्करण: 2014, पृ.69
13. वही, पृष्ठ सं-79
14. हरनोट, एस. आर., कीलें, भागादेवी का चायघर (कहानी-संग्रह), वाणी प्रकाशन, दरियागंज (नई दिल्ली), प्रथम संस्करण: 2019, पृष्ठ सं-12
15. हरनोट, एस. आर., अभी, लिटन ब्लाक गिर रहा है (कहानी-संग्रह), आधार प्रकाशन, पंचकूला (हरियाणा), प्रथम संस्करण: 2014, पृष्ठ सं-12
16. वही, पृ.17
17. हरनोट, एस. आर., कीलें(कहानी-संग्रह), वाणी प्रकाशन, दरियागंज (नई दिल्ली), प्रथम संस्करण: 2019, फ्लैप



FOOD-SNATCHING BEHAVIOUR IN ANTS

¹KHOKAN NASKAR AND ²SRIMANTA KUMAR RAUT

¹Department of Zoology, Achhruram Memorial College, Jhalda,
Purulia-723202, West Bengal, India

²Ecology and Ethology Laboratory, Department of Zoology, University of Calcutta, 35,
Ballygunge Circular Road, Kolkata - 700019, India

¹. E-mail : khokan24@gmail.com | 2. E-mail : srimantakraut@gmail.com

*Corresponding author

Received - 12.05.2020

Revised - 07.06.2020

Accepted - 02.07.2020

ABSTRACT

Foraging behaviour of the ants Anoplolepis gracilipes, Camponotus compressus, Crematogaster subnuda, Meranoplus bicolor, Monomorium pharaonis, Pheidole roberti and Tetraponera rufonigra was studied following supply of different food items in the open foraging ground with a view to note the interactions, if any. It is revealed that, in spite of available foods at the supplying sites Paratrechina longicornis, Pheidole roberti, Anoplolepis gracilipes and Tetraponera rufonigra are habituated to face the food-snatching operations initiated either by the foragers of the same species belonging to different colonies or by the other competing species who are very much involved in sharing the food resources from the same foraging area. Food-snatching event is associated with the abrupt and brutal attack by the snatcher ant on the ants carrying food to their nest. Thus, fighting in most cases was inevitable and many of the food-transporting ant individuals were seen injured severely. The food snatching behaviour exhibited by these ant species was not only to ensure the need of their food but also a strategy to treat the competing ant species psychologically by imposing fearful threat, as a dominant species, not to visit the said foraging ground again, in future.

Key words:- Ants, Foraging, Food-snatching, Tricks

INTRODUCTION

Ants forage at large here and there in their foraging area (Vowler 1955, Carroll and Janzen 1973, Traniello 1989, Sumpter and Beekman 2003, Wrege et al. 2005, Prabhakar et al. 2012, Li et al. 2014, Gathalkar and Sen 2018). Though there exists niche segregation it is very common to note the different ant species in foraging act side by side in certain spots (MacArthur and Levins 1967, Gordon 1995, Cerdá et al. 1998, Detrain et al. 2000, Albrecht and Gotelli 2001, Saar et al. 2018). As the availability of food resources, especially in view to the need of the colony members, varied to a great extent in respect to foraging area because of seasons competition both at the intra and interspecies levels is inevitable (Rust et al. 2000, Sanders and Gordan 2000, Bestelmeyer 2003, Grover et al. 2007, Cook et al. 2011, Pinto et al. 2018). Accordingly, ants have developed various devices like robbing and/or stealing by developing the dominating behavioural tricks over other neighbouring ant species (Lynch et al. 1980, Yamaguchi 1995, Breed et al. 2012, McGlynn et al. 2015, Paul and Annagiri 2018). Breed and coworkers (2012) discussed at length on the cleptobiosis in social insects in consideration with the phenomenon of theft of food among animals.

We are engaged in studying the different aspects of bioecology of the ants occurring in

NASKAR AND RAUT

the south-western region of the state West Bengal, India since 2010. And, in the meantime we did our best to report the food searching, food examination, food selection, food preference, foraging activities, food–transporting mechanisms, necrophagy as well as on some factors influencing foraging in *Camponotus compressus*, *Crematogaster subnuda*, *Pheidole roberti*, *Tetraponera rufonigra*, *Monomorium pharaonis*, *Anoplolepis gracilipes*, *Meranoplus bicolor* and *Paratrechina longicornis* ants (Naskar and Raut 2014a, b, c, 2015a, b, c, d, e, f, 2016a, b, c, 2018a, b, 2019).

However, in course of studies we paid due attention to note the food-snatching behaviour in a number of ant species in their common foraging area where we offered different types of food items experimentally, to note their foraging behaviour under such circumstances. Surprisingly, we had the opportunity to record a number of food-snatching events in the open foraging ground either on way of fighting or through the exercise of aggressive dominant power, one over other-be it member of the same species or different species, with a view to ensure their foraging success by hook or crook. As there exists, virtually no report on the said aspect of the ants we are describing the same in this article with a view to add further information on the tricky food collection behaviour in the foraging ground contrast to food robbing from the neighbouring nests or at the entry point of these nests by certain cunning ants.

MATERIALS & METHODS

For experimental studies on different aspects of food-selection, feeding, food transporting, and foraging activities in different ant species who are habituated to forage in the grounds in the south-western zone of West Bengal, India different types of food fragments viz. sugar cubes and fragments of sugarmade materials with different colouration, biscuit fragments, piece of nuts, dry fish, freshly dead mosquitoes, mustard seeds, coriander seeds, aniseeds, cumin seeds, chocolate fragments of different number and sizes as the cases applicable were offered at several locations in the foraging ground at different hours of the study of the study dates during the period of last 12 years at frequent intervals. Apart from other behavioural activities we paid due attention to note the ants who were victimized by other individuals of the same or different species at the time of food examination, food selection, food transportation because of aggression but abrupt attack with a view to snatch the food from the transporters on way of their movement towards the nest. Also, we noted the behaviours exhibited by the victimized ants and their food-snatcher ants in course of interactions, in respect to food-snatching events at per date and hours of the day concerned.

Photographs have been taken into account to visualize the facts the ants exhibited during their food-snatching operation. The experiments were carried out at Garia, Kolkata (South 24 parganas) as well as in and around the Achhruram Memorial College campus, Jhalda, Purulia, West Bengal, India.

RESULTS

During the study period of the total trials, 22 food-snatching events have been noted on different dates and hours of the study days (Table 1). The ant species involved in the food-snatching activities were *Pheidole roberti*, *Paratrechina longicornis*, *Anoplolepis gracilipes* and *Tetraponera rufonigra*.

DISCUSSION

Cleptobiosis is an well established behaviour in many animals including social insects (Breed et al. 2012). Also furtive behaviour in some foraging ants *Ectatomma ruidum* have also been noted by McGlynn and coworkers (2015). Moreover, interspecific competition through food robbing did not escape the sight of Yamaguchi (1995) in the harvester ant *Messor aciculatus*. All the above

mentioned behaviours have been developed in ants depending on the scarcity of food and/or to avoid trouble in searching and transporting the food materials to the colony. Undoubtedly, such types of behavioural adaptability is deviation from the normal nature of food searching, food selection and food transportation in ants. Such adaptabilities though have been triggered through the practice of aggressive foraging behaviour (Lynch et al. 1980, Yamaguchi 1995, Cerdá et al. 1998, Gathalkar and Sen 2018, Pinto et al. 2018). But, in this context the climax is attributed not only through the development of a distinct behavioural caste for robbing food from the conspecific nest and/or removing the food from the foragers at the entry point of their nest but also by developing the tricks for brood theft to get a good number of slaves to serve as foragers and colony maintainers (Paul and Annagiri 2018).

It is most likely that cleptobiosis in social insects is derived evolutionarily from established foraging behaviours (Breed et al. 2012) but the basic information in strengthening the said idea is being supplied through the present findings on the food-snatching behaviour in the ants *Ph. roberti*, *Pa. longicornis*, *A. gracilipes*, *T. rufonigra* during foraging in open ground. As the ants *Pa. longicornis* or *A. gracilipes* inhibited other ant species either to procure a food item or to carry the same to their nest at the spot where many more food items were available for their choice it is apparent that certain ant species, being members of the same foraging ground are motivated not to allow other species to share the resource. And, under any situation when these ants were finding the opportunity to transport the food to their nest these stranger ants, being in contact, did not care to snatch the food item either forcibly through a strong bite to the food item or abruptly attacking the ant or ants who are engaged in single or cooperative food-transporting mechanism (Czaczkes et al. 2010, Czaczkes and Ratnicks 2013, McCreery and Breed 2014, Naskar and Raut 2015, 2018a, b). Of course, dominant nature of a species influences habits of resource removal (Lynch et al. 1980, Yamaguchi 1995, Cerdá et al. 1998) from the other less dominant ant species it is well evident that, depending upon the physical ability of the food-transporter and the food-snatcher fighting is obvious as have been noted in course of food-snatching events between *Pa. longicornis*, *A. gracilipes* or between *Ph. roberti* and *Pa. longicornis*, or between *T. rufonigra* and *Pa. longicornis*. Mysteriously, in some interactions the snatchers were successful to drive away the food-carrying individuals or injured them heavily but did not procure the said food item. This indicates that the competitors attack these ants, not in all cases, to snatch the food item but to teach them a lesson of torture, brutal action and deprivation of food resources if they again visit the concerned foraging area. Simply, its an attempt to keep the competitors under psychological pressure.

In the present study it is also clear that food snatching though a common behavioural phenomenon in ants is not customarily an interspecific event. This sort of behaviour is also common between the members of the same species as could be revealed from the fact of food-snatching event exhibited by *A. gracilipes*. But, it is sure that these ants belong to different colonies. However, it is surprising that, being driven away by the snatcher ant the depriver ant, under certain instances, is tuned to return to the spot of interaction to collect the food item which she dropped on the ground during the attack, and was not taken away by the snatcher. This sort of behaviour the ants perhaps, admitted through their experience, as in some cases food item may not be procured by the snatcher ant. Though, according to Lynch and coworkers (1980) resource removal by a behaviourally subordinate species are reduced in the presence of a dominant species *Prenolepis imparis*, the present findings indicate that, under certain circumstances the weaker or less dominant species may have the opportunity to minimise the rate of reduction of loss of food

NASKAR AND RAUT

in course of foraging.

Thus, it is concluded that cleptobiosis in ants is originated from snatching habit and successively modified through thieving/stealing, robbing and brood-thieving to ensure easy success in obtaining food resources.

ACKNOWLEDGEMENT

The authors are thankful to the Head of the Department of Zoology, University of Calcutta and to the Principal, Achhruram Memorial College, Purulia for the facilities provided. The ant specimens were identified by the Zoological Survey of India, Kolkata, India.

Table 1. Food-snatching events in ants.

| Date of observation | Timing of observation | Description of food snatching events |
|---------------------|-----------------------|--|
| July 20, 2010 | 8.15 AM | A <i>Pheidole roberti</i> was carrying a piece of dry fish to her nest. On way a <i>Paratrechina longicornis</i> suddenly attacked her. <i>Ph. roberti</i> left the food piece and moved away. The <i>Pa. longicornis</i> , then picked up the said piece of dry fish and was moving towards her destination. But, the said <i>Ph. roberti</i> came back quickly to follow the <i>Pa. longicornis</i> . Soon she approached the said ant and attacked her ferociously. They fought for 2 minutes and finally <i>Pa. longicornis</i> moved away leaving the food item at the fighting spot. The said fish-food piece was then carried by <i>Ph. roberti</i> safely to her nest. |
| July 21, 2010 | 8.30 AM | An <i>Anoplolepis gracilipes</i> was on her way by pushing a piece of dry fish. On way a <i>Pa. longicornis</i> attacked her and tried to snatch the said fish piece from her. The fish piece was dropped on the ground because of tug of war for 95 seconds. But, in the meantime three more <i>Pa. longicornis</i> assembled there and took part in fighting with the <i>A. gracilipes</i> . Suddenly three more <i>A. gracilipes</i> joined in the interaction process and fighting was continued for another two minutes. But, finally all the four <i>A. gracilipes</i> left the fighting spot and the original snatcher <i>Pa. longicornis</i> carried the said dry fish piece successfully to her destination. |
| | 8.43 AM | An <i>A. gracilipes</i> was on way to her nest pushing a piece of dry fish. Of on a sudden she was encircled by many <i>Pa. longicornis</i> individuals. Immediately one <i>Pa. longicornis</i> started pulling the fish piece from the <i>A. gracilipes</i> . But she was rigid to hold the said fish piece under her grip on way of biting the same strongly. Just after 35 seconds the other members of <i>Pa. longicornis</i> tried to attack her from all sides and then the food piece was out of the grip of <i>A. gracilipes</i> . The <i>Pa. longicornis</i> who was engaged in snatching the fish piece initially was able to move out of the battle field. The <i>A. gracilipes</i> being injured somehow escaped the dangerous situation and went away. Of the fighting <i>Pa. longicornis</i> three individuals quickly moved and joined with the fish-piece carrying <i>Pa. longicornis</i> to enable easy transportation of the same to their nest. |
| August 04, 2010 | 8.49 AM | An <i>A. gracilipes</i> was pulling a dry fish fragment to her nest. On the way she came across another <i>A. gracilipes</i> individual who tried to pull the said fish fragment in opposite direction (Fig 1.). The said event was continued for two minutes. Thereafter the original carrier ant stopped pulling activity and moved to the opposite end of the fish fragment where the rival <i>A. gracilipes</i> was trying to snatch the fish fragment. They started fighting. In the meantime, a <i>Pa. longicornis</i> took the opportunity to carry away the said fish fragments which was laid on the ground. |
| August 09, 2010 | 8.53 AM | There were some sugar cubes at the supplied site. Eight <i>Pa. longicornis</i> assembled there and were engaged in examining the sugar cubes. Mean while a big <i>A. gracilipes</i> appeared and started fighting with these <i>Pa. longicornis</i> . The <i>A. gracilipes</i> was compelled to leave the spot. Then each <i>Pa. longicornis</i> individual was seen to carry a sugar cube individually to their destination. But of on a sudden a large sized <i>A. gracilipes</i> was seen to attack these <i>Pa. longicornis</i> individuals. To save their life <i>Pa. longicornis</i> dropped the sugar cubes on the ground and moved hurriedly elsewhere. All the sugar cubes were procured by <i>A. gracilipes</i> |
| October 06, 2015 | 07.55 AM | <i>Ph. roberti</i> were assembled at the site of food supplied spot. They were just on way of carrying the sugar cubes. Suddenly five <i>Pa. longicornis</i> appeared there and attacked the <i>Ph. roberti</i> individuals who were carrying the sugar cubes. Consequently fighting started and <i>Ph. roberti</i> were dispersed. The sugar cubes were procured by <i>Pa. longicornis</i> |

PROC. ZOOL. SOC. INDIA

| | | |
|-------------------|----------|--|
| October 27, 2015 | 09.58 AM | A <i>Tetraponera rufonigra</i> came in contact of the supplied sugar cubes. She checked five sugar cubes and then picked up one sugar cube with a view to carry the same to the nest. Just at that time a <i>Pa. longicornis</i> attacked her. The <i>T. rufonigra</i> dropped the sugar cube and started fighting with <i>Pa. longicornis</i> . After two minutes <i>T. rufonigra</i> was able to collect that sugar cube to carry the same to her nest. There were still six sugar cubes at the site and <i>Pa. longicornis</i> then, bite one of these sugar cubes to carry the same to her nest. |
| November 08, 2015 | 05.18 PM | An <i>A. gracilipes</i> drove away two <i>Pa. longicornis</i> while they were carrying a piece of pink sugar fragment on way of pulling and pushing system to their nest. The dropped sugar fragment was carried safely to the nest by the <i>A. gracilipes</i> . |
| November 09, 2015 | 09.26 AM | At the site a <i>Pa. longicornis</i> was eating a piece of murki (fragmented flat rice soaked with molasses) following examination of the supplied food items. In the meantime an <i>A. gracilipes</i> appeared there and forcibly drove away the <i>Pa. longicornis</i> (Fig 2.). Then <i>A. gracilipes</i> carried the said murki piece to her nest. |
| | 09.28 AM | Two <i>Pa. longicornis</i> were carrying a piece of white sugar fragment to their nest. Suddenly an <i>A. gracilipes</i> gave a strong bite to the said sugar fragment and lifted the same while these two <i>Pa. longicornis</i> had no alternative but to leave the sugar fragment. Side by side, at a close distance another <i>A. gracilipes</i> was also seen to snatch a piece of yellow sugar fragment from two <i>Pa. longicornis</i> . |
| November 10, 2015 | 09.35 AM | Three <i>Pa. longicornis</i> were jointly transporting a piece of yellow sugar fragment. They were forcibly detached from the food fragment by an <i>A. gracilipes</i> who picked up the said sugar fragment and moved towards her nest. |
| | 09.37 AM | An <i>A. gracilipes</i> attacked two <i>Pa. longicornis</i> who were on their way to the nest to deposit a sugar fragment. <i>Pa. longicornis</i> failed to resist the attack and thus the sugar particle was snatched by the <i>A. gracilipes</i> . |
| November 11, 2015 | 08.00 AM | A <i>Pa. longicornis</i> was carrying a salt grain from the supplied spot. On way she was attacked by an <i>A. gracilipes</i> . <i>Pa. longicornis</i> ran away dropping the salt grain. But <i>A. gracilipes</i> examined the said salt grain and left the place leaving the salt grain as such at the spot. <i>Pa. longicornis</i> came back to the said spot and picked up the salt grain for transporting the same to her nest. |
| | 09.24 AM | A <i>Pa. longicornis</i> was on her way to nest with a piece of pink sugar fragment. Suddenly an <i>A. gracilipes</i> attacked her and snatched away the sugar fragment. |
| November 12, 2015 | 09.19 AM | An <i>A. gracilipes</i> chased a <i>Pa. longicornis</i> , who was carrying a piece of pink sugar fragment, suddenly and ferociously. The <i>Pa. longicornis</i> dropped the sugar fragment and quickly moved away. The snatcher transported the said sugar fragment to her destination. |
| | 09.22 AM | A <i>Pa. longicornis</i> was pulling a biscuit fragment. But on way an <i>A. gracilipes</i> chased her. She left the biscuit fragment and moved away. But, the <i>A. gracilipes</i> did not collect the said biscuit fragment and left the place. The said <i>Pa. longicornis</i> came back to the spot and took the biscuit fragment to transport the same to her nest. |
| | 09.23 AM | A <i>Pa. longicornis</i> was pulling a piece of white sugar fragment. She was attacked by an <i>A. gracilipes</i> on way of movement towards her nest. They fought for a while and the <i>Pa. longicornis</i> left the place leaving the sugar fragment. The said sugar fragment was carried by <i>A. gracilipes</i> to her nest. |
| | 04.01 PM | A <i>Pa. longicornis</i> examined the offered food items at the site. She then, selected a piece of pink sugar fragment. She was pulling the same to her nest but on the way an <i>A. gracilipes</i> came in contact with the sugar fragment and started pulling the same in opposite direction. The interaction was continued for 80 seconds when another <i>A. gracilipes</i> joined in the tug of war. The sugar fragment was detached by <i>Pa. longicornis</i> and these two <i>A. gracilipes</i> carried the sugar fragment jointly to their nest. |
| | 04.18 PM | A yellow sugar fragment was carrying by two <i>A. gracilipes</i> . One of them was pushing and the other one was pulling the said sugar fragment. Of on a sudden comparatively healthier <i>A. gracilipes</i> appeared and gave a strong bite to the sugar fragment at the lateral side. She then lifted the same and moved to her destination. |

NASKAR AND RAUT

| | | |
|-------------------|----------|--|
| November 13, 2015 | 09.08 AM | One <i>Pa longicornis</i> was pulling a "batasa" (made of sugar) fragment from the offered site. She was attacked by an <i>A. gracilipes</i> on the way (Fig 3.). <i>A. gracilipes</i> very promptly snatched the batasa fragment and hurriedly moved towards her nest. |
| | 09.16 AM | One <i>A. gracilipes</i> chased a <i>Pa. longicornis</i> , on the way, who was pushing a piece of white sugar fragment. <i>A. gracilipes</i> injured <i>Pa. longicornis</i> by damaging her legs through repeated biting. Consequently, <i>Pa. longicornis</i> failed to move forward and <i>A. gracilipes</i> snatched away the sugar fragment. |
| | 09.21 AM | A piece of chocolate fragment was pulling by an <i>A. gracilipes</i> . A <i>Pa. longicornis</i> coming in contact with the chocolate fragment started to pull the same in opposite direction with a view to snatch the same (Fig 4.). But, <i>A. gracilipes</i> was able to manage her movement in a befitting manner to escape the chaser. |



Fig. 1 Food-snatching act by an *A. gracilipes* from another *A. gracilipes*

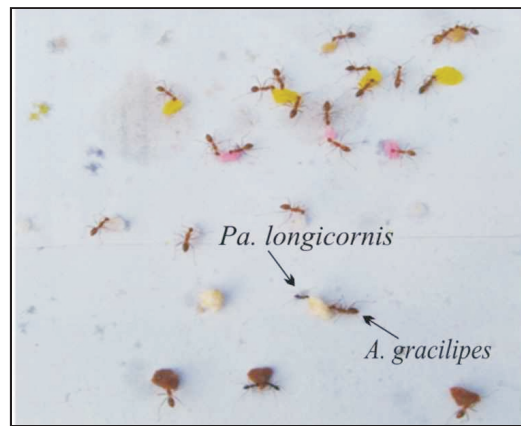


Fig. 2 An *A. gracilipes* snatching a murki fragment from a *Pa. longicornis*.



Fig. 3 An *A. gracilipes* snatching a batasa fragment from a *Pa. longicornis*



Fig. 4 A *Pa. longicornis* snatchin a chocolate fragment from a *A. gracilipes*

REFERENCES

- Albrecht, M and Gotelli, N. J. 2001:** Spatial and temporal niche partitioning in grassland ants. *Oecologia* 117:404-412.
- Bestelmeyer, B. T. and Wiens, J.A. 2003:** Scavenging ant foraging behavior and variation in the scale of nutrient redistribution among semi arid-grasslands. *J. Arid Environ* 2003, 53 (3): 373-386.
- Breed, M. D., Cook, C. and Krasnec, M. O. 2012:** Cleptobiosis in Social Insects. *Psyche* Article 1D484765, 7 pages doi:10.1155/2012/484765.
- Carroll, C. R. and Janzen, D. H. 1973:** Ecology of foraging by ants. *Annu. Rev. Ecol. Evol. Syst.* 1973, 4: 231-257.
- Cerdá, X., Retana, J., Manzaneda, A. 1998 :** The role of competition by dominants and temperature in the foraging of subordinate species in Mediterranean ant communities. *Oecologia* 1998, 117: 404-412.
- Cook, S. C., Eubank, M. D. Gold, R E and Behrner, S. T. 2011 :** Seasonality directs contrasting food collection behavior and nutrient regulation strategies in ants. *PLoS ONE* 2011, 6(9): e25407 doi:10.1371/journal.pone.0025407.
- Czaczkes, T. J., Nouvellet, P., Ratnieks, F. L. W. 2010 :** Cooperative food transport in the Neotropical ant, *Pheidole oxyops*. *Insectes Soc.* 2010, 58: 153-161.
- Czaczkes, T. J. and Ratnieks, F. L. W. 2010 :** Cooperative transport in ants (Hymenoptera: Formicidae) and elsewhere *Myrmecol. News* 2013, 18: 1-11.
- Detrain, C., Tasse, O., Versaen, N. and Pasteels, J. M. 2000. :** A field assessment of optimal foraging in ants: tail patterns and seed retrieval by the European harvester ant, *Messor barbarus*. *Insectes Soc.* 2000, 47: 56-62.
- Gathalkar, G and Sen. A. 2018 : Foraging and predatory activities of ants. *Intech Open*, 2018, DOI:10.5772/intechopen.78011.
- Gordon, D. M. 1995:** The development of an ant colony's foraging range. *Anim. Behav.* 1995, 49: 649-659.
- Grover, C. D., Kay, A. D., Monson, J. A., Marsh, T. C. and Holway D. A. 2007 :** Linking nutrition and behavioural dominance: carbohydrate scarcity limits aggression and activity in Argentine ants. *Proc. R. Soc. Sec B Biol. Sci.* 2007, 274:2951-2957.
- Li, L., Peng, H., Kurths, G., Yang, Y. and Hans, J. S. 2014 :** Chaos - order transition in foraging behaviour of ants. *Proc. Natl. Acad. Sci., USA* 2014, 111(23):8392-8397.
- Lynch, J. F., Balinsky, E. C., Vail, S. G. 1980 :** Foraging patterns in three sympatric forest ant species, *Prenolepis imparis*, *Paratrechina melanderi* and *Aphaenogaster rudis* (Hymenoptera: Formicidae). *Ecol. Entomol.* 1980, 5: 353-361.
- MacArthur, R. and Levins, R. 1967 :** The limiting similarity, convergence, and divergence of coexisting species. *Am. Nat.* 1967, 101: 377-385.
- McCreery, H. F., and Breed, M. D. 2014 :** Cooperative transport in ants; a review of proximate mechanisms. *Insectes Soc.* 2014, 61: 99-110.
- McGlynn, T. P., Graham, R., Wilson, J., Emerson, J., Jandt, J. M. and Jahren A. H. 2015 :** Distinct types of foragers in the ant *Ectatomma ruidum* typical foragers and furtive thieves.

NASKAR AND RAUT

- Anim. Behav.* 2015, 109: 243-247.
- Naskar, K. and Raut, S. K. 2014a** : Food searching and collection by the ants *Pheidole roberti* Forel. *Discovery*. 2014a, 32: 6-11.
- Naskar, K. and Raut, S. K. 2014b** :Judicious foraging by the ants *Pheidole roberti* Forel. *Proc. Zool. Soc.* 2014b, 68: 131-138.
- Naskar, K. and Raut, S. K. 2014c** :Ants forage haphazardly: a case study with *Pheidole roberti* Forel. *Int. J. Sci. Nat.* 2014c, 5: 719-722.
- Naskar, K. and Raut, S. K. 2016d** :Ants' foraging, a mystery. *Int. j. innov. Sci. Res.* 2015a, 4 (2): 064-067.
- Naskar, K. and Raut, S. K. 2015b** Foraging interactions between the Reddish brown ants *Pheidole roberti* and the Black ants *Paratrechina longicornis* *IJRBS*. 2015b, 3 (3): 183-189.
- Naskar, K. and Raut, S. K. 2015c** :Available food and ant's response. *IJESTR*, 2015c, 4 (4): 368-372.
- Naskar, K. and Raut, S. K. 2015d** :Food-carrying strategy of the ants *Pheidole roberti*. *Int. j. Tech. Res. and Appl.* 2015d, 3(3): 55-58.
- Naskar, K. and Raut, S. K. 2015c**:Foraging behaviour following food contact in the ants *Pheidole roberti*. *GJBAHS*, 2015e, 4 (2): 21-24.
- Naskar, K. and Raut, S. K. 2015f**:Mysterious foraging of Pharaoh ant *Monomorium pharaonis*. *Int. J. Appl Eng. Res.* 2015f, 5(7): 67-71.
- Naskar, K. and Raut, S. K. 2016a** :Ants' food examination. *Proc. Zool. Soc.* 2016a, 70 (2): 119-131.
- Naskar, K. and Raut, S. K. 2016b** : Winter quarter-induced foraging in ants. *GJBB*. 2016b, 5 (3): 318-323.
- Naskar, K. and Raut, S. K. 2016c** : Does colour of the food attract ants? *Proc. Zool. Soc.* 2016c, 71(1): 25-29.
- Naskar, K. and Raut, S. K. 2018a** : Food-induced food-transporting strategies of the ants *Ph. roberti* and *Pa. longicornis* ; in *Entomology : Current Status and Future Strategies*. Ganguly, A. and K. Naskar (eds), 2018a, 125-133, Daya Publishing House, (Astral Int. Pvt. Ltd.), New Delhi.
- Naskar, K. and Raut, S. K. 2018b** : Genesis and significance of cooperative transport in ants. *GJBB*. 2018b, 7(4): 633-637.
- Naskar, K. and Raut, S. K. 2019** :Ant's necrophagy on ants. *GJBB*. 2019, 8(4): 335-339.
- Paul, B. and Annagiri, S. Tricks of the trade: Mechanism of brood theft in an ant. *PLoS One*. 2018, 13 (2): e0192144. Doi:10.1371/journal.pone0192144.
- Pinto, V., Reddy, M. S., Pratheepa, M. and Verghese, A. 2018** : Incidence of aggressive territoriality between two ant species: *Camponotus compressus* Fab and *Oecophylla smaragdina* Fab (Hymenoptera: Formicidae). *Curr. Sci.* 111(12): 2044-2046.
- Prabhakar, B., Dektar, K. N. and Gordon, D. M. 2012** :The regulation of ant colony foraging activity without spatial information. *PLoS Comput. Biol.* 8 (8) E1002670.doi : 10.1371/journal.pcbi.1002670

PROC. ZOOL. SOC. INDIA

- Rust, M. K., Reinson, D. A., Paine, E. and Blum, L. J. 2000:** Seasonal activity and bait preferences of Argentine ant (Hymenoptera: Formicidae). *J. Agri. Urban Entomol.* 17(4): 201-212.
- Saar, M., Subach, A., Reato, I, Liber, T., Pruitt, J. N. and Scharf, I. 2018:** Consistent differences in foraging behavior in 2 sympatric harvester ant species may facilitate coexistence. *Curr. Zool.* 64(5): 653-661.
- Sanders, N. J. and Gordan, D.M. 2000:** The effects of inter-specific interaction on resource use and behaviour in a desert ant. *Oecologia.* 125(3): 436-443.
- Sumpter, D. J. T and Beekman, M. 2003:** From nonlinearity to optimality: pheromone trail foraging by ants. *Anim. Behav.* 66: 273-280.
- Traniello, G. F. A. 1989:** Foraging strategies of ants. *Ann. Rev. Entomol.* 1989, 34: 191-210.
- Vowler, D. M. 1995:** The foraging of ants. *The British J. Anim. Behav.* 1955, 3(1): 1-13.
- Wrege, P. H., Wikelski, M., Mandal, J. T., 2005.** Rassweiler and Couzin, J. D. Antbirds parasitize foraging army ants. *Ecology.* 86 (3): 555-559.
- Yamaguchi, T. 1995:** Interspecific competition through food robbing in the harvester ant, *Messor aciculatus* (Fr. Smith), and its consequences on colony survival. *Insectes Soci.* 1995, 42: 89-101.



A preliminary study on the juvenile stages of *Tenebrio molitor* Linnaeus, 1758 (Coleoptera: Tenebrionidae) and *Sphenarium purpurascens* Charpentier, 1842 (Orthoptera: Pyrgomorphidae) as exploitable nutraceutical resources

Arijit Ganguly¹ · Jose Manuel Pino Moreno²

Received: 31 May 2020 / Accepted: 10 February 2021
© African Association of Insect Scientists 2021

Abstract

Being rich in nutrients insects are potential nutraceutical resources. In the present study, we have selected the 8th instar larval stages of *Tenebrio molitor* and 5th instar nymphal stages of *Sphenarium purpurascens*, because these are the most sought after stages in the edible insect market in various states of the Mexican Republic. We have estimated their proximate composition and mineral contents and compared them with red meat and white meat. *S. purpurascens* has been found to be rich in protein and energy, whereas *T. molitor* contains maximum amount of fat and energy that are even better than that of red and white meat. Both of them also contain higher amount of minerals compared to red and white meat. It has been further observed that only 500g of insect flour can provide almost all the minerals in question, whereas the same amount of red and white meat can provide merely three of them. Thus, insects should be exploited as a source of nutraceuticals, more in depth study is necessary in this aspect though.

Keywords *T. molitor* · *S. purpurascens* · Nutraceuticals · Grub · Nymph

Introduction

The Indian Ayurveda and Hippocrates have reverberated the same opinion that our food should be our medicine (Wildman 2001; El-Sohaimy 2012), so it is necessary to practice a healthy feeding habit. Workers from around the world have developed an interest on the analyses of nutrient compositions of our common victuals and their possible influence on human health (Srividya et al. 2010). In this context a relatively new term “nutraceuticals” has been emerged, coined by Stephen De Felice from two different words “nutrient”, and “pharmaceuticals” (De Felice 1995; Biesalski 2001). Such products could be anything from dietary supplements, isolated nutrients, and herbal products to genetically engineered stuffs (Pandey et al. 2010). Later

on, various workers from different parts of the world have ushered information on the nutraceutical and medicinal compounds in various food materials. However, most of them are from plant related products; even though a few works on the animal products also have been reported (Barrera and Moreno 2018) the information is inadequate until now.

Very recently, insects have emerged as a potential food source for human and livestock (van Huis 2013). They definitely have a huge potential to be instated as a good nutraceutical resource that could be utilised as food additive for both human and in livestock industries. Nevertheless, the information is lagging far behind. Although authors like Ramos-Elorduy (2000), Costa Neto et al. (2006), Pino et al. (2009) have evaluated the medicinal and nutraceutical properties of insects such as grasshoppers, roaches, beetles, flies, bees and wasps, in China, Mexico, Brazil, Cuba etc. we need to get even more information in this aspect.

Keeping this idea in mind, in the present work we have selected the 8th instar larval stages of *Tenebrio molitor* Linnaeus, 1758 and 5th instar nymphal stages of *Sphenarium purpurascens* Charpentier, 1842, because these are the most

✉ Arijit Ganguly
arijitganguly87@yahoo.co.in

¹ Department of Zoology, Achhruram Memorial College, Jhalda, Purulia, India

² Department of Entomology, Institute of Zoology, National Autonomous University of Mexico, Mexico City, Mexico

sought after stages in the edible insect market in various states of the Mexican Republic, like the State of Mexico, Michoacán, Puebla, Oaxaca, Tlaxcala, etc. (van Huis et al. 2013). *T. molitor* is a coleopteran insect whose juvenile stage is known as “yellow meal worm”. This species is indigenous to Europe but now is distributed worldwide and considered as a serious pest of stored grains. In Mexico this insect is commonly used to feed companion animals owing to its nutritional value and ease of handling in captive conditions (van Huis 2013). Various authors have reported about their nutritional quality and they have found 43–65% crude protein, 7–32% fat, 20–27% carbohydrate and 213–247 Kcal/100g of energy, depending upon the developmental stage of the insects (Ravzanaadii et al. 2012; Heidari-Parsa et al. 2018). On the other hand, *S. purpurascens* is a short horn grasshopper species, which is also a serious pest of grain crop plants, and has been the most demanded edible insect resource for native Mexican people who consume them as “chapulines” since ancient times. In Mexico, chapulines are either toasted on a comal, and devoured along with “tortillas” and “pasilla chili sauce”, or just seasoned with salt and lemon (van Huis 2013). Authors like Ramos-Elorduy et al. (2012), Torruco-Uco et al. (2019), Celeste et al. (2020) have reported the nutritional contents of this insect species. They are reported to contain 60–64% crude protein, 11–15% fat, 20–25% carbohydrate and 384–403 Kcal/100g of energy depending on whether the experiments were carried out on nymphal or adult stage. Both the insect species are also reported to be rich in fatty acids, amino acids, vitamins and minerals (Virginia et al. 2015; Feng, 2018; Liu et al. 2020). In the present work, we have focused on the estimation of the proximate composition and mineral content of these two edible insects. Additionally we have made an attempt to compare our obtained results with that of red meat and white meat from the literature, and finally commented the consumption of how much of these insects can fulfill the demand of daily mineral consumption of an average healthy human being.

Materials and methods

Sampling of test insects

Collection of adult *S. purpurescens* was carried out in corn crop lands located in Tepotzotlán state of Mexico, which were then assembled, labeled and identified according to the key proposed by Márquez (1962). Then they were stocked in the insect rearing facility of our laboratory. When eggs hatched, nymphs were transferred to plastic boxes measuring 38cm × 30cm × 20cm and reared on a mixed diet of pesticide free fresh foliage of lettuce (*Lactuca sativa* L.), cabbage (*Brassica oleracea* L.), corn (*Zea maize* L.), and alfalfa (*Medicago sativa* L) in a set up following the

method described by Haldar et al. (1999). When the insects grew up to 5th instar nymphal stages, 600 individuals were separated for chemical analyses.

We have a population of rice bran fed *T. molitor* maintained since 1980s in the mass production insectaria of Entomology Laboratory, Department of Zoology, Institute of Biology of the Autonomous University of Mexico (UNAM). For chemical analyses 2,500 individuals of 8th instar larval stage were segregated.

Chemical analyses

The insects were oven dried at 70–80°C for about 48 hours until the weight became constant. Moisture free samples were then crushed into powder form using a mixer grinder, and 100g dry samples of each species were subjected to proximate composition, whereas 5g were used for mineral estimation following the procedure of AOAC (Helrich 1990). Crude protein was estimated by Kjeldahl (AOAC 988.05), fat was estimated using soxhlet apparatus (AOAC 920.39), crude fiber was estimated using acid-alkali digestion (AOAC 962.09), ash was estimated using a muffle furnace (AOAC 942.05), and nitrogen free extract was calculated by difference method. The energy was determined by an oxygen bomb calorimeter according to the method as mentioned in Anand et al. (2008). Determination of minerals (i.e. K, Mg, Zn, Fe, Cu and Na) was carried out using the AOAC method 968.08. For this purpose, 5 g of sample was weighed in a beaker, and 10 mL of concentrated nitric acid was added to it, heated for an hour until a translucent color was obtained. The solution was then cooled, recovered and filtered in a volumetric flask. De-ionized distilled water was added to this solution to make it 25 mL “stock solution”. Then the mineral contents were determined by atomic absorption spectrophotometry with the Perkin Elmer atomic absorption, model 2380. Calcium and phosphorus were determined using the hydride generation technique coupled to atomic absorption spectrophotometry. For calcium AOAC method 927.02, and for phosphorus AOAC method 965.17 was employed. All the chemical analyses were carried out in triplicate in the Laboratory of Animal Nutrition and Biochemistry of the Faculty of Veterinary Medicine and Zootechniques of UNAM.

Nutritional value of red and white meat

We have consulted various research articles (mentioned in Table 1, and Table 2) to obtain the nutritional values of different red meat and white meat resources. We have considered the mean values published in all the papers for each type of meat and tabulated the average data along with the nutrient quality of the selected insects.

Table 1 Proximate composition and energy content of the larval stages of *S. purpurascens* and *T. molitor* along with red meat and white meat

| Sample | Crude Protein (%) | Ether Extract (%) | Ashes (%) | Raw Fiber (%) | Nitrogen-free Extract (%) | Gross energy Kcal/100g | Source |
|--------------------------------------|-------------------|-------------------|-------------|---------------|---------------------------|------------------------|--|
| <i>Sphenarium purpurascens</i> nymph | 67.8±0.076b | 11.47±0.180b | 4.87±0.043c | 10.51±0.144c | 4.65±0.076b | 393.03±4.367b | Lab analysis |
| <i>Tenebrio molitor</i> grub | 47.76±0.068a | 38.29±0.122c | 2.77±0.038b | 6.91±0.162b | 4.24±0.059b | 552.37±6.082c | Lab analysis |
| Red meat | 82.76±14.150b | 12.37±4.073a | 1.16±0.842a | 0.079±0.007a | 2.32±0.382a | 127±5.611a | Adeniyi et al. (2011), Karakök et al. (2010), Bohrer (2017) |
| White meat | 80.59±13.212b | 10.92±3.567a | 1.96±0.614a | 0.082±0.004a | 2.79±0.264a | 121±6.203a | Adeniyi et al. (2011), Al-Yasiri et al. (2017), Karakök et al. (2010), Bohrer (2017) |

Results are mean ± SD. Different letters within a column shows significant different values (One-way ANOVA, $P < 0.01$, Tukey's posthoc test)

Statistical analyses

The results were calculated as mean ± SD. For statistically comparing the obtained data between the two selected insect species and the conventional meat sources one-way analysis of variance (ANOVA) was carried out with the significance level of $P < 0.01$ followed by Tukey's posthoc test. All the calculations were carried out using Microsoft Excel 2007, and Past, version 3.26.

Results

The proximate composition of *S. purpurascens* and *T. molitor* along with red meat (i.e., beef, lamb, veal, pork etc.) and white meat (i.e. broiler chicken, quail, turkey etc.) are depicted in Table 1. It is not surprising to find out that red meat and white meat are having maximum amount of crude

protein (about 82% and 80% respectively). Nevertheless, *S. purpurascens* also has more than 67% protein content, while *T. molitor* is having the least amount (just above 47%) of the same. On the contrary, *T. molitor* contains more than 38% of crude fat which is significantly higher than that of *S. purpurascens* as well as the red and white meat. Crude fiber is present in the highest amount in *S. purpurascens* followed by *T. molitor* (more than 10% and 6% respectively), while both red and white meat have negligible amount of the same. This exact trend is evident in case of ashes too (more than 4% for *S. purpurascens*, more than 2% for *T. molitor*, more than 1% for red meat, and nearly 2% for white meat). NFE also is in greater amount in the insects (over 4% in both). *T. molitor* contains maximum gross energy followed by *S. purpurascens* (more than 552 Kcal/100g, and nearly 393 Kcal/100g respectively), while red meat and white meat are having just over 120 Kcal/100g of gross energy.

Table 2 Mineral content of the larval stages of *S. purpurascens* and *T. molitor* along with red meat and white meat

| Sample | P (mg/Kg) | K (mg/Kg) | Ca (mg/Kg) | Mg (mg/Kg) | Zn (mg/Kg) | Fe (mg/Kg) | Cu (mg/Kg) | Na (mg/Kg) | Source |
|---------------------------------------|----------------|----------------|---------------|--------------|------------|------------|------------|--------------|--|
| <i>Sphenarium purpurascens</i> nymphs | 7562.8±312.1c | 10824.3±441.5c | 2120.7±103.8d | 1107.1±10.7c | 171.7±3.4d | 113.6±3.1c | 53.3±1.2d | 447.5±8.2a | Lab analysis |
| <i>Tenebrio molitor</i> grubs | 10118.9±214.2d | 10318.1±352.6c | 612.6±21.3c | 3714.4±32.5d | 132.2±2.8c | 75.7±3.6b | 22.4±0.8c | 1706.2±11.4c | Lab analysis |
| Red Meat | 2621.5±209.7b | 4417.9±102.7b | 74.2±15.9a | 320.3±27.1b | 38.1±11.8b | 19.8±5.1a | 1.3±0.3a | 615.3±61.1b | Wyness et al. (2011), Williams (2007), Bohrer (2017) |
| White meat | 1753.2±117.4a | 2120.2±226.9a | 132.3±16.1b | 177.5±25.2a | 17.1±7.6a | 18.4±6.2a | 2.9±0.8b | 677.5±39.3b | Jokanović et al. (2014), Bohrer (2017) |

Results are mean ± SD. Different letters within a column shows significant different values (One-way ANOVA, $P < 0.01$, Tukey's posthoc test)

Table 3 Daily mineral demand and amount of red meat, white meat and insect flour needed to attain that demand

| Minerals | Daily demand(mg) According to FDA (2019) and FAO/WHO (2004) in adults | Supply | | | |
|----------|---|--------------|---------------|---------------------------|----------------------|
| | | By red meat | By white meat | By <i>S. purpurascens</i> | By <i>T. Molitor</i> |
| P | 600-800 | About 300g | About 400g | About 100g | About 70g |
| K | 4500-4700 | About 1100g | About 2200g | About 400g | About 400g |
| Ca | 1000-1200 | About 20000g | About 12000g | About 500g | About 2000g |
| Mg | 400-420 | About 1400g | About 2200g | About 400g | About 150g |
| Zn | 1.97-3.37 | About 70g | About 140g | About 20g | About 20g |
| Fe | 8-11 | About 500g | About 500g | About 100g | About 150g |
| Cu | 9-10 | About 7500g | About 3500g | About 200g | About 500g |
| Na | 1300-1500 | About 2200g | About 2200g | About 3000g | About 800g |

Table 2 shows a comparative representation of various minerals present in *S. purpurascens* and *T. molitor* along with pooled data of the same present in red meat and white meat. It is evident that the insects are a much better source of Zn, Fe, and Cu, compared to red meat and white meat, on the contrary in case of Na the least amount is present in *S. purpurascens* (slightly over 447 mg/Kg) even though *T. molitor* has the peak value of more than 1706 mg/Kg.

Table 3 shows the daily demand of the minerals in question by human, and the amount of dry mass of insects as well as red meat and white meat that can fulfill the daily need of the minerals. These values were obtained from the information already mentioned in Table 2, and presented as an approximation. According to Table 3, the daily demand of phosphorus (P) is 600-800 mg, and from Table 2 we get the content of P in *S. purpurescens* which is about 7562.8 mg/Kg. So, it is clear that 100g of *S. purpurescens* will provide about 756.28mg of the said mineral which is within the prescribed range. The approximate estimations for the other cases have

been derived in the same manner. It is evident from the table that 500g of both red and white meat can fulfill the need of P, Zn, and Fe. In contrast, 500g of dry biomass of *S. purpurescens* can fulfill the daily demand of almost all the minerals in question only leaving Na. The situation is almost similar in case of *T. molitor* also, where 500g could provide the daily demand of six of them only leaving Ca and Na. In Table 4, the deficiency maladies of the minerals in question are depicted. It is evident that these mineral deficiencies are mostly related to weak bone, debility, weak heart, and deprived immunity.

Discussion

Anand et al. (2008) have evaluated the proximate composition of four edible grasshoppers from India. In their study, it is found that these grasshoppers have protein content of around 63-65%. Our study follows the same pattern as *S. purpurascens* is having protein

Table 4 Deficiency maladies of the minerals selected for the present study

| Minerals | Deficiency maladies | References |
|----------|---|---|
| P | Rickets, Osteomalacia, Osteoporosis | FAO/WHO(2004); Kestenbaum and Tilman (2010) |
| K | Hypokalemia, leads to weakness | FAO/WHO 2004, Lanham-New et al. 2012 |
| Ca | Osteoporosis, Memory loss, cramps, confusion | FAO/WHO (2004); Tulchinsky (2010), Kestenbaum and Tilman (2010) |
| Mg | Nausea, fatigue, irregular heart rhythm, poor memory, anxiety | FAO/WHO (2004); Kestenbaum and Tilman (2010) |
| Zn | Apetite loss, stunted growth, poor immune function, delayed sexual maturity, diarrhea, eye and skin lesions, hair loss, poor wound healing, weight loss | FAO/WHO (2004); Tulchinsky (2010) |
| Fe | Tiredness, pale skin, shortness of breath, head ache, palpitation, dry hair and skin, tongue and mouth soreness, restless legs, brittle fingernails, anemia | FAO/WHO (2004); Tulchinsky (2010) |
| Cu | Fatigue, weak and brittle bones, memory related problems, improper walking, cold sensitivity, pale skin, impaired vision, grey hair | Tsugutoshi (2004); Krupanidhi et al. (2008); Angelova et al. (2011) |
| Na | Nausea, Head ache, confusion, weakness | FAO/WHO 2004; Bellows and Moore 2013 |

slightly over 67%. However, energy content of those grasshoppers varies from 465–566 Kcal/100g, which is much higher than *S. purpurascens*. Sanchez-Muros et al. (2015) and Jajic et al. (2019) report protein percentage of *T. molitor* ranging from around 55–58% which is higher than our findings. Additionally, in their work the range of crude fat is in between 25 and 30%, which is lower than that of our findings. In any case, it is a proved fact that insects are not only a good source of protein, they are actually a better fat and energy source as well, compared to conventional meat resources (Kouřimská and Adámková, 2016).

Many edible insects have been found to be rich in iron content, and sometimes could have even more than in beef (Kinyuru et al. 2015). Our results also show this exact trend. According to van Huis (2013) the iron contents of mopane worms and *Locusta migratoria* range from 31 to 77 mg and 8 to 20 mg per 100 g of dry weight, respectively. Iron deficiency is one of the world's most widespread nutritional disorders; consequently, in developing countries anemia is extremely prominent in children and pregnant women (Mawani et al. 2016). Therefore, edible insects could be exploited to improve the status of iron deficiency (Kinyuru et al. 2015). Among conventional foods major source of Zn and Cu are oyster and beef, and the Zn content of oyster ranges in around 132mg/Kg (Kim et al. 2017). Our work supports this view as the content of Cu has been found to be much higher in the insects in comparison with red meat. Kim et al. (2017) evaluated five edible insects from Korea, but they have reported mealworm to have 11.4 mg/Kg of Cu, which is much less than our findings. The same authors have reported 27.2 mg/Kg of Cu in the grasshopper *Oxya chinensis*, but our chosen species of grasshopper *S. purpurescens* contains over 53 mg/Kg of Cu. Na and K are essential electrolytes that play important roles in physiology, such as nervous coordination. As reported by Ooninx et al. (2010), and Hyun et al. (2012), insects are a rich source of minerals such as sodium, potassium, calcium, phosphorus and magnesium. Our results are also in concert with this statement as it is evident here also that these minerals are in much higher amount in the selected insects compared to red meat and white meat. Ca, P, and Mg are essential elements of bone (Palacios 2006). The main conventional source of Ca is milk that contains 900–1300 mg/Kg of this element. It is evident that *T. molitor* is a slightly better source of Ca than meat, but *S. purpurascens* has an amount, which is almost double, compared to the amount of Ca in milk. However, Mg and P contents are found to be highest in *T. molitor*, whereas K content is almost similar in both the two insects where both the red meat and white meat contain a much lower amount of K.

Conclusion

Grasshopper and mealworm farming is a fast growing economy in various countries like China, Singapore, and Thailand. Recently US and UK based companies are also emerging. The prime goal of the insect farms is to provide protein rich food for human and livestock consumption. But from our findings, we could conclude that in addition to protein only a handful of insect flour is enough to provide ample amount of fat and energy, as well as they could act as a food additive that can supplement the minerals and keep the deficiency related maladies at bay. Thus, insects make a potential resource of nutraceuticals which demands further in depth research that will eventually encourage people to set up farms with different other insects, ultimately creating job opportunity.

Acknowledgements The authors thank the technical assistant of the Laboratory of Animal Nutrition and Biochemistry of the Faculty of Veterinary Medicine and Zootechniques of UNAM for extending kind helping hand regarding all the chemical analyses.

Authors' contributions AG and JMPM both have equal contribution for the preparation of this manuscript

Declarations

Consent for publication The authors confirm that both of them have consent for publication of this manuscript in its present form.

Conflicts of interest The authors state that there is no conflict/competing interest as far as their knowledge is concerned.

References

- Adeniyi OR, Ademosun AA, Alabi OM (2011) Proximate composition and economic values of four common sources of animal protein in South-western Nigeria. *Zootecnia Trop* 29:231–234
- Al-Yasiry ARM, Kiczorowska B, Samolińska W (2017) Nutritional value and content of mineral elements in the meat of broiler chickens fed *Boswellia serrata* supplemented diets. *J Elem* 22:1027–1037. <https://doi.org/10.5601/jelem.2017.22.1.1294>
- Anand H, Ganguly A, Haldar P (2008) Potential value of Acridids as high protein supplement for poultry feed. *Int J PoulSci* 7:722–725
- Angelova M, Asenova S, Nedkova V, Koleva-Kolarova R (2011) Copper in the human organism. *TJS* 9:88–98
- Barrera AIA, Moreno JMP (2018) Nutraceutical and Medicinal Insects: An Unexplored Research Field. In: Ganguly A, Naskar K (eds) *Entomology: Current Status and Future Strategies*, 1st edn. Daya Publishing House, Astral International, New Delhi, India, pp 137–168
- Bellows L and Moore R (2013) Sodium and the Diet. *Food and Nutrition Series, Health. Colorado state university extensión. Fact Sheet No. 9.354. pp 5.*

- Biesalski HK (2001) Nutraceuticals: the link between nutrition and medicine. In: Wildman REC (2001) Handbook of Nutraceuticals and Functional Foods, 1st edn. CRC press, Taylor and Francis, New York pp 1–9.
- Bohrer BM (2017) Review: Nutrient density and nutritional value of meat products and non-meat foods high in protein. Trends Food Sci Tech 65:103–112
- Celeste CIH, Acosta-Estrada B, Chuck-Hernández C, Serrano-Sandoval SN, Guardado-Félix D, Pérez-Carrillo E (2020) Nutritional content of edible grasshopper (*Sphenarium purpurascens*) fed on alfalfa (*Medicago sativa*) and maize (*Zea mays*). CyTA J Food 18:257–263. <https://doi.org/10.1080/19476337.2020.1746833>
- Costa Neto EM, Ramos-Elorduy J, Pino MJM (2006) Los insectos medicinales de Brasil: primeros resultados. Bol Soc & Ent Arag 38:395–414
- De Felice LS (1995) Thenutraceutical revolution, its impact on food industry. Trends Food Sci Tech 6:59–61
- El-Sohaimy SA (2012) Functional Foods and Nutraceuticals-Modern Approach to Food Science. World Appl Sci J 20:691–708. <https://doi.org/10.5829/idosi.wasj.2012.20.05.66119>
- FAO/WHO (2004) Vitamin and mineral requirements in human nutrition: report of a joint FAO/WHO expert consultation, Bangkok, Thailand, 21–30 September 1998. FAO/WHO, Rome
- FDA (2019) Interactive nutrition facts label. USFDA. https://www.accessdata.fda.gov/scripts/interactivenutritionfactslabel/factsheets/vitamin_and_mineral_chart.pdf. Accessed on 28 Dec 2019
- Feng S (2018) *Tenebrio molitor* L., entomophagy and processing into ready to use therapeutic ingredients: a review. J Nutr Health Food Eng 8:280–285
- Haldar P, Das A, Gupta RK (1999) A laboratory based study on farming of an Indian grasshopper *Oxya fuscovittata* (Marschall) (*Orthoptera: Acrididae*). J Orth Res 8:93–97. <https://doi.org/10.2307/3503431> <https://www.jstor.org/stable/3503431>
- Heidari-Parsa S, Imani S, Fathipour Y, Kheiri F, Chamani M (2018) Determination of yellow mealworm (*Tenebrio molitor*) nutritional value as an animal and human food supplementation. Arthropods 7:94–102
- Helrich K (1990) Official methods of analysis of the Association of Official Analytical Chemists. A.O.A.C, Philadelphia, USA
- Hyun SH, Kwon KH, Park KH, Jeong HC, Kwon O, Tindwa H, Han YS (2012) Evaluation of nutritional status of an edible grasshopper, *Oxya chinensis formosana*. Entomol Res 42:284–290
- Jajic I, Popovic A, Urosevic M, Krstovic S, Petrovic M, Guljas D (2019) Chemical composition of mealworm larvae (*Tenebrio molitor*) reared in Serbia. ContAgr 68:23–27. <https://doi.org/10.2478/contagri-2019-0005>
- Jokanović MR, Tomović VM, Jović MT, Škaljac SB, Šojić BV, Ikonić PM, Tasić TA (2014) Proximate and Mineral Composition of Chicken Giblets from Vojvodina (Northern Serbia). Int J Nutr Food Eng 8:986–989
- Karakök SG, Ozogul Y, Saler M, Ozogul F (2010) Proximate analysis. Fatty acid profiles and mineral contents of meats: a comparative study. J Muscle Foods 21:210–223
- Kestenbaum B, Tilman BD (2010) Disorders of Calcium, Phosphate, and Magnesium metabolism. In: Floege J, Johnson RJ, Feehally J (eds) Comprehensive clinical nephrology, 4th edn. Mosby, Elsevier, USA, pp 130–148
- Kim KS, Weaver CM, Choi MK (2017) Proximate composition and mineral content of five edible insects consumed in Korea. CyTA J Food 15:143–146. <https://doi.org/10.1080/19476337.2016.1223172>
- Kinyuru JN, Mogendi JB, Riwa CA, Ndung'u NW, (2015) Edible insects—a novel source of essential nutrients for human diet: Learning from traditional knowledge. Anim Front 5:14–19
- Kouřimská L, Adámková A (2016) Nutritional and sensory quality of edible insects. NFS J 4:22–26
- Krupanidhi S, Sreekumar A, Sanjeevi CB (2008) Copper & biological health. Indian J Med Res 128:448–461
- Lanham-New SA, Lambert H, Freassetto L (2012) Nutrient information: Potassium. Adv Nutr 3:820–821. <https://doi.org/10.3945/an.112.003012>
- Liu C, Masri J, Perez V, Maya C, Zhao J (2020) Growth performance and nutrient composition of mealworms (*Tenebrio molitor*) fed on fresh plant materials supplemented diets. Foods 9:1–10
- Márquez MC (1962) Estudio de las especies del género *Sphenarium* basado en su genitalia (*Acrididae: Orthoptera*), con la descripción de una especie nueva. An Inst Biol Univ Nac Auton Mex Ser Zoo 1–2:247–265
- Mawani M, Ali SA, Bano G, Ali SA (2016) Iron Deficiency Anemia among women of reproductive age, an Important Public Health Problem: Situation Analysis. Reprod Syst Sex Disord 5:1–6. <https://doi.org/10.4172/2161-038X.1000187>
- Ooninx DGAB, van Itterbeeck J, Heetkamp MJW, van den Brand H, van Loon JJA, van Huis A (2010) An exploration on greenhouse gas and ammonia production by insect species suitable for animal or human consumption. PLoS One 5:1–7
- Palacios C (2006) The role of nutrients in bone health, from A to Z. Crit Rev Food Sci Nutr 46:621–628
- Pandey M, Verma RK, Shubhini AS (2010) Nutraceuticals: new era of medicine and health. AJPCR 3:11–15
- Pino MJM, Ángeles CS, García A (2009) Substancias curativas encontradas en insectos nutraceuticos y medicinales. Entomol Mex 8:256–261
- Ramos-Elorduy J (2000) La etnoentomología actual en México en la alimentación humana, en la medicina tradicional y en el reciclaje y alimentación animal. Mem XXXV Cong Nac de Ent, pp 3–46.
- Ramos-Elorduy J, Moreno JMP, Camacho VHM (2012) Could Grasshoppers Be a Nutritive Meal? Food Nutr Sci 3:164–175
- Ravzanaadii N, Kim SH, Choi WH, Hong SJ, Kim NJ (2012) Nutritional value of mealworm, *Tenebrio molitor* as food source. Int J Indust Entomol 25:93–98
- Sanchez-Muros MJ, de Haro C, Sanz A, Trenzado CE, Villareces S, Barroso FG (2015) Nutritional evaluation of *Tenebrio molitor* meal as fish meal substitute for tilapia (*Oreochromis niloticus*) diet. Aquac Nutr 21:1–14
- Srividya AR, Nagasamy V, Vishnuvarthan VJ (2010) Nutraceutical as medicine. Pharmanest 1:132–145
- Torrucó-Uco JG, Hernández-Santos B, Herman-Lara Martínez-Sánchez CE, Juárez-Barrientos JM, Rodríguez-Miranda, (2019) Chemical, functional and thermal characterization, and fatty acid profile of the edible grasshopper (*Sphenarium purpurascens* Ch.). Eur Food Res Technol 245:285–292. <https://doi.org/10.1007/s00217-018-3160-y>
- Tsugutoshi A (2004) Copper deficiency and the clinical practice. Jpn Med Assoc J 47:365–370
- Tulchinsky TH (2010) Micronutrient deficiency conditions: Global Health Issues. Public Health Rev 32:243–255
- van Huis A (2013) Potential of insects as food and feed in assuring food security. Annu Rev Entomol 58:563–583. <https://doi.org/10.1146/annurev-ento-120811-153704>
- van Huis A, Itterbeeck JV, Harmke K, Mertens E, Halloran A, Muir G, Vantomme P (2013) Edible insects: future prospects for food and feed security. Food and Agriculture Organization of the United Nations, Rome, Italy
- Virginia MR, Quirino-Barreda T, García-Núñez M, Díaz-García R, Sánchez-Herrera K, Schettino-Bermudez B (2015) Grasshoppers *Sphenarium purpurascens* Ch. Source of proteins and essential amino acids. J Chem Chem Eng 9:472–476. <https://doi.org/10.17265/1934-7375/2015.07.008>

Wildman REC (2001) Handbook of Nutraceuticals and Functional Foods. CRC Press, Taylor and Francis, New York
Williams P (2007) Nutritional composition of red meat. *Nutr Diet* 64:S113–S119. <https://doi.org/10.1111/j.1747-0080.2007.00197.x>

Wyness L, Weichselbaum E, O'Connor A, Williams EB, Benelam B, Riley H, Stanner S (2011) Red meat in the diet: an update. *Nutr Bull* 36:34–77

*On the biomass production of
Spathosternum prasiniferum prasiniferum
(Walker, 1871) (Orthoptera: Acrididae) as
a potential insect to feed the livestock*

**Arijit Ganguly, Parimalendu Haldar &
Dipak Kr. Mandal**

**International Journal of Tropical
Insect Science**

e-ISSN 1742-7592

Int J Trop Insect Sci
DOI 10.1007/s42690-020-00328-z



Your article is protected by copyright and all rights are held exclusively by African Association of Insect Scientists. This e-offprint is for personal use only and shall not be self-archived in electronic repositories. If you wish to self-archive your article, please use the accepted manuscript version for posting on your own website. You may further deposit the accepted manuscript version in any repository, provided it is only made publicly available 12 months after official publication or later and provided acknowledgement is given to the original source of publication and a link is inserted to the published article on Springer's website. The link must be accompanied by the following text: "The final publication is available at link.springer.com".



On the biomass production of *Spathosternum prasiniferum prasiniferum* (Walker, 1871) (Orthoptera: Acrididae) as a potential insect to feed the livestock

Arijit Ganguly¹ · Parimalendu Haldar² · Dipak Kr. Mandal²Received: 22 June 2020 / Accepted: 9 October 2020
© African Association of Insect Scientists 2020

Abstract

In recent times short horn grasshoppers (i.e. acridids) have been emerged as a potential nutrient resource for livestock in India. But it is necessary to attempt their mass production for a sustainable supply which is also cost effective. In this context the present work aimed to evaluate the ability of annual production of *Spathosternum prasiniferum prasiniferum* (Walker, 1871). The insects were reared in captivity in natural condition without the aid of any environmental chamber that has been used in all the previous works. For estimation of biomass nymphal survival percentage, number of egg pods laid per female, number of eggs hatched per pod, sex ratio, energy content and dry body weight of adult individuals were taken into consideration. Then projected annual biomass was calculated from the obtained results. The findings were encouraging because we have estimated about 66,326 individuals, or 3.55 Kg of dry biomass i.e. 82,234.33 KJ of energy after one year starting from only one pair. Even though the probable annual biomass was found to be lower than the previous works, still it was a good amount, and heartening for mass scale production. Thus we have concluded the work with a notion that this might encourage small scale start up even by poor farmers who are unable to procure environmental chamber. However, other species should be explored in future that can produce a higher biomass.

Keywords Insect farming · Annual biomass · *Spathosternum prasiniferum prasiniferum*

Introduction

It is estimated that by the year 2050 there will more than nine billion people on earth and because of this global population boom and due to over-exploitation of food there will be a great scarcity of conventional protein sources (Kouřimská and Adámková 2016). In this context it is a must to look for alternatives (Madau et al. 2020). In recent times insects are emerging as an unconventional nutritionally rich food resource where anti-nutritional growth retardants are present in tolerance limit (Das and Mandal 2014). The ubiquitous presence made these marvel creatures a frequent ingredient in common

victuals from time immemorial throughout the world (Imathiu 2020). Nevertheless, only in recent days they are getting serious attention from the scientific community. Many workers established that insects are high in nutrients and energy, and many of them could be cultivated as mini-livestock (Zhou and Han 2006; Alexander et al. 2017). But accepting insects as food is not always very easy for any mature person having western influenced upbringing who consider these creatures as “poor man’s food”; and because of this social taboo we observe repugnance in consuming insects among the western and western influenced communities (Rodríguez-Miranda et al. 2019). In this context they could be used as an alternative nutrient supplement for the livestock industry.

Various workers have successfully used insects as alternative protein source for poultry, fish and pigs (Yen 2015). Among insects, the order Orthoptera (i.e. grasshoppers and crickets) has been found to contain about 43.9% to 77.1% protein with the highest quantity in *Melanoplus mexicanus* (Saussure, 1861) and 14.05 KJ to 21.88 KJ of energy where *Blaberus* sp. showed the best value (Ramos-Elorduy et al. 2012). Workers like Anand et al. (2008a) and Das and

✉ Arijit Ganguly
arijitganguly87@yahoo.co.in

¹ Department of Zoology, Achhruram Memorial College, Purulia, Jhalda, West Bengal 723202, India

² Department of Zoology, Visva Bharati University, Santiniketan, West Bengal 731235, India

Mandal (2013) effectively utilized the acridid grasshopper *Oxya* sp. as poultry feed. Likewise, Ganguly et al. (2014) proved acridid grasshoppers to be suitable to feed ornamental fishes, while Ghosh and Mandal (2019) reported lucrative results when these short-horn grasshoppers were used as a supplementary nutrient in table fish feed. However, any food resource needs to be produced in mass scale for sustenance. Therefore, acridid mass production is very much needed.

To address this issue Haldar and Nandy (1997) first attempted mass rearing of *Hieroglyphus banian* (Fabricius, 1798), *Acrida exaltata* (Walker, 1859), and *Oxya* sp. Later, Das et al. (2002) did a mass culture study on *Oxya fuscovittata* (Marschall, 1836). Anand et al. (2008b) compared the mass production abilities of *O. fuscovittata* and *S. pr. prasiniferum*. Das et al. (2012) successfully cultured *Oxya hyla hyla* (Surville, 1831). The results proved *O. hyla hyla*, *O. fuscovittata*, and *S. pr. prasiniferum* are the major candidate species for mass culture. According to them both the *Oxya* species have higher potential of mass production in comparison with *S. pr. prasiniferum*. It should be noted that all these studies utilized environmental chamber so that the insects could be reared in optimum temperature, photo period, and humidity. But, we should keep in mind that many poor farmers who are interested to start acridid farming would not be able to procure sufficient amount of environmental chambers. And those who could afford such apparatus will have huge start up cost.

Considering this scenario, the present work was designed to evaluate the mass production ability of the oligophagous short-horned grasshopper (i.e. acridid) *S. pr. prasiniferum* which is comparatively a less studied species. Das and Mandal (2013) opined that this insect species could be an alternative nutrient resource. Their study revealed that this grasshopper species contains more than 65% crude protein, 7% fat, and over 6% of carbohydrate on dry matter basis. The energy content was reported to be 2347 KJ/100 g. Additionally they were also found to be rich in fatty acids, amino acids, vitamins and minerals, where anti-nutritional factors like oxalate, tannin, and phytin were present in significantly low titer. Ganguly et al. (2013) reported that *S. pr. prasiniferum* is one of the most abundant tetravoltine (i.e. completing four generations in a year) acridid species in the state of West Bengal in India, where the present work was conducted. According to that report their gestation period is about four weeks, nymphal duration is about 40–50 days, and adult duration is about 30–40 days. They start copulating soon after reaching maturity, and start laying egg pods within 8–12 days of adulthood. Thus it is observed that *S. pr. prasiniferum* can complete four generations annually. This oligophagous insect may affect the entire winter crop (sown during June–August and harvested in November–January), and summer seedlings of sorghum and wheat (Sown during January–February and harvested in April–May) in the state of

West Bengal, India. As it was evident that these insects mainly target plants under Poaceae family, in our work also they were reared on four food plants of the same family, and nymphal survival and reproductive potential was estimated. Then their probable annual biomass was calculated from those data assuming a single pair as a starting point. The entire study had been conducted in natural condition during May, 2019 to August, 2019, and without the use of environmental chamber. The prime goal of this study was to get an idea whether there will be sufficient biomass even if environmental chambers are not used in acridid farms.

Material and methods

Stocking of *S. pr. prasiniferum*

Fifty adult males and fifty females of *S. pr. prasiniferum* were collected from the grasslands of Santiniketan, West Bengal, India. They were stocked in 5 plastic boxes measuring 38 cm × 30 cm × 20 cm with 10 males and 10 females in each. For rearing purpose leaves of *Cynodon dactylon* (L.) Pers. was offered to the insects in a set up as described by Haldar et al. (1999). Taxonomic identification up to sub-species level was confirmed with the help of the authentic guidebook of Bhowmik (1986), published by the Zoological Survey of India.

Food plants

Seeds of *Sorghum halepense* (L.) Pers., *Triticum aestivum* L., and *Oryza sativa* L. were bought from the local market and sowed in the “Entomology Experimental Plot” in the Department of Zoology campus of Visva Bharati University. No pesticides were administered to the food plants. When the seedlings emerged fresh leaves were clipped and offered to the insects in the experimental sets each day. The common “Durva grass” *C. dactylon* was abundant in the same pesticide free experimental plot and they were also clipped and offered to the sets afresh each day.

Experimental set up

The experiment was conducted in 12 plastic boxes as we have used one food plant per set and there were four food plants in triplicates. Rearing was done by the same Haldar et al. (1999) method. Each box measured 38 cm × 30 cm × 20 cm, and was fitted with nylon mesh of about 1 mm wide pore size for proper aeration. The bottoms of the boxes were covered with 5 cm deep sterilized sand that was previously boiled in water in 100 °C for ten minutes. Each day some water was sprinkled to keep the sand moist so that the humidity of the experimental boxes could be maintained. When eggs hatched out from the

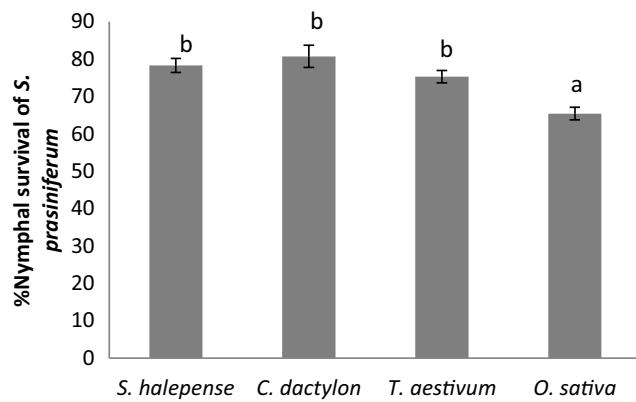


Fig. 1 % Nymphal survival of *S. prasiniferum* fed with different food plants. Values are means \pm SD. **Note:** Values with different letters are significantly different ($F = 30.41$, $P < 0.01$, one-way ANOVA, Tukey's pair-wise test)

stock sets, same day hatched 492 fledglings were randomly selected and placed in the experimental sets with 41 individuals in each.

Estimation of selected parameters

For the computation of annual biomass production, parameters like nymphal survival, number of egg pods laid per female, number of eggs hatched per pod, sex ratio, dry body weight, and energy content of adult individuals were taken into consideration. For the estimation of dry body mass 51 adult males and 51 adult females were separately collected from stock sets and freeze killed followed by oven drying at 60 °C until the weight became constant. Finally they were weighed individually and the mean values of their dry body masses were expressed in grams. After that the dry insect carcass was crushed in powder form by a mixer grinder and mixed with fixed proportion of benzoic acid as burning agent to make pellets weighing 1 g. Later, the mixed pellets were charged with digital oxygen bomb calorimeter (model EIE-220A, EIE Instruments Pvt. Ltd., Ahmedabad, India) and energy was expressed in terms of KJ/100 g. Sex ratio was estimated by random sampling of 1000 individuals from the grasslands of Santiniketan by sweeping technique and number of males and females were calculated separately. Other estimations were made in the experimental set up. Nymphal survival was expressed as percentage of nymphs reaching adulthood. When first copulating pair was observed in all the boxes, they were regularly checked for counting number of egg

pods along with the number of adult females in each. Thus average number of egg pods laid per female was estimated. Known amount of egg pods (usually 8–10) were kept inside sterilized moist sand in 80 ml plastic cups fitted with nylon net at the top. When hatching started, numbers of fledglings were calculated, recorded, and were transferred to the stock sets. When there were no hatching recorded for 30 days it was assumed no more eggs to be hatched; then average number of eggs hatched per pod was estimated.

Computation of projected annual biomass

For the computation of total biomass produced in a year we started with a single pair. Multiplying the total egg pods laid per female and eggs hatched per pod we got the probable number of fledglings hatched from one female. Then the mortality percentage was subtracted to obtain total number of insect attaining adulthood. Later, they were separated as male and female groups according to their sex ratio that we obtained from our field sampling data. Thus we have reached to total number of adult males and females in the first generation. We followed the same pattern to attain the total number of individuals in three subsequent generations owing to the tetra-voltinity of *S. pr. prasiniferum*. The total annual production of males and females were obtained by adding the numbers of all the four generations. Finally, the numbers were separately multiplied with individual dry body weight, and energy.

Statistical analyses

Data were presented as means \pm SD. Food plant specific difference between nymphal survivals, egg pods laid per female, and eggs hatched per pod were subjected to one way analysis of variance (ANOVA) taking food plants as independent variable. Mean separations were conducted by Tukey's pair-wise test where ANOVA showed significant difference. Disparity between mean dry weight of adult males and females were obtained by independent t test. All the analyses were performed at 95% confidence level (i.e. $\alpha = 0.05$) using Microsoft excel, and Past version 3.20.

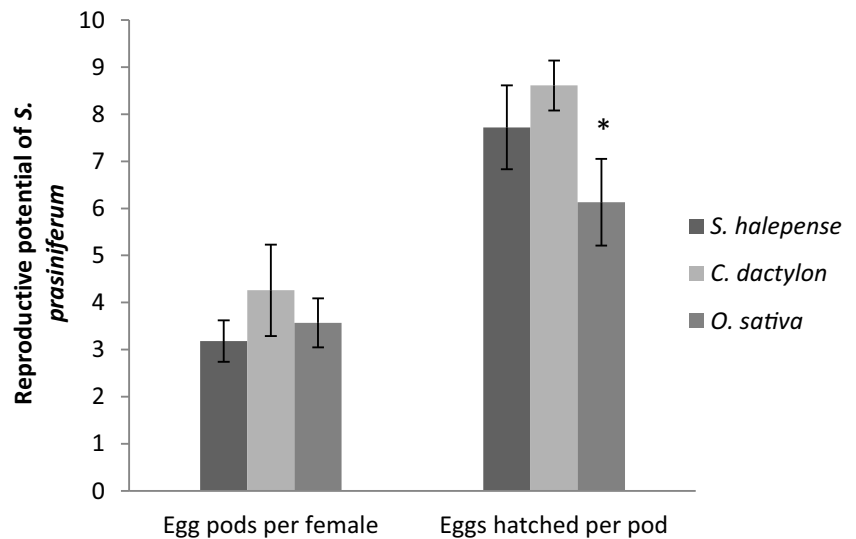
Results

Percentage of nymphal survival is summarized in Fig. 1. *C. dactylon* fed groups had the highest mean survival

Table 1 One way ANOVA table of nymphal survival

| Source of Variation | SS | df | MS | F | P value | F crit |
|---------------------|----------|----|----------|----------|----------|----------|
| Between Groups | 406.9347 | 3 | 135.6449 | 30.41212 | 0.000101 | 4.066181 |
| Within Groups | 35.6818 | 8 | 4.460225 | | | |
| Total | 442.6165 | 11 | | | | |

Fig. 2 Reproductive potential of *S. prasiniferum* fed with different food plants. Values are means \pm SD. **Note:** Asterisk (*) shows significant lower value in *O. sativa* fed groups compared to *C. dactylon* fed ones (F = 7.4, $P < 0.05$, one-way ANOVA, Tukey's pair-wise test). Other values are insignificant



(80.73%), even though it did not vary significantly from the results of *S. halepense* and *T. aestivum* fed groups ($P > 0.05$, Tukey's pair-wise test). On the other hand *O. sativa* fed groups showed significant low survival (65.41%) compared to the other three plant fed groups (F = 30.41, $P < 0.01$, one-way ANOVA, Tukey's pair-wise test, Table 1). Reproductive potential of *S. pr. prasiniferum* is depicted in Fig. 2. Here it should be noted that *T. aestivum* fed groups did not lay any egg pod. Highest number of egg pods were observed in *C. dactylon* fed groups (i.e. 4.26) and the lowest value of 3.18 was recorded in the *S. halepense* fed sets. However, in this case statistical analysis did not show any significant difference (F = 1.916, $P = 0.227$, one-way ANOVA, Table 2). Nevertheless, the parameter of eggs hatched per pod showed statistically significant result in one way ANOVA (F = 7.401, $P < 0.05$, Table 3). Here, the highest mean value 8.61 was observed in *C. dactylon* fed groups. Mean separation by Tukey's pair-wise test revealed that the result of *S. halepense* and *C. dactylon* fed groups did not vary significantly ($P > 0.05$), however *O. sativa* fed groups showed the lowest mean value of 6.13 which was significantly lower than *C. dactylon* fed groups ($P < 0.05$). In this study *C. dactylon* fed groups almost always showed better survival and reproductive potential. Hence we have selected those results for the computation of projected annual biomass production. Figure 3 represents the mean dry weight of adult males and females that were 0.045 g and 0.065 g respectively. Independent t test revealed that females always had higher dry mass than that of

males ($P < 0.05$) owing to their robustness. Finally, the energy content was observed to be 2316.46 KJ per 100 g of dry biomass.

For the calculation of sex ratio 1000 individuals were randomly collected from the grasslands near the campus of Zoology department of Visva Bharati University, santiniketan. Among them 572 were recorded to be males and 428 were females. Thus we have calculated the ratio as—♂:♀ = 572:428 = 5.7:4.3.

In the present study we considered the tetravoltinity to calculate the probable annual biomass, which was computed for four generations starting with a single male and female pair (Fig. 4). It is already mentioned that we have selected the results of *C. dactylon* fed groups for this calculation. It is evident from Fig. 2 that average number of egg pods laid per female is 4.26, while eggs hatched per pod is 8.61. So from one female we can expect $4.26 \times 8.61 = 36.68$ fledglings. Then we considered the nymphal survival percentage to estimate the total number of individuals reaching adulthood. The nymphal survival percentage of *C. dactylon* fed groups was 80.73. So, it was assumed that 80.73% of 36.68 i.e., about 29.61 individuals will reach maturity. Then we divided this number according to sex ratio of ♂:♀ = 5.7:4.3 to obtain 16.88 males and 12.13 females, and thus completed the first cycle. The second cycle started with 12.13 females and we followed the same pattern up to fourth generation that we used to compute the first one. Lastly the total number of males and females were summed up and we obtained a total of about

Table 2 One way ANOVA table of egg pods laid per female

| Source of Variation | SS | df | MS | F | P value | F crit |
|---------------------|--------|----|--------|----------|----------|----------|
| Between Groups | 1.7946 | 2 | 0.8973 | 1.916079 | 0.227252 | 5.143253 |
| Within Groups | 2.8098 | 6 | 0.4683 | | | |
| Total | 4.6044 | 8 | | | | |

Table 3 One way ANOVA table of eggs hatched per pod

| Source of Variation | SS | df | MS | F | P value | F crit |
|---------------------|---------|----|--------|----------|----------|----------|
| Between Groups | 9.4706 | 2 | 4.7353 | 7.401219 | 0.023994 | 5.143253 |
| Within Groups | 3.8388 | 6 | 0.6398 | | | |
| Total | 13.3094 | 8 | | | | |

37,806 males and 28,520 females to be produced in one year. After multiplying these numbers with respective dry weights we obtained 1.7 Kg of male and 1.85 Kg of female dry biomass or 3.55 Kg of total annual dry biomass. Lastly, total annual biomass in terms of energy was estimated by multiplying the energy content (2316.46 KJ/100 g) with the total dry mass (3.55 Kg) and we obtained 82,234.33 KJ.

Discussion

Acridid biomass is directly proportional to nymphal survival, fecundity and fertility, which are well dependent on the food plants on which these insects feed. Hence, a suitable food plant ought to be found out for a sustainable farming of acridids as mini-livestock. In this context, Ganguly et al. (2010) first reported *S. halepense* to be a suitable food plant for the mass rearing of *O. fuscovittata*. Later, Das et al. (2012) evaluated the nutritional ecology of *O. hyla hyla* and *S. pr. prasiniferum* where three different grasses like *Dactyloctenium aegyptium* (L.) Willd., *C. dactylon*, and *Brachiaria mutica* (Forssk.) Stapf were fed to them. In their study the authors reported *B. mutica* to be the best food plant followed by *C. dactylon*. Ganguly et al. (2013) studied life history, growth rates, food consumption and utilization indices of *S. pr. prasiniferum* fed with different food plants. According to them *S. halepense* followed by *C. dactylon* gave the best results. In the present work we have estimated nymphal survival and reproductive potential of the same insect with the same food plants, and we obtained *C. dactylon* and *S. halepense* to be the best ones. Considering all the parameters we could easily conclude that these two plants are the best choice for mass rearing of this insect.

On the other hand, although acridids are considered to be paddy pest, *O. sativa* fed groups did not show good results. In a similar work Nzekwu and Akingbohunge (2002) reported that nymphal duration of *Oedalues nigeriensis* Uvarov, 1926 was very low when fed with *Seteria gracilipes* Hubbard and *Axonopus compressus* (Sw.) P. Breauv. Hence it is evident that food plants are an important prerequisite for the livelihood of acridid species (Riffat and Muhammad 2007; Riffat and Wagan 2007; Das et al. 2012). In the present study higher nymphal survival was obtained in *C. dactylon* followed by *S. halepense* and highest nymphal mortality was observed in

O. sativa fed groups. This occurred may be because of the interaction between the nutritional demand of the insect and nutrients present in the plants. While studying the nutritional ecology of *O. fuscovittata*, Ganguly et al. (2010) reported nutritional quality of *S. halepense*, *C. dactylon*, *T. aestivum* and *O. sativa*. According to their result, *S. halepense* contained maximum amount of crude protein, and fat (more than 15% and 3% of dry body weight respectively). *C. dactylon* fell next in terms of crude protein that was about 11.5%. *C. dactylon* and *T. aestivum* shared similar protein and fat contents, but the latter had higher carbohydrate (84.43%) and very low crude fiber (2.27%). On the other hand *O. sativa* contained the lowest amount of protein (just over 6%). The nutritional values were very much aligned with the results obtained in the present case. It is a well known fact that dietary nitrogen can impact survival and reproductive potential of acridids (Rode et al. 2017). In the present work we have obtained least nymphal survival percentage in *O. sativa* fed groups as the protein content was the lowest in this plant. Apart from survival, food plants also have significant effect on the fecundity and fertility. While describing the importance of choice of food plants Awmack and Leather (2002), and Branson (2006) mentioned that host plant quality can directly affect insect reproductive strategies like egg size, quality and allocation of resources to eggs; even choice of oviposition sites may be influenced by plant quality. In the present work *T. aestivum* fed groups were observed to be unable to produce any egg pod. Relatively higher amount of carbohydrate and significantly low fiber content might be a cause behind this. Egg pods laid per female did not vary significantly between

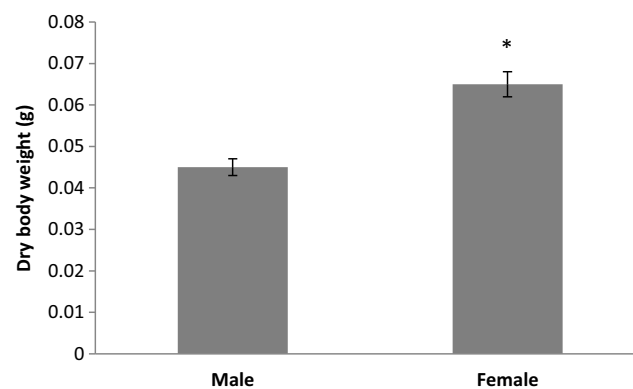
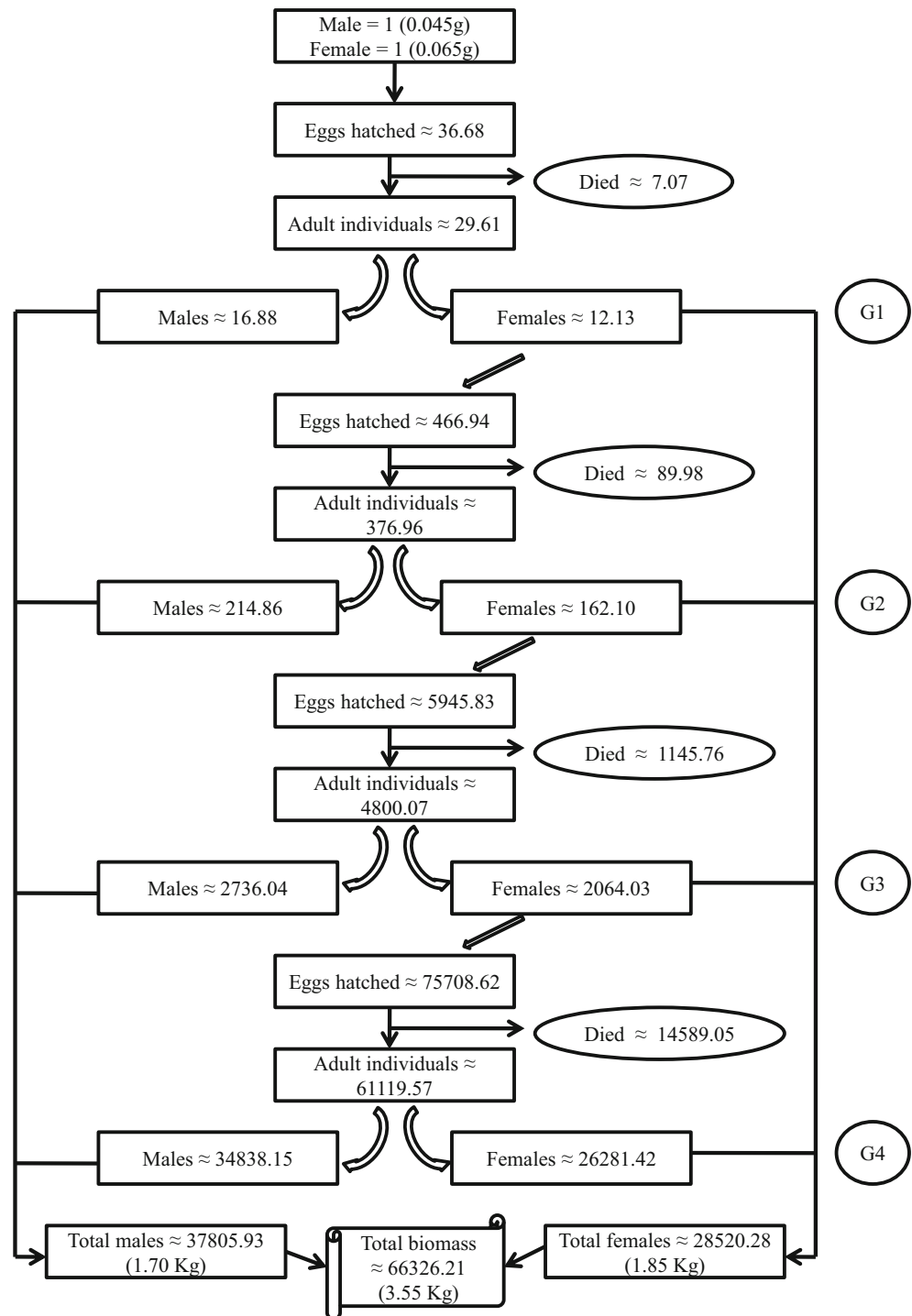


Fig. 3 Mean dry body weight (g) of adult males and females. Values are means \pm SD. **Note:** Asterisk (*) shows significant higher mean dry weight in female *S. pr. prasiniferum* ($P < 0.05$, independent t test)

the other three plant-fed groups, but the mean number of eggs hatched per pod was the lowest in *O. sativa* fed sets. These findings have also been supported by Abdel-Rahman (2001), and Das et al. (2002). The results of the present study clearly showed food plant specific variations in nymphal survival, fecundity and fertility that may directly affect mass production, and *C. dactylon* fed groups had the capacity to produce the highest biomass.

The mass production of *S. pr. prasiniferum* was attempted by Anand et al. (2008b) and Das et al. (2012). Both of these two works projected around 10 Kg of dry biomass annually assuming a single pair as a starting point which was fairly higher than our finding of 3.55 Kg. Here it should be noted that we did not use any environmental chamber for the present study. We should also mention that even this lower biomass is encouraging because if we could obtain more than three

Fig. 4 The conceptual model of projected annual biomass of *S. prasiniferum* starting with a single pair and fed with *C. dactylon*



kilograms of dry biomass only from one pair annually, we could produce hundreds of kilograms of *S. pr. prasiniferum* biomass in an insect mini-livestock farm with bigger area. We hope that our findings will hearten the farmers at the grassroots level to take up insect farming as a start-up since they will obtain a good biomass even without environmental chamber. However, other acridid species such as *Oxya* sp. should be given trial in future because of their ability to produce higher biomass and find out whether they can also provide better production without the aid of environmental chamber.

Lastly it should be noted that in the present study the rearing had been done for only one generation and the same trend was utilized for the calculation of the annual biomass. However, practically this could not be the case in nature. Insect production is very much dependant on temperature, photoperiod and humidity, that cannot be the same throughout the year (Ma et al. 2017). Thus, survival, growth, life span, and reproductive potential will have season wise variation that may lead to a quite different biomass with respect to the findings of the present study. Nevertheless, the present work mainly focused on whether mass production of *S. pr. prasiniferum* is possible without using any costly apparatus. The findings were much encouraging and demand future works on the assessment of the economical aspects of acridid farm building, maintenance and production cost which was out of the scope of this paper. We conclude with the hope that in near future realistic acridid grasshopper farms might be built where a tangible annual biomass will be attained to feed the livestock.

Acknowledgements The authors thank the Head, Department of Zoology, Visva Bharati University for providing laboratory facilities to conduct this study. The University Grants Commission, Govt. of India, is acknowledged for providing financial assistance.

Authors' contributions AG DKM and PH have equal contribution for the preparation of this manuscript.

Data availability Not applicable.

Compliance with ethical standards

Declaration of competing interest The authors declare that they have no known competing interests with respect to this paper.

Ethics approval Not applicable.

Consent to participate Not applicable.

Consent for publication All the three authors have consent for publication of this manuscript in its present form.

Code availability Not applicable.

References

- Abdel-Rahman KM (2001) Food consumption and utilization of the grasshopper *Chrotogonus lugubris* Blanchard (Orthoptera, Acridoidea, Pyrgomorphidae) and its effect on the egg deposition. *J Cent Eur Agric* 2:263–270
- Alexander P, Brown C, Arneth A, Dias C, Finnigan J, Moran D, Rounsevell MDA (2017) Could consumption of insects, cultured meat or imitation meat reduce global agricultural land use? *Glob Food Sec* 15:22–32. <https://doi.org/10.1016/j.gfs.2017.04.001>
- Anand H, Das S, Ganguly A, Haldar P (2008a) Biomass production of acridids as possible animal feed supplement. *J Environ Sociobiol* 5: 181–190
- Anand H, Ganguly A, Haldar P (2008b) Potential value of acridids as high protein supplement for poultry feed. *Int J Poul Sci* 7:722–725
- Awmack CS, Leather SR (2002) Host plant quality and fecundity in herbivorous insects. *Annu Rev Entomol* 47:817–844. <https://doi.org/10.1146/annurev.ento.47.091201.145300>
- Bhowmik HK (1986) Grasshopper fauna of West Bengal. Zoological Survey of India, Calcutta
- Branson DH (2006) Life history responses of *Ageneotettix deorum* (Scudder) (Orthoptera: Acrididae) to host availability and population density. *JK Entom Soc* 79:146–155. <https://doi.org/10.2317/0501.11.1>
- Das M, Mandal SK (2013) Assessment of nutritional quality and anti-nutrient composition of two edible grasshoppers (Orthoptera: Acrididae) - a search for new food alternative. *IJMPS* 3:31–48
- Das M, Mandal SK (2014) *Oxya hyla hyla* as an alternative protein source for Japanese quail. *Int Sch Res Notices* 2014:1–14. <https://doi.org/10.1155/2014/269810>
- Das A, Das S, Haldar P (2002) Effect of food plants on growth rate and survivality of *Hieroglyphus banian* (Fabricius) (Orthoptera: Acrididae), a major paddy pest in India. *Appl Entomol Zool* 37: 207–212. <https://doi.org/10.1303/aez.2002.207>
- Das M, Ganguly A, Haldar P (2012) Annual biomass production of two acridids (Orthoptera: Acrididae) as alternative food for poultry. *Span J Agric Res* 10:671–680. <https://doi.org/10.5424/sjar/2012103-222-11>
- Ganguly A, Chakravorty R, Sarkar A, Haldar P (2010) Johnson grass [*Sorghum halepense* (L.) Pers.] A potential food plant for attaining higher biomass in acridid farms. *Philipp Agric Scientist* 93:329–336
- Ganguly A, Chakravorty R, Haldar P (2013) Assessment of consumption utilization and growth of *Oedaleus abruptus* (Thunberg) and *Spathosternum prasiniferum prasiniferum* (Walker) (Orthoptera: Acrididae) fed with various food plants in laboratory conditions. *Ann Soc Entomol Fr* 49:160–171. <https://doi.org/10.1080/00379271.2013.810027>
- Ganguly A, Chakravorty R, Sarkar A, Mandal DK, Haldar P, Ramos-Elorduy J, Moreno JMP (2014) A preliminary study on *Oxya fuscovittata* (Marschall) as an alternative nutrient supplement in the diets of *Poecillia sphenops* (Valenciennes). *PLoS One* 9:1–7. e111848. <https://doi.org/10.1371/journal.pone.0111848>
- Ghosh S, Mandal DK (2019) Nutritional evaluation of a short-horned grasshopper, *Oxya hyla hyla* (Serville) meal as a substitute of fishmeal in the compound diets of rohu, *Labeo rohita* (Hamilton). *Jo BAZ* 80: 1–8. <https://doi.org/10.1186/s41936-019-0104-4>
- Haldar P, Nandy NC (1997) Feasibility of grasshopper farming in West Bengal—a review on laboratory based studies. *J Inter Des* 1:160–161
- Haldar P, Das A, Gupta RK (1999) A laboratory based study on farming of an Indian grasshopper *Oxya fuscovittata* (Marschall) (Orthoptera: Acrididae). *J Orth Res* 8:93–97. <https://doi.org/10.2307/3503431>
- Imathiu S (2020) Benefits and food safety concerns associated with consumption of edible insects. *NFS J* 18:1–11. <https://doi.org/10.1016/j.nfs.2019.11.002>

- Kouřimská L, Adámková A (2016) Nutritional and sensory quality of edible insects. *NFS J* 4:22–26
- Ma L, Wang X, Liu Y, Su MZ, Huang GH (2017) Temperature effects on development and fecundity of *Brachmia macroscopa* (Lepidoptera: Gelechiidae). *PLoS One* 12:1–12. <https://doi.org/10.1371/journal.pone.0173065>
- Madau A, Arru B, Furesi R, Pulina P (2020) Insect farming for feed and food production from a circular business model perspective. *Sustainability* 12:1–15. <https://doi.org/10.3390/su12135418>
- Nzekwu AN, Akingbohunge AE (2002) The effect of various host plants on nymphal development and egg production in *Oedaleus nigeriensis* Uvarov (Orthoptera: Acrididae). *J Orthop Res* 11:185–188. [https://doi.org/10.1665/1082-6467\(2002\)011\[0185:TEOVHP\]2.0.CO;2](https://doi.org/10.1665/1082-6467(2002)011[0185:TEOVHP]2.0.CO;2)
- Ramos-Elorduy J, Moreno JMP, Camacho VHM (2012) Could grasshoppers be a nutritive meal? *Food Nutr Sci* 3:1–12. <https://doi.org/10.4236/fns.2012.32025>
- Riffat S, Muhammad SW (2007) Some studies of growth, development and fecundity of grasshopper *Hieroglyphus oryzivorus* Carl, (Orthoptera: Acrididae) on food plants in Sindh. *Pak Entomol* 29:9–13
- Riffat S, Wagan MS (2007) The effect of food plants on the growth rate fecundity and survivality of grasshopper *Hieroglyphus nigrorepletus* I. Bolivar (Orthoptera: Acrididae) a major paddy pest in Pakistan. *J Biol Sci* 30:27–32. <https://doi.org/10.3923/jbs.2007.1282.1286>
- Rode M, Lemoine NP, Smith MD (2017) Prospective evidence for independent nitrogen and phosphorus limitation of grasshopper (*Chorthippus curtipennis*) growth in a tallgrass prairie. *PLoS One* 12. <https://doi.org/10.1371/journal.pone.0177754>
- Rodríguez-Miranda J, Alcántar-Vázquez JP, Zúñiga-Marroquín T, Juárez-Barrientos JM (2019) Insects as an alternative source of protein: a review of the potential use of grasshopper (*Sphenarium purpurascens* Ch.) as a food ingredient. *Eur Food Res Technol* 245:2613–2620. <https://doi.org/10.1007/s00217-019-03383-0>
- Yen AL (2015) Foreword: why a journal of insects as food and feed? *J Insects as Food Feed* 1:1–2. <https://doi.org/10.3920/JIFF2015.x001>
- Zhou J, Han D (2006) Proximate amino acid and mineral composition of pupae of the silkworm *Antheraea pernyi* in China. *J Food Compos Anal* 19:850–853. <https://doi.org/10.1016/j.jfca.2006.04.008>

Publisher's note Springer Nature remains neutral with regard to jurisdictional claims in published maps and institutional affiliations.



Special Issue on "Medicinal Chemistry"

J. Indian Chem. Soc.,
Vol. 97, August 2020, pp. 1287-1294

Zinc and copper homeostasis is crucial to maintain the cellular health and their role in viral diseases including COVID-19

Sneha Mondal^a, Sounik Manna^b, Tarun Kr. Barik^c and Santi M. Mandal^{*d}

^aDepartment of Chemistry, Visva-Bharati, Santiniketan-731 235, India

^bDepartment of Microbiology, Midnapore College (Autonomous), Paschim Medinipur-721 101, West Bengal, India

^cDepartment of Physics, Achhruram Memorial College, Jhalda, Purulia-723 202, West Bengal, India

^dCentral Research Facility, Indian Institute of Technology Kharagpur, Kharagpur-721 302, West Bengal, India

E-mail: mandalsm@gmail.com

Manuscript received online 02 July 2020, accepted 28 July 2020

Both, zinc and copper play important roles in human metabolic processes. In humans, zinc (Zn) is required directly for the chemical catalysis and/or maintaining the structure of nearly 10% of total body proteins. It plays a significant role not only in immune defence but also takes part in DNA and protein synthesis, growth and development throughout the life span as well as in tissue repair. On the other hand, copper (Cu) is crucial to strengthen the skin, epithelial tissue, connective tissue and blood vessels. Cu helps to increase the level of haemoglobin, melanin and myelin in our body. Both of these trace metals possess antioxidant like properties. However, it is necessary to balance the optimal concentration of Zn or Cu in blood serum to avoid the associated organ damage. Excess zinc intake increases the incidence of chronic kidney disease (CKD) which is harmful to normal renal function and thus elevated the risk of prostate cancer. Similarly, the one and only reason for heart, kidney and liver failure including Wilson disease is the excess amount of copper. Both of these trace metals are responsible to deal with brain diseases. Thus, there are many "faces" of Zn and Cu in the maintenance of cellular network including immunomodulatory regulation and infection prevention. Zinc appears to inhibit the enzymatic processes of viral protease and polymerase, as well as different physical processes for instance virus attachment, inflammation, and viral uncoating. Ideally, the clinicians should monitor zinc status of the individuals and advice for the supplements when necessary, otherwise deficiency of these micronutrients could lead to the onset of severe secondary diseases.

Keywords: Zinc, copper, immunomodulatory, signalling network, viral infection.

Introduction

It has been estimated that nearly two to four grams of zinc (Zn) is distributed throughout the human body¹. Even though copper (Cu) is considered as the third most abundant trace metal [next to iron and zinc], its total amount in the human body ranges only between 75–100 mg². Zinc and copper ions are involved with numerous aspects of cellular metabolism via electrochemical oxidation and reduction reactions. The proportion of copper to zinc is clinically more significant than the concentration of both of these trace metals³. Like oxidation and reduction reactions in electrochemical cell, copper and zinc metal ions play similar role in presence of human cell plasma, where the electron movement occurred in Zn and Cu through an electrically conducting

pathway as an electromagnetic wave – leading to a better model for the cellular neurotransmission process.

Zn has versatile functions in physical improvement, enzymatic catalysis and signal transduction of biological system. Under certain circumstances the attachment of zinc to membrane is followed by binding with redox-active metals (like iron and copper), not only but also zinc acts as an essential component of both intracellular and extracellular Cu/Zn superoxide dismutase (Cu/Zn-SOD). The behaviour of zinc like an antioxidant is controlled by means of various regulators such as NF- κ B, p53, AP-1, and some other enzymatic actions during cellular signal transduction at multiple cell levels. Several studies have shown that Zn supplement is helpful to improve the pathological conditions⁴.

Zn is a crucial metal indispensable for proper assembly and progress for functioning of nearly about 2800 macromolecules and more than 300 enzymes. Around 83% of zinc proteins carry out enzymatic catalysis in prokaryotic organisms⁵. Eukaryotic organisms also use Zn for various biological purposes such as the regulation of zinc-related proteins in catalytic reactions (47%), DNA transcription (44%), protein transport (5%), and signalling pathways (3%). Zn is essential in stabilization of the membrane construction mechanism, and it supports to maintain membrane integrity against damages due to changes in osmotic potential, platelet aggregation, and other progressions⁶. Subsequently, the extensive shortage of Zn is associated with several health consequences for example weaknesses, growth and development retardation while it is required for proper immune, reproductive, and neurosensory systems^{4,5}.

Importance of zinc in human biochemical reactions:

Zinc does not contribute to redox active reaction under physiological conditions in contrast to other transition metals. It is designated as the second most abundant trace metal, found in eukaryotes second only to iron. It operates as a Lewis acid to receive a pair of electrons. Zinc remains as a stable ion in an organic medium and it is reported to be a perfect metal cofactor for reactions like proteolysis and the hydration of carbon dioxide with the necessity of redox-stable ion. The crystallization of insulin with zinc was the first proof of Zn-proteins/peptides combination⁷, while the zinc finger motif was first identified within the transcription factor TFIIIA of *Xenopus*. Human genome encodes almost 10% of the zinc proteins, which remarkably points out the physiological importance of zinc in cellular biology. After the initial recognition of zinc from erythrocyte carbonic anhydrase, it has been reported to appear within all six classes of enzymes defined in the enzyme commission (EC). The functioning of several enzymes, transcriptional factors, and other proteins shows an essentiality towards zinc; there exists a possible interaction between these proteins and Zn through definite regions like zinc-finger, LIM, RING finger domains etc. In the interior part of protein structure, zinc is coordinated by nitrogen, oxygen, and sulfur atoms with distinct coordination numbers⁸. It is suggested from zinc proteome analysis that nearly 9% of proteins in eukaryotes are zinc proteins with the number significantly enhanced in higher organisms. The number of zinc-binding motifs in zinc proteomes is governed by the intramo-

lecular zinc binding sites although it is a difficult task to recognize them⁹.

Physiological role of zinc in immune homeostasis:

The essentiality of zinc was first predicted in the year of 1869 while studying the growth of *Aspergillus niger*. At length of time, consistent growth of plants, rats and birds was found to be regulated by an indispensable role of Zn. Subsequently, different hazardous problems like immune deficiency, diarrhoea, alopecia, brain dysfunctions, uncoordinated healing process of wound, loss of appetite, liver disease, chronic inflammation, certain neuropsychological abnormalities such as emotional instability, irritability, and depression etc. are triggered by zinc deficiency, although up to 1961, zinc was not considered as a vital micronutrient for human body. Maximum zinc deficit cases are identified from the elderly, vegans/vegetarians people or the individual with chronic diseases like lymphopenia, liver cirrhosis or inflammatory bowel disease, defective lymphocyte responses from the developing countries like Africa and Asia while its global approximation varies from 17% to 20%. Mainly, zinc tends to be accumulated in the skeletal muscles and bones¹⁰. So, for the maintenance of proper Zn-balance in our body, zinc intake is necessary in our diet on a daily basis keeping it in mind that excess may be harmful. Different health related aspects like eye lesion and wound in skin, disorder in taste, alopecia, impaired immune function, deceleration in growth may arise from zinc deficiency while the excessive Zn-intake shows toxicity such as nausea, vomiting, fever, headaches and chronic kidney disease (CKD). Zinc supplementation is potential enough to reduce the occurrence of pneumonia in children from developing countries, diarrhoea, infections and to improve immunity¹¹. It is also useful in boosting the growth of children and in reducing impaired vision as well as the muscle atrophy¹². Zn also successfully reduced the time scale of symptoms caused by rhinovirus. Herpes simplex virus (HSV) infection can be effectively treated with zinc sulfate¹³. Infection caused by rhinovirus can be successfully inhibited by binding of zinc to virion. Reproductive cycle of HIV-1 virus¹⁴, vaccinia virus¹⁵, and polioviruses can also be hindered with *in vitro* zinc treatment. It was evidenced that zinc at its lowest concentration (10 μ M), showed 800-fold reduction in RSV virus when studied *in vitro*. Zn transporters function as intracellular signal transducers and Zn also acts like a neuromodulator in synaptic transmission. Zn homeostasis is

Mondal *et al.*: Zinc and copper homeostasis is crucial to maintain the cellular health and their role in viral diseases *etc.*

maintained by a number of Zn transporters which signifies proper cellular functioning.

Zinc homeostasis in human body:

There are two different types of intracellular zinc pools (i) protein-bound zinc and (ii) loosely bound Zn²⁺ i.e. “free” zinc. Very small amount of zinc exists as free-zinc ions due to toxicity of zinc within cells and majority of zinc belongs to the first type. Mature human body possesses nearly 2–3 g zinc. Skeletal muscle cells can store upto 60% zinc, nearly 30% zinc is accumulated in case of bone cells, 5% in the cells of liver and skin while the rest 2–3% in other tissues. Less than 1% of the total body zinc is derived from blood serum. The albumin protein combines loosely with nearly 80% of serum zinc and the other 20% is tightly combined with α₂-macroglobulin protein^{16,17}. Human body can adjust with a ten-fold increased Zn, consumed on a daily basis for the maintenance of homeostasis. Almost, nearly 0.1% of the whole Zn is added in regular diet (breast milk for children). The strict regulation of Zn absorption from food mainly occurs in the duodenum and jejunum; the absorption rises up to 90% when there is inadequate accessibility of dietary Zn. In case of excess Zn intake, it is released from the gastrointestinal tract and is also discarded through shedding off mucosal epithelial cells¹⁸ and renal excretion¹⁹. Generally, in mammals, over 30 proteins, together with ZnT and ZIP transporters, function properly to maintain systemic zinc homeostasis; however, humoral mediators have not been recognized in case of zinc mediated metabolism (Fig. 1).

Distribution of zinc within cell:

Nearly 50% zinc is distributed within cell cytoplasm, 30–

40% in nucleus and 10% in membrane²⁰. Total cellular zinc concentration varies between 10–100 μM range while the cytosolic concentration fluctuates between picomolar and low nanomolar range. In case of intracellular organelles, mitochondrial free zinc concentration have been quantified as 0.14 pM²¹, 0.2 pM concentration have been reported from mitochondrial matrix²², 0.9 pM from ER, and approximately 0.2 pM from the Golgi²³, although elevated level of zinc (~300 pM and 5 nM) concentrations have been reported from mitochondria and the ER²⁴. So, the zinc balance is maintained through a complex sequence of uptake, distribution, storage, and efflux along with a central role of ZnT and ZIP transporters at cellular and subcellular level. Both of these transporters cause movement of zinc between vesicles and organelles of cell cytosol, leads to buffer disorder, a condition which is termed as “buffering” and “muffling”²⁵.

Distribution of zinc within cellular vesicles/granules:

Excess amount of labile zinc is considered as chelating agent due to its accumulation within cells and tissues. Release of zinc from synaptic vesicles is predicted within the range of approximately 100 to 300 μM. Beside, soft tissues (200 nmol/g wt on average), zinc tends to be aggregated within the tissues of prostate gland at a 3- to 15-fold higher range than the range reported from other²⁶. However, a massive reduction of higher zinc level found in prostate cancer and carcinoma is an indication of its significance in metabolic activity of prostate gland. Accumulation of higher concentration of zinc within the β-cells of pancreas is mandatory for crystallization of insulin molecule. Correspondingly, higher zinc content is also reported from GH containing dense-core secretory granules of anterior pituitary cell line, epithelial and myoepithelial cells of submandibular salivary gland, sperm cells, exocrine cells of pancreas, pigment epithelial cells of retina, paneth cells of intestine and mast cells. Various processes occur within subcellular compartments due to zinc accumulation. At the time of meiotic maturation from prophase I to metaphase, higher amount of zinc is introduced and concentrated within the cortical granules of oocytes, necessary for growth detention following meiosis I. During egg activation, accumulated zinc is discarded from the oocyte to reduce zinc bioavailability immediately after intracellular calcium oscillations, termed as “zinc spark”²⁷. Zinc also tends to be aggregated within subcellular compartments during specific pathological situations.

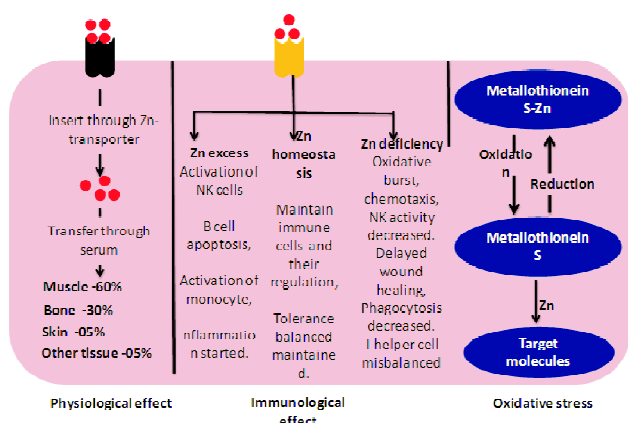


Fig. 1. Schematic representation of immuno-physiological effect of Zn homeostasis in cell.

Metallothionein and MTF-1 – storing house of zinc within cytosol:

61–68 amino acids together with 20–21 cysteines form MTs, which can combine up to 7 equivalents of zinc as well as another metal cations with a valence of two. 5–15% of zinc is tied up by MTs located in the cytosol. Approximately 12 MTs from humans and 4 MTs from mice are reported. In case of mammals, the MT molecule is divided into two zinc binding domains: α and β domains. MTs also serve as zinc acceptors and donors. In the promoter region of MTs excess zinc can tie up metal-response element-binding transcription factor-1 (MTF-1) and metal response element (MRE, 5'-TGCRcNCGGCC-3')²⁸ leading to a significant increase in MT-I and MT-II expression in mice. In vertebrates MT genes are induced in response to zinc by metal-responsive transcription factor-1 (MTF-1) comprising 6 C₂H₂ zinc finger motifs which show a significant contribution towards zinc sensing and metal responsive transcriptional activation. Zinc finger motif also acts as DNA-binding domains with increased level of cellular zinc. MTF-1 maintains zinc homeostasis to increase the transcription of host genes – MTs, *ZnT1*, and *ZnT2*^{28–30}, which are related with the reduction of zinc induced toxicity as well as additional suppression of a set of genes such as zinc transporter *ZIP10*. But in later situation, Pol II movement is physically spoiled. MTF-1 is indispensable for liver development of embryo.

Antiviral effect of zinc:

Several *in vitro* studies have suggested the antiviral nature of zinc where concentrations are necessary for the measurement of antiviral activity. Antiviral zinc concentrations can extend upto mM concentrations whereas human plasma zinc concentration ranges between 10–18 μ M. The antiviral potency of zinc depends on its availability although it is definitely virus-specific (Fig. 2). The details of antiviral effects of zinc are given below:

Herpesviridae: Restriction of the protein ubiquitination pathway can inhibit the herpes simplex virus reproduction and a reduction in NF- κ B activity accompanied by zinc ionophore pyrithione. Remarkably a decreased repetition as well as extent of disease outbreak was revealed from the performance of several relevant zinc application studies in humans^{31,32}. The effectiveness of recent implementation, along with *in vitro* studies indicates the coating of entire HSV virus particle by unbound zinc to prevent infection. Mechanisti-

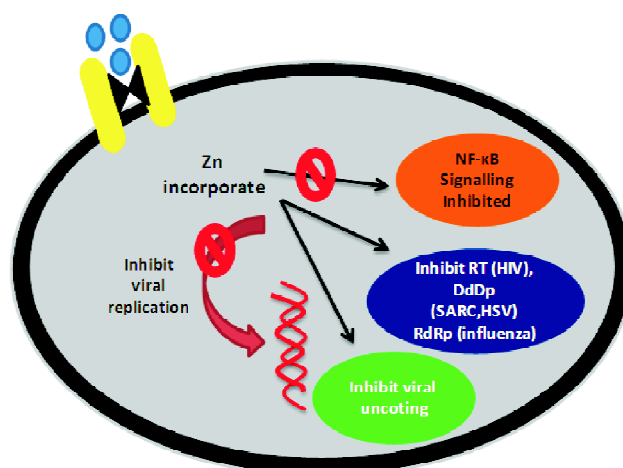


Fig. 2. Schematic representation of the mechanistic approach of Zn as antiviral agent.

cally, zinc ions retard Human alphaherpesvirus 3, usually referred to as the varicella-zoster virus by their *in vitro* inactivation. Both HSV and Varicella-Zoster virus, the members of *Alphaherpesvirinae* subfamily, are genetically related, and possess identical inhibition strategy.

Picornaviridae: Before 1980, it was revealed that zinc can inhibit picornavirus, encephalomyocarditis virus (EMCV), poliomyelitis causing virus – poliovirus, foot and mouth disease virus (FMDV). In case of coxsackievirus B3 which belongs to picornaviridae family, zinc hinders the autocatalysis to encode 3C protease from its precursor 3CD protease to inhibit viral polyprotein processing³³. Zinc seems to bind and alter the viral polyprotein tertiary structure of EMCV³³.

Flaviviridae: Flaviviruses are mainly transmitted by insects. Mosquito-borne diseases caused by dengue virus and West Nile virus, as well as the hepatotropic virus such as hepatitis C virus are grouped under flaviviridae family. *In vitro* studies confirmed the diminished level of HCV replication (mainly inhibition of HCV RdRp) (approximately 50% by 100 μ M ZnSO₄) by zinc salts; however, in case of *E. coli*, the IC₅₀ value is near about 60 μ M³⁴.

Togaviridae: Togaviruses mainly involve the viruses which are transmitted by arthropod vectors like mosquitoes in the Semliki forest, Western equine encephalomyelitis causing agent, and Chikungunya virus. Receptor-mediated endocytosis, with the subsequent virus and endosomal membrane fusion, as well as the release of new virion particle into the cytoplasm are the steps involved in viral replication.

Mondal *et al.*: Zinc and copper homeostasis is crucial to maintain the cellular health and their role in viral diseases *etc.*

Zinc has been revealed as an efficient inhibitor of Semliki forest virus and sindbis virus's membrane fusion using liposomal vesicle³⁵, RBCs³⁶, and BHK Strain 21. To inhibit membrane fusion step of viral replication process, at low endosomal pH, zinc ions form a complex with one (i.e. envelope glycoprotein 1) of the two enveloped glycoproteins of virus through specific histidine residue³⁷.

Retroviridae: Viruses belonging to retroviridae family are identified on the basis of their capability for the transcription of RNA into DNA utilizing reverse transcriptase (RT) and therefore permitting incorporation of new DNA into the host cell genome. The integrated genome of virus called provirus within host cell DNA thus becomes the major barrier to virus healing pathway specifically for HIV-1, with the production of specific infection within host deprived of any symptom i.e. remains dormant. It is well established that there is a correlation between the cellular concentration of Zn ion and CD4⁺ T cells count in HIV infection³⁷. The inhibition of the HIV-1 protease³⁸, and viral transcription was reported to be inhibited by zinc. However, stimulation of zinc influx into monocytes by HIV remains inconsistent.

Papillomaviridae: HPVs, the oncogenic viruses, can stimulate proliferation in basal epithelial cells, give rise to swelling. Although cutaneous swelling is limited as well as non-dangerous, genetic variants of HPV (HPV-16 and -18) are the main source of cancer that occurs in the cells of the cervix³⁹. E6 and E7 genes of HPV encode oncoproteins and both of them are important components for cell proliferation and apoptosis by reviving the degeneration of tumour suppressor's p53 and pRB, respectively⁴⁰. Although nuclear zinc appears to boost up HPV replication, treatment with exogenic zinc (CIZAR, zinc chloride and citric acid anhydrous) can successfully prevents construction of E6 and E7 genes and regain the role of tumour suppressor's p53 and pRB causing cell death of cervical malignant cells. Although down regulating mechanism of E6 as well as E7 expression by zinc is unknown, but zinc induction may lead up to a barrier in different part of viral life cycle.

Zn-Cu homeostasis in health:

It has been reported that a competition between copper and zinc absorption occurs in small intestine⁴¹. After binding with protein metallothionein, both of these elements are absorbed by the cells facing the small intestine. Over expression of metallothionein production in the enterocytes is due

to Excessive zinc ingestion. After tie up of zinc or copper with metallothionein, its movement through the enterocyte gets blocked. Zinc absorption is regulated by stimulating the synthesis of this protein. Copper possesses a higher affinity for metallothionein than zinc⁴² and so it displaces zinc from metallothionein and thus undergoes a preferential binding to the metallothionein, with leftover in the enterocytes; when the intestinal cells are discarded, they lost in faces. Thus, due to mucosal blockage zinc gives rise to a negative copper balance. Failure to mobilize adsorbed Cu from the intestinal cells forms the basis of Menkes syndrome. High doses of zinc given for a longer period in patients, causes an abnormality with Wilson disease which is decreased by the incorporation of Cu into ceruloplasmin by the reduction in biliary excretion of Cu⁴³. Myeloid hyperplasia has been shown in the bone marrow due to zinc-induced copper deficiency. Oral zinc ingestion causes suspiciously high toxicity comparative to copper – a process to influence copper deficiency. In case of humans, multiple antagonistic side effects involve a reduction in copper-dependent enzymes for instance superoxide dismutase, ceruloplasmin, and cytochrome c oxidase; fluctuations in immunological constraints, cholesterol, and its lipoprotein distribution.

Zinc and copper are the most important element which act as ion cofactor in receptors, proteins, different enzymatic reactions and hormones⁴⁴. This Zn-Cu duo can reduce the oxidative stress by stimulation of metallothionein synthesis to form structural ions of SOD⁴⁵⁻⁴⁷. This duo has the essential role in redox potential mechanism and their imbalanced ratio may be the main cause for an improved susceptibility to oxidative damage⁴⁸⁻⁵⁰, although acute Zn depletion causes a decrease in innate and adaptive immunity, chronic insufficiency with increased inflammation⁵¹. Contrarily, excess Cu may be related with an inflammatory response, though it is not clear whether copper has pro-oxidant or antioxidant like effects. Deactivation of unbound radical as well as prevention of associated damage promoted by the antioxidant properties of copper. In opposition to that, unbound radical induced cellular damage may be triggered by the pro-oxidant like behaviour of copper. This is because ceruloplasmin, as the key copper-containing protein, has been exposed to act both as an antioxidant and pro-oxidant in different situations⁵².

Maintenance of the dietary ratio of copper-zinc is very important as higher intake of Zn can affect Cu absorption

and the raised levels have been reported to introduce a negative impact on health status. Zinc acts as a signalling molecule to promote different types of cellular proliferation and growth. If the Zn level decreases with the increased level of Cu, intracellular and extracellular anti-oxidant defence mechanism will be highly affected. According to a research, metabolic and endocrine alterations with enhanced aging might be an indication of "survival" reactions to genotoxic stress that could stimulate tumorigenesis⁵³.

Physiochemical effect of Zn on COVID-19:

Since December 2019, there was a rapid outbreak of a virus named as severe acute respiratory syndrome coronavirus 2 (SARS-CoV-2), causing coronavirus disease-19 (COVID-19) to almost every country of the world. But until now there is no inhibition strategy to keep control of SARS-CoV-2 infection due to lack of approved vaccines or pharmaceutical therapies. Due to the role of zinc as immune modulator in infection as well as its nature like antiviral agents, it is regarded as one of the optional treatments for COVID-19. Inhibition of proteolytic processing of replicase polyproteins by Zn was reported previously. In fact, it was shown that zinc can inhibit the RNA dependent RNA polymerase (RdRp) activity of Hepatitis E virus. Moreover, it was also shown that zinc ionophores blocked coronavirus RdRp activity as well as coronavirus replication⁵⁴. Chloroquine (CQ) and hydroxychloroquine (HCQ), which are generally prescribed for the treatment of malaria and associated inflammatory conditions, might be an alternative tactic because both of these drugs behave like weak bases with an elevated pH level and tend to accumulate within endosomes, lysosomes, or golgi vesicles⁵⁵. In case of SARS-CoV-2, during the replication procedure within host cell, specifically the increased pH of lysosomes, could restrict the pH-dependent phases like membrane fusion and viral uncoating. This elevated pH within intracellular compartments seems to inhibit SARS-CoV-2 replication, because it requires acidification of endosomes for appropriate functioning. Therefore, it is assumed that an inhibiting effect of CQ and HCQ might be important for the treatment of SARS-CoV-2 infected patients. Earlier findings revealed that chloroquine as a zinc ionophore, increases Zn²⁺ flux into the cell⁵⁶. Treatment with zinc supplementation without chloroquine shows some positive effects in treatment⁵⁷. Theoretically, such effectiveness of Zn with substantial lower toxicity may also be detected by means of additional zinc

ionophore activity of quercetin and epigallocatechin-gallate⁵⁸. Targeting Zn ions in viral protein structure is another approach for modulation of COVID-19. Zn helps in protein destabilization of MERS-CoV and SARS-CoV⁵⁹. Zn-ejecting agents (e.g. antialcoholism drug disulfiram) may be used as potential antiviral agents for SARS-CoV-2 treatment by ejecting Zn²⁺ from the predicted target site to inhibit viral replication. SARS-CoV-2 utilizes angiotensin-converting enzyme 2 (ACE2) for entry into host cells. So, modification of ACE2 receptor was also thought as the potential therapeutic strategy in COVID-19. It is also reported the susceptibility of 100 μM zinc to reduce the activity of recombinant human ACE-2 in rat lungs. The consequence of zinc on SARS-CoV-2 and ACE2 interaction appeared to be only imaginary even though this concentration is close to the physiological values of total zinc⁶⁰. Impaired mucociliary clearance caused by HCoV 229E, induced ciliary dyskinesia although neither HCoV 229E nor HCoV-OC43 infection triggered a substantial reduction in ciliary beat frequency. Improvement of length of cilia from bronchial epithelium of Zn-deficient rats⁶¹, as well as increased ciliary beat frequency was boosted by Zn supplementation. We therefore postulate that zinc supplement will enhance nCoV-2019 induced dysfunction via mucociliary clearance.

Conclusion

There is a well-organized system within human body for proper management and regulation of vital trace metals. But once this system fails to operate accurately, anomalous levels of trace metals can be a significant threat to human health. Zinc as a vital trace element, performs many fundamental activities of cellular metabolism, significant to all forms of life. Generally, over 300 enzymes possess the essentiality of zinc for their proper functioning. This trace metal is also assisted with improved immune mechanism, faster wound curing, synthesis of DNA or protein and cell division. The antioxidant like properties of zinc may defend against faster aging. On the other hand, copper permits many critical enzymes to function properly and thus achieves an important place in metabolism. It basically maintains the firmness of skin, blood vessels, epithelial and connective tissue all over the body. It also takes part in the production of hemoglobin, myelin, melanin and collagen. Copper behaves both as an antioxidant and a pro-oxidant. Zinc acts like an intracellular signalling molecule with an important role in cell-mediated

Mondal *et al.*: Zinc and copper homeostasis is crucial to maintain the cellular health and their role in viral diseases *etc.*

immune response and oxidative stress. At the same time, zinc deficiency is the cause of many long-term illnesses which is needed to be altered to evade complications. Different types of diseases can be prevented with supplements, and at the same time certain types of medications cause disturbed Cu and Zn concentrations which may results in onset of other diseases. Therefore, it is very much necessary to keep a well-maintained balance between Zn and Cu than their individual concentration in blood serum.


References

- M. Dardenne, J. M. Pleau, B. Nabama, P. Lefancier, N. Denien, J. Choay and J. F. Bach, *Proc. Natl. Acad. Sci. USA*, 1982, **370**, 5373.
- M. S. Willis, S. A. Monaghan, M. L. Miller, R. W. McKenna and W. D. Perkins, *et al.*, *Am. J. Clin. Pathol.*, 2005, **123**, 125.
- J. Osredkar and N. Sustar, *J. Clinic. Toxicol.*, 2019, **S3**, 001.
- A. Hamnett and R. J. Mortimer, *J. Electroanal. Chem. Interfacial. Electrochem.*, 1987, **234**, 185.
- J. Osredkar and N. Sustar, *J. Clinic. Toxicol.*, 2011, **S3**, 001.
- S. R. Lee, *Oxid. Med. Cell. Longev.*, 2018, **2018**, 9156285.
- D. A. Scott and A. M. Fisher, *J. Clin. Invest.*, 1938, **17**, 725.
- T. Kochanczyk, A. Drozd and A. Krezel, *Metallomics.*, 2015, **7**, 244.
- C. Andreini, I. Bertini and A. Rosato, *Acc. Chem. Res.*, 2009, **42**, 1471.
- M. J. Jackson, "Physiology of Zinc: General Aspects", Springer Publishers, London, 1989, pp. 1-14.
- Z. A. Bhutta, R. E. Black, K. H. Brown, J. M. Gardner, S. Gore,
- A. Hidayat, F. Khatun, R. Martorell, N. X. Ninh, M. E. Penny, J. L. Rosado, S. K. Roy, M. Ruel, S. Sazawal and A. Shankar, *J. Pediatr.*, 1999, **135**, 689.
- Age-Related Eye Disease Study Research Group, *Arch Ophthalmol.*, 2001, **119**, 1417.
- A. Wahba, *Acta Dermatol. Venerol.*, 1980, **60**, 175.
- Y. H. Haraguchi, S. Sakurai, B. M. Hussain and H. Hoshino, *Antivir. Res.*, 1999, **43**, 123.
- E. Katz and E. Margalith, *Antimicrob. Agents. Chemother.*, 1981, **19**, 213.
- M. J. Jackson, Springer, 1989, pp. 1-14.
- J. P. Barnett, C. A. Blindauer, O. Kassar, S. Khazaipoul, E. M. Martin, P. J. Sadler and A. J. Stewart, *Biochim. Biophys. Acta*, 2013, **1830**, 5456.
- C. M Taylor, J. R. Bacon, P. J. Aggett and I. Bremner, *Am. J. Clin. Nutr.*, 1991, **53**, 755.
- M. Hambidge and N. F. Krebs, *Annu. Rev. Nutr.*, 2001, **21**, 429.
- H. Rink, *Biofactors*, 2014, **40**, 27.
- J. G. Park, Y. Qin, D. F. Galati and A. E. Palmer, *ACS Chem. Biol.*, 2012, **7**, 1636.
- B. J. McCranor, R. A. Bozym, M. I. Vitolo, C. A. Fierke, L. Bambrick, B. M. Polster, G. Fiskum and R. B. Thompson, *J. Bioenerg. Biomembr.*, 2012, **44**, 253.
- Y. Qin, P. J. Dittmer, J. G. Park, K. B. Jansen and A. E. Palmer, *Proc. Natl. Acad. Sci. USA.*, 2011, **108**, 7351.
- P. Chabosseau, E. Tuncay, G. Meur, E. A. Bellomo, A. Hessels, S. Hughes, P. R. Johnson, M. Bugliani, P. Marchetti, B. Turan, A. R. Lyon, M. Merckx and G. A. Rutter, *ACS Chem. Biol.*, 2014, **9**, 2111.
- R. A. Colvin, W. R. Holmes, C. P. Fontaine and W. Maret, *Metallomics.*, 2010, **2**, 306.
- M. C. Franz, P. Anderle, M. Burzle, Y. Suzuki, M. R. Freeman, M. A. Hediger and G. Kovacs, *Mol. Aspects. Med.*, 2013, **34**, 735.
- A. M. Kim, M. L. Bernhardt, B. Y. Kong, R. W. Ahn, S. Vogt, T. K. Woodruff and T. V. O'Halloran, *ACS Chem. Biol.*, 2011, **6**, 716.
- G. W. Stuart, P. F. Searle and R. D. Palmiter, *Nature*, 1985, **317**, 828.
- L. A. Lichten, M. S. Ryu, L. Guo, J. Embury and R. J. Cousins, *PLoS One.*, 2011, **6**, e21526.
- H. R. Godfrey, N. J. Godfrey, J. C. Godfrey and D. Riley, *Altern. Ther. Health Med.*, 2001, **7**, 49.
- B. B. Mahajan, M. Dhawan and R. Singh, *Indian J. Sex. Transm. Dis. AIDS*, 2013, **34**, 32.
- S. Shishkov, T. Varadinova, P. Bontchev, C. Nachev and E. Michailova, *Met. Based Drugs*, 1996, **3**, 11.
- S. A. Read, G. Parnell, D. Booth, M. W. Douglas, J. George and G. Ahlenstiel, *J. Viral Hepat.*, 2018, **25**, 491.
- J. Corver, R. Bron, H. Snippe, C. Kraaijeveld and J. Wilschut, *Virology*, 1997, **238**, 14.
- E. Zaitseva, A. Mittal, D. E. Griffin and L. V. Chernomordik, *J. Cell. Biol.*, 2005, **169**, 167.
- C. Y. Liu and M. Kielian, *J. Virol.*, 2012, **86**, 3588.
- E. Mocchegiani and M. Muzzioli, *J. Nutrition*, 2000, **130**, 1424S.
- Y. Haraguchi, H. Sakurai, S. Hussain, B. M. Anner and H. Hoshino, *Antiviral Res.*, 1999, **43**, 123.
- K. Hoppe-Seyler, F. Bossler, J. A. Braun, A. L. Herrmann and F. Hoppe-Seyler, *Trends. Microbiol.*, 2018, **26**, 158.
- S. N. Bae, K. H. Lee, J. H. Kim, S. J. Lee and L. O. Park, *Biochem. Biophys. Res. Commun.*, 2017, **484**, 218.
- E. R. Broun, A. Greist, G. Tricot and R. Hoffman, *JAMA*, 1990, **264**, 1441.
- V. Yuzbasiyan-Gurkan, A. Grider, T. Nostrant, R. J. Cousins and G. J. Brewer, *J. Lab. Clin. Med.*, 1992, **120**, 380.
- N. Kumar, "Fifty Neurological Cases from Mayo Clinic", Oxford University Press, Oxford, England, 2004, 131.
- J. C. Fleet, "Biochemical and Physiological Aspects of Hu-

- man Nutrition", Philadelphia, PA, Saunders, 2000.
46. M. Fukuoka, E. Tokuda, K. Nakagome, Z. Wu, I. Nagano and Y. Furukawa, *J. Inorg. Biochem.*, 2017, **175**, 208.
 47. J. C. Rutherford and A. J. Bird, *Eukaryot Cell.*, 2004, **3**, 1.
 48. N. Saydam, T. K. Adams, F. Steiner, W. Schaffner and J. H. Freedman, *J. Biol. Chem.*, 2002, **277**, 20438.
 49. M. Soinio, J. Marniemi, M. Laakso, K. Pyörälä, S. Lehto and T. Rönnemaa, *Diabetes Care.*, 2007, **30**, 523.
 50. A. Ceriello, *Metabolism*, 2000, **49**, 27.
 51. L. O. Klotz, K. D. Kröncke, D. P. Buchczyk and H. Sies, *J. Nutr.*, 2003, **133**, 1448.
 52. P. Bonaventura, G. Benedetti, F. Albarède and P. Miossec, *Autoimmun. Rev.*, 2015, **14**, 277.
 53. S. Bo, M. Durazzo and R. Gambino, *et al.*, *J. Nutr.*, 2008, **138**, 305.
 54. B. Schumacher, G. A. Garinis and J. H. Hoeijmakers, *Trends Genet.*, 2008, **24**, 77.
 55. A. J. W. Velthuis, S. H. E. van denWorm, A. C. Sims, R. S. Baric, E. J. Snijder and M. J. van Hemert, *PLoS Pathog.*, 2010, **6**, e1001176.
 56. J. M. Rolain, P. Colson and D. Raoult, *Int. J. Antimicrob. Agents*, 2007, **30**, 297.
 57. J. Xue, A. Moyer, B. Peng, J. Wu, B. N. Hannafon and W. Q. Ding, *PLoS One*, 2014, **9**, e109180.
 58. M. Guastalegname and A. Vallone, *Clin. Infect. Dis.*, 2020.
 59. H. Dabbagh Bazarbachi, G. Clergeaud, I. M. Quesada, M. Ortiz, C. K. O'Sullivan and J. B. Fernandez Larrea, *J. Agric. Food Chem.*, 2014, **62**, 8085.
 60. M. H. Lin, D. C. Moses, C. H. Hsieh, S. C. Cheng, Y. H. Chen, C. Y. Sun and C. Y. Chou. *Antiviral Res.*, 2018, **150**, 155.
 61. R. Speth, E. Carrera, M. Jean-Baptiste, A. Joachim and A. Linares, *FASEB J.*, 2014, **28**, 1067.
 62. A. Darma, R. G. Ranuh, W. Merbawani, R. A. Setyoningrum, B. Hidajat, S. N. Hidayati, A. Andaryanto and S. M. Sudarmo, *Indones Biomed. J.*, 2020, **12**, 78.

REVIEW

Electrochemical communication in biofilm of bacterial community

Sounik Manna¹ | Chandan Ghanty² | Piyush Baidara³ | Tarun Kr. Barik⁴ |
Santi M. Mandal¹ 

¹Central Research Facility, Indian Institute of Technology Kharagpur, Kharagpur, West Bengal, India

²Department of Chemistry, School of Science, OP Jindal University, Raigarh, Chhattisgarh, India

³Department of Microbiology and Immunology, University of Arkansas for Medical Sciences, Little Rock, Arkansas

⁴Department of Physics, Acchuram Memorial College, Jhalda, West Bengal, India

Correspondence

Santi M. Mandal, Central Research Facility, Indian Institute of Technology Kharagpur, Kharagpur, West Bengal 721302, India.

Email: mandalsm@gmail.com

Abstract

Electrochemical communication during biofilm formation has recently been identified. Bacteria within biofilm-adopt different strategies for electrochemical communication such as direct contact via membrane-bound molecules, diffusive electron transfer via soluble redox-active molecules, and ion channel-mediated long-range electrochemical signaling. Long-range electrical signals are important to communicate with distant members within the biofilm, which function through spatially propagating waves of potassium ion (K^+) that depolarizes neighboring cells. During propagation, these waves coordinate between the metabolic states of interior and peripheral cells of the biofilm. The understanding of electrochemical communication within the biofilm may provide new strategies to control biofilm-mediated drug resistance. Here, we summarized the different mechanisms of electrochemical communication among bacterial populations and suggested its possible role in the development of high level of antibiotic resistance. Thus, electrochemical signaling opens a new avenue concerning the electrophysiology of bacterial biofilm and may help to control the biofilm-mediated infection by developing future antimicrobials.

KEYWORDS

antibiotic resistance, bacterial biofilm, electrochemical signaling, membrane potential

1 | INTRODUCTION

Bacteria are the unicellular organisms; they lack intracellular membrane compartmentalization, but they possess an outer cell envelope [1]. The extracellular membrane of the bacteria plays an important role in their overall physiology. The outer cell surface of bacteria mediates exchange processes and adhesive properties. Such processes involve different types of electrochemical and immunological interactions occurring on the cell

membrane. These different types of interactions help in cell growth, cell division, and biological communication. The bacterial outer surface is formed by different macromolecular components such as carboxylate, phosphate, and amino group that are ionized in different environmental conditions (e.g., pH) [2]. Such ionization processes are responsible for an electrostatic interaction on the cell periphery [1]. Bacteria are present in aqueous nutrient environments, and therefore they must be hydrated outside to transport nutrient and waste particles

Sounik Manna and Chandan Ghanty contributed equally to this study.

[3]. Physicochemical factors of bacterial surfaces, such as electrostatic charge, are important with respect to overall polarity, to maintain and protect the hydrophilicity of bacterial cell surface for essential functioning of the cell. The net surface charge of a bacterial cell can be measured on the basis of zeta potential [4]. Zeta potential is the electrical potential of the common boundary between the bacterial surface and the aqueous environment [5]. Zeta potential can be measured by calculating cellular electrophoretic movement in an electric field [1]. Recently, Czerwińska-Główka and Krukiewicz [6] have summarized the electrochemical methods to characterize the biofilm over conventional techniques for monitoring their growth and development.

When bacterial cells are cultured at different physiological conditions (with varying pH), the cell surface acquires a net negative electrostatic charge [1], as shown in Figure 1. Positive counterions first attach to the negatively charged surface, forming a rigid layer called the Stern layer. The surface continues to attract more positive ions, but now these counterions experience repulsion from other counterions in the vicinity and by the Stern layer itself. Again, there is a competition between counterion neutralization and molecular motion, and as a result of such competition, an interfacial electrical diffuse layer is formed. Stern layer and diffuse layer are together called a double layer [7]. In the inner region, the Stern layer contains the surface charge as well as electrostatically bound counterions. The outer region extends into the aqueous environment, which contains a more diffuse distribution of anions and cations. This condition

of the environment with varying pH contributes to electrostatic interactions between the cells and other charged surfaces [8]. Measurement of zeta potential can provide an approximate measure of the potential of the Stern layer in bacteria.

The bacterial outer cell envelope consists of different ionized phosphoryl and carboxylate molecules, which are the cause of bacterial net electronegativity as the surface charge. In Gram-positive bacteria, the cell wall is formed by peptidoglycan, which influences inner electronegativity, because there exist substituted phosphoryl groups, with teichoic and teichuronic acid residues as substituents, as well as unsubstituted carboxylate groups [9]. In contrast, Gram-negative bacterial peptidoglycan is encapsulated within the periplasmic space and the outer membrane. Therefore, these are not exposed to the extracellular environment. However, in Gram-negative bacteria, phosphoryl and 2-keto-3-deoxyoctonate carboxylate groups of lipopolysaccharide, present in the outer membrane, serve as the negative electrostatic surface charge, which is present in the outer region of the outer membrane [10]. In Gram-positive and -negative bacteria, although different surface layers are found in the exterior of the cell walls, they similarly affect cell surface charge properties at physiological pH. Extracellular polysaccharides are present in the bacteria, which are naturally acidic in nature and may be attached with the cell surface as relatively compact capsules. In contrast, diffuse slime layers, which are loosely associated with the cell surface, consist of symmetric paracrystalline arrays, which are visible only with the help of electron

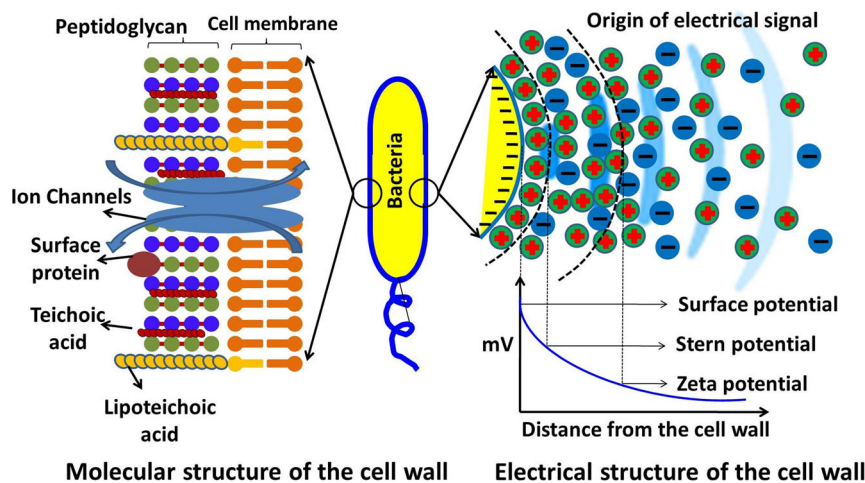


FIGURE 1 The molecular and electrical structure of the cell wall. The molecules present in the bacterial membrane play a role in the production of electric charge on the cell wall. A double-layer (Stern layer and diffuse layer) structure of a bacterial cell, which is cultured at different physiological conditions, is presented. Positive counterions first attach to the negatively charged surface and form a rigid layer called the Stern layer. The surface continues to draw more positive ions, but these counterions experience repulsion from other counterions in the surrounding area and by the Stern layer itself. So, there is a competition between counterion neutralization and molecular motion; such competition results in the formation of an interfacial electrical diffuse layer

microscopy [11]. They are formed by divalent cation-stabilized protein or glycoprotein subunits, which are associated noncovalently in a lateral way on the cell wall surface in an extensive diversity of bacteria. These charged components of the bacterial membrane have created the basis of electrochemical communication between the inner and outer surface [12].

Often some bacteria grow by adhering to each other, and they also adhere to a fixed surface to form bacterial biofilm. These adherent cells are submerged in a slime layer. Bacteria within biofilm can communicate their behavior through different forms of coordination [13–16]. Quorum sensing is a way for the cell-to-cell signaling process in bacteria [17]. Recently, it has been established that bacterial cell-to-cell communication mechanism is dependent on ion channel-mediated electrical signaling [18]. This electrical signaling has enabled cell-to-cell communication within a biofilm community [16,18]. It has been observed that *Bacillus subtilis* biofilm can energetically communicate extracellular potassium signals, which creates electrical waves that spread through the biofilm and organize metabolic states, thereby accumulating cooperative ability [16,18]. This K⁺ channel-mediated electrical signaling communication occurs between the interior and peripheral cells. The electrical signal is generated by different organisms, and its attraction seems to be a genetic mechanism that allows cross-species interactions.

On the other hand, the peptidoglycan layer is broader than Gram-negative bacteria, whereas the lipopolysaccharide layer in Gram-positive bacteria is just vice versa. Bacteria require proton motive force for their growth and sustainability. The proton motive force is produced in the bacterial cell membrane during energy generation. This proton motive force in the inner membrane produces bacterial electrochemical signaling and generates the potential charges in the membrane [19]. In the free-living planktonic state, bacteria have the ability to form the biofilm, and sessile cells adhere to the substrate and strengthen the biofilm [20].

However, electrical signals can control the direct bacterial motility by changing the membrane potential. Such long-range electrical signaling could deliver a generic mechanism for bacterial societies and control the motile behavior of unsociable cells.

2 | DIFFERENT PHYSIOLOGICAL PROCESSES OF BACTERIAL ELECTRICAL COMMUNICATION

To maintain the optimum cell function of a unicellular organism, it is important to control the interfacial

physiology of these organisms. Ionized phosphoryl and carboxylate substituents are present on the outer cell envelope of macromolecules, due to which bacterial cell surfaces have a net negative electrostatic charge. The major electrical signaling communication in biological systems is the action potential in neurons, which is communicated by ion channels [21]. Several years of research on ion channels have provided important insights into the structural basis of such neuronal signaling [22,23]. In particular, the prokaryotic K⁺ channels *kcsA* provided the first physical information on ion discernment and conductance [24]. Recently, it has been documented that bacteria have many significant classes of other ion channels such as chloride channel, sodium channels, ionotropic glutamate receptors, and calcium-gated potassium channels [25–28]. However, the inherent role of ion channels in bacteria has mostly remained unclear [29,30]. Different types of ion channels present in bacteria are not only responsible for cellular processes, but these ion channels are also responsible for electrochemical communication between their own environments. These ion-specific channels of bacteria also have unique functions like extreme acid-resistant response and osmoregulation [31]. It also remains indistinct that these ion channels can maintain other unique functions in prokaryotes. The study of the bacteria in their native background, the biofilm community, may reveal new signs about the function of ion channels in bacteria. Bioelectrochemistry is a very well-known phenomenon in human system, but in bacteria, bioelectric currents particularly exist in an agglomerated form in the biofilm. During biofilm formation, bacteria are able to produce electric field at the time of their movement and they jump due to the amount of electric potential on the biofilm [6].

3 | ELECTROCHEMICAL COMMUNICATION DURING BIOFILM FORMATION

Bacterial biofilm are prearranged communities comprising billions of densely crowded cells. Such communities can display an interesting macroscopic three-dimensional coordination [32–34]. Usually, biofilm are formed under different environmental stress situations including nutrient limitation [35]. In any group of microorganisms in a biofilm, cells are stuck to each other and often to a surface. A slimy extracellular matrix is composed of extracellular polymeric substances (EPS), in which the adherent cells are embedded. In the biofilm, the cells produce the EPS, which are typically a polymeric cluster of DNA, lipids, extracellular

polysaccharides, and proteins. When bacterial communities grow larger, due to the high growth of the peripheral cells in the biofilm, the nutrient supply of the interior cells becomes inadequate. When there is nutrient deficiency, the interior cells are protected by the peripheral cells, which remain in a critical situation for the survivability due to the presence of different external challenges. In a bacterial community, an important confrontation occurs between the opposing stresses for biofilm growth and upholding the capability of protected (interior) cells. The identification of electrochemical communication mechanisms present in the bacterial biofilm community is responsible for the sustainability of the protected interior cells, which is important to understand biofilm development [36].

However, it is not clear how microscopic bacteria can successfully interconnect in large distances. To examine this question, scientists have studied *B. subtilis* microbial community, revealing that these bacteria show metabolic oscillations activated by nutrient limitation conditions [16]. The oscillatory dynamics results from long-range metabolic co-dependence among the cells in the interior and periphery of the biofilm [16]. Specifically, the interior and peripheral cells of the biofilm share ammonium ions but compete for glutamate. Therefore, biofilm growth stops intermittently due to the increase in nutrient availability for the protection of interior cells. Remarkably, glutamate and ammonium ions are both charged metabolites, which leads to cellular uptake of these compounds, which is recognized by the proton motive force and transmembrane electrical potential. In bacterial motility, membrane potential plays a common role in their communication [37,38]. Consequently, the metabolic coordination in the biofilm community among the interior and peripheral cells might be involved in electrochemical signaling.

For the measure of electrical signaling, scientists used the fluorescent cationic dye thioflavin T to quantify the membrane potential within the bacterial biofilm community. Within the biofilm community, thioflavin T is used for the measurement of global alternations in membrane potential. Thioflavin T is a highly positively charged molecule and it is attracted to cells due to the negative membrane potential of the bacterial cell. The experimental result shows that thioflavin T increases inside the cell when the cell becomes more negative, and thus thioflavin T is inversely related to the membrane potential [18]. These membrane potential oscillations are highly coordinated among the most distant areas of the biofilm. Actually, biofilm community or bacterial cells can transfer charge particles in their membrane, which occurs only for electrochemical signaling communication.

4 | BACTERIAL ION CHANNEL-MEDIATED ELECTRICAL SIGNALING

The ion channels of the bacterial membrane possess different ion-transferring mechanisms by the electrochemical signal. It is evidenced that YugO (K^+ channel) in *B. subtilis* is important for biofilm formation [39]. This potassium flux pump has an intracellular TrkA domain, which is regulated by the metabolic state of the cell [40–42]. For better understanding the hypothesis, wild-type and YugO-deleted mutant strains were used, which revealed that extracellular K^+ increased for the wild-type strain, but not for the mutated strain. Consequently, the metabolic limitation could form the primary trigger for YugO activation. Specifically, the fundamental metabolic oscillations are determined by glutamate limitation [16], which is due to the release of K^+ and the elimination of glutamate. The neighboring cells become depolarized due to the presence of K^+ outside the cells, restraining glutamate uptake, which creates additional nitrogen limitation, and thus metabolic stress is generated. These cyclic consequences occur due to cell–cell transmission of the potassium signal. These findings hypothesized that glutamate limitation can trigger potassium signal via the YugO potassium channel [43].

In *B. subtilis*, YugO also has a role in the active propagation of the potassium signal. Wild-type and YugO mutant strains have transient bursts of external K^+ concentration (300-mM KCl). As can be predicted, K^+ causes short-term membrane potential depolarization in both strains. However, in the wild-type strain, this primary depolarization is naturally monitored by a protracted hyperpolarization phase, which was not observed in the YugO mutant strain. This period of hyperpolarization is complemented by an increase in extracellular K^+ ions. This YugO was triggered by intracellular potassium, because when an equal concentration of sorbitol (an uncharged solute) was used, but it did not stimulate an equal response, producing purely osmotic effects. Therefore, YugO seems to have a role in propagating the extracellular potassium signal within the biofilm [18].

The K^+ channel shows the electrochemical activity and the mechanism is experimentally observed in the form of propagating pulses of electrical activity. A temporary depolarization is monitored by hyperpolarization in reaction to native proliferations in extracellular potassium concentration. Additionally, the model demonstrates that long-range proliferation of these excitations does not show a decrease in the amplitude of membrane potential oscillations. The bacterial cells release intracellular potassium when they are in a metabolically stressed condition, and this extracellular potassium generates more metabolic

stress on neighboring cells. *B. subtilis* cotransported glutamate with two protons by the GltP transporter, and this process is influenced by the proton motive force [37]. Potassium-mediated depolarization of the membrane potential can permanently decrease the electrical module of the proton motive force, [44] and thus lower glutamate acceptance and intracellular ammonium retention [37,38]. Consequently, this potassium-intermediated signaling could proliferate metabolic stress on distant cells. With the increase of cells in glutamine, the response to extracellular potassium can be reduced. Glutamate and ammonium requirement can be compensated by two main factors: an uncharged metabolite and a favored nitrogen source [45]. Hence, potassium-mediated ion channel of bacteria is formed by an electrical signal that controls the metabolic stress. In *Bacillus* sp., the YugO channel transfers the ion and creates an effective electrical communication between distant cells [26].

5 | CROSS-SPECIES COMMUNICATION

Biofilm refer to the compressed relationship of microorganisms and their environment. The chemical signaling mechanism in a bacterial communication network is quorum sensing. Recently, it has been revealed that electrical signaling is mediated through the ion channels of bacterial cells. Long-range behavior of bacteria is also influenced by their signaling mechanism. As a result, in a bacterial community, long-range cross-species communication has been possible. This considerable result has provided a new example to examine the complex coexistence of biofilm societies and distant cells, with a probable scope of application in synthetic biology.

In bacterial motility, membrane potential plays a common role in signal communication [46]. Therefore, a new suggestion is that the process of attraction based on persuading alterations in membrane potential can apply to other bacteria as well. To answer this hypothesis, scientists studied the interaction of *Pseudomonas aeruginosa* cells with the pre-existing *B. subtilis* biofilm and demonstrated that the motile *P. aeruginosa* cells are intermittently attracted to the *B. subtilis* biofilm during electrical oscillations. It has been experientially proved that a difference in the period of electrical signaling within the biofilm is directly coordinated by the period of *P. aeruginosa* magnetism to the biofilm edge. This implies that the mechanism of electrically arbitrated attraction is not restricted to *B. subtilis* cells, therefore allowing cross-species interaction also [43].

Bacterial ion channels generated long-range electrochemical signals; for example, K^+ channel generates a

rapid response in the cell motility, because any biochemical synthesis or any complex signaling networks are not required in this response. This study also proposes a new hypothesis that cross-species signaling occurs in long range and is generic in nature, where no exact receptor or signaling pathways are required. The result of this effort leads to many motivating questions concerning the result of the newly invented signaling procedure over the quorum-sensing bacterium in the multifaceted coexistence of the biofilm communities and neighboring cells [43,46,47].

The bacterial ion channel-mediated signaling mechanism results in a quick response in cell motility of even physically distant cells, due to its individuality on a multifaceted signaling network. Consequently, due to distant species electrochemical signaling, bacteria from diverse species are involved and incorporated in a pre-existing biofilm. Therefore, the complex coexistence of a biofilm with its neighboring cross-species societies has led to an increase in many fascinating features of the signaling mechanism in the secretive microorganism community.

6 | ELECTRICAL COMMUNICATION DURING INTERSPECIES-SPECIFIC CROSSTALK

When an electron is moved between different species of microbes, is known as interspecies electron transfer (IET) mechanism. This IET mechanism has been established on the basis of obliging behaviors and community purposes. IET mechanisms depend on the circulation of redox chemical species or direct interaction in cell aggregates. Following IET, bacteria generate their membrane potential and proton motive force as one of their communicative way among bacterial communities [48].

In growing biofilm, bacteria surrender their freedom and settle into large stationary societies. Suel and colleagues grew a biofilm of *B. subtilis* to understand the communication process within the bacterial cells with the outer cells, when to divide or relax. The biofilm of *B. subtilis* were treated with fluorescent markers that were energized by potassium and sodium ions, and the potassium marker lit up, as ions flowed out of starved cells. The biofilm cells also released K^+ , refreshing the signal, when the ions reached closer to them. The signal flowed outward in this way until it reached the biofilm's edge, and in response to the signal border, cells stopped dividing until the intramural cells received a feed, after which they stopped releasing potassium. Suel's team then created mutant bacteria without potassium channels, and they found that the mutant cells did not grow in the same stop-start manner of wild-type

cells. Like neurons, to communicate electrical signals, bacteria evidently use K^+ [18,43,47].

The significant flow of electrons through a small cable is called an electric current. In bacteria, the pili act as nanowires, which transfer electrons to the surrounding environment. Flagella are the extracellular projection of bacteria, which transfer electrons to electrodes, which are called bacterial nanowires. Bacterial nanowire formation was established by atomic force and transmission electron microscopy and by electrochemical techniques, and its conductive nature was investigated. It can be observed from analyzing marine bacteria that live in the mud at the bottom of the sea that an electric current is propagated through the layers of mud. Cyclic voltammetry (CV) and electrochemical impedance spectroscopy (EIS), nondestructive voltammetry techniques, suggest that bacterial nanowires could be the source of electrons, which may be used in various applications, for example, microbial fuel cells, biosensors, organic solar cells, and bioelectronic devices. Underneath the layer of mud, bacteria generate energy, and the electrons thus released reach the top layer, where they subsequently react with O_2 . These electrons travel a distance of 12 mm, which is 10,000 times of body length of bacteria [16,43,46].

In contrast, *Bacillus* sp. uses a K^+ channel to convert free-swimming cells to their static society. Remarkably, the bacteria attract not only *Bacillus* sp. but also other dissimilar species. Bacteria seem to live in diverse communities, not just in monocultures. These two *Bacillus* species exchange potassium signals, and two *Bacillus* biofilm can “time-share” nutrients also. In an experiment, where two bacterial communities have been employed and allowed to utilize glutamate, the biofilm are allowed to ingest the desired nutrients more professionally. As a result of the sharing of two different bacterial communities, the biofilm grew more rapidly than they could have if the bacteria had consumed the nutrients without the interference of any other bacteria [18]. When the ion channel was modified, they gave weaker signals in the biofilm community and they were not properly able to coordinate their feeding and grew more slowly. Therefore, it is clear that the same species of different bacteria also communicate by generating electrochemical signals [44].

7 | ELECTRICAL COMMUNICATION DURING INTRASPECIES-SPECIFIC CROSSTALK

Bacteria within biofilm communities can organize their behavior through cell-to-cell signaling. However, it remains uncertain if these signals can stimulate the

behavior of distant cells that are not part of the community. In *B. subtilis* biofilm community, there is a K^+ channel-mediated electrical signaling communication between the interior and peripheral cells. An electrochemical potassium signal is generated inside the biofilm, which alters the membrane potential of distant cells, thus leading to their motility [16,18].

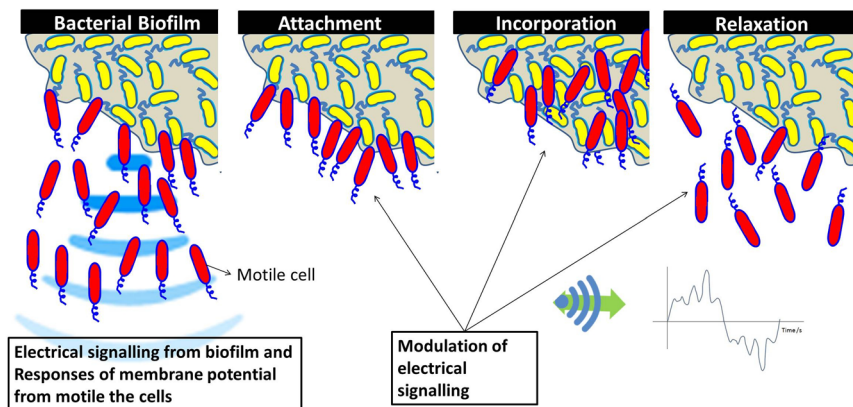
This electrical signal is generated by different organisms, and the attraction seems to be a generic mechanism that allows cross-species interactions. *B. subtilis* biofilm released the electrical signal by its ion channel and *P. aeruginosa* cells became attracted to this electrical signal. Through the long-range electrical signaling, the cells of the bacterial community can coordinate their own behavior and also affect the behavior of different bacteria at a particular distance [43,46].

The communication mechanisms between the biofilm and distant cells occur between the evolutionarily distant bacteria, and are therefore not restricted to cells from a single species. In a biofilm community, the effect of extracellular K^+ on membrane potential is communal among all cells, and therefore communication is physical in nature (Figure 2). The long-range cross-species signaling is generic and it does not require specific receptors or any signaling mechanism. Stimulatingly, due to cross-species attraction, bacteria from a different species can be assimilated into a pre-existing biofilm. In cross-species bacterial community, they have different membrane potential and thus generate electrochemical signal by their membrane ion channels. This electrochemical signal might be their way of communication [16,18,43].

8 | ELECTROCHEMICAL SIGNALING VIA MEMBRANE POTENTIAL AND RESISTANCE DEVELOPMENT

In recent years, bacterial electrophysiology has been demonstrated to have important roles in the various physiological processes like cellular proliferation, electrochemical communication, persister cell formation, and antibiotic resistance [49–52]. Electrochemical signaling via K^+ channels, together with resultant membrane potential, which is specific for different bacterial communities, is a way of electrochemical communication in bacterial biofilm. Biofilm formation is also stimulated by a variety of natural products including surfactin, which induces potassium leakage that triggers multicellularity. Potassium leakage stimulates a membrane protein kinase, KinC, which regulates the genes involved in the biofilm formation [53]. Interestingly, surfactin possesses antimicrobial activities, but it generates the chances for

FIGURE 2 Migration, attachment, incorporation, and relaxation of motile cells in biofilm, depending on the modulation in electrochemical signaling in bacterial biofilm community



resistance development against itself and other antimicrobials by induction of genes involved in biofilm formation via potassium leakage. In addition, potassium leakage results in depolarization of membrane potential that might play role in resistance development against positively charged antimicrobials. Next, bacterial biofilm formation and cell-to-cell communication within biofilm have already been reported for their role in the development of drug resistance [47,54]. Electrochemical signaling in bacterial biofilm has also demonstrated to have a role in cell-to-cell communication via differences in membrane potential [18,43]. However, a direct link between electrochemical signaling in bacterial biofilm and its role in drug resistance development is missing.

During IET in bacterial biofilm, which is important for cell-to-cell communication, a high membrane potential is generated in biofilm, which is key to biofilm matrix production [55]. Furthermore, it has been shown that bacterial membrane potential dynamics in biofilm facilitates electrical signaling in both intra- and intercellular levels. This membrane potential derived from electrical signaling is found to be proportional to cellular proliferation capacity [51]. The increase in membrane potential induces a higher cellular proliferation, which helps in the development of resistance and required antimicrobials that are more potent. In a recent report, it has been confirmed that K^+ transport system of *Staphylococcus aureus* plays an important role in resistance development against aminoglycoside antibiotics and cationic antimicrobial peptides [56]. In conclusion, here we have suggested that disruption of electrochemical signaling by targeting bacterial cell membrane potential could be a promising alternative to confront the rapid emergence of multidrug resistance [57].

9 | CONCLUSION

Electrophysiology is a well-known branch of neurosciences. In the recent past, multiple studies have

shown that bacterial communities like biofilm utilize electrochemical signals for communication, based on the fundamentals of electrophysiology. K^+ channels are the major channels that help in long-distance electrochemical communication in biofilm and in developing a dynamic membrane potential across interior and peripheral cells within the biofilm. This resultant dynamic potential propagated in the form of electrical pulses between the distant cells of biofilm induces biofilm formation. The electrochemical communication within biofilm may also be involved in the measurement of electrical resistance or development within the bacterial communities by membrane depolarization and induction of multicellularity. Therefore, electrochemical control of biofilm may develop as a potential biofilm treatment strategy and confront multidrug-resistant biofilm-forming bacterial pathogens.

CONFLICT OF INTERESTS

The authors declare that there are no conflict of interests.

ORCID

Santi M. Mandal  <http://orcid.org/0000-0002-0119-7138>

REFERENCES

- [1] Mozes N, Rouxhet PG. Microbial hydrophobicity and fermentation technology. In: Doyle RJ, Rosenberg M, editors. Microbial cell surface hydrophobicity. Washington, DC: American Society for Microbiology; 1990. p. 75-105.
- [2] Kureisaite-Ciziene D, Varadajan A, McLaughlin SH, Glas M, Montón Silva A, Luirink R, et al. Structural analysis of the interaction between the bacterial cell division proteins FtsQ and FtsB. *mBio*. 2018;9:01346-18.
- [3] Beveridge TJ, Graham LL. Surface layers of bacteria. *Microbiol Rev*. 1991;55:684-705.
- [4] Wilson WW, Wade MM, Holman SC, Champlin FR. Status of methods for assessing bacterial cell surface charge properties based on zeta potential measurements. *J Microbiol Methods*. 2001;43:153-64.
- [5] Saito T, Takatsuka T, Kato T, Ishihara K, Okuda K. Adherence of oral streptococci to an immobilized agent. *Arch Oral Biol*. 1997;42:539-45.

- [6] Czerwinska-Glowkaa D, Kurkiewicz K. A journey in the complex interactions between electrochemistry and bacteriology: from electroactivity to electromodulation of bacterial biofilms. *Bioelectrochemistry*. 2020;131:10740.
- [7] Howard JJ, Perkyns JSB, Pettitt M. The behavior of ions near a charged wall-dependence on ion size, concentration, and surface charge. *J Phys Chem B*. 2010;114:6074-83.
- [8] Brown MA, Bossa GV, May S. Emergence of a Stern layer from the incorporation of hydration interactions into the Gouy-Chapman model of the electrical double layer. *Langmuir*. 2015;42:11477-83.
- [9] Beveridge TJ. The bacterial surfaces: general considerations towards design and function. *Can J Microbiol*. 1988;34:363-72.
- [10] Nikaido H. Molecular basis of bacterial outer membrane permeability revisited. *Microbiol Mol Biol Rev*. 2003;67:593-656.
- [11] Dominique HL, Christopher JJ, Wozniak DJ. Bacterial extracellular polysaccharides in biofilm formation and function. *Microbiol Spectr*. 2015;3:3.
- [12] Sleytr UB, Schuster B, Egelseer E, Pum D. S-layers: principles and applications. *FEMS Microbiol Rev*. 2014;38:823-64.
- [13] Shapiro JA. Thinking about bacterial populations as multicellular organisms. *Ann Rev Microbiol*. 1998;52:81-4.
- [14] Waters CM, Bassler BL. Quorum sensing: cell-to-cell communication in bacteria. *Annu Rev Cell Dev Biol*. 2005;21:319-46.
- [15] Brameyer S, Bode HB, Heermann R. Languages and dialects: bacterial communication beyond homoserine lactones. *Trends Microbiol*. 2015;23:521-3.
- [16] Liu J, Prindle A, Humphries J, Gabalda-Sagarra M, Asally M, Lee DY, et al. Metabolic co-dependence gives rise to collective oscillations within biofilms. *Nature*. 2015;523:550-4.
- [17] Miller MB, Bassler BL. Quorum sensing in bacteria. *Annu Rev Microbiol*. 2001;55:165-99.
- [18] Prindle A, Liu J, Asally M, Ly S, Garcia-Ojalvo J, Suel GM. Ion channels enable electrical communication in bacterial communities. *Nature*. 2015;527:59-63.
- [19] Bradbeer C. The proton motive force drives the outer membrane transport of cobalamin in *Escherichia coli*. *J Bacteriol*. 1993;175:3146-50.
- [20] Rollet C, Gal L, Guzzo J. Biofilm-detached cells, a transition from a sessile to a planktonic phenotype: a comparative study of adhesion and physiological characteristics in *Pseudomonas aeruginosa*. *FEMS Microbiol Lett*. 2009;290:135-42.
- [21] Liu J, Martinez-Corral R, Prindle A, Lee DD, Larkin J, Gabalda-Sagarra M, et al. Coupling between distant biofilms and emergence of nutrient time-sharing. *Science*. 2017;356:638-42.
- [22] Hille B. Ion channels of excitable membranes. Washington, DC: University of Washington, Sinauer Associates, Inc.; 2001.
- [23] MacKinnon R. Potassium channels and the atomic basis of selective ion conduction. *Biosci Rep*. 2004;24:75-100.
- [24] Doyle DA. The structure of the potassium channel: molecular basis of K1 conduction and selectivity. *Science*. 1998;28:69-77.
- [25] Ren D, Navarro B, Xu H, Yue L, Shi Q, Clapham D. A prokaryotic voltage-gated sodium channel. *Science*. 2001;294:2372-5.
- [26] Iyer R, Iverson TM, Accardi A, Miller C. A biological role for prokaryotic ClC chloride channels. *Nature*. 2002;419:715-8.
- [27] Jing X, Yang Y, Ai Z, Chen S, Zhou S. Potassium channel blocker inhibits the formation and electroactivity of *Geobacter* biofilm. *Sci Total Environ*. 2020;705:135796.
- [28] Chen GQ, Cui C, Mayer ML, Gouaux E. Functional characterization of a potassium-selective prokaryotic glutamate receptor. *Nature*. 1999;402:817-21.
- [29] Kuo MMC, Haynes WJ, Loukin SH, Kung C, Saimi Y. Prokaryotic K1 channels: from crystal structures to diversity. *FEMS Microbiol Rev*. 2005;29:961-85.
- [30] Saimi Y, Loukin SH, Zhou XL, Martinac B, Kung C. Ion channels in microbes. *Methods Enzymol*. 1998;294:507-24.
- [31] Martinac B, Buechner M, Delcour AH, Adler J, Kung C. Pressure-sensitive ion channel in *Escherichia coli*. *Proc Natl Acad Sci USA*. 1987;84:2297-301.
- [32] Costerton JW, Stewart PS, Greenberg EP. Bacterial biofilms: a common cause of persistent infections. *Science*. 1999;284:1318-22.
- [33] Wilking JN, Zaboradaev V, Volder MD, Losick R, Brenner MP, Weitz DA. Liquid transport facilitated by channels in *Bacillus subtilis* biofilms. *Proc Natl Acad Sci USA*. 2013;110:848-52.
- [34] Payne S, Li B, Cao Y, Schaeffer D, Ryser MD, You L. Temporal control of self-organized pattern formation without morphogen gradients in bacteria. *Mol Syst Biol*. 2013;9:697.
- [35] Hall-Stoodley L, Costerton JW, Stoodley P. Bacterial biofilms: from the natural environment to infectious diseases. *Nature Rev Microbiol*. 2004;2:95-8.
- [36] Vlamakis H, Aguilar C, Losick R, Kolter R. Control of cell fate by the formation of an architecturally complex bacterial community. *Genes Dev*. 2008;22:945-53.
- [37] Tolner B, Ubbink-Kok T, Poolman B, Konings WN. Characterization of the proton/glutamate symport protein of *Bacillus subtilis* and its functional expression in *Escherichia coli*. *J Bacteriol*. 1995;177:2863-9.
- [38] Boogerd FC, Ma H, Bruggeman FJ, van Heeswijk WC, Garcia-Contreras R, Molenaar D, et al. AmtB-mediated NH₃ transport in prokaryotes must be active and as a consequence regulation of transport by GlnK is mandatory to limit futile cycling of NH₄(+)/NH₃. *FEBS Lett*. 2011;585:23-8.
- [39] Lundberg ME, Becker EC, Choe S. MstX and a putative potassium channel facilitate biofilm formation in *Bacillus subtilis*. *PLOS One*. 2013;8:e60993.
- [40] Cao Y, Pan Y, Huang H, Jin X, Levin EJ, Kloss B, et al. Gating of the TrkH ion channel by its associated RCK protein TrkA. *Nature*. 2013;496:317-22.
- [41] Roosild TP, Miller S, Booth IR, Choe S. A mechanism of regulating transmembrane potassium flux through a ligand-mediated conformational switch. *Cell*. 2002;109:781-91.
- [42] Schlosser A, Hamann A, Bossemeyer D, Schneider E, Bakker EP. NAD1 binding to the *Escherichia coli* K1-uptake protein TrkA and sequence similarity between TrkA and domains of a family of dehydrogenases suggest a role for NAD1 in bacterial transport. *Mol Microbiol*. 1993;9:53343-543.
- [43] Humphries J, Xiong L, Liu J, Prindle A, Yuan F, Arjes HA, et al. Species-independent attraction to biofilms through electrical signaling. *Cell*. 2017;168:200-9.
- [44] Krulwich TA, Sachs G, Padan E. Molecular aspects of bacterial pH sensing and homeostasis. *Nature Rev Microbiol*. 2011;9:330-43.
- [45] Fisher SH. Regulation of nitrogen metabolism in *Bacillus subtilis*: vive la difference. *Mol Microbiol*. 1999;32:223-32.

- [46] Majumdar S, Pal S. Cross-species communication in bacterial world. *J Cell Commun Signal*. 2017;11:187-90.
- [47] Qi L, Li H, Zhang C, Liang B, Li J, Wang L, et al. Relationship between antibiotic resistance, biofilm formation, and biofilm-specific resistance in *Acinetobacter baumannii*. *Front Microbiol*. 2016;7:483.
- [48] Katoa S, Hashimoto K, Watanabe K. Microbial interspecies electron transfer via electric currents through conductive minerals. *Proc Natl Acad Sci USA*. 2012;109:10042-6.
- [49] Verstraeten N, Knapen WJ, Kint CI, Liebens V, van den Bergh B, Dewachter L, et al. O₂ and membrane depolarization are part of a microbial bet-hedging strategy that leads to antibiotic tolerance. *Mol Cell*. 2015;59:9-21.
- [50] Damper PD, Epstein W. Role of the membrane potential in bacterial resistance to aminoglycoside antibiotics. *Antimicrob Agents Chemother*. 1981;20:803-8.
- [51] Stratford JP, Edwards CLA, Ghanshyam MJ, Malyshev D, Delise MA, Hayashi Y, et al. Electrically induced bacterial membrane-potential dynamics correspond to cellular proliferation capacity. *Proc Natl Acad Sci U S A*. 2019;116:9552-7.
- [52] Sultana ST, Call DR, Beyenal H. Eradication of *Pseudomonas aeruginosa* biofilms and persister cells using an electrochemical scaffold and enhanced antibiotic susceptibility. *NPJ Biofilms Microbiomes*. 2016;2:2.
- [53] López D, Fischbach MA, Chu F, Losick R, Kolter R. Structurally diverse natural products that cause potassium leakage trigger multicellularity in *Bacillus subtilis*. *Proc Natl Acad Sci USA*. 2009;106:280-5.
- [54] Hirakawa H, Tomita H. Interference of bacterial cell-to-cell communication: a new concept of antimicrobial chemotherapy breaks antibiotic resistance. *Front Microbiol*. 2013;4:114.
- [55] Qin Y, He Y, She Q, Larese-Casanova P, Li P, Chai Y. Heterogeneity in respiratory electron transfer and adaptive iron utilization in a bacterial biofilm. *Nat Commun*. 2019;10:3702.
- [56] Gries CM, Bose JL, Nuxoll AS, Fey PD, Bayles KW. The Ktr potassium transport system in *Staphylococcus aureus* and its role in cell physiology, antimicrobial resistance and pathogenesis. *Mol Microbiol*. 2013;89:760-73.
- [57] Goldberg K, Sarig H, Zaknoon F, Epanand RF, Epanand RM, Mor A. Sensitization of Gram-negative bacteria by targeting the membrane potential. *FASEB J*. 2013;27:3818-26.

How to cite this article: Manna S, Ghanty C, Baindara P, Barik TK, Mandal SM. Electrochemical communication in biofilm of bacterial community. *J Basic Microbiol*. 2020;60:819–827.
<https://doi.org/10.1002/jobm.202000340>



Prospect of nanotechnology: A brief review

Tarun Kumar Barik^{*a}, Santi M. Mandal^b, Soma Mitra (Banerjee)^c, Gopal Chandra Maity^d,
Gourisankar Roymahapatra^e and Tuhin Shubhra Santra^f

^aDepartment of Physics, Achhruram Memorial College, Jhalda, Purulia-723 202, West Bengal, India

^bCentral Research Facility, Indian Institute of Technology Kharagpur, Kharagpur-721 302, West Bengal, India

^cDepartment of Physics, University of Gour Banga, Malda-732 103, West Bengal, India

^dDepartment of Chemistry, Abhedananda Mahavidyalaya, Sainthia-731 234, Birbhum, West Bengal, India

^eSchool of Applied Science and Humanities, Haldia Institute of Technology, Haldia-721 657, West Bengal, India

^fDepartment of Engineering Design, Indian Institute of Technology Madras, Chennai-600 036, India

E-mail: tarun.barik2003@gmail.com

Manuscript received online 18 November 2020, revised and accepted 30 November 2020

Nanotechnology has offered a great improvement in science, engineering, medicine, biomedical engineering, food technology, packing technologies, clothes, robotics, and computing from the beginning of twenty-first century. As the maximum potential of scientific discovery always contains some good and bad effects in human civilization, nanotechnology is not an exception among them. The major drawbacks consist of economic disruption and possible threats to security, privacy, health, and environmental hazards, etc. The advancements and benefits of nanotechnology are discussed along with different drawbacks in health-related problems due to their extensive application in medicine, food, agriculture, etc., are summarized. Besides, it highlights the social-economic disruption due to rapid use of nanotechnology. The nanopollution, not only affects human beings but also influences the existence of other living beings like microorganisms, animals and plants, which are also briefly reviewed. The safety and security of nanotechnological developments, current policies, regulation status, challenges and future trends using nanomaterials in humans are demonstrated. In conclusion, while nanotechnology offers more efficient power sources, faster and modern kinds of computers and life-saving medical treatments but some negative issues and limitations are prominent due to their toxicity. Finally, rapid research on nanotechnology bounds to think twice before any advanced technological applications on its safety and security aspect will revolutionize the whole world in near future.

Keywords: Progress in nanotechnology, nanotoxicity, nanopollution, human health, safety.

Introduction

Nanoscience are the emerging field in modern technology with numerous applications in biomedical and manufacturing of new smart materials¹. In the last two decades, nanotechnology integrates with the mechanical and electronic engineering to develop micro/nano-electromechanical systems (MEMS/NEMS) devices, which have diverse applications in different fields of science and engineering. These devices are potentially applicable for different sensing, actuating as well as biomedical analysis purposes². Recently quantum dots have acquired much attention in biological fields owing to its unique size, tunable light absorption and

emission properties³. Further, biocompatible nanomaterials have many applications in biomedical purposes such as orthopedic, cardiovascular, contact lenses, catheter, prosthetic replacement, etc.^{4,5}. Past three decades, extensive research has been carried out to develop nanomedicine and nanoscience based biomedical sensor and instruments^{6,7}. Metallic nanoparticles have unique optical, electrical and biological properties, that have attracted significant attention in applications, like catalysis, ultrasensitive chemical and biological sensors, bio-imaging, targeted drug delivery and fabrication⁸⁻¹⁵. It also comprise of large surface area to volume ratio, unique quantum size, having excellent magnetic proper-

ties, heat conductivity additionally to some catalytic and antimicrobial properties¹⁶. Nanoparticles are often synthesized via various chemical and physical routes like chemical reduction^{17–19}, photochemical reduction^{20–24}, electrochemical reduction^{25,26}, heat evaporation^{27,28}, etc. A series of reducing agents like sodium or potassium borohydrate, hydrazine and salts of tartrate, or organic ones like sodium citrate, vitamin-C, or amino acids are used to get oxidized. Several studies have reported shape and size dependency of silver nanoparticles formation on capping agents like dendrimer²⁹, chitosan³⁰, ionic liquid³¹, and poly(vinylpyrrolidone) PVP³². These capping agents control the nanoparticle growth via reaction confinement within the matrix or through preferential adsorption on specific crystal facets. But, these approaches are costly and hazardous, with the involvement of toxic, non-environment-friendly agents. Hence, evaluation of the risk of these nanoparticles to human health becomes critical. Multiple studies have shown the increase of leukocytes number, neutrophils, in the lungs and bronchoalveolar lavages during airway exposure of nanoparticles in *in vivo* models of inflammation. The neutrophil counts act as biomarkers for inflammation. Therefore, selection of a synthesis route that minimizes the toxicity and increases the stability of nanoparticle leads to enhanced biomedical applications of silver and gold nanoparticles. The development of better experimental procedures for the synthesis of nanoparticles employing variety of chemical compositions and controlled polydispersity offers considerable advancement³³. Methods of nanoparticle fabrication through different physical and chemical process as mentioned above have their demerits as they produce enormous environmental contaminations and unsafe byproducts. Thus, there's a necessity for "green chemistry" that ensures clean, non-toxic, and environment-friendly nanoparticles production³⁴. Nowadays nanomaterials are produced by industries for commercial applications with enormous benefits. While there lies an enormous potential of nanomaterials for fulfilling human requirements, likewise it also correspond to potential risks to human health³⁵.

In recent times, eco-friendly approaches have been developed to engineer stable nanoparticles with intelligible morphology and configured constricted sizes³⁶. Additionally, owing to the high demand for precious metals like silver and gold and their oxides is of great significance and interest^{37,38}.

Bio-inspired synthesis of nanoparticles is an advanced, cost-effective, environment-friendly approach over chemical and physical methods, without any inclusion of high pressure, energy, temperature, and toxic chemicals³⁹. For example, plant leaf extract is used for the biosynthesis of silver and gold nanoparticles for pharmaceutical and biomedical applications, without employing any toxic chemicals in the synthesis protocols⁴⁰. Eco-friendly acceptable reducing and capping agents are considered to be an effective one for "green" synthesis nanoparticles⁴¹. The fabrication process also necessitates the use of non-toxic solvents to make eco-friendly. Generally in this technique, microwave retains a constant temperature of the solvent systems. In conventional extraction techniques hexane, ethanol and water are used for the collection of bioactive molecules⁴². But hexane and ethanol are immensely problematic due to their instability as well as environmental and health hazards⁴³. To overcome this problem, researchers developed the supercritical fluid (SCF) extraction technology to avoid toxic organic solvents in green technology. SCF possesses physical properties intermediate between CO₂ gas and a liquid at a temperature and pressure above of its critical point. Supercritical CO₂ is non-polar, non-toxic, non-flammable, and has low critical temperature. In this regard, nanomaterials, including metal nanoparticles, carbon nanotubes, quantum dots, and other active nanomaterials can be used to develop biosensors against a broad spectrum of microorganisms for the formulation of a new generation of antimicrobial agents. Among noble metals, silver (Ag) and gold (Au) nanoparticles synthesis via marine algae are used as a broad-spectrum antimicrobial agent towards a variety of pathogens in the biomedical field⁴⁴. Many microorganisms are used for the synthesis of nanoparticles such as cyanobacteria, eukaryotic algae, and fungi. Biosynthesis of nanoparticles by plant extracts are better source in comparison to the various biological processes often considered as eco-friendly substitutes of chemical and physical methods^{1,5}. Seaweeds with rich in organic and inorganic is used widely in agriculture, pharmaceutical, biomedical, and nutraceutical industries for consisting high amount of vitamins and minerals^{45,46}. Among several genera of microalgae, *Spirulina platensis* is blue-green algae of the cyanobacteria family grown in temperate water in the whole world. A blue-green algae has served as food with high protein content and nutritional value from ancient

times⁴⁷. The algae produce novel and potentially useful bioactive compounds^{48,49}. The bioactive materials have gained significant attention in recent years and have been used considerably in the development of new pharmaceutical products, food products, renewable bio-energy and biomedical applications^{50–52}. However, antibiotic resistance is a global issue that lowers these drugs' effectiveness via genetic mutation or gene acquisition. Therefore, new classes of antibiotics with novel structural diversity are required to battle this trend. Now food preservation is dealing with severe concern of microorganisms mediated spoilage along with fall in quality and nutrition worldwide⁵³. Recently, nanoparticles are used in various industries like electronics, aerospace, cosmetics, textile, and even in food. Consequently, the chance of human exposure to nanoparticles is rising, heading towards the time when nanoparticles will eventually be present in blood circulation interacting with immune blood cells.

Advantages and growth of nanotechnology

Recently, research and development in nanotechnology have seen exponential growth due to advantages in different fields like drug delivery, cell imaging, material improvement, medical devices for diagnosis and treatment. More powerful computers are being designed using nonmaterial having faster in speed and consuming very less power, long-life batteries.

The term nanocomputers framed in several ways, using mechanical, electronic, biochemical, or quantum nanotechnology. Circuits consisting of carbon nanotubes can maintain the computer system more advance. Carbon nanotubes are also commercially used in sports equipment, with light weight and high strength. Nanoparticles in fabrics improve the water-resistance, stain resistance, and flame resistance, without putting on extra weight, stiffness, or thickness of the fabric⁵⁴. Nanoparticles are used in medical products for dermal, oral or inhalation applications. Tiny insize, corresponds to higher surface area of nanomaterials offering greater strength, stability, chemical, physical, and biological activity. The carbon-based nanomaterials (fullerenes and nanotubes) are employed in thin films, coatings, and electronics. The metal-based nanomaterials (nanosilver, nanogold) and metal oxides (titanium dioxide (TiO₂)) are useful for food, cosmetics, and drug-related products. The dendrimers are nano-poly-

mers, an ideal candidate for drug delivery. Composites such as nanoclays are formed with a combination of nanoparticle with other particles. Many beverage bottles are made up of plastics with nanoclays. The nanoclay reinforcement increases penetration resistance to oxygen, carbon dioxide, moisture and thus increases shelf life and thus nanoclays are also being used in packaging. It helps to improve vehicle fuel efficiency and corrosion resistance by using diamond-like-nanocomposite (DLN) materials that are lighter, stronger, and high chemical resistant^{55,56}. The DLN film exhibits biocompatibility in nature, which have potential applications as a coating material for biomedical purpose. Few nanoparticles are also used in water filter technology that can remove heavy metals, kill viruses and bacteria. These cost-effective, portable water-treatment systems are ideal for the improvement of drinking water quality in developing countries. Now a day, most sunscreens also contain nanoparticles for effective absorption of light including the more dangerous ultraviolet range and pass the other wavelengths, which is healthy for skin. Recently, nanosensors are able to detect a toxic chemical at very low levels, for example, single molecule detection, out of billions of molecules^{57,58}. In medical science, the detection of single biomolecules has tremendous applications for DNA/RNA sequencing and disease analysis. The nanobiosensors can be used to precisely identify particular cells or substances in the body for different diagnostics purposes. Current research is focused on preparing the smaller, highly sensitive and cost-efficient biosensors. The new biosensors are updated to even detect odors specific diseases for medical diagnosis, pollutant detection, and gas leaks for environmental protection.

Nanoparticles in pharmaceutical products facilitate improved absorption within the human body along with easy delivery, often in association with medical devices. For example, magnetite, a metal oxide has great potential applications in nanomedicine. Nanoparticles can assist targeted delivery of chemotherapy drugs to specific cells, i.e. cancer cells. Superparamagnetic iron oxide nanoparticles (SPIONs) and ultra-small superparamagnetic iron oxide (USPIO) have also proved its significance for targeted drug delivery⁵⁹. Nanoparticles can improve the water-solubility of weakly soluble drugs. It can increase drug half-life, modify pharmacokinetics, perk up bioavailability, diminish drug metabolism, assist to controlled and targeted drug delivery, and also com-

bined drug delivery^{60–64}. According to the data by the International Agency for Research on Cancer (IARC), estimates nearly 13.1 million deaths due to cancer by 2030. It is obvious that the low survival rate occurs not because of scarcity of potent, natural, or synthetic antitumor agents but owing to inadequate drug delivery systems. This develops the requirement of technology advancement to need to develop carriers and delivery systems, capable of targeted and efficient delivery of the chemotherapeutic agents without unwanted systemic side effects⁶⁵. The solid lipid nanoparticles and nano-emulsions are the most employed lipid-based drug delivery particles. However, nanosilver based commercial products are capturing market.



Fig. 1. Technological tsunami due to nanotechnology.

The newly developed nanomaterials for theranostics are being employed alone or in association with “classical” drugs, e.g. cytostatic drugs, or antibiotics. Theranostics is a combined term for nanomaterials with diagnostic and therapeutic properties⁶⁴. Fig. 1 shows Technological tsunami occurs due to nanotechnology in the fields of energy storage, defense and security, metallurgy and materials, electronics, optical engineering and microelectromechanical systems (MEMS), biomedicine and drug delivery, agriculture, food science, cosmetics and paints, textile, etc.⁶⁶. According to Zion market research analysis in 2017⁶⁷, there is a rapid increase

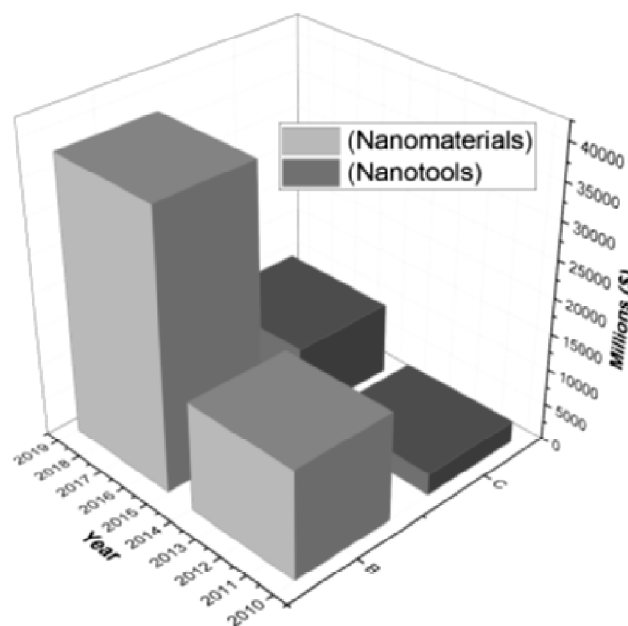


Fig. 2. Global nanotechnology review for nanomaterials, nanotools and nanodevices market from 2011 to 2017 (in Million USD).

of global nanomaterials market volume (in kilo tons) and revenue (in USD Billion), which is estimated from 2014 to 2022, is shown in Fig. 2(a). Other statistical surveys from two different agencies (see Fig. 2(b) and Fig. 2(c) (BCC research)) also confirmed the rapid increase of global nanotechnology market of nanomaterials, nanotools and nanodevices, etc.^{68,69}. Some important key points are summarized below about the advantages and growth of nanotechnology. The key benefits of nanotechnology are:

- (i) Reduction of size of any material, machine or equipment.
- (ii) Reduction of amount of energy and resource.
- (iii) Helps to clean up the existing nano-pollution.
- (iv) Able to secure economy once it can be fully implemented.
- (v) Can alter the basic of technology for human, in its matured phase.
- (vi) Early stage detection of some diseases.
- (vii) Improvement of the drug therapeutic index by increasing efficacy and/or reducing toxicities.
- (viii) Targeted delivery of drugs in tissue-, cell- or organelle-specific manner.

- (ix) Enabling sustained or stimulus-triggered drug release.
- (x) More sensitive cancer diagnosis and imaging.
- (xi) Better pharmaceutical properties like stability, solubility, and half-life of drug molecules.
- (xii) Approaches to develop synthetic vaccines.

Limitations of nanotechnology

Nanomaterials are being employed in different industries and everyday life. Therefore, the interplay of nanomaterials and human surroundings is worth scientific exploration. Nanomaterials with several benefits can be toxic in nature. Various studies also confer with the above-mentioned effects, indicating the potential toxicological effects on human environment⁶⁰. Different toxic and hazardous effects of nanotechnology are briefly discussed below.

Potential routes for nanomaterials to enter into human body:

Nanomaterials can enter into human body in various ways. Potential routes nanomaterials entry into human body are ingestion, inhalation and skin absorption⁷⁰. Many nanomaterials are employed in drug transport or cell imaging via intravenous entry to the human body. In the body, nanomaterials are translocated throughout the body by blood circulation. For the purpose, the nanoparticles must fulfill the requirement of permeability across the barrier of blood vessel wall. Absorption through the skin serves as an alternate route of entry for nanoparticles inside a human body. The skin is the largest organ of the human body, provides a large surface area for interactions with the external environment. TiO₂ nanoparticles can take either route for entry i.e. the lungs or gastrointestinal tract. Nanomaterials can enter into the body through skin due to various reasons, such as use of medicine, cosmetics, ointments and use of clothes containing nanomaterials, occupational contact in industry etc. Soaps, shampoos, toothpaste, hair gels, creams, and some cosmetics containing the nanosilver, which can enter into the body through skin. Cream or solution containing silver nanoparticles is used for treatment of wounds, burns, etc. to prevent infections and damaged skin and the size of nanoparticles drive the penetrating ability in cell. The smaller the nanoparticle, has a greater penetrating ability. The inhaled particulate matter gets accumulate in human respiratory tract, while one major portion of those inhaled particles gets deposited in the lungs. Nanoparticles also have

the potential to travel across the placenta in pregnant women to the fetus along with other organs i.e. brain, liver, spleen and induce lung inflammation and heart disease⁷⁰. The pulmonary inflammation is due to the inhalation of nano-sized urban particulate matter appear due to the oxidative stress, imposed by these particles in the cells^{60,71,72}. The first reported nanoparticle is nano-silver, which can damage DNA molecules. Silver nanoparticles have the most harmful effects on the most sensitive biological groups^{60,73–76}. This nanoparticle can penetrate into blood through the skin. Silver binds with the thiol group of some proteins. If silver complexes with thiol groups are located near-skin region, it gets readily available to get reduced either by visible or UV light into metallic nanosilver particles. This results in immobilization of silver nanoparticles in the skin. Further, the effect of nano copper-induced renal proximal tubule necrosis in kidneys has been reported by Liao and Liu⁷⁷.

Toxicity of nanomaterials:

Greater the human exposure of nanomaterials presents in environment, greater is the harmful effect on human health. The assessment of the cytotoxicity of nanomaterials assists in proper elucidation of their biological activity. Gerloff *et al.*⁷⁸ reported the cytotoxicity of various nanoparticles such as zinc oxide (ZnO), SiO₂, and TiO₂ on human Caco-2 cells. Shen *et al.*⁷⁹ showed the human immune cells are prone to toxicity due to ZnO nanoparticles⁸⁰. The ZnO nanoparticles damage mitochondrial and cell membranes in rat kidney ultimately leading to nephrotoxicity⁸⁰. Generally, nanomaterial toxicity mechanism comprises reactive oxygen species formation and genotoxicity. But as described earlier, toxicity of ZnO nanoparticles particularly affects immune cells. Various nanomaterials with their diverse sizes alter mitochondrial function. For example, ZnO nanoparticles generate Zn²⁺ ions, which disrupts charge balance in electron transport chain in the mitochondria and therefore triggers reactive oxygen species generation. Nanosilver particle has a genotoxic effect. Nanosilver (~20 nm) has a genotoxic effect on human liver HepG2 and colon Caco2 cells. It has also increased mitochondrial injury as well as loss of double-stranded DNA helix in both cell types⁸¹. TiO₂ nanoparticles inhalation, resulted in pulmonary overload in rats and mice with inflammation^{82,83}. The cytotoxic and genotoxic effects of TiO₂ nanoparticles on human lung have been reported by Jugan *et al.*⁸⁴. TiO₂ nanoparticles are genotoxic and it can induce pathological

damage of the liver, kidney, spleen, and brain. Du *et al.* reported cardiovascular toxicity of silica nanoparticles in rats⁸⁵. The surface coating of quantum dots causes toxicity to the skin cells including cytotoxicity and immunotoxicity⁸⁶. Nanosilver is used in wound dressings, affects both keratinocytes and fibroblasts. Fibroblasts show higher sensitivity towards nanosilver than by keratinocytes. Again, iron oxide nanoparticles rapidly get endocytosis on cultured human fibroblasts and interrupt the function. Citrate/gold nanoparticles have shown toxicity on human dermal fibroblasts⁸⁷. Carbon nanotubes have high toxicity and produce harmful effects on human. The nanoparticles can penetrate into the lungs, then reached blood and act as barrier for the circulation of blood into brain. They can also enter inside other organs like bone marrow, lymph nodes, spleen, or heart. Sometimes, nanoparticles can incite inflammation along with oxidant and antioxidant activities, oxidative stress, and change in mitochondrial distribution. These effects depend on the type of nanoparticles and their concentrations⁶⁹. Copper nano particles (diameter 40 nm and 60 nm) have harmful effect on brain cell at low concentration. It activated the proliferation of the endothelial cells in brain capillaries. Ag nanoparticles (25, 40, or 80 nm) influenced the blood-brain barrier, causing a proinflammatory reaction, which might induce a brain inflammation with neurotoxic effect. Smaller Ag nanoparticles (25 nm and 40 nm diameter) can induce cytotoxic effect at a greater rate compared to larger nanoparticles. Nanoparticles also have harmful effects on the brain cell of the mouse and rat. The high concentration of nanoparticles can affect brain blood fluxes, with consequent cerebral edema. Pathogenic effects of Ag-nanoparticles (25, 40, and 80 nm diameter), Cu-nanoparticles (40 and 60 nm) and Au-nanoparticles (3 and 5 nm) on the blood-brain barrier of pig have been reported⁸⁸. Silver nanoparticles (45 nm) influenced the acetylcholine activity via nitric oxide generation; it induces hyperactivity of rat tracheal smooth muscle⁸⁹. It is also reported that Ag-nanoparticles (25 nm) produced an oxidative stress after the injection into the mouse. The nanoparticles were aggregated in the kidneys, lungs, spleen red pulp and in the nasal airway, with no observable morphological changes apart from nasal cavity⁹⁰.

Very few cells do not undergo morphological changes after withstanding the air-liquid interface culture for an extended duration. Au-nanoparticles (5 nm and 15 nm diameter) penetrated into the mouse fibroblasts, where they re-

mained stocked. Only the presence of 5 nm Ag-nanoparticles disrupted cytoskeleton resulting in narrowing and contraction of cells. Many engineered nanomaterials, such as TiO₂, magnetite iron, CeO₂, carbon black, SWCNTs, and MWCNTs, also might cause different levels of inflammatory reactions, including enhanced pro-inflammatory cytokines expression, target inflammation-related genes, and micro-granulomas formation^{91,92}. The intra-tracheal administration of MWCNTs with variable length and iron content in hypertensive rats Led to the lung inflammation with increased blood pressure and lesions in abdominal arteries along with accumulation in multiple organs i.e. liver, kidneys, and spleen post 7 days and 30 days exposure⁹³. Maneewatttanapinyo *et al.* studied acute toxicity of colloidal silver nanoparticles administered in laboratory mice and observed neither any mortality any acute toxicity symptoms after a limited dose of 5.000 mg/kg post 14 days of oral administration. No differences could be observed in among groups after hematological and biochemical assessment and the histopathological study. The instillation of silver nanoparticles at the concentration of 5.000 ppm developed a transient eye irritation for 24 h. The application of these nanomaterials on skin did not produce any micro or macroscopic toxicity⁹⁴. The schematic mechanism of silver nanoparticles toxicity in human body is shown in Fig. 3⁹⁵. Liver and spleen are maximum exposed organs to nanomaterials owing to the prevalence of phagocytic cells in the reticuloendothelial system. Also, the organs with high blood flow such as kidneys and lungs can be affected.

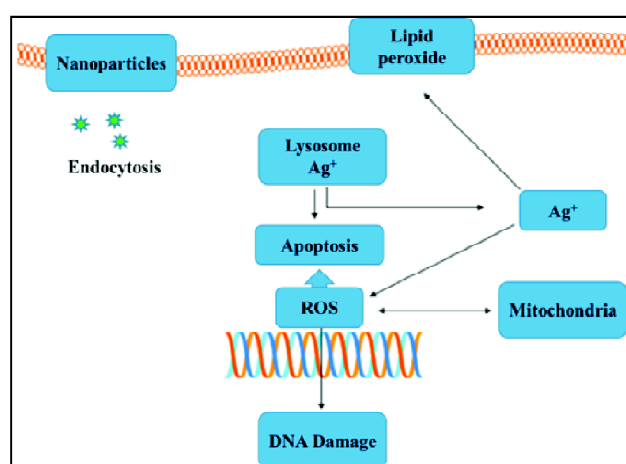


Fig. 3. Mechanism of silver nanoparticles toxicity (Abbreviations: NPs – nanoparticles; ROS – reactive oxygen species; Ag⁺ – silver ions) Redrawn from⁹⁵.

Health hazards in human:

In spite of having many benefits and uses the nanomaterials may cause health hazards to humans owing to very small size. The large absorption surface of lung, the thinner air-blood barrier, and comparatively less inactivation of enzymes leads to faster entry for particles into the systemic blood circulation at higher drug concentrations. Additionally, intentional uptake, exposure of particles carried by the wind from the environment, and nanoparticles released at manufacturing units may also cause health hazards for human. Usually, the biological effects of nanomaterials are based on their size, composition, shape and also on their electronic, magnetic, optical, and mechanical properties. Presently, the influence of nanotechnology on human health and environment is still controlled. Most of the studies assessed the outcomes of unintentional and accidental exposure (inhalation, medical procedures, or accidental ingestion) and focused on local effects only^{66,67}. Though, along with introducing nanomaterial-based biomedical procedures, it is mandatory to analyze their toxicity at a systemic level. Centuries before, Paracelsus said, "everything is a poison, and nothing is a poison, it is only a matter of a dose". For nanomaterials, it is applicable in both the aspects of dose and particle size⁶⁸. There is a huge demand for the use of nanomaterials in various applications, ranging from diagnostic technology, bio-imaging, to gene/drug delivery⁹⁶⁻⁹⁸. Therefore, intended or unintended human exposure to nanomaterials is unavoidable and has greater prospects of exposure in the future. Therefore, a branch of science is developing, named "nanotoxicology", the study of toxicity of nanomaterials. Nanotoxicology assess the role and safety of nanomaterials on human health. Several anthropogenic sources like power plants, internal combustion engines and other thermo-degradation reactions also generate nanoparticles and therefore develop the need to assess them as well⁶⁹.

Hazards in nanomedicine:

The nanomaterials represent a variety of biomedical applications, however, there is some potential risks factor related to the toxic issue. For example, cytotoxicity, genotoxicity, oxidative stress and inflammation have been reported on *in vitro* and *in vivo* models for testing nanoparticles. The difference in the size of nanomaterial and bulk comes with the differences in properties and toxicity as well. Nanomaterials are tremendously beneficial yet can be toxic. Ag, ZnO, or

CuO nanoparticles are frequently used as bactericides⁷⁹. But waste disposal in the environment can also negatively affect non-target organisms.

Hazards in medical instrumentation:

Nanomaterials are involved in medical interventions like prevention, diagnosis, and treatment of diseases. With development of science and technology, more accurate and multi functional medical diagnostic equipment are being fabricated for easy and safe operation. The 'lab-on-a-chip' technology facilitates instantaneous point-of-care testing, enhancing the standards of medical care. Nanomaterial based thin films on implant surfaces improve the wear and resist infection. But until now, these medical nanodevices are not 100% hazard free due to manufacturing processes, not following guidelines of nanotoxicity and also operating without the assessment of long term effects of nanotoxicity.

Hazards in food product:

Nanotechnology is used to produce advanced food products and smart packaging technology⁹⁹⁻¹⁰¹. In this way, the possibility of direct exposure of nanomaterials with human beings is enhanced and different types of long-term or short-term toxicity may occur^{102,103}. Nanoparticles and diamond-like nanocomposite (DLN) thin films are used in food packaging to reduce UV exposure and prolonged shelf life. Due to very few articles being reported in this area, further research is needed to fully explore the potential use of these nanoparticles for food products and medical treatments.

Environmental nanopollution and its effect in society:

Environment conservation is a challenging task. Its vastness and complexity make this even more difficult. As the production of nanomaterials is growing multiple issues concerning nanotechnology arise as environmental pollution and industrial exposure. Nanoparticles serve as pollutants in diesel exhaust or welding fumes, presenting new toxicological mechanisms^{104,105}. It also makes us face pollution in macro, micro, and nano-scale. New branches of electronics are also creating new sources of occupational exposure hazard. The circumstances produce new challenges for both classical toxicology and nanotoxicology. Though nanotechnology is improving the living standard, simultaneous increase in water and air pollution has also occurred. As the origin of this pollution lies in nanomaterials hence termed as "nanopollution". Nanopollution is extremely lethal to both

underwater flora and fauna and organisms living on soil. The pollutants can enter in human body in multiple ways. Cellular mechanisms can get affected by nanomaterial toxicity, which mainly comprises reactive oxygen species generation and genotoxicity^{105,106}. The nanoparticle's exposure on humans can occur unintentionally by environmental particles (e.g. air pollution) and deliberately because of a diversity of consumer products, cosmetics, and medical products containing nanoparticles. The release of nanoparticles during the manufacturing process may result in exposure on workers via dermal, oral, and inhalation routes. Exposure to air pollutants, such as ultrafine particles, is known to cause inflammatory air-way diseases and also cardiovascular problems in humans¹⁰⁷. Pope *et al.*¹⁰⁸ stated that even very very low amount of ambient nanoparticle exposure, have a momentous consequence on mortality. To decrease nanopollution, scientists and researchers used nanotechnology to develop nanofilters, which can eliminate almost all airborne particles¹⁰⁹.

Economic and social disruption due to rapid use of nanotechnology:

As the speed of nanotechnology development is growing, as a consequence the job opportunities are decreasing, arising the problem of unemployment in fields like industrial sector, manufacturing, and traditional farming¹¹⁰. Nanotechnology-based devices and machines have replaced humans to furnish the job more rapidly and efficiently, which has pointed out the importance of manpower in the field of practical work. Increasing growth and instant performance of nanotechnology have compromised the worth of commodities like diamond and oil. As an alternative technology i.e. nanotechnology has a detrimental effect on the demand as substitutes have more efficiency and do not need fossil fuels. Diamonds are losing the worth due to greater availability from nanotechnology-based fabrication methods. Currently, manufacturing companies are equipped for the production of the bulk of these products at a molecular scale, followed by disintegration to create new components.

At present, nanotechnology involves high investment technologies; raising the cost daily. The high cost is the resultant of intricate molecular structure and processing charges of the product. The whole process makes it difficult for manufacturers to randomly produce dynamic products using nanotechnology. Currently, it is an unaffordable business

owing to huge pricing of nanotechnology-based machines. Hence, nanotechnology can also bring financial risks as manufacturers have to invest large sum of money for setting up nanotech plants. The manufacturers have to face a huge loss if by any chance the manufactured products fail to satisfy the customers. Alternate options such as recovery of the original product or maintenance of the nanomaterials are also a costly and tedious affair. Further, nanotechnology does not leave any byproducts or residues, generally basis for the small industries, therefore creating huge risk of extinction for small scale industries. As an outcome, the quantity of sub-products of coal and petroleum is deteriorating. Another gigantic threat (like Covid-19 pandemic situation), which is born with the arrival of nanotechnology. It can make the easy accessibility of bio-chemical weapons or nano-bio engineered biological weapons. Nanotechnology is making these weapons more powerful and destructive. Unauthorized criminal bodies or corrupt politicians can steal the formulations and may reach these hazardous weapons easily and they can easily destroy our civilization¹¹¹.

Effect of nanotechnology on microorganisms, animals, and plants:

Some nanomaterials are not only hazardous to human beings but are also harmful to the existence of different microorganisms, animals, and plants. Man-made nanopollution is very much unsafe for living microorganisms, animals, and plants under the water or on the earth. As a result, many microorganism's families have completely disappeared from the world. Recently, due to rapid application of nanotechnology in the agriculture sector without proper nanotoxicological analysis, many plants are directly exposed to nanotoxicity and animals are indirectly exposed. Thus, in last two decades, a vast number of valuable plants and animals are completely disappeared from our world.

Key points about limitations of nanotechnology:

Some key points about limitations of nanotechnology are summarized below:

- (i) Still at its infancy stage.
- (ii) More research and developmental work need to be done.
- (iii) Expensive technology till now.
- (iv) Creates environmental nanopollution.
- (v) Huge initial cost for implementation.

(vi) Resistance from culture perspective, activists, journalists and even within the government.

(vii) Knowledge limitation from many industries and misperception among many fields about its capabilities.

(viii) Nanomaterials are not regulated by the government.

(ix) Requirement of large investment and research but yield is still a limiting factor.

(x) Some nanoparticles may be toxic to humans.

(xi) Nanotechnology made weapons are more powerful and more destructively increasing the explosion potential.

(xii) Lack of employment in the fields of traditional farming, manufacturing, and industrial sector.

Safety and security of nanotechnological developments

Nanotechnology is an extensively expanding field. Researchers, scientists, and engineers are getting high success to produce nano-materials and take the advantages of improved properties, such as higher strength, lighter weight, increased electrical conductivity, and chemical reactivity with respect to their macro equivalents¹¹². Human health concerns are also growing due to nanomaterials. The attempts of technological manipulations raise vocational risk to the workers in case of accidental exposures. Major cases of poisoning occur during coatings on the products. These micro or nano particles penetrate inside the brain, while in contact with humans and to lungs during inhalation. So it is matter of ethical issue. The problem can be addressed by using nanoscale materials to overcome the negative effects of micro or nano particles coatings in industry and health sectors. Academic and industry experts suggest that there exists ambiguity regarding the toxic effects of releasing nanoparticles into the environment. It is also noteworthy that, there is a lack of knowledge of nanoparticles interactions with humans and environment. Similar to most of the emerging technologies nanotechnology and nanochemistry industries have both benefits and challenges. To get maximum benefits the challenges must be overcome, managed and endured. Mesoporous silicates, alone or in combination with other inorganic or organic counterparts have been extensively explored for targeted drug delivery and cancer treatment. Even though the long-term toxicity of the nanoparticles is subjected to controversies and doubts, the use of gold and silver nanoparticles have provided more advantages in comparison to other actual alternatives (cytostatics). Conse-

quently, there is a growing interest in developing *in vitro* assays for nanotoxicology study¹¹³, it is strongly encouraged to use primary human cells as a source for *in vitro* study with nanoparticles since different origins of cancerous cell lines complicate data interpretation for human risk evaluation. Till now, the environmental effects and the toxicity of nanomaterials to organisms are in infancy state. The evaluation methods need to be cost-effective rapid, and quantity efficient.

Current policy and regulation status

The social implications of nanotechnology comprise of many fundamental aspects like ethics, privacy, environment, and security. Occasionally, the negative impacts on environment are too adverse to handle that the people simply give up. However, nanoscience researchers are still optimistic to see light of hope on the other side of the tunnel. Environmental clean-up is possible via design and manipulation of atomic and molecular scale of materials. It would develop cleaner energy production, energy efficiency, water treatment, and environmental remediation. Nanoscale fluid dynamics deciphers flow of nanoparticles in environment as a result of interactions with biological and environmental systems. Researchers are keen to understand the transportation of nanomaterials in association with environmental contaminants through groundwater systems. For food authenticity, safety, and traceability, every food company should need to use smart labels at stronger and innovative functional lightweight packaging. Now, each developed and developing countries have a separate policy and regulation for the use of nanotechnological products and applications. Explicit initiatives on nanotechnology must be needed to pledge that, the prospects provided by nanotechnology are not misused and research does not become bitty. The ambiguity, complication, and diversity of nanotechnology mean that any such initiative should not be a strictly predetermined closed program. Flexibility will be needed to stay side by side of development as they arise.

Challenges and future trends in using nanomaterials in humans

Nanotechnology-based production uses very little manpower, land, maintenance and it is cost-effective, high productivity with modest requirements of materials and energy. The extensively growing field offers scientists and engineers

a great opportunity to manipulate or alter the materials at nanoscale to yield benefit of enhanced material characteristics like enhanced strength, lightweight, higher electrical conductivity, and chemical activity in comparison to their large-scale counterparts. However, for biomedical applications, the toxicity evaluation of nanomaterials should be performed. Broadly, detailed physicochemical characterization of nanomaterial should be performed before and during any toxicity study. Important properties that can control nanomaterial-induced toxicity, including size and shape of the nanomaterials, coating, chemical composition, crystal growth, nanomaterials purity, structure, surface area, surface chemistry, surface charge, agglomeration, and solubility should also be taken care. Measurements should be performed in full stable state of nanomaterials in the most relevant test medium, i.e. aggregation status and ion release from metallic nanomaterials. Various engineered materials should be tested for their multidisciplinary tiered toxicity using diverse models and experiments^{114,115}. Therefore, the first step in the genotoxicity is an assessment of physicochemical properties of nanomaterials. The validation of the proposed tiered approaches is still waiting for future. The researchers are continuously trying to increase the relevant database with an increasing number of publications (papers, reviews, or even patents) every year¹¹⁶, particularly market share of the nanotechnology products is also growing up to thousands of billions of Euros¹¹⁷. Balanced use of the nanotechnologies/nanomaterials must be arranged, to optimize the opportunities/risks factors. Further research related to the size and shape, capping agents, receptors immobilization onto the metal nanoparticles are still a matter of keen interest with high necessity. Surface plasmon resonance can be tuned by varying sizes, shape of the nanomaterials and different surface functionalization of both silver and gold nanoparticles can reduce the toxicity and enhance a variety of biomedical applications in future. For example, CNT toxicity can be reduced via functionalization, surface coating, and stimulation of the autophagic flux. The amino functionalization decreases the CNT toxicity to the cells¹¹⁸, along with albumin coating for SWCNTs¹¹⁹.

Conclusions

Nanoparticles can enter and get distributed around the human body very easily. After entering into human, it moves within the body and creates cellular toxicity. Then it attacks

respiratory system, cardiovascular system, brain, skin, gut, and other organs. Again, some nanomaterials kill harmful bacteria within body and some of them kill good bacteria and live-cell of human body. Nanoparticles with different substances are used in SIM cards of cell phones or sunscreens. When these are used, free nanoparticles get released in the environment (air, water or soil). Engineering fields like civil and electronics also create new occupational health risks; making new potentially toxic nanomaterials. The toxicity of nanoparticles depends on their shape, size, and chemical composition. Centuries before, Paracelsus quoted, "everything is a poison, and nothing is a poison, it is only a matter of a dose". In regards to nanomaterials, the quotes hold value for both dose and particle size. The new interdisciplinary investigations explore the potentially harmful effects of these useful NPs and help in environmental preservation. Owing to smaller size the inhalation of nanomaterials imposes harmful effects on human health. The inhalation causes severe injury to the lungs and can also become fatal. The deterioration of lungs can be observed even after 60 s of nanoparticle inhalation. Therefore, for sustainable nanotechnology development, it is mandatory to evaluate and spread knowledge about the short term and long term exposure benefits and hazards for nanomaterials. To conclude, nanotechnology has the potential to impact society, both positively or negatively. Its consumers, producers and dealers include all the members of the society and all stakeholders; so we should collectively raise the voice in its various growth and commercialization phases. Currently, nanotechnology is in its infancy stage with a significant lack of awareness about its effects on humans and the environment. As civilization moves forward, the vital query is: how should we manage the risks and uncertainties of this emergent technology? Is anyhow COVID-19 pandemic situation manmade? If not, we can face such type of situations due to careless application of nanotechnology in different fields. However, all these limitations can be overcome itself by the rapid research on each such suspected fields of nanotechnology.

References

1. T. S. Santra, F-G. Tseng and T. K. Barik, *J. Nanopharmaceutics Drug Deliv.*, 2014, **2**, 1.
2. A. R. Jha (ed.), "MEMS and nanotechnology-based sensors and devices for communications, medical and aerospace applications", CRC Press, 2008.

3. I. L. Medintz, H. T. Uyeda, E. R. Goldman and H. Mattoussi, *Nat. Mater.*, 2005, **4(6)**, 435.
4. Y. Oshida (ed.), "Bioscience and bioengineering of titanium materials", Elsevier Science, eBookISBN: 9780080467191, 2006.
5. T. S. Santra, F.-G. Tseng and T. K. Barik, *Am. J. Nano Res. Appl.*, 2014, **2**, 5.
6. N. Savithamma, M. L. Rao, S. Ankanna and P. Venkateswarlu, *Int. J. Pharma. Sci. and Res.*, 2012, **3(4)**, 1141. <http://dx.doi.org/10.13040/IJPSR.0975-8232>.
7. P. S. Chikramane, A. K. Suresh, J. R. Bellare and S. G. Kane, *Homeopathy*, 2010, **99**, 231.
8. K. Aslan, Z. Leonenko, J. R. Lakowicz and C. D. Geddes, *J. Phys. Chem. B*, 2005, **109**, 3157.
9. J. J. Diao and Q. Cao, *AIP Adv.*, 2011, **1**, 012115. <https://doi.org/10.1063/1.3568815>.
10. J. K. Lim, K. Imura, T. Nagahara, S. K. Kim and H. Okamoto, *Chem. Phys. Lett.*, 2005, **412**, 41.
11. E. Hutter and D. Maysinger, *Microsc. Res. Tech.*, 2011, **74**, 592.
12. G. Schider, R. Krenn, A. Hohenau, H. Ditlbacher, A. Leitner, R. Aussenegg, L. Schaich, I. Puscasu, B. Monacelli and G. Boreman, *Phys. Rev. B: Condens. Matter Mater. Phys.*, 2003, **68**, 155427.
13. X. Lou, Y. Zhang, J. Qin and Z. Li, *Chem. - A Eur. J.*, 2011, **17**, 9691.
14. J. M. Pingarrón, P. Yáñez-Sedeño and A. González-Cortés, *Electrochim. Acta*, 2008, **53**, 5848.
15. C. D. Geddes, A. Parfenov, I. Gryczynski and J. R. Lakowicz, *Chem. Phys. Lett.*, 2003, **380**, 269.
16. M. Ra, A. Gade, S. Gaikwad, P. D. Marcato and N. Durán, *J. Braz. Chem. Soc.*, 2012, **23**, 14.
17. D. G. Yu, *Colloids Surfaces B: Biointerfaces*, 2007, **59**, 171.
18. Y. Tan, Y. Wang, L. Jiang and D. Zhu, *J. Colloid Interface Sci.*, 2002, **249**, 336.
19. C. Petit, P. Lixon and M. P. Pileni, *J. Phys. Chem.*, 1993, **97**, 12974.
20. S. A. Vorobyova, A. I. Lesnikovich and N. S. Sobal, *Coll. Surf. A*, 1999, **152**, 375.
21. K. Mallick, M. J. Witcomb and M. S. Scurrrell, *Mater. Chem. Phys.*, 2005, **90**, 221.
22. S. Kéki, J. Török, G. Deák, L. Daróczi and M. Zsuga, *J. Colloid Interface Sci.*, 2000, **229**, 550.
23. M. P. Pileni, *Pure Appl. Chem.*, 2000, **72(1-2)**, 53.
24. Y. P. Sun, P. Atorngitjawat and M. J. Meziari, *Langmuir*, 2001, **17**, 5707.
25. Y. C. Liu and L. H. Lin, *Electrochem. Commun.*, 2004, **6**, 1163.
26. G. Sandmann, H. Dietz and W. Plieth, *J. Electroanal. Chem.*, 2000, **491**, 78.
27. C. H. Bae, S. H. Nam and S. M. Park, *Appl. Surf. Sci.*, 2002, **197-198**, 628.
28. A. B. Smetana, K. J. Klabunde and C. M. Sorensen, *J. Colloid Interface Sci.*, 2005, **284**, 521.
29. K. Esumi, R. Isono and T. Yoshimura, *Langmuir*, 2004, **20**, 237.
30. A. Murugadoss, A. Khan and A. Chattopadhyay, *J. Nanoparticle Res.*, 2010, **12**, 1331.
31. H. Zhang, X. Li and G. Chen, *J. Mater. Chem.*, 2009, **19**, 8223.
32. Y. Sun and Y. Xia, *Science*, 2002, **298**, 2176.
33. R. Bhattacharya and P. Mukherjee, *Adv. Drug Deliv. Rev.*, 2008, **60**, 1289.
34. D. Raghunandan, P. A. Borgaonkar, B. Bendegumble, M. D. Bedre, M. Bhagawanraju, M. S. Yalagatti, D. S. Huh and V. Abbaraju, *Am. J. Anal. Chem.*, 2011, **02**, 475.
35. R. K. Bera, S. M. Mandal and C. R. Raj, *Lett. Appl. Microbiol.*, 2014, **58(6)**, 520.
36. K. Kathiresan, S. Manivannan, M. A. Nabeel and B. Dhivya, *Colloids Surfaces B: Biointerfaces*, 2009, **71**, 133.
37. Y. Konishi, T. Tsukiyama, K. Ohno, N. Saitoh, T. Nomura and S. Nagamine, *Hydrometallurgy*, 2006, **81**, 24.
38. E. Castro-Longoria, A. R. Vilchis-Nestor and M. Avalos-Borja, *Colloids and Surfaces B: Biointerfaces*, 2011, **83(1)**, 42.
39. D. S. Goodsell (ed.), "Bionanotechnology: Lessons from Nature", ISBN: 978-0-471-41719-4, 2004.
40. N. S. Thakur, B. P. Dwivedee, U. C. Banerjee and J. Bhaumik (ed.), "Bioinspired Synthesis of Silver Nanoparticles: Characterisation, Mechanism and Applications", eBook ISBN9781315370569, CRC Press, 2016.
41. J. Xie, J. Y. Lee, D. I. C. Wang and Y. P. Ting, *ACS Nano.*, 2007, **1**, 429.
42. M. Hayes (ed.), "Marine Bioactive Compounds: Sources, Characterization and Applications", DOI: 10.1007/978-1-4614-1247-2_2, Springer Science+Business Media, LLC, 2012
43. G. Wenqiang, L. Shufen, Y. Ruixiang and H. Yanfeng, *Nat. Prod. Res.*, 2006, **20**, 992.
44. D. Fawcett, J. Verduin, M. Shah, S. Sharma and G. E. J. Poinern, *J. Nanoscience*, Article ID 8013850, 2017, DOI: 10.1155/2017/8013850.
45. S. Cox, N. Abu-Ghannam and S. Gupta, *Int. Food Res. J.*, 2010, **17**, 205.
46. M. De Pádua, P. S. G. Fontoura and A. L. Mathias, *Brazilian Arch. Biol. Technol.*, 2004, **47**, 49.
47. P. Kumari, M. Kumar, V. Gupta, C. R. K. Reddy and B. Jha, *Food Chem.*, 2010, **120**, 749.
48. S. Ravikumar, S. Krishnakumar, S. J. Inbaneson and M. Gnanadesigan, *Archives of Applied Science Research*, ISSN 0975-508X, 2010, **2(6)**, 273.

Barik et al.: Prospect of nanotechnology: A brief Review

49. S. Krishnakumar, J. Premkumar, R. Alexis Rajan and S. Ravikumar, *Int. J. Appl. Bioengineering*, 2011, **5(2)**, 12.
50. P. Manivasagan, J. Venkatesan and S.-K. Kim (ed.), "Marine Algae: An Important Source of Bioenergy Production", eBook ISBN9780429076282, CRC Press, 2015.
51. S. Ermakova, M. Kusaykin, A. Trincone and Z. Tatiana, *Front. Chem.*, 2015, **3**, 39.
52. J. Venkatesan, I. Bhatnagar, P. Manivasaga, K. H. Kang and S.-K. Kim, *Int. J. Biol. Macromol.*, 2015, **72**, 269.
53. A. M. Fayaz, K. Balaji, M. Girilal, R. Yadav, P. T. Kalaiichelvan and R. Venketesan, *Nanomedicine*, 2010, **6(1)**, 103.
54. G. Roymahapatra, Towels Made of Nano Cloth - An Alternative Concept, 'Charoibeti', published on the occasion of 14th Years Celebration of Education and Health Day organized by 'Smile', 12th January, 2018
55. T. S. Santra, T. K. Bhattacharyya, F. G. Tseng and T. K. Barik, *AIP Adv.*, 2012, **2**, 022132.
56. T. S. Santra, T. K. Bhattacharyya, P. Patel, F. G. Tseng and T. K. Barik, *Surf. Coatings Technol.*, 2011, **206**, 228.
57. T. S. Santra, C. H. Liu, T. K. Bhattacharyya, P. Patel and T. K. Barik, *J. Appl. Phys.*, 2010, **107**, 124320.
58. T. S. Santra, T. K. Bhattacharyya, P. Mishra, F. G. Tseng and T. K. Barik, *Science of Advanced Materials*, 2012, **4(1)**, 110, doi.org/10.1166/sam.2012.1258.
59. D. De, S. M. Mandal, J. Bhattacharya, S. Ram and S. K. Roy, *Journal of Environmental Science and Health. Part A, Toxic/Hazardous Substances and Environmental Engineering*, 2009, **44(2)**, 155.
60. S. M. Mandal, W. F. Porto, D. De, A. Phule, S. Korpole, A. K. Ghosh, S. K. Roy and O. L. Franco, *The Analyst*, 2014, **139(2)**, 464.
61. R. Singh and J. W. Lillard, *Exp. Mol. Pathol.*, 2009, **86(3)**, 215.
62. A. Z. Wang, R. Langer and O. C. Farokhzad, *Annu. Rev. Med.*, 2012, **63**, 185.
63. T. W. Prow, J. E. Grice, L. L. Lin, R. Faye, M. Butler, W. Becker, E. M. T. Wurm, C. Yoong, T. A. Robertson, H. P. Soyer and M. S. Roberts, *Adv. Drug Deliv. Rev.*, 2011, **63(6)**, 470.
64. J. Xie, S. Lee and X. Chen, *Adv. Drug Deliv. Rev.*, 2010, **62(11)**, 1064.
65. L. Brannon-Peppas and J. O. Blanchette, *Adv. Drug Deliv. Rev.*, 2004, **56**, 1649.
66. <https://www.iberdrola.com/innovation/nanotechnology-applications>.
67. <https://www.zionmarketresearch.com/news/nanomaterials-market>.
68. <https://www.statista.com/statistics/1073886/global-market-value-nanotechnology>.
69. [https://www.bccresearch.com/pressroom/nan/global-nanotechnology-market-to-reach-\\$64.2-billion-in-2019](https://www.bccresearch.com/pressroom/nan/global-nanotechnology-market-to-reach-$64.2-billion-in-2019).
70. A. Elsaesser and C. V. Howard, *Adv. Drug Deliv. Rev.*, 2012, **64(2)**, 129.
71. T. Papp, D. Schiffmann, D. Weiss, V. Castranova, V. Vallyathan and Q. Rahman, *Nanotoxicology*, 2008, **2**, 9.
72. G. Oberdörster, E. Oberdörster and J. Oberdörster, *Environ. Health Perspect.*, 2005, **113**, 823.
73. S. A. Love, M. A. Maurer-Jones, J. W. Thompson, Y.-S. Lin and C. L. Haynes, *Annu. Rev. Anal. Chem.*, 2012, **5**, 181.
74. M. Ahamed, M. S. AlSalhi and M. K. J. Siddiqui, *Clin. Chimica Acta*, 2010, **411**, 1841.
75. A. Manke, L. Wang and Y. Rojanasakul, *Biomed Res. Int.*, 2013, **2013**, 1.
76. C. Beer, R. Foldbjerg, Y. Hayashi, D. S. Sutherland and H. Autrup, *Toxicol. Lett.*, 2012, **208**, 286.
77. M. Y. Liao and H. G. Liu, *Environ. Toxicol. Pharmacol.*, 2012, **34**, 67.
78. K. Gerloff, C. Albrecht, A. W. Boots, I. Frster and R. P. F. Schins, *Nanotoxicology*, 2009, **3**, 355.
79. C. Shen, S. A. James, M. D. De Jonge, T. W. Turney, P. F. A. Wright and B. N. Feltis, *Toxicol. Sci.*, 2013, **136**, 120.
80. G. Yan, Y. Huang, Q. Bu, L. Lv, P. Deng, J. Zhou, Y. Wang, Y. Yang, Q. Liu, X. Cen and Y. Zhao, *J. Environ. Sci. Heal., Part A*, 2012, **47**, 577.
81. S. C. Sahu, J. Zheng, L. Graham, L. Chen, J. Ihrle, J. J. Yourick and R. L. Sprando, *J. Appl. Toxicol.*, 2014, **34**, 1155.
82. M. Semmler, J. Seitz, F. Erbe, P. Mayer, J. Heyder, G. Oberdörster and W. G. Kreyling, *Inhal. Toxicol.*, 2004, **16**, 453.
83. J. Ferin, G. Oberdörster and D. P. Penney, *Am. J. Respir. Cell Mol. Biol.*, 1992, **6**, 535.
84. M. L. Jugan, S. Barillet, A. Simon-Deckers, S. Sauvaigo, T. Douki, N. Herlin and M. Carrière, *J. Biomed. Nanotechnol.*, 2011, **7**, 22.
85. Z. Du, D. Zhao, L. Jing, G. Cui, M. Jin, Y. Li, X. Liu, Y. Liu, H. Du, C. Guo, X. Zhou and Z. Sun, *Cardiovasc. Toxicol.*, 2013, **13**, 194.
86. H. Shi, R. Magaye, V. Castranova and J. Zhao, *Part. Fibre Toxicol.*, 2013, **10**, 1.
87. R. Landsiedel, L. Ma-Hock, T. Hofmann, M. Wiemann, V. Strauss, S. Treumann, W. Wohlleben, S. Gröters, K. Wiench and B. Van Ravenzwaay, *Fibre Toxicol.*, 2014, **11**, 16.
88. W. J. Trickler, S. M. Lantz-Mcpeak, B. L. Robinson, M. G. Paule, W. Slikker, A. S. Biris, J. J. Schlager, S. M. Hussain, J. Kanungo, C. Gonzalez and S. F. Ali, *Drug Metab. Rev.*, 2014, **46**, 224.
89. C. González, S. Salazar-García, G. Palestino, P. P. Martínez-Cuevas, M. A. Ramírez-Lee, B. B. Jurado-Manzano, H. Rosas-Hernández, N. Gaytán-Pacheco, G. Martel, R. Espinosa-Tanguma, A. S. Biris and S. F. Ali, *Toxicol. Lett.*, 2011, **207**, 306.

90. M. B. Genter, N. C. Newman, H. G. Shertzer, S. F. Ali and B. Bolon, *Toxicol. Pathol.*, 2012, **40**, 1004.
91. H. Tsuda, J. Xu, Y. Sakai, M. Futakuchi and K. Fukamachi, *Asian Pac. J. Cancer Prev.*, 2009, **10**, 975.
92. E. J. Park, H. Kim, Y. Kim, J. Yi, K. Choi and K. Park, *Toxicology*, 2010, **275**, 65.
93. R. Chen, L. Zhang, C. Ge, M. T. Tseng, R. Bai, Y. Qu, C. Beer, H. Autrup and C. Chen, *Chem. Res. Toxicol.*, 2015, **28**, 440.
94. P. Maneewattanapinyo, W. Banlunara, C. Thammacharoen, S. Ekgasit and T. Kaewamatawong, *J. Vet. Med. Sci.*, 2011, **73**, 1417.
95. S. Clichici and A. Filip, "in vivo Assessment of Nanomaterials Toxicity", in: *Nanomater. - Toxic. Risk Assess.*, InTech, 2015, 93.
96. P. Shinde, A. Kumar Kavitha, K. Dey, L. Mohan, S. Kar, T. K. Barik, J. Sharifi-Rad, M. Nagai and T. S. Santra, "Physical approaches for drug delivery", in: *Deliv. Drugs*, Elsevier, 2020, 161.
97. T. S. Santra, P. C. Wang, H. Y. Chang and F. G. Tseng, *Appl. Phys. Lett.*, 2013, **103**, 233701.
98. A. K. Narasimhan, S. B. Lakshmi, T. S. Santra, M. S. R. Rao and G. Krishnamurthi, *RSC Adv.*, 2017, **7**, 53822.
99. C. Silvestre, D. Duraccio and S. Cimmino, *Prog. Polym. Sci.*, 2011, **36(12)**, 1766.
100. S. D. F. Mihindukulasuriya and L. T. Lim, *Trends Food Sci. Technol.*, 2014, **40(2)**, 149.
101. B. S. Sekhon, *Nanotechnol. Sci. Appl.*, 2010, **4(3)**, 1.
102. V. K. Bajpai, M. Kamle, S. Shukla, D. K. Mahato, P. Chandra, S. K. Hwang, P. Kumar, Y. S. Huh and Y. K. Han, *J. Food Drug Anal.*, 2018, **26(4)**, 1201.
103. Q. Chaudhry, M. Scotter, J. Blackburn, B. Ross, A. Boxall, L. Castle, R. Aitken and R. Watkins, *Food Addit. Contam. - Part A: Chem. Anal. Control. Expo. Risk Assess.*, 2008, **25(3)**, 241.
104. R. K. Ibrahim M. Hayyan, M. A. Alsaadi, A. Hayyan and S. Ibrahim, *Environ. Sci. Pollut. Res.*, 2016, **23**, 13754.
105. P. Mehndiratta, A. Jain, S. Srivastava and N. Gupta, *Environ. Pollut.*, 2013, **2(2)**, 49.
106. B. Zhang, H. Misak, P. S. Dhanasekaran, D. Kalla and R. Asmatulu, *Am. Soc. Eng. Educ.*, 2011, **1845(1)**, 1.
107. V. C. Van Hee, J. D. Kaufman, G. R. Scott Budinger and G. M. Mutlu, *Am. J. Respir. Crit. Care Med.*, 2010, **181**, 1174.
108. A. C. Pope, R. T. Burnett, D. Krewski, M. Jerrett, Y. Shi, E. E. Calle and M. J. Thun, *Circulation*, 2009, **120**, 941.
109. N. Bernd, *Nanotechnology*, 2005, **39(5)**, 106A.
110. S. Wood, A. Geldart and R. Jones, *TATuP-Zeitschrift Für Tech. Theor. Und Prax.*, 2003, **12**, 7.
111. A. Khan, Ethical and social implications of nanotechnology, *QScience Proc.*, 2015. <https://doi.org/10.5339/qproc.2015.elc2014.57>.
112. Encyclopedia of Nanotechnology, 2012. <https://doi.org/10.1007/978-90-481-9751-4>.
113. S. Arora, J. M. Rajwade and K. M. Paknikar, *Toxicol. Appl. Pharmacol.*, 2012, **258**, 151.
114. K. Savolainen, H. Alenius, H. Norppa, L. Pylkkänen, T. Tuomi and G. Kasper, *Toxicology*, 2010, **269**, 92.
115. A. Kumar and A. Dhawan, *Arch. Toxicol.*, 2013, **87**, 1883.
116. Scopus-Document search Signed in, (n.d.). <https://www.scopus.com/search/form.uri?display=basic> (accessed June 9, 2020).
117. Nanomaterials: Toxicity and Risk Assessment - Google Books, (n.d.). <https://books.google.co.jp/books/> (accessed June 9, 2020).
118. W. Chen, Q. Xiong, Q. X. Ren, Y. K. Guo and G. Li, *Neural Regen. Res.*, 2014, **9**, 285.
119. Y. Liu, L. Ren, D. Yan and W. Zhong, *Part. Part. Syst. Charact.*, 2014, **31**, 1244.

ISSN : 2319-5282

EDU CARE

A Multidisciplinary International
Peer Reviewed/Refereed Journal

Vol. IX, Number - 8

January-December, 2020

Chief Editor

Dr. S. Sabu

Principal, St. Gregorios Teachers' Training College, Meenangadi P.O.,
Wayanad District, Kerala-673591. E-mail: drssbkm@gmail.com

Co-Editor

S. B. Nangia

A.P.H. Publishing Corporation

4435-36/7, Ansari Road, Darya Ganj,

New Delhi-110002

Children Education During COVID-19 Pandemic and Related NSS Activities

Dr. Tarun Kumar Barik*

ABSTRACTS

During the COVID-19 pandemic, we are facing a serious living and learning crisis. Children and youth of primary, secondary and higher secondary school age were out of school. Actually, COVID-19 threatens the education system from a bad to worst situation day by day and creates a gigantic shock to all education systems in our lifetimes. Different crisis and approach to recover children's education system from this hazardous emergency situation and related NSS activities have been summarized in this article. The schools, colleges and universities need proper master plan to start reopening and stabilizing the education system slowly but more carefully. The present analysis suggests to emphasis on the maintenance of hygiene level, following digital systems and regular basis online counseling of school children are required on priority basis. School authorities are most responsible to upgrade their digital systems timely and make a long-term resilience in our education system. NSS volunteers play a prime role to spread the awareness through online and one to one personal communication about the importance of hand hygiene, respiratory hygiene, social distancing, importance of mask wearing in the public places and also the importance of COVID-19 vaccination.

Keywords: COVID-19; Hygiene, Online Education, NSS

INTRODUCTION

The shocking pandemic outbreak of coronavirus disease -2019 (COVID-19) is a severe threat to our human society. COVID-19 is caused by a new type corona virus, SARS-CoV-2 (Severe acute respiratory syndrome coronavirus 2) and in the case of infection, most of the people fall sick with mild to moderate symptoms. It becomes deadly serious when virus transmitted to lungs and subsequently occurred complications like acute respiratory failure. The virus spread easily among people by person to person contact (within about 6 feet, or nearly 2 meters), by the droplets released from coughing, sneezing or talking of infected person. Till now, COVID-19 patient's complications, risk factors and prevention strategies are announced and well documented. Researchers through worldwide have already discovered COVID-19 vaccines; most of them have completed phase-3 clinical trials successfully. Doctors are trying to manage the symptomatic treatment to increase the recovery rate. However, whole World is following the lockdown based option of prevention strategy by staying home as much as possible to stop the spreading in our community. It is recommended to work from home. It is going for long days that will make an immense problem in our society or nation. This is the era of World Wide Web (www), where maximum work can complete by the help of web based technologies. Therefore, the educational systems have the major role in this period to grow up our nation in a required standard. The Post-COVID emergence or ongoing the pandemic scenario have multidirectional consequences on various spheres of life apart from deterioration of human health. The economical

cost associated with COVID-19 pandemic is very high as it inferred from high costs of medical and intensive care, loss of productive working days, major impact on travel and tourism, ban on export of agricultural product from affected regions, etc. Similarly, if the growths of educational systems become weaken that can't be compensated by means of anything else. Students' mental health is also very much important for his learning, appearance and attitude. In this critical situation, the roles of teachers are extraordinarily important to save our student's health and growth our nation.

SHARING OF KNOWLEDGE ON HEALTH AND HYGIENE

Hygiene is the attitude, behaviour and practices for the protection of health consequently healthy living. Poor health hygiene practices are the major cause of several communicable diseases in developing countries, the primary causes of morbidity and mortality among young or school children are the acute respiratory and intestinal infections [1]. School is the only place where students acquire not only education but also provoke their attitude, behaviour and environment. The United Nations Children's Fund (UNICEF) confirmed that knowledge, attitudes, and practices (KAP) are the basic principle of hygiene. Simple hygienic process by washing hands with soap is poorly practiced in India and almost no culture in any school, college or university systems. It is necessary to prepare real hand washing facilities including enough knowledge in awareness which may lead to some changes in behaviour and attitude. Lack of resources like soap, sanitizing material, and very poor sanitizing system in educational institutes in India may be the main reasons not to develop their attitude and behavior.

Recent awareness regarding the pandemic outbreak of coronavirus disease (COVID-19) is extremely important due to its pathogenic and contamination nature because it is caused by a virus SARS-CoV-2. Currently, COVID-19 has caused global health concern. Human to human transfer by contact or through the aerosols from sneezing and coughing is widely confirmed. To reduce the transmission of current outbreak, lockdown emergency is going on including banned the international and domestic flights and social distancing etc. World health Organization (WHO) gives a general advice on how to comply with "social distancing" while also fulfilling family and work responsibilities and provides guidance on the hygiene measures to protect someone from infected patients. All the students must have to follow the points in future and make their attitude to continue with these habits:

- Wash hands with soap and water before and after meal for at least 20 seconds.
- Wash hands with soap and water after toilet and urination.
- Maintain good respiratory hygiene (covers mouth and nose when coughing or sneezing and immediately disposes of tissues and wash hands).
- Use alcohol-based (>70%) hand sanitizers when necessary.
- Provide basic knowledge about how sanitizers and soap kills the virus (SARS-CoV-2).
- Avoid touching eyes, nose and mouth.
- Clean and disinfect surfaces you use often such as bench tops, desks and doorknobs
- Increase the amount of fresh air by opening windows or changing air conditioning
- Frequent cleaning of work surfaces and touch points such as door handles etc.
- Use mask when it is necessary to go outside.

The maintenance of personal hygiene is of great importance to decrease the trouble of not only COVID-19 but also from any other infectious diseases.

Emphasis on Home School

Recently, the COVID-19 pandemic has altered the education system all over the world. Globally due to pandemic situation, billions of students are out of their usual classrooms teaching. As a result education has changed noticeably, with the characteristic rise of e-learning, whereby teaching is

Accessed remotely on digital platforms. Recent research suggests that online learning has been shown to increase retention of information, and take less time [2]. While some people believe that unplanned and rapid move to online learning – without proper training, insufficient bandwidth, and little preparation – will result in a poor user experience that is un-conducive to sustain growth. In the other hands, others believe that a new hybrid model of digital education will emerge with significant benefits. According to Wang Tao, Vice President of Tencent Cloud and Vice President of Tencent Education "The integration of information technology in education will be further accelerated as online education will eventually become an integral component of school education". Again, according to Dr. Amjad, a professor at the University of Jordan, who has been using Lark to teach his students, says, "It has changed the way of teaching. It enables me to reach out to my students more efficiently and effectively through chat groups, video meetings, voting and also document sharing, especially during this pandemic. My students also find it is easier to communicate on Lark. I will stick to Lark even after coronavirus, I believe traditional offline learning and e-learning can go hand by hand." [2] There are, however, challenges to overcome online learning. Some students do not have reliable internet access and/or technology struggle to participate in digital learning; this gap is seen across countries and between income brackets within countries. Hence, schools, college, ministry or government authorities should think about this matter seriously in near future for uniform learning [2]. For those, who do have access to the right technology, there is evidence that learning online can be more effective in a number of ways. Some research shows that on average, students learn 25-60% more material when learning online compared to only 8-10% in a classroom. This is mostly due to the students being able to learn faster online; e-learning requires 40-60% less time to learn than in a traditional classroom setting because students can learn at their own swiftness, go back and re-reading, skipping, or accelerating through concepts as they choose [2]. But the effectiveness of online learning varies amongst age groups. BYJU's Mrinal Mohit says "Over a period, we have observed that clever integration of games has demonstrated higher engagement and increased motivation towards learning especially among younger students, making them truly fall in love with learning". It is clear that this pandemic has completely disrupted the education system, while some worry that the hasty nature of the transition online may have hindered the goal, others plan to make e-learning part of their 'new normal' after experiencing the benefits first-hand [2]. Like, e-commerce post-SARS, it is yet to see an inflection point for rapid innovation occurs in the case of e-learning post-COVID-19.

The horror of Covid-19 outbreak has shut-down schools, college and universities in India. Preliminary data analysis about online teaching indicates that it is a non-starter for most students and institutions in India. Maximum student of India comes from backward class of rural or urban area, where less possibility of access home internet. Actually, it is easy to connect to one set of students, reaching others through the internet would be tough. The digital divide should be evident in teaching resources but every student must have access to it. Few privileged educational institutions in India have good platform of e-learning because of their maximum students come from a creamy society but other have to struggle with inequality for successful implementation of digital drive of e-learning at home. However, internet access at home is pitifully low in India. This is a combination of low internet coverage in India as well as the fact that many households do not own smart phones that can get them on the internet. As the Covid-19 infections rise in India, and there is justified pressure to keep educational institutions closed, one must be mindful of these numbers when suggesting online teaching. While the long-term strategies may involve increasing internet connectivity, or subsidizing data on mobiles, it would seem that device ownership is as much a worry, especially for children coming from rural places. If universities remain closed for a long time, it is important for the universities to subsidize cheap smart phones for students

to get on with the business of teaching. This is in addition to any subsidies that need to be paid for bandwidth (assuming that it is a surmountable problem). Without such help, online teaching is a non-starter for most institutes of India. Central- and state-government, different NGOs and every hearty peoples of India should come forward and work together to solve this inequality in the post pandemic situation and should fulfill the dream of digital India.

At the time of nationwide lockdown schools, colleges and universities are depending on the online mode of teaching in order to maintain the continuity of education. Schools are launching apps, conducting classes over Google meet/ Google Hangouts / Zoom / Teams, and sending interactive worksheets and videos for learning in WhatsApp or facebook groups. Even though Internet-based teaching is the most appropriate stop-gap arrangement now, it has highlighted the inequalities in the education system in major portion of India. A majority of the student population is being left out in the pursuit of basic education. Many schools, colleges and universities of India are using WhatsApp or facebook groups, to connect to their students or guardians. Teachers have been asked to make WhatsApp group of all parents in their respective classes and send those lessons so that students can learn at home. Teachers are taking help from the central government's digital learning portal DIKSHA, which has lessons in multiple languages for all classes from primary to UG/PG. Some teachers are also making videos on practical concepts and these videos are then shared on the WhatsApp groups to connect to their students. As for example, nearly 50% school students (of class-V to Class-XII) and 75% college or university students of Medinipur municipality, Paschim Medinipur, West Bengal, India are accessing this facility. The students below the class-V of the above locality have accessed e-learning facilities only 20%. On the other hand, the situation of rural students of Paschim Medinipur district is very bad compared to students of urban area [This is the approximate data survey by the author in his district]. Table-I shows the list of e-learning resources, platforms and educational applications to help parents, teachers, school/college/university administrators, and students during the COVID-19 outbreak [3].

Resource Generation by Teachers

School teachers have to be more conscious about their teaching and course work generation. It may not be the same as in practical class teaching. School teachers can sign up to provide their teaching material to enrolled students with full and free access or make web based industry partners. They must be careful about a long-term plan for web based virtual learning classes and accordingly design their course work. Few important points are discussed below to sharing the knowledge and resource management-

- **Design an online course-** Develop online course tutorial for classroom, planning and designing online lessons following modern and advanced educational tools.
- **Be an online tutor-** Self practice necessary training to teaching about online education processes. Follow several online teaching modules like Online Learning Technology Landscape, e-learning management tools, and communication and creation tools.
- **Directory of open educational resources-** There are over 7000 resources on higher education, open schooling, teacher education, and technical and vocational skills development. anyone can take help.
- **Open resources for english language teaching** is intended to support classroom activities for teachers.
- **COL's Institutional repository** provides access to a large number of resources on online learning and guides to help teachers plan, design, develop and offer quality online learning.
- **Digital/ WhatsApp and Facebook educator Information hub** may consider engaging with your students on WhatsApp and make group. Be part of what's happening around the world in real-time, no matter where you are.

BUILD UP THE LONGER-TERM RESILIENCE OF EDUCATION SYSTEMS

It is commonly accepted that countries demand well-built education systems that advocate knowledge, life skills, and social consistency. However, systems sometimes fail to deliver education services in adverse situation such as natural disaster, political crisis, health epidemic, invasive violence, and armed quarrel etc. Ironically, education can also lend a hand to take the edge off the risks of such hardship and help students to succeed over the situation despite of unremitting challenges. This is one aspect of the kind of pliability of individuals, communities, and the institutions that providing development to convalesce and understanding positive change in the face of hardship. The Education Resilience Approaches (ERA) program applied by World Bank Group (WBG) is an important tool in facing this hardship [5]. This program is designed to provide relative analysis of resilience processes in education system based on local statistics on adversity, school-neighbourhood relations, education policies, and services in adverse situation. Several countries have been using 'Systems Approach for Better Education Results (SABER)' to analyze various aspects of their education systems [6]. WBG launched the 'Education Sector Strategy 2020: Learning for All', in 2011, with the aim to 'Invest early, invest smartly, and invest for all [7]. The strategy "holds that investments in education should achieve learning for all because growth, development and poverty reduction depend on the knowledge and skills that people acquire, not the number of years that they sit in a classroom." The main theme of SABER is to provide 'Learning for All' by targeting on three main pillars (i) "Public access to systematic, accurate, and comparable data on the quality of countries' education policies and the quality of implementation of those policies", (ii) "Awareness and utilization of these data by countries and development partners in sector analyses, policy dialogue, and planning processes", (iii) "More informed global discussion and debate about strengthening education systems to increase countries' learning for all". These areas are supposed to take part in a big role in education system reforms on both for a country and global level also. There are thirteen domains that are currently evaluated through SABER, and education resilience is a major domain among these. The thirteen areas are- (i) Early Childhood Development (ECD), (ii) Education Management and Information Systems (EMIS), (iii) Education Resilience (ERA), (iv) Engaging the Private Sector (EPS), (v) Equity and Inclusion (E&I), (vi) Information and Communication Technologies (ICT), (vii) School Autonomy and Accountability (SA&A), (viii) School Finance (SF), (ix) School Health and School Feeding (SH&SF), (x) Student Assessment (SA), (xi) Teachers (T), (xii) Tertiary Education (TE), (xiii) Workforce Development (WFD). The initial focus of SABER is to evaluate education environments by investigating the existing documented education policies. Then assess the efficacy of these policies and institutions in practice at the classroom level, and to identify policy implementation gaps within and across countries. SABER then propose a new tool to explicate the linkages between these gaps to explore an overall systems approach. Knowledge regarding human development and learning has grown at a rapid pace; the opportunity to shape more effective educational practices has also increased.

Even before the COVID-19 pandemic, the world was living a learning crisis. Before the pandemic, 258 million children from primary and secondary-school age, were out of school education system. Another adverse impact is of low schooling quality which means many students, who were in school learned too little. It can be defined as 'Learning Poverty'. The Learning Poverty rate in low-and middle-income countries was 53 % percent before COVID-19 pandemic, meant that more than half of all 10-year-old children couldn't read and comprehend a simple story. Even worse, the most underprivileged children had the worst access to schooling leads to highest dropout rates, and the largest learning deficits. It proves that, the world was already far behind the target of 'Sustainable Development Goal (SDG)', which include, "all girls and boys complete

free, equitable and quality primary and secondary education " The COVID-19 pandemic added new challenges in this context. The pandemic has created a deep impact on education by closing schools almost everywhere in the world. It has impacted nearly 1.57 billion learners out of school and 191 country-wide school closures, impacting 91.3% of the world's total enrolled learners as per UNESCO estimation up to April 20, 2020. Drop-out rates across the globe are likely to rise as a result of this massive disruption to education access [8, 9]. It has created a severe dent to all education systems in our lifetimes. The damage will become even more rigorous as the COVID-19 pandemic will be translated into global recession. Out of school, children are more likely to be exposed to risks like child labor, family violence, forced marriage, trafficking and exploitation and so many. For the most vulnerable children, education is life saving drug, it also inculcate hope for a brighter future. However, it is possible to counter this damage, and to turn emergency in to opportunity. The first step is to manage effectively with the school closures, by protecting health, safety and doing what they can to prevent students' learning loss using remote learning. Secondly, countries need to start planning for reopening of school with a proper framework. That means preventing dropout, ensuring healthy school conditions, and using new techniques to promote rapid learning recovery, once the students are back in school. Teachers have a major role in framing out the new system, within the school as well as the government systems, and also to implement them effectively at earliest. And during the Lockdown, continuing education through alternative learning pathways must also be a top priority right now, to ensure the interruption to education is as limited as possible. We urgently need to support teachers, parents/caregivers, innovators, communications experts and all those who are positioned to provide education, whether through radio programmes, home-schooling, online learning and other innovative approaches

REGULAR BASIS ONLINE COUNSELING

The pandemic has radically changed the concept of traditional education in the past few months and virtual learning will be the new future of education. Before the pandemic, technology was just considered as a means of entertainment. Today, keeping teachers and the students engaged in learning process has become the priority during lockdown, and virtual classes have proved to be helpful in these difficult times. This powerful medium has diversified the field of teaching. Earlier, teachers were not so familiar with online teaching at the school level, except for the computer lectures. Now, along with teachers, every profession has chosen the virtual platform, providing precious opportunities to both new learners and experts. There appears to be no deficiency of online resources of academic value. And therefore, online teaching is more an opportunity than a challenge for teachers today. Mental health of students is the topic of major concern during COVID-19 pandemic, especially when school and colleges and other academic institutes are closed due to 'LOCK DOWN'. The overall education is not only dependent on academic curriculum but also on his mental health. Disturbances in the mental health have an extreme negative impact to a student and also on the community. Today's student is the future citizen of the country; contributing to the development of a nation by serving various roles like teacher, engineers, doctors, nurse etc. Hence, the mental health of the students has to be given at most importance. Till date, there is no proven treatment to manage the Novel corona virus disease, though some vaccines are in trial, lockdown is the only option available to slowdown the rate of spreading the infection by restricting community-infection path. In this process, all the education institutes suddenly were declared 'locked down'. The students were in different phases of their academic year. It is well known that the students experience lots of stress especially before and during the examinations [10,11].

Table-1: The list of e-learning resources, platforms and educational applications below to help parents, teachers, school/college/university administrators, and students during the COVID-19 outbreak [3].

| System management systems | Systems built for use on basic mobile phones | External repositories of distance learning solutions | Massive Open Online Course (MOOC) Platforms | Self-directed learning content | Mobile reading applications | Collaboration platforms that support live-video communication | Tools for teachers to create digital learning content |
|--|--|--|--|--|---|---|--|
| 1 Century Tech 2 ClassDojo 3 Edmodo 4 Edraak 5 EdStep 6 Google Classroom 7 Moodle 8 Kaltura 9 Paper Airplanes 10 Schoology 11 Seesaw 12 Skooler | 1. Cell-Ed 2. Eneza Education 3. Funzi 4. KalOS 6. Ubongo 7. Ustad Mobile | 1. UNHCR 2. UNEVOC Resources 3. Organisation International de la Francophonie 4. Koulu.me 5. Keep Learning Going 6. Global Business Coalition for Education 7. European Commission Resources 8. EdSurge 9. Education Nation 10. Brookings Common Sense Education Commonwealth of Learning | 1. Allson 2. Canvas 3. Coursera 4. European Schoolnet Academy 5. EdX 6. ICourse 7. Future Learn 9. Icourses 10. TED-Ed Earth School 11. Udemy 12. XuotangX | 1 British Council 2. Byju's 3. Code It 4. Code.org 5. Code Week 7. Discovery Education 8. Duolingo 9. Edraak 10. Facebook Got Digital 11. Feed the Monster 12. GooKle 13. Khan Academy 14. KilKit School 15. Lab X change 16. Minds park 17. Mosoteach 18. Music Crab 19. OneCourse 20. Polyup 21. Quizlet 22. Siyavula 23. Smart 24. History 25. YouTube | 1 African Storybook 2. Biblioteca 3 Digital del Institute Latinoamericano de la Comunicación Educativa 5. Global Digital Library 6. Interactive 7. Learning Program 8. Reads 9. Room to Read 10. Story Weaver 11. World reader | 1 Dingtalk 2 Lark 3 Hangouts Meet 4 Teams 5. Skype 6. eChat Work 7. Whats App 8 Zoom | 1 Trelo 2 Soap 3 Peer Desk 4 Nearpod 5 Kaltura 6 Edi Casa 7 Ed Puzzle 8. Buncha 9. Thing Ink |

The students were preparing the examinations especially the entrance examinations for years together. For example, in India, NEET is the common entrance examination to enter into the professional colleges. Students will be preparing for this exam since two years as the scores will decide their admission criteria. Some students might be allotting an extra year to get through the entrance examinations. These students are in high anxiety because their pre-examination

phase will prolong till they complete their examination, further, as there is no proclamation of the date of exam, there is quiet improbability about their future. Parents may add up more anxiety to the system, as they are equally undergoing stress regarding their kid's career in future. Though many of the educational institutes have launched online classes, adaptation of the student to the sudden change from habitual teaching method to a new system is stressful. This is true chiefly in case of the slow learners. The fear of corona pandemic will add up to their stress. There for, the need of psychiatrist, in this circumstance to keep the mental balance of the students is extremely necessary. Every educational institution may think of establishing a mental health cell, or student counseling centre that comprises of psychiatrist(s) or psychologist(s) with a proper management system. Regular online counseling should be planned along with the online teaching classes. Importance should be given to counsel the parents with equal importance along with students. Regular monitoring of the stress levels using different online tools can be done to prevent the student to enter into the state of depression. And teacher who is a pivot of this whole system, simultaneously be counseled in handling the students with the new teaching process. The student should be priory convinced that there will not be any loss of academic year. The entrance examinations may be planned to conduct online as majority of the universities/ institutes throughout the world is already following the same. The counseling cell should also monitor the students even after the lockdown as it takes time for the students to normalize himself after the long, unexpected break of his studies. Continuous monitoring, offering counseling to the needy students will help to keep the students mentally sound and do well in personal and professional life. For example, to uphold student's mental health during the lockdown the Student Counseling Unit (SCU) of Unit-Fort Hare University (UFHU) has moved its services to an online platform [13]. By visiting the SCU facebook page, students are able to engage with qualified Psychologists in a safe and confidential space. The SCU of UFH University is managed by a psychologist on a daily basis. The platform allows psychologists from the unit to participate in live chats and offer one-on-one assistance via private online sessions. Psychological advice on how to manage lockdown related stress and anxiety is also shared on the page. The SCU also suggested their students to stay connected with their peers, share study materials and approaches in order to feel connected with like-minded people. They also suggested some following tips [13] to their students to remove stress during and make one feel goal-directed during lockdown.

- To prepare a special routine during lockdown and maintain it.
- Planning of study sessions and including break time.
- Self-care is an important aspect
- Never stay in empty stomach, intake meal in regular time
- Drink sufficient water time to time
- Listening to good music and engaging in dance once in a while can have a positive impact on mental health
- Not spending too much time on social media, especially at night, as this may lead to sleep problems and fatigue.

In our India, Calcutta University has started free online psychological counseling [14] service for all its students to beat any stress during the COVID-19 lockdown. The university has also issued a circular with the name and number of the faculty members whom the students may call at specified time slots for counselling services. Thirteen teachers - five from the Department of Psychology and eight from the Department of Applied Psychology - provide counseling session to students of undergraduate and postgraduate courses available for 12 hours daily.

REACHING TO CHILDREN OF MIGRANT LABOUR

Refugees, displaced and migrant children, often fall between the cracks as national policies do not necessarily include these helpless groups. They must be included and provided for in global responses to this crisis. While we are practising social distancing, and trying to practice stay at home, in the hope of a better tomorrow, there is a possibility that a significant number of children would appear as victims of such measures. One impact would be an increase in the number of child workers. Along with the health crisis, the pandemic has generated a huge shock on the economic and labour market. And millions of child labour would be in vulnerable condition which needs serious attention. According to ILO (International Labour Office) the Global Estimates of Child Labour: Results and Trends (2012-2016) presented in Geneva in 2017 [16], there were 152 million child labourers worldwide, of which 73 million were in hazardous work. Among these 152 million, 68 million are boys (58%) and 64 million are girls (42%). Among these children, 48% are 5-11 years-olds, 28% are 12-14 years-olds and only 24% are 15-17 years-olds. In another statistics, 70.9% of these children were engaged in Agriculture sector, 11.9% in Industry and 17.2% in Service sector. If we do address this issue with immediate and accelerated efforts, we are going to lose the battle of eliminating all forms of child labour by 2025, a commitment under the SDG. And the bare fact is that a very large number of children in child labour are completely deprived of education.

Children of the age group 5-14 years, there are 36 million are in child labour who are out of school, which is 32 per cent of all those in child labour in this age range. It is one of the most important indicators to address of the impact of child labour on sustainable livelihood prospects. The crisis created by the pandemic of COVID-19, will push millions of vulnerable children into child labour, specially the children of migratory labour. The Government of India has also declared for a countrywide school closure. UNESCO also estimates that around 32 crore learners are had an effect of it, of which 16.2 crore are boys 15.8 crore are girls. The bulk of these students are enrolled in primary and secondary schools (86%), followed by tertiary (10%) and pre-primary (4%) level of education [8]. Governments have adopted a variety of hi-tech, low-tech and no tech solutions to ensure the continuity of learning during this period. Most of the focus has been on online learning platforms, though nearly half of our country has no internet access. We can't think about internet access of children living in remote village, staying at foot-path or in slams. The MHRD (Ministry of Human Resource Development) of Govt. of India has suggested that all schools should connect their students through digital platforms to compensate for the loss of school hours. But the issue is that, as of now, mostly private schools (Generally CBSE and ICSE affiliated schools) and selected Govt. schools like Kendriya Vidyalaya have started online classrooms. However, most state government schools do not have the technology and equipment to provide online teaching. Moreover, the majority of students do not have access to internet, smart phones or a computer. Therefore, a large number of children studying in public schools remain cut off from online education. This will inexplicably affect children who already experience barriers in accessing education. This includes children with disabilities, students in remote locations, children of migrant workers, and children from the poor family. The millions of children who will be victims of the COVID-19 pandemic need immediate attention from states and communities. The starting point should be the parents; coordinated policy efforts should be taken income support to all informal sector workers, migrant workers to stimulate their family needs. As a direct measure, states should prioritise efforts to provide education for all children, using all available technology. But school teachers have a vital role to address this issue. Teachers have the direct relation with students in education process. So, they will take initiative to discuss with school authorities and need to ensure that every student will have lunch at home until schools open. Special efforts should be taken to identify children

orphaned due to COVID-19, and arrangements of shelter and foster care for them should be made on a priority basis. Apart from teaching process, teachers have a role to support the Govt. policies adopted during this pandemic period. States are also working on food distribution to all Govt. school children. For example, while Kerala and Delhi government are delivering food packets as a part of mid-day meals for government school children at their doorsteps, West Bengal and Andhra Pradesh are providing dry rations to children. But distribution of foods in terms of food packets or dry rations can be smoothly organized with the help of teachers. Another hard problem for migrant children is to adopt the language of education. As their parents are migrant labour, they have to move around with their parents, thorough the India, which is multilingual country. In COVID-19 pandemic, when most of the migrant labours are coming back to their home state, both students and teacher will face a problem to use the common language for education. Kerala [16] can be a model in this situation. Kerala's economy is dependent on migrants. Kerala sending out large numbers of workers overseas (2.4 million in 2013, based on a May 2018 report by the Centre for Development Studies) it needs migrants from other Indian states for Kerala's economic activities. The exact number of migrants coming to Kerala is unknown. According to 2017 estimations by CMID, (Centre for Migration and Inclusive Development, an Ernakulam-based non-profit organization) as much as 11% of the population of Kerala) would be migrant and the figure may turn to 3.5 - 4 million. The Kerala government has been more proactive compared to other states to address situation as their economy is directly relate to it. There are three types of migrant workers at Kerala; those who come for work and settle down, those who look for work temporarily, and seasonal migrants, and the migrant due to natural calamities. The migrant student drop-out rate depends on the nature of migration. The problem starts with the language barrier first. Kerala Govt. through Sarva Shiksha Abhiyan (SSA) has appointed a large number of volunteer to help those students understand Malayalam, which is the medium of education in all Govt. schools. Those measures will no doubt respond to the emergency created by COVID-19 directly or indirectly to some extent. However, it is clear that more needs to be done to prevent children from lapsing into child labour and teacher as a main pillar of education system, has a major role to address this situation.

ROLE OF NSS VOLUNTEERS IN COVID-19 OUTBREAK

Maximum schools, colleges and universities of India have National Service Scheme (NSS) volunteers since 1969. The number of NSS volunteers was 40,000 in 1969 and 3.8 million in March 2018. A NSS volunteer is a student of school or college or university who has enrolled his/her name in the National service Scheme. The roles of the NSS volunteers are very significant according to the National Service Scheme because they are the main beneficiaries of the programme. It provides the opportunity to the youth students of class-XI and XII in schools and graduate and post graduate students of colleges and university level of India to take part in various community service activities and programmes. The slogan of NSS is NOT ME BUT YOU [4]. The NSS programme aims to encourage social welfare in students, and to provide service to society without bias. NSS volunteers work to ensure that everyone who is needy gets help to enhance their standard of living and lead a life of dignity. In doing so, volunteers learn from people in adopted villages how to lead a good life despite a shortage of resources. The first thing NSS provide is to develop their own thought process by doing community services. Society is a group of persons who may have different ideology. NSS volunteers work to ensure skills and dedication build it a homogenous ideological group. NSS volunteers also provide help in natural and man-made disasters by providing food, clothing and first aid to the disaster victims. NSS volunteers take care of cleanliness, blood donation, health awareness issues, child education, and many other activities. NSS is always trying to bring smiles on innocent faces through empowering the

education. In this way NSS makes its volunteer a good human being. While studying, these volunteers undertake community development activities which help to build their personality and develop the belongingness towards the society. The NSS volunteers are performing the role as a bridge between the education system and the community which is helpful for the nation building. They are developing their qualities of leadership, skills to become an organizer, and an administrator to attain the multi-faceted development of their personality as a whole. Whenever there is a need, NSS volunteers appear themselves to serve the nation. NSS volunteers always take up relief and rescue operations on priority whenever a natural disaster occurs in any part of the country. It may be in the form of environment enrichment, malnutrition, immunization, or the issue of natural disaster; NSS volunteers are becoming the saviors for the victims [17].

Recently, Maximum NSS volunteers with their NSS programme officers and coordinators have completed iGOT (Integrated Govt. Online Training) courses about COVID-19 pandemic on DIKSHA platform. There are different iGOT courses about COVID-19 like Basic of COVID-19, Infection Prevention and Control, Clinical Management of COVID-19, ICU Care and Ventilation Management, Infection Prevention through PPE, Management of COVID-19 cases, Quarantine and Isolation, Psychological support of patients with COVID-19 etc. The trained volunteers are also trying to attract the attention of younger students of the school, college or university towards these courses about Covid-19 outbreak awareness activity.

National Service Scheme (NSS) volunteers in India have taken up different awareness activities about basic infection, prevention and control of COVID-19 in war-footing basis to the common people during the lockdown period of COVID-19 pandemic. Different NSS units across the India are fully involved in the relief activities to the poor. The NSS volunteers are sanitising the affected area, preparing food packets for the flood victims, running common kitchen and distributing medicines. The NSS volunteers and other functionaries are distributing food packets to the affected people at various places and are also helping in rescue operations with the health workers. They are collecting items like dry ration, drinking water, clothes, soaps, medicines, sanitary napkins, milk powder, washing powders, hand wash, sanitizers etc. These volunteers work tirelessly to mobilise relief materials and work for the smooth distribution of the collected materials in the affected area in close coordination with the district administration. They are also collecting money for the PM Relief Fund or CM Relief Fund of different states of India. As for example, Md. Salauddin Ansari, a NSS volunteer (Fig. 1) of Achhram Memorial College, Jhalda, Purulia, West Bengal, India participated in different COVID-19 related activities [see Fig.-1] to aware and help the common people. At present about 32000 NSS volunteers are enrolled in this programme in 426 universities of India covering about 32000 persons. NSS nodal or programme officers circulate and forward materials including Covid-19 awareness guide, packet book and awareness posters etc to all NSS volunteers and then they in turn forward these materials through email, whatsapp and other social media platforms to all other NSS volunteers and students of University /Directorate /College /schools /institutions to propagate the right messages on Corona virus and clear all myths, misconceptions, stigma & discrimination about Covid-19. At this critical juncture, NSS play the prime role to spread the awareness through one to one personal communication about the importance of hand hygiene, respiratory hygiene and minimum 1 meter social distancing in the public places. Students of the National Service Scheme are not discouraged by the lockdown, and are doing their bit by spreading awareness on Covid-19 via posters, videos, quizzes, etc. The NSS coordinators are performing their responsibility by spreading awareness about mask preparation, hand sanitizer preparation or the simple practices such as using gloves and even ways to handle those under home quarantine. Also some educational institutions have started creating quizzes or webinar about COVID-19.



Fig.1: Some COVID-19 related NSS activities performed by Md. Salauddin Ansari, NSS volunteer (unit-III) of Achhruram Memorial College, Jhalda, Purulia, West Bengal, India.

REFERENCES

1. <https://www.scielosp.org/scielo.php?lng=en>
2. <https://www.weforum.org/agenda/2020/04/coronavirus-education-global-covid19-online-digital-learning/>
3. <https://en.unesco.org/covid19/educationresponse/solutions>

1. <https://www.researchgate.net/publication/319111111>
2. <https://www.researchgate.net/publication/319111111>
3. <https://www.researchgate.net/publication/319111111>
4. <https://www.researchgate.net/publication/319111111>
5. <https://www.researchgate.net/publication/319111111>
6. <https://www.researchgate.net/publication/319111111>
7. <https://www.researchgate.net/publication/319111111>
8. <https://www.researchgate.net/publication/319111111>
9. <https://www.researchgate.net/publication/319111111>
10. <https://www.researchgate.net/publication/319111111>
11. <https://www.researchgate.net/publication/319111111>
12. <https://www.researchgate.net/publication/319111111>
13. <https://www.researchgate.net/publication/319111111>
14. <https://www.researchgate.net/publication/319111111>
15. <https://www.researchgate.net/publication/319111111>
16. <https://www.researchgate.net/publication/319111111>
17. <https://www.researchgate.net/publication/319111111>
18. <https://www.researchgate.net/publication/319111111>
19. <https://www.researchgate.net/publication/319111111>
20. <https://www.researchgate.net/publication/319111111>

Basics of Foam Science – A Brief Review

| Article History | |
|--|-------------|
| Received: | 19. 01.2021 |
| Revision: | 31. 01.2021 |
| Accepted: | 12.02.2021 |
| Published: | 25.02.2021 |
| Author Details | |
| Tarun Kumar Barik | |
| Authors Affiliations | |
| Department of Physics, Achhruram Memorial College, Jhalda, Purulia-723202, West Bengal, India | |
| Corresponding Author* | |
| Tarun Kumar Barik | |
| How to Cite the Article: | |
| Tarun Kumar Barik (2021). Basics of Foam Science – A Brief Review .IAR J Eng Tech, 2(1), 55 -64. | |

Abstract: Wet foam is a very common example of soft matter. In wet foam, molecules are more structured than in liquids but more random than they are in solids. Recently, physics of foam has become a rapidly developing branch in science and engineering. A deeper understanding is crucial for many technological applications of wet foam. Hence, in this article, the basic structure and properties of foam are reviewed based on the literature survey of published research work. Some research works, available in the literature, in which optical probes have been used to study the structure, properties and dynamics of foam. In this article, wet foam is used to study the basic structure and properties of foam for better understanding. Raman Spectroscopy and Diffusing wave Spectroscopy have been used on wet foam to establish its structure and properties are also reported. Finally, in conclusion, recent scientific, technological and commercial applications and future prospects of wet foam are proposed to build impulse on the wet foam science more to enrich our day to day life with the modern concepts of nanofoam technology. Recently, due to rapid increase of nanotechnology, different metallic (Cu, Au, Ni, Pt, Pd etc.) or nonmetallic (C) solvent-assisted nanofoam have modernized the structure, properties of foam science and hence have accelerated its day to day technological applications.

Keywords: Wet foam, Rheology, Coarsening, Liquid drainage, Collapse, Raman Spectroscopy, Diffusing wave spectroscopy, nanofoam.

INTRODUCTION:

Imagine opening a carbonated cold drink bottle or a soda can after shaking it: almost instantaneously, gas bubbles rise and crowd together at the surface of the liquid forming a soft foam. Inside the bottle or can, carbon dioxide is dissolved in liquid at high pressure. Shaking of the container results in the creation of a large number of little bubbles as the agitation unbinds the carbonation from the solution. By opening the container, these gas bubbles rise to the liquid surface to release carbon dioxide into the surrounding air. Similar incident also occurs at the time of washing or shaving with soap. These are the common examples of sort lasting wet foam. The history of foam can be traced from the publication in 1873 titled *Statique Experimentale et Theorique des Liquides soumis aux seules Forces Moleculaires* by the Belgian physicist Joseph Antoine Ferdinand Plateau (Plateau, J.A.F. 1873). This book summarizes the previous history of foam research and also presents author's own work, which laid the foundation for the future studies. Soft foam is a very common example of soft matter (a matter which is neither liquid nor solid, but something in between). In foam, molecules are more structured than in liquids but more random than they are in solids. Foam physics has become a rapidly developing branch in science. This is due to the fact that the physics of foam is, as yet, ill-understood. Further, a deeper understanding is crucial for many technological applications of foam. There are a number of models are available in the literature to simulate the bubble growth in foam in two or three dimensions, its bubble size distribution and most essential properties of foam (Glazier, J. A. Glazier, J. A. *et al.*, 1990; Lim, K. S., & Barigou, M. 2005; Magrabi, S. A. *et al.*, 1999; Monsalve, A., & Schechter, R. S. 1984; Lemlich, R. 1978; Hutzler, S., & Weaire, D. (2000; Ganan-Calvo, A. M *et al.*, 2004; Kabla, A. *et al.*, 2007; Gardiner, B. S. *et al.*, 1999; Gardiner, B. S. *et al.*, 2000; Sun, B. *et al.*, 2015; & Tenneti, S. *et al.*, 2013). There are also a lot of experiments with wet foam in the literature to establish its essential properties (Feitosa, K. *et al.* 2006; Saint-Jalmes, A. *et al.*, 2000; Barik, T. K., & Roy, A. 2009; Bandyopadhyay, P. *et al.*, 2008; & Barik, T. K. *et al.*, 2009). Recently, carbon nanofoam is one of the lightest solid materials known today, having a density of ~ 2 mg/cm³. It has an extremely high surface area and is a good electrical insulator. It is fairly transparent, quite brittle and can withstand very high temperature. Highly uniform samples of carbon nanofoam from hydrothermal sucrose carbonization were studied by helium ion microscopy (HIM), X-ray photoelectron spectroscopy (XPS), and Raman spectroscopy (Frese, N. *et al.*, 2016). Facile synthesis of Ni nanofoam using aqueous solutions at room temperature is studied for flexible and low-cost non-enzymatic glucose sensing (Iwu, K. O. *et al.*, 2016). Once more, hierarchical NiCo₂O₄ nanosheets are grown on Ni nanofoam as high-performance electrodes for supercapacitors (GAO, G. *et al.*, 2015). Cu nanofoams are also fabricated using a simple powder-metallurgy method which is useful for potential energy applications (Jo, H. *et al.*, 2014). Bimetallic Pd/Pt nanostructures deposited on Cu nanofoam substrate by galvanic replacement are also fabricated as an effective electrocatalyst for hydrogen evolution reaction (Rezaei, B. *et al.*, 2015). Gold nanofoams were synthesized in the Deep Eutectic Solvent (DES) with no templates, seeds, or additives (Jia, H. *et al.*, 2015). Thus, there are many such foam with different advanced technological applications are reported in recent literature, but this article is focused to study the basic structure and properties of foam.

Basic Structure of foam:

Foam is a two-phase cellular structure either of gas and liquid (liquid foam) or of gas and solid (solid foam). Here, in this article, we shall concentrate only on

liquid foam. Liquid foam consists of a collection of gas bubbles surrounded by thin liquid films. A typical microscope image of wet foam (Gillette shaving foam) is shown in Fig. 1.



Fig. 1: A typical microscope image of Gillette shaving foam.

For better stability, some surface active substances (i.e. surfactants) are used while preparing liquid foam. There are mainly two types of liquid foam depending upon its liquid content (a) *dry foam* has less liquid and consists of thin films between bubbles. These bubbles take the form of polyhedral cells and have a poly-disperse distribution and (b) *wet foam*, which has high liquid content. All bubbles in wet foam are spherical in shape and nearly mono-disperse at the initial state. In a statistical analysis of bubble size distribution using Gillette shaving foam shows coarsening of bubbles and the change in bubble size distribution in wet foam with ageing. It also shows an increase in polydispersity of foam with ageing and the growth of larger bubbles at the cost of the smaller bubbles, during ageing (Barik, T. K., & Roy, A. 2009). In a foamy network, the three liquid films from three nearby bubbles meet to form a scalloped-triangular channel, which is known as Plateau border. Only four Plateau borders meet at a region shared by four neighboring bubbles making equal

angles and this region is known as the vertex. In foam, the Plateau borders and vertices form a continuous network. The law of Plateau defines few rules, which are necessary to obtain an equilibrium configuration of a foamy network. These rules are:

- **Rule 1:** For dry foam, three films of three nearby bubbles intersect at a time with an angle of 120° to each other. In two dimensions, this applies to the lines, which define the cell boundaries.
- **Rule 2:** For dry foam, four bubbles meet and form a symmetric tetrahedral vertex. The angle between the films is called the Maraldi angle.
- **Rule 3:** In wet foam, Plateau border joins the adjacent films by smooth surfaces.
- Typical schematic diagrams of dry and wet foam with the construction of the corresponding Plateau border network are shown in Fig. 2.

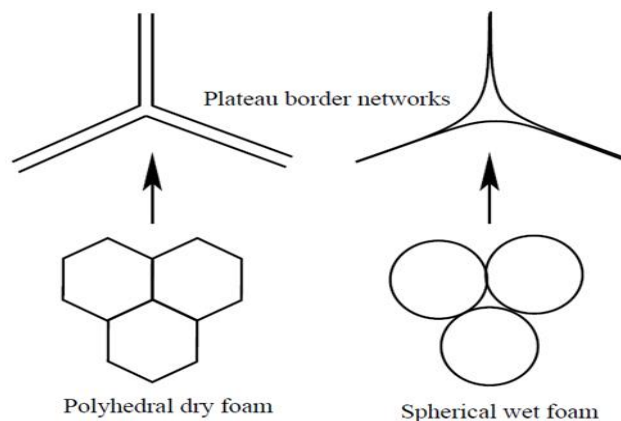


Fig. 2: Schematic representations of dry and wet foam with Plateau border network.

In dry foam, the polyhedral bubbles are with slightly curved edges and faces. Any polyhedron (whose closed surface is topologically equivalent to that of a sphere) in three dimensional space obeys Euler's theorem, $U - E + F = 2$, where, U , E and F are the number of vertices, edges and faces of the polyhedron, respectively. For dry foam bubbles, the polyhedral geometry is further restricted by Plateau's rules. The coordination numbers of Plateau's laws enforce $2E = 3U$ and therefore, $E = 3F - 6$ follows for any foam polyhedron. In other words, for

polyhedra in foam any of the three quantities U , E and F determines the other two. The fascinating properties of foam arise from its topological changes via T1 and T2 processes. While in the T1 process, a fourfold vertex dissociates into a stable threefold vertex (Fig. 3(a)), a three-sided cell may disappear by the T2 process, as shown in Fig. 3(b) [26]. With this introduction to the basic structure of wet foam, its essential properties are discussed in brief below.

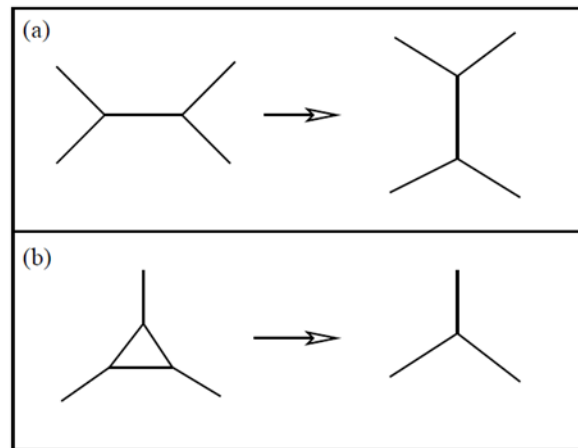


Fig. 3: Schematic representations of topological changes in liquid foam via (a) T1 process and (b) T2 process (Dennin, M., & Knobler, C. M. 1997)

Properties of foam:

To study the properties of foam, we have chosen wet foam for easy understanding. In the following sections of this article, the four most essential properties of foam: (i) Rheology, (ii) Coarsening, (iii) Liquid drainage and (iv) Collapse, are briefly reviewed. A study about the structure and dynamics of wet foam using optical probes are also reported in the following sections.

Rheology:

Foam has unique rheological properties. The mechanical response of liquid foam to an applied force is complex, exhibiting both elastic and viscous character (Kraynik, A. M. 1988). Under low applied shear stress, foam behaves like an elastic solid. However, with an increase in stress it becomes progressively plastic; beyond a certain yield stress, the foam flows along with topological changes. The flow is intermittent and mediated by non-linear rearrangement events in which several neighboring gas bubbles suddenly hop from one tightly packed configuration to another. Such characteristics of foamy structure strongly depend on the bubble size, liquid fraction, viscosity and interfacial tension. The schematic stress-strain relation for the liquid foam is shown in Fig. 4.

Both two and three dimensional foam can be accurately simulated using various models (Weaire, D., & Hutzler, S. 1999). The computer simulation results provide the correlation between the shear modulus and gas/liquid fraction in the tightly packed gas bubbles (Bolton, F., & Weaire, D. 1990; Feng, S. *et al.*, 1985; Hutzler, S. *et al.*, 1995; Princen, H. M., & Kiss, A. D. 1986). For example, the model based on bubble-bubble interaction takes into account the pair-wise quadratic potential energies for connecting bubbles in the low compression limit. The bubble-scale model, proposed by Durian and his co-workers, explains the foam mechanics by solving the equation of motion of the individual disk (two dimensional projection of spheres) and assuming a harmonic potential for interaction between the bubbles (Durian, D. J. 1995; & Durian, D. J. 1997). The effect of liquid flow under low shear has been taken into account by including the viscous term. The model provides a connection between the complex macroscopic rheological behavior of foam and its underlying microscopic structure. Other models are also available in the literature, in which, the various aspects of the stress-strain relation have been dealt with (Glazier, J. A., & Weaire, D. 1992; Weaire, D., & McMurtry, S. 1996; Khan, S. A., & Armstrong, R. C. 1986; Jabarkhyl, S. *et al.*, 2020; Ptaszek, P. 2013).

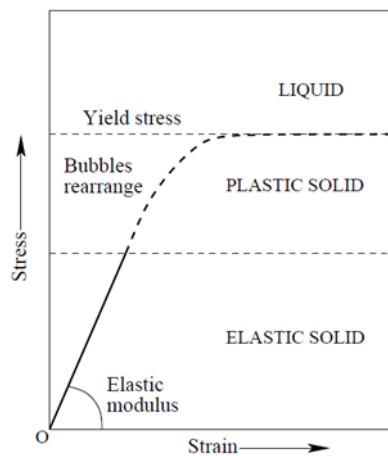


Fig. 4: A schematic diagram of the stress-strain relation for liquid foam.

Coarsening:

Foams are of broad scientific interest for their ability to fill space efficiently with a random packing of bubbles and for the coarsening of this disordered structure with time. Coarsening is the gradual change of

foam structure due to gas diffusion through the films from smaller bubbles to larger bubbles following the well-known Laplace-Young law. This law relates the pressure difference to the mean curvature for a surface in equilibrium. From Laplace-Young law, the

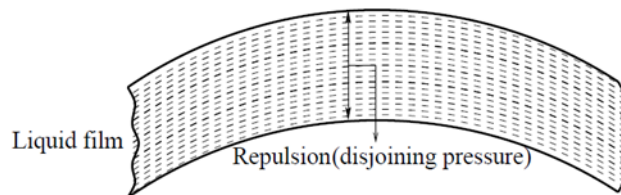


Fig 5: The mutual repulsion (disjoining pressure) between the two surfaces of a thin liquid film.

Balance in pressure difference inside a bubble, ΔP , can be expressed as: $\Delta P = \frac{2\alpha}{r}$; where α is the surface tension of liquid film and r is the mean local radius of curvature of the film surface. r is related to the two principal curvatures r_1 and r_2 as: $\frac{2}{r} = \frac{1}{r_1} + \frac{1}{r_2}$. For wet foam, the bubbles are spherical and hence $r_1 = r_2$. At equilibrium, the Laplace pressure is balanced by the disjoining pressure of the films, which originates from the mutual repulsion between the two surfaces of the thin liquid film (see Fig. 5). In case of wet foam the gas diffusion takes place only through the liquid films not through the Plateau borders (In Ref. [20], see p. 98). The increase in the average bubble size with time can be obtained from the fact that the rate of change of a bubble's volume is proportional to its surface area and to its Laplace pressure difference with respect to a certain mean or critical bubble radius r_c .

Thus,

$$\frac{dr^d}{dt} \propto r^{d-1} \left(\frac{1}{r_c} - \frac{1}{r} \right),$$

for any dimension d . for $d=3$,

$$\frac{dr}{dt} \propto \left(\frac{1}{r_c} - \frac{1}{r} \right).$$

Thus, the large bubbles, $r > r_c$, grow in size, whereas the smaller bubbles $r < r_c$ shrink. If r_a be the average bubble radius, then we have

$$\frac{dr_a}{dt} \propto \frac{1}{r_a},$$

Which implies that $r_a(t) \sim t^{\frac{1}{2}}$. In general, the time-scale of evolution of the average bubble radius can be expressed as:

$$r_a \propto (t - t_0)^{\frac{1}{2}}$$

Where, t_0 is an initial constant. For an infinite foam network the coarsening process has no end. Thus, one can identify the asymptotic scaling behavior of foam with ageing. In 1952, von Neumann demonstrated that the time evolution of bubbles in a two dimensional

foam only depends on the number of its sides, n , rather than on the size or shape of the bubbles (Von Neumann, J. 1952). The rate of change of area, A_n , of the n th bubble is given by the von Neumann's law

$$\frac{dA_n}{dt} = \frac{2\pi}{3} \alpha k(n - 6),$$

where, α and k are the permeability constant and surface tension for the liquid films. The significance of the above equation for $n = 6$, is that the area of the hexagonal bubbles remain constant until they encounter a topological change. A number of models are available

in the literature to simulate the bubble growth in foam in two or three dimensions (Bolton, F., & Weaire, D. 1990; Glazier, J. A., & Weaire, D. 1992; Patzek, T. W. 1993; Avron, J. E., & Levine, D. 1992; & Feitosa, K. *et al.*, 2006).

Liquid drainage:

The liquid between the bubbles can drain out in response to gravity or due to adjacent film rupture to settle into a equilibrium profile. This phenomenon is known as drainage. For fairly dry foams, the liquid is distributed in (a) the flat films that separate two neighboring bubbles, (b) the long Plateau borders and (c) the scalloped-tetrahedral vertices (Bikerman, J. J. 1973; Prud'homme, R. K., & Khan, S. A. 1996; & Weaire, D. *et al.*, 1997). During drainage, the flow of liquid out of foam is assumed to be confined to the network of Plateau borders and/or vertices and it slows down as equilibrium is approached. Due to the density mismatch between gas and liquid, the bubbles rise and collect at the top and the liquid accumulates at the bottom. The liquid also flows because of the capillary effect, which is related to the gradient of liquid fraction in a column of foam. Such a gradient of liquid fraction implies an existence of a pressure gradient in the liquid foam. Thus, a capillary flow is induced by bringing liquid from high liquid fraction regions to regions with low liquid fraction. Liquid drainage in a column of wet foam has been modeled by non-linear partial differential drainage equation, which expresses liquid conservation as it flows in response to gravity, capillarity and viscous forces (Weaire, D. *et al.*, 1997; Bhakta, A., & Ruckenstein, E. 1997; & Koehler, S. A. *et al.*, 1998). However, the analytical solutions of the nonlinear equation can only be obtained by ignoring the capillary term. Durian *et al.*, designed an experiment, minimizing the capillary effect during drainage, to verify the drainage equation (Saint-Jalmes, A. *et al.*, 2000). A generalized drainage equation for arbitrary shape of the container is also available in Ref. (Saint-Jalmes, A. *et al.*, 2000). The complex draining action in a wet foam prompted many experiments in which the drained liquid has been measured as a function of time.

In the experiments based on 'forced drainage', a constant input of external liquid at the top of the foam column maintains a constant flow of liquid throughout the foam. On the other hand, for 'free drainage' experiments, no external liquid is added on the top of foam surface. Free drainage is the unavoidable fate of aqueous foams under earth's gravity (Bikerman, J. J. 1973; & Prud'homme, R. K., & Khan, S. A. 1996). Drainage of liquid in wet foam has been studied using various optical techniques, like absorption or transmission measurements. A detailed review is available in (Saint-Jalmes, A. 2006). Free drainage with slow as well as fast coarsening of gas is a coupled phenomenon in wet foam (Saint-Jalmes, A. 2006; & Patzek, T. W. 1993). In spite of a thorough endeavor to understand the free drainage process in wet foam, the problem is still not well understood (Saint-Jalmes, A. *et al.*, 1999).

Collapse:

Usually, most liquid foams do not last for long, as the bubbles collapse by the rupture of the exposed liquid films. Many factors like liquid drainage, coarsening, evaporation, impurities and additives are responsible for foam collapse. The study of foam collapse has a great practical importance because it deals with the stability of the film. Topological change in foam structure due to the bubble growth by film rupturing is less studied in the literature and remains very poorly understood. A crucial feature of liquid foam is that it irreversibly evolves with time. The spherical bubbles in fresh foam take the form of polyhedra while minimizing the energy of the system. The evolution of the bubbles in foam with time can be described by the above four mutually coupled mechanisms.

Measurement of properties of wet foam with light:

Structure and properties of foam have been probed extensively using various optical techniques. Here we mention some of the earlier works, where light has been used to measure the size, wetness, movement of bubbles and other properties of foam. Diffusing wave spectroscopy (DWS) is the most commonly used optical tool to study the behavior of foam (Miri, M. F., & Stark, H. 2004; Gittings, A. S., & Durian, D. J. 2006; Gopal, A. D., & Durian, D. J. 1999; & Höhler, R. *et al.*, 2003). This technique is an extension of Dynamic light scattering technique for a strongly scattered medium, where the propagation of light is described by the diffusion approximation (Weitz, D. A. *et al.*, 1993). The autocorrelation function of the multiple scattering of light is calculated by dividing the photons into separate diffusive paths. The distribution of these paths and the

probability that the photon will follow a path of a given length is determined through the diffusion equation of light. The total correlation function is then determined by summing the contributions from all possible paths with weighted probabilities, assuming that each path is uncorrelated with the other path. The fluctuations of the transmitted scattered light result from the variation in total optical path length. The decay of the temporal autocorrelation function of the intensity of the scattered light, which reflects the temporal evolution of the path length, provides the dynamics of the medium. DWS has been extensively used to study bubble size and liquid fraction in wet foam. Using this technique the static transmission coefficient (T) of light through foam of a given thickness has been measured. Diffusion of light is characterized by the transport mean free path, l^* , of the transmitted light. It has been shown that

$$T \approx \frac{5l^*}{3L}$$

(considering the large thickness of the foam, L , and no absorption of light by foam). Using this relation, average bubble diameter d_a can be estimated from the relation $l^* = (3.5 \pm 0.5)d_a$ (Saint-Jalmes, A. *et al.*, 1999). The scaling behavior of the bubble growth, discussed in the above section-3, has been verified experimentally with the average bubble diameter growing in time as \bar{r}^z , with $z = 0.45 \pm 0.05$ (Durian, D. J. *et al.*, 1991). It is reported that the changes in the packing conditions during the coarsening process give rise to a dynamical process that also exhibits temporal scaling. In Ref. (Vera, M. U. *et al.*, 2001), Vera *et al.*, used the multiple scattering of light by aqueous foam to study the coupling between drainage and coarsening mechanisms. Other than confirming the fact that the transport mean free path is proportional to the bubble diameter, authors have shown that the liquid fraction in foam is proportional to $\frac{1}{l^*}$. Furthermore, DWS is a potential tool to study the viscoelastic behavior of foam (Mason, T. G. *et al.*, 1997). The technique has also been applied to model foam subjected to shear stress. The observed data reflect the local rearrangement events in the foam (Earnshaw, J. C., & Wilson, M. 1995). Along DWS, various other optical techniques have been used to study the behavior of wet foam. The change in the degree of depolarization of a collimated, polarized incident light on non-absorbing foams has been studied by Wong *et al.*, (2002). It is observed that the denser media (with a large number of bubbles) tend to depolarize the incident beam more. The degree of depolarization can be correlated to the bubble size distribution in wet foam. Durian and his coworkers used the photon channelling experiments to study the absorptivity and liquid fraction in foams (Gittings, A. S. *et al.*, 2004). The authors added a dye to the continuous liquid phase for the absorption of diffuse photons in the

aqueous foams and studied the absorption mechanisms under different experimental conditions.

Study Wet foam by Raman scattering:

In this thesis, we have studied the properties of the soft Gillette shaving foam, using an optical spectroscopic technique, based on Raman scattering. Raman spectroscopy is a powerful noninvasive tool to probe the structure and dynamics of a system at the molecular level. Our aim is to investigate, if this technique can be used to study the effect of ageing on molecular structure and to characterize the stability of wet foam. In addition, Raman scattering is caused by deformation/stretching of different vibrational bonds of molecules. Thus, if macroscopic and microscopic properties in foam are related, one expects that the analysis of Raman line profiles can be used to probe the elastic properties of wet foam, indirectly, by studying its molecular behavior. The main hindrance in using Raman spectroscopy to probe wet foam arises due to multiple scattering of light within the bubbles, which masks the Raman signal from the foamy structure, to a large extent. The signal to noise ratio in the spectrum is always poor in this case. Thus, in the literature, we do not find too many articles on Raman studies of wet foam. The most significant one is by Goutev and Nickolov (1996), where the authors have studied the microstructure of stable three-dimensional foam on the basis of its molecular behavior. Based on Raman measurements of foam, authors have shown that (a) two distinct phases can exist in wet foam|a lamellar phase (with an ordered multilayer structure of surfactant molecules) and an isotropic phase, (b) in fresh foam small bilayer lamellae are dispersed in foam films and with ageing they self-organize around the bubble in large shell-like bilayer structures. It is to be noted that the quantitative estimates of the structure and properties

of liquid foam depend on the liquid fraction and the chemical constituents. However, the generic features are expected to remain same for all. Since, the other groups have worked on various aspects of foam using Gillette shaving foam as their sample (Durian, D. J. *et al.*, 1991a; Durian, D. J. *et al.*, 1991b; Earnshaw, J. C., & Jaafar, A. H. (1994; Goutev, N., & Nickolov, Z. S. 1996), it is preferable to use the same material for further investigation while using a new experimental technique. Therefore, we have chosen the Gillette foam in our work. The basic ingredients of Gillette shaving foam are triethanolamine stearate with small amount (< 1%) of sodium lauryl sulphate, polyethylene glycol lauryl ether and emulsified liquid hydrocarbon gases. These ingredients are kept in an aqueous solution under high pressure. The foam is produced after expansion of the above mixture in air. It is reproducible and stable over the duration required for an optical measurement. For Raman measurements this commercial foam offers an extra advantage|when laser light is incident on foam it undergoes multiple scattering. In order to obtain the optimum Raman signal, the mean free path, l^* , [$\cong 3.5 \times$ average diameter of the bubbles (d_a)] of light within the foam should be comparable with the slit-width of the spectrometer collecting the scattered light (Nieto, M. I. *et al.*, 2014). The mean diameter of bubbles in fresh Gillette shaving foam is close to $30 \mu\text{m}$ and the maximum diameter, which we have studied, is $\approx 350 \mu\text{m}$ |comparable with the slit-width of our spectrometer ($\cong 100 \mu\text{m}$) in order of magnitude. Below we discuss the basic principle of Raman scattering and also the instrument used by us for the Raman measurements. Different recent researches on wet foam have explained the gross properties of wet foam in light of its characteristic molecular structure using Raman spectroscopy. They have related the observed shift in the low frequency Raman peak position of the methylene rocking mode with the variation in internal stress in the system. The analysis of Raman data over the range between 1000 cm^{-1} and 1450 cm^{-1} indicates the gradual structural change of wet foam from all-trans conformation to crystalline structure with ageing (Kraynik, A. M. 1988). Drainage of water from wet foam is discussed and in addition to free water molecules, which drain out with ageing of foam, water clusters of only a few water molecules are also present in foam. It is also shown that the correlation between the internal stress and the characteristics of a vibrational mode in wet foam. Thus the capability of the Raman spectroscopy to reveal the crystallinity in foamy materials is established (Bandyopadhyay, P. *et al.*, 2008; & Barik, T. K. *et al.*, 2009).

In conclusion, the basic structure and properties of wet foam are reviewed in the light of present scientific literature to reveal interesting essential properties of wet foam. The optical probes (specially, Raman spectroscopy and Diffusing wave spectroscopy) used to study the wet foam are also briefly discussed. There are huge applications of solid foam compared to wet foam reported in the literature. Similarly, recent researches suggest that wet foam has also the huge possibilities in different technological applications like fire extinguishing, food processing, commercial chemicals and cosmetics, agricultural fields, biomedical fields, environmental safety and toy-making industries etc. (Nieto, M. I. *et al.*, 2014; Takahashi, M. *et al.*, 2009; & Subagyono, D. J. *et al.*, 2011). Recently, the higher density foams like carbon nanofoam, however, show an advanced graphitization degree and a stronger sp^3 -type electronic contribution, related to the inclusion of sp^3 connections in their surface network (Frese, N. *et al.*, 2016). Again, by employing Ni nanofoam flexible and highly sensitive glucose sensors have been produced on a plastic substrate with excellent performances (Iwu, K. O. *et al.*, 2016). A high-performance electrode for supercapacitors is also designed and synthesized by growing electroactive NiCo_2O_4 nanosheets on conductive Ni nanofoam (Gao, G. *et al.*, 2015). Again, Cu nanofoams are also very much useful for potential energy application (Jo, H. *et al.*, 2014). The gold nanofoams with no capping agents have more catalyst active sites and excellent catalytic efficiency (Jia, H. *et al.*, 2015). The main objective of this article is to review the structure and properties of foam to attract more research attention towards foam technology and develop this field for more scientific, technological and commercial applications for our day to day life. Diffusing wave spectroscopy and Raman spectroscopy are quick and noninvasive tool to measure the strain and hence, the stability of a wet foam (Bandyopadhyay, P. *et al.*, 2018; & Barik, T. K. *et al.*, 2009) and hence, these spectroscopic techniques can act as optical probe to study the properties of foam. Some papers use Gillette shaving foam to study wet foam characteristics. But, the composition of commercial shaving foams (like Gillette foam) is quite complex and its physicochemical properties are ill defined; it is worth to study the wet foam using simple foamy materials with well controlled composition, specially made in a laboratory. Further experiments on known surfactants will also indicate if the observed behavior of the wet foam originates from the characteristics of the surfactant itself or from its foamy structure (Jabarkhyl, S. *et al.*, 2020; de Moraes, E. G., & Colombo, P. 2014; & Zhao, J. *et al.*, 2018). Furthermore, using the experimental method stated in (Bandyopadhyay, P. *et al.*, 2018) at different heights of the column of foam, one can experimentally study the coupling between coarsening and drainage of liquid in wet foam.

CONCLUSION:

Acknowledgement:

The author wishes to acknowledge Prof. Anusree Roy, Department of Physics and Meteorology, Indian Institute of Technology, Kharagpur, India for her helpful discussions and guidance.

REFERENCES:

1. Avron, J. E., & Levine, D. (1992). Geometry and foams: 2D dynamics and 3D statics. *Physical review letters*, 69(1), 208.
2. Bandyopadhyay, P., Ojha, A. K., Barik, T. K., & Roy, A. (2008). Drainage and water clusters in Gillette foam. *Journal of Raman Spectroscopy: An International Journal for Original Work in all Aspects of Raman Spectroscopy, Including Higher Order Processes, and also Brillouin and Rayleigh Scattering*, 39(7), 827-831.
3. Barik, T. K., & Roy, A. (2009). Statistical distribution of bubble size in wet foam. *Chemical engineering science*, 64(9), 2039-2043.
4. Barik, T. K., Bandyopadhyay, P., & Roy, A. (2009). Probing Internal Stress and Crystallinity in Wet Foam via Raman Spectroscopy. *International Journal of Modern Physics B*, 23(19), 3913-3924.
5. Bhakta, A., & Ruckenstein, E. (1997). Decay of standing foams: drainage, coalescence and collapse. *Advances in Colloid and Interface Science*, 70, 1-124.
6. Bikerman, J. J. (1973). *Foams*, (Springer-Verlag, New York, 1973).
7. Bolton, F., & Weaire, D. (1990). Rigidity loss transition in a disordered 2D froth. *Physical review letters*, 65(27), 3449.
8. de Moraes, E. G., & Colombo, P. (2014). Silicon nitride foams from emulsions. *Materials Letters*, 128, 128-131.
9. Dennin, M., & Knobler, C. M. (1997). Experimental studies of bubble dynamics in a slowly driven monolayer foam. *Physical review letters*, 78(12), 2485.
10. Durian, D. J. (1995). Foam mechanics at the bubble scale. *Physical review letters*, 75(26), 4780.
11. Durian, D. J. (1997). Bubble-scale model of foam mechanics: mMelting, nonlinear behavior, and avalanches. *Physical Review E*, 55(2), 1739.
12. Durian, D. J., Weitz, D. A., & Pine, D. J. (1991a). Multiple light-scattering probes of foam structure and dynamics. *Science*, 252(5006), 686-688.
13. Durian, D. J., Weitz, D. A., & Pine, D. J. (1991b). Scaling behavior in shaving cream. *Physical Review A*, 44(12), R7902.
14. Earnshaw, J. C., & Jaafar, A. H. (1994). Diffusing-wave spectroscopy of a flowing foam. *Physical Review E*, 49(6), 5408.
15. Earnshaw, J. C., & Wilson, M. (1995). Strain-induced dynamics of flowing foam: an experimental study. *Journal of Physics: Condensed Matter*, 7(5), L49.
16. Feitosa, K., Halt, O. L., Kamien, R. D., & Durian, D. J. (2006). Bubble kinetics in a steady-state column of aqueous foam. *EPL (Europhysics Letters)*, 76(4), 683.
17. Feitosa, K., Halt, O. L., Kamien, R. D., & Durian, D. J. (2006). Bubble kinetics in a steady-state column of aqueous foam. *EPL (Europhysics Letters)*, 76(4), 683.
18. Feng, S., Thorpe, M. F., & Garboczi, E. (1985). Effective-medium theory of percolation on central-force elastic networks. *Physical Review B*, 31(1), 276.
19. Frese, N., Mitchell, S. T., Neumann, C., Bowers, A., Götzhäuser, A., & Sattler, K. (2016). Fundamental properties of high-quality carbon nanofoam: from low to high density. *Beilstein journal of nanotechnology*, 7(1), 2065-2073.
20. Ganán-Calvo, A. M., Fernandez, J. M., Marquez Oliver, A., & Marquez, M. (2004). Coarsening of monodisperse wet microfoams. *Applied physics letters*, 84(24), 4989-4991.
21. Gao, G., Wu, H. B., Ding, S., Liu, L. M., & Lou, X. W. (2015). Hierarchical NiCo₂O₄ nanosheets grown on Ni nanofoam as high-performance electrodes for supercapacitors. *Small*, 11(7), 804-808.
22. Gardiner, B. S., Dlugogorski, B. Z., & Jameson, G. J. (1999). The evolution of defects in a two-dimensional wet foam. *Journal of Physics: Condensed Matter*, 11(28), 5437.
23. Gardiner, B. S., Dlugogorski, B. Z., & Jameson, G. J. (2000). The steady shear of three-dimensional wet polydisperse foams. *Journal of non-newtonian fluid mechanics*, 92(2-3), 151-166.
24. Gittings, A. S., & Durian, D. J. (2006). Gaussian and non-Gaussian speckle fluctuations in the diffusing-wave spectroscopy signal of a coarsening foam. *Applied optics*, 45(10), 2199-2204.
25. Gittings, A. S., Bandyopadhyay, R., & Durian, D. J. (2004). Photon channelling in foams. *EPL (Europhysics Letters)*, 65(3), 414.
26. Glazier, J. A., & Weaire, D. (1992). The kinetics of cellular patterns. *Journal of Physics: Condensed Matter*, 4(8), 1867.
27. Glazier, J. A., Anderson, M. P., & Grest, G. S. (1990). Coarsening in the two-dimensional soap froth and the large-Q Potts model: a detailed comparison. *Philosophical Magazine B*, 62(6), 615-645.
28. Gopal, A. D., & Durian, D. J. (1999). Shear-induced "melting" of an aqueous foam. *Journal of Colloid and Interface Science*, 213(1), 169-178.
29. Goutev, N., & Nickolov, Z. S. (1996). Raman studies of three-dimensional foam. *Physical Review E*, 54(2), 1725.

30. Hilgenfeldt, S., Koehler, S. A., & Stone, H. A. (2001). Dynamics of coarsening foams: accelerated and self-limiting drainage. *Physical review letters*, 86(20), 4704.
31. Höhler, R., Labiausse, V., & Cohen-Addad, S. (2003). High-resolution diffusing-wave spectroscopy using optimized heterodyne detection. *JOSA A*, 20(11), 2179-2184.
32. Hutzler, S., & Weaire, D. (2000). Foam coarsening under forced drainage. *Philosophical magazine letters*, 80(6), 419-425.
33. Hutzler, S., Weaire, D., & Bolton, F. (1995). The effects of Plateau borders in the two-dimensional soap froth III. Further results. *Philosophical Magazine B*, 71(3), 277-289.
34. In Ref. [20], see p. 98.
35. Iwu, K. O., Lombardo, A., Sanz, R., Scirè, S., & Mirabella, S. (2016). *Sens Actuators B*. 224, 764–771.
36. Jabarkhyl, S., Barigou, M., Badve, M., & Zhu, S. (2020). Rheological properties of wet foams generated from viscous pseudoplastic fluids. *Innovative Food Science & Emerging Technologies*, 64, 102304.
37. Jia, H., An, J., Guo, X., Su, C., Zhang, L., Zhou, H., & Xie, C. (2015). Deep eutectic solvent-assisted growth of gold nanofoams and their excellent catalytic properties. *Journal of Molecular Liquids*, 212, 763-766.
38. Jo, H., Cho, Y. H., Choi, M., Cho, J., Um, J. H., Sung, Y. E., & Choe, H. (2014). Novel method of powder-based processing of copper nanofoams for their potential use in energy applications. *Materials Chemistry and Physics*, 145(1-2), 6-11.
39. Kabla, A., Scheibert, J., & Debregeas, G. (2007). Quasi-static rheology of foams. part 2. continuous shear flow. *Journal of Fluid Mechanics*, 587, 45-72.
40. Khan, S. A., & Armstrong, R. C. (1986). Rheology of foams: I. Theory for dry foams. *Journal of non-newtonian fluid mechanics*, 22(1), 1-22.
41. Koehler, S. A., Stone, H. A., Brenner, M. P., & Eggers, J. (1998). Dynamics of foam drainage. *Physical Review E*, 58(2), 2097.
42. Kraynik, A. M. (1988). Foam flows. *Annual Review of Fluid Mechanics*, 20(1), 325-357.
43. Lemlich, R. (1978). Prediction of changes in bubble size distribution due to interbubble gas diffusion in foam. *Industrial & Engineering Chemistry Fundamentals*, 17(2), 89-93.
44. Lim, K. S., & Barigou, M. (2005). Pneumatic foam generation in the presence of a high-intensity ultrasound field. *Ultrasonics sonochemistry*, 12(5), 385-393.
45. Magrabi, S. A., Dlugogorski, B. Z., & Jameson, G. J. (1999). Bubble size distribution and coarsening of aqueous foams. *Chemical engineering science*, 54(18), 4007-4022.
46. Mason, T. G., Gang, H., & Weitz, D. A. (1997). Diffusing-wave-spectroscopy measurements of viscoelasticity of complex fluids. *JOSA A*, 14(1), 139-149.
47. McDaniel, J. G., Akhatov, I., & Holt, R. G. (2002). Inviscid dynamics of a wet foam drop with monodisperse bubble size distribution. *Physics of Fluids*, 14(6), 1886-1894.
48. Miri, M. F., & Stark, H. (2004). The role of liquid films for light transport in dry foams. *EPL (Europhysics Letters)*, 65(4), 567.
49. Monsalve, A., & Schechter, R. S. (1984). The stability of foams: Dependence of observation on the bubble size distribution. *Journal of colloid and interface science*, 97(2), 327-335.
50. Nieto, M. I., Santacruz, I., & Moreno, R. (2014). Shaping of dense advanced ceramics and coatings by gelation of polysaccharides. *Advanced Engineering Materials*, 16(6), 637-654.
51. Patzek, T. W. (1993). Self-similar collapse of stationary bulk foams. *AIChE journal*, 39(10), 1697-1707.
52. Plateau, J.A.F. (1873). *Statique Experimentale et Theorique des Liquides soumis aux seules Forces Moleculaires*, (Gauthier-villars, Paris, 1873), 2 vols.
53. Princen, H. M., & Kiss, A. D. (1986). Rheology of foams and highly concentrated emulsions: III. Static shear modulus. *Journal of colloid and interface science*, 112(2), 427-437.
54. Prud'homme, R. K., & Khan, S. A. (1996). *Experimental results on foam rheology* (p. 217). Marcel Dekker, New York.
55. Ptaszek, P. (2013). The non-linear rheological properties of fresh wet foams based on egg white proteins and selected hydrocolloids. *Food research international*, 54(1), 478-486.
56. Rezaei, B., Mokhtarianpour, M., & Ensafi, A. A. (2015). Fabricated of bimetallic Pd/Pt nanostructure deposited on copper nanofoam substrate by galvanic replacement as an effective electrocatalyst for hydrogen evolution reaction. *International Journal of Hydrogen Energy*, 40(21), 6754-6762.
57. Saint-Jalmes, A. (2006). Physical chemistry in foam drainage and coarsening. *Soft Matter*, 2(10), 836-849.
58. Saint-Jalmes, A., Vera, M. U., & Durian, D. J. (1999). Uniform foam production by turbulent mixing: new results on free drainage vs. liquid content. *The European Physical Journal B-Condensed Matter and Complex Systems*, 12(1), 67-73.

59. Saint-Jalmes, A., Vera, M. U., & Durian, D. J. (2000). Free drainage of aqueous foams: container shape effects on capillarity and vertical gradients. *EPL (Europhysics Letters)*, 50(5), 695.
60. Saint-Jalmes, A., Vera, M. U., & Durian, D. J. (2000). Free drainage of aqueous foams: container shape effects on capillarity and vertical gradients. *EPL (Europhysics Letters)*, 50(5), 695.
61. Subagyono, D. J., Liang, Z., Knowles, G. P., Webley, P. A., & Chaffee, A. L. (2011). PEI modified mesocellular siliceous foam: A novel sorbent for CO₂. *Energy Procedia*, 4, 839-843.
62. Sun, B., Tenneti, S., & Subramaniam, S. (2015). Modeling average gas–solid heat transfer using particle-resolved direct numerical simulation. *International Journal of Heat and Mass Transfer*, 86, 898-913.
63. Takahashi, M., Menchavez, R. L., Fuji, M., & Takegami, H. (2009). Opportunities of porous ceramics fabricated by gelcasting in mitigating environmental issues. *Journal of the European Ceramic Society*, 29(5), 823-828.
64. Tenneti, S., Sun, B., Garg, R., & Subramaniam, S. (2013). Role of fluid heating in dense gas–solid flow as revealed by particle-resolved direct numerical simulation. *International Journal of Heat and Mass Transfer*, 58(1-2), 471-479.
65. Vera, M. U., Saint-Jalmes, A., & Durian, D. J. (2001). Scattering optics of foam. *Applied optics*, 40(24), 4210-4214.
66. Von Neumann, J. (1952). *Metal Interfaces*, (Am. Soc. for Metals, Cleveland, 1952), p. 108.
67. Weaire, D., & Hutzler, S. (1999). *The Physics of Foams*, (Oxford University Press, Oxford, 1999), pp. 215-217.
68. Weaire, D., & McMurry, S. (1996). Some fundamentals of grain growth, in *Solid State Physics: Advances in Research and Applications*, H. Ehrenreich and F. Spaepen (Editors) (Academic Press, Boston, 1997), Vol. 50.
69. Weaire, D., Hutzler, S., Verbist, G., & Peters, E. A. J. F. (1997). A review of foam drainage. *Advances in chemical Physics*, 102, 315-374.
70. Weitz, D. A., Zhu, J. X., Durian, D. J., Gang, H., & Pine, D. J. (1993). Diffusing-wave spectroscopy: The technique and some applications. *Physica Scripta*, 1993(T49B), 610.
71. Wong, B. T., & Mengüç, M. P. (2002). Depolarization of radiation by non-absorbing foams. *Journal of Quantitative Spectroscopy and Radiative Transfer*, 73(2-5), 273-284.
72. Zhao, J., Yang, C., Shimai, S., Guan, X., Zhou, G., Zhang, J., ... & Wang, S. (2018). The effect of wet foam stability on the microstructure and strength of porous ceramics. *Ceramics International*, 44(1), 269-274.



Short Communication

Dual macrocyclic chemical input based highly protective molecular keypad lock using fluorescence in solution phase: A new type approach

Monaj Karar^a, Provakar Paul^a, Rajib Mistri^b, Tapas Majumdar^{a,*}, Arabinda Mallick^{c,*}^a Department of Chemistry, University of Kalyani, Nadia, West Bengal 741235, India^b Department of Chemistry, Achharam Memorial College, Purulia, West Bengal 723202, India^c Department of Chemistry, Kazi Nazrul University, Asansol, West Bengal 713340, India

ARTICLE INFO

Article history:

Received 12 January 2021

Received in revised form 11 February 2021

Accepted 13 February 2021

Available online 20 February 2021

Keywords:

Chemical input

Fluorescence

Keypad lock

Opto-chemical password

ABSTRACT

Generally, the non-bonding interactions provide the stability to the host-guest complexes without affecting the molecular identity of macrocyclic host and guest (probe) molecules. As a result, macrocyclic-based systems are far more deserving candidates over the ionic systems, as the chance of chemical bleaching is suitably dodged due to the weaker non-bonding interaction. The present article intends to highlight an unconventional and completely innovative designing strategy to validate the operation of a highly protective opto-chemical keypad lock driven by the macrocyclics. Herein, we have utilized the reversible photoswitching phenomenon between two prototropic forms (cationic and neutral) of Harmine (HM) regulated by the dual macrocyclic components, CTAB and β -CD. Most interestingly, methodology provides the choice of the selection of emission detector one at a time between two available emission channels (416 and 365 nm), which have been considered as the "optical inputs". Substantial emission intensities of the probe at the respective emission channels have been treated as the "optical outputs". On the basis of a cautious literature survey, we anticipate that, this kind of designing for a highly protective opto-chemical security device driven by the macrocyclic "chemical inputs" has never explored yet.

© 2021 Elsevier B.V. All rights reserved.

1. Introduction

As representative of superior alternative of the silicon based modern computing technology, numerous molecular interactions with versatile analytes based smart molecular systems having potential to execute binary logic operations are attracting special attentions in recent times [1–7]. Several researchers developed and utilized various small molecular systems as the multipurpose building blocks for multidimensional digital applications like data storage [8–10] and data processing [11–14], switches [15,16], wires [17,18], and molecular machines [19–22]. One of the premium applications of molecular logic circuits is its implementation for the designing of password protected molecular security devices and specifically molecular keypad locks [23,24].

Information protections at the molecular level assisted by extremely secure keypad locks are capable to create and process strong passwords for separate end-users. Currently used security devices utilize silicon-based electronic circuits that need the input of password 'keys' manually for protection of data against illegal information invasion. Limited numbers of keys/digits reduce the level of security of the current

security gadgets. Compared to current silicon-based password systems that use limited alphabets (A-Z), characters (@,%,# etc.) and numbers (0-9) as input keys, opto-chemical molecular security devices were expected to be more secure as they needed to be operated through optical parameters and chemicals as input keys. These newer opto-chemical security systems are evolving as next-generation security gadgets, as hackers require the exact information of the chemical component (s) used in a particular device along with exact optical parameter(s). Endless optical and chemical options and countless possibilities of their combinations make opto-chemical security systems extremely complex and almost impossible to crack, over the conventional silicon-based password circuitry.

Counteracting the social stipulation, scientists engaged themselves with enormous efforts to design keypad locks at the molecular level based on the photo-physical responses [23–26]. These keypad locks are generally constructed based on different optical responses received from the interactions of probe molecules with ions/molecules. In this context, we note that among large number of available molecular keypad lock reports, the use of macrocyclic component/s in molecular logic arena are feeble [27–31]. To the best of our knowledge concern, only one report [30] of chemical security device based on macrocyclics as the chemical inputs is available till date.

Previously, we have studied and reported the structural switching of the cationic and neutral forms of Harmine, HM (Scheme 1) in presence

* Corresponding authors.

E-mail addresses: tapasmju@gmail.com (T. Majumdar), ampcju@yahoo.co.in (A. Mallick).

of CTAB and β -CD in water medium [32,33]. Our current investigation utilizes the same probe (HM) for the construction of molecular keypad lock by using the fluorescence responses upon interaction between macrocyclic components with HM, individually and sequentially. Forward and reverse structural switching of HM upon sequential interactions with CTAB followed by β -CD (macrocyclic 'inputs') resulted in changes of the associated fluorescence intensities at 365 nm & 416 nm (optical 'outputs'). Among many possibilities, a different set of input-output combinations have compiled to produce different sets of passwords. Interaction of macrocyclics with the probe molecule is assumed non-covalent [34–36]. In comparison to the previously reported macrocyclic based keypad lock [30], we propose our lock system seems to be more superior, appealing, and more realistic since it can generate, process, and authenticate a series of passwords accessible for different end-users.

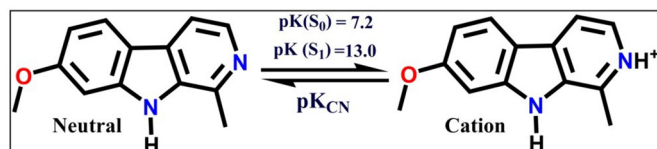
2. Materials and methods

HM and β -CD were procured from Aldrich (Missouri, USA) and used as received. Surfactant, CTAB was procured from Lancaster (England) and used as received. HPLC grade water was used throughout the experiments. Steady-state fluorescence experiments were carried out on Hitachi F-7000 spectrofluorometer (Tokyo, Japan) keeping the slit ratio 1 (Ex. slit = 5 nm, Em. slit = 5 nm) and PMT voltage at 500V. For all fluorescence measurements, a cuvette of 10 mm width was utilised. Concentration of stock HM was 0.335 mM. Pre-weighted β -CDs were gradually added into the cuvette owing to its very low solubility in water, and sonicated for plenty times to obtain thermally equilibrated homogeneous solutions. All other fluorescence measurements were also carried out after proper thermal equilibration of the resultant solution in quartz cuvette through suitably stirred on a magnetic stirrer. Throughout the experiments, temperature was kept constant at 300 K.

3. Results and discussion

It is well established in our previous report that addition of macrocyclic components in a proper chronology leads to switching between the cationic and neutral forms of HM in water medium [33]. In lieu of further detailing, to design the molecular keypad lock, in this present report we have only considered the typical emission spectral changes of HM after the sequential interactions with CTAB and β -CD. In water medium, with λ_{exc} of 300 nm, pure HM exhibited a sharp single emission band at 416 nm, accounted well for its cationic form [37]. With gradual increase of macrocyclic CTAB micelles concentrations, drastic changes in the emission properties of HM were observed. Initial intensity of the existing 416 nm cationic band significantly decreased with simultaneous appearance of a new blue-shifted band close to 365 nm, through a discrete isoemissive point. As per the existing literature, this 365 nm band is well elucidated for the neutral form of HM [36]. Interestingly, with further addition of another macrocyclic component, β -CD within the micelle bound HM, the initial cationic band at 416 nm was almost restored with the outlay of neutral band at 365 nm i.e., almost reverse switching of spectral response was observed (Fig. 1).

In this report, our proposed opto-chemical lock operates through manual entry of a five-digit password and its successive authentication



Scheme 1. Molecular structure of HM with indicated neutral and cationic forms.

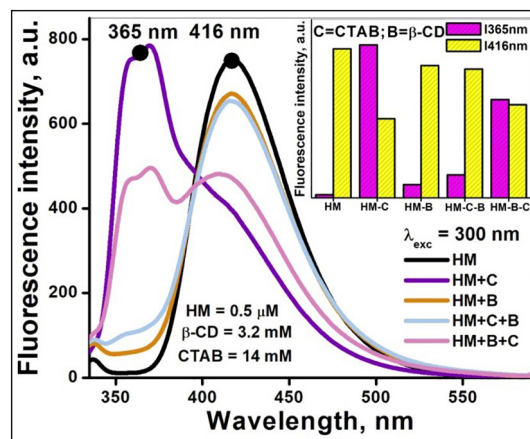


Fig. 1. Fluorescence spectral responses of HM in water upon interactions with CTAB and β -CD sequentially; [HM] = 0.5 μ M; [CTAB] = 14 mM; [β -CD] = 3.2 mM; λ_{exc} = 300 nm; temp. = 300 K.

by the system i.e., the end-user needs to press exactly five input keys in correct sequence for successful password authentication. To construct and track the primary operational trajectory of a functional password, the most important directive is one needs to press 'D4 or D3' key initially, and after each successive entry of chemical inputs, 'C or B', on the system (Fig. 2). Therefore, according to the assigned trajectory of this opto-chemical security device, a general format of the opto-chemical password must follow the sequence as 'D4 or D3' at first, then 'C or B', again 'D4 or D3' key, again 'B or C' and finally 'D4 or D3' again to complete and generate a unique optical pattern as the output response. After each pressing of the optical input key, excitation light (λ_{exc} = 300 nm) must remain "ON" for a pre-fixed time. Within this time-window, corresponding emission must be recorded at the step-correlated detector. Finally, corresponding to that emission intensity, a bar would be generated at the recorder. Ultimately, after completion of a 5-digit password entry, following the proper password trajectory (Fig. 2), a bar pattern would be generated at the recorder.

The back-to-back entry of similar kinds of input keys i.e. optical (D3/D4) or chemical (C/B) during the course of a password entry led to the violation of the preset trajectory pattern embedded within the system. For example, if the end-user does not follow the password format and presses D4/D3 key immediately after entering D3 key or C/B key after entering B key. It would ultimately lead to an erroneous opto-chemical trajectory that will mismatch with the preset password

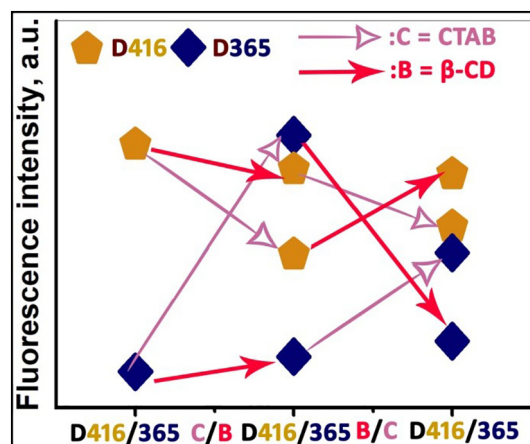


Fig. 2. Password trajectory of the HM system with some specific sequence of password entry. Some typical password recognition patterns have been displayed herein.

trajectory stored within the system. At those situations, the system would display an “error” message, immediately after the wrong entry and alert the administrator for an unauthorized attempt for access. Therefore, it will be an additional advantage of this proposed opto-chemical security device over the conventional chemical password systems [23–25,30,38] that the system could be programmed to alert the administrator for any incorrect key pressing at any step, even before the completion of the password entry, smartly minimizing the chances of password hack through trials.

Ultimately, tracking the above-described guidelines for password compositions, the dual macrocyclics tuned HM system would be able to construct, recognize and authenticate 16 distinct passwords with respective 16 unique emission intensity bar patterns (Fig. 3). These exclusive passwords as the combinations of optical and chemical input keys could be assigned to different end-users for login and other authentication purposes. Any arbitrary entry of opto-chemical input keys beyond the pre-assigned password to a particular end-user must fail to generate an exclusive pattern at the recorder. Only a valid opto-chemical password entry with the correct sequence without any error at any step would successfully operate the lock. Therefore, our proposed system is quite flexible and robust to support and authenticate unique passwords for different end-users on the single chemical platform.

In tune with these advantages, against the illegal invasion this proposed macrocyclics driven opto-chemical security system would perform a dual defence mechanism. At first, during the course of password entry the end-user requires to match/follow the preset password trajectory or exact password sequence of the input keys and secondly it is required to put the exact assigned opto-chemical password, in order to open the lock. If any anomaly found at any step during the course of password entry, the system will alert the administrator. With these

absolute advantages, our proposed macrocyclic component based molecular security device is more promising, versatile, and highly secure compared to so far reported macrocyclics driven lock [30] through supporting a greater number of passwords for multiple users and a step-wise monitoring feature preventing unauthorized access through adopting trials.

In tune with our previous report [37], to illustrate the operational principle of the proposed macrocyclic based molecular keypad lock, let us have a look at the detailed operational mechanism. Suppose an end-user has been assigned with a five-digit password '23452' for login purpose. Now, the end-user needs to press the input keys of that password in the proper sequence. Incipiently, upon pressing the “ON” button the lock starts working. Then the end-user enters the password '23452' on the physical PIN pad of the lock. As the first character of the password '2' is entered, the system is so programmed that it recognizes it as 'D3' input and the detector responsible to measure the emission of HM at 365 nm gets activated. Similarly, the next consecutive four keys, '3', '4', '5' & '2' of the password could be assigned as 'C', 'D4', 'B' & 'D3' input keys, respectively, to the system. As the user enters these password keys in sequence, the system performs next four sequential and independent operations. Complete five-step operations performed by the system could be presented as follows: Step 1) pressing of key '2': system measures the emission intensity of pure HM at 365 nm and at the recorder subsequent bar is generated; Step 2) pressing of key '3': incorporation of CTAB within the HM takes place; Step 3) pressing of key '4': the system monitors the emission of HM-CTAB complex at 416 nm and the corresponding bar is generated at the recorder; Step 4) pressing of key '5': addition of β -CD to the HM-CTAB solution takes place; Step 5) finally, pressing of key '2': the emission intensity of HM-CTAB- β -CD solution is measured at 365 nm and the corresponding

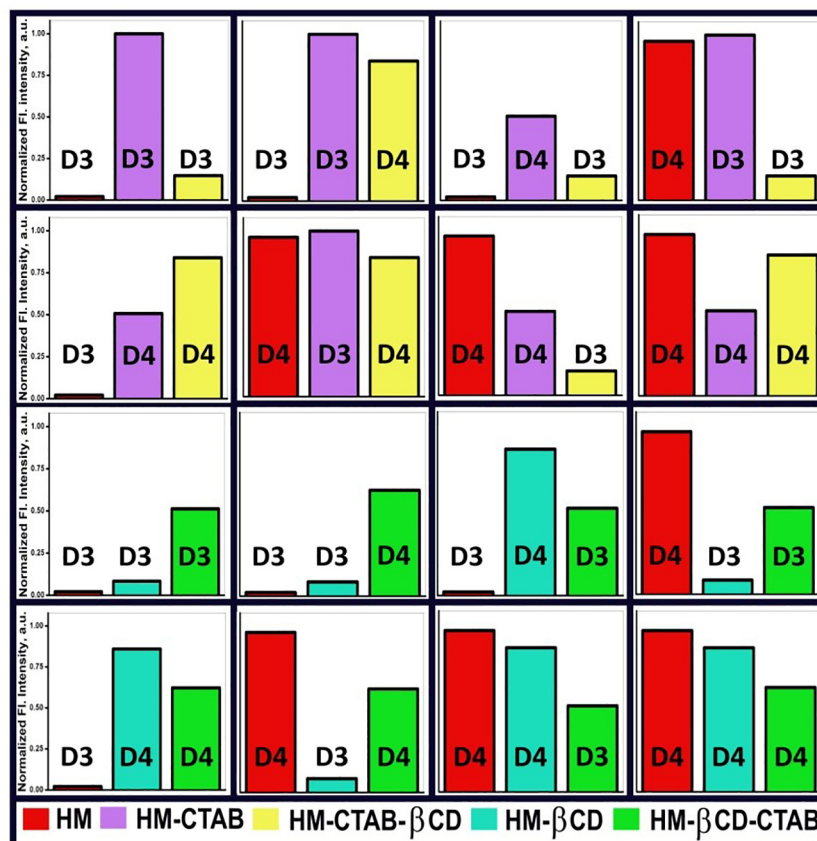


Fig. 3. Derived combinational bar patterns for passwords considering output responses of HM at 365 and 416 nm and altering chemical (CTAB and β -CD) and optical (D4 and D3) inputs; those, in turn, could authenticate the respective opto-chemical passwords.

bar is recorded with the sequence. After successful entry of the complete password, a unique pattern is generated at the recorder with a set of three bars, guided by the stepwise entry of individual and alternate chemical and optical inputs. These unique bar patterns resulting from sequential chemical and optical inputs (Fig. 3) ultimately make different distinct passwords recognized and authenticated by the system to open the lock.

Other arbitrary entry of password keys by unauthorized users would not be validated as the system fails to generate recognizable and authenticated bar patterns at the recorder and ultimately denies the access. Moreover, the lock would not respond if the end-user uses a password less than five digit. Further, if the end-user enters the input keys of the password assigned to him/her in any other arbitrary way (say 24352); the system will immediately alert the administrator as it would fail to meet the stipulated opto-chemical trajectory. A pictorial layout of the above said operational mechanism is given below (Fig. 4).

Virtue of this security device lies in the fact that all possible bar patterns generated following the above-prescribed guidelines are unique and easily distinguishable against each password (Fig. 3). Beyond such 16 possible unique input-output guided bar patterns, the versatility of the keypad lock could be enhanced farther by increasing the number of unique passwords. If we consider the repeated additions of the same substrate at the two addition steps then the allowed and unique passwords should be 32. Further, considering "addition of nothing" at each addition step as a third option, as many as 72 different and unique passwords could be generated. Hitherto, round about all the reported molecular keypad locks were proposed based on the interactions of a particular molecule with a specific set of ions [23–25]. In the ionic environment, it was observed that the structural switching of the main device molecule from one state to another was about irreversible and the molecule more or less lose its originality after only a few cycles of operations. Compared to such ionic components based molecular lock,

the superiority of our proposed macrocyclics driven molecular keypad lock is that the structural switching of our device molecule is completely guided by macrocyclic induced non-ionic chemical environments and the interactions are purely non-covalent rather guided by mildly electrostatic and hydrogen-bonding interactions.

4. Conclusion

A new concept to design molecular keypad lock has been demonstrated on the dynamic switching of HM between cationic and neutral prototropic forms in the presence of macrocyclic chemical inputs, CTAB and β -CD. Since, HM generates dual-band ratiometric emission responses during such differential interactions, the choice of a detector for emission intensity measurement, either at 416 nm or at 365 nm, were considered as optical inputs and designated as D4 or D3, respectively. Finally, different set of emission intensities at the specified wavelengths were considered as optical outputs. Stepwise changes in the intensity values next to the entry of a full-course opto-chemical password were so arranged with step sequencing that specific bar patterns were created against each individual password. Reported macrocyclics based opto-chemical password protection system features formidable security characteristics in terms of non-identifiable chemical and optical elements, error detection during password entry along with reversibility, reusability, energy efficiency, and rapid response. This report might be sighted as a wide-ranging tactic towards the designing of molecular security devices for a category of molecules, specifically, other members of the β -carboline family like, harmaline, norharmaline, proving similar optical switchability as that of HM, in course of differential interactions with these macrocyclic inputs.

Author contributions

TM and AM conceived the idea and coordinated the project. MK,PP, RM carried out the experiments. TM and MK prepared the graphics. TM and AM co-wrote the manuscript.

Declaration of Competing Interest

"There are no conflicts to declare."

Acknowledgements

Research reported in this paper was supported by Department of Science and Technology, Govt. of India under the award number of DST YSS/2015/000904, dated 17-Nov-2015 sanctioned to Tapas Majumdar. Authors also thank University of Kalyani for funding through DST PURSE and DST-FIST (level-2, SR/FST/CS-II/2019/96, Dt. 07.01.2020) programs. M. K. gratefully acknowledges CSIR, Govt. of India for his senior research fellowship. P. P. sincerely acknowledges CSIR, Govt. of India for his junior research fellowship.

References

- [1] A.P. de Silva, H.Q.N. Gunaratne, C.P. McCoy, A molecular photoionic AND gate based on fluorescent signalling, *Nature* 364 (1993) 42–44.
- [2] L.M. Adleman, Molecular computation of solutions to combinatorial problems, *Science* 266 (1994) 1021–1024.
- [3] V. Balzani, M. Venturi, A. Credi, *Molecular Devices and Machines: A Journey into the Nanoworld*, Wiley-VCH, Weinheim, 2003.
- [4] A.P. de Silva, M.R. James, B.O.F. McKinney, D.A. Pears, S.M. Weir, Molecular computational elements encode large populations of small objects, *Nat. Mater.* 5 (2006) 787–790.
- [5] R. Beckman, E. Johnston-Halperin, Y. Luo, J.E. Green, J.R. Heath, Bridging Dimensions: demultiplexing ultrahigh-density nanowire circuits, *Science* 310 (2005) 465–468.
- [6] J.E. Green, J.W. Choi, A. Boukai, Y. Bunimovich, E. Johnston Halperin, E. Delonno, Y. Luo, B.A. Sheriff, K. Xu, Y.S. Shin, H.R. Tseng, J.F. Stoddart, J.R. Heath, A 160-kilobit molecular electronic memory patterned at 10^{11} bits per square centimeter, *Nature* 445 (2007) 414–417.

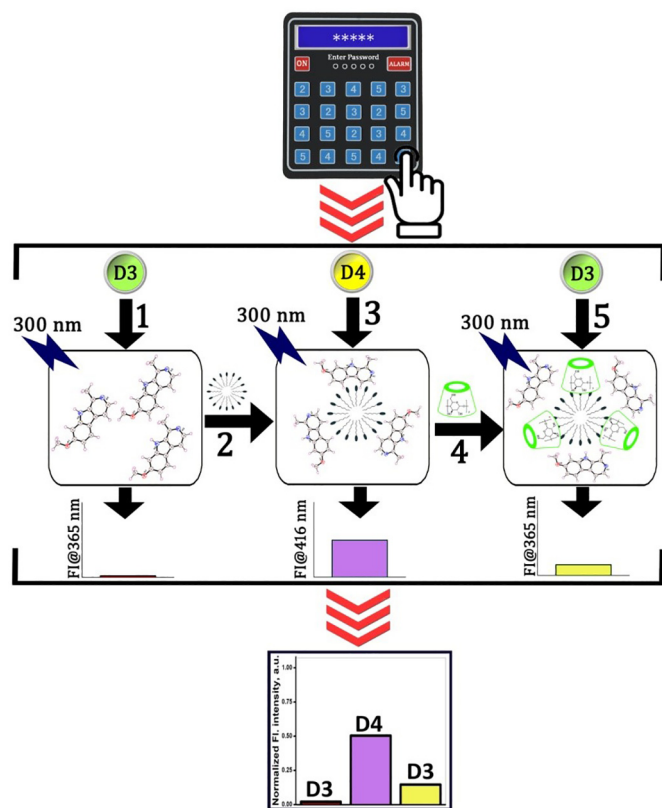


Fig. 4. Operational layouts of the proposed keypad lock considering an authenticated specific five-digit password, '23452', as an example.

- [7] M. Karar, P. Paul, B. Biswas, A. Mallick, T. Majumdar, Excitation wavelength as logic operator, *J. Chem. Phys.* 152 (2020) 075102–075110.
- [8] M. Irie, Diarylethenes for memories and switches, *Chem. Rev.* 100 (2000) 1685–1716.
- [9] J.Y. Jiang, S. Wang, W.F. Yuan, L. Jiang, Y.L. Song, H. Tian, D.B. Zhu, Highly fluorescent contrast for rewritable optical storage based on photochromic bisthiénylene-bridged naphthalimide dimer, *Chem. Mater.* 18 (2006) 235–237.
- [10] S.J. Lim, J. Seo, S.Y. Park, Photochromic switching of excited-state intramolecular proton-transfer (ESIPT) fluorescence: A unique route to high-contrast memory switching and nondestructive readout, *J. Am. Chem. Soc.* 128 (2006) 14542–14547.
- [11] D. Margulies, G. Melman, A. Shanzer, Fluorescein as a model molecular calculator with reset capability, *Nat. Mater.* 4 (2005) 768–771.
- [12] Y.C. Zhou, H. Wu, L. Qu, D.Q. Zhang, D.B. Zhu, A new redox-resettable molecule-based half-adder with tetrathiafulvalene, *J. Phys. Chem. B* 110 (2006) 15676–15679.
- [13] U. Pischel, Chemical approaches to molecular logic elements for addition and subtraction, *Angew. Chem. Int. Ed.* 46 (2007) 4026–4040.
- [14] J. Andreasson, S.D. Straight, S. Bandyopadhyay, R.H. Mitchell, T.A. Moore, A.L. Moore, D. Gust, Molecular 2:1 digital multiplexer, *Angew. Chem. Int. Ed.* 46 (2007) 958–961.
- [15] P.R. Ashton, V. Balzani, J. Becher, A. Credi, M.C.T. Fyfe, G. Matternsteig, S. Menzer, M.B. Nielsen, F.M. Raymo, J.F. Stoddart, M. Venturi, D.J. Williams, A three-pole supramolecular switch, *J. Am. Chem. Soc.* 121 (1999) 3951–3957.
- [16] A.P. de Silva, H.Q.N. Gunaratne, T. Gunnlaugsson, A.J.M. Huxley, C.P. McCoy, J.T. Rademacher, T.E. Rice, Signaling recognition events with fluorescent sensors and switches, *Chem. Rev.* 97 (1997) 1515–1566.
- [17] R. Ziessel, A. Harriman, Building photoactive molecular-scale wires, *Coord. Chem. Rev.* 171 (1998) 331–339.
- [18] A. Harriman, R. Ziessel, Making photoactive molecular-scale wires, *Chem. Commun.* (1996) 1707–1716.
- [19] N. Koumura, R.W.J. Zijlstra, R.A. van Delden, N. Harada, B.L. Feringa, Light-driven unidirectional molecular rotor, *Nature* 401 (1999) 152–155.
- [20] C.D. Mao, W.Q. Sun, Z.Y. Shen, N.C. Seeman, A nanomechanical device based on the B–Z transition of DNA, *Nature* 397 (1999) 144–146.
- [21] C.P. Collier, E.W. Wong, M. Belohradsky, F.M. Raymo, J.F. Stoddart, P.J. Kuekes, R.S. Williams, J.R. Heath, Electronically configurable molecular-based logic gates, *Science* 285 (1999) 391–394.
- [22] M. Asakawa, P.R. Ashton, V. Balzani, A. Credi, G. Matternsteig, O.A. Matthews, M. Montalti, N. Spencer, J.F. Stoddart, M. Venturi, Electrochemically induced molecular motions in pseudorotaxanes: a case of dual-mode (Oxidative and Reductive) dethreading, *Chem. Eur. J.* 3 (1997) 1992–1996.
- [23] D. Margulies, C.E. Felder, G. Melman, A. Shanzer, A molecular keypad lock: A photochemical device capable of authorizing password entries, *J. Am. Chem. Soc.* 129 (2007) 347–354.
- [24] W. Sun, C. Zhou, C.H. Xu, C.J. Fang, C. Zhang, Z.X. Li, C.H. Yan, A fluorescent-switch-based computing Platform in defending information risk, *Chem. Eur. J.* 14 (2008) 6342–6351.
- [25] S. Kumar, V. Luxami, R. Saini, D. Kaur, Superimposed molecular keypad lock and half-subtractor implications in a single fluorophore, *Chem. Commun.* (2009) 3044–3046.
- [26] J. Andre Asson, U. Pischel, Molecules for security measures: from keypad locks to advanced communication protocols, *Chem. Soc. Rev.* 47 (2018) 2266–2279.
- [27] U. Pischel, V.D. Uzunova, P. Remon, W.M. Nau, Supramolecular logic with macrocyclic input and competitive reset, *Chem. Commun.* 46 (2010) 2635–2637.
- [28] M. Karar, P. Paul, S. Paul, B. Haldar, A. Mallick, T. Majumdar, Dual macro-cyclic component based logic diversity, *Dyes Pigments* 174 (2020) 108060–108066.
- [29] A.P. de Silva, I.M. Dixon, H.Q.N. Gunaratne, T. Gunnlaugsson, P.R.S. Maxwell, T.E. Rice, Integration of logic functions and sequential operation of gates at the molecular-scale, *J. Am. Chem. Soc.* 121 (1999) 1393–1394.
- [30] C.P. Carvalho, Z. Dominguez, J.P. Da Silva, U. Pischel, A supramolecular keypad lock, *Chem. Commun.* 51 (2015) 2698–2701.
- [31] B. Daly, T.S. Moody, A.J.M. Huxley, C. Yao, B. Schazmann, A. Alves-Areias, J.F. Malone, H.Q.N. Gunaratne, P. Nockemann, A.P. de Silva, Molecular memory with downstream logic processing exemplified by switchable and self-indicating guest capture and release, *Nat. Commun.* 10 (2019) 49.
- [32] M. Karar, S. Paul, A. Mallick, T. Majumdar, Interaction behavior between active hydrogen bond donor-acceptors as a binding decoration for anion recognition: experimental observation and theoretical validation, *Chemistryselect* 2 (2017) 2815–2821.
- [33] M. Karar, S. Paul, A. Mallick, T. Majumdar, Shipment of a photodynamic therapy agent into model membrane and its controlled release: A photophysical approach, *Chem. Phys. Lipids* 210 (2018) 122–128.
- [34] A. Chakraborty, D. Seth, P. Setua, N. Sarkar, Photoinduced electron transfer reaction in polymer-surfactant aggregates: photoinduced electron transfer between N,N-dimethylaniline and 7-amino coumarin dyes, *J. Chem. Phys.* 128 (2008) 204510.
- [35] P. Das, A. Mallick, A. Chakraborty, B. Haldar, N. Chattopadhyay, Effect of nanocavity confinement on the rotational relaxation dynamics: 3-acetyl-4-oxo-6,7-dihydro-12H indolo-[2,3-a] quinolizine in micelles, *J. Chem. Phys.* 125 (2006). 044516.
- [36] D. Chakraborty, A. Chakraborty, D. Seh, N. Sarkar, Effect of alkyl chain length and size of the headgroups of the surfactant on solvent and rotational relaxation of Coumarin 480 in micelles and mixed micelles, *J. Chem. Phys.* 122 (2005) 184516.
- [37] T. Majumdar, B. Haldar, A. Mallick, A strategic design of an opto-chemical security device with resettable and reconfigurable password based upon dual channel two-in-One chemosensor molecule, *Sci. Rep.* 7 (2017) 42811–42817.
- [38] M. Karar, P. Shit, B. Halder, A. Mallick, T. Majumdar, Multifunctional logic applications of a single molecule: a molecular photo-switch performing as simple and complex gates, memory element, and a molecular keypad lock, *Chemistryselect* 3 (2018) 5277–5282.



REVIEW

Supported Transition Metal Catalysts for Organic Fine Chemical Synthesis: A Review

RAJIB MISTRI*^{ORCID} and BIDYAPATI KUMAR^{ORCID}

Department of Chemistry, Achhruram Memorial College, Jhalda, Purulia-723202, India

*Corresponding author: E-mail: rajibmistri@yahoo.co.in

Received: 9 October 2020;

Accepted: 8 December 2020;

Published online: 16 February 2021;

AJC-20239

Transition metal catalysts play an important role for synthesis of industrially and laboratory important organic fine chemicals to control the selectivity, activity and stability. In this review, we focus on mainly transition metal based supported catalyst, mainly oxide supported catalyst for heterogeneous catalytic hydrogenation and oxidation of some synthetically important organic molecules. First we discuss the industrially important catalytic organic synthetic reactions. This is followed by the role of supported metal catalysts in the heterogeneous synthetic catalytic reactions with specific attention to hydrogenation and oxidation of organic molecules. The role of base metals and noble metals in monometallic and bimetallic catalysts are then discussed. Some synthetic routes for preparation of oxide supported metal catalysts are also discussed. Finally, a general discussion of the metal-support interaction (MSI) in oxide supported metal catalysts is made.

Keywords: Heterogeneous catalyst, Transition metal, Oxidation, Hydrogenation, Important organic molecules.

INTRODUCTION

A chemical industry is in need of technology having maximum activity as well as selectivity towards organic synthetic reactions. Similarly, the requirement is also to adopt “clean” chemical processes having minimum impact on the environment. Hydrogenation and oxidation of organic functional group with high activity and selectivity is one of such requirement. Heterogeneous catalysis plays an important role in wide variety of industrial processes. The most important synthetic use of heterogeneous catalysts are for common synthetic organic transformation. The heterogeneous catalysts can be either oxides [1-6] or metals [7-11]. Most synthetically useful catalytic processes are run over metal catalysts [10-12]. The metal catalyst can be composed of a single metallic component or a mixture of metals [12]. Either of these types can be supported or unsupported. Metal catalysts are used primarily for hydrogenation, hydrogenolysis, isomerization and oxidation reactions, *etc.* [13-16].

The catalytic activity of dispersed metals on an oxide support is influenced by a number of factors. These include size, shape, extent of dispersion, relative amount of metals present, chemical nature of support and strength of interaction between

the support and metal [17]. A support can alter the behaviour of metal in a number of ways. Several explanations have been given to understand enhanced activity of metal doped oxide supported catalysts [18]. They are easily prepared and can be characterized without too many difficulties. Due to this, metal catalysts are generally preferred for basic research. The active catalytic species is believed to be finely dispersed metal particles of sizes in the nano region. Lots of research works have been done on metal-support interaction in supported metal catalysts. Yet the exact nature of active site and the exact role of the support in terms of metal-support interaction are less understood.

Synthetically important organic reaction: Organic synthesis is a key step for the preparation of fine chemicals, pharmaceuticals, agrochemicals, food additives, dyes and pigments. An important factor in developing synthetic reactions is choosing the reaction route to the final product. Catalytic routes have been proven to be one of the most effective ways in simplifying the reaction routes to these compounds by increasing selectivity and reducing waste and hazardous materials handling [19-21]. Additionally, reactions should proceed under mild conditions to reduce the costs of energy. The ultimate aim is of course to adopt a green synthetic route for organic transformations. In

this context, good catalyst performance can be characterized by: (i) high activity and selectivity; (ii) little or no alteration of activity and selectivity with time; (iii) low sensitivity of activity and selectivity to contaminant in the feedstock; and (iv) favourable separation properties.

Organic synthetic chemists are in search of more active, selective and environmentally benign catalyst for their synthesis applications. Alkylation or arylation of aromatic or aliphatic, dehydrogenation, dehydration, hydrogenation, selective oxidation and isomerization are important organic synthesis reactions. A number of new precious catalysts are used for this type of synthetic reactions [22-24].

The alkylation of aromatic compounds is extensively used in the synthesis of various intermediates, fine chemicals and petrochemicals [25]. The necessary feature of this reaction is the replacement of the hydrogen atom of aromatic compound containing alkyl group derived using an alkylating agent. If acid catalyst is used, a replacement occurs in the aromatic ring and base catalyst replaced at side chain of the ring [26]. The commercial alkylations are acid catalyzed [25,27,28]. These include acidic halides such as AlCl_3 , BF_3 , acidic oxides, HF , H_2SO_4 [27], H_3PO_4 and zeolites [28]. The intramolecular isomerization and the transfer alkyl groups between aromatic molecules are also catalyzed by acid catalysts [29-31].

Dehydrogenation of aromatic hydrocarbons (ethylbenzene, diethylbenzene) and alcohols are also industrially important. The ethylbenzene dehydrogenation (EBDH) products are styrene and H_2 [32,33]. Iron oxide is mainly used as a catalyst for the production of styrene [32]. The incorporation of V, Ce and Mo improved the catalytic properties of iron oxide [34]. Catalytic

dehydrogenation of primary and secondary alcohols gives corresponding aldehydes and ketones [34,35]. A large number of solid metal oxide catalysts have been effectively used for alcohol dehydrogenation [36,37]. Most of the oxide catalysts possess also dehydration activity and in some of them, such as alumina, the dehydration predominates [35]. The ratio of the dehydration and dehydrogenation depends on catalyst preparation and its purity. However, some exhibit only dehydrogenation activity, such as oxides of copper, zinc, chromium, iron, *etc.* [36-40]. Metals are also used as dehydrogenation catalysts. Copper is used most frequently, while silver is applied in the combined dehydrogenation-oxidative dehydrogenation processes for production of formaldehyde from methanol or acetaldehyde from ethanol. Noble metals Pt, Pd, Ru, Ir can also be used as oxidative-dehydrogenation catalysts [41-43].

Hydrogenation is the addition of H_2 molecule to a multiple bond ($\text{C}=\text{C}$, $\text{C}\equiv\text{C}$, $\text{C}=\text{O}$, $\text{C}=\text{N}$, $\text{C}\equiv\text{N}$, $\text{N}=\text{O}$, $\text{N}=\text{N}$, $\text{N}\equiv\text{N}$, *etc.*) to reduce it to a lower bond order (Fig. 1). Catalysts are required for the reaction to be usable as the non-catalytic hydrogenation takes place only at very high temperatures.

Platinum, rhodium, palladium and ruthenium form various highly active catalysts and operate at low hydrogen pressures and low temperatures [44-46]. Moreover, inexpensive metal catalysts, based on nickel (such as Raney nickel [47,48] and Urushibara nickel [49]) are established as economical alternatives for expensive catalysts. However, they often provide slow catalysis or operate at high temperatures. Two broad families of catalysts, homogeneous and heterogeneous, are simultaneously important for catalytic hydrogenation. The rhodium based Wilkinson's catalyst and the iridium based Crabtree's homo-

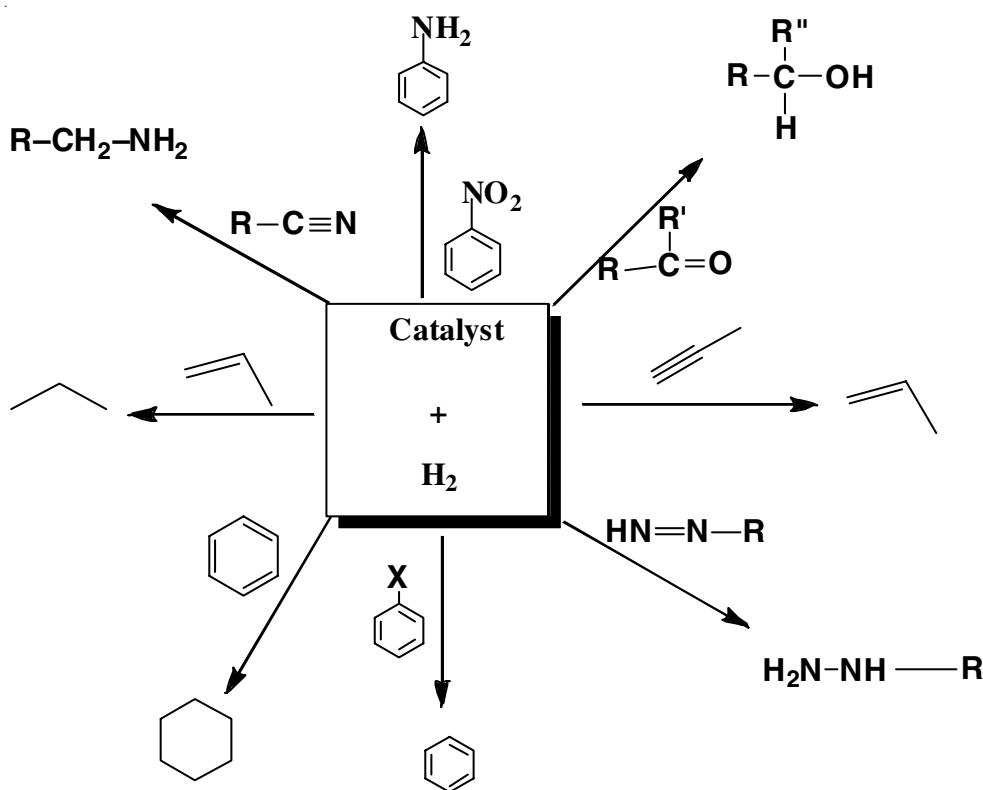


Fig. 1. Common hydrogenation reactions

geneous catalyst are exclusively used as hydrogenation catalyst [50-53].

Heterogeneous catalysts for hydrogenation are more common in industrial synthetic reactions. As in homogeneous catalysts, the activity of the catalyst is adjusted through changes in the environment around the metal, *i.e.* coordination sphere. Different faces of a crystalline heterogeneous catalyst show distinct activities. Similarly, the activity of the heterogeneous catalysts are affected by their supports, *i.e.* the material on which the heterogeneous catalyst is bound [53,54]. A number of new precious catalysts such as Pd/C [55], Pt/C [56] and immobilized Rh [57] catalyst have been successfully commercialized in recent years.

Selective oxidation of functional group is another industrially important catalytic reaction (Fig. 2). Catalytic oxidation in the liquid phase is widely used in bulk chemicals manufacture [58] and become increasingly important in the synthesis of fine chemicals.

A traditional process involving stoichiometric inorganic oxidants is receiving increasing environmental pressure [59]. Generally, in the liquid phase, catalytic oxidation employs soluble complexes or metal salts combined with inexpensive and clean oxidants such as O_2 , H_2O_2 , or RO_2H [20,21].

However, compared with their homogeneous counterparts, heterogeneous catalysts present the advantage of facile recycling and recovering. Large-scale selective oxidation is based on heterogeneous metallic catalysts. Silver is exclusively used as an epoxidation catalyst for the production of ethylene epoxide

from ethylene. Palladium is used as oxidative coupling catalyst for the production of vinyl acetate from ethylene and acetic acid. Cu, V, Mn, Ru, *etc.* are also used as oxidation catalysts for the cycloalkanes, cycloalkenes, benzene and benzyl alcohol [26,60-62].

Common organic hydrogenation reactions: The most common use of catalysts in organic synthesis is the hydrogenation of functional groups. The number of books and reviews published in this area underscores the synthetic importance of these reactions [63-66]. Hydrogenation is commonly a chemical reaction between molecular hydrogen (H_2) and another compound or element, usually in the presence of a catalyst. Hydrogenation of organic functional groups can be categorized into (a) addition of hydrogen across single bonds leading to cleavage of functional groups (hydrogenolysis), (b) addition of hydrogen to unsaturated groups as, for example, in the hydrogenation of ketone to alcohol and (c) removal of oxygen by hydrogen, for example, aromatic nitro to aniline (Fig. 3). Alkenes, alkynes, aromatics, heteroaromatics, ethers, ketones, esters, acids and amides can all be hydrogenated to industrially or synthetically important chemicals.

Catalytic hydrogenation can either be heterogeneous or homogeneous. Metal salts and complexes have provided some homogeneous hydrogenating agents [67-70]. The major disadvantage of the large-scale utilization of metal salts and complexes is their high cost. Due to the inefficient and stoichiometric nature of reactions, for hydrogenation, large quantities of metals or metal salts are required. Furthermore, separating products

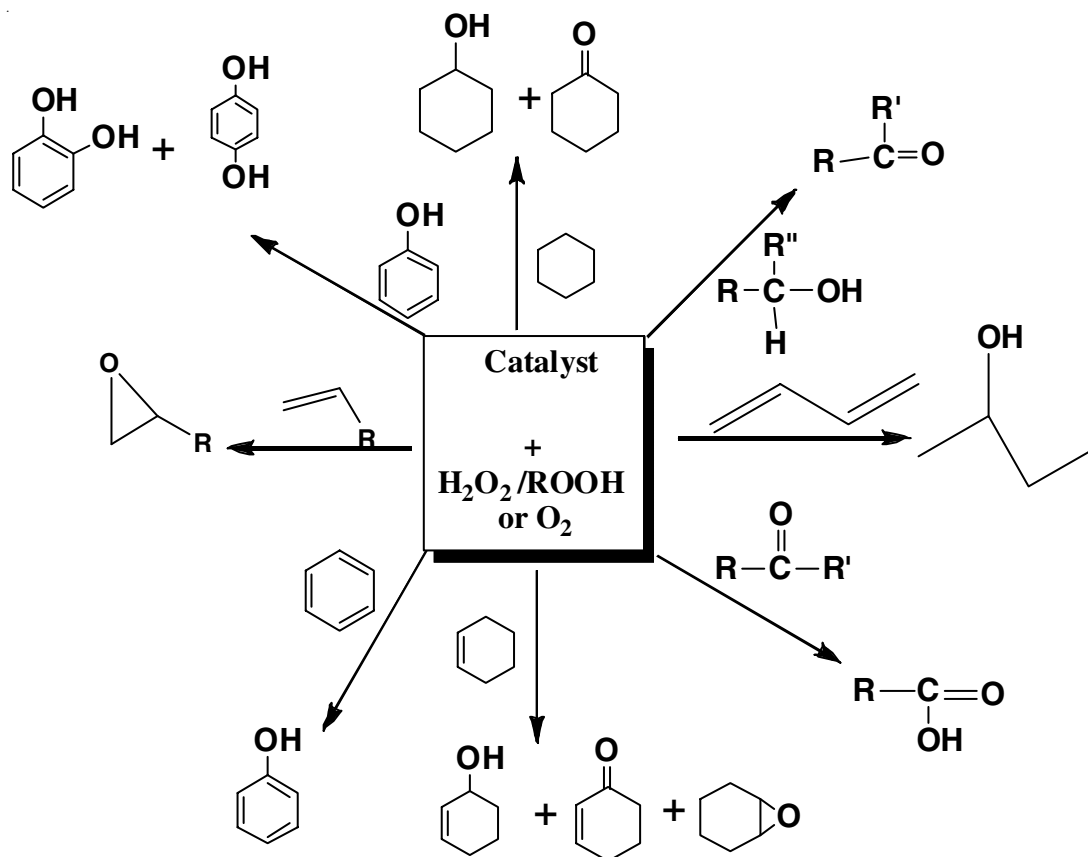


Fig. 2. Common oxidation reactions

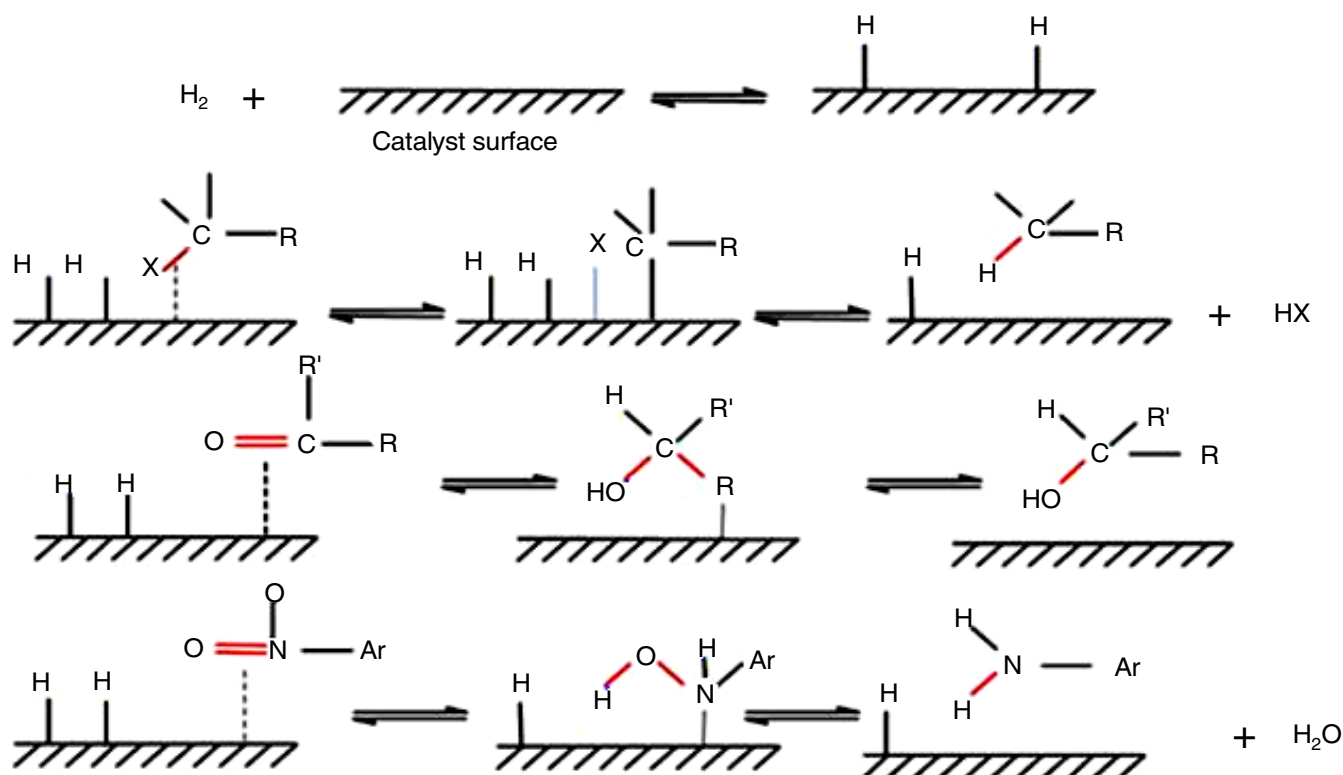


Fig. 3. Catalytic hydrogenation of organic functional groups *via* (a) hydrogenolysis, (b) hydrogen addition and (c) oxygen removal by hydrogen [R, R' = alkyl group; Ar = Aryl group and X = halogen]

from large volumes of metal complex or salt solutions can be inefficient and laborious. These disadvantages can be eliminated by using supported or unsupported heterogeneous metal catalysts, which leads to the easy separation of products and catalysts from reaction mixtures.

Metal-based catalysts are the most active for heterogeneous transfer hydrogenation. Palladium is highly active for the hydrogenation of alkynes or alkenes into alkanes and most commonly used catalyst for hydrogenolyses (benzylic and allylic C=O and C=N bonds, carbon-halogen and het=het, where het = N,O). For the hydrogenation of double bonds (C=N, C=C, and C=O), platinum is highly active [71,72]. When Pt is used, hydrogenolysis does not occur [17]. Under mild conditions, rhodium based catalysts are employed for the hydrogenation of aromatic compounds [73]. By contrast, at high pressures and temperatures, ruthenium usually is employed for the hydrogenation of carbonyl functional groups and aromatic compounds. Nickel, especially Raney nickel, is suitable for the hydrogenation of nitriles to amines and carbonyl groups (ketones and aldehydes) [74]. Under rather harsh conditions, copper-based catalysts are utilized in the hydrogenation of esters into the corresponding alcohols [75].

The catalytic activity of metals depends mainly on three factors (i) catalyst selection, (ii) reaction medium, (ii) reaction condition [76]. The order of the influence of these factors on selectivity is, in general, catalyst > reaction medium > reaction conditions. Catalyst selection depends on metal selection, chemical composition of support, catalyst particle size, particle morphology and oxidation state of metal. The metal influences both the characteristic adsorption/desorption and the surface

reaction. So a right choice of metal is very important for an efficient catalytic reaction. Supports interact with the metal, which influences its structural (morphology and size) and electronic properties, thereby results a lot of catalytic reactions. The rate of the hydrogenation reaction depends on metal particle size and shape or morphology. The smaller the particles, the larger the surface area and thus the activity increases. The catalytic hydrogenation reactions are mainly run in liquid solvent medium. The solvent polarity and hydrogen adsorption capacity and acidity of the medium influence the catalytic reactions. The activity can also depend on the reaction temperature and pressure.

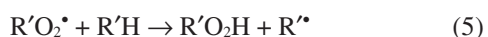
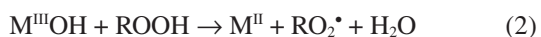
Metal catalysts can be finely divided, pure bulk metal, a skeletal or porous type (Raney Ni), nanoparticles and metals dispersed on different supports or carriers such as inorganic oxides (BaSO_4 , CaCO_3 , SiO_2 and Al_2O_3), carbon (charcoal), polymer, asbestos and zeolites. Some variations found in the metal catalytic activity in supported and free finely divided (blacks) forms result from various ageing treatments and preparation methods. Finely divided metals forms are prone to agglomeration, and in the long run, lose the catalytic activity. This agglomeration can even be accelerated through substrate action or substrate polymerization onto catalysts [77]. Metal precipitation on the support surface is advantageous because it results in a more uniform cluster or particle size of atoms than unsupported metals do and because it provides a large active surface area for the given metal mass (high specific surface density). Metal nanoparticles supported on mesoporous silicas [78,79], hydroxylapatites [80], porous carbons [81,82], zeolite [83], alumina [84] and titanium oxides [85] have been reported

to be highly active for various hydrogenation reactions. The direct synthesis of nanoparticles is limited and preparatory procedures are difficult. So supported metal catalysts are useful for hydrogenation reactions.

Hydrogenation of molecules containing single functional group is a common synthetic transformation. The selective hydrogenation of one functional group in presence of other groups is very important for the synthesis of industrially important chemicals. But if the functional groups have relatively similar or close activities, selectivity can sometimes be achieved by manipulating reaction condition or using proper catalysts. Therefore, recent research effort has been focused strongly on maximizing the catalytic efficiency of the precious metal catalyst by optimizing their physico-chemical properties [86,87], forming alloy structures [72], developing new catalyst supports [88], adding promoters [89,90] and modifying the metal-support interactions [91]. Both heterogeneous [92] and homogeneous metal catalysts [93] have been used in hydrogenation reactions for several decades.

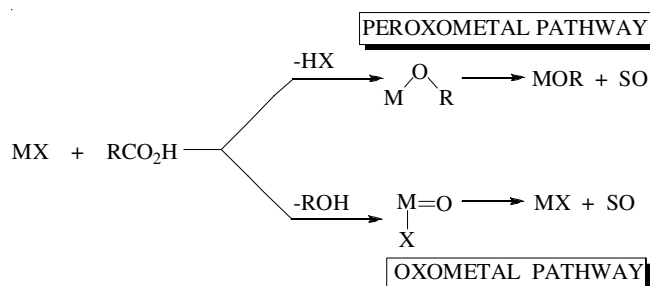
Common organic oxidation reaction: Like hydrogenation, the oxidation of organic functional groups is an important synthetic reaction [58,59]. Most oxidation reactions are run using inorganic oxidants such as permanganate and chromium oxide. The disposal of their reduction products is environmentally unacceptable [20,21]. In the manufacture of bulk chemicals, catalytic oxidation has become very important due to its low impact on the environment. The conversions of alkenes, alkanes, alcohols, ketones, epoxides and aromatic compounds into the more valuable oxygen containing materials are important synthetic reactions in industries [58-62].

Many reactions are run either in vapour phase or in liquid phase and the reaction conditions are usually specific for the production of specific products. Various new catalytic systems have been developed for the oxidation in gas phase and in liquid phase using organic peroxides, H₂O₂ or O₂ as an oxidant [81-83]. The catalytic oxidation reactions are run either by free radical auto-oxidation process or by oxygen transfer process. One-electron oxidants, *e.g.*, Cu(II), Mn(III), Co(III), Ce(IV), Fe(III), *etc.* catalyze free radical auto-oxidation processes by promoting the decomposition of alkyl hydroperoxides into chain initiating alkoxy and alkyl peroxy radicals in one-electron transfer processes (**Scheme-I**, reactions 1 and 2). Strictly speaking the metal ion acts as an initiator of free radical auto-oxidation, which proceeds further *via* reactions 3-5, which does not involve the catalytic species.



Scheme-I: Mechanism of metal catalyzed auto-oxidation

Metal ions which catalyze oxygen transfer reactions with H₂O₂ or RO₂H can be divided into two types based on the active intermediate: a peroxometal or an oxometal complex [92] (**Scheme-II**). Peroxometal pathway is usually favoured over early transition elements with *d*⁰ configuration, *e.g.* Mo(VI), W(VI), V(V) and Ti(IV). On the other hand, over the late or first row transition elements, *e.g.* Cr(VI), V(V), Mn(V), Ru(VI), Ru(VIII) and Os(VIII), the oxometal pathway is usually followed. Some elements, *e.g.* vanadium involve both oxometal and peroxometal pathways depending on the substrate.



Scheme-II: Peroxometal vs. oxometal pathways [92]

Heteroatom oxidations and olefin epoxidation are the reactions involving peroxometal routes. By contrast, oxometal species exhibit the broader range of activities, such as allylic and benzylic oxidations. Peroxometal routes do not involve a change in the metal oxidation state, *i.e.*, activity is not restricted to only variable valence elements and the metal behaves as a Lewis acid. By contrast, the oxometal pathway involves a two-electron redox reaction of metal ions. Furthermore, most metals that catalyse oxygen transfer through oxometal or peroxometal pathways can catalyze one-electron transfer by using peroxides. Consequently, free radical processes frequently compete to a lesser or greater extent with oxygen transfer. When alkyl hydroperoxides are employed as oxidants, heterolytic *versus* homolytic processes are distinguished by using a suitable investigated molecule [93]. The unsupported metals usually form soluble peroxo complexes with H₂O₂ or peroxide so these reactions, in reality, homogeneously catalyzed [94]. Separations of the final products thus become very difficult. Supporting the metals in inorganic oxides (such as SiO₂, Al₂O₃) [95,96] or zeolite [96-98] only served to facilitate the dissolution of the metal species by dispersing the metal over the surface of the support and making it more accessible to the peroxides.

Different types of oxide supported metal catalysts such as Fe/MgO [99], Fe/Al₂O₃ [100], Co/Fe₂O₃ [101], Cu/Al₂O₃ [102], Cu/SiO₂ [103], V/SiO₂ [104] and Mn/Al₂O₃ [105] have been reported to be efficient systems for the production of industrially and chemically important products. These catalysts are usually prone to deactivation before the oxidation is completed. The deactivations are thought to be caused by either oxidation of the metals or blocking the active metal surface by the strong adsorption of the reaction byproducts or decrease of active metal component through metal leaching during oxidation.

A number of procedures have been employed to minimize this deactivation. Most of the early work in this area used large

amount of large sized metal particles [106]. These larger metal particles are more resistant to oxidation than the smaller particles present on the supports [107]. In addition, the large quantity of catalyst ensures that some active species will still be available towards the end of the reactions. The adsorption of byproducts can be eliminated by using more selective catalyst or changing solvent or reaction conditions [108]. Adding another metal particle/s significantly reduce the deactivation [109-112]. The metal leaching can be controlled by using proper support where metal support interaction is strong [113]. The metal leaching is also resisted by adopting specific preparation procedure and incorporating with other metals [114]. Association of two or more active metals can perform well in a reaction system with the enhanced degree of interaction of the components over a support with new redox and acid properties [115].

Selective oxidations *via* heterogeneous catalysis occupy a predominant place in both science of catalysis and synthetic based modern industry. These processes, such as benzene to phenol, benzyl alcohol to benzaldehyde, cyclohexane or cyclohexene to corresponding alcohols and carbonyl compounds have been extensively studied [116-119]. Ru, Pd, Mn, Fe, Co, Ni, V and Cu supported catalysts have been extensively used as catalyst for this type of reaction with H₂O₂ or *tert*-butyl hydrogen peroxide (TBHP) as the oxidant [120-122]. Still there are a large number of opportunities to develop suitable supported metal catalysts for this type of reaction.

Supported metal catalysts in organic synthetic reaction:

Catalytic reaction can be run over supported or unsupported metal catalysts. The active sites on a heterogeneous catalyst are found on its surface. Usually, the efficient catalysts have a large catalytically active surface exposed to the reaction medium. One way to maximizing the active surface of a catalyst is it can be used as a very fine powder as unsupported catalyst. The unsupported metals are found in variety of forms; single crystals, colloids, powders, blacks, skeletal and nanoparticles. Single crystals were used somewhat routinely in the early catalytic research for developing the mechanism in vapour phase reactions [123]. Since most of the synthetic reactions are run in liquid phase these single crystal metal catalysts find little use in the study of synthetic reactions. Black or powder is a metallic powder obtained by the reduction of metal salt or condensation of metal vapour [47]. But they are usually composed of relatively large particles having a low surface area and poor activity [17,48]. Skeletal metals are produced by leaching out one component of an alloy and leaving the active species behind in the form of porous materials having a high surface area [47-49]. However, heating of unsupported catalysts usually results in sintering or agglomeration of the small particles into larger, less efficient entities [124]. The most common way to minimizing metal catalyst sintering is to distribute the active component over a porous, thermostable, inert support. The support may be inorganic oxides, active carbon, polymers and zeolites.

Catalysts with a supported metal comprise 0.1-20 wt.% metal from group 8 or 9, which is dispersed on the support surface, usually a high-surface area oxide [125]. These catalysts are widely used in industries and research laboratories. Because an active metallic phase exists as extremely small particles

with a dispersion degree (*i.e.*, the fraction of atoms exposed to the surface) of 10-100%, these catalysts are effective. These catalysts are widely separated from each other and firmly anchored to supports. Thus, they do not readily sinter or coalesce.

The activity of the dispersed catalyst particles in these supported catalysts is influenced by a number of factors, primarily the relative amount of catalytically active materials present, the surface area of the support, nature of the support and the strength of support-catalyst particles interaction. Metal catalysts with a low metal loading are generally composed of very small crystallites widely scattered over the surface of the support. Such crystallites generally have a high dispersion and the metal is efficiently used as catalyst. As the metal load increases, the crystallites become close to each other and frequently get larger in size. Thus the crystallites are become more resistant to thermal sintering. Obviously, if the catalyst crystallites are come in contact to each other then thermal coalescence can be expected to take place with a resulting loss of active surface area. The low metals loaded highly dispersed catalysts provide a maximum surface area per unit mass of metal. While the catalysts having larger number of catalyst particles spread over the support surface also provide a maximum metal surface area per volume of catalyst.

Generally noble metal catalysts have low metal loads and high metal dispersion, while catalysts containing the less expensive base metals have higher metal loadings. The surface area of a support is directly related to pore size, distribution and volume. The maximum surface area for the support or catalyst is the best possible arrangement. The surface area is not only associated with external surface of the particles but also with the surface of all the pores within the particles. A particle with small diameter pores will have a higher surface area than one with larger diameter pores having both the same total pore volume.

In case of vapour phase reaction involving molecules, catalyst particles having a large number of smaller pores and higher surface areas are preferred. Reactions of larger molecules are usually run in a liquid medium. For such reactions catalysts having smaller pores are inefficient since the diffusion restraints would severely hinder the reaction. Catalysts have larger pores with the catalytically active sites located near the surface of the support particles. So diffusion of the reactants to the active sites will not be a significant factor in the reaction.

Synthetic routes to oxide supported metal catalysts:

The metal components are dispersed over the oxide support by various methods that include impregnation, precipitation and coprecipitation, deposition precipitation, ion-exchange, sol-gel, incipient wetness impregnation, spray drying, freeze drying, *etc.* [126,127]. However, all these processes are involved and sometimes require special equipment and are time consuming. Patil *et al.* [128,129] introduced a novel technique, the single-step solution combustion method, which involved the combustion of the metal salts with organic fuels, for the preparation of different fluorite, perovskite, spinel and mixed oxides [130,131].

Some advantages and disadvantages associated with the conventional methods which are coprecipitation and deposition-

precipitation are beneficial for synthesizing catalysts having high metal loadings (*e.g.* >10 wt.%) and those having low metal loadings of 0.01-5 wt.%, respectively. A limited coprecipitation cannot be applied to SiO₂ but supports Al₂O₃ because these hydroxide precursors or metal oxides cannot be coprecipitated using noble metal hydroxides. The sol-gel method can be used instead of coprecipitation for the SiO₂ support. Deposition-precipitation can be applied to basic metal oxides having the point of zero charge (PZC) of >5 pH. On the surfaces of supports of acidic metal oxide having PZC of < pH 5, noble metal hydroxides cannot be precipitated.

Metal-support interaction in supported metal catalysts:

The concept of a metal-support interaction (MSI) is one of the oldest in heterogeneous catalysis. Initially, it was thought that the support material is inert and serves simply as a vehicle for keeping the catalytically active species separated and thus, minimizes sintering. This is accomplished because catalyst crystallinities are formed some type of chemical bond to the support material by so they are not free to migrate across the surface and agglomerate or coalesce with other crystallinities to form larger particles. Since, the catalyst particles are anchored to the support through some form of bonding the support can, potentially, also influence the activity of the catalyst [132].

This support effect can be assumed as taking place in two distinct ways. First, the support could modify the electronic character of the catalyst particles. This could affect the adsorption and reaction characteristic of the catalytically active sites. Another possibility is that the shape of geometry of the catalyst particles. The electronic effect could change the activity of the sites on the surface while geometric effect would modify the number of active sites present. The first specific suggestion of how the catalytic properties of a metal might be influenced by the support came about 85 years ago by Adadurov (1935). He proposed that metals would be polarized by the surface of oxides containing highly charged cations [133]. The catalytic property of the supported metal catalyst is strongly influenced by the metal support interaction [134-136]. According to Bond's proposition, the metal-support interactions are of three types, namely strong (SMSI), medium (MMSI) and weak (WMSI) [137]. As has been discussed, the SMSI is ascribed to transition metals supported on reducible oxides like CeO₂, TiO₂, BaTiO₃, *etc.* [138-143]. The metal-support interaction is increased with more reducible support. The weak metal-support interaction (WMSI) is generally associated with non-reducible oxides such as SiO₂, Al₂O₃, ZrO₂, *etc.* [144-147]. But the classification is not so straightforward. There are instances of SMSI effect in non-reducible oxide supports [148,149]. The difference between the two categories lies in the facts that MSI is induced under more severe conditions and the property of the catalyst is less pronounced in case of nonreducible oxides.

The catalytic activity of noble metals is decreased significantly as the metal-support interaction increase with reducible support. Several explanations are given for the deactivation behaviour associated with SMSI [150,151]. Four models are proposed for the origin of SMSI, namely, electron transfer, morphological effects, alloying and decoration [152]. Even after extensive studies, a fundamental understanding of the origin

of the SMSI effect remains unclear and it is still a subject of current research [153].

Conclusion

From the foregoing discussion, it is suggested that there is lot of scope towards design of effective catalytic formulations. The preparation of industrially or synthetically important active catalyst for hydrogenation and oxidation reactions has been the constant motivation of researchers in this area of catalysis as outlined above. Inorganic oxide supported noble or base metal catalysts are extensively used as active catalyst for the synthetic organic reactions. It must be kept in mind that the sources of noble metal are limited and also the extraction procedure is costly, which in turn increases the cost of noble metals or its salts. Thus, urge is to reduce the amount of noble metal in the catalyst. But this should not affect the catalyst activity adversely. Conventional dispersion of metal component as zero-valent metal gives rise to finely dispersed nanocrystallinities of size ~3-5 nm on oxide surface. Further reduction of metal crystallinities size to ~1 nm will further increase the dispersion with lower amount of metal doping and hence the rate of reaction will be enhanced. Whatever may be the size of the crystallite, only the metal atoms at the surface of it takes part in chemisorption and catalytic action. The highest possible dispersion with highest activity can be achieved by dispersing each metal atom at the surface, which is not possible by the conventional methods of dispersing metals since due to metal-metal interaction, agglomerated metal crystallites are formed in the end. Thus the catalyst is multiphasic in nature. To make use of each metal atom as the adsorption site, the metal atoms should be placed at particular lattice positions. If the metals are substituted in support lattice in the form of metal-ion by using proper support or proper catalytic preparation methods, then the predominant electronic interaction will be a strong ionic interaction between metal ion and the oxide support. This means that substitution of metal ion in the support lattice is to be achieved forming single phase metal-ion substituted oxide. The metal ions in its positive oxidation state can easily be reduced by other oxidizable substances. Therefore, if the metal is dispersed as ionic form and if one is able to keep the oxidation state in positive state, in principle oxidation can be carried out over such ionically dispersed catalyst. The questions which automatically arise are: (i) How to substitute metal in its ionic form; and (ii) whether the catalytic capability would be the same in its oxidized state and in the zero-valent metallic state? So it is still challenging to prepare an efficient catalyst for synthetically important organic reactions in 21st century.

CONFLICT OF INTEREST

The authors declare that there is no conflict of interests regarding the publication of this article.

REFERENCES

1. T. Curtin, J.B. Mcmonagle, M. Ruwet and B.K. Hodnett, *J. Catal.*, **142**, 172 (1993); <https://doi.org/10.1006/jcat.1993.1199>
2. M. do Ce'v Costa, R. Taveres, W. Motherwell and M.J.M. Curto, *Stud. Surf. Sci. Catal.*, **78**, 639 (1993).

3. A. Servino, J. Vital and L.S. Lobo, *Stud. Surf. Sci. Catal.*, **78**, 685 (1993).
4. L. Posner and R. L. Augustine, *Chem. Ind.*, **62**, 531 (1995).
5. J. Kobayashi, T. Shimizu and K. Inamura, *Chem. Lett.*, **21**, 211 (1992); <https://doi.org/10.1246/cl.1992.211>
6. F. Cavani, G. Centi, F. Parrinello and F. Trifiro, *Stud. Surf. Sci. Catal.*, **31**, 227 (1987).
7. F. Sondheimer and S. Wolfe, *Can. J. Chem.*, **37**, 1870 (1959); <https://doi.org/10.1139/v59-274>
8. A.A. Wismeijer, A.P. Kieboom and H. van Bekkum, *Recl. Trav. Chim. Pays Bas*, **105**, 129 (1986); <https://doi.org/10.1002/recl.19861050406>
9. K. Heyns and H. Paulsen, *Newer Methods of Preparative Organic Chemistry*, Interscience: New York, vol. II, p. 303 (1963).
10. R. Egli and C.H. Eugster, *Helv. Chim. Acta*, **58**, 2321 (1975); <https://doi.org/10.1002/hlca.19750580814>
11. R.W. Clayton and S.V. Norval, *Catalysis*, **3**, 70 (1980); <https://doi.org/10.1039/9781847553140-00070>
12. A. Roberti, V. Ponce and W.M.H. Sachtler, *J. Catal.*, **28**, 381 (1973); [https://doi.org/10.1016/0021-9517\(73\)90131-0](https://doi.org/10.1016/0021-9517(73)90131-0)
13. H.A. Smith and R.G. Thompson, *Adv. Catal.*, **9**, 727 (1957); [https://doi.org/10.1016/S0360-0564\(08\)60225-4](https://doi.org/10.1016/S0360-0564(08)60225-4)
14. P.N. Rylander, N. Rakonczka, D. Steele and M. Bollinger, *Engelhard Ind. Tech. Bull.*, **4**, 95 (1963).
15. W. Reeve and J. Christian, *J. Am. Chem. Soc.*, **78**, 860 (1956); <https://doi.org/10.1021/ja01585a042>
16. A.A. Alshaheri, M.I.M. Tahir, M.B.A. Rahman, T.B.S.A. Ravooof and T.A. Saleh, *Chem. Eng. J.*, **327**, 423 (2017); <https://doi.org/10.1016/j.cej.2017.06.116>
17. R.L. Augustine, *Heterogeneous Catalysis for the Synthetic Chemist*, Marcel Decker: New York, p. 153 (1996).
18. S. Bernal, J.J. Calvino, M.A. Cauqui, J.M. Gatica, C. Larese, J.A. Pérez Omil and J.M. Pintado, *Catal. Today*, **50**, 175 (1999); [https://doi.org/10.1016/S0920-5861\(98\)00503-3](https://doi.org/10.1016/S0920-5861(98)00503-3)
19. S. Bernal, J.J. Calvino, M.A. Cauqui, J.M. Gatica, C. Larese, J.A. Pérez Omil and J.M. Pintado, *Appl. Catal. A Gen.*, **209**, 125 (2001); [https://doi.org/10.1016/S0926-860X\(00\)00750-X](https://doi.org/10.1016/S0926-860X(00)00750-X)
20. E.L. Pires, J.C. Magalhaes and U. Schuchardt, *Appl. Catal. A Gen.*, **203**, 231 (2000); [https://doi.org/10.1016/S0926-860X\(00\)00496-8](https://doi.org/10.1016/S0926-860X(00)00496-8)
21. R.S. da Cruz, J.M. de Souza e Silva, U.I. Arnold and U. Schuchardt, *J. Mol. Catal. Chem.*, **171**, 251 (2001); [https://doi.org/10.1016/S1381-1169\(01\)00111-X](https://doi.org/10.1016/S1381-1169(01)00111-X)
22. Kirk-Othmer, *Encyclopedia of Chemical Technology*, Wiley: New York, edn 4 (1991).
23. H. Pines, *The Chemistry of Catalytic Hydrocarbon Conversions*, Academic Press: New York (1981).
24. N.Y. Chen, W.E. Garwood and R.H. Heck, *Ind. Eng. Chem. Process Des. Dev.*, **26**, 706 (1987); <https://doi.org/10.1021/ie00064a014>
25. F.G. Dwyer and P.J. Lewis, in eds.: J.J. McKetta and W.A. Cunningham, *Encyclopedia of Chemical Processing and Design*, Marcel Dekker: New York, vol. 20, p. 77 (1997).
26. G. Ertl, H. Knozinger and J. Weitkamp, in: *Hand book of Heterogeneous Catalysis*, Marcel Decker, New York, vol. 5 (1995).
27. G.A. Olah, *Fridel-Crafts Chemistry*, Wiley: New York (1973).
28. W.L. Lenneman, R.D. Hites and V.I. Komarewsky, *J. Org. Chem.*, **19**, 463 (1954); <https://doi.org/10.1021/jo01368a028>
29. M.B. Welch, *Zinc Aluminate Double Bond Isomerization Catalyst and Process for its Production*, US Patent 4692430 (1986).
30. P. Wimmer, H.-J. Buysch and L. Puppe, *Process for the Preparation of Thymol*, US Patent 5030770 (1991).
31. S. Velu and S. Sivasanker, *Res. Chem. Intermed.*, **24**, 657 (1998); <https://doi.org/10.1163/156856798X00555>
32. J. Stell, *Oil Gas J.*, **99**, 74 (2001).
33. J. Weitkamp and Y. Traa, in eds.: G. Ertl, H. Knozinger and J. Weitkamp, *Handbook of Heterogeneous Catalysis*, VCH: Weinheim, vol. 4, p. 2039 (1997).
34. K.K. Kearby in eds.: P. Emmett, *Catalysis*, Rheinhold: New York, vol. III, p. 469 (1955).
35. E.H. Lee, *Catal. Rev.*, **8**, 285 (1974); <https://doi.org/10.1080/01614947408071864>
36. R. Connor, K. Folkers and H. Adkins, *J. Am. Chem. Soc.*, **54**, 1138 (1932); <https://doi.org/10.1021/ja01342a042>
37. A.H. Blatt, *Organic Syntheses*, vol. 2, p. 142 (1943).
38. K. Weissermel and H.J. Arpe, *Industrielle Organische Chemie*, VCH, Weinheim, edn 4 (1994).
39. T. Hirano, *Appl. Catal.*, **26**, 81 (1986); [https://doi.org/10.1016/S0166-9834\(00\)82543-9](https://doi.org/10.1016/S0166-9834(00)82543-9)
40. I.E. Wachs and R.J. Madix, *Surf. Sci.*, **76**, 531 (1978); [https://doi.org/10.1016/0039-6028\(78\)90113-9](https://doi.org/10.1016/0039-6028(78)90113-9)
41. M.A. Barteau, M. Bowker and R.J. Madix, *Surf. Sci.*, **94**, 303 (1980); [https://doi.org/10.1016/0039-6028\(80\)90009-6](https://doi.org/10.1016/0039-6028(80)90009-6)
42. T. Mallat, T. Allmendinger and A. Baiker, *Appl. Surf. Sci.*, **52**, 189 (1991); [https://doi.org/10.1016/0169-4332\(91\)90047-N](https://doi.org/10.1016/0169-4332(91)90047-N)
43. T. Mallat, E. Orglmeister and A. Baiker, *Chem. Rev.*, **107**, 4863 (2007); <https://doi.org/10.1021/cr0683663>
44. J. Wang, L. Huang and Q. Li, *Appl. Catal. A Gen.*, **175**, 191 (1998); [https://doi.org/10.1016/S0926-860X\(98\)00216-6](https://doi.org/10.1016/S0926-860X(98)00216-6)
45. B. Cornils and E. Wiebus, *Chemtech*, **33** (1999).
46. V.L. Khilnani and S.B. Chandalia, *Org. Process Res. Dev.*, **5**, 257 (2001); <https://doi.org/10.1021/op9900380>
47. H. Adkins and G. Krsek, *J. Am. Chem. Soc.*, **70**, 412 (1948); <https://doi.org/10.1021/ja01181a501>
48. M. Yadav and R.K. Sharma, *Curr. Opin. Green Sustain. Chem.*, **15**, 47 (2019); <https://doi.org/10.1016/j.cogsc.2018.08.010>
49. Y. Urushibara, *Bull. Chem. Soc. Jpn.*, **26**, 280 (1952); <https://doi.org/10.1246/bcsj.25.280>
50. A.M. Bennett and A.P. Longstaff, *Chem. Ind.*, 846 (1965).
51. A.J. Birch and D.H. Williamson, *Organic Reactions*, **24** (1976).
52. B.R. James, *Homogeneous Hydrogenation*, John Wiley & Sons: New York, (1973).
53. R.H. Crabtree, *Acc. Chem. Res.*, **12**, 331 (1979).
54. J.H. Kang, L.D. Menard, R.G. Nuzzo and A.I. Frenkel, *J. Am. Chem. Soc.*, **128**, 12068 (2006); <https://doi.org/10.1021/ja064207p>
55. P. Ehrburger and P.L. Walker, *J. Catal.*, **55**, 63 (1978); [https://doi.org/10.1016/0021-9517\(78\)90187-2](https://doi.org/10.1016/0021-9517(78)90187-2)
56. W.F. Newhall, *J. Org. Chem.*, **23**, 1274 (1958); <https://doi.org/10.1021/jo01103a009>
57. J.W. Bozzelli, Y.M. Chen and S.C. Chuang, *Chem. Eng. Commun.*, **115**, 1 (1992); <https://doi.org/10.1080/00986449208936024>
58. R.A. Sheldon and J.K. Kochi, *Metal Catalyzed Oxidations of Organic Compounds*, Academic Press: New York (1981).
59. R.A. Sheldon and R.S. Downing, *Appl. Catal. A Gen.*, **189**, 163 (1999); [https://doi.org/10.1016/S0926-860X\(99\)00274-4](https://doi.org/10.1016/S0926-860X(99)00274-4)
60. R.L. Augustine, *Catalytic Hydrogenation, Techniques and Application in Organic Synthesis*, Dekker: New York (1965).
61. S. Parashar and S. Khare, *React. Kinet. Mech. Catal.*, **127**, 469 (2019); <https://doi.org/10.1007/s1144-019-01559-z>
62. R.L. Augustine, *Catal. Rev.*, **13**, 285 (1976); <https://doi.org/10.1080/00087647608069940>
63. P.N. Rylander, in: *Hydrogenation Methods*, Academic Press: New York (1985).
64. M. Freifelder, *Practical Catalytic Hydrogenation*, Wiley-Interscience: New York (1971).
65. A.P.G. Kieboom and F. van Rantwijk, *Hydrogenation and Hydrogenolysis in Synthetic Organic Chemistry*, Delft University Press, Delft (1977).
66. F. Zaera, *ACS Catal.*, **7**, 4947 (2017); <https://doi.org/10.1021/acscatal.7b01368>
67. S.A. Mahood and P.V. Schaffner, in eds.: A. H. Blatt, *Organic Synthesis*, Wiley: New York, vol. 11, p. 160 (1969).
68. O. Kamm, in eds.: A.H. Blatt, *Organic Synthesis*, Wiley: New York, vol. 11, p. 445 (1948).
69. H.E. Bigelow and D.B. Robinson, in eds.: E.C. Horning: *Organic Synthesis*, Chapman and Half Loncn, vol. 111, p. 103 (1955).
70. H.E. Bigelow and A. Palmer, in eds.: A.H. Blatt, *Organic Syntheses*, Wiley: New York, vol. 11, p. 57 (1969).

71. H. Hattori, *Chem. Rev.*, **95**, 537 (1995); <https://doi.org/10.1021/cr00035a005>
72. T. Punniyamurthy, S. Velusamy and J. Iqbal, *Chem. Rev.*, **105**, 2329 (2005); <https://doi.org/10.1021/cr050523v>
73. G. Gilman and G. Cohn, *Adv. Catal.*, **9**, 733 (1957); [https://doi.org/10.1016/S0360-0564\(08\)60226-6](https://doi.org/10.1016/S0360-0564(08)60226-6)
74. H. Hauptmann and W.F. Walter, *Chem. Rev.*, **62**, 347 (1962); <https://doi.org/10.1021/cr60219a001>
75. H. Adkins, *Organic Reaction*, vol. VIII, p. 1 (1994).
76. R.A.W. Johnstone, A.H. Wilby and I.D. Entwistle, *Chem. Rev.*, **85**, 129 (1985); <https://doi.org/10.1021/cr00066a003>
77. J.R. Weir, B.A. Patel and F.R. Heck, *J. Org. Chem.*, **45**, 4926 (1980); <https://doi.org/10.1021/jo01312a021>
78. W. Zhou, J.M. Thomas, D.S. Shephard, B.F.G. Johnson, D. Ozkaya, T. Maschmeyer, R.G. Bell and Q. Ge, *Science*, **280**, 705 (1998); <https://doi.org/10.1126/science.280.5364.705>
79. V. Hulea, D. Brunel, A. Galarneau, K. Philippot, B. Chaudret, P.J. Kooyman and F. Fajula, *Micropor. Mesopor. Mater.*, **79**, 185 (2005); <https://doi.org/10.1016/j.micromeso.2004.10.041>
80. C.M. Ho, W.Y. Yu and C.M. Che, *Angew. Chem. Int. Ed.*, **43**, 3303 (2004); <https://doi.org/10.1002/anie.200453703>
81. L. Fabre, P. Gallezot and A. Perrard, *J. Catal.*, **208**, 247 (2002); <https://doi.org/10.1006/jcat.2002.3567>
82. E. Crezee, B.W. Hoffer, R.J. Berger, M. Makkee, F. Kapteijn, A. Jacob and J.A. Moulijn, *Appl. Catal. A Gen.*, **251**, 1 (2003); [https://doi.org/10.1016/S0926-860X\(03\)00587-8](https://doi.org/10.1016/S0926-860X(03)00587-8)
83. M.L. Kantam, B.P.C. Rao, B.M. Choudary and B. Sreedhar, *Adv. Synth. Catal.*, **348**, 1970 (2006); <https://doi.org/10.1002/adsc.200505497>
84. B. Kusserow, S. Schimpf and P. Claus, *Adv. Synth. Catal.*, **345**, 289 (2003); <https://doi.org/10.1002/adsc.200390024>
85. A.T. Bell, *Science*, **299**, 1688 (2003); <https://doi.org/10.1126/science.1083671>
86. J. Zhang, K. Sasaki, E. Sutter and R.R. Adzic, *Science*, **315**, 220 (2007); <https://doi.org/10.1126/science.1134569>
87. V.R. Stamenkovic, B. Fowler, B.S. Mun, G. Wang, P.N. Ross, C.A. Lucas and N.M. Markovic, *Science*, **315**, 493 (2007); <https://doi.org/10.1126/science.1135941>
88. S.H. Joo, S.J. Choi, I. Oh, J. Kwak, Z. Liu, O. Terasaki and R. Ryoo, *Nature*, **412**, 169 (2001); <https://doi.org/10.1038/35084046>
89. T.W. Hansen, J.B. Wagner, P.L. Hansen, S. Dahl, H. Topsøe and C.J.H. Jacobsen, *Science*, **294**, 1508 (2001); <https://doi.org/10.1126/science.1064399>
90. R. Mistri, J. Llorca, B.C. Ray and A. Gayen, *J. Mol. Catal. Chem.*, **376**, 111 (2013); <https://doi.org/10.1016/j.molcata.2013.04.018>
91. Q. Fu, H. Saltsburg and M. Flytzani-Stephanopoulos, *Science*, **301**, 935 (2003); <https://doi.org/10.1126/science.1085721>
92. J.V. Porcelli, *Catal. Rev.*, **23**, 151 (1981); <https://doi.org/10.1080/03602458108068073>
93. W.M.H. Sachtler, C. Backx and R.A. Van Santen, *Catal. Rev.*, **23**, 127 (1981); <https://doi.org/10.1080/03602458108068072>
94. R.K. Grasselli, *ACS Symp. Ser.*, **222**, 317 (1983); <https://doi.org/10.1021/bk-1983-0222.ch025>
95. M.G. Noppenhuis, A. Baiker, P. Barnickel and A. Wokaun, *Appl. Catal. A Gen.*, **85**, 157 (1992); [https://doi.org/10.1016/0926-860X\(92\)80149-7](https://doi.org/10.1016/0926-860X(92)80149-7)
96. A. Sakthivel and P. Selvam, *J. Catal.*, **211**, 134 (2002); [https://doi.org/10.1016/S0021-9517\(02\)93711-5](https://doi.org/10.1016/S0021-9517(02)93711-5)
97. M.L. Neidig and K.F. Hirsekorn, *Catal. Comm.*, **12**, 480 (2011); <https://doi.org/10.1016/j.catcom.2010.10.024>
98. R.A. Sheldon, *Top. Curr. Chem.*, **164**, 21 (1993); https://doi.org/10.1007/3-540-56252-4_23
99. P.A. MacFaul, I.W.C.E. Arends, K.U. Ingold and D.D.M. Wayner, *J. Chem. Soc., Perkin Trans. II*, 135 (1997); <https://doi.org/10.1039/a606160e>
100. I.W.C.E. Arends, K.U. Ingold and D.D.M. Wayner, *J. Am. Chem. Soc.*, **117**, 4710 (1995); <https://doi.org/10.1021/ja00121a031>
101. R.A. Sheldon, in eds.: R. Ugo, *Aspect of Homogeneous Catalysis*, Reidel, Dordrecht, vol. 4, p. 1 (1981).
102. J. Sobczak and J.J. Ziolkowski, *React. Kinet. Catal. Lett.*, **11**, 359 (1979); <https://doi.org/10.1007/BF02079726>
103. R.A. Sheldon, in eds.: S. Patai, *The Chemistry of Functional Groups-Peroxides*, Wiley: New York, p. 161 (1982).
104. R.A. Sheldon and J. Dakka, *Catal. Today*, **19**, 215 (1994); [https://doi.org/10.1016/0920-5861\(94\)80186-X](https://doi.org/10.1016/0920-5861(94)80186-X)
105. M.G. Clerici, *Stud. Surf. Sci. Catal.*, **78**, 21 (1993); [https://doi.org/10.1016/S0167-2991\(08\)63301-7](https://doi.org/10.1016/S0167-2991(08)63301-7)
106. C. Ferrini and H.W. Kouwenhoven, *Stud. Surf. Sci. Catal.*, **55**, 53 (1990); [https://doi.org/10.1016/S0167-2991\(08\)60133-0](https://doi.org/10.1016/S0167-2991(08)60133-0)
107. N.K. Renuka, *J. Mol. Catal. Chem.*, **316**, 126 (2010); <https://doi.org/10.1016/j.molcata.2009.10.010>
108. H.H. Monfared and Z. Amouei, *J. Mol. Catal. Chem.*, **217**, 161 (2004); <https://doi.org/10.1016/j.molcata.2004.03.020>
109. H. Kanzaki, T. Kitamura, R. Hamada, S. Nishiyama and S. Tsuruya, *J. Mol. Catal. Chem.*, **208**, 203 (2004); [https://doi.org/10.1016/S1381-1169\(03\)00516-8](https://doi.org/10.1016/S1381-1169(03)00516-8)
110. J. Okamura, S. Nishiyama, S. Tsuruya and M. Masai, *J. Mol. Catal. Chem.*, **135**, 133 (1998); [https://doi.org/10.1016/S1381-1169\(97\)00298-7](https://doi.org/10.1016/S1381-1169(97)00298-7)
111. K. Heynes and H. Paulsen, in eds.: W. Forest and F.K. Kirchner, *Newer Methods of Preparative Organic Chemistry*, Academic Press: New York, vol. 2, p. 303 (1963).
112. M. Boudart, A. Aldag, J.E. Benson, N.A. Dougharty and C. Girvin Harkins, *J. Catal.*, **6**, 92 (1966); [https://doi.org/10.1016/0021-9517\(66\)90113-8](https://doi.org/10.1016/0021-9517(66)90113-8)
113. T. Mallat and A. Baiker, *Catal. Today*, **19**, 247 (1994); [https://doi.org/10.1016/0920-5861\(94\)80187-8](https://doi.org/10.1016/0920-5861(94)80187-8)
114. T. Mallat and A. Baiker, *Appl. Catal. A Gen.*, **79**, 41 (1991); [https://doi.org/10.1016/0926-860X\(91\)85005-1](https://doi.org/10.1016/0926-860X(91)85005-1)
115. T. Mallat, A. Baiker and L. Botz, *Appl. Catal. A Gen.*, **86**, 147 (1992); [https://doi.org/10.1016/0926-860X\(92\)85145-2](https://doi.org/10.1016/0926-860X(92)85145-2)
116. T. Miyahara, H. Kanzaki, R. Hamada, S. Kuroiwa, S. Nishiyama and S. Tsuruya, *J. Mol. Catal. Chem.*, **176**, 141 (2001); [https://doi.org/10.1016/S1381-1169\(01\)00242-4](https://doi.org/10.1016/S1381-1169(01)00242-4)
117. I.W.C.E. Arends and R.A. Sheldon, *Appl. Catal. A Gen.*, **212**, 175 (2001); [https://doi.org/10.1016/S0926-860X\(00\)00855-3](https://doi.org/10.1016/S0926-860X(00)00855-3)
118. X. Liu, J. He, L. Yang, Y. Wang, S. Zhang, W. Wang and J. Wang, *Catal. Commun.*, **11**, 710 (2010); <https://doi.org/10.1016/j.catcom.2010.01.026>
119. K.T. Makhmudov, R.A. Alieva, S.R. Gadzhieva and F.M. Chyragov, *J. Anal. Chem.*, **63**, 435 (2008); <https://doi.org/10.1134/S1061934808050055>
120. L. Lin, J. Liuyan and W. Yunyang, *Catal. Commun.*, **9**, 1379 (2008); <https://doi.org/10.1016/j.catcom.2007.11.041>
121. M.R. Morales, B.P. Barbero and L.E. Cadus, *Appl. Catal. B*, **74**, 1 (2007); <https://doi.org/10.1016/j.apcatb.2007.01.008>
122. H. Liu, Z. Fu, D. Yin, D. Yin and H. Liao, *Catal. Commun.*, **6**, 638 (2005); <https://doi.org/10.1016/j.catcom.2005.06.002>
123. S.K. Pardeshi and R.Y. Pawar, *Mater. Res. Bull.*, **45**, 609 (2010); <https://doi.org/10.1016/j.materresbull.2010.01.011>
124. J.W. Geus, *Stud. Surf. Sci. Catal.*, **16**, 1 (1983); [https://doi.org/10.1016/S0167-2991\(09\)60006-9](https://doi.org/10.1016/S0167-2991(09)60006-9)
125. G.C. Bond, *Acc. Chem. Res.*, **26**, 490 (1993); <https://doi.org/10.1021/ar00033a006>
126. F.J. Janssen, in eds.: G. Ertl, H. Knozinger and J. Weitkamp, *Hand Book of Heterogeneous Catalysis*, VCH, Weinheim, vol. 1, p.191 (1997).
127. G. Y. adachi and T. Masui, in eds.: A. Trovarelli, *Catalysis by Ceria and Related Materials*, Imperial College Press: London, p. 52 (2002).
128. M.M.A. Sekar, S.S. Manoharan and K.C. Patil, *J. Mater. Sci. Lett.*, **9**, 1205 (1990); <https://doi.org/10.1007/BF00721893>

129. K.C. Patil, S.T. Aruna and S. Ekambaram, *Curr. Opin. Solid State Mater. Sci.*, **2**, 158 (1997);
[https://doi.org/10.1016/S1359-0286\(97\)80060-5](https://doi.org/10.1016/S1359-0286(97)80060-5)
130. K. Suresh and K.C. Patil, eds.: K.J. Rao, Perspective in Solid State Chemistry, Narosa Publishing House: New Delhi, p. 376 (1995).
131. A. Gayen, K.R. Priolkar, P.R. Sarode, V. Jayaram, M.S. Hegde, G.N. Subbanna and S. Emur, *Chem. Mater.*, **16**, 2317 (2004);
<https://doi.org/10.1021/cm0401261>
132. G.C. Bond and R. Burch, eds.: G.C. Bond and G. Webb, A Specialist Periodical Report: Catalysis, The Royal Society of Chemistry, London, vol. 6, 27 (1983).
133. S.A. Stevenson, G.B. Raupp, J.A. Dumesic, S.J. Tauster and R.T.K. Baker, eds.: S.A. Stevenson, G.B. Raupp, J.A. Dumesic, S.J. Tauster R.T.K. Baker and E. Ruckenstein, Metal-Support Interaction in Catalysis, Sintering and Redispersion, Van Nostrand-Reinhold, New York, p. 3, (1987).
134. J.G. Dickson, L. Katz and R. Ward, *J. Am. Chem. Soc.*, **83**, 3026 (1958);
<https://doi.org/10.1021/ja01475a012>
135. J.H. Sinfelt, *J. Phys. Chem.*, **68**, 344 (1964);
<https://doi.org/10.1021/j100784a023>
136. G.M. Schwab, *Advances Catalysis*, Academic Press: Orlando, FL, vol. 1, (1978).
137. G.C. Bond, *Metal-Support and Metal Additive Effect in Catalysis*, Elsevier Scientific Pub. Co.: Amsterdam, (1982).
138. S.J. Tauster, S.C. Fung and P.L. Garten, *J. Am. Chem. Soc.*, **100**, 170 (1978);
<https://doi.org/10.1021/ja00469a029>
139. L.E. Oi, M.-Y. Choo, H.V. Lee, H.C. Ong, S.B.A. Hamid and J.C. Juan, *RSC Advances*, **6**, 108741 (2016);
<https://doi.org/10.1039/C6RA22894A>
140. A.K. Datye, D. Kalakkad, M.H. Yao and D.J. Smith, *J. Catal.*, **155**, 148 (1995);
<https://doi.org/10.1006/jcat.1995.1196>
141. C. Hardacre, R.M. Ormerod and R.M. Lambert, *J. Phys. Chem.*, **98**, 10901 (1994);
<https://doi.org/10.1021/j100093a036>
142. S. Bernal, G. Blanco, J.M. Gatica, C. Larese and H. Vidal, *J. Catal.*, **200**, 411 (2001);
<https://doi.org/10.1006/jcat.2001.3210>
143. S. Penner, D. Wang, D.S. Su, G. Rupprechter, R. Podloucky, R. Schlögl and K. Hayek, *Surf. Sci.*, **532-535**, 276 (2003);
[https://doi.org/10.1016/S0039-6028\(03\)00198-5](https://doi.org/10.1016/S0039-6028(03)00198-5)
144. N.R. Socolova, *Colloids Surf. A Physicochem. Eng. Asp.*, **239**, 125 (2004);
<https://doi.org/10.1016/j.colsurfa.2003.11.037>
145. K.D. Ghuge and G.P. Babu, *J. Catal.*, **151**, 453 (1995);
<https://doi.org/10.1006/jcat.1995.1047>
146. D.C. Koningsberger and M. Vaarkamp, *Physica B*, **208-209**, 633 (1995);
[https://doi.org/10.1016/0921-4526\(94\)00776-R](https://doi.org/10.1016/0921-4526(94)00776-R)
147. D.E. Ramaker, J. de Graaf, J.A.R. van Veen and D.C. Koningsberger, *J. Catal.*, **203**, 7 (2001);
<https://doi.org/10.1006/jcat.2001.3299>
148. H. Praliaud, *J. Catal.*, **72**, 394 (1981);
[https://doi.org/10.1016/0021-9517\(81\)90028-2](https://doi.org/10.1016/0021-9517(81)90028-2)
149. T. Ren-Yuam, W. Rong-An and L. Li-Wu, *Appl. Catal.*, **10**, 163 (1984);
[https://doi.org/10.1016/0166-9834\(84\)80101-3](https://doi.org/10.1016/0166-9834(84)80101-3)
150. J.P. Belzunegui, J. Sanz and J.M. Rojo, *J. Am. Chem. Soc.*, **112**, 4066 (1990);
<https://doi.org/10.1021/ja00166a069>
151. J.P. Belzunegui, J. Sanz and J.M. Rojo, *J. Am. Chem. Soc.*, **114**, 6749 (1992);
<https://doi.org/10.1021/ja00043a019>
152. S.A. Stevenson, G.B. Raupp, J.A. Dumesic, S.J. Tauster and R.T.K. Baker, eds.: S.A. Stevenson, G.B. Raupp, J.A. Dumesic, S.J. Tauster R.T.K. Baker and E. Ruckenstein, Metal-Support Interaction in Catalysis, Sintering and Redispersion, Van Nostrand-Reinhold: New York, p. 77 (1987).
153. S.J. Tauster, eds.: R.T. Baker, S.J. Tuaster and J.A. Dumesic, Strong Metal-Support Interactions, ACS Symposium, Series No. 298, ACS, Washington DC, p. 1 (1986).

Contents lists available at [ScienceDirect](https://www.sciencedirect.com)

International Journal of Geoheritage and Parks

journal homepage: <http://www.keaipublishing.com/en/journals/international-journal-of-geoheritage-and-parks/>

Exploring the potential for development of Geotourism in Rarh Bengal, Eastern India using M-GAM

Manoj Kumar Mahato*, Narayan Chandra Jana

Department of Geography, The University of Burdwan, West Bengal, India

ARTICLE INFO

Article history:

Received 28 September 2020

Received in revised form 21 April 2021

Accepted 19 May 2021

Available online xxxxx

Keywords:

Rarh Bengal

Geotourism

Geosites

Potential

Modified Geosite assessment model

ABSTRACT

The Rarh Bengal of India has huge potential for development of geotourism due to its diverse landscape consisting of hills, dome shaped inselbergs, tors, dams, badlands, springs, waterfall, ravines etc. The combination of vast dense forest and diverse flora and fauna with various geomorphic features has created a prosperous and complex geodiversity in the Rarh region. However, the potential of geotourism in the region has not yet fully developed. The main objective of this study is to emphasize the potential for geotourism in the Rarh region of West Bengal and to determine the existing status and geotourism prospective of geosites in this region. In this paper, the authors have proposed an inventory of geosites in the Rarh region and analyzed the vast potential of geotourism among them. A comparative analysis of the selected sites has been carried out by applying the Modified Geosite Assessment Model (M-GAM), which has exposed the most suitable geosites for the development of future geotourism. The M-GAM provided the significant assessment of both Main Values and Additional Values of the sites according to the status of each sub-indicator in the valuation model assumed by tourists. The results of this study reveal information about the major aspects of the development of each geosites and identify which sites need more attention and better management in future, so that the region becomes much attractive to larger number of tourists and becomes a well-known geotourism destination.

© 2021 Beijing Normal University. Publishing services by Elsevier B.V. on behalf of KeAi Communications Co. Ltd. This is an open access article under the CC BY-NC-ND license (<http://creativecommons.org/licenses/by-nc-nd/4.0/>).

1. Introduction

The “geotourism: approach was developed in the late 1980s after the recognition by the geologists of schools, universities and museums in United Kingdom (Hose, Markovi, Komac, & Zorn, 2011). The term “geotourism” has been invented rather recently and was first coined in 1995 by Thomas A Hose, Professor of Earth Science at the University of Bristol in the United Kingdom (Antic & Tomic, 2017; Grover & Mahanta, 2018). According to Thomas A Hose (2005), the definition of geotourism is “to ensure the value and social preservation of geological and geomorphological sites and their materials and to provide interpretative facilities and services for the use of students, tourists and other casual recreationalists” (Hose, 2005, p 27; Hose, 1997, p 2955). This definition clearly represents that the key focus of geotourism is on interpretation, promotion and preservation, which are all significant elements for the development of geotourism. According to Newsome and Dowling (2010), geotourism is an arrangement of natural area tourism that specially focuses on landscape and geology and their interpretation, promotion and conservation with the help

* Corresponding author.

E-mail address: mahatomanojkumar16@gmail.com. (M.K. Mahato).

<https://doi.org/10.1016/j.ijgeop.2021.05.002>

2577-4441/© 2021 Beijing Normal University. Publishing services by Elsevier B.V. on behalf of KeAi Communications Co. Ltd. This is an open access article under the CC BY-NC-ND license (<http://creativecommons.org/licenses/by-nc-nd/4.0/>).

Please cite this article as: M.K. Mahato and N.C. Jana, Exploring the potential for development of Geotourism in Rarh Bengal, Eastern India using M-GAM, International Journal of Geoheritage and Parks, <https://doi.org/10.1016/j.ijgeop.2021.05.002>

of appreciation and education. The definition of geotourism has evolved throughout the years, and Hose and Vasiljevic gave an updated version of definition in 2012 (Jonic, 2018). According to them “geotourism is the providing of informative and service facilities for geosites and geomorphosites and their surrounding topography together through their allied in-situ and ex-situ artifacts, to build of constituency for their conservation by making appreciation, learning and research for current and future generations” (Hose & Vasiljevic, 2012, p 25; Jonic, 2018, p 113). The definition and the approach of geotourism (Hose, 1995) was accepted and endorsed by UNESCO in its preliminary geopark documentation (Hose et al., 2011; Patzack & Eder, 1998).

Geotourism is a nature of tourism that renovates its activities (Pereira, da Cunha, & Nascimento, 2018), involving abiotic ingredients (geology, landscape, geomorphic forms, climate etc.), biotic components (flora & fauna) and culture (Dowling, 2013; Wulung & Rajoendah, 2019). Geotourism is a comparatively new phenomenon based on old ideas about tourism and belongs to a category of special interest tourism (Antic & Tomic, 2017). In the general sense, geotourism signifies the upgrade and protection of geological heritage care of tourism through the education and interpretation (Tomic, 2016). This is a new emerging type of tourism that environmentally innovative (Dowling, 2013). It promotes geosites into a tourist destination and preserves the geodiversity with the understanding of earth science. It has been proposed that greater concentration should be given to environmentally innovative forms of tourism, which encourage both environmental and social obligation (Paskova, 2012). Geotourists travel individually or in groups and they may visit whether these are natural areas or built-up areas, they opt the areas that have geological attraction for tourism.

Rarh Bengal Region is a toponym for an area in the Indian subcontinent (Faridi, 2013), which lies between the Ganges Delta on the east and Chhotanagpur Plateau on the west. The Rarh Bengal Region is very rich in terms of geodiversity existing in numerous forms. This province is very rich with numerous hills, dome-shaped inselbergs, tors, dams, badlands, springs, waterfall and ravines, which is located in a relatively small area. Besides, this territory is well-known lateritic landscape endowed with lots of geoarchaeological sites (Chakrabarty & Mandal, 2019). These sites are outstanding representatives of this area's geodiversity. Geotourism sites usually consist of all geological, geomorphological and pedological values produced through the formation of the Earth's crust (Djurovic & Mijovic, 2006). All of these values are being present in the region of Rarh Bengal in India, which has made this territory extremely promising for the development of geotourism in the future. Therefore, we can say that the Rarh Bengal Region is underdeveloped in agriculture and industry, if geotourism was developed here, the region may be economically dependent on the combined influence of agriculture, industry and geotourism.

The main objective of this study is to explore the potential of geotourism in the Rarh Bengal of eastern India and to identify the most suitable geosites for the development of geotourism. This study is based on the Modified Geosite Assessment Model (M-GAM) provided by Tomic and Bozic (2014). M-GAM is a modified version of GAM (Geosite Assessment Model) by Vujicic et al. (2011), where incorporate the opinions of the visitors or tourists (Pal & Albert, 2018; Tomic & Bozic, 2014). M-GAM has been used to compare the existing status of selected sites and compare their geotourism potential.

This model has been applied to eleven geosites in the Rarh Bengal of eastern India. The results of the analysis provide information on major areas of improvement and identify which areas need more attention and better management in future so that the region can become a recognized geotourism destination, which will be able to mesmerize a large number of tourists in the future years to come. So keeping in view of the above discussion, this paper has given emphasis an enquiry about how the geosites are more potential for geotourism in Rarh Bengal.

2. Materials and methods

2.1. Study area

Rarh Bengal is a major part of the physiographical divisions of West Bengal, which lies between the Chhotanagpur Plateau in the west of India and the Ganges Delta in the east of India. The Rarh Bengal is located in the southwestern part of the Indian state of West Bengal, bounded by latitudes of 21°39'43" N to 24°35'51"N and longitudes of 85°49'27" E to 88°28'43"E (Fig. 1). Purulia, Bankura, Jhargram, Birbhum, Paschim Bardhaman, Purba Bardhaman and Paschim Medinipur are located in Rarh Bengal. In addition, promotion of geotourism can generate employment opportunities for towards pandering rural economy in these districts of Rarh Bengal. Rarh Bengal is diversified with number of hills, dome-shaped inselbergs, tor topography, undulating upland, valleys, erosional plain and ravines; the regions is characterized by lateritic land surface and sub-tropical monsoon type of climate with very high day temperatures during the summer months reaching up to 47 °C (Purulia district in January 2020) (IMD, Kolkata). The region is not favorable for agricultural development and any capital-intensive industry due to the deficit of adequate water. However, the area has great potentially for tourism promotion (Chakrabarty & Mandal, 2018, 2019) because of its richness in terms of geodiversity existing in numerous forms.

The proposed geosites inventory comprises eleven geosites located throughout the Rarh Bengal in India (Fig. 1. & Table 1). In addition to these geosites, many other sites can be included in the geotourism activities. However, priority should be given to the eleven selected geosites at the initial stage of geotourism development in this region, as they already have some infrastructural necessities for tourism development along with their attractiveness and accessibility.

2.2. Methodology

The methodology of this study is based on the Modified Geosite Assessment Model (M-GAM), provided by Tomic and Bozic (2014). The M-GAM method has developed based on previous geosite assessment methods established by different authors

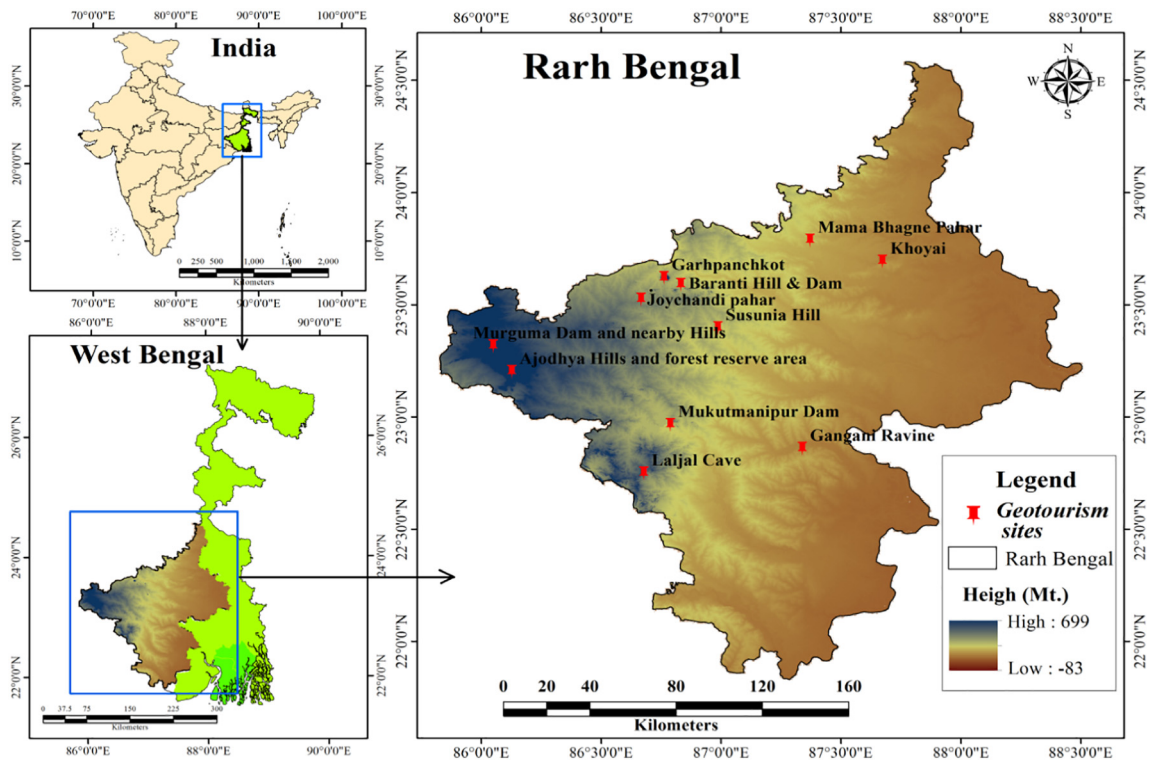


Fig. 1. Location of proposed geotourism sites of the Rarh Bengal.

Table 1

Proposed geosites in the Rarh Bengal of eastern India.

| Geosites label | Geosites name | Geographical location |
|------------------|---------------------------------------|--|
| GS ₁ | Ajudhya Hills and forest reserve area | 23°06'25.53"N to 23°21'30.46"N 85°57'22.53"E to 86°14'08.87"E |
| GS ₂ | Murguma Dam and nearby Hills | 23°18'54.29"N to 86°03'01.24"E |
| GS ₃ | Joychandi Pahar | 23°31'21.07"N to 86°40'01.08"E |
| GS ₄ | Baranti Hill & Dam | 23°35'20.19"N to 86°49'58.16"E |
| GS ₅ | Garhpanchkot | 23°37'06.65"N to 86°45'45.60"E |
| GS ₆ | Susunia Hill | 23°23'42.51"N to 86°59'14.76"E |
| GS ₇ | Mukutmanipur Dam | 22°57'50.07"N to 86°47'20.39"E |
| GS ₈ | Laljal Cave | 22°44'55.24"N to 86°40'43.88"E |
| GS ₉ | Gangani Ravine | 22°51'28.68"N to 87°20'22.96"E |
| GS ₁₀ | Khoyai | 23°41'30.43"N to 87°40'23.32"E |
| GS ₁₁ | Mama Bhagne Pahar | 23°47'06.98"N to 87°22'19.50"E |

(Bruschi & Cendrero, 2005; Coratza & Giusti, 2005; Erhartic, 2010; Hose, 1997; Jonic, 2018; Pereira, Pereira, & Caetano Alves, 2007; Pralong, 2005; Reynard, 2008; Reynard, Fontana, Kozlik, & Scapozza, 2007; Serrano & Gonzalez-Trueba, 2005; Tomic, 2011; Tomic, Markovic Slobodan, Antic, & Tesic, 2020; Vukovic & Antic, 2019). It combines the views of both side's tourists and experts with equal importance, in such a way, no one is favored in the evaluation process (Tomic et al., 2020; Vukovic & Antic, 2019). The M-GAM has been efficaciously tested and applied several times for the appraisal of various geosites (Bozic, Tomic, & Pavic, 2014; Boskov et al., 2015; Antic & Tomic, 2017; Ticar et al., 2018; Vukoicic, Milosavljevic, Valjarevic, Nikolic, & Sreckovic-Batocanin, 2018; Antic, Tomic, & Markovic, 2019).

The M-GAM contains two basic indicators: Main Values (MV) and Additional Values (AV), which are furthermore divided into 12 and 15 sub-indicators respectively and each indicator is individually denoted by a value from 0.00 to 1.00. This category is created due to two common types of values: the Main Values - which are mostly generated by the natural properties of the geosite and the Additional Values - these are mostly human-induced and created by modifications in its use by visitors. The Main Values consist of three groups of sub-indicators: (i) scientific/educational values (VSE), (ii) scenic/aesthetic values (VSA) and (iii) protection (VPr). In addition, Additional Values are divided into two groups of sub-indicators: (iv) functional values (VFn) and (v) touristic values (VTr). The structure of indicators and sub-indicators of Main Values and Additional Values are shown in Table 2a and grades values in Table 2b.

Table 2a
The structure of M-GAM.

| Indicators/Sub-indicators | Description |
|---|---|
| Main Values (MV) | |
| Scientific/Educational value (<i>VSE</i>) | |
| (1) Rarity | Number of closest identical sites |
| (2) Representativeness | Didactic and exemplary features of the site due to its own value and general configuration |
| (3) Knowledge on geoscientific issues | Number of papers written in recognized journals, theses, exhibitions and other publications |
| (4) Level of interpretation | Levels of explanatory potential on Geological and geomorphological processes, phenomena, shapes and stages of scientific knowledge |
| Scenic/Aesthetic values (<i>VSA</i>) | |
| (5) Viewpoints | Number of viewpoints accessible by pedestrian path. Everyone must present a specific perspective and be located less than 1 km from the site. |
| (6) Surface | Surface means the entire surface of the site. The quantitative relationship of each site with other sites is considered. |
| (7) Surrounding landscape and nature | The quality of the panoramic view, the presence of water body and natural vegetation, the absence of human-induced degradation, the vicinity of urban areas, etc. |
| (8) Environmental fitting of sites | The level of contrast with nature, the contrast of color, the presence of size and shapes, and so on. |
| Protection (<i>VPr</i>) | |
| (9) Current condition | Current state of geosite |
| (10) Protection level | State of protection by local groups, state govt., national govt., international organizations, etc. |
| (11) Vulnerability | Vulnerability level of geosite |
| (12) Suitable number of visitors | The proposed number of visitors entering the geosite at the same time according to the space, vulnerability and existing status of the geosite. |
| Additional values (AV) | |
| Functional values (<i>VFn</i>) | |
| (13) Accessibility | Opportunities of approaching to the site |
| (14) Additional natural values | Number of extra natural values in the radius of 5 km (geosites are also included) |
| (15) Additional anthropogenic values | Number of auxiliary anthropogenic values in the radius of 5 km |
| (16) Vicinity of emissive centers | Proximity to emissive centers |
| (17) Vicinity of important road network | Proximity to important road networks within a radius of 20 km |
| (18) Additional functional values | Parking services and facilities, gas station, mechanical facilities etc. |
| Touristic values (<i>VTr</i>) | |
| (19) Promotion | Level and number of promotional agencies and resources |
| (20) Organised visits | Total number of organised visits to the geosite annually |
| (21) Vicinity of visitors centers | Proximity to the visitor center on the geosite |
| (22) Interpretative panels | Interpretative features of text, graphics, size and volume of material, quality and decoration of surroundings etc. |
| (23) Number of visitors | Number of annual visitors |
| (24) Tourism infrastructure | Additional infrastructural facilities for tourists (internal pathways, resting spaces, drinking water facilities, garbage cans, toilets etc.) |
| (25) Tour guide service | If existing, their level of skill, knowledge of local and foreign languages (speaking), explanatory skills etc. |
| (26) Hostelry service | Hostelry service near to the geosite |
| (27) Restaurant service | Hotel and restaurant service near to the geosite |

The sum of the grades 0.00 to 1.00 of the 12 sub-indicators of Main Values and 15 sub-indicators of Additional Values are defined using the following simple equation (Eq. 1):

$$M - GAM = MV + AV \tag{1}$$

Where, *MV* represents Main Values and *AV* represents Additional Values. Since the Main Values and Additional Values contain 3 and 2 groups of sub-indicators, so the values are determined by these two equation:

$$MV = VSE + VSA + VPr \tag{2}$$

$$AV = VFn + VTr \tag{3}$$

This model is done for each sub-indicator after which the values are added up according to the M-GAM equation but this time due to the adding of the importance factor (*Im*), it indicates a more objective and accurate result finally. Visitors in the same way like the experts, determine a numerical value of this parameter for the Main Values and Additional Values of each of these

Table 2b
Grades values of M-GAM.

| Sub-indicators | Grades (0.00–1.00) | | | | |
|----------------|---|--|--|--|---|
| | 0.00 | 0.25 | 0.50 | 0.75 | 1.00 |
| 1 | Common | Regional | National | International | The only occurrence |
| 2 | None | Low | Moderate | High | Utmost |
| 3 | None | Local publications | Regional publications | National publications | International publications |
| 4 | None | Processes are moderate level, but the detection is difficult to interpret to non-experts | Good examples of processes, but difficult to interpret to non-experts | Processes are moderate level, but easy to interpret to the average visitor | Good examples of processes and easy to interpret to the average visitor |
| 5 | None | 1 | 2 to 3 | 4 to 6 | > 6 |
| 6 | Small | – | Medium | – | Large |
| 7 | – | Low | Medium | High | Utmost |
| 8 | Unfitting | – | Neutral | – | Fitting |
| 9 | Completely damaged (due to the various activities of human) | Extremely damaged (due to the natural processes) | Moderate level of damaged (with necessary geomorphological features are preserved) | Slightly damaged | No damage |
| 10 | None | Local | Regional | National | International |
| 11 | Irrevocable (with the probability of total loss) | High (can be damaged simply) | Moderate (can be damaged by any of the natural processes or human activity) | Less (can only be harmed by human activity) | None |
| 12 | 0 | 1 to 10 | 11 to 20 | 21 to 50 | > 50 |
| 13 | Unreachable | Low (walking with special equipment through expert tourist guide) | Moderate (via bicycles and other means of transport that uses muscle power) | High (by car) | Utmost (by bus, train, helicopter, etc.) |
| 14 | None | 1 | 2 to 3 | 4 to 6 | > 6 |
| 15 | None | 1 | 2 to 3 | 4 to 6 | > 6 |
| 16 | > 100 km | 100 to 50 km | 50 to 25 km | 25 to 5 km | < 5 km |
| 17 | None | Local | Regional | National | International |
| 18 | None | Low | Medium | High | Utmost |
| 19 | None | Local | Regional | National | International |
| 20 | None | < 12 per year | 12 to 24 per year | 24 to 48 per year | > 48 per year |
| 21 | > 50 km | 50 to 20 km | 20 to 5 km | 5 to 1 km | < 1 km |
| 22 | None | Low quality | Medium quality | High quality | Utmost quality |
| 23 | None | Low (< 5000) | Medium (5001 to 10,000) | High (10,001 to 100,000) | Utmost (> 100,000) |
| 24 | None | Low | Medium | High | Utmost |
| 25 | None | Low | Medium | High | Utmost |
| 26 | >50 km | 25 to 50 km | 10 to 25 km | 5 to 10 km | < 5 km |
| 27 | >25 km | 10 to 25 km | 5 to 10 km | 1 to 5 km | < 1 km |

sub-indicators. These numeric values are marked as 0.00, 0.25, 0.50, 0.75 and 1.00. The importance factor (*Im*) is determined as follows:

$$Im = \frac{\sum_{k=1}^K Iv_k}{K} \tag{4}$$

Where, *Iv_k* is the assessment or score for each sub-indicator given by a visitor, whereas *K* is total number of visitors. Here the value of *Im* can be any value from 0.00 to 1.00.

Finally, the equation of M-GAM is presented as follows:

$$M-GAM = MV + AV$$

Where, $MV = \sum_{i=1}^n Im_i * MV_i$ (5)

$$AV = \sum_{i=1}^n Im_i * AV_i \tag{6}$$

The M-GAM equation shows that the values of the *Im* of each sub-indicator determined individually by the visitors are multiplied by the values of each sub-indicator given by the experts. In this way, the value of each sub-indicator in the model is determined.

Survey was conducted in March 2019 to study various geotourist sites and calculated the importance factor (*Im*) for each sub-indicator in this model. The questionnaire contained 27 sub-indicators or questions and every visitor was questioned to rate the importance of all sub-indicator on a five-point Likert scale (ranging from 0.00 to 1.00), it was done in the same way as the experts did. A total of 164 visitors completed the questionnaire. However, the main fact is that all the geosites of Rarh Bengal have not yet become such a popular tourist destination and the analyzed Baranti hill and dam, Khoyai and Laljal cave are not visited by more than 500 visitors every year. Thus, it can be said that the size of the sample is sufficient for judgment and decision-making.

3. Results and discussion

For this study, previously described eleven geosites of the Rarh Bengal were evaluated by applying the M-GAM method. The final results of this assessment are shown in Tables 3 and 4 as well as in Fig. 2. The comprehensive analysis of the results is comprised the assessment of the Main Values and Additional Values of the geosites. The Main Values contain 12 sub-indicators of geosites associated with scientific/educational values (*VSE*), scenic/aesthetic values (*VSA*) and protection (*VPr*). The Additional Values contain 15 sub-indicators of geosites related to functional values (*VF_n*) and tourist values (*VTr*).

Table 4 and Fig. 2 show that the Main Values of Ajodhya Hills and forest reserve area is highest, which is 9.21, followed by Garhpanchkot is 9.00, Mukutmanipur Dam is 9.00 and Gangani Ravine is 8.65 respectively. All these geosites have extremely high scientific/educational values (*VSE*) and scenic/aesthetic values (*VSA*), especially in case of rarity (*SIMV₁*), representativeness (*SIMV₂*), level of interpretation (*SIMV₄*), viewpoints (*SIMV₅*), surrounding landscape and nature (*SIMV₇*) and environmental fitting of sites (*SIMV₈*); while *SIMV₂* and *SMIV₅* at Mukutmanipur Dam, *SIMV₄* at Garhpanchkot and *SIMV₅* at Gangani Ravine are slightly lower. These four geosites have the highest Main Values due to the high values of the importance factor (*Im*) for these sub-indicators. Although the Susunia Hill has the best in representativeness (*SIMV₂*), environmental fitting of sites (*SIMV₈*), accessibility (*SI_{AV₁}*), annual number of organised visits (*SI_{AV₈}*) and tourism infrastructure (*SI_{AV₁₂}*), it is at a lower end of scale in geotourism development due to its lower Main Values. The main reason for this is the very low scenic/aesthetic values (*VSA*), especially the surface (*SIMV₆*) is very low, the surrounding landscape and nature (*SIMV₇*) is moderate and there are no separate viewpoints except a temple and a spring in the hill. Similarly, the main reason for the lesser Main Values (6.00) in Laljal Cave is resulted from the lower scenic/aesthetic values (*VSA*) (1.31). Khoyai also has very low scenic/aesthetic (*VSA*) (1.73) and protection (*VPr*) (1.60) values, so its Main Value is very low (5.95). Moreover, for Murguma Dam and nearby Hills Joychandi Pahar, Baranti Hill & Dam and Mama Bhagne Pahar, the values of all the main indicators present a consistent level in terms of its different values i.e., scientific/educational values (*VSE*), scenic/aesthetic values (*VSA*) and protection (*VPr*).

The geosites with the lowest Main Values are Susunia Hill (5.67), Khoyai (5.95) and Laljal Cave (6.00). The values of the sub-indicators underlying to Main Values of these geosites, such as surface (*SIMV₆*), knowledge on geo-scientific issues (*SIMV₃*), viewpoints (*SIMV₅*) and surrounding landscape and nature (*SIMV₇*) are very low, although knowledge on geo-scientific issues (*SIMV₃*) is much higher in the Laljal Cave due to its geological significance. The main reason why visitors visit these geosites is that these are located on the way to other important geosites in the area. The sites like Susunia Hill, Joychandi Pahar, Baranti Hill & Dam and Garhpanchkot are located side by side, so tourists visit all the sites together. Tourists visit Khoyai as it is located near important cultural center like the Santiniketan.

In terms of protection values (*VPr*), these four geosites i.e., Ajodhya Hills and forest reserve area, Murguma Dam and nearby Hills, Garhpanchkot and Mukutmanipur Dam have the highest protection values (*VPr*), each of which has the equal value (2.51). These four are followed by Joychandi Pahar (2.36), Gangani Ravine (2.36), Baranti Hill & Dam (2.34), Mama Bhagne Pahar (2.29) and Susunia Hill (2.12) etc. respectively. The four geosites with the highest protection values are protected on a national level, and they are located in rural environment far away from the urban center, so they do not suffer any damage. Khoyai is the site with the lowest protection values (*VPr*), which is 1.60. Even though it is under national level of protection, the values of current condition (*SIMV₉*) and vulnerability (*SIMV₁₁*) are much lower due to the presence of excessive erosion prone lateritic soil.

In terms of Additional Values, the highest value is seen in the Ajodhya Hills and forest reserve area (8.17), which is followed by Joychandi Pahar (7.57), Mukutmanipur Dam (7.02),

Garhpanchkot (6.64), Gangani Ravine (6.22) etc. respectively. Although the functional values (*VF_n*) of these sites are almost the same, the greater disparity in tourist values (*VTr*) has led to diversity among them. In addition, Laljal Cave and Baranti Hill & Dam are located in very remote areas, so the value of their all sub-indicators in the Additional Values (*AV*) is much lower.

In case of functional values (*VF_n*), Garhpanchkot, Khoyai, Ajodhya Hills and forest reserve area, Gangani Ravine, Joychandi Pahar and Mama Bhagne Pahar have highest values, which are 3.35, 3.03, 3.00, 2.94, 2.90 and 2.85 respectively. There are ample facilities to reach these six sites, they are connected to the important road network of national highways and state highways and the location away from the big urban centers has increased their functional values (*VF_n*). Therefore, their values of accessibility (*SI_{AV₁}*), vicinity of important road network (*SI_{AV₅}*) and vicinity of emissive centers (*SI_{AV₄}*) are at the utmost or greatest level on the five-point Likert scale. Moreover, the score of additional functional values (*SI_{AV₆}*) of these sites ranges from high to the utmost. To reach the three sites of Laljal Cave, Baranti Hill & Dam and Murguma Dam and nearby Hills, visitors has to take private car on rural roads, which are inaccessible to big buses; again during the rainy season no visitors can go due to the bad condition of the road, so their functional values is lowest.

Lastly, from the point of view of tourist values (*VTr*), it can be seen that its values is the lowest in Laljal cave (0.58), which is followed by Baranti Hill & Dam (1.83), Khoyai (1.93), Mama Bhagne Pahar (2.08), Susunia Hill (2.45) and Murguma Dam and nearby Hills (2.51) etc. respectively. Although promotion (*SI_{AV₇}*), annual number of organised visits (*SI_{AV₈}*) and annual number of visitors (*SI_{AV₁₁}*) are present in lower range at Laljal cave, but others sub-indicators of tourist values (*VTr*) are completely

Table 3

Sub-indicators values given by experts for each analyzed geosite.

| Main indicators/sub-indicators | Values given by experts (0 to 1) | | | | | | | | | | | Im | Total value | | | | | | | | | | | |
|---|----------------------------------|-----------------|-----------------|-----------------|-----------------|-----------------|-----------------|-----------------|-----------------|------------------|------------------|------|-----------------|-----------------|-----------------|-----------------|-----------------|-----------------|-----------------|-----------------|-----------------|------------------|------------------|------|
| | GS ₁ | GS ₂ | GS ₃ | GS ₄ | GS ₅ | GS ₆ | GS ₇ | GS ₈ | GS ₉ | GS ₁₀ | GS ₁₁ | | GS ₁ | GS ₂ | GS ₃ | GS ₄ | GS ₅ | GS ₆ | GS ₇ | GS ₈ | GS ₉ | GS ₁₀ | GS ₁₁ | |
| Main values | | | | | | | | | | | | | | | | | | | | | | | | |
| (I) Scientific/Educational values (VSE) | | | | | | | | | | | | | | | | | | | | | | | | |
| 1. Rarity (SIMV ₁) | 1.00 | 0.50 | 1.00 | 0.75 | 1.00 | 0.50 | 1.00 | 1.00 | 1.00 | 1.00 | 0.75 | 1.00 | 0.95 | 0.95 | 0.48 | 0.95 | 0.71 | 0.95 | 0.48 | 0.95 | 0.95 | 0.95 | 0.71 | 0.95 |
| 2. Representativeness (SIMV ₂) | 1.00 | 1.00 | 0.75 | 1.00 | 1.00 | 0.75 | 1.00 | 1.00 | 1.00 | 1.00 | 0.50 | 0.50 | 0.79 | 0.79 | 0.79 | 0.59 | 0.79 | 0.79 | 0.79 | 0.59 | 0.79 | 0.79 | 0.40 | 0.40 |
| 3. Knowledge on geo-scientific issues (SIMV ₃) | 1.00 | 0.50 | 1.00 | 0.75 | 1.00 | 0.50 | 1.00 | 0.75 | 1.00 | 1.00 | 0.75 | 1.00 | 0.66 | 0.66 | 0.33 | 0.66 | 0.50 | 0.66 | 0.33 | 0.66 | 0.50 | 0.66 | 0.66 | 0.33 |
| 4. Level of interpretation (SIMV ₄) | 1.00 | 1.00 | 1.00 | 0.50 | 0.75 | 0.50 | 1.00 | 0.50 | 1.00 | 1.00 | 1.00 | 1.00 | 0.85 | 0.85 | 0.85 | 0.85 | 0.43 | 0.64 | 0.43 | 0.85 | 0.43 | 0.85 | 0.85 | 0.85 |
| (II) Scenic/aesthetic values (VSA) | | | | | | | | | | | | | | | | | | | | | | | | |
| 5. Viewpoints (SIMV ₅) | 1.00 | 0.50 | 0.50 | 0.50 | 1.00 | 0.50 | 0.75 | 0.50 | 0.50 | 0.25 | 0.50 | 0.50 | 0.83 | 0.83 | 0.42 | 0.42 | 0.42 | 0.83 | 0.42 | 0.62 | 0.42 | 0.42 | 0.21 | 0.42 |
| 6. Surface (SIMV ₆) | 1.00 | 0.75 | 0.50 | 0.50 | 1.00 | 0.00 | 1.00 | 0.00 | 1.00 | 0.50 | 0.50 | 0.50 | 0.84 | 0.84 | 0.63 | 0.42 | 0.42 | 0.84 | 0.00 | 0.84 | 0.00 | 0.84 | 0.42 | 0.42 |
| 7. Surrounding landscape and nature (SIMV ₇) | 1.00 | 1.00 | 0.75 | 1.00 | 1.00 | 0.50 | 1.00 | 0.50 | 1.00 | 0.25 | 0.50 | 0.50 | 0.91 | 0.91 | 0.91 | 0.68 | 0.91 | 0.91 | 0.46 | 0.91 | 0.46 | 0.91 | 0.23 | 0.46 |
| 8. Environmental fitting of sites (SIMV ₈) | 1.00 | 1.00 | 1.00 | 1.00 | 1.00 | 1.00 | 1.00 | 0.50 | 1.00 | 1.00 | 1.00 | 1.00 | 0.87 | 0.87 | 0.87 | 0.87 | 0.87 | 0.87 | 0.87 | 0.87 | 0.44 | 0.87 | 0.87 | 0.87 |
| (III) Protection (VPr) | | | | | | | | | | | | | | | | | | | | | | | | |
| 9. Current condition (SIMV ₉) | 1.00 | 1.00 | 1.00 | 1.00 | 1.00 | 0.75 | 1.00 | 1.00 | 1.00 | 0.50 | 0.75 | 0.75 | 0.89 | 0.89 | 0.89 | 0.89 | 0.89 | 0.67 | 0.89 | 0.89 | 0.89 | 0.45 | 0.67 | |
| 10. Protection level (SIMV ₁₀) | 0.75 | 0.75 | 0.75 | 0.75 | 0.75 | 0.75 | 0.75 | 0.50 | 0.75 | 0.75 | 0.75 | 0.75 | 0.67 | 0.50 | 0.50 | 0.50 | 0.50 | 0.50 | 0.50 | 0.50 | 0.34 | 0.50 | 0.50 | 0.50 |
| 11. Vulnerability (SIMV ₁₁) | 0.75 | 0.75 | 0.50 | 0.75 | 0.75 | 0.75 | 0.75 | 0.50 | 0.50 | 0.25 | 0.75 | 0.58 | 0.44 | 0.44 | 0.29 | 0.44 | 0.44 | 0.44 | 0.44 | 0.44 | 0.29 | 0.29 | 0.15 | 0.44 |
| 12. Suitable number of visitors (SIMV ₁₂) | 1.00 | 1.00 | 1.00 | 0.75 | 1.00 | 0.75 | 1.00 | 0.75 | 1.00 | 0.75 | 1.00 | 0.68 | 0.68 | 0.68 | 0.68 | 0.51 | 0.68 | 0.51 | 0.68 | 0.51 | 0.68 | 0.51 | 0.68 | |
| Additional values | | | | | | | | | | | | | | | | | | | | | | | | |
| (I) Functional values (VFn) | | | | | | | | | | | | | | | | | | | | | | | | |
| 13. Accessibility (SIAV ₁) | 1.00 | 0.75 | 1.00 | 0.75 | 1.00 | 1.00 | 1.00 | 0.75 | 1.00 | 1.00 | 1.00 | 0.87 | 0.87 | 0.65 | 0.87 | 0.87 | 0.87 | 0.87 | 0.87 | 0.65 | 0.87 | 0.87 | 0.87 | 0.87 |
| 14. Additional natural values (SIAV ₂) | 1.00 | 0.50 | 0.50 | 0.50 | 1.00 | 0.50 | 0.75 | 0.50 | 0.75 | 0.25 | 0.50 | 0.50 | 0.67 | 0.67 | 0.34 | 0.34 | 0.34 | 0.67 | 0.34 | 0.50 | 0.34 | 0.50 | 0.17 | 0.34 |
| 15. Additional anthropogenic values (SIAV ₃) | 1.00 | 1.00 | 0.75 | 0.50 | 1.00 | 1.00 | 0.75 | 0.25 | 0.50 | 1.00 | 0.50 | 0.48 | 0.48 | 0.48 | 0.36 | 0.24 | 0.48 | 0.48 | 0.36 | 0.12 | 0.24 | 0.48 | 0.48 | 0.24 |
| 16. Vicinity of emissive centers (SIAV ₄) | 0.00 | 0.00 | 0.50 | 0.25 | 0.50 | 0.25 | 0.00 | 0.25 | 0.50 | 0.75 | 0.75 | 0.71 | 0.00 | 0.00 | 0.36 | 0.18 | 0.36 | 0.18 | 0.00 | 0.18 | 0.36 | 0.53 | 0.53 | |
| 17. Vicinity of important road network (SIAV ₅) | 0.75 | 0.75 | 0.75 | 0.50 | 0.75 | 0.50 | 0.75 | 0.50 | 0.75 | 0.75 | 0.75 | 0.74 | 0.56 | 0.56 | 0.56 | 0.37 | 0.56 | 0.37 | 0.56 | 0.37 | 0.56 | 0.56 | 0.56 | |
| 18. Additional functional values (SIAV ₆) | 1.00 | 0.50 | 1.00 | 0.50 | 1.00 | 1.00 | 1.00 | 0.25 | 1.00 | 1.00 | 0.75 | 0.42 | 0.42 | 0.21 | 0.42 | 0.21 | 0.42 | 0.42 | 0.42 | 0.11 | 0.42 | 0.42 | 0.42 | 0.32 |
| (II) Tourist values (VTr) | | | | | | | | | | | | | | | | | | | | | | | | |
| 19. Promotion (SIAV ₇) | 0.75 | 0.75 | 1.00 | 0.50 | 0.75 | 0.50 | 0.75 | 0.50 | 1.00 | 0.75 | 0.75 | 0.56 | 0.42 | 0.42 | 0.56 | 0.28 | 0.42 | 0.28 | 0.42 | 0.28 | 0.56 | 0.42 | 0.42 | |
| 20. Annual number of organised visits (SIAV ₈) | 1.00 | 0.50 | 1.00 | 0.25 | 0.75 | 1.00 | 0.75 | 0.25 | 1.00 | 0.50 | 0.50 | 0.62 | 0.62 | 0.31 | 0.62 | 0.16 | 0.47 | 0.62 | 0.47 | 0.16 | 0.62 | 0.31 | 0.31 | |
| 21. Vicinity of visitors centres (SIAV ₉) | 1.00 | 0.50 | 0.25 | 0.00 | 0.25 | 0.25 | 0.00 | 0.00 | 0.25 | 0.00 | 0.00 | 0.81 | 0.81 | 0.41 | 0.20 | 0.00 | 0.20 | 0.00 | 0.00 | 0.00 | 0.20 | 0.00 | 0.00 | 0.00 |
| 22. Interpretive panels (SIAV ₁₀) | 1.00 | 0.00 | 0.75 | 0.00 | 0.50 | 0.25 | 1.00 | 0.00 | 0.75 | 0.25 | 0.50 | 0.76 | 0.76 | 0.00 | 0.57 | 0.00 | 0.38 | 0.19 | 0.76 | 0.00 | 0.57 | 0.19 | 0.38 | |
| 23. Annual number of visitors (SIAV ₁₁) | 1.00 | 0.50 | 0.75 | 0.25 | 1.00 | 0.50 | 0.75 | 0.25 | 0.75 | 0.50 | 0.75 | 0.58 | 0.58 | 0.29 | 0.44 | 0.15 | 0.58 | 0.29 | 0.44 | 0.15 | 0.44 | 0.29 | 0.44 | |
| 24. Tourism infrastructure (SIAV ₁₂) | 0.75 | 0.00 | 1.00 | 0.50 | 0.75 | 0.75 | 1.00 | 0.00 | 0.50 | 0.25 | 0.75 | 0.70 | 0.53 | 0.00 | 0.70 | 0.35 | 0.53 | 0.53 | 0.70 | 0.00 | 0.35 | 0.18 | 0.18 | |
| 25. Tour guide service (SIAV ₁₃) | 0.00 | 0.00 | 0.50 | 0.00 | 0.00 | 0.25 | 1.00 | 0.00 | 0.00 | 0.00 | 0.00 | 0.63 | 0.00 | 0.00 | 0.32 | 0.00 | 0.00 | 0.16 | 0.63 | 0.00 | 0.00 | 0.00 | 0.00 | |
| 26. Hostelry service (SIAV ₁₄) | 1.00 | 0.50 | 1.00 | 0.25 | 0.00 | 0.00 | 0.25 | 0.00 | 0.00 | 0.00 | 0.00 | 0.73 | 0.73 | 0.37 | 0.73 | 0.18 | 0.00 | 0.00 | 0.18 | 0.00 | 0.00 | 0.00 | 0.00 | |
| 27. Restaurant service (SIAV ₁₅) | 1.00 | 1.00 | 0.75 | 1.00 | 1.00 | 0.25 | 1.00 | 0.00 | 0.75 | 0.75 | 0.50 | 0.72 | 0.72 | 0.72 | 0.54 | 0.72 | 0.72 | 0.18 | 0.72 | 0.00 | 0.54 | 0.54 | 0.36 | |

GS₁ - Ajothya Hills and forest reserve area, GS₂ - Murguma Dam and nearby Hills, GS₃ - Jyochandi Pahar, GS₄ - Baranti Hill & Dam, GS₅ - Garhpanchkot, GS₆ - Susunia Hill, GS₇ - Mukutmanipur Dam, GS₈ - Laljal Cave, GS₉ - Gangani Ravine, GS₁₀ - Khoyai, GS₁₁ - Mama Bhagne Pahar.

Table 4
Overall position of the analyzed geosites by using M-GAM.

| Geosites label | Geosites name | Main Values | | Additional Values | | Field |
|------------------|---------------------------------------|--------------------|----------|-------------------|----------|-----------------|
| | | VSE + VSA + VPr | Σ | VFn + VTr | Σ | |
| GS ₁ | Ajodhya Hills and forest reserve area | 3.25 + 3.45 + 2.51 | 9.21 | 3.00 + 5.17 | 8.17 | Z ₃₂ |
| GS ₂ | Murguma Dam and nearby Hills | 2.45 + 2.83 + 2.51 | 7.79 | 2.23 + 2.51 | 4.74 | Z ₂₁ |
| GS ₃ | Joychandi Pahar | 3.05 + 2.39 + 2.36 | 7.80 | 2.90 + 4.67 | 7.57 | Z ₂₂ |
| GS ₄ | Baranti Hill & Dam | 2.42 + 2.62 + 2.34 | 7.38 | 1.99 + 1.83 | 3.82 | Z ₂₁ |
| GS ₅ | Garhpanchkot | 3.04 + 3.45 + 2.51 | 9.00 | 3.35 + 3.29 | 6.64 | Z ₃₂ |
| GS ₆ | Susunia Hill | 1.82 + 1.74 + 2.12 | 5.67 | 2.65 + 2.45 | 5.1 | Z ₂₂ |
| GS ₇ | Mukutmanipur Dam | 3.25 + 3.24 + 2.51 | 9.00 | 2.71 + 4.31 | 7.02 | Z ₃₂ |
| GS ₈ | Laljal Cave | 2.66 + 1.31 + 2.03 | 6.00 | 1.76 + 0.58 | 2.34 | Z ₂₁ |
| GS ₉ | Gangani Ravine | 3.25 + 3.04 + 2.36 | 8.65 | 2.94 + 3.28 | 6.22 | Z ₃₂ |
| GS ₁₀ | Khoyai | 2.62 + 1.73 + 1.60 | 5.95 | 3.03 + 1.93 | 4.96 | Z ₂₁ |
| GS ₁₁ | Mama Bhagne Pahar | 2.53 + 2.16 + 2.29 | 6.98 | 2.85 + 2.08 | 4.93 | Z ₂₁ |

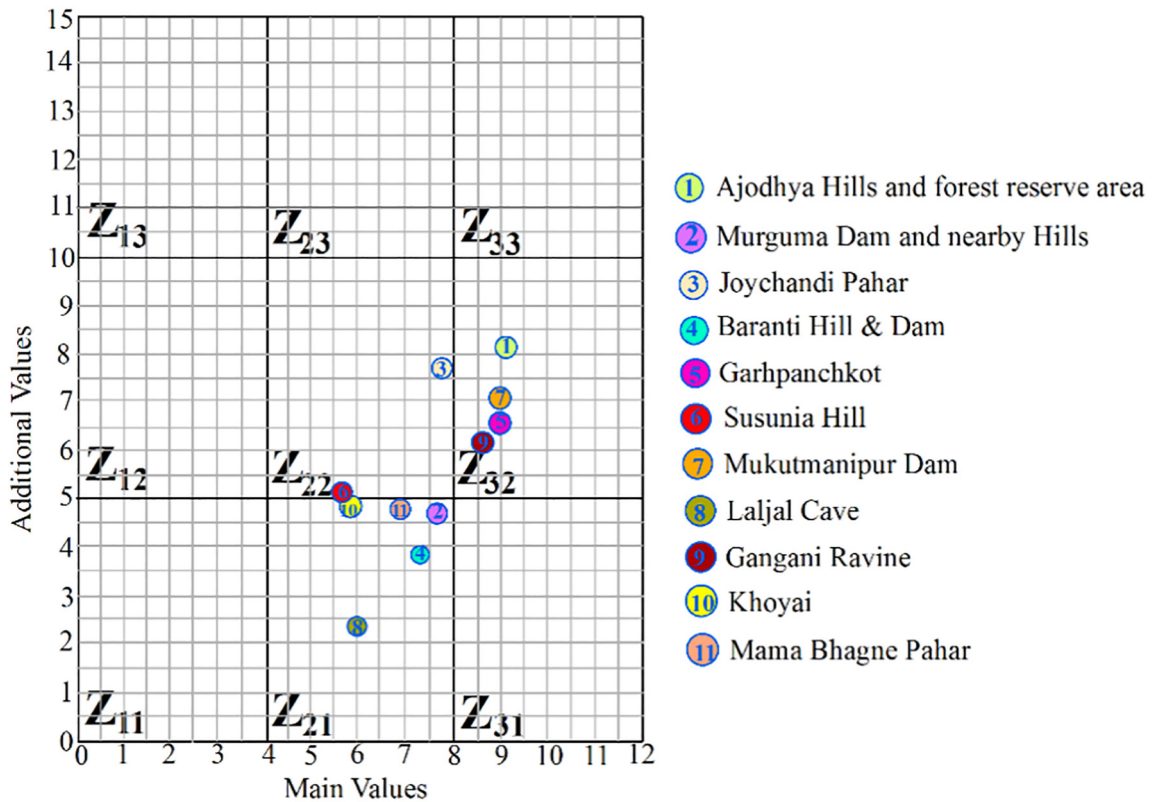


Fig. 2. Position of the analyzed geosites in the M-GAM matrix.

absent. On one hand, there are not any tourist guide, hostelry service, interpretive panels and such tourism infrastructure. On the other hand, the sites with higher tourist values (*VTr*) are Ajodhya Hills and forest reserve area (5.17), Joychandi Pahar (4.67), Mukutmanipur Dam (4.31), Garhpanchkot (3.29) and Gangani Ravine (3.28). These sites attract a large number of tourists and organizations every year in the autumn, winter and spring seasons as they have high quality restaurants service including government youth hostels and also have promotions from national to international level. Tourist guides of different languages are available in Joychandi Pahar and Mukutmanipur Dam, but they are inexperienced in foreign languages.

Based on the Main Values and Additional Values, all the sites of Rarh Bengal have been divided into three groups of sites with the help of M-GAM matrix (Fig. 2). The first group has the highest Main Values and moderate Additional Values, it includes Ajodhya Hills and forest reserve area, Mukutmanipur Dam, Gangani Ravine, and Garhpanchkot, all positioned in the Z₃₂ field of the matrix. The second group comprises sites with moderate Main Values and lowest Additional Values, which is located in the Z₂₁ field of the matrix in Fig.2. These sites are Murguma Dam and nearby Hills, Baranti Hill & Dam, Mama Bhagne Pahar, Khoyai and Laljal Cave. The third group has the moderate Main Values and moderate Additional Values, it includes Joychandi Pahar and Susunia Hill and is located in the Z₂₂ field of the matrix in Fig.2.

The key feature of M-GAM matrix is that sites with higher Main Values and higher Additional Values are suitable sites for the successful development of geotourism. Again, the sites with lower Main Values and lower Additional Values are not suitable sites for the development of geotourism. On the other hand, the sites that have lower Additional Values but the Main Values especially the scientific/educational values (VSE) and scenic/aesthetic values (VSA) of which are higher, can also have the possibility to develop geotourism by improving other necessary sub-indicators through further more investment (Bozic et al., 2014; Bozic & Tomic, 2015; Jonic, 2018; Tomic et al., 2020; Vukovic & Antic, 2019).

Based on the M-GAM matrix, it can be said that the first group sites located in the Z_{32} fields have great potential for the development of geotourism. It is seen that out of these, the Ajodhya Hills and forest reserve area has highest probability for the development of geotourism, as it has vast area based on hilly and forested environment with more view points, improved transportation and communication facilities, government hostelry service, restaurant service etc. Looking at the overall results, it can be concluded that all the sites located in Z_{32} can attract a larger number of tourists through the improvement of promotional activities, basic tourism infrastructure, visitor centers and tourist guide services etc. Located under Z_{22} field but at the edge of Z_{32} field, the Joychandi Pahar has potentiality of geotourism like the first group sites. In the Z_{21} field, the Main Values of Murguma Dam and nearby Hills and Baranti Hill & Dam are greater than 7.00, so it is possible for these sites to develop geotourism by improving the values of sub-indicators of these sites.

4. Conclusion

In the view of above discussion, it can be concluded that Rarh Bengal in eastern India has many notable geosites with a lot of potential for the development of geotourism. The sites in this region already have all the natural elements required for the development of geotourism, but most of the sites lack tourist facilities. The M-GAM method evaluates the assessment of both Main Values and Additional Values of each site according to their importance for tourists and the ultimate results has revealed that there is plenty of room for geotourism improvement in these sites, especially in terms of the tourist values. It explicitly refers to the investment for the improvement of tourism infrastructure based on the development of tourism as well as the enhancement of management and planning. In addition, with all those enhancement as well as embodying the promotional activities, these geosites could attract more visitors every year, which can benefit local community by creating new jobs and incomes towards strengthening the local economy. However, the geotourism development at these sites needs to strictly adhere to the principles of sustainable development as they belong to hilly and forested environments.

Credit author statement

Narayan Chandra Jana; Introduction
 Manoj Kumar Mahato; Study Area
 Manoj Kumar Mahato; Methodology
 Manoj Kumar Mahato and Narayan Chandra Jana; Objective of the study
 Manoj Kumar Mahato and Narayan Chandra Jana; Results and discussion
 Manoj Kumar Mahato and Narayan Chandra Jana; Conclusion
 Manoj Kumar Mahato; Computation of Tables and Mapping in softwares
 Manoj Kumar Mahato; Photo-plates

Declaration of Competing Interest

None.

References

- Antic, A., & Tomic, N. (2017). Geoheritage and geotourism potential of the Homolje area (eastern Serbia). *Acta Geoturistica*, 8(2), 67–78.
- Antic, A., Tomic, N., & Markovic, S. B. (2019). Karst geoheritage and geotourism potential in the Pek River lower basin (Eastern Serbia). *Geographica Pannonica*, 23(1), 32–46.
- Boskov, J., Kotrla, S., Jovanovic, M., Tomic, N., Lukic, T., & Rvovic, I. (2015). Application of the preliminary geosite assessment model (GAM): The case of the Bela Crkva municipality (Vojvodina, North Serbia). *Geographica Pannonica*, 19(3), 146–152.
- Bozic, S., & Tomic, N. (2015). Canyons and gorges as potential geotourism destinations in Serbia: Comparative analysis from two perspectives – General geotourists' and pure geotourists'. *Open Geosciences*, 7, 531–546.
- Bozic, S., Tomic, N., & Pavic, D. (2014). Canyons as potential geotourism attractions of Serbia – Comparative analysis of Iazar and Uvac canyons by using M-GAM model. *Acta Geoturistica*, 5(2), 18–30.
- Bruschi, V. M., & Cendrero, A. (2005). Geosite evaluation. Can we measure intangible values? *II Quaternario*, 18(1), 293–306.
- Chakrabarty, P., & Mandal, R. (2019). Geoarchaeosites for geotourism: A spatial analysis for Rarh Bengal in India. *Geo Journal of Tourism and Geosites*, 25(2), 543–554.
- Chakrabarty, P., & Mandal, T. (Eds.). (2018). *Tourism and sustainability: A geographical study in the Rarh Region of West Bengal*. Kolkata: Anjan Publisher.
- Coratza, P., & Giusti, C. (2005). Methodological proposal for the assessment of the scientific quality of geomorphosites. *II Quaternario*, 18(1), 307–313.
- Djurovic, P., & Mijovic, D. (2006). Geoheritage of Serbia-representative of its total geodiversity. *Collection of papers*, 54, 5–18.
- Dowling, R. K. (2013). Global Geotourism – An emerging form of sustainable tourism. *Czech Journal of Tourism*, 2(2), 59–79.
- Erhartic, B. (2010). Geomorphosite assessment. *Acta Geographica Slovenica*, 50(2), 295–319.
- Faridi, R. (2013). Rahr Plains of West Bengal, India. (August 18, 2013), from <https://rashidfaridi.com/2013/08/18/rahr-plains-of-west-bengal-india/>

- Grover, A. K., & Mahanta, B. N. (2018). Geotourism potential in Arunachal Pradesh – A preliminary appraisal. *Indian Journal of Geosciences*, 72(4), 345–360.
- Hose, T. A. (1995). Selling the story of Britain's stone. *Environmental Interpretation*, 10(2), 16–17.
- Hose, T. A. (1997). Geotourism – Selling the Earth to Europe. In P. G. Marinos, G. C. Koukis, G. C. Tsiambaos, & G. C. Stournaras (Eds.), *Engineering geology and the environment* (pp. 2955–2960). Rotterdam: A. A. Balkema.
- Hose, T. A. (2005). *Geo-Tourism-Appreciating the deep side of landscapes in Novelli. Niche tourism; contemporary issues, trends and cases*. Oxford, UK: Elsevier Science Ltd, 27–37<https://silo.pub/niche-tourism-contemporary-issues-trends-and-cases.html>.
- Hose, T. A., Markovi, S. B., Komac, B., & Zorn, M. (2011). Geotourism - A short introduction. *Acta Geographica Slovenica*, 51(2), 339–342.
- Hose, T. A., & Vasiljevic, D. A. (2012). Defining the nature and purpose of modern geotourism with particular reference to the United Kingdom and South-East Europe. *Geoheritage*, 4, 25–43.
- Jonic, V. (2018). Comparative analysis of Devil's town and Bryce Canyon geosites by applying the modified Geosite assessment model (M-GAM). *Researches Review DGTH*, 47(2), 113–125.
- Newsome, D., & Dowling, R. K. (Eds.). (2010). *Geotourism: The tourism of geology and landscape*. Oxford: Goodfellow Publishers.
- Pal, M., & Albert, G. (2018). Comparison of geotourism assessment models: And experiment in Bakony-Balaton UNSECO global Geopark, Hungary. *Acta Geoturistica*, 9(2), 1–13.
- Paskova, M. (2012). Tourism Environmentalism. *Czech Journal of Tourism*, 1(2), 77–113.
- Patzack, M., & Eder, W. (1998). UNESCO GEOPARK, a new programme – A new UNESCO label. *Geologica Balcania*, 28, 3–4.
- Pereira, L. S., da Cunha, L. S., & Nascimento, M. L. A. (2018). Emergence of geotourism activity at Joao Pessoa municipality and South Coast of Paraiba (Na Brazil). *Sustainable Geoscience and Geotourism*, 1, 1–10.
- Pereira, P., Pereira, D., & Caetano Alves, M. I. (2007). Geomorphosite assessment in Montesinho Natural Park (Portugal). *Geographica Helvetica*, 62, 159–168.
- Pralong, J. P. (2005). A method for assessing the tourist potential and use of geomorphological sites. *Geomorphologie: Relief, Processus, Environnement*, 3, 189–196.
- Reynard, E. (2008). Scientific research and tourist promotion of geomorphological heritage. *Geografia Fisica e Dinamica Quaternaria*, 31, 225–230.
- Reynard, E., Fontana, G., Kozlik, L., & Scapozza, C. (2007). A method for assessing "scientific" and "additional values" of geomorphosites. *Geographica Helvetica*, 62, 148–158.
- Serrano, E., & Gonzalez-Trueba, J. J. (2005). Assessment of geomorphosites in natural protected areas: The Picos de Europa National Park (Spain). *Geomorphologie: Relief, Processus, Environnement*, 3, 197–208.
- Ticar, J., Tomic, N., Breg Valjavec, M., Zorn, M., Markovic, S. B., & Gavrilov, M. B. (2018). Speleotourism in Slovenia: Balancing between mass tourism and geoheritage protection. *Open Geosciences*, 10(1), 344–357.
- Tomic, N. (2011). The potential of lazard canyon (Serbia) as a geotourism destination: Inventory and evaluation. *Geographica Pannonica*, 15(3), 103–112.
- Tomic, N. (2016). *Geoheritage of the middle and lower Danube Region in Serbia: Inventory, geo-conservation and geotourism*. Ph. D. thesis Serbia: University of Novi Sad.
- Tomic, N., & Bozic, S. (2014). A modified geosite assessment model (M-GAM) and its application on the lazard canyon area (Serbia). *International Journal of Environmental Research*, 8(4), 1041–1052.
- Tomic, N., Markovic, S. B., Antic, A., & Tesic, D. (2020). Exploring the potential for geotourism development in the Danube region of Serbia. *International Journal of Geoheritage and Parks*, 8, 123–139.
- Vujcic, M., Vasiljevic, D., Markovic, S., Hose, T. A., Lukic, T., Hadzic, O., & Janicevic, S. (2011). Preliminary geosite assessment model (gam) and its application on Fruska gora mountain, potential geotourism destination of Serbia. *Acta Geographica Slovenica*, 51(2), 361–377.
- Vukoicic, D., Milosavljevic, S., Valjarevic, A., Nikolic, M., & Sreckovic-Batocanin, D. (2018). The evaluation of geosites in the territory of National Park "Kopaonik" (Serbia). *Open Geosciences*, 10, 618–633.
- Vukovic, S., & Antic, A. (2019). Speleological approach for geotourism development in Zlatibor County (West Serbia). *Turizam*, 23(1), 53–68.
- Wulung, S. R. P., & Rajoendah, M. I. K. (2019). Sustainable tourism development through geotourism route planning: A case study of natuna island. *Paper presented at the First Sustainable Tourism National Seminar, STP Mataram*.

‘এবং মত্হয়া’-বিশ্ববিদ্যালয় মঞ্জুরী আয়োগ (U.G.C.- CARE List) অনুমোদিত

তালিকার অন্তর্ভুক্ত। ২০২০ সালে প্রকাশিত ৮৬ পৃ.

তালিকার ৬০ পৃ. এবং ৮৪ পৃ. উল্লেখিত।

এবং মত্হয়া

(বাংলা ভাষা, সাহিত্য ও গবেষণাধর্মী মাসিক পত্রিকা)

২২ তম বর্ষ, ১২৫ সংখ্যা, অক্টোবর, ২০২০

সম্পাদক

ডা. মদনমোহন বেরা

কে.কে. প্রকাশন

গোলকুঁয়াচক, মেদিনীপুর, প.বঙ্গ।

| | |
|--|-----|
| ১২. নাটক : স্বরূপ, নানারূপ ও গণযোগ | |
| :: দেবজ্যোতি শীট | ১৪ |
| ১৩. অভিব্যক্তি : রায় বাংলার এক শিলাচর্চা কেন্দ্র | |
| :: সমর কান্তি চক্রবর্তী | ১০২ |
| ১৪. 'দর্পণ' নাটকে নারীর আর্ত-ক্রন্দন | |
| :: সৌমেন পুরকাহিত | ১১২ |
| ১৫. পুরুলিয় লেখকি এসাইলাম : কুষ্ঠরোগ, চিকিৎসাবিধি ও মিশনারী | |
| :: জয়ন্ত মাজিগোপ | ১২০ |
| ১৬. 'মহত্তর'-এর বিপর্যয় ও মানব প্রতিক্রিয়া : অহেয়ণ | |
| :: কঙ্করী কর | ১৩২ |
| ১৭. উদ্যোগপতি বাঙালি : অষ্টদশ-ঊনবিংশ শতাব্দী | |
| :: অচিত্র দে | ১৪০ |
| ১৮. মুর্শিদাবাদ জেলার লোকপূজার আঙ্গিকে সোলেনীর গান | |
| :: টুকটুকি হালদার | ১৪৮ |
| ১৯. গিরিশ ও গিরীশ : সমানামী দুই নাটককার | |
| :: সিদ্ধার্থ চক্রবর্তী | ১৬৩ |
| ২০. সংস্কৃত নাট্যোৎপত্তি | |
| :: মধুমিতা জানা | ১৭৯ |
| ২১. রবীন্দ্রনাটকের জনতা : 'রাজা ও রাণী' থেকে 'তপতী' | |
| :: তময় সিংহ মহাপাত্র | ১৮৪ |
| ২২. 'সিরাভূদীন' আমাদের কবিতা : পাঠকের অনুভবে | |
| :: দেবারতি দে | ১৯২ |
| ২৩. দ্বন্দ্ব, দ্বন্দ্বিকতা : বাঙালির মনীষায় ও বাংলা সাহিত্যে | |
| :: অমিতাভ মুখোপাধ্যায় | ২০০ |
| ২৪. মানবপ্রয়াস ও ভগবৎকৃপার যৌথ অভিযান | |
| :: বানানী বর্মন | ২০৭ |
| ২৫. কেবি অবদ্রীতানন্দ ও বৃহত্তর মানভূমের কুমার | |
| :: ডম প্রকাশ সিংহদেও | ২১৩ |
| ২৬. 'তিলোত্তমা মঞ্জুমাধার-এর উপন্যাসে পুরাতনের বর্ণনায় প্রতিফলন : প্রসঙ্গ 'অর্জুন ও চারকন্যা' | |
| :: মঞ্জুরী বিশ্বাস | ২২৯ |

| | |
|---|-----|
| ২৭. কুমুদরঞ্জন মাহিকের প্রবন্ধে গ্রাম সমাজের রূপ ও রূপান্তর | |
| :: সবাট কুমার পাল | ২২৫ |
| ২৮. 'নক্সী কাঁথার মাঠ' এবং 'রূপসী বাংলা' : বঙ্গ প্রকৃতির রূপের বিচিত্র আলোক্য | |
| :: বাপি দত্ত | ২৩০ |
| ২৯. কমল কুমার মুখোপাধ্যায়ের গল্প 'মতিলাল পাদরী' : | |
| ধর্ম বিশ্বাসের আড়ালে মানবিক চেতনা | |
| :: বেরী পাত্র (সোমস) | ২৩৫ |
| ৩০. সরলা দেবী চৌধুরাণী : উপনিবেশিক বঙ্গের বিপ্লবী আন্দোলনের অন্যতম উপগাতা | |
| :: চিত্ত সেন পরামানিক | ২৪৫ |
| ৩১. 'কথা'র মধ্যে 'বাদ'-এর স্বেচ্ছত বিচার | |
| :: প্রিয়ঙ্কা মাহতি (দাস) | ২৫৩ |
| ৩২. রবীন্দ্রসঙ্গীত : যুক্তিগত থেকে নৈবেদ্যিক অভিযাত্রা | |
| :: সুকান্ত চক্রবর্তী | ২৬৭ |
| ৩৩. কান্দীদাসী মহাভারতে রাজনৈতিক ও মানোত্তমিক দ্বন্দ্ব | |
| :: সৌমিতা মুখাঙ্কী | ২৭৪ |
| ৩৪. 'উদ্যোগ পর্ব' : এক বিশেষ সময়ের ইতিবৃত্তে ঝরাও জীবন | |
| :: বৈশাখী কুণ্ডু | ২৮২ |
| ৩৫. রবীন্দ্র ছোটগল্পে প্রতীবাদী নারী | |
| :: তাহামিজা খাতুন | ২৮৭ |
| ৩৬. 'দুঃখ তোমার যুচবে করে?' রবীন্দ্রনাথ | |
| :: ড. অরুণ সরকার | ২৯৪ |
| ৩৭. বাংলা মঙ্গলকাব্যে অস্তিত্বের সংকট | |
| :: ড. শান্তনু ভট্টাচার্য | ৩০৩ |
| ৩৮. বাংলা থিয়েটারে নারী : ঊনিশ শতক | |
| :: ড. বিপ্লবকুমার মণ্ডল | ৩১৪ |
| ৩৯. পাঠ্যপুস্তক রচয়িতা রবীন্দ্রনাথ | |
| :: ড. অচিনা দগুপাঠ | ৩২৪ |
| ৪০. প্রকৃতি ও প্রকৃতির দ্বন্দ্ব অতীন বন্দ্যোপাধ্যায়ের উপন্যাস | |
| :: ড. সুরভকুমার দে | ৩৩৩ |
| ৪১. এমন দিন হবে হবে তারা : প্রসঙ্গ 'বীরাঙ্গনা কাব্য'র তারা চরিত্র | |
| :: ড. শান্তনু চট্টোপাধ্যায় | ৩৪৩ |

অভিব্যক্তি : রাঢ় বাংলার এক শিল্পচর্চা কেন্দ্র

সময় কালি চক্রবর্তী

বন্দর অঙ্গ ঝাঁকুড়া। জেলার ছোট গ্রাম চন্দ্রহার। লোকমুখে তা বর্তমান ছান্দাড় বা ছান্দার। অতেনা অজানা অখ্যাত গ্রামটির সুখ্যাতি আজ বিধ্বজেড়া। ছান্দার আজ জেলার ভৌগোলিক গভী পেরিয়ে পৃথিবীর মানচিত্রে স্থান করে নিয়েছে।

মনে প্রশ্ন জাগতেই পারে কেন? কী আছে এখানে? ইত্যাদি ইত্যাদি...। উত্তর লুকিয়ে আছে নেপথ্য কাহিনির অন্তরালে।

আমরা জানি, বর্তমানে প্রতি মুহূর্তে অতীতকে পিছনে ফেলে অভিজ্যতের দিকে অগ্রসর হয়ে চলেছে। আজ থেকে চার দশকেরও কিছু পূর্বে এমন একজন ব্যক্তি এখানে এসেছিলেন যার তুলনা হয় না। জহুরী চোখে তিনি বুঝতে পেরেছিলেন, রাঢ় বাংলার এক রুক্ষ মাটি তাও একদিন সোনার ফসল ফলবে। আর পঁচাত্তরের মতো সাপাশাটা আটপোরে জীবন যাপন করলেও তিনি ছিলেন কিছুটা ব্যতিক্রমী। অদম্য উৎসাহী, অক্লান্ত পরিশ্রমী, বাস্তববাদী, সত্যনাস্তানী, রামকৃষ্ণ ভাবদর্শে অনুপ্রাণিত, সুন্দরের পূজারী, শিল্প সংস্কৃতি মনস্ত দুয়দুটি সম্পন্ন মানুষটি তিলতিল করে গড়ে তুলেছিলেন তাঁর স্বপ্নের শিল্পচর্চা কেন্দ্র ‘অভিব্যক্তি’।

সৌম্যকান্তি চেহারার আপাদমস্তক স্মারিত বহুকাঠিন অথচ কুসুম কোমল হৃদয়ের নীরব শিল্পী কম্যোগী, সন্ন্যাসী বীরপুরুষটি আর কেউ নন, তিনি হলেন এই প্রতিষ্ঠানের (অভিব্যক্তি) প্রাণ প্রতিষ্ঠাতা— উৎপল চক্রবর্তী।

রাঢ় বাংলার এক অখ্যাত নন্দন কাননে যে শিল্প প্রতিষ্ঠানটি পথ হয়েছিল; তার নামকরণ ছিল শ্রী চক্রবর্তীর মস্তিষ্ক প্রসূত ভাবনা। যার অর্থ মনের ভাব প্রকাশ করা।

প্রসঙ্গক্রমে মিশাইলমান প্রাক্তন রাষ্ট্রপতি ড. এ. পি. জে. আব্দুল কালামের বিখ্যাত উক্তি স্মরণ করে বলা যায় উৎপলবাবু যুগিয়ে স্বপ্ন দেখতেন না, স্বপ্ন তাঁকে ঘুমতে দিত না?

দেশভাগের সময় ওপার-বাংলা থেকে এপার বাংলায় এসে কোলকাতায় বসবাস। পেশার টানে ঝাঁকুড়ায় আসা, শিল্পের নেশায় ঝাঁকুড়াকে ভালোবাসা। একাধারে তিনি ছিলেন— বিশিষ্ট শিক্ষক, কল্পনাপ্রবণ শিল্পী, ভাস্কর, গীতিকার, সুরকার, গায়ক, লেখক, প্রাবন্ধিক, কবি, সাহিত্য অনুরাগী, সুবক্তা প্রভৃতি জগের অধিকারী। আখ্যাতোলা কাজপাণ্ডা মানুষটি জীবনের শেষ দিন পর্যন্ত ঝাঁকুড়ার লাল মাটির সৌন্দর্যকে মানুষকে ভালবেসে ও ভালবাসা পেয়ে তিনি মানুষের হৃদয়ে নাম

লিখতে পেরেছিলেন।

বহুমুখী প্রতিভার উৎপল চক্রবর্তীর জীবন খাতার প্রতি পাতায়, জড়িয়ে থাকা আলোর পথযাত্রীর পথে ঝাঁকে, চড়াই-উৎসাহ, যাত-প্রতিযাত, সুখ-দুঃখ, হাসি-কান্না, ভালো-মন্দ প্রভৃতি ধ্বংসীয় ছন্দেভরা নানারঙের রামধনু আঁক-ময়ূরকণ্ঠ দিনগুলির কথা, স্মৃতিচারণের মাধ্যমে নানান টুকরো টুকরো ঘটনা নিয়ে একটি জীবন্ত কোলাজ তৈরি করার চেষ্টা করেছিলেন।

উৎপল চক্রবর্তীর পিতৃত্বমি ছিল বাংলাদেশের বড়ভা জেলার কুসুমী গ্রামে। পিতা স্বর্ণিত অমল চক্রবর্তী ছিলেন সরকারী কর্মচারী। মাতা শবিতা দেবী ছিলেন গৃহবধু। পাঁচ ভাইবোনোর মধ্যে তিনিই জ্যেষ্ঠপুত্র। এক শিক্ষিত স্বচ্ছল সম্ভ্রান্ত পরিবারের সুসন্তান। তিনি ১৩ই জ্যেষ্ঠ, ১৩৪৫ বঙ্গাব্দে অবিভক্ত দিনাজপুর জেলার বালুরঘাট শহরে (মাতুলালয়) জন্মগ্রহণ করেন। শৈশব, কৈশোর ও ছাত্রজীবন সেখানেই অভিব্যাহিত হয়। কলেজে পাঠরত অবস্থায় ট্যান্ড্রিও চালিয়েছেন।

বাবা শনিবারের চিঠি, অচলপত্র, যুগান্তর প্রভৃতি পত্র-পত্রিকায় লিখতেন, মা ভালো গান জানতেন। সেখান থেকেই উৎপলবাবুর লেখাকৌশি ও সঙ্গীতের প্রেরণা পান। আদর করে মা ডাকতেন কেটো বলে।

মালদার দামোদরপুর প্রাথমিক বিদ্যালয়ের শিক্ষকরূপে তিনি কর্মজীবন শুরু করেন। তারপর নদিয়ার মহেশগঞ্জ হাইস্কুল, ২৪ পরগণার বিরাটীর খালিসাকোটা বিদ্যালয়। এক বৎসর শিক্ষকপদস্থলের রবীন্দ্র রচনাবলী বিভাগে কাজ করেন। পরে বাণীপুর ২নং শিক্ষক শিক্ষণ মহাবিদ্যালয়ের অধ্যাপক ছিলেন। সেখান থেকে ১৯৬৮ সালে ঝাঁকুড়া জেলার ছান্দার জুনিয়ার বেসিক ট্রেনিং কলেজে অধ্যাপক হিসাবে যোগদান করেন।

কিছুদিনের জন্য এই জেলার সাবডাকোন বেসিক ট্রেনিং সেন্টারের ভারপ্রাপ্ত অধ্যক্ষের পদ অলংকৃত করেছিলেন। পুনরায় ফিরে এসে অধ্যক্ষপদ পদে যোগদান করতে তাঁর বিবেকে বাঁধে। পরাধীনতার নাগপাশ মুক্ত জীবনানন্দের জন্য ১৯৮৯ সালে স্বেচ্ছাবসর নিলেন। তারপর থেকে অভিব্যক্তিই হয়ে উঠল তাঁর ধ্যান জ্ঞান ও সাধনার কমতিধ। শিল্পের নেশায় বৃন্দ হয়ে যেতে ঝঠেন সৃষ্টি সুখের উদ্দেশ্যে।

মালদায় ঢাকায় করার সময় প্রায়ই গৌড় যেতেন। গৌড়েই গড়বেন শিল্প দেউল এমনটাই তাঁর প্রথম ইচ্ছা। পরে ভাবনা পাশ্টে হল বাণীপুর। অবশেষে তা পূর্ণিত পেল ঝাঁকুড়ার ছান্দারে।

সময়টা ১৯৭২, উত্তর ২৪ পরগণার বাণীপুরে থাকাকালীন ‘সেন্টার ফল কালচারাল অ্যাক্টিভেশন’ তথা আলোর সারণী পত্রিকার সম্পাদক শ্রী সঞ্জীব সরকারের আমন্ত্রণে কোলকাতার সেন্টপলস ক্যাথিড্রাল চার্চ প্রাঙ্গণে যুব উৎসবে চিত্র প্রদর্শনীর জন্য একটি সংস্থা গঠন করেন, সঙ্গে ছিলেন শিল্পী ও পুরণবেষক নীহার ঘোষ এবং রাম বসু।

সেই সময় উৎপলবাবু বদলী হয়ে আসেন ছান্দারের (JBT) সেন্টারে। এখানকার সাবেকী সংস্কৃতি তাঁকে উদ্ভুদ্ধ করে। ১৯৭৪ সালে তিনি বঙ্গ সংস্কৃতি সংকলনে ছাত্র-ছাত্রীদের হাতের কাজ এবং লোকগানের অনুষ্ঠান করেন। উক্ত সংকলনে ত্রয়সী প্রশংসা পান।^{১৫} এছাড়াও ছান্দারের উৎপলবাবু তাঁর পক্ষে-শিল্পে গুরুত্বপূর্ণ বাকুড়ার মাটিতে বহুকৃতিসন্তান জন্মগ্রহণ করেছেন। তাদের মধ্যে যামিনী রায় ও রামকিশোরের মতো দিকপাল শিল্পী ও ভাস্করের কথা মাথায় রেখে শ্রী চক্রবর্তী এখানে একটি শিল্প প্রতিষ্ঠান গড়ার পরিকল্পনা করেছিলেন। এমন সময় গ্রামের বিশিষ্ট সমাজসেবী শ্রী শশাঙ্ক শেখর মুখোপাধ্যায় তাঁর সুযোগ্যপুত্র প্রাক্তন বিধায়ক শ্রী মাণিক মুখোপাধ্যায়ের সঙ্গে পরিত্যম ঘটে এবং এই বিষয়টি নিয়ে একপ্রস্থ আলোচনা হয়। প্রস্তাবটি জনহিতকর। তাই তাঁরা একটি স্থায়ী প্রতিষ্ঠান গড়ার জন্য সাহায্যের হাত বাড়িয়ে দেন। প্রথমে ১ বিঘা ও ছটাক এবং পরে কিছু অংশ সর্বস্বত্বল্যে প্রায় দেড় বিঘা জমি দান করেন, যা বেলিয়াতোড় থেকে ৩ কিমি দূরে বাকুড়া বর্মান রাস্তার ধারে JBT কলেজের ঠিক উল্টোদিকে অবস্থিত। জমির পাশেই দুটি সারর এবং মহাশয়ান রয়েছে।^{১৬}

শুরু হল পথচলী—

২৬ শে ডিসেম্বর ১৯৭৭ সালে জমি জরিপ হয়। ঝান-ঝেদ ভরা পলাশ খেজুর প্রভৃতি গাছ ও বুনো খোপা ঝাড় কেটে চলে সাবাই অভিযান। এতে অংশ নেয় ‘সব পেয়েছি’ আশ্রয়ের ছেলে-মেয়েরা, ৭৬, ৭৭ এবং ৭৮ বর্ষের পর প্রসিক্ষণরত শিক্ষক, প্রশিক্ষক, স্থানীয় কয়েকটি ক্লাবের সদস্যবৃন্দ এবং শুভাকাঙ্ক্ষী ব্যক্তিগণ। সবই চলত উৎপলবাবুর নির্দেশমতো। এখানে রাজারাম খাঁড়া, বৃন্দাবন কর ও শুধাংশু চন্দের নাম বিশেষভাবে প্রাঙ্গিক হয়ে পড়ে। কেননা এরা বাড়ি ছেড়ে দিন রাত এক করে মাটি কামাড়ে পড়ে ছিলেন প্রতিষ্ঠানটি গড়ার জন্য।^{১৭} ছোড়া অর্থাৎ উৎপলবাবু তাঁদের ব্যয়ভার বহন করতেন।^{১৮} প্রথমে একটি রিক্ত খেজুর গাছকে কেন্দ্র করে গড়ে ওঠে চলাঘর, গোলঘর। তারপর একে একে আরও কয়েকটি ঘর। সবই ছিল ছিটেবেড়ার তৈরি। অভিজাতিকর জনপ্রিয় গোলঘর অর্থাৎ প্রদর্শন কক্ষের কথায় একটা কাঁচা বাড়ির দেওয়ালের উপর তালপাতার ছাউনি। ছাউনির বাইরের অর্ধাংশ সাঁজোলা রমণীরা মাটির সঙ্গে খড় পুড়িয়ে গোবরের সঙ্গে তা মিশিয়ে কাল রং এর প্রলেপ (পেচার) দেয়, বাকী উপরের অর্ধাংশে কাল পেরমাটির প্রলেপ। দেওয়ালের গায়ে সুদৃশ্য আলপনার মাধ্যমে গ্রাম বাংলার লোক সংস্কৃতিকে তুলে ধরা হয়েছে।^{১৯} গোলঘর সংলগ্ন ঠাকুর ঘরে শ্রীরামকৃষ্ণদেবের মাটির ভাস্কর্য গড়েন উৎপল চক্রবর্তী স্বয়ং। প্রতিদিন সেখানে প্রার্থনা ও সন্ধ্যারিত হয়। চতুঃসীমা বরাবর বেড়া বা রিদ দেওয়া হয়। মূল প্রবেশ পথে বাঁশের তৈরি গেট বানানো হয়। ১৯৭৮ সালের ১০ই মার্চ (ঠাকুরের জন্মতিথি উপলক্ষে)

অভিজাতিক (চাক ও কারুশিল্প এবং লোক সংস্কৃতি কেন্দ্র) কে আনুষ্ঠানিক ভাবে সর্বসাধারণের জন্য উন্মুক্ত করে দেওয়া হয়। প্রতি বৎসর এই নির্দিষ্ট প্রতিষ্ঠা দিবস হিসাবে পালিত হয়।

গোলঘরের ঠিক সামনেই চট্টগ্রাম বিঙ্গবের সুবর্ণজয়ন্তীর প্রতীক ভাস্কর্যটিও উৎপলবাবুর তৈরি। ১৯৮০ সালের ১৫ই নভেম্বর সেটি উদ্বোধন করে চট্টগ্রাম বিঙ্গবের অন্যতম সদস্য বিপ্লবী গণেশ ঘোষ।^{২০} ভাস্কর্য উন্মোচনের পর তিনি একটি অমুখ চারা রোপন করেছিলেন যা আজ মহিষ্কররূপে মুক্তমণ্ডের মাঝখানে মাথা উঁচু করে নীলাকাশ ঘূরন করে চারিদিকে সিন্ধু ছায়া দান করছে।

গোলঘর সহ অভিজাতিকর গ্রাঙ্গন জুড়ে একে একে বেশ কয়েকটি গৃহ গড়ে উঠেছে। গৃহগুলি নির্মাণের পিছনে অনেক ঘটনা, অনেকের সাহায্য ও অবদান রয়েছে। স্থানাভাবে বিস্তারিত বর্ণনা না করতে পারলেও সংক্ষিপ্ত পরিচিত তুলে ধরলাম।

১. প্রথম আলো-সর্বপ্রথম যে খেজুরগাছকে ঘিরে চলাঘর তৈরি হয়েছে (১৯৭৮খ্রি:)
২. অভিব্যক্তি— গ্রাঙ্গনী কক্ষ (গোলঘর) ১৯৭৮ খ্রি:।
৩. আতিথ্য— যেখানে সবাই এসে বসেন (১৯৭৯ খ্রি:।
৪. রূপসাগর— যেখানে আলোচনা সভা ও ঘরোয়া অনুষ্ঠান হয়।
৫. রামকিশোর ভবন— দ্বিতীয় গ্যালারী (১৯৮০ খ্রি:।
৬. যামিনী ভবন— তৃতীয় গ্যালারী (১৯৮৪ খ্রি:।
৭. অমল সবিতা ভবন— উৎপলবাবুর পিতামাতার স্মৃতিতে (১৯৯০ খ্রি:।
৮. আরশি নগর— পূর্বতন শশাঙ্ক রমণীবালা ভবন (১৯৯০) নবরূপে (২০১৩)।
৯. হুমঘর— কন্নীরা যেখানে রাত্রে থাকেন (১৯৯১ খ্রি:।
১০. বইবাহিক— বই রাখার ঘর (১৯৯২) নবরূপে (২০১৩ খ্রি:।
১১. ফিরোদ প্রসাদ বিদ্যাবিনোদ মুক্তমণ্ড— ১৯৯২ খ্রি:।
১২. চন্দ্রহার— চতুর্থ গ্যালারী (১৯৯৯ খ্রি:।
১৩. এসো স্নান করি (আনচান)— স্নানঘর (১৯৯৯ খ্রি:।
১৪. পাবির নীড়ের মতো— জীবনানন্দ দাস জন্মশতবর্ষ স্মরণে (১৯৯৯ খ্রি:।
১৫. পঞ্চবর্তী— ছান্দার গ্রামপঞ্চায়েত নির্মিত বটতলার সভাঘর (২০০৯ খ্রি:।
১৬. ফকিরের অতিথি— রবীন্দ্রনাথ ঠাকুরের জন্ম সাধ শতবর্ষ স্মরণে (২০১০ খ্রি:।
১৭. মা সারদা ভবন— স্মৃনী বিবেকানন্দের সাধ শতবর্ষ স্মরণে (২০১২ খ্রি:।

এছাড়াও—
চিনাইস ও রাজহাঁসদের জন্য— খাঁচা হাসপাতাল
পাখিদের জন্য— পাখিখানা
মাছেদের জন্য— মাংসালয়

ধরগোসের জন্য— শস্যব্যস্ত
পায়রাদের জন্য— কেপোতায়

কোলকাতার একাডেমি অফ ফাইন আর্টসে ‘অভিব্যক্তি’ বেশ কয়েকবার চার ও কার্ফিশিষের প্রদর্শনী করেছে। একবার প্রদর্শনীর উদ্বোধক ছিলেন প্রখ্যাত ভাস্কর রামকিশোর বেইজ। সেই প্রদর্শনীতে আসেন তৎকালীন কেন্দ্রীয় হস্তশিল্প নিগমের পূর্বাঞ্চলীয় অধিকর্তা কল্যাণ দে। তাঁরই ব্যবস্থাপনায় অভিব্যক্তিতে একে একে চালু হয় স্টেট খোদাই ও অন্যান্য শিল্প চর্চার কাজ এবং প্রতিষ্ঠানটি হস্তশিল্পের সরকারী স্বীকৃতি পায়। পরে এগিয়ে আসে জেলা প্রশাসনের কর্তৃপক্ষ। সেইসময় রাজ্যপাল সৈয়দ নরুল হাসান ‘অভিব্যক্তি’ পরিদর্শনে এলেন তাঁর প্রচেষ্টায় পূর্বাঞ্চলীয় সংস্কৃতি কেন্দ্রের সঙ্গে যোগাযোগ আরো নিবিড় মজবুত হয়।

চিত্রকলা ও কার্ফ শিল্পচর্চার ক্ষেত্রে পরীক্ষা নিরীক্ষা চলতে থাকে। স্টেট, বীশ, বেলামালা ও ধানের কাজে সফলতা আসে। শিল্প চর্চার পাশাপাশি সঙ্গীত, সাহিত্য এবং লোকসংস্কৃতি চর্চাও চলতে থাকে। গ্রাম পরিচিতি নিয়ে প্রকাশিত হয় অভিব্যক্তি গ্রন্থমালা। বিভিন্নস্থানে হস্তশিল্পের কর্মশালাও আয়োজন করা হয়।

রাজ্য চারুকলা পর্ষদ, রাজ্য সঙ্গীত একাডেমী, পূর্বাঞ্চল সংস্কৃতিকেন্দ্র, লোকসংস্কৃতি ও আদিবাসী সংস্কৃত কেন্দ্র, রাজ্য স্কুদ ও কুটির শিল্পদপ্তর, কেন্দ্রীয় হস্তশিল্প বোর্ড, বাংলা নাটক উটকম, শময়িতা মঠ প্রভৃতি বিভিন্ন সংস্থার সহায়তায় নানাবিধ হস্তশিল্প এবং সঙ্গীতের কর্মশালা অনুষ্ঠিত হয়েছে।^{১১}

বাংলার লোকশিল্প ছাড়াও বিহারের মধুবনী শিল্প, মধ্যপ্রদেশের গোনদ উপজাতির শিল্প, পটচিত্র, আদিবাসী চিত্র, বেলামালা বীশ, টেরাকোটা কাঠ, পাথরখোদাই, স্টেট খোদাই, ভেঁকরা শিল্প, শঙ্খশিল্প, টেরাকোটা বিন্যাসের কাজ, গয়নাবাড়ি প্রভৃতি বিভিন্ন বিষয়ে এখন থেকে প্রায় হাজার খানের বেশি শিল্পী প্রশিক্ষণ নিয়েছেন। তাছাড়া ফিল্ডের গোর্টা (SHG) মহিলাদের নিয়মিত প্রশিক্ষণ দেওয়া হয়।

এখানকার প্রশিক্ষণপ্রাপ্ত শিল্পকর্মীরা রাজ্য ও রাজ্যের বাইরে নিজেরা ফিল্ডের হয়ে কাজ করছেন। উদাহরণ স্বরূপ বলা যায় কেঞ্জেকুড়ায় সুধাংশু চন্দের ‘তিনেত্রী শিল্পশ্রম’ বীশ শিল্পের এক বিখ্যত প্রতিষ্ঠান। রাজারাম খাঁড়া গোড়াবাড়ীতে গড়েছেন ‘আঁকাজোকা’, শিবারণ তুং এর স্বামীজি কার্ফিশিল্প কেন্দ্র তালান্দায়, নবগ্রামে সঞ্জিবের প্রতিস্থবি, চুয়ামাসিনার পবন গোহার, সমারেন্দ্র মালিয়াডায়, এমনি করে বিবেক সাঁতারার মতো অনেক মানুষ বঙ্গভূতে কর্মে লিপ্ত রয়েছেন।

তাই বলতে বিধা নেই অভিব্যক্তির কর্মক্ষেত্র মানুষের অন্ন-বস্ত্র ও বাসস্থান অর্থাৎ জীবন জীবিকার সন্ধান দেয়। এখানকার গ্রামীণ মহিলারা বেল থেকে বেলামালা কেটে অর্ধোপার্জন করেন। কেউ আবার কুটির শিল্পের সাহায্যে সংসার প্রতিপালন করেন। অতএব অভিব্যক্তি যে মানুষের আর্থ-সামাজিক চাহিদা পূরণে সহায়ক ভূমিকা পালন করে চলছে— সে বিষয়ে বিন্দুমাত্র সন্দেহ নেই।

সাধারণ তুচ্ছ ফেলে দেওয়া জিনিসপত্র থেকে অসাধারণ চোখ ধাঁধানো শিল্পকর্ম তৈরি করাই তো শিল্পীর কাজ। এই প্রতিষ্ঠানের শিল্পীরা গ্রামীণ স্থানীয় মেলা, জেলা বা রাজ্য এমনি কি তিনরাজ্যে শিল্পমেলায় শিল্পের পসর্যা নিয়ে হাজির হন। যেমন— বিশ্বপুত্র মেলা, মেদিনীপুর, রানীপুর, কলকাতা (হস্তশিল্প মেলা), ভুবনেশ্বর, চণ্ডীগড়, দিল্লী প্রভৃতি। ১৯৯০ সালে দিল্লীর প্রগতি ময়দানে ভারতবর্ষ বাণিজ্য মেলা বা Trade Fair ‘অভিব্যক্তি’ অংশগ্রহণ করে দেশের মধ্যে দ্বিতীয় স্থান অর্জন করেছিল। প্রথম হয়েছিল রাজস্থান, তৃতীয় কেরল।^{১২}

‘অভিব্যক্তি’-র শিল্পকর্ম দেখতে, পাওয়া যাবে বাঁকড়া, বর্ধমান, বালুরঘাট (দক্ষিণ দিনাজপুর), কালিয়াগঞ্জ (উত্তর দিনাজপুর), মালদহ, পশ্চিম মেদিনীপুর, হুগলী, আরামবাগ, কোলকাতা প্রভৃতি স্থানে। বর্তমানে আরো বিভিন্ন স্থানে চলছে।

শুধু শিল্পচর্চা নয়, সাহিত্য ও সঙ্গীতের জগতেও প্রতিষ্ঠানটি বিশেষভাবে নজর কেড়েছে। সাহিত্য রচনার ছোড়দার (প্রতিষ্ঠানের কর্ণধার) মুন্সিয়ানার তারিক করতেই হয়। তিনি বেশ কিছু পত্রিকার প্রচ্ছদ অলংকরণ করেছেন। অন্যান্য সদস্যদেরও কিছু বই এবং প্রকাশিত হয়েছে ‘অভিব্যক্তি গ্রন্থমালা’।

এখানে উৎপল চক্রবর্তী প্রণীত পুস্তকগুলির কথাই উল্লেখ করলাম—

১. আমার স্বপ্নের মুখ (কবিতা)— মিঞালয়
২. জ্বালিবাস কিছু অনুভব (কবিতা সংকলন)— ‘কবিতা দর্শনিনে’
৩. পাথুলিপি করে আয়োজন— লিটিল ম্যাগাজিনে লাহরুরী— বেলিয়াতোড়
৪. দৈতকর্ষ (সহলোক কাঙ্গীনাথ দাস)— মিঞালয়
৫. আমি আছি (গল্প সংকলন)
৬. আমি সাক্ষ্যকার (গল্প)— দীপ প্রকাশক
৭. যা মনে হয় (প্রবন্ধ সংকলন)— অমর ভারতী
৮. বিপুল রাজধানী (ইতিহাস ভ্রমণ)— অমর ভারতী (১ ও ২ একত্রে)
৯. একটি পাবক শিখা (কিংবদন্তীর গল্প)— বিশ্বজ্ঞান
১০. অগ্নাংসব (উপন্যাস)— কবিতা পাবিক
১১. বিলুপ্ত রাজধানী (অখণ্ড)— অমর ভারতী
১২. পরচর্চা (২য় খণ্ড)— অমর ভারতী
১৩. পরচর্চা (২য় খণ্ড)— ব্রাহ্মী প্রকাশন (দুর্গাপুর)
১৪. কিছু সৌভাগ্যের স্মৃতি— একুশ শতক

সঙ্গীতের ক্ষেত্রেও প্রতিষ্ঠানটির অসাধারণ অবদান রয়েছে। এখানকার সঙ্গীত শিল্পীরা বিভিন্ন স্থানে বেতার, দূরদর্শন, সঙ্গীত পরিবেশন করেছেন। তাছাড়া এখান থেকে অভিব্যক্তির মান- ১ এবং ২ (ক্যাসেট ও সিডি), গানের ধারণাতলয় (সিডি) প্রকাশিত হয়েছে।

এছাড়াও দূরদর্শনে ‘অভিব্যক্তি’ অংশ নিয়েছে। রয়েছে বেশ কিছু তথ্যচিত্র।

অভিযাত্রিক সংগ্রহশালায় ঐতিহ্যমণ্ডিত দুষ্প্রাপ্য সংগ্রহ রয়েছে। এই প্রতিষ্ঠানে স্থানমধ্যম ব্যক্তিগণের আগমন ঘটেছে। তাদের মধ্যে সাহিত্যিক, ভাস্কর ও চিত্রশিল্প, সঙ্গীতশিল্প, নৃত্যশিল্প, নাটক ও চলচ্চিত্র তারকা, পরিচালক, আবিষ্কারক, ক্রীড়াবিদ, শিক্ষাবিদ, সাংবাদিক প্রমুখ ব্যক্তিত্বরা। রাজ্যপাল থেকে আরম্ভ করে স্থানমধ্যম নারী দামী এবং সাধারণ মানুষের মতামত, উক্তি ও যুক্তি। অভিযাত্রিক ডায়েরিতে সংরক্ষিত আছে। সম্প্রতি ‘অভিযাত্রিক স্থান’ প্রদানের ব্যবস্থা করা হয়েছে। কোলকাতা, মেদিনীপুর, বঁকুড়া, বিষ্ণুপুর, ছান্দাড, বেতিরাতোড, হাটগ্রাম, নয়াতিহি, শুশুনিয়া, আনানগোল থেকেই অনেকেই সংরক্ষিত হয়েছেন।

প্রখ্যাত সাহিত্যিক সুনীল গঙ্গোপাধ্যায় বলেছিলেন— ‘এখানে এখন সুন্দর ধামকে দাঁড়িয়েছে। আক্ষরিক অর্থেই নীলগোহিতের এই বক্তব্য অনুভব করা যায় অভিযাত্রিতে পদাঙ্গণের মাধ্যমে। প্রবেশদ্বার বা তোরণের দুপাশে দুটি ঘোড়া আগম্বক অতিথিবৃন্দকে স্বাগত জানাচ্ছে। আর ‘বঁকুড়ার ঘোড়া’, নাম জনগোষ্ঠা, সেকথা নতুন করে বলার অপেক্ষা রাখে না। পাঁচমুড়া, সৈদ্যা থেকে আরম্ভ করে বেলেতোড়ের ধর্মরাজের ঘোড়া সহ আজ পর্যন্ত ১৮ ধরনের ডিজাইনের ঘোড়া স্বীকৃতিলাভ করেছে।^{১০} আনন্দের বিষয় হল এই ১৮ নম্বর ঐতিহ্যবাহী ঘোড়ার রূপকার উৎপল চক্রবর্তী। উৎপলবাবুর অধ্যয়নের ঘোড়া আজ দিগন্তে ছুটেছে।

প্রবেশ করলেই চোখে পড়বে একটি জলছবি। ছোট জলাশয়, সেখানে হাঁস, সাপ, নৌকা ইত্যাদি। সবই শিল্পীর তৈরি। বিষ্ণুপুরের ঐতিহ্যবাহী লঠন। শিল্পগুরু অবনীঠাকুরের কাঁচম কুঁচম অবলম্বনে কিছু শিল্পকর্ম। সোজা নাকের ভগায় গোলঘর বা প্রদর্শনী কথা এবং ঠাকুরঘর। পাশেই অক্রপনগর ও অন্যান্য ঘর। প্রাক্নজুড়ে ছড়িয়ে রয়েছে বেশ কিছু ভাস্কর্য, গোলঘরের সামনে উৎপলবাবুর মর্মমূর্তি ও ভিত্তিহীন।

এখানকার শিল্পীদের চিত্র, ভাস্কর্য, মুরাল ও বিভিন্ন শিল্পকর্মগুলি দর্শকদের দৃষ্টি আকর্ষণ করবে। শিল্পী শ্যামাপন পানের উৎপল চক্রবর্তীর আবক্ষমূর্তিটি জীবন্ত হয়ে উঠেছে। রূপসাগর ভবনের উত্তর দেওয়ালে শিল্পী মহাদেব মুখার্জীর মুরাল বা ফ্রেস্টোটি আসাধারণ। শিউলী তলায় অসিত দাসের ‘দুটি হাত’ (একহাতে তুলি, অপর হাতে প্যাগেট) ভাস্কর্যটি শিল্প চর্চাক্ষেত্রের ইঙ্গিতবাহী। খরগোশের ঘর (শশবাত্ত) এর কাছে রামমোহন শীটের ‘ঝাঙুদার’ পরিবেশ পরিকল্পনার বাতী ছড়াচ্ছে। অভিযাত্রিক উঠানের দীনমাপন ভাস্কর্যগুলি শিল্পী প্রদীপ তুং-এর হাতে গড়া।

প্রদর্শনী কথা অর্থাৎ গোলঘরের দেওয়াল চিত্র ও নক্সাগুলি গ্রামীণ লোকশিল্প ধারা তথা জীবনযাত্রার কথা স্মরণ করিয়ে দেয়। চিত্রাঙ্কন করেছেন প্রবীন শিল্পী সুধাংশু চন্দ, তাঁকে সহযোগিতা করেছেন লোক স্থপন কর্মকার। লোকের তৈরি একজোড়া কাগাজের বাঘ (মুখোশ শিল্প) উৎপলবাবু প্রদর্শনিকক্ষে সযত্নে রেখেছেন। আট গ্যালারিতে উৎপলবাবুর বেশ কয়েকটি ছবি ও ভাস্কর্য রয়েছে। সুধাংশু চন্দের তৈরি

বেলগানার দুর্গাপ্রতিমা, ছায়া খোমের ধানের কাজ, এছাড়া কাঁচম কুঁচম বঁশ, বাড, পাথর, শঙ্খশিল্প, টোকাটো প্রভৃতি শিল্পকর্ম রয়েছে। এককথায় শিল্প প্রতিভার বিস্তারণ ঘটেছে।

অফিসরুম, ডাইনিংহল, বাউজারীওয়াল সহ বিভিন্ন স্থানে সুস্থির বর্ধন, উত্তম পান, দীপক বাউরী ও শিল্পার্থীদের হাতের কাজগুলি দৃষ্টি নন্দন। আশা করি ভ্রমণ বিলাসী, নিম্নপ্রমী পর্যটক (Tourist) ‘অভিযাত্রিক’র এই সমস্ত Folk Art & Traditional Art গুলি কিছুটা হলেও মনের চাহিদা পূরণ করতে সক্ষম হবে।

মহাবতী দেবী তাই বলেছিলেন— ‘পশ্চিমবঙ্গ জুড়ে একলাখ অভিযাত্রিক হোক’। আর সমবেশ বনুর কথায় ‘অভিযাত্রিক যে মানুষটি যৌবনে ছোট-খাটো ছুরা ব্যাপিকে তোয়াস্বাই করতেন না, তিনি বর্ধকে দুরারোগ্য ক্যান্সারে মুহামান হয়ে পড়েন। বেসরকারী নার্সিং হোমে ভর্তি করা হলেও শেষরক্ষা হয়নি। ১৩ই জ্যেষ্ঠ ১৪২৪ বঙ্গাব্দের অভিশপ্ত দিনে মাত্র ৭৯ বৎসরে মৃত্যুর সঙ্গে পাঞ্জা লাড়ে পরান্ত হন। যেহে গেল বীরবোদ্ধার রথের ঢাকা। নেমে এলো গভীর শোকের ছায়া। প্রতিষ্ঠানের প্রাঙ্গণ জুড়ে যে দ্বীপাশিখা এতদিন প্রাজ্ঞালিত হয়ে আলোকের বর্ণধারায় ভরিয়ে দিত তা নিষ্পত্ত তমাস্বহন হয়ে পড়ল।

অভিযাত্রিতে উৎপলবাবুর নিধর দেহ শায়িত রাখা হয়। শোকার্ভ পরিবেশে অপ্রসিক্ত নয়নে আপামর জনতা তাঁকে অতিম শ্রদ্ধাঞ্জলি অর্পন করেন। পরে ছান্দার পরিক্রমা করে শবদেববাহী শকটটি (স্বর্গরথ) কোলকাতার উদ্দেশ্যে পাড়ি দেয়। ছোড়দের ইচ্ছানুসারে রতনবাবুর ঘাটেই তাঁর অস্ত্যষ্টিক্রিয়া সম্পন্ন করা হয়।

প্রাকৃতিক নিয়মে শিল্পার মৃত্যু ঘটে কিন্তু তাঁর সৃষ্টিগুলো চির অমর। তাই আমরা অভিযাত্রিক প্রাঙ্গণ জুড়ে এখনো তাঁর অদৃশ্য উপস্থিতি অনুভব করি। মনে হয় যেন শিল্পীরসিক্ত তৃণপরে লেগে রয়েছে তাঁর পদরেণু। ব্যবস্তু প্রতিটি আপবাব পরে মমতামাখা স্নেহের পরশ। সৃষ্টি আলো যেন হাতছানি দিয়ে ডাকেছে। উচ্ছ্বাসিত আলোকমঞ্জরী পঙ্কবিত পুষ্প সৌরতে মুখরিত সিদ্ধ সমীরণ... সততাই যেমন উৎপলময়।

দুরদর্শী মানুষটি জীবদশায় অনুভব করেন তাঁর অবতরমানে প্রতিষ্ঠানটি দৃষ্টিভরা জ্বর দখল করতে পারে। তাই তিনি সিজান্ত গ্রহণ করেন তাঁর সাজানো বাগানটি উপযুক্ত কোন প্রতিষ্ঠানের হাতে তুলে দেনেন। যাঁরা এর মর্ম বোধন, যস নিয়ে নতুন করে ফুল ফোটাবেন। যেমন ভাবনা, তেমনিই কাজ। তিনি বঁকুড়া বিশ্ববিদ্যালয়ের উপাচার্য মাননীয় দেবনারায়ণ বন্দ্যোপাধ্যায়ের সঙ্গে যোগাযোগ করেন। প্রতিষ্ঠানের কর্ণধারস্বয়ের আলোচনায় তিনি খুশি। তাই নিয়ম ও আইন মেনে দানপত্রের দলিল এবং অভিযাত্রিক দায়িত্বভার ছী চক্রবর্তী ছী বন্দ্যোপাধ্যায়ের হাতে তুলে দেন। আইস-চ্যাংকলার উৎপলবাবুর এই মহতি দানকে যথাযোগ্য মর্যাদার সঙ্গে গ্রহণ করে এবং দায়িত্ব পালনের প্রতিশ্রুতি দেন। এরপর অভিযাত্রিক বঁকুড়া

বিধবিদ্যালয়ের অন্তর্ভুক্ত হয়।^{১৪}

২০১৪ সালে বিশ্ববিদ্যালয় স্থাপিত হয় এবং ২০১৭ সালে অভিযুক্তি গ্রহণ করে শুরু হয় অভিযুক্তির দ্বিতীয় অধ্যায় বিশ্ববিদ্যালয় পর্ব। উৎপলবাবুর দীর্ঘদিনের ইচ্ছে ছিল এখানে একটি আর্ট কলেজ গড়ার। তাঁর সেই স্বপ্নকে বাস্তবায়িত করার লক্ষ্যে উপাচার্য ব্রতী হন। বীকুজা বিশ্ববিদ্যালয়ের ৪র্থ ক্যাম্পাস হিসাবে এখানে প্রতিষ্ঠিত হন—‘যামিনী রায় ইনস্টিটিউট অফ আর্ট এন্ড কালচার’। ২০১৮ সালের ১০ই মার্চ প্রতিষ্ঠা দিবস ‘অভিযুক্তি’ এবং ‘বিশ্ববিদ্যালয়ের’ যৌথ উদ্যোগে পালিত হয়।^{১৫}

উৎপল চক্রবর্তীর প্রয়াণের পর বিশ্ববিদ্যালয় কর্তৃপক্ষ একতৃষ্ণ পরিচালনা নিয়ে চেলে সাজান। তাই কৃষ্ণেন্দু শেঠ নামে একজন যোগ্য ব্যক্তিকে তিনি ইনচার্জ হিসাবে নিয়োগ করেন। কৃষ্ণেন্দুবাবু অভিযুক্তির প্রাক্তন থেকে নবীনদের সঙ্গে যোগাযোগ করে সমস্ত বিষয় ঞ্চনেন, বুঝনেন ও জাননেন। তারপর স্টাডি করে পুরানো ঐতিহ্যের অস্তিত্ব অপরিবর্তনশীল রেখে নিজের মতো করে ভাস্পা গড়ার খেলার সোতে উঠলেন। বর্তমানে অভিযুক্তি নবরূপে, নবরাজে সুসজ্জিত। যা চকচকে প্রতিষ্ঠান উপহার দেবার জন্য—দেবনারায়ণ বাবু এবং নিম্বার শেঠকে অভিনন্দন, ধন্যবাদ জানাতেই হয় সেই সঙ্গে প্রত্যক্ষ ও পরোক্ষভাবে যুক্ত সকলকে স্যালুট।

নব কলেজের প্রতিষ্ঠানটি ৯টি বিখ্যের পাঠক্রম চালু করে চলেছে। যেকোন বয়সের উচ্চ মাধ্যমিক উত্তীর্ণরা ১ বছরের সার্টিফিকেট কোর্স করার সুযোগ পানেন। বর্তমান শিক্ষাবর্ষে Art এবং Santali Folk ক্লাস শুরু হয়েছে।

সম্প্রতি একাধিক শিক্ষাবিদ মূদুর অস্ট্রেলিয়া থেকে উড়ে আসেন বীকুজা বিশ্ববিদ্যালয়ের এই প্রতিষ্ঠানে। তারা হলেন—

Prof. Jonathan Sweet (University of Deakin)

Prof. Bill Ashcroft (University of New South Wales)

Prof. Helen Springle (University of New South Wales)

Prof. Paul Sharrad (University of Wollongong)

Prof. Eileen Chanin (Australian National University)

প্রতিষ্ঠানের শিক্ষীদের হস্তশিল্প প্রদর্শনে মুগ্ধ, লোকসঙ্গীতের সুরের মুহূর্তনায় আশ্বত, Folk Dance দর্শনে অজিত এবং Instrument স্পর্শ করে বাকরুদ্ধ হয়ে পড়েন। আরেগা ঘন চিত্রে অস্ট্রেলিয়া সফরের আমন্ত্রণ জানান। এতে দুই দেশের মধ্যে শিক্ষা ও সংস্কৃতির আদান প্রদান সম্পৃক্ত হবে শিক্ষাজগৎ। এ যেন প্রথম চলেই কিংজাত। অথবা অভিযুক্তির মুকুট নতুন পালক যুক্ত হন।

পরিশেষে তাই বলতেই হয় যতদিন ‘অভিযুক্তি’ থাকবে ততদিন উৎপল চক্রবর্তীর নাম স্মরণের লেখা থাকবে।

তথ্যসূত্র :

1. APJ Abdul Kalam, SPIRIT OF INDIA, RAJPAL : Delhi, 5th Edition-2014, P. 96.
2. কৃষ্ণেন্দু শেঠ, অভিযুক্তি সংবাদ, বীকুজা বিশ্ববিদ্যালয়, ২০১৯, পৃ. ২৫।
3. তদেব, ২০১৯, পৃ. ০৪।
4. কৃষ্ণেন্দু শেঠ, ২০২০, পৃ. ০৫।
5. ড. শ্যামলী দাস, বীকুজার জনশিল্পধারা ও শিল্পী সমাজ, প্রান্তর, ২০১৫, পৃ. ১৬২।
6. কৃষ্ণেন্দু শেঠ, অভিযুক্তি সংবাদ, বীকুজা বিশ্ববিদ্যালয়, ২০১৯, পৃ. ২৩।
7. কৃষ্ণেন্দু শেঠ, অভিযুক্তি সংবাদ, বীকুজা বিশ্ববিদ্যালয়, ২০২০, পৃ. ৪১।
8. কৃষ্ণেন্দু শেঠ, অভিযুক্তি সংবাদ, বীকুজা বিশ্ববিদ্যালয়, ২০১৯, পৃ. ৭৫।
9. কৃষ্ণেন্দু শেঠ, অভিযুক্তি সংবাদ, বীকুজা বিশ্ববিদ্যালয়, ২০২০, পৃ. ১৮।
10. কৃষ্ণেন্দু শেঠ, অভিযুক্তি সংবাদ, বীকুজা বিশ্ববিদ্যালয়, ২০২০, পৃ. ১৮।
11. কৃষ্ণেন্দু শেঠ, অভিযুক্তি সংবাদ, বীকুজা বিশ্ববিদ্যালয়, ২০২০, পৃ. ৮৫।
12. নির্বাণ আশ, চিত্র প্রকাশ, রক্তকরবী, ২০০৬, পৃ. ৬১।
13. কৃষ্ণেন্দু শেঠ, অভিযুক্তি সংবাদ, বীকুজা বিশ্ববিদ্যালয়, ২০১৯, পৃ. ২৬।
14. কৃষ্ণেন্দু শেঠ, অভিযুক্তি সংবাদ, বীকুজা বিশ্ববিদ্যালয়, ২০২০, পৃ. ২৭।
15. কৃষ্ণেন্দু শেঠ, অভিযুক্তি সংবাদ, বীকুজা বিশ্ববিদ্যালয়, ২০২০, পৃ. ২০।

পত্রপত্রিকা :

1. পশ্চিমবঙ্গ (বীকুজা জেলা সংখ্যা), তথ্য ও সংস্কৃতি দপ্তর, পশ্চিমবঙ্গ সরকার।
2. যুগান্তর- ২৯.০৮.১৯৮২- তথ্যকেন্দ্র, অভিযুক্তি।
3. কোম্পানি টাইমস- ০৬.০২.১৯৮৯, রাজিৎ বন্দ্যোপাধ্যায়, শিল্পীর গণকীর্ণ নয় শিল্পকলার পূর্ণাঙ্গ পরিচিতি জরুরি।
4. আনন্দবাজার পত্রিকা- ২৮.১১.১৯৮৮, শিল্পরসিক।
5. গণশক্তি- ১৩.০৮.১৯৯৬, তথ্যকেন্দ্র প্রদর্শনী, একইবৃত্তে গ্রাম ও শহর।

কৃতজ্ঞতা স্বীকার :

1. কৃষ্ণেন্দু শেঠ, অভিযুক্তির অফিসার-ইন-চার্জ (বীকুজা বিশ্ববিদ্যালয়)।
2. শুধুগুণ চন্দ, অভিযুক্তির প্রাক্তনী, কারু, বেলামজা ও বাঁশ শিল্পী।
3. সুধীর বর্দন, অভিযুক্তির কর্মী।

Spectroscopic investigation of complex nuclear excitations in ^{66}Ga

U. S. Ghosh,¹ S. Rai,^{1,*} B. Mukherjee^{1,†} A. Biswas,¹ A. K. Mondal,¹ K. Mandal,¹ A. Chakraborty,¹ S. Chakraborty^{1,2,‡}
 G. Mukherjee³, A. Sharma⁴, I. Bala,⁵ S. Muralithar⁵, and R. P. Singh⁵

¹Department of Physics, Siksha-Bhavana, Visva-Bharati, Santiniketan, West Bengal 731235, India

²Department of Physics, Institute of Science, Banaras Hindu University, Varanasi 221005, India

³Variable Energy Cyclotron Centre, 1/AF Bidhannagar, Kolkata 700064, India

⁴Department of Physics, Himachal Pradesh University, Shimla 171005, India

⁵Inter University Accelerator Centre (IUAC), Aruna Asaf Ali Marg, New Delhi 110067, India



(Received 23 November 2019; revised 5 July 2020; accepted 29 July 2020; published 24 August 2020)

In-beam spectroscopic technique using the fusion evaporation reaction $^{52}\text{Cr}(^{18}\text{O}, 1p3n)$, at a beam energy of 72.5 MeV, was employed to explore the structural phenomena in ^{66}Ga , mainly at intermediate and high spins. The experimental setup involved an array of 14 Compton suppressed Ge clover detectors, placed around the target position to detect emitted γ rays from excited states. A new level scheme has been proposed, which is enriched with more than 20 new transitions and is extended up to an excitation energy ≈ 12 MeV. A few observed intermediate spin states of ^{66}Ga are discussed in the framework of coupling of single-particle configurations with the vibrational core of ^{64}Zn . Shell model calculations have also been performed with two different interactions, viz., jj44bpn and jun45pn , for the interpretation of the observed level structure in ^{66}Ga .

DOI: [10.1103/PhysRevC.102.024328](https://doi.org/10.1103/PhysRevC.102.024328)

I. INTRODUCTION

Complex excitations, including single-particle and collective ones, have been observed in Zn [1–8], Ga [9–12], and Ge [13,14] isotopes, manifesting various shapes, which are explained by simple theoretical models like the shell model, the interacting Boson model, and cranked Nilsson Strutinsky calculations. Nuclear level structures in $^{65,67}\text{Ga}$ are explained in the framework of the interacting boson-fermion plus broken pair model (IBFBPM), where low and medium spin negative parity yrast states are explained as originating from the coupling of one quasiproton of the negative parity $1f$ or $2p$ orbital with the multiphonon vibrational states of ^{64}Zn and ^{66}Zn , respectively. High spin states in the former two nuclei are mainly of three-quasiparticle nature, originating from coupling of one proton with a broken neutron pair excitations. A similar study on ^{63}Ga and ^{65}Ga by Weiszflog *et al.* [9] revealed rotational-like structures built on $9/2^+$ and $19/2^{(-)}$ states in both nuclei. Angular momenta of the rotational states, built on the $9/2^+$ states, were reported to be generated from the alignment of a neutron pair in the $g_{9/2}$ orbital. As the $g_{9/2}$ orbital is occupied by a single proton, proton crossing is blocked by the Pauli exclusion principle. All the observations in $^{63,65,67}\text{Ga}$ suggest that a large variety of phenomena emerge out of the competition between single-particle and collective excitations, consisting of both

vibrational and rotational degrees of freedom. Interestingly, in ^{68}Ga , high spin states, viz., 9^+ , 11^+ , 13^+ , were compared respectively with $9/2^+$, $13/2^+$, $17/2^+$ energy states of ^{67}Ga by Singh *et al.* [12]. Configurations of these states in ^{67}Ga were stated to be built predominantly from one $\pi g_{9/2}$ quasiproton plus phonon configuration coming from the vibrational core of ^{66}Zn . Alternatively, it can be understood that 11^+ and 13^+ states of ^{68}Ga originate from the couplings of 9^+ ($\pi g_{9/2} \otimes \nu g_{9/2}$) state of ^{68}Ga with multiphonon vibrational states of ^{66}Zn .

In order to understand how this coupling of phonons with single particles qualifies to yield the measured energy values, we have compared some already existing data with the coupling configurations. Intermediate spin states of $^{63,65,67}\text{Ga}$, viz., $13/2^+$, $17/2^+$ and $21/2^+$ [9,11], are compared with $2_1^+ \otimes 9/2^+$, $4_1^+ \otimes 9/2^+$ and $6_1^+ \otimes 9/2^+$ coupled states, respectively, in Fig. 1. As is evident from the figure, observed states $13/2^+$, $17/2^+$, and $21/2^+$ of ^{63}Ga are very close in energy respectively to those states originating from couplings of 2_1^+ , 4_1^+ , and 6_1^+ core states of ^{62}Zn [4] with the $9/2^+$ state of ^{63}Ga . Similarly, in the case of ^{65}Ga and ^{67}Ga , core states are the multiphonon vibrational states of ^{64}Zn [7] and ^{66}Zn [15], respectively. In the case of ^{65}Ga , good agreement is observed for $13/2^+$ and $17/2^+$ states but some discrepancy appears at $21/2^+$, whereas in ^{67}Ga only the $13/2^+$ state is in close proximity to the core-coupled state. This could be due to the significant contribution arising from residual interaction between the core and the particle with increasing spin and mass number.

So, situated in between ^{65}Ga and ^{67}Ga , ^{66}Ga is expected to have a similar kind of systematics and intermediate spin states will have complex structures, with contributions from

*Presently at Department of Physics, Salesian College, Siliguri Campus, Siliguri 734001, India.

[†]buddhadev.mukherjee@visva-bharati.ac.in

[‡]Presently at IUAC, New Delhi, India.

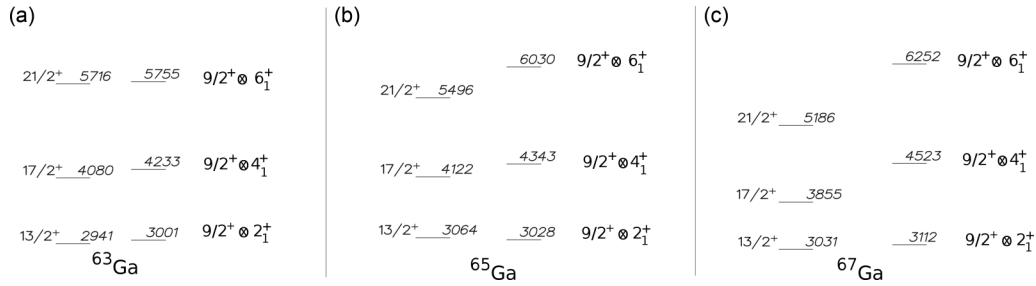


FIG. 1. (a) Energy values of the observed $13/2^+$, $17/2^+$ and $21/2^+$ states in ^{63}Ga (data taken from Ref. [9]) are compared with the sum energy values of $9/2^+$ state (of ^{63}Ga) coupled to, respectively, 2_1^+ , 4_1^+ , and 6_1^+ vibrational states of ^{62}Zn [4] forming, respectively, coupled states $13/2^+$, $17/2^+$, and $21/2^+$ in ^{63}Ga . Here, energy values are quoted in keV. (b) Same as panel (a) but for ^{65}Ga , which has core states originating from ^{64}Zn [7] and $9/2^+$, $13/2^+$, $17/2^+$ and $21/2^+$ states from ^{65}Ga [9,11]. (c) Same as panel (a) but for ^{67}Ga , which has core states originating from ^{66}Zn [15] and $9/2^+$, $13/2^+$, $17/2^+$ and $21/2^+$ states of ^{67}Ga [11]. Please see text for details.

both single-particle and collective excitations. This kind of investigation on observed levels in $^{66,68}\text{Ga}$ has been performed and is described later in detail in the discussion section.

Earlier studies on ^{66}Ga were done with modest detector setups using electron-capture decay and reactions like $^{64}\text{Zn}(\alpha, p n \gamma)$, $^{63}\text{Cu}(\alpha, n \gamma)$, $^{64}\text{Zn}(\alpha, d)$, $^{66}\text{Zn}(p, n \gamma)$, $^{66}\text{Zn}(^3\text{He}, t)$, and $^{56}\text{Fe}(^{13}\text{C}, p 2 n \gamma)$, which were used to explore only low and medium spin states [16–23]. The most recent study by Bhattacharjee *et al.*, [10] was performed using 15 Compton suppressed Ge clover detectors; the level scheme was extended up to $21^{(+)}$. Two bandlike structures were observed, with the positive and negative parity bands being described to have originated from $\nu(g_{9/2})^3(f_{5/2})^2 \otimes \pi(g_{9/2})^1(f_{5/2})^2$ and $\nu(g_{9/2})^2(f_{5/2})^1 \otimes \pi(g_{9/2})^1(f_{5/2})^2$ configurations, respectively. As in $^{63,65}\text{Ga}$ and ^{65}Zn , the role of the $g_{9/2}$ neutron pair appears to be very significant in ^{66}Ga , as its alignment along the rotational axis generates the angular momenta of the high spin states in the bands. Here, we report on an experimental investigation on medium and high spin excitations of ^{66}Ga as well as its shell model description mainly at low and intermediate spin values.

II. EXPERIMENTAL DETAILS AND DATA ANALYSIS

In the fusion-evaporation reaction, an ^{18}O beam at 72.5 MeV was obtained from the 15-UD pelletron accelerator [24] at the Inter University Accelerator Centre (IUAC), New Delhi. An isotope of ^{52}Cr of thickness 1 mg/cm² (isotopic abundance $\approx 99\%$), backed by 7 mg/cm² gold, was used as target. The emitted γ rays were detected in coincidence with 14 Compton suppressed high-purity germanium (HPGe) clover detectors of the Indian National Gamma Array (INGA) [25]. Detectors were placed at three different angles, viz., 123° , 148° , and 90° with respect to the beam direction. Time-stamped data were collected in list mode with the help of the computer-aided measurement and control (CAMAC) based data acquisition software CANDLE [26]. Different symmetric and angle dependent E_γ - E_γ matrices from coincidence data were constructed using analysis packages, viz., RADWARE [27] and INGASORT [28]. More details about the target, experimental setup, and data analysis procedure can be found in Refs. [5,29]. Multipolarity of a transition was determined from the DCO ratio (R_{DCO}) [30], which in the present INGA

geometry is defined as

$$R_{DCO} = \frac{I_{\gamma_1} \text{ at } 148^\circ \text{ gated by } \gamma_2 \text{ at } 90^\circ}{I_{\gamma_1} \text{ at } 90^\circ \text{ gated by } \gamma_2 \text{ at } 148^\circ},$$

where I_{γ_1} is the measured intensity of γ_1 when the gating transition is γ_2 . The expected R_{DCO} values for the stretched quadrupole and the dipole transitions are ≈ 1.0 (2.0) and ≈ 0.5 (1.0), for pure quadrupole (dipole) gates respectively. In this work, R_{DCO} values are measured by using stretched $E2$ gates of 1189 ($9_1^+ \rightarrow 7_1^+$), 1268 ($9_2^+ \rightarrow 7_2^+$), 947 ($13_1^+ \rightarrow 11_1^+$), 1058 ($15^+ \rightarrow 13_2^+$), and 1002 keV ($14_1^- \rightarrow 12_3^-$) of ^{66}Ga . Electric or magnetic nature of γ -ray transitions was determined from the polarization measurement [31,32], which was analyzed by constructing two asymmetric matrices, one with perpendicular and the other with parallel scattered events (i.e., the events with γ rays scattered perpendicular or parallel to the emission plane) of 90° detectors in one axis and corresponding γ rays detected at all angles on another axis. The asymmetry parameter was calculated as

$$\Delta_{\text{asym}} = \frac{a(E_\gamma)N_\perp - N_\parallel}{a(E_\gamma)N_\perp + N_\parallel},$$

where $a(E_\gamma)$ represents the experimental asymmetry correction factor for clover detectors at 90° of the present INGA setup and was determined from the ratio of the parallel (N_\parallel) and the perpendicular (N_\perp) scattered events obtained from an unpolarized source. It is defined as

$$a(E_\gamma) = \frac{N_\parallel(\text{unpolarized})}{N_\perp(\text{unpolarized})}.$$

The value of the asymmetry correction factor for the present detector setup is found to be $\approx 1.03(2)$ in the energy range ≈ 0.1 – 1.5 MeV using the standard ^{152}Eu radioactive source. Electric (magnetic) type transitions will have positive (negative) polarization asymmetry (Δ_{asym}) value, while a near zero value of Δ_{asym} indicates that there is a strong admixture. Figures 2 and 3 represent, respectively, the plots of R_{DCO} and polarization asymmetry values for different transitions belonging to ^{66}Ga , which were observed in the measurements.

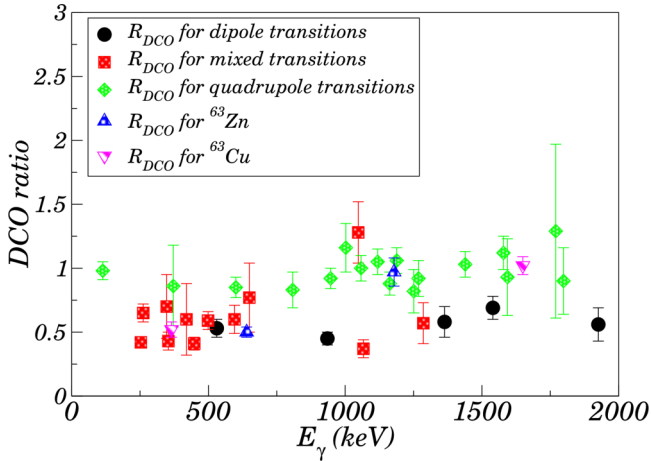


FIG. 2. R_{DCO} values for different transitions of ^{66}Ga (gated by different $E2$ transitions as mentioned in the text and in Table I) along with those of selected transitions having definite multiplicities, viz., of ^{63}Cu ($E_\gamma = 365$ and 1650 keV respectively, for $7/2^- \rightarrow 5/2^-$ and $13/2^+ \rightarrow 9/2^+$ transitions) and ^{63}Zn ($E_\gamma = 640$ and 1179 keV respectively, for $9/2^+ \rightarrow 7/2^-$ and $17/2^+ \rightarrow 13/2^+$ transitions), populated in the fusion evaporation reaction. The latter four transitions are used to fix the reference values in the current analysis and to validate the same. For ^{63}Cu and ^{63}Zn the gating transitions are 342 ($17/2^+ \rightarrow 13/2^+$) and 882 keV ($13/2^+ \rightarrow 9/2^+$) stretched $E2$ type, respectively.

III. RESULTS AND DISCUSSION

A new level scheme of ^{66}Ga (Fig. 4) has been proposed in the present work, which is based on the coincidence relationship, relative intensity balance, angular correlation, and polarization measurements of the emitted γ rays. Almost all the transitions reported previously are observed in this measurement. New transitions are marked with asterisks in the level scheme. A total of 21 new transitions and 20 new

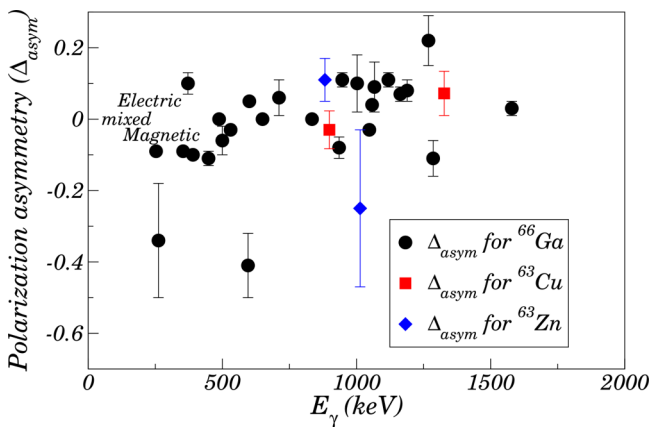


FIG. 3. Polarization asymmetry values (Δ_{asym}) for different transitions in ^{66}Ga , measured in the present experiment. Here, the asymmetry values of 1013 keV ($7/2^- \rightarrow 5/2^-$) and 882 keV ($13/2^+ \rightarrow 9/2^+$) transitions of ^{63}Zn and 899 ($7/2^- \rightarrow 5/2^-$) and 1327 keV ($7/2^- \rightarrow 3/2^-$) transitions of ^{63}Cu are also plotted for the same purpose as in the DCO plot (Fig. 2).

levels have been placed in the level scheme. Transitions which are in coincidence are shown in the typical gated spectra (Fig. 5). Here, the gated spectra are generated through a “logical AND” of the two single gates, which is a feature available in RADWARE.

The 44 ($1^+ \rightarrow 0^+$) and 22 keV ($2^+ \rightarrow 1^+$) γ -ray transitions, which decay respectively from the 44 ($I^\pi = 1^+$) and 66 keV ($I^\pi = 2^+$) states, as were reported previously [16,17], are not observed in the present work as the energies are below the measured energy threshold of the γ -ray spectrometer, we used. So, the ground 0^+ state is not shown in the new level scheme. Najam *et al.* [20] argue, in part, for a spin of 2 for the state at 66 keV based on the absence of feeding from a 0^+ parent in electron-capture decay, as noted by de Boer *et al.* [33]. Morand *et al.* [17] subsequently considered the argument strengthened somewhat based on lifetime measurements made in other works that suggested that the 22 and 44 keV γ rays are $M1$ in nature, and thus that the 2^+ assignment is firm. There is a conflict between those authors and Evaluated Nuclear Structure Data File (ENSDF) evaluators regarding this firm 2^+ spin-parity assignment. However, lifetimes likely do not adequately distinguish between $1^+ \rightarrow 1^+$ and $2^+ \rightarrow 1^+$ $M1$ transitions. So, these are probably considered to be weak arguments by ENSDF evaluators and they also continue to show the state at 66 keV as $(2)^+$. To keep things simple in this work, we have followed the assignment of Refs. [20] and [17], and multiplicities of the higher spin states are determined based on this assignment.

In this work the DCO ratios of many transitions are determined using 1189 keV ($9^+ \rightarrow 7^+$) $E2$ gate. Multipolarity of the 1189 keV γ ray is adopted from the literature [10]. Determination of multipolarity of all the transitions (as given in Table I) was not possible using a single gate, so other transitions, which are stretched quadrupole in the 1189 keV $E2$ gate, are used for this purpose.

Here, the states with energies 863 , 414 , and 162 keV decay in cascade respectively by strong 448 , 253 , and 96 keV γ rays to the 2^+ state at 66 keV. The measured value of the DCO ratio (R_{DCO}) of 96 keV, and also the measured R_{DCO} and polarization asymmetry (Δ_{asym}) of 253 and 448 keV γ rays suggest 3^+ , 4^+ , and 5^+ spin-parity assignments for 162 , 414 , and 863 keV states respectively. Measured R_{DCO} and Δ_{asym} of 834 and 935 keV transitions suggest a 5^+ spin-parity assignment for the 1350 keV state.

Figure 5(a) indicates that the height of the 834 keV peak is about one third of that of 935 keV peak. These transitions decay from the 1350 keV level and have been found to be present in the spectrum gated on 1189 and 1540 keV transitions that feed the 1350 keV level. However, the measured intensity of the 935 keV transition indicates that the size of this transition is significantly larger in the table than is seen in the figure. This anomaly in branching is suggestive of the possible presence of a weak doublet 834 keV transition which could neither be properly identified nor be placed in the level scheme due to the lack of sufficient statistics.

The state at 516 keV is assigned with a spin-parity 4^+ , depending upon the measured R_{DCO} and Δ_{asym} of the depopulating 354 keV γ ray. The state at 1463 keV decays to that at 863 keV (5^+) by a strong 601 keV γ -ray transition. Measured

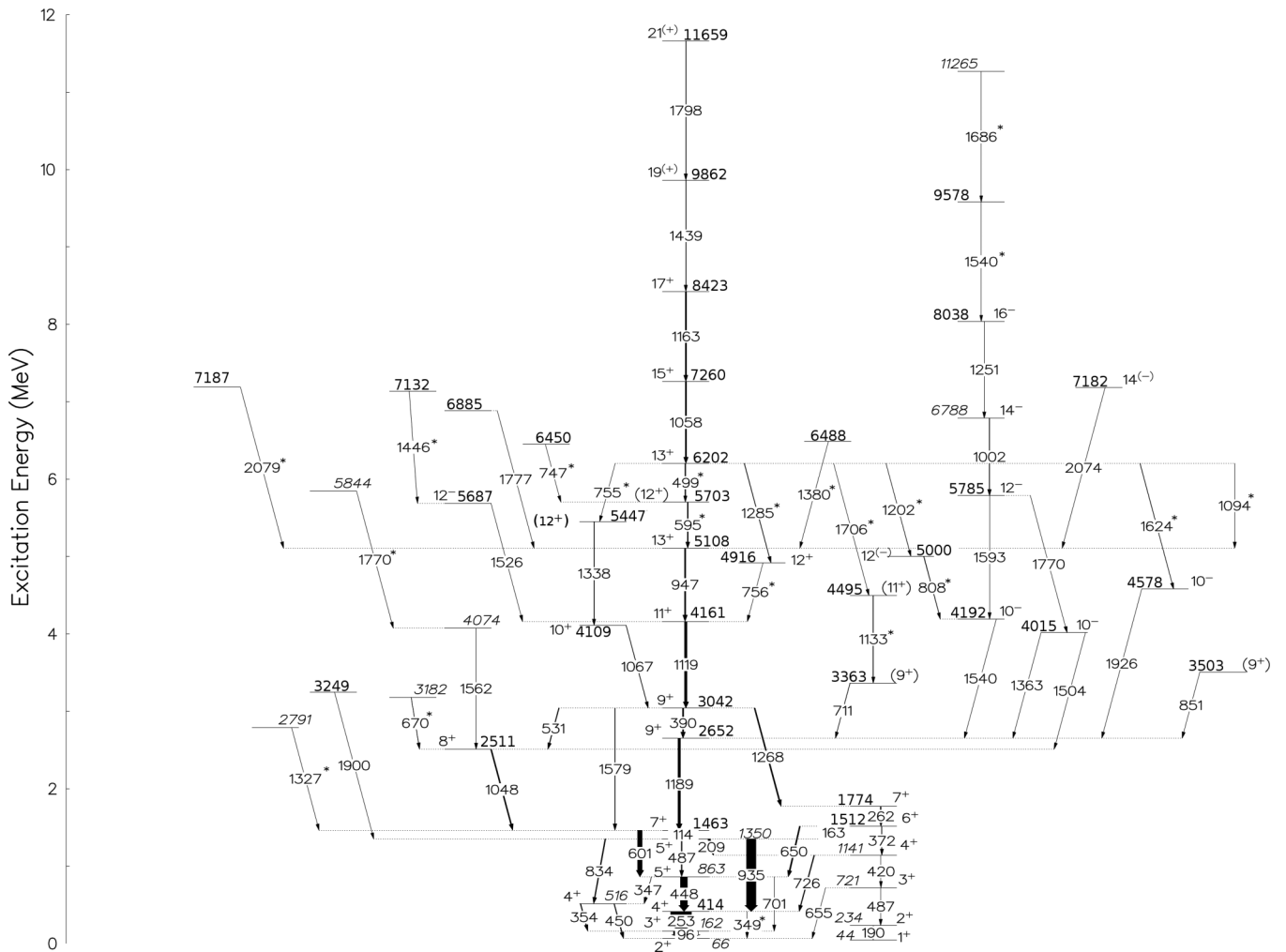


FIG. 4. Proposed level scheme of ^{66}Ga . Widths of the arrows are proportional to the relative intensity of the respective transition observed in the present experiment. New transitions are marked with asterisks. The energies in the figure are in keV.

R_{DCO} and Δ_{asym} of the 601 keV transition suggest quadrupole nature of this γ ray, so a spin-parity 7^+ is assigned to the 1463 keV state. This state at 1463 keV is fed by a strong 1189 keV γ -ray transition depopulating the state at 2652 keV. Previous observations predicted $E2$ nature for the 1189 keV transition, so the state at 2652 keV is assigned with a 9^+ spin-parity value. The state at 3042 keV is depopulated by 390, 531, 1268, and 1579 keV γ rays to states at 2652 (9^+), 2511, 1774, and 1463 keV (7^+), respectively. Measured R_{DCO} and Δ_{asym} of the 1048 keV γ ray suggest 8^+ spin-parity for the state at 2511 keV, so measured values of those for 531 and 1579 keV transitions suggest a spin-parity value of 9^+ for the state at 3042 keV. As a result, the 390 keV ($9^+ \rightarrow 9^+$) transition could be assumed to be dipole in nature, though it has $R_{DCO} \approx 1.0$. This is possible, as the $\Delta I = 0$ transition will have the same angular correlation as that of a quadrupole one.

A negative polarization asymmetry value has been obtained for the 390 keV γ ray that decays from the 3042 keV level. Combining the measured values of polarization asymmetry and the corresponding DCO ratio, the $\Delta I = 0$, 390 keV transition can be characterized as a magnetic dipole type with the probable presence of a very small admixture of $E2$

component. Hence, the assignment of $M1(+E2)$ multipolarity has been made for the 390 keV transition. The measured R_{DCO} and Δ_{asym} values of 1268 and 262 keV γ rays suggest 7^+ and 6^+ spin-parities for 1774 and 1512 keV states, respectively.

We would also like to mention here that the peak height of 1268 keV transition as can be seen from Figs. 5(c)–5(e) is not in accordance with that of the 1579 keV γ ray as far as the measured intensities of the two transitions are concerned (see Table I). Both the transitions decay from 3042 keV level and the measured intensities suggest that the height of the 1268 keV peak should be more than that of the 1579 keV peak in the gated spectra of Figs. 5(c)–5(e) obtained with the gating transitions that feed the 3042 keV level. It is worthwhile mentioning that the quoted intensities of Table I for the 1268 and 1579 keV branches have been obtained from the gated spectrum of the 253 keV γ -ray lying below the 3042 keV level. The analysis of the gated spectrum provides clear indication of a larger peak area of the 1268 keV transition in comparison to that of the 1579 keV transition. The anomalies in the peak count for 1268 and 1579 keV transitions between the top gated and bottom gated coincidence spectra may possibly reflect a missing

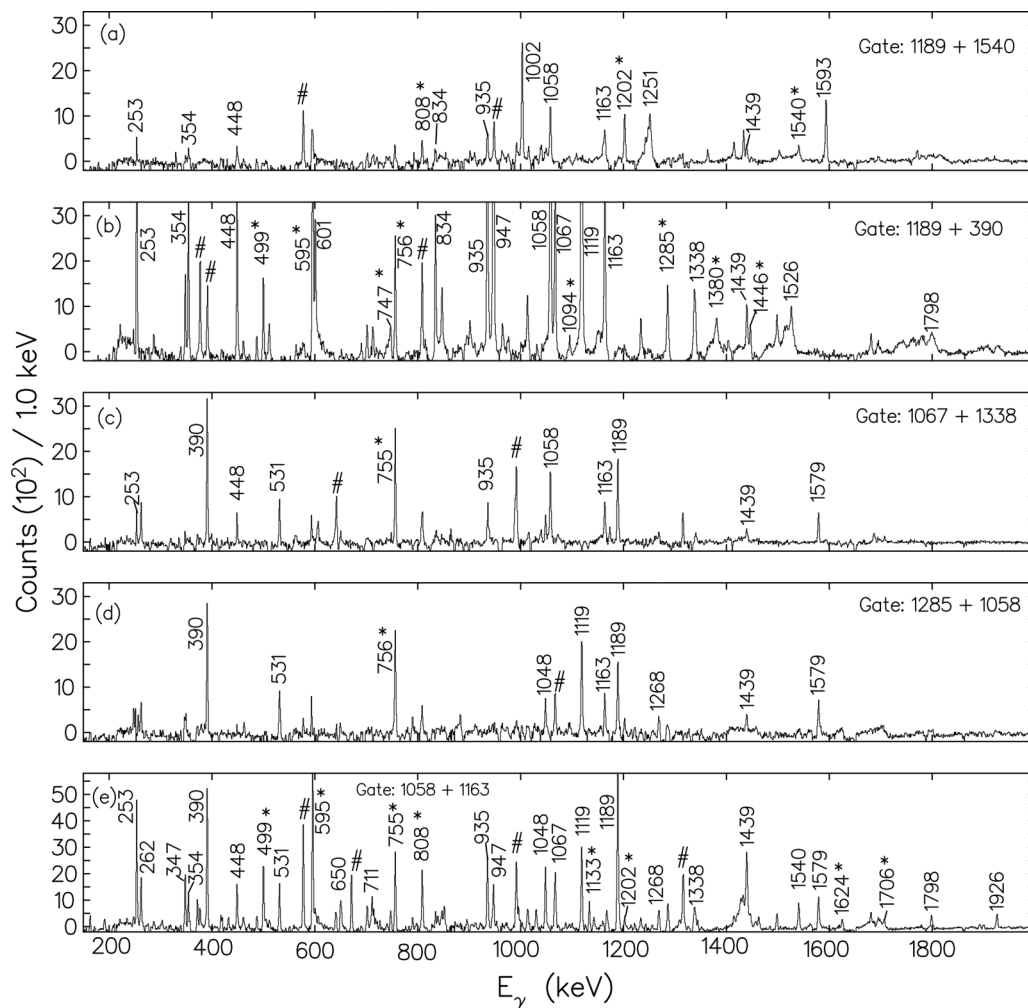


FIG. 5. Background subtracted γ - γ coincidence spectra for ^{66}Ga in the sum gates of (a) 1189 ($9^+ \rightarrow 7^+$) and 1540 keV ($10^- \rightarrow 9^+$), (b) 1189 ($9^+ \rightarrow 7^+$) and 390 keV ($9^+ \rightarrow 9^+$), (c) 1067 ($10^+ \rightarrow 9^+$) and 1338 keV ($12^{(+)} \rightarrow 10^+$), (d) 1285 ($13^+ \rightarrow 12^+$) and 1058 keV ($15^+ \rightarrow 13^+$), and (e) 1058 ($15^+ \rightarrow 13^+$) and 1163 keV ($17^+ \rightarrow 15^+$) γ rays. New transitions are marked by asterisks (*). The inset of (e) contains the portion of 1058 + 1163 keV gated spectrum (from 1600 to 1800 keV in energy in the x axis, and 0 to 800 in counts in the y axis), which is expanded to show the presence of newly observed (weak) 1624 and 1706 keV γ rays. A few strong peaks are marked with “#” symbols indicating contaminant γ rays or ones which could not be placed in the level scheme.

1268 keV doublet transition. This missing weak doublet transition is probably in coincidence with the 253 keV γ ray and not in coincidence with either the cascade transitions of 1285, 1058, and 1163 keV or the cascade transitions of 1067 and 1338 keV. However, the doublet nature of the 1268 keV transition could not be confirmed from the present analysis.

Spin-parities of both 1141 and 721 keV states are assigned to be 4^+ and 3^+ , depending upon the measured R_{DCO} of 372 and 420 keV γ rays. Here, the measured R_{DCO} and Δ_{asym} of 372 keV suggest $E2$ nature for this transition. No information regarding the spin-parity of the 1141 keV state was given by previous work. Also, the state at 721 keV was assigned with a tentative spin 3 but definite positive parity [i.e., $(3)^+$] in Ref. [10], but, as mentioned, we assign definite spin-parity to this state, from the derived multipolarity nature of 372 ($E2$) and 420 keV ($M1/E2$) transitions. The 44 and 234 keV states are reported to be 1^+ and 2^+ by previous observations [10,16,17,20,23]. Due to weak intensities of 190

and 487 keV γ rays, measurement of R_{DCO} and Δ_{asym} of these two transitions, depopulating the 234 and 721 keV states respectively, was not possible.

Measured R_{DCO} and Δ_{asym} of 1363 keV transition predicts its dipole nature to be of electric type, therefore a 10^- spin-parity is assigned to the state at 4015 keV. Following the measured R_{DCO} and Δ_{asym} of the 1540 keV γ ray and a previous assignment [10], a 10^- spin-parity value is confirmed for the state at 4192 keV.

Here, a notable fact is that the 935 keV γ -ray transition depopulating the 1350 keV (5^+) state is visible in the spectrum gated by 1189 and 1540 keV γ rays [panel (a), Fig. 5], while 601 keV γ -ray depopulating the 1463 keV (7^+) state is not. However, this 601 keV transition is also in coincidence with the 1189 and 1540 keV γ rays and has a strong peak area with sufficient statistics. This 7^+ state is an isomeric state with a half-life of 57 ns. If the coincidence time window used during the experiment was small compared to the 57 ns half-life then

TABLE I. Values of the level energy (E_i) in keV, γ -ray energy (E_γ) in keV, initial spin-parity (I_i^π) \rightarrow final (I_f^π), intensity (I_γ), DCO ratio (R_{DCO}), polarization asymmetry (Δ_{asym}) and multipolarity assignment of the γ -ray transitions, as obtained in ^{66}Ga .

| Level energy ^a E_i (keV) | Gamma-ray energy E_γ (keV) | Initial \rightarrow final spin-parity $I_i^\pi \rightarrow I_f^\pi$ | Relative intensity I_γ | DCO ratio R_{DCO} | Polarization asymmetry Δ_{asym} | Assignment |
|--|--------------------------------------|--|----------------------------------|------------------------|--|---------------|
| 161.5(4) | 95.9(3) | $3^+ \rightarrow (2)^+$ | 100 | 0.62(7) ^b | | ($M1 + E2$) |
| 234.02(23) | 190.21(23) | $2^+ \rightarrow 1^+$ | 0.21(7) | | | |
| 414.4(4) | 252.93(24) | $4^+ \rightarrow 3^+$ | 87.76(95) | 0.42(4) ^b | -0.09(1) | $M1 + E2$ |
| | 348.61(23) ^h | $4^+ \rightarrow (2)^+$ | | | | |
| 515.5(4) | 353.83(18) | $4^+ \rightarrow 3^+$ | 2.50(27) | 0.43(7) ^b | -0.09(1) | $M1 + E2$ |
| | 450.36(12) | $4^+ \rightarrow (2)^+$ | 3.04(29) | | | |
| 720.8(3) | 486.74(20) ^h | $3^+ \rightarrow 2^+$ | | | | |
| | 655.37(18) | $3^+ \rightarrow (2)^+$ | 0.20(4) | | | |
| 862.6(4) | 347.39(28) | $5^+ \rightarrow 4^+$ | 0.53(19) | 0.70(25) ^b | | $M1 + E2$ |
| | 448.22(19) | $5^+ \rightarrow 4^+$ | 29.82(53) | 0.41(5) ^b | -0.11(2) | $M1 + E2$ |
| | 701.1(3) | $5^+ \rightarrow 3^+$ | 0.68(12) | | | |
| 1140.8(4) | 419.7(4) | $4^+ \rightarrow 3^+$ | 0.21(7) | 0.60(28) ^c | | $M1 + E2$ |
| | 726.40(19) | $4^+ \rightarrow 4^+$ | 2.75(22) | | | |
| 1349.5(4) | 208.62(10) | $5^+ \rightarrow 4^+$ | 0.71(13) | | | |
| | 486.94(15) | $5^+ \rightarrow 5^+$ | 3.88(24) | 0.96(29) ^b | -0.03(2) | ($M1 + E2$) |
| | 834.13(13) | $5^+ \rightarrow 4^+$ | 3.29(38) | 0.52(7) ^b | ≈ 0 | ($M1 + E2$) |
| | 934.89(16) | $5^+ \rightarrow 4^+$ | 40.96(68) | 0.45(5) ^b | -0.08(3) | $M1$ |
| 1463.3(4) | 113.70(24) | $7^+ \rightarrow 5^+$ | 12.33(34) | 0.98(7) ^b | | Q |
| | 600.67(10) | $7^+ \rightarrow 5^+$ | 18.21(94) | 0.85(8) ^b | +0.05(1) | $E2$ |
| 1512.2(4) | 162.5(3) | $6^+ \rightarrow 5^+$ | 1.93(27) | 0.54(13) ^c | | (D) |
| | 371.69(30) | $6^+ \rightarrow 4^+$ | 1.17(18) | 0.86(32) ^c | +0.10(3) | $E2$ |
| | 649.52(13) | $6^+ \rightarrow 5^+$ | 5.02(37) | 0.77(27) ^c | ≈ 0 | $M1 + E2$ |
| 1773.9(4) | 261.68(16) | $7^+ \rightarrow 6^+$ | 3.45(22) | 0.65(7) ^c | -0.34(16) | $M1 + E2$ |
| 2511.3(4) | 1047.90(11) | $8^+ \rightarrow 7^+$ | 4.41(32) | 1.28(24) ^d | -0.03(2) | $M1 + E2$ |
| 2651.9(4) | 1188.64(12) | $9^+ \rightarrow 7^+$ | 11.83(33) | 1.06(10) ^d | +0.08(3) | $E2$ |
| 2790.7(5) | 1327.36(22) | | 0.35(10) | | | |
| 3042.1(4) | 390.24(12) | $9^+ \rightarrow 9^+$ | 6.06(26) | 1.08(8) ^b | -0.10(1) | $M1(+E2)$ |
| | 530.72(17) | $9^+ \rightarrow 8^+$ | 2.25(21) | 0.53(7) ^d | -0.03(1) | $M1$ |
| | 1268.20(16) | $9^+ \rightarrow 7^+$ | 4.88(25) | 0.92(14) ^d | +0.22(7) | $E2$ |
| | 1578.87(15) | $9^+ \rightarrow 7^+$ | 3.26(21) | 1.12(13) ^d | +0.03(2) | $E2$ |
| 3181.7(5) | 670.40(17) | | 0.90(14) | | | |
| 3249.1(7) | 1899.6(5) ^h | | | | | |
| 3362.8(5) | 710.92(24) | $(9^+) \rightarrow 9^+$ | 0.72(16) | 1.11(26) ^b | -0.06(5) | ($M1 + E2$) |
| 3503.0(6) | 851.1(4) | $(9^+) \rightarrow 9^+$ | 0.31(11) | 1.12(44) ^b | | ($M1 + E2$) |
| 4015.2(4) | 1363.41(10) | $10^- \rightarrow 9^+$ | 0.40(8) | 0.54(8) ^b | +0.03(2) | $E1$ |
| | 1503.79(18) | $10^- \rightarrow 8^+$ | 0.23(8) | 1.07(60) ^f | | (Q) |
| 4073.8(4) | 1562.48(13) | | 0.60(8) | | | |
| 4109.0(4) | 1066.81(14) | $10^+ \rightarrow 9^+$ | 1.16(14) | 0.37(7) ^b | +0.09(7) | $M1 + E2$ |
| 4160.7(4) | 1118.70(16) | $11^+ \rightarrow 9^+$ | 10.66(29) | 1.05(10) ^b | +0.11(2) | $E2$ |
| 4192.0(4) | 1540.08(14) | $10^- \rightarrow 9^+$ | 0.53(8) | 0.69(9) ^e | +0.10(2) | $E1^s$ |
| 4495.3(5) | 1132.5(3) | $(11^+) \rightarrow (9^+)$ | 0.66(7) | 1.07(36) ^b | | (Q) |
| 4577.5(5) | 1925.58(17) | $10^- \rightarrow 9^+$ | 0.49(8) | 0.56(13) ^b | | $E1^s$ |
| 4916.2(5) | 755.58(12) | $12^+ \rightarrow 11^+$ | 0.95(10) | | | |
| 5000.0(5) | 808.08(24) | $12^{(-)} \rightarrow 10^-$ | 0.87(18) | 0.83(14) ^b | | Q |
| 5107.5(5) | 946.75(12) | $13^+ \rightarrow 11^+$ | 5.90(22) | 0.92(8) ^b | +0.11(2) | $E2$ |
| 5446.9(5) | 1337.75(18) | $(12^+) \rightarrow 10^+$ | 0.88(12) | 0.85(27) ^b | | (Q) |
| 5686.5(5) | 1525.80(22) ^h | $12^- \rightarrow 11^+$ | | | | |
| 5703.0(5) | 595.45(13) | $(12^+) \rightarrow 13^+$ | 3.56(50) | 0.60(11) ^d | -0.41(9) | $M1 + E2$ |
| 5785.3(4) | 1593.28(15) | $12^- \rightarrow 10^-$ | 0.32(9) | 0.93(30) ^b | | $E2^s$ |
| | 1770.04(12) | $12^- \rightarrow 10^-$ | 0.87(25) | 1.29(68) ^f | | $E2$ |
| 5844.0(5) | 1770.22(25) ^h | | | | | |
| 6201.8(4) | 498.77(19) | $13^+ \rightarrow (12^+)$ | 2.17(29) | 0.59(7) ^d | -0.06(4) | $M1 + E2$ |
| | 754.81(18) | $13^+ \rightarrow 12^{(+)}$ | 0.57(7) | | | |
| | 1094.4(4) ^h | $13^+ \rightarrow 13^+$ | | | | |
| | 1201.85(17) | $13^+ \rightarrow 12^{(-)}$ | 0.59(10) | 0.57(15) ^b | | ($D + Q$) |

TABLE I. (Continued).

| Level energy ^a E_i (keV) | Gamma-ray energy E_γ (keV) | Initial→final spin-parity $I_i^\pi \rightarrow I_f^\pi$ | Relative intensity I_γ | DCO ratio R_{DCO} | Polarization asymmetry Δ_{asym} | Assignment |
|--|--------------------------------------|--|----------------------------------|------------------------|---|------------|
| | 1285.69(17) | $13^+ \rightarrow 12^+$ | 1.10(3) | 0.57(16) ^b | -0.11(5) | $M1 + E2$ |
| | 1624.34(23) | $13^+ \rightarrow 10^-$ | 0.55(10) | | | |
| | 1706.5(3) | $13^+ \rightarrow (11^+)$ | 0.20(7) | | | |
| 6449.9(5) | 746.87(22) ^h | | | | | |
| 6487.7(5) | 1380.23(23) ^h | | | | | |
| 6787.7(5) | 1002.41(16) | $14^- \rightarrow 12^-$ | 1.89(22) | 1.16(19) ^b | +0.10(8) | $E2$ |
| 6884.9(5) | 1777.39(23) ^h | | | | | |
| 7132(3) | 1445.8(26) | | 0.35(10) | | | |
| 7181.5(11) | 2074 ^{h,i} | $14^{(-)} \rightarrow 13^+$ | | | | |
| 7186.5(11) | 2079 ^{h,i} | | | | | |
| 7259.7(5) | 1057.87(12) | $15^+ \rightarrow 13^+$ | 5.05(30) | 1.00(10) ^b | +0.04(1) | $E2$ |
| 8038.4(5) | 1250.67(19) | $16^- \rightarrow 14^-$ | 0.57(14) | 0.82(17) ^f | | Q |
| 8422.6(6) | 1162.9(4) | $17^+ \rightarrow 15^+$ | 4.05(20) | 0.88(9) ^b | +0.07(2) | $E2$ |
| 9578.4(11) | 1540 ^{h,i} | | | | | |
| 9861.6(7) | 1438.95(20) | $19^{(+)} \rightarrow 17^+$ | 0.72(11) | 1.03(10) ^e | | Q |
| 11264.9(12) | 1686.44(11) | | 0.34(9) | | | |
| 11659.3(7) | 1797.7(3) | $21^{(+)} \rightarrow 19^{(+)}$ | 0.67(11) | 0.90(26) ^e | | Q |

^aLevel energies are obtained from least-squares fit to the γ energies using the GTOL code [22].

^bGate on $E2$, 1189 keV.

^cGate on $E2$, 1268 keV.

^dGate on $E2$, 947 keV.

^eGate on $E2$, 1058 keV.

^fGate on $E2$, 1002 keV.

^gCorroborated also with Ref. [10].

^hIntensity measurement was not possible due to low statistics.

ⁱ γ -energy error of 1 keV was assumed to get least-squares fit level energy.

some of that coincidence intensity would be lost, but it was ≈ 250 ns. So, coincidence time window is probably not the reason behind this. The reason for the disappearance of the 601 keV transition in the sum gate of 1189 and 1540 keV γ rays is not confirmed in this work.

A positive parity band was observed by the authors of Ref. [10], and was reported to be built on the 11^+ state, consisting of 947, 1058, 1163, 1439, and 1799 keV γ rays depopulating, respectively, states at 5108 (13^+), 6167 (15^+), 7330 (17^+), 8769 ($19^{(+)}$), and 10568 keV ($21^{(+)}$). Now, it is evident in the gated spectra (Fig. 5) that 1058, 1163, and 1439 keV γ rays are in coincidence with 1338 and 1067 keV transitions. So, a new linking transition of 755 keV (6202 \rightarrow 5447 keV) has been placed connecting former transitions with 1338 and 1067 keV transitions depopulating the states at 5447 and 4109 keV, respectively. As a result, the previously reported positive parity yrast band has been modified and the energy values of the states depopulated by 1058, 1163, 1439, and 1798 keV γ rays have been changed to 7260 (15^+), 8423 (17^+), 9862 ($19^{(+)}$), and 11 659 keV ($21^{(+)}$) respectively. The state at 5108 keV decays to the 9^+ (3042 keV) state via two strong 947 and 1119 keV γ rays in cascade. The measured values of R_{DCO} and Δ_{asym} of the former two transitions suggest 13^+ and 11^+ spin-parity values for states at 5108 and 4161 keV, respectively.

The state at 6202 keV, which is newly observed in this work, decays mainly by fragmented γ rays of 755, 499, 1094, 1285, 1202, 1624, and 1706 keV energy to the states at 5447,

5703, 5108, 4916, 5000, 4578, and 4495 keV, respectively. The fragmented decay pattern of the former state suggests that the wave function corresponding to this state is of complex nature. This state decays to that at 5108 keV (13^+) via the cascade of two newly observed 499 and 595 keV γ rays as well as by the direct 1094 keV transition. Measured values of the DCO ratio of newly observed 1202 and 808 keV transitions suggest a spin value of 13 for the state at 6202 keV, while the measured values of DCO ratio and polarization asymmetry of 499 and 595 keV transitions confirm positive parity for this state. The state at 5703 keV is assigned with a tentative spin-parity 12^+ , based on the assigned spin-parities of the states at 6202 and 5108 keV, and further it is confirmed by the measured DCO ratio and polarization asymmetry values of 499 and 595 keV transitions.

Measured values of DCO ratio and polarization asymmetry of 595 keV γ ray do suggest a 14^+ spin-parity value for the state at 5703 keV. But in that case measured values of DCO ratio and polarization asymmetry of 499 keV transition would suggest 15^+ spin-parity for the 6202 keV state. As a result, many of the γ -ray transitions depopulating this 6202 keV state would have ambiguous multipolarities; for example, the 755 keV γ ray would be $M3$ in nature and the 1624 keV one would be $E5$ in nature. So, a tentative 12^+ spin-parity is assigned to the 5703 keV state.

The state at 6202 keV also decays to that at 4161 keV via the cascade of 1285 and 756 keV γ rays, and the measured values of DCO ratio and polarization asymmetry of the

1285 keV γ ray predict a spin-parity of 12^+ for the state at 4916 keV. Interestingly, the state at 6202 keV decays to that at 4578 keV via a 1624 keV $E3$ type γ ray. The $E3$ type transition is observed for the first time in this nucleus in the present work, but, due to very low intensity of this γ ray, measurements of R_{DCO} and Δ_{asym} were not possible.

Here, an important fact is that the 499 and 595 keV transitions should have similar peak areas when gated from above, but the 595 keV γ ray appears with a nearly double peak area compared to the 499 keV γ -ray as is evident from gated spectrum (e) of Fig. 5. This could be due to the presence of a 595 keV doublet or could reflect missing transitions, which is not confirmed by the present observation.

The spin-parities of the states at 8423 and 7260 keV are estimated to be 17^+ and 15^+ , respectively, from the observed stretched electric quadrupole nature of both the depopulating 1163 and 1058 keV γ rays. The measured R_{DCO} value of the 1439 keV γ ray suggests stretched quadrupole nature of this transition but, as polarization measurement was not possible due to low intensity of this transition, a tentative positive parity is assigned to the state at 9862 keV. The state at 11 659 keV is assigned $21^{(+)}$ spin-parity value, based on the measured R_{DCO} value of the 1798 keV transition.

Placement of the state at 5447 keV was tentative in previous work [10], but its presence is confirmed in the present experiment, as we could detect the depopulating 1338 keV γ ray in strong coincidence with the 1067 keV transition and other strong and weak transitions in cascade, as shown in the gated spectra (Fig. 5).

The 5446 keV level decays through a single branch of the 1338 keV transition. The level is found to be populated very weakly in the present experiment. Hence, the extracted DCO value of the 1338 keV transition is associated with a large uncertainty and a tentative (12^+) assignment has been made for the 5446 keV level.

The state at 3363 keV is assigned with a tentative spin-parity of (9^+) based on the measured values of R_{DCO} and Δ_{asym} of the 711 keV transition decaying from the 3363 keV level. Previously, it was assigned as 10^+ [10]. The measured values of R_{DCO} and Δ_{asym} for the 711 keV transition suggest that the state at 3363 keV could perhaps be assigned with a spin-parity value of 11^- , but in that case the 711 keV γ ray would be of $M2$ multipolarity which is supposed to be less probable. Here, the measured uncertainty in R_{DCO} also suggests that the 711 keV transition may have considerable mixing, so a tentative ($M1 + E2$) multipolarity is assigned to this γ ray and the state at 3363 keV is assigned tentatively with (9^+) spin-parity. Following the same assumption, the state at 3503 keV is also assigned tentatively with 9^+ spin-parity, though it is depopulated by the 851 keV γ ray which has $R_{DCO} \approx 1.0$. The state at 3363 keV is connected to that at 6202 keV via two newly observed γ rays in cascade, i.e., 1133 and 1706 keV. The new state at 4495 keV is assigned with a tentative spin-parity 11^+ , on the basis of the measured value of DCO ratio of the 1133 keV γ ray transition. The negative parity state at 8038 keV decays to that at 4192 keV by 1251, 1002, and 1593 keV γ rays in cascade. Measured R_{DCO} and Δ_{asym} predict stretched quadrupole nature of electric type for the 1002 keV γ ray and the measured R_{DCO} for 1251

and 1593 keV transitions suggest quadrupole nature. The negative-parity band has been extended up to an excitation energy ≈ 11 MeV by placing two new transitions, viz., of 1540 and 1686 keV, in cascade above the state at 8038 keV.

The 9^+ state of ^{66}Ga at 2652 keV has a single-particle origin from contributions of both the $1g_{9/2}$ proton and $1g_{9/2}$ neutron. So, the coupling of the 9^+ state with the 2^+ , 3^+ , 4^+ , 6^+ , and 8^+ states of ^{64}Zn , which has one proton and one neutron less than ^{66}Ga , can produce, respectively, 11^+ , 12^+ , 13^+ , 15^+ , and 17^+ states of ^{66}Ga . In order to search for the possibility of such coupling, we have compared (Fig. 6) the observed energy states with 11^+ , 12^+ , 13^+ , 15^+ , and 17^+ spin-parity values of ^{66}Ga with those originating from coupling of 9^+ state (at 2652 keV) of ^{66}Ga with 2^+ , 3^+ , 4^+ , 6^+ , and 8^+ states of ^{64}Zn [7,22]. In Fig. 6, a similar comparison is made in ^{68}Ga , for standardization purpose. In ^{68}Ga , the energies of 9^+ , 11^+ , 13^+ , 15^+ , and 17^+ states are taken from Ref. [12] and the National Nuclear Data Center (NNDC) [34]. In the case of ^{68}Ga , coupled states are coming from the coupling of the 9^+ state of ^{68}Ga at 2894 keV with 2_1^+ , 2_2^+ , 4_1^+ , 6_1^+ , and 8_1^+ states of ^{66}Zn [15]. As is evident from Fig. 6, the observed states are in close proximity in energy with the coupled states in the case of ^{68}Ga , compared to ^{66}Ga . Variation in energy with spin for the observed states follows the same pattern as that of the coupled states, in the case of ^{68}Ga , but does not follow the pattern in the case of ^{66}Ga . The energy states at 12^+ and 17^+ are lower in energy with respect to $9^+ \otimes 3_1^+$ and $9^+ \otimes 8_1^+$ coupled states, respectively, whereas the energy values of yrast 11^+ , 13^+ , and 15^+ states are higher than those of $9^+ \otimes 2_1^+$, $9^+ \otimes 4_1^+$, and $9^+ \otimes 6_1^+$ coupled states, respectively. All the observed states are lower in energy values compared to the coupled states, in the case of ^{68}Ga . The reason behind this behavior could be due to the complex interaction nature between the core and particles in the case of ^{66}Ga compared to ^{68}Ga . As far as the residual interactions between the core and particles are concerned, we may infer from this observation that ^{66}Zn is behaving more as a pure core than ^{64}Zn . This nature of the vibrating core, in the case of ^{68}Ga , gives rise to a platform for more simple kinds of excitations at intermediate and high spins, compared to ^{66}Ga . Therefore, a complex nature of excitations in ^{66}Ga draws special attention to explore the fundamental single-particle configurations related to its structure.

IV. SHELL MODEL CALCULATIONS

In order to understand the observed nuclear structure in ^{66}Ga , shell model calculations have been performed in the present work using two different interactions, viz., jun45pn [35] and jj44bpn [36]. The shell model code NUSHELLX@MSU [37] was used for this purpose. With the ^{56}Ni core, the valence space for the calculation consists of $2p_{3/2}$, $1f_{5/2}$, $2p_{1/2}$, and $1g_{9/2}$ proton and neutron orbitals. The effective Hamiltonian jun45pn [35] has been obtained from a realistic interaction based on the Bonn-C potential, with a total of 133 two-body matrix elements and four single-particle energies modified empirically so as to fit 400 experimental energy values of 69 nuclei with mass numbers $A = 63$ –96. In the derivation of this effective Hamiltonian, experimental

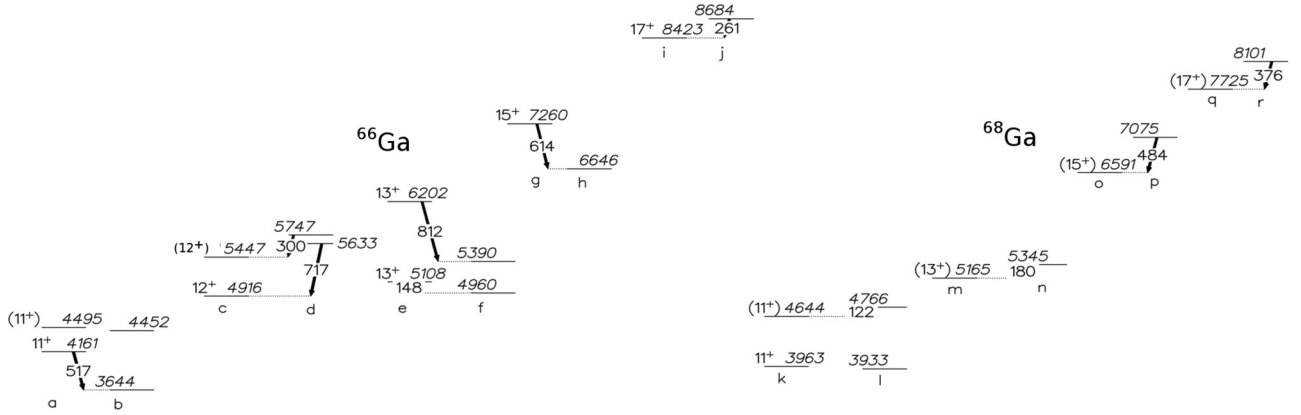


FIG. 6. A comparison of observed states with coupled states in $^{66,68}\text{Ga}$. Panel a: Observed energy states of 11_1^+ and 11_2^+ in ^{66}Ga obtained from the present experiment. Panel b: Calculated sum energy of the 9_1^+ state of ^{66}Ga (2652 keV, observed in the present experiment) plus 2_1^+ , 2_2^+ of ^{64}Zn [7,22], producing coupled states 11_1^+ and 11_2^+ of ^{66}Ga . Similarly, panels (c and d), (e and f), (g and h), and (i and j) for different mentioned states in ^{66}Ga . Here, the observed states compared are 11^+ , 12^+ , 13^+ , 15^+ , and 17^+ of ^{66}Ga . Panel k: Observed energy states of 11_1^+ and 11_2^+ in ^{68}Ga [12]. Panel l: Calculated sum energy of 9^+ state of ^{68}Ga [12] plus 2_1^+ , 2_2^+ of ^{66}Zn [15], producing coupled states 11_1^+ and 11_2^+ of ^{68}Ga . Similarly, panels (m and n), (o and p), and (q and r) for different mentioned states in ^{68}Ga . Here, the observed states compared are 11^+ , 13^+ , 15^+ , and 17^+ of ^{68}Ga . Each arrow represents the energy difference between the observed and coupled states (true for all pairs > 100 keV apart, for visualization purpose). See text for details.

data are not taken from $N = Z$ nuclei, specifically the Ni and Cu isotopes, because the model space may not be sufficient to describe the collectivity expected in these nuclei. The single-particle energies for this Hamiltonian are -9.8280 , -8.7087 , -7.8388 , and -6.261 MeV, respectively for the $2p_{3/2}$, $1f_{5/2}$, $2p_{1/2}$, and $1g_{9/2}$ orbitals. The effective Hamiltonian jj44bnp, due to Brown and Lesitskiy [36], is a realistic interaction based on the Bonn-C potential, which has been obtained by fitting binding energies and excitation energies in the Ni, Cu, and Zn isotopes and nuclei close to $N = 50$. The single-particle energies are taken to be -9.6566 , -9.2859 , -8.2695 , and -5.8944 MeV for the $2p_{3/2}$, $1f_{5/2}$, $2p_{1/2}$, and $1g_{9/2}$ orbitals, respectively. Previous calculations for ^{63}Zn [5], ^{63}Cu [29], and $^{60,62,64,66}\text{Zn}$ [38] with similar interaction and model space have produced very good agreements.

Observed levels in the present experiment, which are assigned with definite or tentative spin-parities, are compared with shell model calculations in Fig. 7. Those observed levels which are not assigned with spin-parities are not compared with calculated levels. The dominant particle configurations, constituting the wave functions of the levels, are represented in Tables II and III.

We have calculated occupation probabilities of protons and neutrons for two different interactions, and the results of these calculations are presented in Figs. 8–13. The wave function of a shell model state is the superposition of different orbitals included in the valence space, and occupation probability corresponding to an orbital indicates the fraction of the total number of valence nucleons (either protons or neutrons) occupying that particular orbital. So, an occupation probability gives the strength of individual contributions of different orbitals ($2p_{3/2}$, $1f_{5/2}$, $2p_{1/2}$, and $1g_{9/2}$ orbitals in the present calculation) of both the protons and neutrons in the total wave function.

Shell model calculations with jj44bnp interaction predict the first 1^+ state at just 27 keV higher in energy value with

respect to the observed value, but it is 142 keV higher in energy value as obtained by using the jun45pn interaction. So, the jj44bnp interaction produces the energy of the 1^+ state better than the jun45pn interaction. The energy of the first excited 3^+ state is better predicted by the jun45pn interaction than by the jj44bnp interaction but both fail to produce the energy value of the second excited 3^+ state, giving a result ≈ 350 keV lower in energy than the experimental value. The configuration of the first excited 3^+ state is predicted to be $[\pi(p_{3/2})^3]_{j_p=3/2} \otimes [v(f_{5/2})^3(p_{3/2})^4]_{j_v=5/2}$ (probability $\approx 13\%$) by jun45pn (Table III). Energies of the first and the second excited 5^+ states are well predicted by the jun45pn interaction, while they are overpredicted by the jj44bnp interaction. The predicted configurations by the jun45pn interaction for these states are $[\pi(f_{5/2})^1(p_{3/2})^2]_{j_p=5/2} \otimes [v(f_{5/2})^3(p_{3/2})^4]_{j_v=5/2}$ (probability $\approx 15\%$) and $[\pi(p_{3/2})^3]_{j_p=3/2} \otimes [v(f_{5/2})^3(p_{3/2})^4]_{j_v=9/2}$ (probability $\approx 11\%$), respectively. Neither interaction could produce the energy values of the first and the second excited 7^+ states, and shell model calculated values are far above the observed values. It is evident from the occupation number plots (Figs. 8 and 9) that significant contributions are coming from the $g_{9/2}$ proton and neutron orbitals in the case of the first 7^+ state, as calculated by the jj44bnp interaction. From the configuration tables of wave functions (Tables II and III), it is clear that the configurations with the highest probability for the first excited 7^+ states are $[\pi(p_{3/2})^1(p_{1/2})^1(g_{9/2})^1]_{j_p=5/2} \otimes [v(f_{5/2})^2(p_{3/2})^4(g_{9/2})^1]_{j_v=9/2}$ (probability $\approx 2\%$) and $[\pi(f_{5/2})^1(p_{3/2})^2]_{j_p=5/2} \otimes [v(f_{5/2})^3(p_{3/2})^4]_{j_v=9/2}$ (probability $\approx 11\%$) as predicted by jj44bnp and jun45pn interactions, respectively. Both interactions predict a full alignment of angular momenta contributed by both types of nucleons, i.e., proton and neutron, in forming the 7_1^+ state. No particular configuration appears to be dominant in forming the wave function for the first 7^+ state; rather, there is large competition between different configurations.

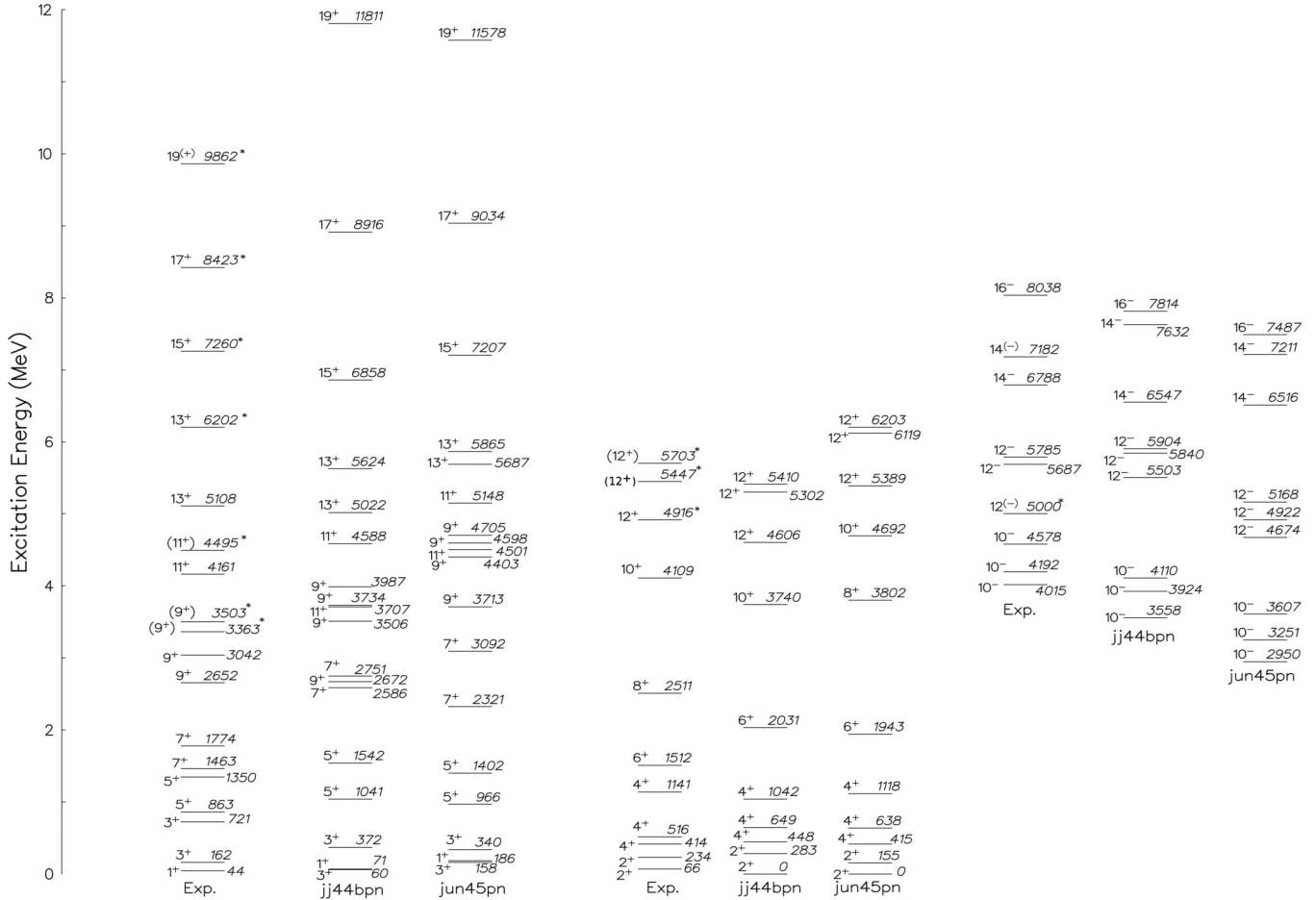


FIG. 7. Comparison of the observed levels of ^{66}Ga with shell model calculations using *jj44bnpn* [36] and *jun45pn* [35] interactions. Newly observed levels in this experiment are identified with asterisks (*). The energies in the figure are in keV.

The first 2^+ excited state is predicted by both interactions to be at 0 keV, whereas the experimental energy value is 66 keV. The second excited 2^+ state is overpredicted by the *jj44bnpn* interaction and is underpredicted by the *jun45pn* interaction. Energy values of the three 4^+ states, as calculated using the *jj44bnpn* interaction, are in moderate

agreement with the observed values, whereas the *jun45pn* interaction predicts the proper value of 415 keV for the first excited 4^+ state, and the second and the third excited 4^+ states are also well predicted by the *jun45pn* interaction in comparison with *jj44bnpn*. Configurations corresponding to these 4^+ states, as given by calculations using *jun45pn*

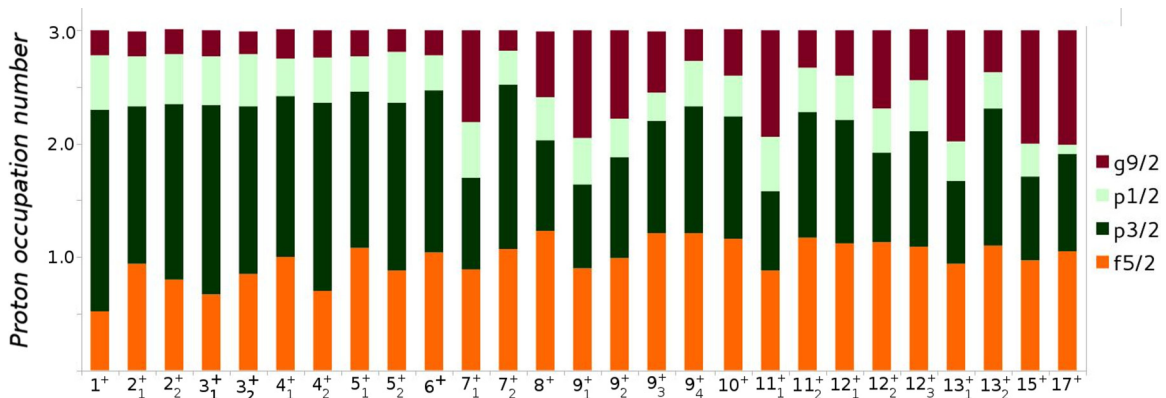


FIG. 8. Calculated occupation probabilities of the $f_{5/2}$, $p_{3/2}$, $p_{1/2}$, and $g_{9/2}$ orbitals for the positive parity states for protons in ^{66}Ga . The occupation probabilities are calculated from the shell model using the *jj44bnpn* interaction. Please see text for details.

TABLE II. Configurations with the highest probabilities of different states in ^{66}Ga , calculated by the shell model using $f_{5/2}p_{g_{9/2}}$ model space with jj44bnp interaction.

| Spin-parity(j^π) | Configuration | Probability |
|------------------------------|---|-------------|
| Positive parity | | |
| 1 ⁺ | $\pi(f_{5/2})^0(p_{3/2})^3(p_{1/2})^0(g_{9/2})^0 \otimes \nu(f_{5/2})^2(p_{3/2})^4(p_{1/2})^1(g_{9/2})^0$ | 9.03 |
| 2 ⁺ | $\pi(f_{5/2})^1(p_{3/2})^2(p_{1/2})^0(g_{9/2})^0 \otimes \nu(f_{5/2})^3(p_{3/2})^4(p_{1/2})^0(g_{9/2})^0$ | 3.59 |
| 3 ₁ ⁺ | $\pi(f_{5/2})^0(p_{3/2})^3(p_{1/2})^0(g_{9/2})^0 \otimes \nu(f_{5/2})^2(p_{3/2})^4(p_{1/2})^1(g_{9/2})^0$ | 3.44 |
| 3 ₂ ⁺ | $\pi(f_{5/2})^1(p_{3/2})^2(p_{1/2})^0(g_{9/2})^0 \otimes \nu(f_{5/2})^4(p_{3/2})^3(p_{1/2})^0(g_{9/2})^0$ | 4.23 |
| 4 ₁ ⁺ | $\pi(f_{5/2})^1(p_{3/2})^2(p_{1/2})^0(g_{9/2})^0 \otimes \nu(f_{5/2})^3(p_{3/2})^4(p_{1/2})^0(g_{9/2})^0$ | 4.32 |
| 4 ₂ ⁺ | $\pi(f_{5/2})^0(p_{3/2})^3(p_{1/2})^0(g_{9/2})^0 \otimes \nu(f_{5/2})^3(p_{3/2})^4(p_{1/2})^0(g_{9/2})^0$ | 5.44 |
| 4 ₃ ⁺ | $\pi(f_{5/2})^1(p_{3/2})^2(p_{1/2})^0(g_{9/2})^0 \otimes \nu(f_{5/2})^3(p_{3/2})^2(p_{1/2})^0(g_{9/2})^2$ | 1.56 |
| 5 ₁ ⁺ | $\pi(f_{5/2})^1(p_{3/2})^2(p_{1/2})^0(g_{9/2})^0 \otimes \nu(f_{5/2})^3(p_{3/2})^4(p_{1/2})^0(g_{9/2})^0$ | 9.33 |
| 5 ₂ ⁺ | $\pi(f_{5/2})^0(p_{3/2})^2(p_{1/2})^1(g_{9/2})^0 \otimes \nu(f_{5/2})^3(p_{3/2})^4(p_{1/2})^0(g_{9/2})^0$ | 4.92 |
| 6 ⁺ | $\pi(f_{5/2})^1(p_{3/2})^2(p_{1/2})^0(g_{9/2})^0 \otimes \nu(f_{5/2})^4(p_{3/2})^3(p_{1/2})^0(g_{9/2})^0$ | 5.17 |
| 7 ₁ ⁺ | $\pi(f_{5/2})^0(p_{3/2})^1(p_{1/2})^1(g_{9/2})^1 \otimes \nu(f_{5/2})^2(p_{3/2})^4(p_{1/2})^0(g_{9/2})^1$ | 1.93 |
| 7 ₂ ⁺ | $\pi(f_{5/2})^1(p_{3/2})^2(p_{1/2})^0(g_{9/2})^0 \otimes \nu(f_{5/2})^3(p_{3/2})^4(p_{1/2})^0(g_{9/2})^0$ | 6.87 |
| 8 ⁺ | $\pi(f_{5/2})^2(p_{3/2})^1(p_{1/2})^0(g_{9/2})^0 \otimes \nu(f_{5/2})^2(p_{3/2})^3(p_{1/2})^0(g_{9/2})^2$ | 2.45 |
| 9 ₁ ⁺ | $\pi(f_{5/2})^0(p_{3/2})^2(p_{1/2})^0(g_{9/2})^1 \otimes \nu(f_{5/2})^2(p_{3/2})^4(p_{1/2})^0(g_{9/2})^1$ | 4.13 |
| 9 ₂ ⁺ | $\pi(f_{5/2})^0(p_{3/2})^2(p_{1/2})^0(g_{9/2})^1 \otimes \nu(f_{5/2})^2(p_{3/2})^3(p_{1/2})^1(g_{9/2})^1$ | 4.24 |
| 9 ₃ ⁺ | $\pi(f_{5/2})^1(p_{3/2})^2(p_{1/2})^0(g_{9/2})^0 \otimes \nu(f_{5/2})^2(p_{3/2})^3(p_{1/2})^0(g_{9/2})^2$ | 5.63 |
| 9 ₄ ⁺ | $\pi(f_{5/2})^1(p_{3/2})^2(p_{1/2})^0(g_{9/2})^0 \otimes \nu(f_{5/2})^2(p_{3/2})^2(p_{1/2})^1(g_{9/2})^2$ | 2.78 |
| 10 ⁺ | $\pi(f_{5/2})^1(p_{3/2})^2(p_{1/2})^0(g_{9/2})^0 \otimes \nu(f_{5/2})^3(p_{3/2})^2(p_{1/2})^0(g_{9/2})^2$ | 4.10 |
| 11 ₁ ⁺ | $\pi(f_{5/2})^2(p_{3/2})^0(p_{1/2})^0(g_{9/2})^1 \otimes \nu(f_{5/2})^4(p_{3/2})^2(p_{1/2})^0(g_{9/2})^1$ | 3.15 |
| 11 ₂ ⁺ | $\pi(f_{5/2})^1(p_{3/2})^2(p_{1/2})^0(g_{9/2})^0 \otimes \nu(f_{5/2})^3(p_{3/2})^2(p_{1/2})^0(g_{9/2})^2$ | 3.73 |
| 12 ₁ ⁺ | $\pi(f_{5/2})^1(p_{3/2})^2(p_{1/2})^0(g_{9/2})^0 \otimes \nu(f_{5/2})^3(p_{3/2})^2(p_{1/2})^0(g_{9/2})^2$ | 8.48 |
| 12 ₂ ⁺ | $\pi(f_{5/2})^1(p_{3/2})^1(p_{1/2})^0(g_{9/2})^1 \otimes \nu(f_{5/2})^2(p_{3/2})^4(p_{1/2})^0(g_{9/2})^1$ | 4.88 |
| 12 ₃ ⁺ | $\pi(f_{5/2})^1(p_{3/2})^1(p_{1/2})^0(g_{9/2})^1 \otimes \nu(f_{5/2})^2(p_{3/2})^4(p_{1/2})^0(g_{9/2})^1$ | 2.11 |
| 13 ₁ ⁺ | $\pi(f_{5/2})^1(p_{3/2})^1(p_{1/2})^0(g_{9/2})^1 \otimes \nu(f_{5/2})^2(p_{3/2})^4(p_{1/2})^0(g_{9/2})^1$ | 5.07 |
| 13 ₂ ⁺ | $\pi(f_{5/2})^1(p_{3/2})^2(p_{1/2})^0(g_{9/2})^0 \otimes \nu(f_{5/2})^1(p_{3/2})^4(p_{1/2})^0(g_{9/2})^2$ | 6.29 |
| 15 ⁺ | $\pi(f_{5/2})^1(p_{3/2})^1(p_{1/2})^0(g_{9/2})^1 \otimes \nu(f_{5/2})^3(p_{3/2})^3(p_{1/2})^0(g_{9/2})^1$ | 10.58 |
| 17 ⁺ | $\pi(f_{5/2})^1(p_{3/2})^1(p_{1/2})^0(g_{9/2})^1 \otimes \nu(f_{5/2})^2(p_{3/2})^3(p_{1/2})^1(g_{9/2})^1$ | 16.62 |
| Negative parity | | |
| 10 ₁ ⁻ | $\pi(f_{5/2})^1(p_{3/2})^2(p_{1/2})^0(g_{9/2})^0 \otimes \nu(f_{5/2})^3(p_{3/2})^3(p_{1/2})^0(g_{9/2})^1$ | 2.76 |
| 10 ₂ ⁻ | $\pi(f_{5/2})^1(p_{3/2})^1(p_{1/2})^1(g_{9/2})^0 \otimes \nu(f_{5/2})^3(p_{3/2})^3(p_{1/2})^0(g_{9/2})^1$ | 3.61 |
| 10 ₃ ⁻ | $\pi(f_{5/2})^1(p_{3/2})^2(p_{1/2})^0(g_{9/2})^0 \otimes \nu(f_{5/2})^3(p_{3/2})^3(p_{1/2})^0(g_{9/2})^1$ | 8.99 |
| 12 ₁ ⁻ | $\pi(f_{5/2})^1(p_{3/2})^2(p_{1/2})^0(g_{9/2})^0 \otimes \nu(f_{5/2})^2(p_{3/2})^4(p_{1/2})^0(g_{9/2})^1$ | 5.51 |
| 12 ₂ ⁻ | $\pi(f_{5/2})^1(p_{3/2})^1(p_{1/2})^1(g_{9/2})^0 \otimes \nu(f_{5/2})^2(p_{3/2})^4(p_{1/2})^0(g_{9/2})^1$ | 6.43 |
| 14 ₁ ⁻ | $\pi(f_{5/2})^2(p_{3/2})^0(p_{1/2})^0(g_{9/2})^1 \otimes \nu(f_{5/2})^3(p_{3/2})^2(p_{1/2})^0(g_{9/2})^2$ | 11.78 |
| 14 ₂ ⁻ | $\pi(f_{5/2})^1(p_{3/2})^1(p_{1/2})^0(g_{9/2})^1 \otimes \nu(f_{5/2})^2(p_{3/2})^2(p_{1/2})^1(g_{9/2})^2$ | 12.58 |
| 16 ⁻ | $\pi(f_{5/2})^1(p_{3/2})^0(p_{1/2})^1(g_{9/2})^1 \otimes \nu(f_{5/2})^3(p_{3/2})^2(p_{1/2})^0(g_{9/2})^2$ | 9.19 |

interaction, are $[\pi(p_{3/2})^3]_{j_p=3/2} \otimes [\nu(f_{5/2})^3(p_{3/2})^4]_{j_v=5/2}$ (probability $\approx 20\%$), $[\pi(f_{5/2})^1(p_{3/2})^2]_{j_p=5/2} \otimes [\nu(f_{5/2})^3(p_{3/2})^4]_{j_v=5/2}$ (probability $\approx 13\%$) and $[\pi(p_{3/2})^3]_{j_p=3/2} \otimes [\nu(f_{5/2})^2(p_{3/2})^4(p_{1/2})^1]_{j_v=7/2}$ (probability $\approx 6\%$). It is evident that first excited 4⁺ state originates from the maximum alignment of proton and neutron angular momenta, whereas the other two 4⁺ states arise from the partial alignment. The 6⁺ excited state is overpredicted in energy value by both interactions. Here, both occupation number plots (Figs. 8–11) and configurations of wave

functions (Tables II and III), show that the 6⁺ state arises mainly due to the occupation of protons and neutrons in $f_{5/2}$ and $p_{3/2}$ orbitals.

With ten valence particles and with large model space, many possible configurations arise for a given total angular momentum, as there are many different ways to distribute valence particles among the $f_{5/2}$, $p_{3/2}$, $p_{1/2}$, and $g_{9/2}$ orbitals which add up to the same spin value. So, a large number of configurations to compete with each other for the construction of the wave function for a particular state, and it is evident

TABLE III. Configurations with the highest probabilities of different states in ^{66}Ga , calculated by the shell model using $f_{5/2}p_{g_{9/2}}$ model space with jun45pn interaction.

| Spin-parity(j^π) | Configuration | Probability |
|------------------------------|---|-------------|
| Positive parity | | |
| 1 ⁺ | $\pi(f_{5/2})^0(p_{3/2})^3(p_{1/2})^0(g_{9/2})^0 \otimes \nu(f_{5/2})^3(p_{3/2})^4(p_{1/2})^0(g_{9/2})^0$ | 12.27 |
| 2 ⁺ | $\pi(f_{5/2})^0(p_{3/2})^3(p_{1/2})^0(g_{9/2})^0 \otimes \nu(f_{5/2})^3(p_{3/2})^4(p_{1/2})^0(g_{9/2})^0$ | 15.02 |
| 3 ₁ ⁺ | $\pi(f_{5/2})^0(p_{3/2})^3(p_{1/2})^0(g_{9/2})^0 \otimes \nu(f_{5/2})^3(p_{3/2})^4(p_{1/2})^0(g_{9/2})^0$ | 12.59 |
| 3 ₂ ⁺ | $\pi(f_{5/2})^0(p_{3/2})^2(p_{1/2})^1(g_{9/2})^0 \otimes \nu(f_{5/2})^3(p_{3/2})^4(p_{1/2})^0(g_{9/2})^0$ | 12.91 |
| 4 ₁ ⁺ | $\pi(f_{5/2})^0(p_{3/2})^3(p_{1/2})^0(g_{9/2})^0 \otimes \nu(f_{5/2})^3(p_{3/2})^4(p_{1/2})^0(g_{9/2})^0$ | 20.43 |
| 4 ₂ ⁺ | $\pi(f_{5/2})^1(p_{3/2})^2(p_{1/2})^0(g_{9/2})^0 \otimes \nu(f_{5/2})^3(p_{3/2})^4(p_{1/2})^0(g_{9/2})^0$ | 12.53 |
| 4 ₃ ⁺ | $\pi(f_{5/2})^0(p_{3/2})^3(p_{1/2})^0(g_{9/2})^0 \otimes \nu(f_{5/2})^2(p_{3/2})^4(p_{1/2})^1(g_{9/2})^0$ | 6.32 |
| 5 ₁ ⁺ | $\pi(f_{5/2})^1(p_{3/2})^2(p_{1/2})^0(g_{9/2})^0 \otimes \nu(f_{5/2})^3(p_{3/2})^4(p_{1/2})^0(g_{9/2})^0$ | 15.20 |
| 5 ₂ ⁺ | $\pi(f_{5/2})^0(p_{3/2})^3(p_{1/2})^0(g_{9/2})^0 \otimes \nu(f_{5/2})^3(p_{3/2})^4(p_{1/2})^0(g_{9/2})^0$ | 10.86 |
| 6 ⁺ | $\pi(f_{5/2})^1(p_{3/2})^2(p_{1/2})^0(g_{9/2})^0 \otimes \nu(f_{5/2})^2(p_{3/2})^4(p_{1/2})^1(g_{9/2})^0$ | 9.90 |
| 7 ₁ ⁺ | $\pi(f_{5/2})^1(p_{3/2})^2(p_{1/2})^0(g_{9/2})^0 \otimes \nu(f_{5/2})^3(p_{3/2})^4(p_{1/2})^0(g_{9/2})^0$ | 11.22 |
| 7 ₂ ⁺ | $\pi(f_{5/2})^0(p_{3/2})^3(p_{1/2})^0(g_{9/2})^0 \otimes \nu(f_{5/2})^4(p_{3/2})^3(p_{1/2})^0(g_{9/2})^0$ | 20.98 |
| 8 ⁺ | $\pi(f_{5/2})^1(p_{3/2})^2(p_{1/2})^0(g_{9/2})^0 \otimes \nu(f_{5/2})^2(p_{3/2})^4(p_{1/2})^1(g_{9/2})^0$ | 10.52 |
| 9 ₁ ⁺ | $\pi(f_{5/2})^0(p_{3/2})^2(p_{1/2})^0(g_{9/2})^1 \otimes \nu(f_{5/2})^4(p_{3/2})^2(p_{1/2})^0(g_{9/2})^1$ | 8.06 |
| 9 ₂ ⁺ | $\pi(f_{5/2})^1(p_{3/2})^2(p_{1/2})^0(g_{9/2})^0 \otimes \nu(f_{5/2})^3(p_{3/2})^4(p_{1/2})^0(g_{9/2})^0$ | 18.88 |
| 9 ₃ ⁺ | $\pi(f_{5/2})^0(p_{3/2})^2(p_{1/2})^0(g_{9/2})^1 \otimes \nu(f_{5/2})^2(p_{3/2})^3(p_{1/2})^1(g_{9/2})^1$ | 5.38 |
| 9 ₄ ⁺ | $\pi(f_{5/2})^1(p_{3/2})^2(p_{1/2})^0(g_{9/2})^0 \otimes \nu(f_{5/2})^3(p_{3/2})^2(p_{1/2})^0(g_{9/2})^2$ | 2.35 |
| and | | |
| | $\pi(f_{5/2})^1(p_{3/2})^2(p_{1/2})^0(g_{9/2})^0 \otimes \nu(f_{5/2})^2(p_{3/2})^3(p_{1/2})^0(g_{9/2})^2$ | 2.35 |
| 10 ⁺ | $\pi(f_{5/2})^1(p_{3/2})^2(p_{1/2})^0(g_{9/2})^0 \otimes \nu(f_{5/2})^2(p_{3/2})^3(p_{1/2})^0(g_{9/2})^2$ | 6.65 |
| 11 ₁ ⁺ | $\pi(f_{5/2})^0(p_{3/2})^2(p_{1/2})^0(g_{9/2})^1 \otimes \nu(f_{5/2})^4(p_{3/2})^2(p_{1/2})^0(g_{9/2})^1$ | 5.05 |
| 11 ₂ ⁺ | $\pi(f_{5/2})^1(p_{3/2})^2(p_{1/2})^0(g_{9/2})^0 \otimes \nu(f_{5/2})^3(p_{3/2})^2(p_{1/2})^0(g_{9/2})^2$ | 5.74 |
| 12 ₁ ⁺ | $\pi(f_{5/2})^1(p_{3/2})^2(p_{1/2})^0(g_{9/2})^0 \otimes \nu(f_{5/2})^3(p_{3/2})^2(p_{1/2})^0(g_{9/2})^2$ | 12.30 |
| 12 ₂ ⁺ | $\pi(f_{5/2})^2(p_{3/2})^1(p_{1/2})^0(g_{9/2})^0 \otimes \nu(f_{5/2})^3(p_{3/2})^2(p_{1/2})^0(g_{9/2})^2$ | 4.12 |
| 12 ₃ ⁺ | $\pi(f_{5/2})^0(p_{3/2})^2(p_{1/2})^0(g_{9/2})^1 \otimes \nu(f_{5/2})^3(p_{3/2})^3(p_{1/2})^0(g_{9/2})^1$ | 6.90 |
| 13 ₁ ⁺ | $\pi(f_{5/2})^1(p_{3/2})^1(p_{1/2})^0(g_{9/2})^1 \otimes \nu(f_{5/2})^4(p_{3/2})^2(p_{1/2})^0(g_{9/2})^1$ | 5.36 |
| 13 ₂ ⁺ | $\pi(f_{5/2})^1(p_{3/2})^2(p_{1/2})^0(g_{9/2})^0 \otimes \nu(f_{5/2})^3(p_{3/2})^2(p_{1/2})^0(g_{9/2})^2$ | 9.39 |
| 15 ⁺ | $\pi(f_{5/2})^1(p_{3/2})^1(p_{1/2})^0(g_{9/2})^1 \otimes \nu(f_{5/2})^4(p_{3/2})^2(p_{1/2})^0(g_{9/2})^1$ | 6.19 |
| 17 ⁺ | $\pi(f_{5/2})^1(p_{3/2})^1(p_{1/2})^0(g_{9/2})^1 \otimes \nu(f_{5/2})^2(p_{3/2})^4(p_{1/2})^0(g_{9/2})^1$ | 15.28 |
| Negative parity | | |
| 10 ₁ ⁻ | $\pi(f_{5/2})^1(p_{3/2})^2(p_{1/2})^0(g_{9/2})^0 \otimes \nu(f_{5/2})^3(p_{3/2})^3(p_{1/2})^0(g_{9/2})^1$ | 9.55 |
| 10 ₂ ⁻ | $\pi(f_{5/2})^1(p_{3/2})^2(p_{1/2})^0(g_{9/2})^0 \otimes \nu(f_{5/2})^3(p_{3/2})^3(p_{1/2})^0(g_{9/2})^1$ | 7.72 |
| 10 ₃ ⁻ | $\pi(f_{5/2})^1(p_{3/2})^2(p_{1/2})^0(g_{9/2})^0 \otimes \nu(f_{5/2})^2(p_{3/2})^3(p_{1/2})^1(g_{9/2})^1$ | 9.51 |
| 12 ₁ ⁻ | $\pi(f_{5/2})^1(p_{3/2})^2(p_{1/2})^0(g_{9/2})^0 \otimes \nu(f_{5/2})^2(p_{3/2})^3(p_{1/2})^1(g_{9/2})^1$ | 14.64 |
| 12 ₂ ⁻ | $\pi(f_{5/2})^1(p_{3/2})^2(p_{1/2})^0(g_{9/2})^0 \otimes \nu(f_{5/2})^2(p_{3/2})^4(p_{1/2})^0(g_{9/2})^1$ | 8.40 |
| 14 ₁ ⁻ | $\pi(f_{5/2})^0(p_{3/2})^2(p_{1/2})^0(g_{9/2})^1 \otimes \nu(f_{5/2})^3(p_{3/2})^2(p_{1/2})^0(g_{9/2})^2$ | 9.04 |
| 14 ₂ ⁻ | $\pi(f_{5/2})^1(p_{3/2})^2(p_{1/2})^0(g_{9/2})^0 \otimes \nu(f_{5/2})^3(p_{3/2})^3(p_{1/2})^0(g_{9/2})^1$ | 12.95 |
| 16 ⁻ | $\pi(f_{5/2})^1(p_{3/2})^0(p_{1/2})^1(g_{9/2})^1 \otimes \nu(f_{5/2})^3(p_{3/2})^2(p_{1/2})^0(g_{9/2})^2$ | 8.12 |

that, for almost all the lower excited states up to 9₃⁺ and 6⁺, as calculated respectively by jun45pn and jj44bpn interactions in ^{66}Ga , the dominant contributions come from the fp shell. It is evident from the wave function tables (Tables II and III) that, up to the 6⁺ spin state, the probability of a particular dominant configuration is significantly larger when calculated using the jun45pn interaction compared to that using jj44bpn.

The energy values of 3₁⁺, 4₁⁺, 4₂⁺, 4₃⁺, 5₁⁺, and 5₂⁺ states, as calculated using the jun45pn interaction, are in better agreement with the experimental values, whereas only that of the 2₂⁺ state calculated using the jj44bpn interaction is in good agreement with the observation. So, as far as the lower excited states are concerned, the jun45pn interaction is more efficient than the jj44bpn interaction in producing the level structure.

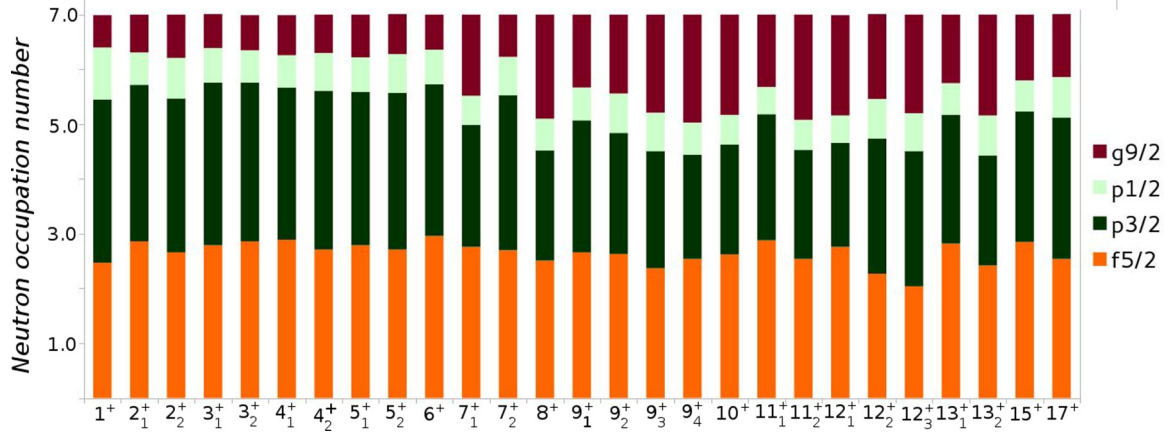


FIG. 9. Calculated occupation probabilities of the $f_{5/2}$, $p_{3/2}$, $p_{1/2}$, and $g_{9/2}$ orbitals for the positive parity states for neutrons in ^{66}Ga . The occupation probabilities are calculated from the shell model using the jj44bnpn interaction. Please see text for details.

The first excited 9^+ state is well reproduced by the jj44bnpn interaction but the other three 9^+ states are overpredicted by the same interaction. Here, all the 9^+ excited states are overpredicted by the jun45pn interaction. Among the different 11^+ , 12^+ , 13^+ , and 15^+ states, the energies of the second 11^+ , second 12^+ , and first 13^+ states, respectively, with configurations $[\pi(f_{5/2})^1(p_{3/2})^2]_{j_p=5/2} \otimes [\nu(f_{5/2})^3(p_{3/2})^2(g_{9/2})^2]_{j_n=17/2}$ (probability $\approx 4\%$), $[\pi(f_{5/2})^1(p_{3/2})^1(g_{9/2})^1]_{j_p=15/2} \otimes [\nu(f_{5/2})^2(p_{3/2})^4(g_{9/2})^1]_{j_n=9/2}$ (probability $\approx 5\%$), and $[\pi(f_{5/2})^1(p_{3/2})^1(g_{9/2})^1]_{j_p=17/2} \otimes [\nu(f_{5/2})^2(p_{3/2})^4(g_{9/2})^1]_{j_n=9/2}$ (probability $\approx 5\%$) are, as predicted by the jj44bnpn interaction, in good agreement with the experimental values, whereas only the energy state of 15^+ with the configuration $[\pi(f_{5/2})^1(p_{3/2})^1(g_{9/2})^1]_{j_p=17/2} \otimes [\nu(f_{5/2})^4(p_{3/2})^2(g_{9/2})^1]_{j_n=13/2}$ (probability $\approx 6\%$) is well reproduced by jun45pn interaction. As far as intermediate and high spin positive parity states are concerned, energy values calculated by both the interactions are in moderate agreement with the observed values but, compared to jun45pn , the jj44bnpn interaction is more able to reproduce the intermediate and high spin structure within the given $f_{5/2}p_{3/2}g_{9/2}$ model space. In all the intermediate and high spin states in ^{66}Ga , contributions to the wave functions are mainly dominated

by the $f_{5/2}$, $p_{3/2}$, and $g_{9/2}$ proton and neutron orbitals, as is obvious from the occupation probability plots and from the tables of configurations.

Higher spin states like 19^+ and above, for which the energy values as calculated by both interactions are greater than 1 MeV compared to the observed values, are not shown in configuration tables or occupation plots. So, it could be argued that a new mode of excitations is appearing at such high spin, which is different from single-particle nature. Large mixing of various orbitals at higher spins, predicted by the shell model calculations, also confirms the nature of a typical onset of collective behavior. A significant contribution, coming from $g_{9/2}$ proton and $g_{9/2}$ neutron orbitals, is very prominent, as reflected in the occupation number plots.

Three 10^- negative parity states are underpredicted in energy by both interactions, and the configurations for these states are mainly contributed from the protons in $f_{5/2}$ and $p_{3/2}$ orbitals and the neutrons in $f_{5/2}$, $p_{3/2}$, and $g_{9/2}$ orbitals. The second and the third 12^- excited states, as calculated by the jj44bnpn interaction, are in good agreement, whereas the first 12^- excited state is overpredicted by the same interaction. Here, all the 12^- states are underpredicted by the jun45pn interaction. The second excited 14^- state is well predicted by the jun45pn

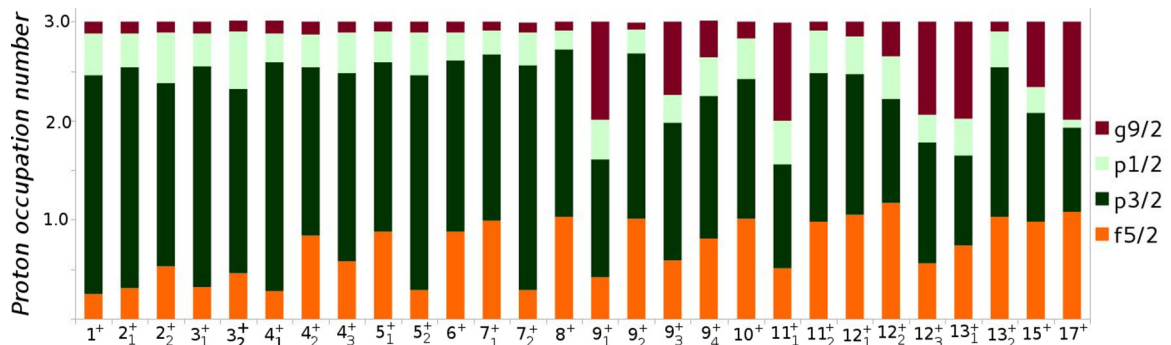


FIG. 10. Calculated occupation probabilities of the $f_{5/2}$, $p_{3/2}$, $p_{1/2}$, and $g_{9/2}$ orbitals for the positive parity states for protons in ^{66}Ga . The occupation probabilities are calculated from the shell model using the jun45pn interaction. Please see text for details.

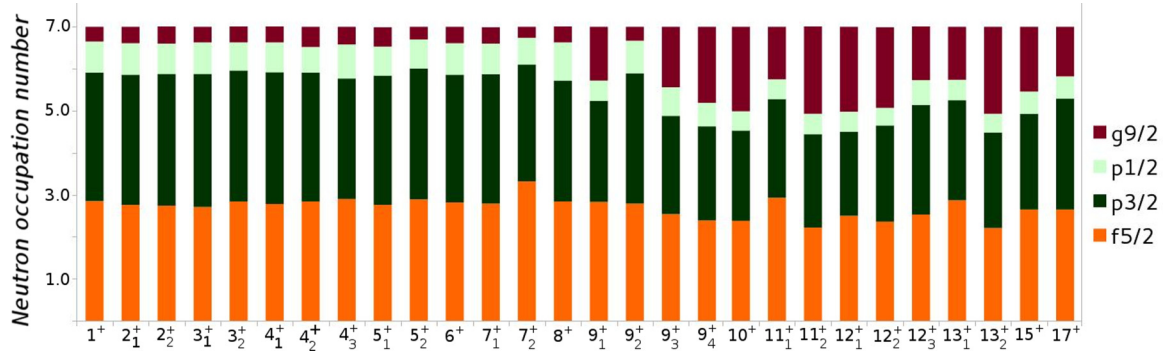


FIG. 11. Calculated occupation probabilities of the $f_{5/2}$, $p_{3/2}$, $p_{1/2}$, and $g_{9/2}$ orbitals for the positive parity states for neutrons in ^{66}Ga . The occupation probabilities are calculated from the shell model using the jun45pn interaction. Please see text for details.

interaction, whereas the first 14^- state is underpredicted by 271 keV in energy. The main configuration of the first excited 14^- state, as predicted by the jun45pn interaction, is $[\pi(p_{3/2})^2(g_{9/2})^1]_{j_p=9/2} \otimes [\nu(f_{5/2})^3(p_{3/2})^2(g_{9/2})^2]_{j_n=19/2}$ and that of second excited 14^- state is $[\pi(f_{5/2})^1(p_{3/2})^2]_{j_p=9/2} \otimes [\nu(f_{5/2})^3(p_{3/2})^3(g_{9/2})^1]_{j_n=19/2}$. So, for the first excited 14^- state, contributions of $g_{9/2}$ orbitals for both protons and neutrons are significantly large with respect to the second 14^- state, and this is also obvious from the occupation number (calculated using the jun45pn interaction) plot (Fig. 13). The energy of the 16^- state is in moderate agreement with the jj44bpn calculation but is well underpredicted by jun45pn. The configuration of this state is mainly originating from protons and neutrons in the $f_{5/2}$, $p_{3/2}$, and $g_{9/2}$ orbitals. The occupation number plots (Figs. 8–13) also suggest that, for both kinds of interaction, the contributions coming from both protons and neutrons in the $g_{9/2}$ orbitals are significantly large for high spin positive and negative parity states. Hence, a variety of structural effects are expected due to the occupancy of the shape driving $g_{9/2}$ orbitals. The low spin positive parity states up to 4^+ are mainly due to the occupation of protons in the $p_{3/2}$ orbital, and those above are due to protons in the $f_{5/2}$ and $p_{3/2}$ orbitals up to spin value $\approx 8\hbar$, as obtained from the calculations using the jun45pn interaction. Significant contributions in wave functions for low spin positive parity states up to 8^+ originate from neutrons occupying the $f_{5/2}$ and $p_{3/2}$ orbitals. For high spin positive (13^+ to 17^+) and negative (14^- and 16^-) parity states, angular momenta are mainly generated by the $(\pi f_{5/2}p_{3/2}g_{9/2})^3 \otimes (\nu f_{5/2}p_{3/2}g_{9/2})^7$ configuration, as predicted by both interactions. It is also

evident from the calculations with both interactions that the participation of the $p_{1/2}$ orbital for the generation of both low and high angular momentum states is insignificant.

V. CONCLUSION

A new level scheme of ^{66}Ga has been proposed in this present work, which is enriched with 21 new transitions and 20 new levels. Some of the previously observed states, without any definite spin-parities, are assigned with definite or tentative values in this work, from the measured values of DCO ratio and polarization asymmetry of depopulating transitions. Multipolarities of many new transitions are determined from the measurements. The level scheme has been extended up to ≈ 11.6 MeV in energy. Some intermediate spin states of ^{66}Ga are explained in the framework of coupling of single-particle configurations with the vibrational core. Shell model calculations have also been performed in $f_{5/2}pg_{9/2}$ model space using two different interactions, viz., jj44bpn and jun45pn. Comparative study shows that the jun45pn interaction is more efficient in explaining the lower excitations than jj44bpn. Both interactions are in moderate agreement in explaining intermediate spin states. With an improved set of the two-body matrix elements and incorporating the full $fpg_{9/2}$ model space, i.e., including the $1f_{7/2}$ orbital for calculations, a more accurate description may be obtained. High spin states above 15^+ are observed to be different from the single-particle nature, and it is probably the collective degrees of freedom that come into play at such high spin. More experimental investigation is required to confirm the nature of the collectivity at such high spin.

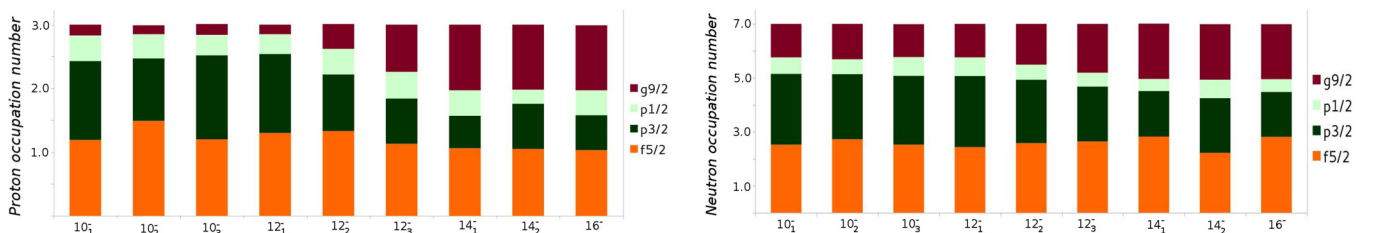


FIG. 12. Calculated occupation probabilities of the $f_{5/2}$, $p_{3/2}$, $p_{1/2}$, and $g_{9/2}$ orbitals for the negative parity states for protons and neutrons in ^{66}Ga . The occupation probabilities are calculated from the shell model using the jj44bpn interaction. Please see text for details.

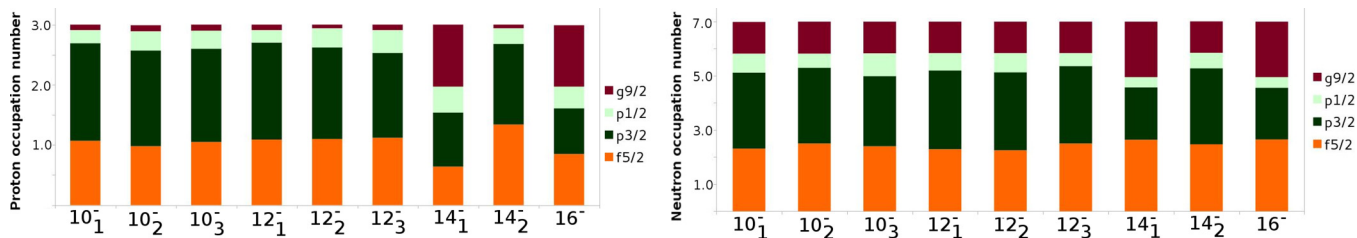


FIG. 13. Calculated occupation probabilities of the $f_{5/2}$, $p_{3/2}$, $p_{1/2}$, and $g_{9/2}$ orbitals for the negative parity states for protons and neutrons in ^{66}Ga . The occupation probabilities are calculated from the shell model using the jun45pn interaction. Please see text for details.

ACKNOWLEDGMENTS

We would like to acknowledge the Pelletron staff of IUAC for providing excellent beams and INGA collaborators for the loan of detectors. Support from the target laboratory and from D. Kanjilal, IUAC is gratefully acknowledged. We would like

to thank S. Nandi (VECC), S. S. Bhattacharjee (TRIUMF, Canada), and R. Garg (IUAC) for their help during the experiment. We would also like to acknowledge financial support from SERB/DST (New Delhi), file No. EMR/2015/000891, IUAC (New Delhi), file No. UFR49318 and DAE-BRNS, Project Sanction No. 37(3)/14/17/2016-BRNS.

-
- [1] C. E. Svensson *et al.*, *Phys. Rev. Lett.* **82**, 3400 (1999).
 [2] L.-L. Andersson *et al.*, *Phys. Rev. C* **79**, 024312 (2009).
 [3] C. E. Svensson *et al.*, *Phys. Rev. Lett.* **79**, 1233 (1997).
 [4] C. E. Svensson *et al.*, *Phys. Rev. Lett.* **80**, 2558 (1998).
 [5] U. S. Ghosh *et al.*, *Phys. Rev. C* **100**, 034314 (2019).
 [6] A. K. Singh *et al.*, *Phys. Rev. C* **57**, 1617 (1998).
 [7] D. Karlgren *et al.*, *Phys. Rev. C* **69**, 034330 (2004).
 [8] B. Mukherjee, S. Muralithar, R. P. Singh, R. Kumar, K. Rani, R. K. Bhowmik, and S. C. Pancholi, *Phys. Rev. C* **64**, 024304 (2001).
 [9] M. Weiszflog *et al.*, *Eur. Phys. J. A* **11**, 25 (2001).
 [10] S. S. Bhattacharjee *et al.*, *Phys. Rev. C* **95**, 054330 (2017).
 [11] I. Dankó *et al.*, *Phys. Rev. C* **59**, 1956 (1999).
 [12] A. K. Singh *et al.*, *Eur. Phys. J. A* **9**, 197 (2000).
 [13] D. Ward *et al.*, *Phys. Rev. C* **63**, 014301 (2000).
 [14] E. A. Stefanova *et al.*, *Phys. Rev. C* **67**, 054319 (2003).
 [15] L. Cleemann *et al.*, *Nucl. Phys. A* **386**, 367 (1982).
 [16] H. H. Bolotin and D. A. McClure, *Phys. Rev.* **180**, 987 (1969).
 [17] C. Morand, M. Agard, J. F. Bruandet, A. Dauchy, A. Giorni, F. Glasser, and T. U. Chan, *Nucl. Phys. A* **308**, 103 (1978).
 [18] C. C. Lu, M. S. Zisman, and B. G. Harvey, *Phys. Rev.* **186**, 1086 (1969).
 [19] J. Timár, T. X. Quang, T. Fényes, Z. Dombrádi, A. Krasznahorkay, J. Kumpulainen, R. Julin, S. Brant, V. Paar, and L. Šimičič, *Nucl. Phys. A* **573**, 61 (1994).
 [20] M. R. Najam, W. F. Davidson, W. M. Zuk, L. E. Carlson, and M. A. Awal, *Nucl. Phys. A* **173**, 577 (1971).
 [21] R. A. Hinrichs, R. Sherr, G. M. Crawley, and I. Proctor, *Phys. Rev. Lett.* **25**, 829 (1970).
 [22] <http://www.nndc.bnl.gov>.
 [23] A. Filevich, A. Ceballos, M. A. J. Mariscotti, P. Thieberger, and E. D. Mateosian, *Nucl. Phys. A* **295**, 513 (1978).
 [24] G. K. Mehta *et al.*, *Nucl. Instrum. Methods Phys. Res. A* **268**, 334 (1988).
 [25] S. Muralithar *et al.*, *Nucl. Instrum. Methods Phys. Res. A* **622**, 281 (2010).
 [26] B. P. Ajith Kumar *et al.*, in *Proceedings of the 44th DAE-BRNS Symposium on Nuclear Physics* (Department of Atomic Energy, Government of India, Mumbai, 2001), p. 390.
 [27] D. C. Radford, *Nucl. Instrum. Methods Phys. Res., Sect. A* **361**, 297 (1995).
 [28] R. K. Bhowmik *et al.*, in *Proceedings of the 44th DAE-BRNS Symposium on Nuclear Physics* (Department of Atomic Energy, Government of India, Mumbai, 2001), p. 422.
 [29] S. Rai *et al.*, *Eur. Phys. J. A* **54**, 84 (2018).
 [30] K. S. Krane *et al.*, *Nucl. Data Tables* **11**, 351 (1973).
 [31] G. Duchene *et al.*, *Nucl. Instrum. Methods Phys. Res. A* **432**, 90 (1999).
 [32] K. Starosta *et al.*, *Nucl. Instrum. Methods Phys. Res. A* **423**, 16 (1999).
 [33] F. W. N. de Boer *et al.*, *Nucl. Phys. A* **158**, 166 (1970).
 [34] E. A. McCutchan *et al.*, *Nucl. Data Sheets* **113**, 1735 (2012).
 [35] M. Honma, T. Otsuka, T. Mizusaki, and M. Hjorth-Jensen, *Phys. Rev. C* **80**, 064323 (2009).
 [36] A. F. Lisetskiy, B. A. Brown, M. Horoi, and H. Grawe, *Phys. Rev. C* **70**, 044314 (2004).
 [37] A. Brown and W. D. M. Rae, *Nucl. Data Sheets* **120**, 115 (2014).
 [38] S. Rai *et al.*, *Int. J. Mod. Phys. E* **25**, 1650099 (2016).

Evolution of collectivity and shape transition in ^{66}Zn

S. Rai ^{1,*} U. S. Ghosh ¹ B. Mukherjee ^{1,†} A. Biswas,¹ A. K. Mondal,¹ K. Mandal ¹ A. Chakraborty ¹
S. Chakraborty ^{2,‡} G. Mukherjee ³ A. Sharma ⁴ I. Bala,⁵ S. Muralithar,⁵ and R. P. Singh ⁵

¹Department of Physics, Siksha-Bhavana, Visva-Bharati, Santiniketan, West Bengal-731235, India

²Department of Physics, Institute of Science, Banaras Hindu University, Varanasi-221005, India

³Variable Energy Cyclotron Centre (VECC), 1/AF Bidhannagar, Kolkata-700064, India

⁴Department of Physics, Himachal Pradesh University, Shimla-171005, India

⁵Inter University Accelerator Centre (IUAC), Aruna Asaf Ali Marg, New Delhi-110067, India



(Received 22 August 2020; accepted 16 November 2020; published 14 December 2020)

Excited states in ^{66}Zn were investigated through the in-beam γ -ray spectroscopic techniques using the $^{52}\text{Cr}(^{18}\text{O}, 2p2n)$ fusion-evaporation reaction at a beam energy of 72.5 MeV. The γ -rays emitted by the de-exciting nuclei were recorded in coincidence mode using the 14 Compton suppressed Ge clover detectors of the Indian National Gamma Array. With 14 new transitions being identified, the level scheme of ^{66}Zn has been extended up to the excitation energy ≈ 12.3 MeV and spin $\approx 17\hbar$. A rotational band, associated with the two quasineutrons from the $1g_{9/2}$ orbital, has been found to exhibit a band crossing with the ground-state band at a spin of $6\hbar$. The evolution of the collectivity and shape transition in this nucleus have been discussed in the framework of the total Routhian surface calculations and in comparison with the neighboring $^{68,70}\text{Ge}$ nuclei.

DOI: [10.1103/PhysRevC.102.064313](https://doi.org/10.1103/PhysRevC.102.064313)

I. INTRODUCTION

Nuclei in the mass region $A \approx 60$ –70 having its Fermi surfaces lying in between that of the $N = Z = 28$ doubly magic ^{56}Ni and the semi-magic $N = 40$ subshell gap are known to exhibit a complex interplay of the single-particle and the collective modes of excitation. While the single particle excitation involves the valence nucleons outside the ^{56}Ni core, the collective excitation has been attributed to the gaps observed in the Nilsson energy diagram at $N = Z = 34$, 36 for the oblate deformation and $N = Z = 38$ for the prolate deformation. In this mass region, the high- j unique parity $1g_{9/2}$ orbital is found to play a major role in the configuration of high spin states and it has been attributed in producing several exciting high spin phenomena [1–8]. Collective structures arising out of the different quasiparticle configurations based on the $\pi 1g_{9/2}$ and/or $\nu 1g_{9/2}$ orbitals have been found to give rise to the different kinds of shape evolution with the increasing spin. In this mass region, the octupole correlations are also expected due to the presence of orbitals satisfying $\Delta L = \Delta J = 3$ criterion, arising out of the $2p_{3/2}$ ($L = 1$) and the $1g_{9/2}$ ($L = 4$) orbitals around the Fermi surface.

Lying in the transitional region encompassing the doubly magic spherical ^{56}Ni and the strongly deformed Sr, Kr isotopes, ^{66}Zn is an interesting candidate for studying the phenomena of shape transitions from the spectroscopic point of view. In the neighboring nuclei, the alignment of the neutrons and protons in the $1g_{9/2}$ orbitals have been observed

leading to the band crossing between the collective structures of different configurations [9–14]. Several superdeformed and terminating bands have been reported in the lighter Zn and other slightly heavier even-even $^{68,70}\text{Ge}$ isotopes [3,4,9–12]. These observations have motivated us for studying the nuclear structure in ^{66}Zn , the latest studies of which date back to the 1970s. Furthermore, most of the previously reported level-structure investigations were performed using the β -decays [15,16], transfer reactions [17] or light-ion induced reactions [18–22] with modest experimental setups. Moreover, Morand *et al.* [23] have measured the lifetimes of a few yrast states in ^{66}Zn via the Doppler shift attenuation method (DSAM), while Cleemann *et al.* [21] have measured lifetimes of some of the negative parity levels using the recoil Doppler method (RDM).

In this article, we report for the first time on the high spin states in ^{66}Zn populated using a heavy-ion induced reaction. The emitted γ -rays were detected with a high resolution and efficient array of high-purity germanium (HPGe) clover detectors. The level scheme of ^{66}Zn has been revisited using the γ - γ coincidence technique and extended significantly in the present work. A collective band based on two $1g_{9/2}$ quasineutrons has been found to exhibit a band crossing with the ground-state band at a spin of $6\hbar$. The evolution of the collectivity and shape transition in this nucleus have been discussed in the framework of the total Routhian surface (TRS) calculation and compared with the neighboring $^{68,70}\text{Ge}$ nuclei, which have similar kind of collective features.

II. EXPERIMENTAL DETAILS AND DATA ANALYSIS

The fusion evaporation reaction $^{52}\text{Cr}(^{18}\text{O}, 2p2n)$ at a beam energy of $E_{\text{lab}} = 72.5$ MeV was used to populate the high

*Present address: Forensic Science Laboratory, 37/1/2 Belgachia Road, Kolkata-700037, India.

†buddhadev.mukherjee@visva-bharati.ac.in

‡Present address: Inter University Accelerator Centre, New Delhi.

TABLE I. Values of the level energies (E_i) in keV, γ -ray energies (E_γ) in keV, initial (I_i^π) \rightarrow final (I_f^π) spin-parity, relative intensities (I_γ), DCO ratio (R_{DCO}), and polarization asymmetry (Δ_{asym}) of the γ -ray transitions as obtained in this work for ^{66}Zn .

| Level energy E_i (keV) | Gamma-ray energy E_γ (keV) | Initial \rightarrow Final spin-parity $I_i^\pi \rightarrow I_f^\pi$ | Relative Intensity ^a I_γ | DCO ratio R_{DCO} | Polarization asymmetry Δ_{asym} | Assignment |
|-----------------------------|--------------------------------------|--|---|-------------------------------|--|---------------|
| 1039 | 1038.91(13) | $2^+ \rightarrow 0^+$ | 100(3) | 1.01(9) ^c | 0.14(4) | $E2$ |
| 1872 | 833.19(19) | $2^+ \rightarrow 2^+$ | 25.72(92) | 0.88(8) ^b | -0.16(6) | $M1(+E2)$ |
| 2450 | 1411.14(15) | $4^+ \rightarrow 2^+$ | $62 < I_\gamma < 69$ | 1.03(13) ^f | 0.12(4) | $E2$ |
| 2764 | 891.91(19) | $4^{(+)} \rightarrow 2^+$ | 3.77(26) | 1.32(27) ^b | | ($E2$) |
| 2826 | 1787.32(13) ^d | $3^{(-)} \rightarrow 2^+$ | < 3 | | | |
| 3077 | 627.20(18) | $(4^+) \rightarrow 4^+$ | 8.00(38) | 0.86(26) ^b | | ($M1$) |
| | 1205.21(14) | $(4^+) \rightarrow 2^+$ | 2.13(21) | 1.01(20) ^b | | ($E2$) |
| 3746 | 668.80(21) | $5^- \rightarrow (4^+)$ | 10.96(47) | 0.77(13) ^b | | ($E1$) |
| | 920.34(17) | $5^- \rightarrow 3^{(-)}$ | 2.81(23) | 1.28(30) ^b | | ($E2$) |
| | 981.72(15) | $5^- \rightarrow 4^{(+)}$ | 2.80(23) | 0.46(20) ^b | | ($E1$) |
| | 1296.34(11) | $5^- \rightarrow 4^+$ | 40.15(140) | 0.57(4) ^b | 0.12(7) | $E1$ |
| 4074 | 328.40(17) | $6^- \rightarrow 5^-$ | 24.80(89) | 0.70(5) ^b | 0.11(9) | $M1 + E2$ |
| 4179 | 1728.67(18) | $6^+ \rightarrow 4^+$ | 13.57(55) | 1.09(13) ^b | 0.13(8) | $E2$ |
| 4250 | 176.34(14) | $7^- \rightarrow 6^-$ | 11.97(50) | 0.76(6) ^b | | $M1 + E2$ |
| | 504.45(15) | $7^- \rightarrow 5^-$ | 23.38(85) | 1.05(9) ^b | 0.08(5) | $E2$ |
| 4812 | 738.45(15) | $(7^-) \rightarrow 6^-$ | 2.33(21) | 0.83(27) ^b | | ($M1 + E2$) |
| 5110 | 860.13(18) ^e | $8^{(-)} \rightarrow 7^-$ | 1.30(18) | | | |
| | 1035.90(17) | $8^{(-)} \rightarrow 6^-$ | 4.20(27) | 1.09(22) ^b | | ($E2$) |
| 5205 | 1026.46(18) | $8^+ \rightarrow 6^+$ | 11.25(48) | 1.06(14) ^b | 0.04(2) | $E2$ |
| | 954.42(21) | $8^+ \rightarrow 7^-$ | 15.23(60) | 0.47(5) ^b | | $E1$ |
| 5463 | 1213.22(14) | $9^- \rightarrow 7^-$ | 17.63(67) | 1.13(13) ^b | 0.08(1) | $E2$ |
| 6075 | 1262.89(15) | $(9^-) \rightarrow (7^-)$ | 2.83(14) | 1.20(27) ^b | | ($E2$) |
| 6291 | 1085.65(10) | $10^+ \rightarrow 8^+$ | 19.75(74) | 1.00(10) ^b | 0.06(4) | $E2$ |
| | 827.80(13) | $10^+ \rightarrow 9^-$ | 3.70(26) | 0.45(10) ^c | | $E1$ |
| 6418 | 1308.15(23) | $\rightarrow 8^{(-)}$ | 1.03(18) | | | |
| 6874 | 1411.11(13) | $11^- \rightarrow 9^-$ | < 4 | 1.10(18) ^c | 0.05(1) | $E2$ |
| 7517 | 1225.56(16) | $12^+ \rightarrow 10^+$ | 13.39(55) | 1.06(16) ^b | | $E2$ |
| | 642.77(16) | $12^+ \rightarrow 11^-$ | 2.64(22) | | | |
| 7613 | 1537.97(19) | $\rightarrow (9^-)$ | 0.65(11) | | | |
| 7918 | 1627.30(24) | $(12^+) \rightarrow 10^+$ | 2.08(10) | 0.78(20) ^f | | ($E2$) |
| 8675 | 1800.63(31) ^e | $(13^-) \rightarrow 11^-$ | < 1 | | | |
| 8889 | 1371.75(22) ^e | $\rightarrow 12^+$ | < 1 | | | |
| 9304 | 1787.13(19) | $14^+ \rightarrow 12^+$ | < 10 | 1.15(28) ^c | | ($E2$) |
| | 1385.58(18) | $14^+ \rightarrow (12^+)$ | 0.77(17) | | | |
| 9823 | 518.74(19) | $(15^+) \rightarrow 14^+$ | 5.90(32) | 0.64(16) ^b | | $M1 + E2$ |
| 10880 | 1575.62(30) | $(16^+) \rightarrow 14^+$ | 1.60(19) | 0.83(14) ^c | | ($E2$) |
| 11187 | 1364.41(21) | $(17^+) \rightarrow (15^+)$ | 0.72(17) | 1.05(66) ^f | | ($E2$) |
| 12278 | 1090.65(18) ^e | $\rightarrow (17^+)$ | < 1 | | | |
| | 1398.41(24) ^e | $\rightarrow (16^+)$ | < 1 | | | |

^aThe quoted error includes the fitting error plus an additional error of 3% taken due to the uncertainties in efficiency, background subtraction, etc.

^bGate on $E2$, 1039 keV.

^cGate on $E2$, 1411 keV.

^dMeasurement of R_{DCO} and Intensity were not possible due to the presence of overlapping γ -energies.

^eMeasurement of R_{DCO} or Intensity were not possible due to the weak statistics.

^fGate on $E2$, 1086 keV.

γ - γ coincidence spectra gated by the 1039, 1411 and 519 keV transitions of ^{66}Zn are shown, respectively, in Figs. 2(a)–2(c), wherein most of the new transitions reported in the present work can be seen.

Apart from the ground-state band structure, the positive parity structures have also been established [19–21], which are weakly populated in the present work. The 1872 keV level

decaying to the yrast 2^+ level by the 833 keV γ -ray transition, has been observed in conformity with the earlier spin-parity assignment 2^+ . This state is fed by a 1205 keV transition and a relatively intense 892 keV transition, both having the quadrupole nature as evident from their DCO ratios. The (4^+) level at 3077 keV is fed by a 669 keV transition of $E1$ nature from the strongly populated 5^- state at 3746 keV. It decays

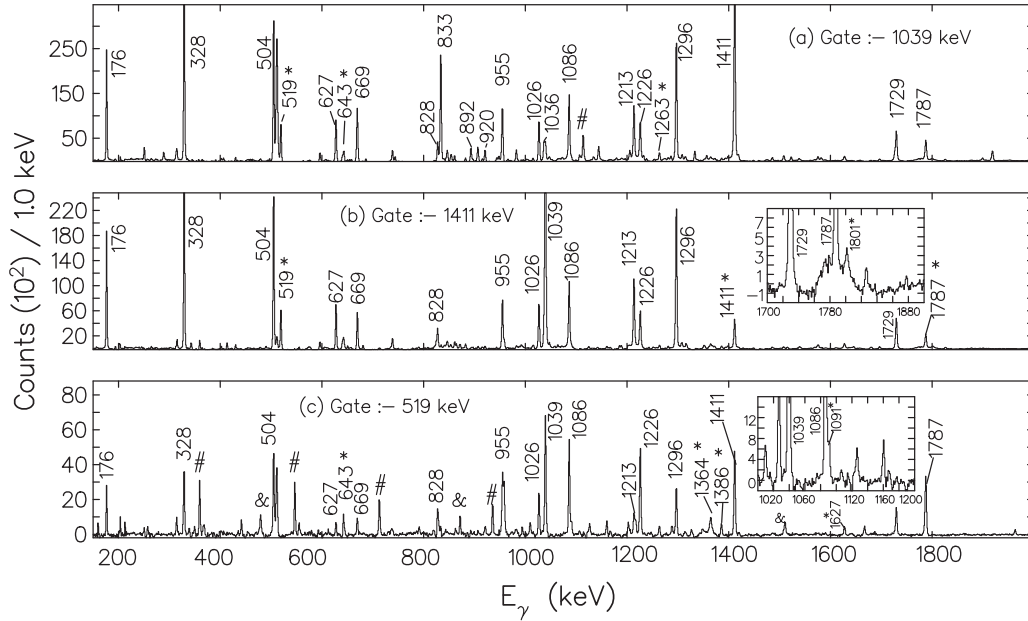


FIG. 2. Background subtracted $\gamma\text{-}\gamma$ coincidence spectra for ^{66}Zn gated on (a) 1039 keV ($2^+ \rightarrow 0^+$), (b) 1411 keV ($4^+ \rightarrow 2^+$), which also contains the contribution from the 1411 keV ($11^- \rightarrow 9^-$) transition. The inset shows the newly identified 1801 keV transition along with the 1729 keV and the 1787 keV transitions, and (c) 519 keV ($(15^+) \rightarrow 14^+$) transition. The inset shows the newly identified 1091 keV transition along with the 1089 keV transition. Here, y-axis represents counts per 1.0 keV. New transitions are marked by the asterisks (*). Strong peaks which are marked with the “#” indicate contaminant γ -rays and those marked by the “&” represent transitions which may belong to ^{66}Zn but could not be placed in the level scheme due to the insufficient coincidence statistics. Here, the contaminant γ -rays are appearing from the $^{61,62}\text{Cu}$ and ^{67}Ga nuclei which are also populated in the same fusion evaporation reaction.

via the 627 keV γ -ray transition to the yrast 4^+ level at the 2450 keV and to the 1872 keV level via the 1205 keV γ -ray transition.

The lowest negative parity state at 2826 keV which was previously established as the 3^- from angular correlation of the de-exciting 1787 keV transition [19], is weakly populated in the present reaction. Due to the presence of an overlapping 1787 keV transition, a firm spin-parity assignment to this state could not be done. This state is fed by a weak 920 keV transition from the 3746 keV level. The 3746 keV level is strongly populated which decays dominantly to the 4_1^+ state. The R_{DCO} and the polarization asymmetry values of the 1296 keV transition feeding the 2450 keV level confirm the 5^- spin-parity assignment to 3746 keV state. Above this level, three strongly populated negative parity states, viz, the 6^- at 4074 keV, 7^- at 4250 keV and the 9^- at 5463 keV, which have been previously established, are confirmed as evident from the electromagnetic nature of the 328, 504, and the 1213 keV transitions, respectively. This sequence is extended by two new levels, one at 6874 keV with the spin-parity 11^- and the other at 8675 keV for which no spin-parity could be assigned due to its weak intensity. The three members of the negative parity sequence i.e, the 7^- , 9^- , and 11^- states are found to be connected to the yrast positive parity states, namely 8^+ , 10^+ , and 12^+ , respectively, by the 955, 828, and 643 keV transitions. A negative parity sequence built on the 6^- , 4074 keV state has been extended with the addition of two new levels at 6075 and 7613 keV. Another cascade of the 1036 and 1308 keV transitions feeding the 6^- level is

observed in accordance with the previous work [20], however spin-parity assignment could not be done for the 6418 keV state due to the weak intensity of the transition decaying from the state. A background subtracted $\gamma\text{-}\gamma$ coincidence spectrum gated by the newly identified 519 keV transition of ^{66}Zn is shown in Fig. 2(c), wherein most of the transitions reported in the present work can be observed.

IV. DISCUSSION

^{66}Zn has two protons and eight neutrons outside the doubly magic core, ^{56}Ni . In the valence configurations, the active orbitals are those of the $N = 3$, $2p_{3/2}$, $1f_{5/2}$, and $2p_{1/2}$ subshells and the $N = 4$, $1g_{9/2}$ intruder subshell. ^{66}Zn , being transitional nucleus, displays a complex spectrum and the description of its level structure from the viewpoint of a single model is difficult. Various theoretical approaches such as the spherical shell-model [35], crude shell model [17], deformed configuration mixing shell-model [36], Hartree-Fock-Bogoliubov calculation [37] and the two-proton cluster vibrator model [21,38] calculations have been used earlier to understand the positive parity and the negative parity level structures in ^{66}Zn .

Using the deformed configuration mixing shell model in the $p_{3/2}f_{5/2}p_{1/2}g_{9/2}$ model space, Ahalpara *et al.* have interpreted fairly well the positive parity high spin states in ^{66}Zn in terms of various configurations [36]. The observation of the sudden dip in the $B(E2)$ value of the $8^+ \rightarrow 6^+$ transition has been attributed to the band crossing between

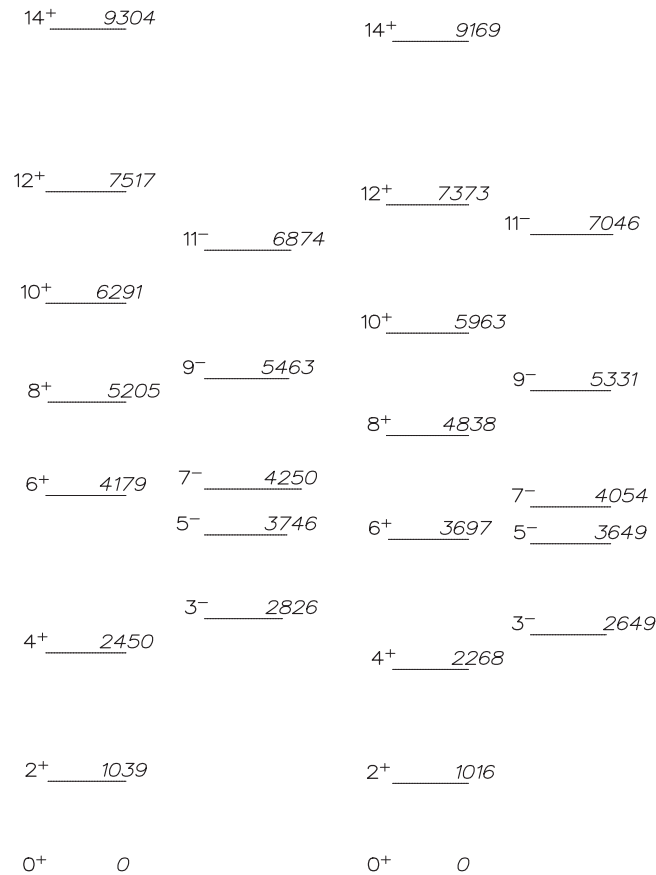


FIG. 3. Comparison of the yrast band and the negative parity level structure of ^{66}Zn (present work) and ^{68}Ge [9]. Numbers along the right side of the levels denote the level energies in keV and that in the left denote the spin(in \hbar)-parity.

the ground-state band and the deformed excited state band arising from the two particle-hole (2p-2h) excitation to the $1g_{9/2}$ orbital [36]. The ground-state band comprising of the $J^\pi = 0^+, 2^+, 4^+, 6^+$ states, has been assigned with the configuration $\pi\nu(p_{3/2}f_{5/2}p_{1/2})^{10}$ and the excited state band comprising of the $8^+, 10^+, 12^+, 14^+$ states to the 2p-2h $(p_{3/2}f_{5/2}p_{1/2})^8(g_{9/2})^2$ configuration. Assuming a configuration of $[\pi(p_{3/2})^2\nu(f_{5/2}p_{1/2})^6]_{6^+} \otimes [\nu(g_{9/2})^2]_{8^+}$, a maximum spin of $14\hbar$ can be obtained and the corresponding (terminating) state has been observed in our work. Beyond this state, a change in the structure or shape transition can be expected which could be predicted by the theoretical calculations. Interestingly, in their calculations, Ahalpara *et al.* predicted the yrast 14^+ level (unobserved experimentally at that time) to lie at ≈ 9.4 MeV, which is very close to the experimentally observed 9.3 MeV level in the present work. In the present investigation, this band is also extended by the placement of the three new connecting γ -ray transitions of 1787, 519 and 1364 keV.

In terms of the level energy, intensity, and decay pattern, a great similarity of the level structure of ^{66}Zn with the neighboring ^{68}Ge isotope is observed. A comparison of the yrast and few negative parity level structure of ^{66}Zn with the isotonic ^{68}Ge is shown in Fig. 3. This kind of

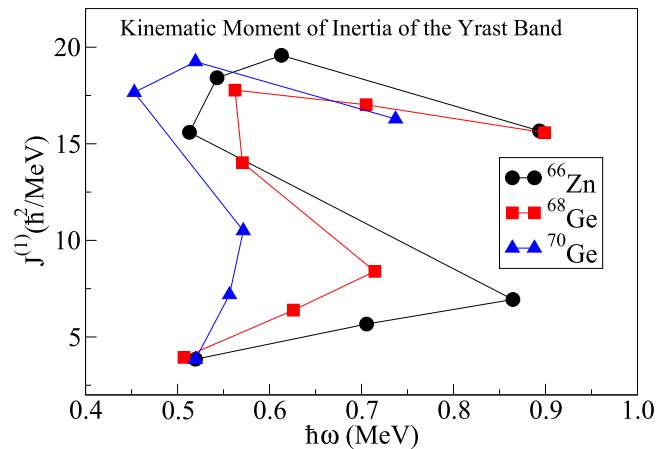


FIG. 4. Variation of the experimentally deduced kinematic moment of inertia as a function of the rotational frequency ($\hbar\omega$) for the yrast positive parity band in ^{66}Zn (present work). The corresponding values of the neighboring $^{68,70}\text{Ge}$ [9–11,14] isotopes are also shown for comparison.

comparison is useful in building the level structure systematics of nuclei in this mass region and in assigning the wave function configurations to the analogous quantum states. In $^{68,70}\text{Ge}$, above the 6^+ state of the ground-state band, two 8^+ states appear leading to the forking of the ground-state band into two quadrupole excited bands [9–11,39]. Theoretical studies [40–42] have suggested this forking phenomena as the band-crossing of the ground-state band with the two excited deformed bands having the two-neutron ($\nu 1g_{9/2}^2$) and the two-proton ($\pi 1g_{9/2}^2$) quasiparticle configurations, respectively. Interestingly in ^{70}Ge , the simultaneous band crossing of the two-neutron aligned configuration and the γ band have been reported leading to the forking of the ground-state band [10].

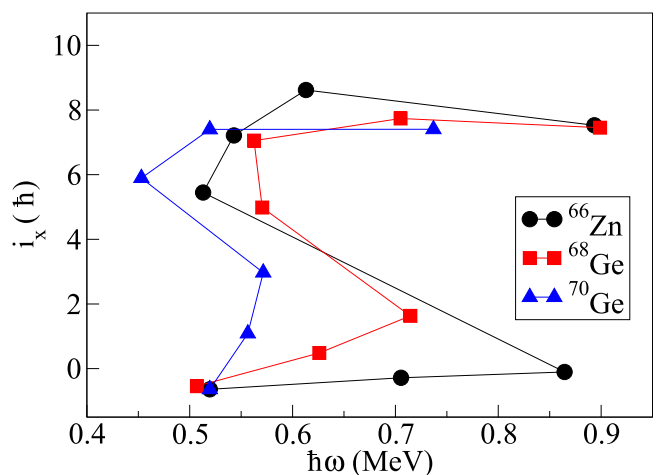


FIG. 5. Experimental alignments of the yrast positive parity band as a function of the rotational frequency for ^{66}Zn (present work) and $^{68,70}\text{Ge}$ [9–11]. The reference rotor, which was subtracted, is based on the Harris parameters, $J_0 = 6.0\hbar^2/\text{MeV}$ and $J_1 = 3.5\hbar^4/\text{MeV}^3$. Please see text for details.

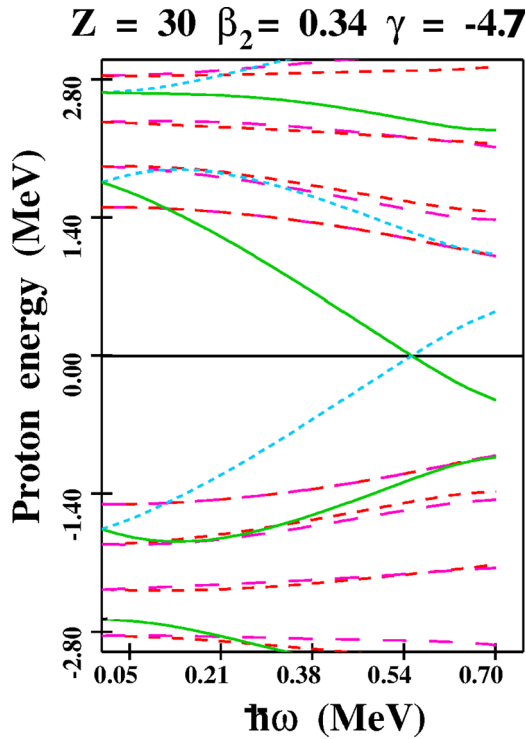


FIG. 6. Calculated quasiparticle Routhians for protons in ^{66}Zn as a function of the rotational frequency $\hbar\omega$ obtained from TRS calculation [44] for $\beta_2 = 0.34$ and $\gamma = -4.7^\circ$. Green and blue lines denote the positive parity, positive signature and positive parity, negative signature, respectively, whereas the red and magenta lines denote the negative parity, positive signature and the negative parity, negative signature respectively. Please see text for more details.

Figures 4 and 5 show the variation of the experimentally deduced kinematic moment of inertia and alignment, respectively, as a function of the rotational energy for ^{66}Zn for the observed yrast positive parity band consisting of 0^+ , 2^+ , 4^+ , 6^+ , 8^+ , 10^+ , 12^+ , and 14^+ states. Here, the kinematic moment of inertia and the alignment are defined, respectively, as $J^{(1)} = i_x/\omega$ and $i = i_x - i_{\text{ref}}$. It is to be noted here, that i_x is the x component (rotational component) of the total angular momentum and i_{ref} corresponds to the value of a reference rotor. The expressions for i_x and i_{ref} are, respectively,

$$i_x = \sqrt{I(I+1) - K^2}$$

and

$$i_{\text{ref}} = (J_0 + \omega^2 J_1)\omega,$$

where K refers to the projection of the total angular momentum on the symmetry axis. J_0 and J_1 represent the Harris parameters. Here, the values of Harris parameters as accepted in this mass region are taken from the Refs. [10,11].

In both figures, the corresponding quantities for the nearby $^{68,70}\text{Ge}$ [9–11] isotopes are also shown for comparison. It is evident that the variation of the kinematic moment of inertia and the alignment as a function of the rotational frequency ($\hbar\omega$) in ^{66}Zn follow the same trend as that in $^{68,70}\text{Ge}$, which in turn indicates a similar intrinsic structure of the observed bands in these three nuclei. The observed backbending in $^{68,70}\text{Ge}$ have been understood to be due to the alignment

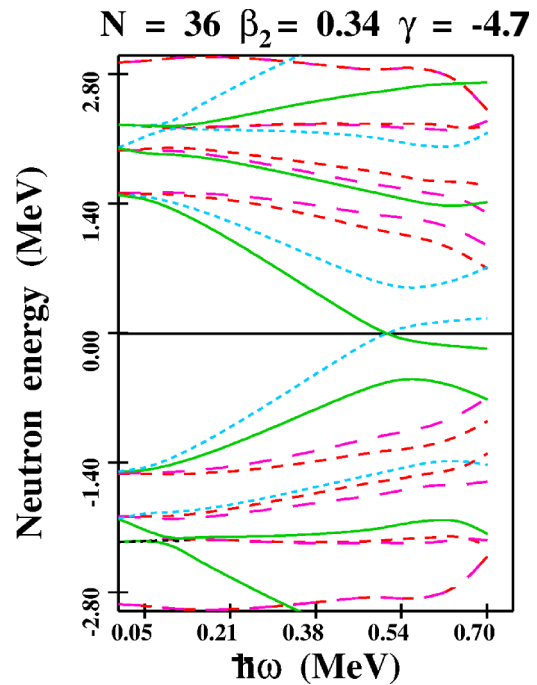


FIG. 7. Same as the Fig. 6 but for the neutrons. Please see text for details.

of a pair of neutrons in the $1g_{9/2}$ orbital [9,10]. As evident from the plots in the Figs. 4 and 5, the first alignment of a pair of neutrons in the $1g_{9/2}$ orbital in $^{68,70}\text{Ge}$ occurs at the frequencies of ≈ 0.60 MeV and ≈ 0.5 MeV, respectively.

The alignment plot for ^{66}Zn indicates that there is a total gain in the alignment of $\approx 8\hbar$ at a frequency of ≈ 0.6 MeV. To understand the observed alignment, quasiparticle Routhians for both the protons and neutrons have been calculated and are plotted, respectively, in the Figs. 6 and 7. The quasi-

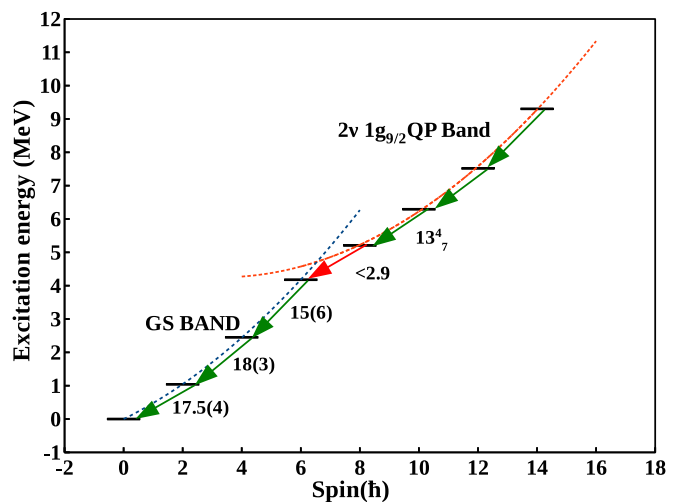


FIG. 8. Excitation energy vs. spin plot for the yrast bands of ^{66}Zn . Reduced transition probabilities $B(E2)$ of the corresponding γ -transitions, which are taken from the literature [43], are also plotted. The dashed lines represent the extrapolation of the bands through the second-order polynomial fitting.

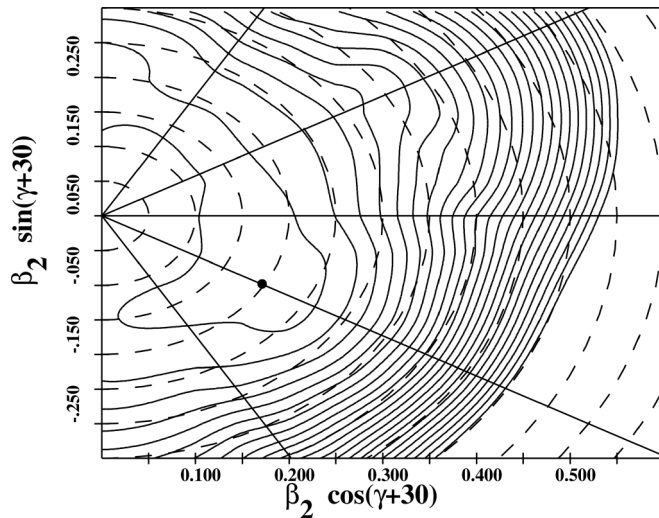


FIG. 9. Contour plots of the TRS calculations in ^{66}Zn for the zero quasiparticle (vacuum) at the rotational frequency ($\hbar\omega$) 0.100 MeV. The energy separation between the two consecutive surface contours is 250 keV.

particle Routhians are calculated using TRS codes based on the Hartree-Fock-Bogoliubov formalism [44], which is discussed later in this manuscript. These plots show that the first crossing of a neutron pair is possible at $\hbar\omega \approx 0.55$ MeV, while that for a pair of protons is feasible at $\hbar\omega > 0.70$ MeV. So, the band built on the 8^+ (5205 keV) state extending to the 14^+ can be understood to be due to the alignment of a pair of neutrons in the $1g_{9/2}$ orbital.

Band crossing has also been reported in the lighter ^{65}Zn isotope, where the two-proton alignment has been found to be responsible for the observed band crossing at a rotational frequency ~ 0.6 MeV [12] with the neutron alignment being blocked. The TRS calculations of ^{65}Zn have predicted that it undergoes a shape transition from a near oblate at lower spin to triaxial at intermediate spin [12]. In ^{66}Zn , the band

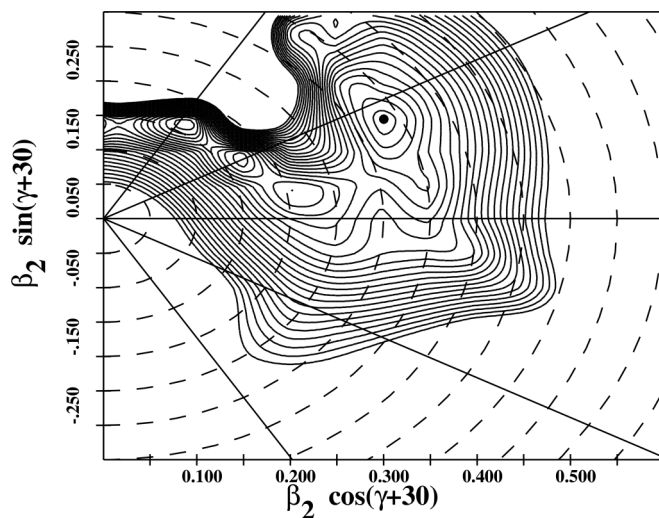


FIG. 10. Same as the Fig. 9 but for the 2ν quasiparticle band (positive parity, positive signature) at $\hbar\omega = 0.5$ MeV in ^{66}Zn .

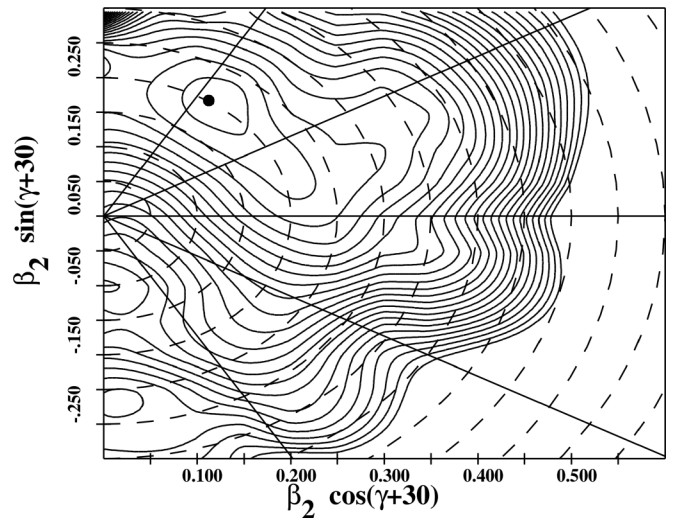


FIG. 11. Contour plots of the TRS calculations for the configuration $\pi(f_{5/2})^2 \otimes \nu(f_{5/2})^3(p_{3/2})^4(g_{9/2})^1$ of the negative parity quadrupole band like structure consisting of the 7^- (4250 keV), 9^- (5463 keV), and 11^- (6874 keV) states in ^{66}Zn at a rotational frequency ($\hbar\omega$) 0.40 MeV. Here, the energy separation between the two consecutive surface contours is 250 keV.

crossing of the ground-state band and the two-quasiparticle band occurs at 6^+ , which is evident from the sudden drop in the $B(E2)$ value (< 2.9 W.u.) for the $8^+ \rightarrow 6^+$, 1026 keV transition [43]. The band crossing is also apparent from the excitation energy vs spin plot for the yrast band illustrated in Fig. 8. The reduced transition probability [$B(E2)$] values for the transitions ($J \rightarrow J-2$) de-exciting along the yrast line, which are taken from the literature [23,43] are also given in the plot. The bands are extrapolated by using a second order polynomial fitting and are given by dashed lines in the plot. The configuration of the two-quasiparticle band is certainly of a two-neutron character, i.e., $(\nu g_{9/2})^2$, as the proton alignment is known to occur at the higher frequencies and one can expect it to undergo a similar shape transition as ^{65}Zn [12] along the positive parity yrast band. However, the two-quasiproton aligned band could not be observed in this nucleus. This may be because of its light nature ($Z = 30, N = 36$), compared to the $^{68,70}\text{Ge}$, leading to the unavailability of the $\pi 1g_{9/2}$ orbital near the proton Fermi surface. The two-neutron quasiparticle structure is well connected to the negative parity states (7^- , 9^- , 11^-), respectively, by the 955, 828, and the 643 keV transitions as seen from the level scheme. This may suggest the fact that these negative parity states also have the similar configurations as the positive parity band.

The TRS calculations for ^{66}Zn have been performed to understand the possible shape evolution using the Woods-Saxon potential. The Hartree-Fock-Bogoliubov code of Nazarewicz *et al.* [44] has been used for the calculations. Equilibrium shapes were calculated in the β_2 - γ plane with the minimization on the β_4 at different values of $\hbar\omega$. Shell corrections have been taken into account and as a residual interaction, the mono pole pairing force has been taken with the strength from Ref. [44]. Figures 9 and 10 show, respectively, the contour plots for the zero quasiparticle and the positive parity, positive

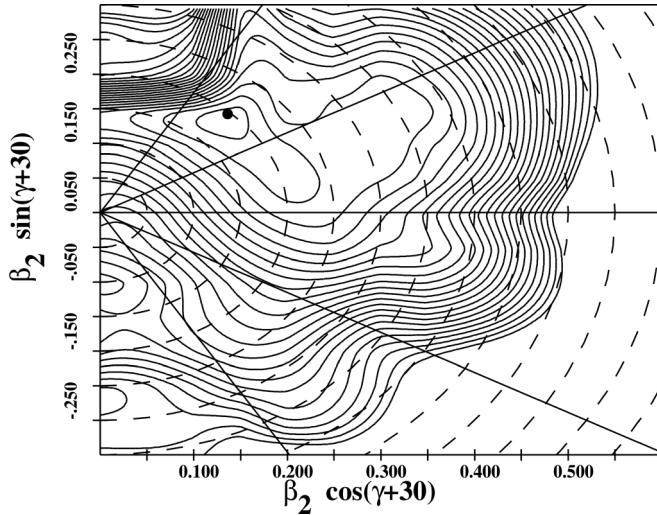


FIG. 12. Same as the Fig. 11 at the rotational frequency ($\hbar\omega$) 0.45 MeV.

signature two neutron quasiparticle sequence in ^{66}Zn . The calculation predicts a collective oblate shape of $\beta_2 \simeq 0.20$ at the lower frequencies up to $\hbar\omega = 0.25$ MeV albeit the flatness of the γ plane indicates a possible triaxial shape as shown in the Fig. 9. With the further increase of the rotational frequency the nucleus becomes more γ soft in nature, which means that the nucleus is triaxial in shape at intermediate spin. At a higher frequency of $\hbar\omega = 0.50$ MeV, it assumes a collective prolate shape having deformation $\beta_2 = 0.34$ ($\gamma \simeq -4^\circ$) as evident from the plot in Fig. 10. These values of $\beta_2 = 0.34$ and $\gamma \simeq -4^\circ$ have been used to calculate the quasiparticle Routhians (Figs. 6 and 7) from which the crossing frequencies are estimated. The TRS calculations thus predict that the alignment of a neutron pair drives the ^{66}Zn nucleus from a collective oblate shape at the ground state via the triaxial shape at the intermediate spin to a collective prolate shape at the high spin.

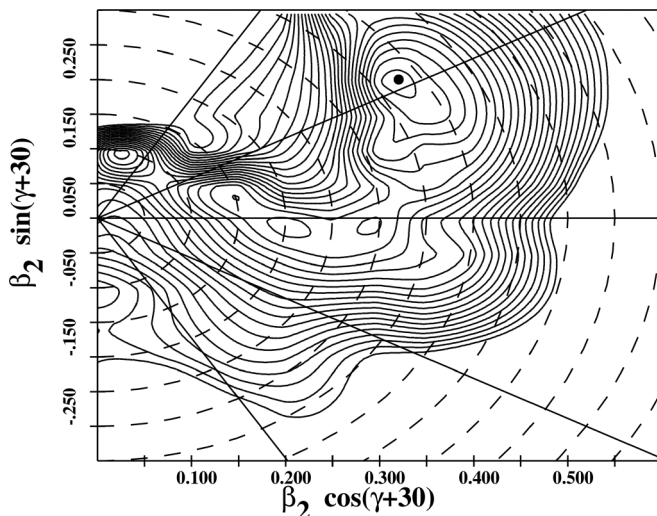


FIG. 13. Same as the Fig. 11 at the rotational frequency ($\hbar\omega$) 0.55 MeV.

The configuration of the negative parity band consisting of the 7^- (4250 keV), 9^- (5463 keV), and 11^- (6874 keV) states is assumed to be of $\pi(f_{5/2})^2 \otimes \nu(f_{5/2})^3(p_{3/2})^4(g_{9/2})^1$. This configuration can generate a maximum angular momentum value of $13\hbar$ which is consistent with the observed highest spin state of the band. Figures 11, 12, and 13 represent the TRS plots for this configuration. As is evident from the plots, the TRS calculations for the negative parity band predict an evolution of shape from a moderately deformed ($\beta_2 \approx 0.20$, $\gamma \approx 23^\circ$) triaxial at $\hbar\omega = 0.40$ MeV to well deformed ($\beta_2 \approx 0.37$, $\gamma \approx 3^\circ$) prolate at $\hbar\omega = 0.55$ MeV.

V. CONCLUSION

Excited states of ^{66}Zn have been studied following their population in a heavy-ion induced fusion-evaporation reaction and using an array of the 14 Compton suppressed clover detectors. Combining the measurement of the energy, angular correlation, linear polarization, intensity and coincidence relationship of the emitted γ -rays, the level scheme of ^{66}Zn has been constructed. With 14 new transitions being identified, the level scheme of this nucleus has been extended up to the excitation energy ≈ 12.3 MeV and a tentative spin of $(17^+)\hbar$. Further, the positive parity [$\pi(p_{3/2})^2\nu(f_{5/2}p_{1/2})^6$] \otimes [$\nu(g_{9/2})^2$] yrast band and the negative parity band corresponding to the $\pi(f_{5/2})^2 \otimes \nu(f_{5/2})^3(p_{3/2})^4(g_{9/2})^1$ configuration have been identified up to their terminating states. A qualitative discussion of the observed band crossing phenomenon and the structure of other levels were presented in the light of various quasiparticle configurations which are based on the existing theoretical studies for this nucleus and the other neighboring nuclei (viz. $^{68,70}\text{Ge}$). TRS calculations predict a shape transition of this nucleus from a collective oblate at $\hbar\omega = 0.10$ MeV to a collective prolate at $\hbar\omega = 0.55$ MeV via triaxial shapes at the intermediate spins along the positive parity yrast band. This shape transition has been attributed to the alignment of a pair of neutron in the $1g_{9/2}$ orbital. Similar TRS calculations corresponding to the negative parity quadrupole band predict an evolution of the shape from the triaxial with a moderate deformation to the prolate with a higher deformation value. Thus, the present study points towards the established fact that the unique parity $1g_{9/2}$ orbital unequivocally plays a major role in the underlying structure of this nucleus as is observed in this work.

ACKNOWLEDGMENTS

The authors thank the operating crew of the Pelletron facility and the target laboratory at IUAC, New Delhi for providing excellent support throughout the experiment. We thank S. Nandi (VECC, Kolkata), S.S. Bhattacharjee (IUAC), and R. Garg (IUAC) for their help during the experiment. Constant encouragement from D. Kanjilal (IUAC) is gratefully acknowledged. We acknowledge the financial assistance received from the IUAC (New Delhi) via Project No. UFR-49318, SERB-DST (India) via Project No. EMR/2015/000891, and DAE-BRNS (India), Project No. 37(3)/14/17/2016-BRNS.

- [1] D. Rudolph *et al.*, *Phys. Rev. L* **80**, 3018 (1998).
[2] C. E. Svensson *et al.*, *Phys. Rev. L* **82**, 3400 (1999).
[3] A. Galindo-Uribarria *et al.*, *Phys. Lett. B* **422**, 45 (1998).
[4] D. Karlgren *et al.*, *Phys. Rev. C* **69**, 034330 (2004).
[5] J. Gellanki *et al.*, *Phys. Rev. C* **86**, 034304 (2012).
[6] M. Albers *et al.*, *Phys. Rev. C* **94**, 034301 (2016).
[7] M. Devlin *et al.*, *Phys. Rev. L* **82**, 5217 (1999).
[8] U. S. Ghosh *et al.*, *Phys. Rev. C* **102**, 024328 (2020).
[9] D. Ward *et al.*, *Phys. Rev. C* **63**, 014301 (2000).
[10] M. Kumar Raju *et al.*, *Phys. Rev. C* **93**, 034317 (2016).
[11] B. Mukherjee *et al.*, *Act. Phys. Hung.: HIP* **13**, 253 (2001).
[12] B. Mukherjee, S. Muralithar, R. P. Singh, R. Kumar, K. Rani, R. K. Bhowmik, S. C. Pancholi, *Phys. Rev. C* **64**, 024304 (2001).
[13] E. A. Stefanova *et al.*, *Phys. Rev. C* **67**, 054319 (2003).
[14] R. A. Haring-Kaye, S. I. Morrow, J. Döring, S. L. Tabor, K. Q. Le, P. R. P. Allegro, P. C. Bender, R. M. Elder, N. H. Medina, J. R. B. Oliveira, and V. Tripathi, *Phys. Rev. C* **97**, 024308 (2018).
[15] A. Gade, H. Klein, N. Pietralla, P. von Brentano, *Phys. Rev. C* **65**, 054311 (2002).
[16] P. M. Endt *et al.*, *Nucl. Phys. A* **575**, 297 (1994).
[17] A. Boucenna, L. Kraus, I. Linck, T. U. Chan, *Phys. Rev. C* **42**, 1297 (1990).
[18] G. P. Couchell *et al.*, *Phys. Rev.* **161**, 1147 (1967).
[19] J. F. Braundet *et al.*, *Phys. Rev. C* **12**, 1739 (1975).
[20] G. F. Neal *et al.*, *Nucl. Phys. A* **280**, 161 (1977).
[21] L. Cleemann *et al.*, *Nucl. Phys. A* **386**, 367 (1982).
[22] B. Erlandsson *et al.*, *Phys. Scr.* **22**, 432 (1980).
[23] C. Morand *et al.*, *J. Phys. Fr.* **38**, 1319 (1977).
[24] D. Kanjilal *et al.*, *Nucl. Instrum. Methods Phys. Res. Sect., A* **328**, 97 (1993).
[25] S. Muralithar *et al.*, *Nucl. Instrum. Methods Phys. Res. Sect., A* **622**, 281 (2010).
[26] B. P. Ajith Kumar *et al.*, in *Proceedings of the 44th DAE-BRNS Symposium on Nuclear Physics* (Department of Atomic Energy, Government of India, Mumbai, 2001), p. 390.
[27] R. K. Bhowmik *et al.*, in *Proceedings of the 44th DAE-BRNS Symposium on Nuclear Physics* (Department of Atomic Energy, Government of India, Mumbai, 2001), p. 422.
[28] D. C. Radford, *Nucl. Instrum. Methods Phys. Res., Sect. A* **361**, 290 (1995).
[29] K. S. Krane *et al.*, *Nucl. Data Tables* **11**, 351 (1973).
[30] K. Starosta *et al.*, *Nucl. Instrum. Methods Phys. Res., Sect. A* **423**, 16 (1999).
[31] R. Palit *et al.*, *Pramana J. Phys.* **54**, 347 (2000).
[32] S. Rai *et al.*, *Eur. Phys. J. A* **54**, 84 (2018).
[33] U. S. Ghosh *et al.*, *Phys. Rev. C* **100**, 034314 (2019).
[34] S. Rai, Ph.D. thesis, Visva-Bharati University (2019).
[35] J. F. A. Van Heinen *et al.*, *Nucl. Phys. A* **269**, 159 (1976).
[36] D. P. Ahalpara *et al.*, *Nucl. Phys. A* **371**, 210 (1981).
[37] S. K. Sharma, *Phys. Rev. C* **22**, 2612 (1990).
[38] V. Lopac and V. Paar, *Nucl. Phys. A* **297**, 471 (1978).
[39] U. Hermkens *et al.*, *Z. Phys. A* **343**, 371 (1992).
[40] A. P. de Lima *et al.*, *Phys. Rev. C* **23**, 213 (1981).
[41] P. A. Dar, R. Devi, S. K. Khosa, J. A. Sheikh, *Phys. Rev. C* **75**, 054315 (2007).
[42] M. Hasegawa, K. Kaneko, T. Mizusaki, *Phys. Rev. C* **70**, 031301(R) (2004).
[43] ENSDF Database, <https://www.nndc.bnl.gov/ensdf>.
[44] W. Nazarewicz *et al.*, *Nucl. Phys. A* **512**, 61 (1990).